CZECH TECHNICAL UNIVERSITY IN PRAGUE

Faculty of Nuclear Sciences and Physical Engineering

FACULTY OF
NUCLEAR SCIENCES
AND PHYSICAL
ENGINEERING
CTU IN PRAGUE

HABILITATION THESIS

Quantum Walks

Martin Štefaňák

Prague, 2017

This thesis is the result of my own work, except where explicit reference is made to the work of others and has not been submitted for another qualification to this or any other university.

Martin Štefaňák

Acknowledgement

I would like to express my sincere gratitude to my colleagues from the Department of Physics, Faculty of Nuclear Sciences and Physical Engineering, Czech Technical University in Prague, in particular, my former PhD. supervisor prof. Igor Jex, Dr. Jaroslav Novotný, Dr. Aurél Gábris and Dr. Václav Potoček, for their contribution to our joint work and for numerous stimulating discussions.

Substantial part of this thesis is based on the results we have obtained together with my students, Ing. Iva Bezděková and Ing. Stanislav Skoupý. I would like to thank them in this way for the fruitful collaboration.

Last but not least, I would like to thank my family and friends for their unflagging support and love.

Abstract

Over the last two decades quantum walks have proven to be a very useful concept in quantum information processing, quantum communication and quantum simulations. The presented thesis reviews our contribution to this field of research. We provide a thorough introduction to methods used for the study of quantum walks and their potential applications. To keep the presentation intelligible we focus on specific examples. In particular, we analyze in detail the properties of homogeneous quantum walks on a one-dimensional lattice with two and three internal states. The application of the obtained results is illustrated on the examples persistence of unvisited sites and quantum transport to an absorbing sink. We also discuss quantum walks on finite graphs and their applications to quantum search and perfect state transfer. Extension of the presented results, which can be found in enclosed published papers, is discussed in detail.

Contents

Notation

$\mathbb{Z}$	set of integers
$\mathbb{C}$	set of complex numbers
$\langle x \rangle$	mean value of a random variable x
Δx	standard deviation of a random variable x
$\mathcal{H}$	separable complex Hilbert space
$l^2(\mathbb{C})$	Hilbert space of square summable complex sequences
$L^2((a,b),dx)$	Hilbert space of square integrable complex function on the interval (a,b)
$\|\psi\rangle$	vector from $\mathcal{H}$
ψ	column vector representing $\|\psi\rangle$ in a particular basis of $\mathcal{H}$
$\langle\psi\|$	linear functional on $\mathcal{H}$
$\langle\phi\|\psi\rangle$	scalar product in $\mathcal{H}$
$\hat{A}$	linear operator on $\mathcal{H}$
A	matrix representation of operator $\hat{A}$ in a particular basis of $\mathcal{H}$
$\hat{I}$	identity operator on $\mathcal{H}$
$\otimes$	tensor product
δ_{ij}	Kronecker delta
$U(n)$	group of $n \times n$ unitary matrices
$f(t) = O(g(t))$	$\|f\|$ is bounded above by g asymptotically, i.e. $\exists\ c,\ t_0 > 0,\ \forall\ t \geq t_0,\ \|f(t)\| \leq cg(t)$
$f(t) = \Omega(g(t))$	f is bounded below by g asymptotically, i.e. $\exists\ c,\ t_0 > 0,\ \forall\ t \geq t_0,\ f(t) \geq cg(t)$
$f(t) = \Theta(g(t))$	f is bounded below and above by g asymptotically, i.e. $f(t) = O(g(t)) \quad \text{and} \quad f(t) = \Omega(g(t))$
$f(t) \sim g(t)$	f is equal to g asymptotically, i.e. $\lim_{t\to\infty} \frac{f(t)}{g(t)} = 1$

Chapter 1

Introduction

Quantum walks [1] emerged during the 1990's as quantum mechanical extensions of classical random walks on a graph or a lattice, although similar ideas appeared already in 1960's in the works of Feynman and Hibbs on discretization of Dirac equation [2] and in the 1980's in the work of Gudder on quantum graphic dynamics [3, 4]. The time evolution of the quantum walk can be either continuous [5] or discrete [6]. In continuous-time quantum walk [5, 7] the evolution of the particle is governed by the Schrödinger equation where the Hamiltonian is given by the discrete Laplacian of the graph. On the other hand, for discrete-time quantum walks the evolution is given by successive application of a unitary evolution operator [6]. In the classical case the discrete-time and continuous-time versions or random walks are equivalent, since we can obtain one from the other by taking an appropriate limit. However, in the quantum case this holds only in several simple cases [8–10], and in general continuous-time and discrete-time quantum walks are not equivalent. Nevertheless, their basic features are similar. Indeed, in both cases coherent evolution of the particle's wave-function manifested in the interference of probability amplitudes results in fundamentally different properties in comparison with the classical random walk. In particular, homogeneous quantum walks on infinite regular lattices spread quadratically faster than their classical counterpart [11]. Indeed, quantum walk is a ballistic process analogous to spreading of light in dispersive media [12], whereas the classical random walk corresponds to a diffusion.

In our work we have focused on the discrete-time quantum walks. Meyer has shown [6] that in order to obtain a non-trivial evolution the particle performing the discrete-time quantum walk cannot be a scalar. A straight-forward way to overcome this constraint is to embed the particle with an additional internal degree of freedom, usually called the coin, which governs the displacements of the particle [11, 13]. This leads us to the coined quantum walk which is the topic of this thesis. Coined quantum walks are naturally defined on regular graphs and lattices. Several variants of coin-less discrete-time quantum walks were proposed. In scattering quantum walks [14–16], which were introduced following the analogy with interferometric networks, the states of the quantum particle corresponds to the directed

edges of the graph. Scattering walks are better suited for graphs with varying vertex degrees than coined quantum walks, however, the two models are fully equivalent as showed in detail in [17, 18]. Another version of coin-less quantum walk was proposed by Szegedy [19] who considered a construction of discrete-time quantum walks based on quantization of classical Markov chains. Certain instances of the Szegedey's model can be converted into the coined quantum walk [20, 21], however, the Szegedy's model is more general. Another formulation of a discrete-time quantum walk dynamics is represented by the staggered quantum walk model [22–26] where the evolution of the particle is governed by reflections that correspond to tessellations of the underlying graph. The staggered quantum walk model was recently proven to be more general than both the coined and the Szegedy's walk [27, 28]. Finally, we note that there is a distinct variant of discrete-time quantum walks, called open quantum walks [29], where the evolution of the walker is driven purely by interactions with the external environment. Open quantum walks are formulated as quantum Markov chains on graphs [30].

The behaviour of quantum walks is usually investigated in the asymptotic limit. For homogeneous translational invariant walks on infinite lattices there exists powerful methods based on Fourier transformation [11]. They allow us to derive in a straightforward way the weak-limit theorems [31] which rigorously prove the ballistic nature of quantum walks. We note that the weak limit theorems can be also derived using the path integral approach [32–34], although with considerably more effort. Homogeneous quantum walks with higher-dimensional coins show additional non-classical effects such as trapping [35–45] where part of the wave-function is captured in the vicinity of the origin. Nevertheless, trapping walks still spread ballistically. Similar effect can be also observed for quantum walks where the translational invariance is broken, e.g. due to point defects [46–50] or restriction of the walk to a half-line [51]. Such walks without translational invariance are significantly more difficult to investigate, however, analytical treatment is still tractable in some cases. For example, the so-called CGMV method [52] which utilizes matrix-valued orthogonal polynomials can be applied to quantum walks on a line [53] or a half-line [54] with position dependent coins. Certain quantum walks with position dependent coins show the effect of Anderson localization [55] manifested by the absence of spreading. Similar effect was observed in quantum walks on a line under the influence of external electric field [56] which implement linearly increasing position dependent phase. The electric field induces either ballistic propagation or Anderson localization, depending on the phase difference per lattice site being a rational multiple of 2π or not. Extending the walk to a 2D lattice allows one to implement artificial magnetic field [57] which shows similar relation between spreading (ballistic/diffusive) and the ratio of magnetic flux through the unit cell to flux quantum (rational/irrational). Great attention has been focused on the influence of external perturbations on the behaviour of quantum walks. It was found that phase noise random in both position and time leads to decoherence and classical behaviour [58, 59]. On the other hand, spatially dependent phase noise results in Anderson localization [60–62]. Another form of external perturbation represented by

randomly disappearing edges leads to quantum walks on dynamical percolation graphs [63]. Asymptotic dynamics of such walks can be treated within the framework of random unitary channels [64–66]. It is highly sensitive to the structure of the percolated graph and boundary conditions [67–69].

Soon after the introduction of quantum walks their potential for quantum information processing was identified [70], in particular, in problems related to graphs. The most promising applications are the quantum walk based algorithms for searching an unsorted database [19, 71–85] which can be formulated as finding a marked vertex of a graph. The quantum walk search offers a quadratic speed-up over its classical counterpart. These results significantly extend the original Grover's search algorithm [86, 87] by representing the database with various graphs structures which might be easier to implement in the future experiments. While the original quantum walk search algorithms were analyzed on symmetric regular lattices or graphs, such as the hypercube or the complete graph, later it was found that high symmetry [88, 89] or connectivity [90] is not required for the optimal runtime of the algorithm. Recently, it was shown [91] that the continuous-time quantum walk search algorithm is optimal for almost all graphs. Quantum walks have been applied to the problem of graph isomorphism testing [92–97] or detecting anomalies in graphs [98–100]. They can be used to achieve quantum state transfer between two vertices of a graph or a lattice [101–106]. Open quantum walks can be used to implement dissipative quantum computation and quantum state engineering [107, 108]. We note that both continuous-time [109] and discrete-time [110] quantum walks were shown to be universal tools for quantum computation, however, the implementation relies on construction of rather complicated graphs and does not seem to be, at least at the moment, suitable for experimental realizations.

Outside of quantum information processing quantum walks were applied to various tasks in the field of quantum simulations. Both continuous-time [111–116] and discrete-time [117–122] quantum walks are natural candidates for modeling of coherent transport on graphs and networks. They are instrumental in discretization of Weyl [123, 124] and Dirac [125–133] equations. Great attention has been recently focused on the abilities of quantum walks to simulate various topological phases of matter [134–145]. The properties of the resulting topologically protected bound states were explored in detail [146, 147].

Wide potential application of quantum walks attracted considerable attention to the design of experimental schemes. Various implementations of quantum walks were proposed, including ion traps [148], neutral trapped atoms [149, 150] and Rydberg atoms [151] in optical lattices, cavity quantum electrodynamics [152, 153], optical cavities [154], linear optics [155, 156], Bose-Einstein condensates [157], arrays of quantum dots [158], semiconductor quantum rings [159], optical angular momentum of light [160], parametric down-conversion in nonlinear crystals [161], or superconducting qubits [162]. For a review on possible realization schemes we refer the reader to [163].

Plenty of successful experimental realizations of quantum walks were reported over the

past decade. Discrete-time quantum walks were implemented in the experiments with optically trapped neutral atoms [164] and ions [165]. The coin degree of freedom is realized by two electronic levels addressed by a laser. A neutral atom experiment was instrumental for simulating the effects of artificial electric fields [166]. Large part of experiments employs interference of light, either coherent or single photons. Continuous-time quantum walks were implemented in integrated wave-guide arrays [168–171]. Discrete-time quantum walks were realized in linear optics experiments mimicking the optical Galton board [172, 173] or beam-displacer interferometers [174, 175]. However, in these schemes the number of required optical elements grows with the desired number of steps of the walk. This can be overcome by utilizing loop architecture and time multiplexing [176], where the position of the walker is encoded into the time of detection. Incorporation of fast-switching programable electro-optical modulators into the optical loops enabled to demonstrate experimentally the effects of decoherence and Anderson localization [177] or a walk on a dynamically percolated graph [178]. Anderson localization was also observed in a walk of two entangled photons in an integrated interferometer array [179]. Effects of topological phases in quantum walks were experimentally demonstrated in a photonic implementation based on optical angular momentum [180] and superconducting circuits [181].

The presented thesis summarizes the work done by the author in the field of quantum walks over the past years. The main body of the text comprises of three Chapters where we illustrate the methods used for analysis of quantum walks and their applications on specific examples. Each Chapter ends with a detailed discussion of extensions of the presented results which can be found in published papers enclosed at the end of the thesis. For easier orientation in the text the author's contributions are listed separately in the bibliography. They are labeled by Roman numerals and ordered chronologically.

The rest of the thesis is organized as follows: Chapter 2 is dedicated to the introduction of analytical methods applicable for homogeneous quantum walks. We briefly introduce coined quantum walks on a line, in particular, the two-state walk with the Hadamard coin (Hadamard walk). This model is used to illustrate the methods of analysis of homogeneous quantum walks, namely the Fourier transformation, stationary phase approximation and the weak-limit theorem. The role of the initial state on the evolution of the Hadamard walk is understood in detail by expressing the derived results in a suitable basis of the coin space. As an example of application of our results we investigate the persistence of unvisited sites. In Chapter 3 the trapping effect and its implications on the behaviour of quantum walks are discussed. We begin with the three-state walk with the Grover coin and investigate the stability of the trapping effect under perturbation of the coin operator. The properties of the derived one-parameter family of walks which preserves the trapping effect are investigated in detail. This model is applied to the study of quantum transport on the ring graph with an absorbing sink. We investigate the restrictions imposed on the transport efficiency by the trapping effect. In Chapter 4 we illustrate the application of quantum walks to perfect

state transfer between two vertices of graph. We discuss the relation between the Grover's search algorithm and the quantum walk search algorithm, and introduce the modification of the latter to achieve perfect state transfer. Finally, we conclude and present an outlook in Chapter 5.

Chapter 2

Analytical Methods for Homogeneous Coined Quantum Walks

2.1 Introduction

In this chapter we review some elementary but highly efficient methods for analyzing the evolution of homogenous coined quantum walks. In particular, we focus on the Fourier analysis [11] and the weak-limit theorem [31]. We describe our contribution to this field, which is a detailed analysis of the role of the initial coin state on the evolution of the quantum walk. The analysis simplifies considerably by choosing a suitable basis of the coin space. We illustrate these methods on the example of the Hadamard walk on a line which was extensively studied in the literature [11, 12, 32, 33, 182–184].

The Chapter is organized as follows: we briefly review the classical random walk on a line and introduce the Hadamard walk as its quantum counterpart in Section 2.2. In Section 2.3 the time evolution of the Hadamard walk is solved with the help of the Fourier transformation. The form of the solution allows us to employ the stationary phase approximation in Section 2.4 to derive some basic properties of the probability distribution generated by the Hadamard walk. We proceed further with the analysis of the probability distribution in Section 2.5 where we derive the weak-limit theorem and the limit density. The dependence of the limit density on the initial condition is investigated in more detail in Section 2.6. The application of the limit density is illustrated on the study of persistence of unvisited sites in Section 2.7. Finally, in Section 2.8 we discuss the extension of the described methods to different models of coined quantum walks which we have considered in [I, V, VI, VII, VIII, IX].

2.2 Hadamard Walk on a Line

Let us first briefly review the classical random walk on a line which is a stochastic process where the particle moves on an integer lattice in discrete time steps. We consider an unbiased

random walk where in each step the particle has two possibilities: it can move from its present position x to the neighboring lattice points $x \pm 1$ with equal probability. Suppose that the particle starts the walk from the origin of the lattice $x = 0$. After the first step, we find it at sites $x = 1$ or $x = -1$ with equal probability one-half. The probability $p(x,t)$ that the particle is at position x at a latter time t is determined by the following recurrence relations

$$p(x,t) = \frac{1}{2}p(x-1,t-1) + \frac{1}{2}p(x+1,t-1), \qquad x \in \mathbb{Z}. \tag{2.1}$$

The solution of the equations (2.1) with the initial condition $p(0,0) = 1$ is given by

$$p(x,t) = \frac{1}{2^t}\binom{t}{\frac{t+x}{2}}, \tag{2.2}$$

where we consider only positions x with the same parity as t. Indeed, the walk is bipartite, i.e. the particle cannot be found at odd (even) position in even (odd) number of steps. We can understand the formula (2.2) in the following way: all random paths connecting the origin and the final destination x in t steps have the same probability $1/2^t$, and the number of such paths is given by the binomial coefficient. Using the formula (2.2) it is straightforward to calculate various attributes of the random walk, e.g. the mean value and the standard deviation of the particle's position. The mean value vanishes since the random walk we consider is unbiased. The standard deviation grows with the square root of the number of steps which corresponds to the fact that the classical random walk is a diffusion process. For large number of steps t we can approximate the exact probability distribution (2.2) with the Gaussian distribution

$$p(x,t) \approx \frac{1}{\sqrt{2\pi t}} e^{-\frac{x^2}{2t^2}},$$

which has a vanishing mean value and a standard deviation $\Delta x = \sqrt{t}$.

Let us now turn to the quantum counterpart of the classical random walk on a line. We consider a propagation of a quantum particle on an integer lattice described by discrete-time unitary evolution. We denote by $|x\rangle, x \in \mathbb{Z}$, the state of the particle being located at the vertex x. These vectors form an orthonormal basis of the position space $\mathcal{H}_P$

$$\mathcal{H}_P = \mathrm{Span}\,\{|x\rangle | x \in \mathbb{Z}\} = l^2(\mathbb{C}), \quad \langle x|y\rangle = \delta_{xy}, \quad \sum_x |x\rangle\langle x| = \hat{I}_P.$$

The propagation of the quantum particle should resemble the classical random walk, where the particle moves from its present position to the nearest neighbours. Instead of choosing the particular direction randomly we would like the quantum particle to evolve into a superposition

$$|x\rangle \longrightarrow |x-1\rangle + |x+1\rangle. \tag{2.3}$$

However, the time evolution according to the rule (2.3) is not unitary, since it does not preserve orthogonality of vectors $|x\rangle$ and $|x \pm 2\rangle$. One possibility to make it unitary is to

consider a quantum particle which has an internal degree of freedom, usually called the coin. This leads us to the coined version of the discrete-time quantum walk [6]. In our particular case the coin has two orthogonal states $|L\rangle$ and $|R\rangle$ which form a basis of the corresponding coin space $\mathcal{H}_C$

$$\mathcal{H}_C = \mathrm{Span}\,\{|L\rangle, |R\rangle\} = \mathbb{C}^2.$$

The complete Hilbert space of such a two-state coined quantum walk on a line is thus given by the tensor product of the position space $\mathcal{H}_P$ and the coin space $\mathcal{H}_C$

$$\mathcal{H} = \mathcal{H}_P \otimes \mathcal{H}_C = l^2(\mathbb{C}) \otimes \mathbb{C}^2.$$

The state of the coin determines the next move of the particle according to the rules

$$|x\rangle|L\rangle \longrightarrow |x-1\rangle|L\rangle, \qquad |x\rangle|R\rangle \longrightarrow |x+1\rangle|R\rangle.$$

This transformation is described by the conditional shift operator $\hat{S}$

$$\hat{S} = \sum_{x=-\infty}^{\infty} \Big(|x-1\rangle\langle x| \otimes |L\rangle\langle L| + |x+1\rangle\langle x| \otimes |R\rangle\langle R| \Big).$$

The time evolution described purely by the shift operator $\hat{S}$ would be trivial, since the part of the initial wave-function with the coin state $|L\rangle$ ($|R\rangle$) will propagate to the left (right) and these two parts will never interfere. In order to achieve a non-trivial time evolution we have to rotate the state of the coin before each application of the shift operator $\hat{S}$. This is mathematically described by the coin operator which in principle can be any unitary acting on the two-dimensional coin space $\mathcal{H}_C$. Moreover, it can be also position and time-dependent. For comparison with the considered classical case where the rules of the evolution do not change we consider the coin operator to be homogeneous in both position and time. We restrict ourselves to a particular choice of the coin given by the Hadamard transformation $\hat{H}$, which is defined by the action on the basis states

$$\hat{H}|L\rangle = \frac{1}{\sqrt{2}}\left(|L\rangle + |R\rangle\right), \qquad \hat{H}|R\rangle = \frac{1}{\sqrt{2}}\left(|L\rangle - |R\rangle\right).$$

This transformation is in the standard basis of the coin space $\{|L\rangle, |R\rangle\}$ represented by the matrix

$$H = \frac{1}{\sqrt{2}} \begin{pmatrix} 1 & 1 \\ 1 & -1 \end{pmatrix}. \tag{2.4}$$

We refer to the two-state quantum walk with this particular choice of the coin operator as the Hadamard walk. The unitary evolution operator $\hat{U}$ which performs a single step of the Hadamard walk is given by

$$\hat{U} = \hat{S} \cdot \left(\hat{I}_P \otimes \hat{H}\right). \tag{2.5}$$

Suppose that the quantum particle starts the walk at the origin with an initial coin state $|\psi_C\rangle$

$$|\psi(0)\rangle = |0\rangle \otimes |\psi_C\rangle. \tag{2.6}$$

The initial coin state $|\psi_C\rangle$ is decomposed into the standard basis of the coin space as

$$|\psi_C\rangle = \psi_L|L\rangle + \psi_R|R\rangle, \tag{2.7}$$

where the amplitudes fulfil the normalization condition

$$|\psi_L|^2 + |\psi_R|^2 = 1.$$

The state of the particle after t steps of the Hadamard walk is given by successive applications of the unitary evolution operator $\hat{U}$ to the initial state

$$|\psi(t)\rangle = \hat{U}^t|\psi(0)\rangle. \tag{2.8}$$

We see that in the quantum case there is no randomness in the time evolution itself - it is the usual unitary evolution of a closed quantum mechanical system. Nevertheless, randomness enters through the measurement. Indeed, if we want to know the position of the particle we have to make a measurement. The probability to find the particle at position x after t steps of the walk is given by the standard quantum mechanical formula

$$p(x,t) = \sum_{i=L,R} |\langle x|\langle i|\psi(t)\rangle|^2,$$

where we sum over the two internal coin states. The state vector after t steps $|\psi(t)\rangle$ can be written as a superposition

$$|\psi(t)\rangle = \sum_{x=-\infty}^{\infty} \Big(\psi_L(x,t)|x\rangle|L\rangle + \psi_R(x,t)|x\rangle|R\rangle \Big), \tag{2.9}$$

where $\psi_{L,R}(x,t)$ are the probability amplitudes of finding the particle at position x with the coin state $|L\rangle$, $|R\rangle$ after t steps of the walk. Let us denote by $\psi(x,t)$ the vector of probability amplitudes corresponding to the position x after t steps, i.e.

$$\psi(x,t) = \left(\psi_L(x,t), \psi_R(x,t)\right)^T.$$

The probability distribution of the particle's position generated by the Hadamard walk is then given by

$$p(x,t) = ||\psi(x,t)||^2 = |\psi_L(x,t)|^2 + |\psi_R(x,t)|^2.$$

For comparison, we show in Figure 2.1 the probability distributions of the classical random walk and the Hadamard walk after $t = 100$ steps. Classical random walk depicted by the

red dots results in a Gaussian distribution with zero mean value and standard deviation proportional to the square-root of the number of steps. Indeed, the classical random walk is a diffusive process. On the other hand, the probability distribution of the Hadamard walk depicted by the black dots is characterized by two dominant peaks on the edges. Due to the choice of the initial coin state $|\psi_C\rangle = |L\rangle$ the peak on the left is more pronounced. Moreover, the standard deviation is proportional to the number of steps, i.e. it grows quadratically faster than in the classical case. The ballistic nature of quantum walks arises from interference of probability amplitudes assigned to different trajectories leading to the same final lattice point. We note that it is important that we let the quantum particle evolve freely and make the position measurement only at the very end. If we perform a position measurement after each step we obtain one classical random path and by making a statistics of such paths we recover a classical random walk.

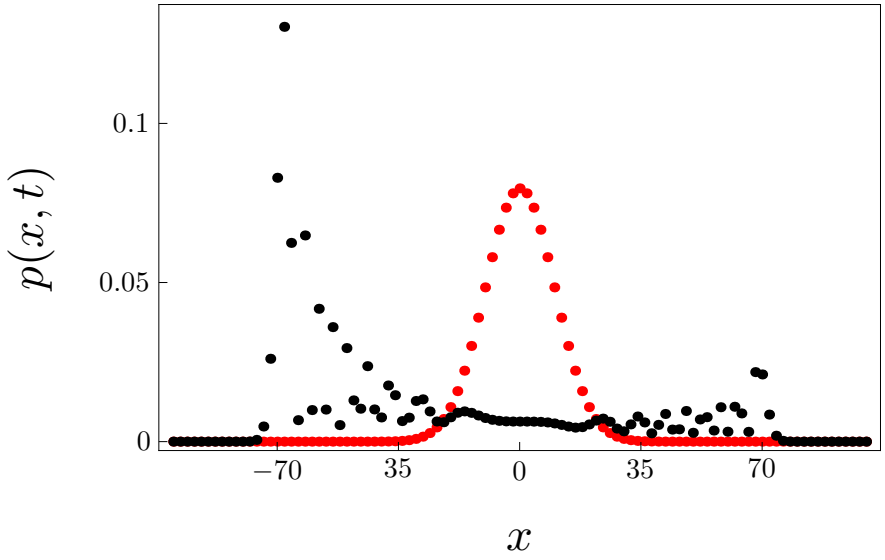

Figure 2.1: The probability distribution $p(x,t)$ of the classical random walk (red dots) and the Hadamard walk (black dots) after 100 steps. We plot $p(x,t)$ only for even x, since after even number of steps the probability to find the particle at odd positions is zero. The width of the distribution is proportional to $\sqrt{t}$ in the classical case and t in the quantum case.

2.3 Fourier Analysis

In this Section we solve the time-evolution equation of the Hadamard walk (2.8) with the help of the Fourier transformation. We follow the approach of [11]. Let us first rewrite the equation (2.8) into a set of equations for the probability amplitudes $\psi(x,t)$. We find that

(2.8) is equivalent to an infinite set of matrix equations

$$\psi(x,t) = H_L\psi(x+1,t-1) + H_R\psi(x-1,t-1), \quad x \in \mathbb{Z}, \tag{2.10}$$

where we have defined the matrices

$$H_L = \frac{1}{\sqrt{2}}\begin{pmatrix} 1 & 1 \\ 0 & 0 \end{pmatrix}, \quad H_R = \frac{1}{\sqrt{2}}\begin{pmatrix} 0 & 0 \\ 1 & -1 \end{pmatrix}.$$

These equations are reminiscent of the time evolution equations of the classical random walk (2.1). However, in (2.10) we transform probability amplitudes instead of probabilities. This difference is at the heart of the quadratically faster growth of the standard deviation for quantum walks in comparison to the classical random walk.

Let us define the Fourier transformation $\hat{F}$ as the isometry between the Hilbert space of the Hadamard walk (i.e. $l^2(\mathbb{C}) \otimes \mathbb{C}^2$) and the Hilbert space of pairs of square integrable complex functions on the unit circle $L^2((0,2\pi),dk) \otimes \mathbb{C}^2$. For $\psi \in l^2(\mathbb{C}) \otimes \mathbb{C}^2$, i.e.

$$\psi = \{\psi(x)\}_{x=-\infty}^{\infty}, \quad \psi(x) \in \mathbb{C}^2, \quad \sum_x ||\psi(x)||^2 < \infty$$

we define its Fourier transformation $\tilde{\psi} \in L^2((0,2\pi),dk) \otimes \mathbb{C}^2$ by

$$\tilde{\psi}(k) = (\hat{F}\psi)(k) = \sum_{x=-\infty}^{\infty} e^{ixk}\psi(x).$$

Multiplying the equation (2.10) by e^{ixk} and summing over all x we find that in the Fourier picture the time-evolution equation reads

$$\tilde{\psi}(k,t) = \tilde{U}(k)\tilde{\psi}(k,t-1), \tag{2.11}$$

where $\tilde{U}(k)$ is the Fourier transformation of the evolution operator $\hat{U}$ which is given by

$$\tilde{U}(k) = D(k)\cdot H, \quad D(k) = \begin{pmatrix} e^{-ik} & 0 \\ 0 & e^{ik} \end{pmatrix}. \tag{2.12}$$

The recurrence relation (2.11) is easily reduced to

$$\tilde{\psi}(k,t) = \tilde{U}(k)^t\tilde{\psi}(k,0), \tag{2.13}$$

where $\tilde{\psi}(k,0)$ is the Fourier transformation of the initial state. Since we consider the initial state of the form (2.6), we find that its Fourier transformation is a k-independent vector ψ_C with components given by the amplitudes of the initial coin state (2.7), i.e.

$$\tilde{\psi}(k,0) = \psi_C = (\psi_L, \psi_R)^T.$$

The time evolution equation (2.13) is readily solved by diagonalizing the matrix $\tilde{U}(k)$. From (2.12) we find that the eigenvalues of $\tilde{U}(k)$ are given by

$$\lambda_1(k) = e^{-i\omega(k)}, \quad \lambda_2(k) = -e^{i\omega(k)},$$

where the phase $\omega(k)$ is determined by the formula

$$\omega(k) = \arcsin\left(\frac{\sin k}{\sqrt{2}}\right). \tag{2.14}$$

The eigenvectors of $\tilde{U}(k)$ corresponding to λ_j can be expressed in the following form

$$\begin{aligned} v_1(k) &= \frac{1}{n_1(k)} \begin{pmatrix} 1 \\ -1 + \sqrt{2} e^{-i\omega(k)+ik} \end{pmatrix}, \\ v_2(k) &= \frac{1}{n_2(k)} \begin{pmatrix} 1 \\ -1 - \sqrt{2} e^{i\omega(k)+ik} \end{pmatrix}. \end{aligned} \tag{2.15}$$

Here the functions $n_i(k)$ represent the normalization factors which equal

$$n_{1,2}(k) = \sqrt{4 - 2\sqrt{2}\cos(k \mp \omega(k))}.$$

The solution of the time-evolution equation in the momentum representation (2.13) is thus given by

$$\tilde{\psi}(k,t) = e^{-i\omega(k)t} v_1(k) f_1(k) + (-1)^t e^{i\omega(k)t} v_2(k) f_2(k), \tag{2.16}$$

where $f_j(k)$ denotes the overlap of the eigenvector $v_j(k)$ with the Fourier transformation of the initial state, i.e.

$$f_j(k) = (v_j(k), \psi_C).$$

Finally, with the help of the inverse Fourier transformation $\hat{F}^{-1}$ defined by

$$\psi(x) = \left(\hat{F}^{-1}\tilde{\psi}\right)(x) = \int_0^{2\pi} \frac{dk}{2\pi} e^{-ixk} \tilde{\psi}(k),$$

we obtain the solution of the time-evolution equation in the position representation in the form

$$\psi(x,t) = \mathcal{I}_1(x,t) + (-1)^t \, \mathcal{I}_2(x,t). \tag{2.17}$$

Here we have defined the integrals

$$\begin{aligned} \mathcal{I}_1(x,t) &= \int_0^{2\pi} \frac{dk}{2\pi} e^{-ixk} e^{-i\omega(k)t} v_1(k) f_1(k), \\ \mathcal{I}_2(x,t) &= \int_0^{2\pi} \frac{dk}{2\pi} e^{-ixk} e^{i\omega(k)t} v_2(k) f_2(k). \end{aligned}$$

This is an exact solution, however, the integrals are difficult to evaluate analytically. Nevertheless, the form of the solution (2.17) allows us to easily identify some basic properties of the probability distribution generated by the Hadamard walk. In particular, we use it to explain the qualitatively different features of the probability $p(x,t)$ in dependence on the relation between $|x|$ and t, as illustrated in Figure 2.2.

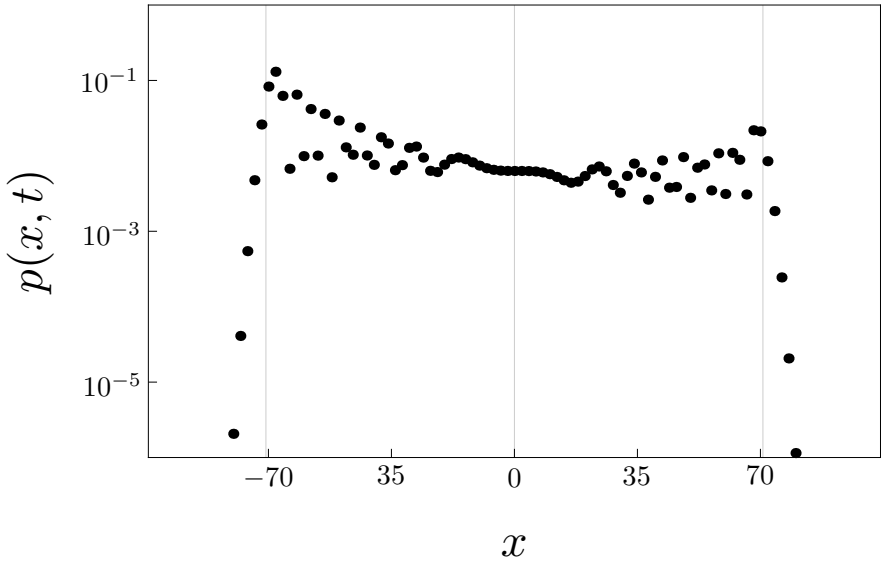

Figure 2.2: Probability distribution of the Hadamard walk with the initial coin state $|\psi_C\rangle = |L\rangle$ after $t = 100$ steps on a logarithmic scale. We clearly observe different regimes of the probability $p(x,t)$ depending on the value of $|x|$. The probability distribution is almost flat for $|x| < 70$. There are significant peaks around positions $x = \pm 70$. Finally, for $|x| > 70$ the probability distribution decreases rapidly.

2.4 Stationary Phase Approximation

Figure 2.2 indicates that there are three distinct regimes of the probability distribution $p(x,t)$ depending on the relation between the number of steps t and the distance from the origin $|x|$. For $|x| \gtrsim 0.7t$ the probability distribution decreases rapidly. Around the points $x \approx \pm 0.7t$ we observe quite dominant peaks. For smaller values of $|x|$ the probability distribution is almost flat. We explain this behaviour by analyzing the asymptotic scaling of the probability distribution. Following the approach of [11] we employ the method of stationary phase [185] to investigate the properties of the integrals $\mathcal{I}_j(x,t)$ for large t. We first rewrite the integrals

into a more suitable form

$$\begin{aligned}\mathcal{I}_1(x,t) &= \int_0^{2\pi} \frac{dk}{2\pi} e^{i\omega_-(k,\frac{x}{t})t} v_1(k) f_1(k), \\ \mathcal{I}_2(x,t) &= \int_0^{2\pi} \frac{dk}{2\pi} e^{i\omega_+(k,\frac{x}{t})t} v_2(k) f_2(k),\end{aligned} \tag{2.18}$$

where we have defined the phases $\omega_\pm$ according to

$$\omega_\pm\left(k, \frac{x}{t}\right) \equiv \pm\omega(k) - \frac{x}{t}k.$$

The asymptotic behaviour of (2.18) can be determined with the stationary phase approximation [185]. Accordingly, the rate of decay is given by the order of the stationary points of the phases $\omega_\pm$. We say that k_0 is a stationary point of ω_j of the order $p-1$ if the first $p-1$ derivatives of ω_j at k_0 vanish and the p-th derivative is non-vanishing. The contribution of such a stationary point k_0 to the integral (2.18) is of the order of $t^{-1/p}$ for large t. If no stationary point within the range of integration exists then the integral decays exponentially with t.

Let us now specify the results for the Hadamard walk. From the expression (2.14) we find that the conditions for k_0 to be a stationary point of the order at least 1 are given by

$$\left.\frac{d\omega_\pm}{dk}\right|_{k_0} = \pm \left.\frac{d\omega}{dk}\right|_{k_0} - \frac{x}{t} = \pm\frac{\cos k_0}{\sqrt{2-\sin^2 k_0}} - \frac{x}{t} = 0. \tag{2.19}$$

The range of the function $\frac{d\omega}{dk} = \frac{\cos k}{\sqrt{2-\sin^2 k}}$ is limited to the interval $\langle -\frac{1}{\sqrt{2}}, \frac{1}{\sqrt{2}}\rangle$. Hence, for $\frac{|x|}{t} > \frac{1}{\sqrt{2}}$ the equations (2.19) do not have a solution, i.e. there are no stationary points of the phases $\omega_\pm$. As follows from the stationary phase approximation, the integrals $\mathcal{I}_j(x,t)$ decay exponentially with t for $|x| > \frac{t}{\sqrt{2}}$. Therefore, the probability distribution $p(x,t)$ also decreases rapidly for $|x| > \frac{t}{\sqrt{2}}$. We illustrate this behaviour in Figure 2.3.

For $\frac{|x|}{t} < \frac{1}{\sqrt{2}}$ the equations (2.19) have solutions $k_{1,2}^\pm$ given by

$$\begin{aligned}\frac{d\omega_+}{dk} &= 0 \quad \Rightarrow \quad k_1^+ = \arccos\left(\frac{\frac{x}{t}}{1-\frac{x^2}{t^2}}\right), \quad k_2^+ = 2\pi - k_1^+, \\ \frac{d\omega_-}{dk} &= 0 \quad \Rightarrow \quad k_1^- = \arccos\left(-\frac{\frac{x}{t}}{1-\frac{x^2}{t^2}}\right), \quad k_2^- = 2\pi - k_1^-.\end{aligned}$$

Moreover, all stationary points $k_{1,2}^\pm$ are of the first order, since the second derivatives of $\omega_\pm$ are non-vanishing as one can readily check from

$$\left|\left.\frac{d^2\omega_\pm}{dk^2}\right|_{k_{1,2}^\pm}\right| = \left(1-\frac{x^2}{t^2}\right)\sqrt{1-2\frac{x^2}{t^2}}.$$

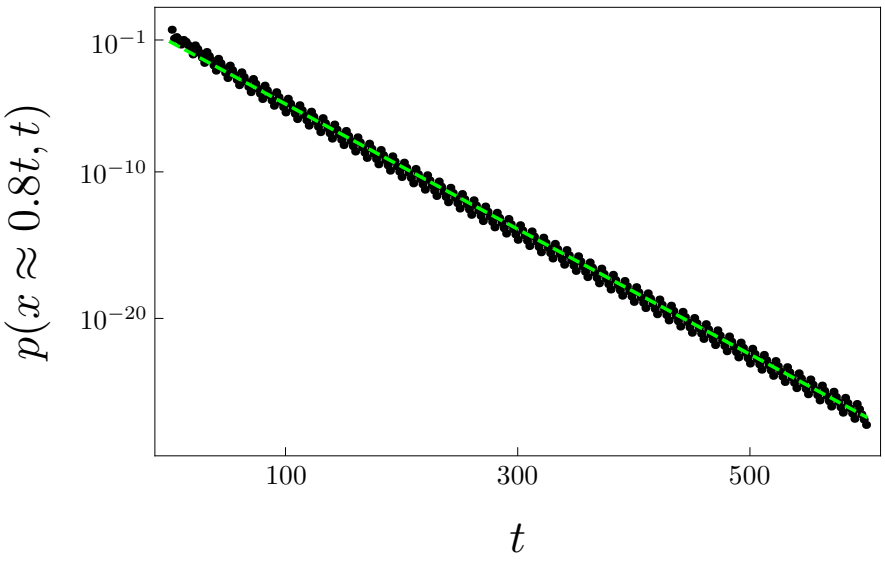

Figure 2.3: Asymptotic scaling of the probability distribution $p(x,t)$ with respect to the number of steps t for $|x| > \frac{t}{\sqrt{2}}$. We have chosen the position x to increase linearly with the number of steps t according to $x \approx 0.8\,t$. The plot uses logarithmic scale to highlight the long-time behaviour. The green dashed line corresponds to the exponential fit $p(x,t) \sim c_1\ e^{-c_2\ t}$.

The stationary phase approximation indicates that for large t the integrals scales according to $\mathcal{I}_j(x,t) = \Theta\left(t^{-\frac{1}{2}}\right)$ for $|x| < \frac{t}{\sqrt{2}}$. The same applies to the probability amplitude $\psi(x,t)$. Hence, for $|x| < \frac{t}{\sqrt{2}}$ the probability behaves like $p(x,t) \sim c\ t^{-1}$. To illustrate this behaviour we plot the probability $p(x,t)$ for a fixed position $x = 0$ as a function of the number of steps t in Figure 2.4.

Finally, let us consider the points $\frac{x}{t} = \pm\frac{1}{\sqrt{2}}$. In this case both the first and the second derivatives of $\omega_\pm$ vanish at $k^\pm_{1,2}$, however, one can check that the third derivatives are non-zero. Hence, for $\frac{x}{t} = \pm\frac{1}{\sqrt{2}}$ the phases $\omega_\pm$ have second order stationary points, and we find that the integrals (2.18) behave as $\mathcal{I}_{2,3}\left(x = \pm\frac{t}{\sqrt{2}}, t\right) = \Theta\left(t^{-\frac{1}{3}}\right)$. This result indicates that in the vicinity of the points $x = \pm\frac{t}{\sqrt{2}}$ the probability distribution behaves like $p(x,t) \sim c\ t^{-\frac{2}{3}}$. Hence, it decays slower than for smaller or larger values of $|x|$ which corresponds to the presence of peaks in the probability distribution. The asymptotic scaling of the probability distribution for $x \approx \frac{t}{\sqrt{2}}$ is illustrated in Figure 2.5.

The distance of the peaks from the origin increases linearly with the number of steps. Hence, one can say that they propagate with a constant velocity which is given by

$$v = \left|\left.\frac{d\omega}{dk}\right|_{k^\pm_{1,2}}\right| = \frac{1}{\sqrt{2}}.$$

This result proves the ballistic spreading of the Hadamard walk on a line. Note that there

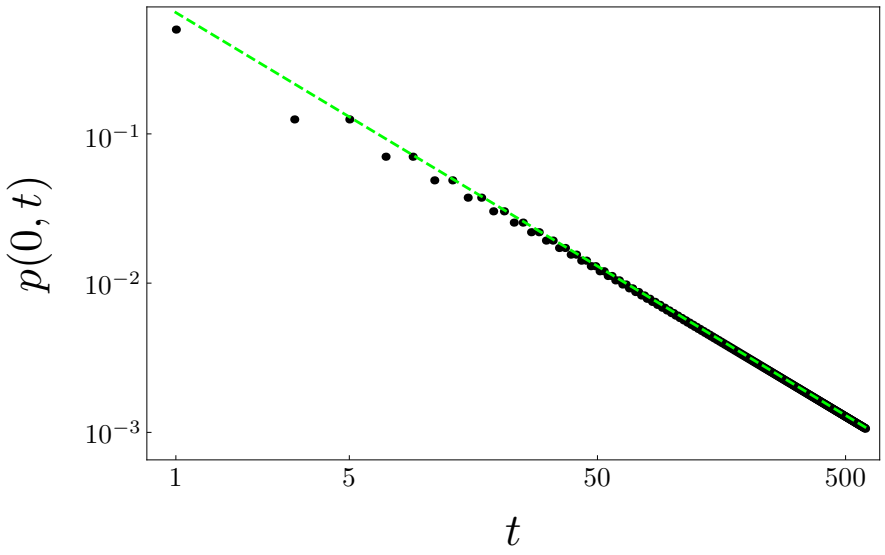

Figure 2.4: Probability to find the particle $p(x,t)$ after t steps for a fixed position $x = 0$. The black dots are obtained from the numerical simulation. The green dashed line is given by the fit $p(x,t) \sim c\, t^{-1}$. We use log-log scale to unravel the asymptotic behaviour of $p(x,t)$.

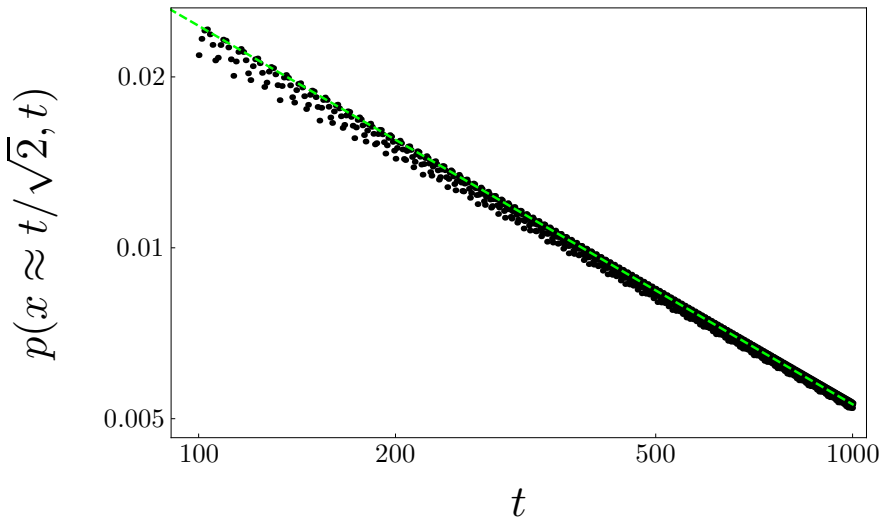

Figure 2.5: Asymptotic scaling of the probability $p(x,t)$ for $x \approx \frac{t}{\sqrt{2}}$. This point corresponds to the position of the peak in the probability distribution after t steps. The black dots are obtained from the numerical simulation. The green dashed line is determined by the fit $p(x,t) \sim c\, t^{-\frac{2}{3}}$. We use log-log scale to unravel the asymptotic behaviour of $p(x,t)$.

is a simple analogy of the spreading of a homogeneous quantum walk on a line with the propagation of a wave in a dispersive medium. Indeed, consider the Fourier variable k as

a wave-number and the phase $\omega(k)$ as frequency. Equation (2.14) represents the dispersion relation. Taking the derivative with respect to k we obtain the group velocity [186]. The wavefront, i.e. the peak in the probability distribution, propagates with the maximal group velocity.

We summarize our observations of a generic probability distribution generated by the Hadamard walk on a line in the Table 2.1.

Distance from the origin	Behaviour of $p(x,t)$
$0 < \lvert x\rvert < \frac{t}{\sqrt{2}}$	$p(x,t) \sim c\ t^{-1}$
$\lvert x\rvert \approx \frac{t}{\sqrt{2}}$	$p(x,t) \sim c\ t^{-\frac{2}{3}}$
$\lvert x\rvert > \frac{t}{\sqrt{2}}$	$p(x,t) \sim c_1\ e^{-c_2\ t}$

Table 2.1: Behaviour of a generic probability distribution $p(x,t)$ in dependence on the relation between $|x|$ and t.

2.5 Weak-limit Theorem

In principle, one can continue with the stationary phase approximation to evaluate higher-order corrections and obtain a more precise description of the probability distribution. However, this procedure is rather tedious. There exists a more straightforward alternative which is based on the observation that the moments of the re-scaled position $\frac{x}{t}$ (or pseudo-velocity) converge in the limit of large number of steps t. To illustrate this behaviour we display in Figure 2.6 the first and the second moment of the random variable $\frac{x}{t}$ as a function of t.

The convergence of moments can be formulated as a week-limit theorem [31]: the pseudo-velocity $\frac{x}{t}$ converges weakly in the asymptotic limit of $t \to +\infty$ to a random variable v. We will prove this statement and derive the explicit form of the probability density of the random variable v, which we refer to as the limit density. We then discuss how the limit density can be used to approximate the probability distribution $p(x,t)$ of the Hadamard walk.

The n-th moment of the pseudo-velocity is given by

$$\left\langle \left(\frac{x}{t}\right)^n \right\rangle = \frac{1}{t^n}\langle \hat{X}^n \rangle = \frac{1}{t^n}\langle \psi(t)|\hat{X}^n|\psi(t)\rangle, \tag{2.20}$$

where the position operator $\hat{X}$ acts on the state vector (2.9) as

$$\hat{X}|\psi(t)\rangle = \sum_{x=-\infty}^{\infty} x \Big(\psi_L(x,t)|x\rangle|L\rangle + \psi_R(x,t)|x\rangle|R\rangle \Big).$$

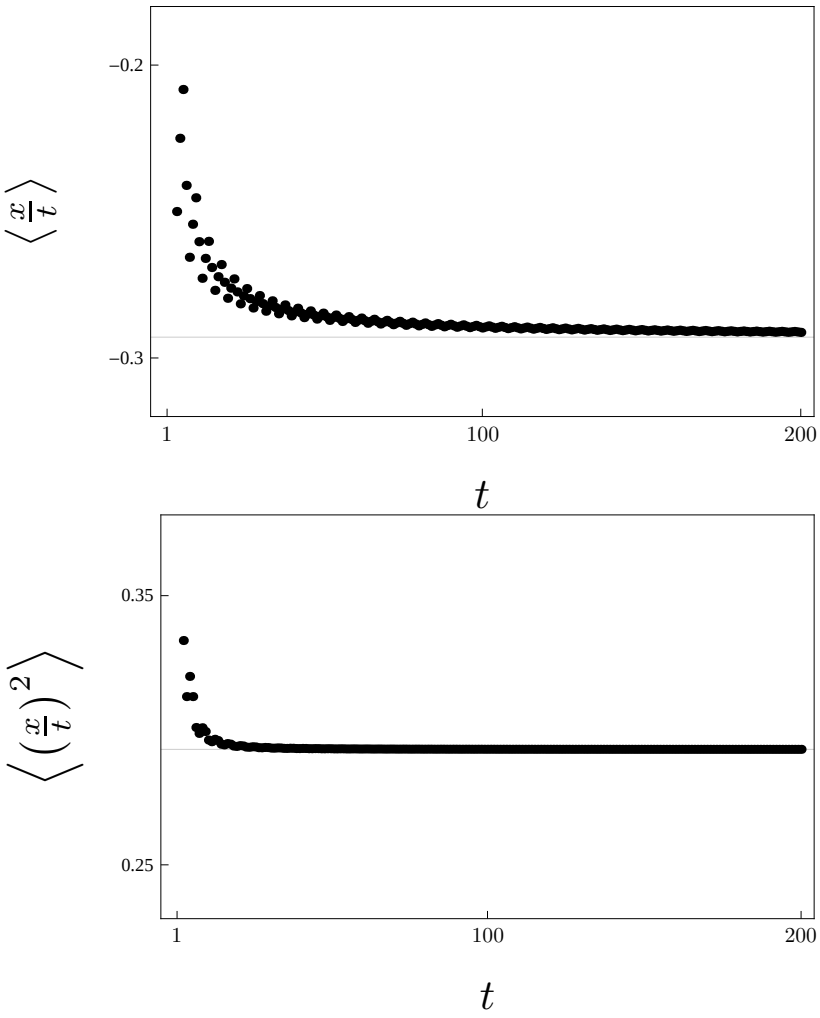

Figure 2.6: First two moments of $\frac{x}{t}$ as a function of the number of steps t. We clearly see that both moments converge to their limiting value. The initial coin state of the Hadamard walk was chosen as $|\psi_C\rangle = |L\rangle$.

The easiest way to evaluate the scalar product in (2.20) is to use the Fourier transformation which turns the position operator $\hat{X}$ into a differential operator with respect to k, i.e.

$$\hat{F}\hat{X}\hat{F}^{-1} = i\frac{d}{dk}.$$

Hence, we find the expression for the n-th moment of the particle's position

$$\langle \hat{X}^n \rangle \;=\; \langle \tilde{\psi}(t)|\hat{F}\hat{X}^n\hat{F}^{-1}|\tilde{\psi}(t)\rangle = \int_0^{2\pi} \frac{dk}{2\pi} \tilde{\psi}^\dagger(k,t) \left(i\frac{d}{dk}\right)^n \tilde{\psi}(k,t), \tag{2.21}$$

where $\tilde{\psi}(k,t)$ is given in (2.16). Let us now turn to the integrand. From the form of the solution in the momentum representation (2.16) we find the relation

$$\left(i\frac{d}{dk}\right)^n \widetilde{\psi}(k,t) = t^n \left(\frac{d\omega}{dk}\right)^n \left(e^{-i\omega(k)t} f_1(k)v_1(k) + (-1)^{t+n} e^{i\omega(k)t} f_2(k)v_2(k)\right) + O(t^{n-1}).$$

The eigenvectors $v_j(k)$ of the evolution operator in the Fourier picture (2.12) satisfy the following orthogonality relations

$$(v_i(k), v_j(k)) = \delta_{ij} \quad \forall k \in (0, 2\pi).$$

This allows us to express the integrand of (2.21) in the form

$$\tilde{\psi}^\dagger(k,t)\left(i\frac{d}{dk}\right)^n \tilde{\psi}(k,t) \;=\; t^n \left(\frac{d\omega}{dk}\right)^n \left(|f_1(k)|^2 + (-1)^n |f_2(k)|^2\right) + O(t^{n-1}).$$

Hence, the moments of the pseudo-velocity $\frac{x}{t}$ are given by

$$\left\langle \left(\frac{x}{t}\right)^n \right\rangle \;=\; \frac{1}{t^n}\langle \hat{X}^n \rangle = \int_0^{2\pi} \frac{dk}{2\pi} \left(\frac{d\omega}{dk}\right)^n \left((-1)^n |f_1(k)|^2 + |f_2(k)|^2\right) + O(t^{-1}). \quad (2.22)$$

With the explicit form of the eigenvectors (2.15) we obtain the following relations

$$\begin{aligned} |f_1(k)|^2 + |f_2(k)|^2 &= 1, \\ |f_1(k)|^2 - |f_2(k)|^2 &= \frac{\left(|\psi_L|^2 - |\psi_R|^2 + \psi_L\overline{\psi_R} + \psi_R\overline{\psi_L}\right)\cos k + \mathrm{Im}\left(\overline{\psi_L}\psi_R - \psi_L\overline{\psi_R}\right)\sin k}{\sqrt{1+\cos^2 k}} \end{aligned}$$

We introduce a new integration variable v defined by

$$v = \frac{d\omega}{dk} = \frac{\cos k}{\sqrt{1+\cos^2 k}}.$$

Inverting this relation we find

$$dk = \frac{dv}{(1-v^2)\sqrt{1-2v^2}}.$$

After some algebra we express the asymptotic values of the moments of pseudo-velocity $\frac{x}{t}$ (2.22) as an integral over the variable v. For even moments we obtain

$$\lim_{t\to\infty} \left\langle \left(\frac{x}{t}\right)^{2n} \right\rangle = \int_{-\frac{1}{\sqrt{2}}}^{\frac{1}{\sqrt{2}}} v^{2n} \frac{dv}{\pi(1-v^2)\sqrt{1-2v^2}}, \quad (2.23)$$

while for odd moments we find

$$\lim_{t\to\infty}\left\langle\left(\frac{x}{t}\right)^{2n+1}\right\rangle = -\int_{-\frac{1}{\sqrt{2}}}^{\frac{1}{\sqrt{2}}} v^{2n+1}\frac{\left(|\psi_L|^2-|\psi_R|^2+\psi_L\overline{\psi_R}+\psi_R\overline{\psi_L}\right)vdv}{\pi(1-v^2)\sqrt{1-2v^2}}. \tag{2.24}$$

We can summarize these results in the form of a weak-limit theorem [31]: the pseudo-velocity $\frac{x}{t}$ converges weakly in the asymptotic limit of $t\to+\infty$ to a random variable v. The limit density of v can be deduced from (2.23) and (2.24) using the method of moments. We find that it is given by [32, 33]

$$w(v) = \frac{\mathcal{M}(\psi_L,\psi_R)}{\pi\left(1-v^2\right)\sqrt{1-2v^2}}, \tag{2.25}$$

where $\mathcal{M}(\psi_L,\psi_R)$ denotes the weight function which depends on the initial coin state

$$\mathcal{M}(\psi_L,\psi_R) = 1-\left(|\psi_L|^2-|\psi_R|^2+\psi_L\overline{\psi_R}+\psi_R\overline{\psi_L}\right)v. \tag{2.26}$$

Since the range of the random variable v is finite the limit density $w(v)$ is determined uniquely. One can easily check that

$$\int_{-\frac{1}{\sqrt{2}}}^{\frac{1}{\sqrt{2}}} w(v)dv = 1,$$

i.e. the density is properly normalized.

We use the limit density $w(v)$ to approximate the exact probability distribution $p(x,t)$ of the Hadamard walk according to

$$p(x,t)\approx\frac{2}{t}w\left(\frac{x}{t}\right). \tag{2.27}$$

The factor of 2 arises from the fact that the Hadamard walk is bipartite, i.e. it occupies only half of the available lattice points at each step. Within this approximation the peaks in the probability distribution $p(x,t)$ correspond to the divergencies of the limit density $w(v)$. Indeed, one can readily see from (2.25) that $w(v)$ diverges for $v\to\pm\frac{1}{\sqrt{2}}$. Hence, $w\left(\frac{x}{t}\right)$ diverges at $x=\pm\frac{t}{\sqrt{2}}$, which coincides with the position of the peaks after t steps. We illustrate the approximation (2.27) for the initial coin state $|\psi_C\rangle=|L\rangle$ in Figure 2.7.

2.6 Change of the Basis in the Coin Space

Let us now investigate the role of the initial coin state $|\psi_C\rangle$ on the shape of the probability distribution in more detail. In principle, this is captured in the limit density through the weight function (2.26), however, the dependence on the initial coin state is rather involved.

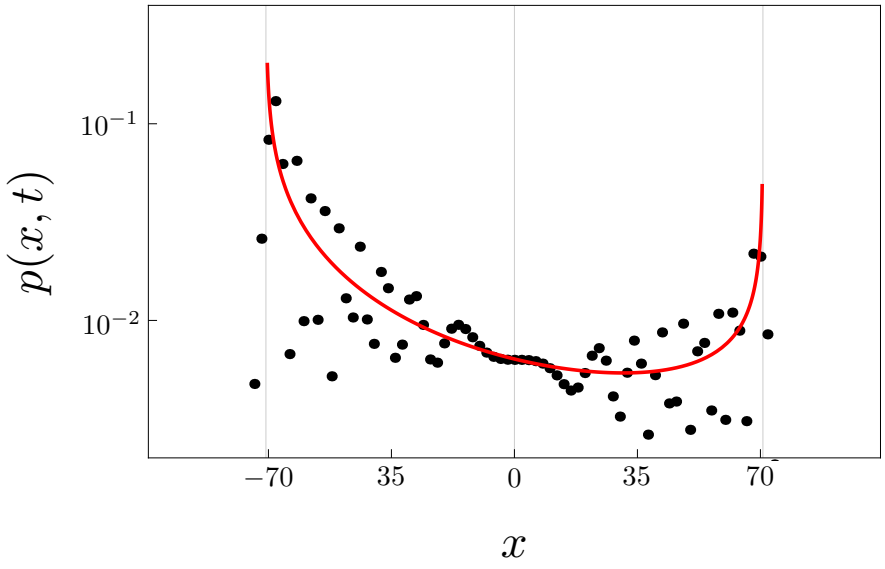

Figure 2.7: The probability distribution after 100 steps of the Hadamard walk for the initial coin state $|\psi_C\rangle = |L\rangle$. The black dots are obtained from the numerical simulation. The red curve corresponds to the approximation (2.27). Notice that the peaks in the probability distribution $p(x,t)$ correspond to the divergencies of the limit density $w(\frac{x}{t})$. The plot is on the log-scale.

Following the approach of [I] we show that the weight (2.26) can be considerably simplified by expressing the initial coin state in a more suitable basis of the coin space.

The weight function $\mathcal{M}(\psi_L, \psi_R)$ depends on the initial coin state through the amplitudes $\psi_{L,R}$ corresponding to the decomposition (2.7) of $|\psi_C\rangle$ into the standard basis of the coin space $\{|L\rangle, |R\rangle\}$. However, we are free to use any basis, and we might find one in which the expression for the weight function (2.26) simplifies. A natural candidate is the basis formed by the eigenvectors of the coin operator $\hat{H}$ which are given by

$$\begin{aligned} |\chi^+\rangle &= \frac{\sqrt{2+\sqrt{2}}}{2}|L\rangle + \frac{\sqrt{2-\sqrt{2}}}{2}|R\rangle, \\ |\chi^-\rangle &= \frac{\sqrt{2-\sqrt{2}}}{2}|L\rangle - \frac{\sqrt{2+\sqrt{2}}}{2}|R\rangle. \end{aligned} \tag{2.28}$$

The vectors $|\chi^\pm\rangle$ satisfy the eigenvalue equations

$$\hat{H}|\chi^\pm\rangle = \pm|\chi^\pm\rangle.$$

Consider the particle starting the walk with the initial coin state $|\psi_C\rangle$ expressed in the eigenvector basis as

$$|\psi_C\rangle = h^+|\chi^+\rangle + h^-|\chi^-\rangle, \tag{2.29}$$

where the amplitudes $h^{\pm}$ satisfy the normalization condition

$$|h^+|^2 + |h^-|^2 = 1.$$

The coefficients of this vector in the standard basis are then given by

$$\begin{aligned} \psi_L &= \frac{\sqrt{2+\sqrt{2}}}{2} h^+ + \frac{\sqrt{2-\sqrt{2}}}{2} h^-, \\ \psi_R &= \frac{\sqrt{2-\sqrt{2}}}{2} h^+ - \frac{\sqrt{2+\sqrt{2}}}{2} h^-. \end{aligned}$$

Substituting these formulas into (2.26) we find that in the new basis the weight function $\mathcal{M}$ acquires a much simpler form

$$\mathcal{M}(h^+, h^-) = 1 - \sqrt{2}\left(2|h^+|^2 - 1\right) v. \tag{2.30}$$

This allows us to get a better understanding of the role of the initial state on the evolution of the quantum walk. First, we see that the coherence of the initial coin state does not influence the shape of the probability distribution or the asymptotic values of the moments of the pseudo-velocity. Indeed, the weight function (2.30) depends only on the probability $|h^+|^2$ of the initial coin state being in the eigenvector $|\chi^+\rangle$. Hence, pure initial coin state (2.29) and a mixed state of the form

$$\hat{\rho}_C = |h^+|^2 |\chi^+\rangle\langle\chi^+| + |h^-|^2 |\chi^-\rangle\langle\chi^-|,$$

result in exactly the same limit density.

Second, we easily find that the eigenvectors $|\chi^{\pm}\rangle$ play a special role since they lead to a non-generic probability distribution with only one peak. Indeed, if we consider $|\chi^+\rangle$ as the initial coin state of the Hadamard walk the weight function reduces to

$$\mathcal{M}(h^+ = 1, h^- = 0) = 1 - \sqrt{2}v.$$

The limit density then has the form

$$w_{|\chi^+\rangle}(v) = \frac{\sqrt{1-\sqrt{2}v}}{\pi\left(1-v^2\right)\sqrt{1+\sqrt{2}v}}. \tag{2.31}$$

We see that the limit density diverges for $v \to -\frac{1}{\sqrt{2}}$, however, for $v \to \frac{1}{\sqrt{2}}$ it tends to zero. Hence, for $|\psi_C\rangle = |\chi^+\rangle$ the resulting probability distribution has only one peak on the left hand side of the lattice. We illustrate this feature in Figure 2.8. Note that for the choice $|\psi_C\rangle = |\chi^-\rangle$ the probability distribution will be the exact mirror image of the one presented in Figure 2.8.

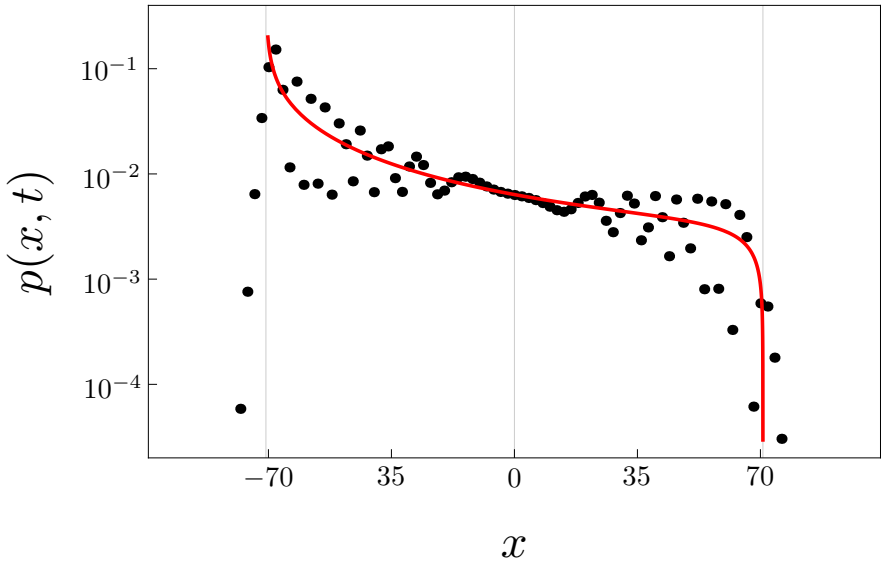

Figure 2.8: The probability distribution after 100 steps of the Hadamard walk for the initial coin state $|\psi_C\rangle = |\chi^+\rangle$. The black dots are obtained from the numerical simulation. The red curve corresponds to the approximation with the limit density (2.31). The choice of the initial coin state $|\chi^+\rangle$ results in a probability distribution with only one peak, in contrast to a generic probability distribution presented Figure 2.7. We use log-scale to unravel the behaviour of the probability distribution near $x \approx 70$.

2.7 Persistence of Unvisited Sites

Finally, let us illustrate the application of the limit density on the example of persistence of unvisited sites [VIII, 187, 188]. Persistence describes the probability that a given site remains unvisited until certain number of steps. For classical random walks on a line and a plane persistence of any site tends to zero for large number of steps. In particular, on one-dimensional lattice persistence obeys an inverse power-law with exponent 1/2, which follows in a straightforward way from the diffusive behaviour of a classical random walk [187]. In the context of quantum walks persistence was first introduced in [188] where persistence of unvisited sites for the Hadamard walk on a line was analyzed. Since measurement has a non-trivial effect on the state of the quantum system, one has to specify a particular measurement scheme to extend the concept of persistence to the domain of quantum walks. The authors of [188] have considered a scheme where the quantum walk is restarted from the beginning after the measurement, and in each iteration one additional step is performed. In this way the effect of measurement on the quantum state is minimized. This measurement scheme was originally introduced in [189] in the context of recurrence of quantum walks, which can be viewed as a complementary event to that of persistence. In [188] it was found that persistence of any site follows an inverse power-law with exponent determined numerically

as $\lambda \approx 0.318$. In contrast to the classical case, no clear connection of the exponent to the ballistic behaviour of the quantum walk was found. We gave analytical explanation of the numerical results found by [188] in the paper [VIII] where we have also extended the study of persistence to different models of quantum walks. Let us now briefly review the approach we have pursued in [VIII].

By persistence of a site x we understand the probability that the particular lattice point remains unvisited until T steps. Since the walk starts at the origin of the lattice we only consider persistence of sites $x \neq 0$. We find that this probability is given by [188]

$$\mathcal{P}_x(T) = \prod_{t=1}^{T}(1 - p(x,t)). \tag{2.32}$$

We are interested in the asymptotic behaviour of persistence for large T. For this purpose we re-write (2.32) in the exponential form

$$\mathcal{P}_x(T) = \exp\left(\ln\left(\prod_{t=1}^{T}(1 - p(x,t))\right)\right) = \exp\left(\sum_{t=1}^{T}\ln(1 - p(x,t))\right).$$

We replace the logarithm by the first order Taylor expansion and arrive at

$$\mathcal{P}_x(T) \approx \exp\left(-\sum_{t=1}^{T} p(x,t)\right). \tag{2.33}$$

Next, we approximate the exact probability $p(x,t)$ with the limit density $w(v)$ according to (2.27) and replace the sum in (2.33) with an integral

$$\mathcal{I}_x(T) = \int_1^T \frac{1}{t} w\left(\frac{x}{t}\right) dt.$$

We obtain the following approximation of persistence

$$\mathcal{P}_x(T) \approx \exp\left(-\mathcal{I}_x(T)\right).$$

Using the form of the limit density of the Hadamard walk (2.25) the integral $\mathcal{I}_x(T)$ can be evaluated explicitly. We find that for large T it grows logarithmically according to [VIII]

$$\mathcal{I}_x(T) \sim \frac{1}{\pi}\ln\left(\frac{T}{|x|}\right).$$

Hence, in the asymptotic regime persistence of site x follows an inverse power-law

$$\mathcal{P}_x(T) \sim c\ \left(\frac{T}{|x|}\right)^{-\frac{1}{\pi}}, \tag{2.34}$$

independent of the initial coin state. The numerical value of the exponent $\lambda = \frac{1}{\pi} \approx 0.318$ coincides with the result obtained in [188].

To illustrate the power-law behaviour (2.34) we display in Figure 2.9 the persistence of site $x = 10$.

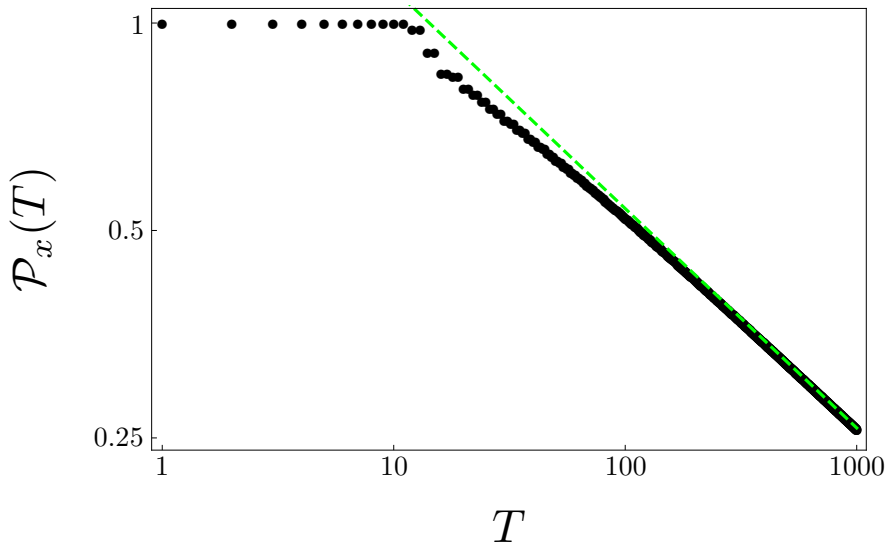

Figure 2.9: Persistence of site $x = 10$ for the Hadamard walk as a function of the number of steps T. The particle starts the walk at the origin with initial coin state $|L\rangle$. The green-dashed line corresponds to the power-law (2.34).

2.8 Discussion

In principle, any homogeneous quantum walk on infinite lattice can be analyzed along the lines we have presented in this Chapter. The Fourier analysis reduces the solution of the time-evolution equation to the diagonalization of a finite-size matrix depending on continuous momentum. However, to find the eigenvalues and eigenvectors of the evolution operator in the Fourier picture analytically is quite a difficult task, especially for quantum walks with more internal degrees of freedom or on higher dimensional lattices. Hence, the limit density in a closed form is known only for several models of quantum walks. Moreover, the dependence of the limit density on the initial coin state is usually rather involved and the complexity increases with growing dimension of the coin space. In this context the simplification of the weight function by a proper choice of the basis of the coin space becomes a crucial point for further analysis of the considered quantum walk and its application.

We have first employed this idea in [I] for the analysis of a quantum walk on a line with two particles. We analyzed the directional correlations between the two particles, i.e. the probability $P_s(t)$ that the particles are after t steps of the walk on the same side of the lattice with respect to the common starting point. We have considered non-interacting particles, i.e. the evolution operator of the two-particle walk has the form

$$\hat{U}^{(2)} = \hat{U} \otimes \hat{U},$$

where $\hat{U}$ is the evolution operator of the two-state Hadamard walk given in (2.5). Never-

theless, the probability distribution of the two-particle walk in general does not factorize into a product of single-particle distributions. Indeed, entangled initial coin states result in non-trivial correlations between the positions of the particles. This makes the dependence of the limit density on the initial coin state in the standard basis of the four-dimensional coin space quite involved. However, the limit density simplifies considerably when the initial coin state is expressed in terms of the basis formed by the eigenvectors of the two-particle coin operator $\hat{H} \otimes \hat{H}$. This basis can be constructed from the eigenvectors of the Hadamard operator (2.28) by taking their tensor product. Expressing the two-particle initial state in the eigenvector basis in the form

$$|\Psi_C\rangle = \sum_{\alpha,\beta=\pm} h_{(\alpha\beta)} |\chi^\alpha\rangle |\chi^\beta\rangle,$$

we found that the limiting value of the directional correlations is given by

$$P_s = \lim_{t\to\infty} P_s(t) = \frac{1}{4}\Big(1 + 2(|h_{(++)}|^2 + |h_{(--)}|^2)\Big).$$

This result shows that the directional correlations for the two-particle Hadamard walk on a line are bounded between $\frac{1}{4}$ and $\frac{3}{4}$. The maximum value is reached when the initial coin state $|\Psi_C\rangle$ is an eigenstate of $\hat{H} \otimes \hat{H}$ with eigenvalue +1, while the minimum value is obtained for $|\Psi_C\rangle$ being an eigenstate corresponding to the eigenvalue -1. In addition, we have analyzed the directional correlations for the walk of non-interacting indistinguishable bosons or fermions. We have shown that it can be reduced to the problem of distinguishable particles with a particular coin state. Finally, we have introduced a two-particle quantum walk with point interactions between the particles by altering the coin operator when the two particles are at the same position. We have indicated by a numerical simulation that for certain point interactions one can exceed the limits of directional correlations for non-interacting particles. This result was later explained analytically in [190].

Quantum walk of two particles on a line, including interactions, was experimentally implemented in [II] using photonic time-multiplexing. The experiment was the first realization of a quantum walk on a non-trivial graph structure, in this case a square lattice. This is mathematically equivalent to a walk of two particles on a line. To simulate the quantum walk of interacting particles one has to alter the coin operator on the diagonal of the square lattice, which corresponds to the two particles being at the same position. In the experiment this was achieved using a fast-switching electro-optical modulator.

We have elaborated on the idea of using the basis of the coin space formed by the eigenvectors of the coin operator for the description of a quantum walk in [V] where we have studied two families of three-state quantum walks on a line which we introduced in [III]. These families of quantum walks exhibit the so-called trapping effect which we discuss in great detail in the following Chapter. In the paper [V] we focused on the role of the initial

coin state and its coherence in controlling the properties of the quantum walk. The use of the basis of the coin space formed by the eigenvectors of the coin operator allowed us to easily identify non-generic solutions which are hidden in the standard basis description. The results of [V] were used extensively in [VII] and [VIII]. In the paper [VII] we have studied the excitation transport to an absorbing center on a ring graph modeled by a discrete-time quantum walk. The results obtained in [V] allowed us to quantify the efficiency of transport in dependence of the initial condition, as we illustrate in the following Chapter. The paper [VIII] was dedicated to the analysis of the asymptotic scaling of persistence of unvisited sites for quantum walks on a line. As we have illustrated on the particular case of the Hadamard walk on a line in Section 2.7, for two-state quantum walks persistence follows an inverse power law, similarly like for the classical random walk. However, for quantum walks there is no connection between the behaviour of persistence and the scaling of the standard deviation. In particular, in [VIII] we have considered two-state quantum walks with the coin

$$C(\rho) = \begin{pmatrix} \rho & \sqrt{1-\rho^2} \\ \sqrt{1-\rho^2} & -\rho \end{pmatrix}, \quad 0 < \rho < 1,$$

which extends the Hadamard walk corresponding to the case $\rho = \frac{1}{\sqrt{2}}$. The coin parameter ρ directly determines the velocity of the peaks. We found that in the asymptotic regime persistence of site x follows an inverse power-law

$$\mathcal{P}_x(T) \sim c \left(\frac{T}{|x|}\right)^{-\lambda},$$

with the exponent

$$\lambda = \frac{\sqrt{1-\rho^2}}{\rho\pi}.$$

Hence, for two-state quantum walks the exponent is determined solely by the coin parameter ρ and it can attain any positive value. For three-state quantum walks the behaviour of persistence can be more involved, as we discuss in the following Chapter.

The analysis of limit distributions and their dependence on the initial coin state was extended further in [VI] to quantum walks with Wigner coins which were introduced in [37]. The authors of [37] have discussed a model of quantum walk on a line where the particle can make $2j + 1$ displacements in each step, where j is a positive integer or half-integer. The coin operator is given by $2j + 1$-dimensional Wigner rotation matrix. The results in [37] were provided in terms of the standard basis of the coin space and their complexity made further analysis of the properties of the quantum walks with Wigner coins quite demanding. In contrast to our previous results for the two-state [I] and three-state quantum walks [V] the eigenvectors of the coin operator do not directly provide the suitable basis. Instead, we have constructed the suitable basis for the two-state model corresponding to $j = \frac{1}{2}$ by explicitly identifying coin states resulting in non-generic densities. From the shape of these

basis vectors we have derived a formula which enabled us to construct a suitable basis for arbitrary j. The simple form of the limit density in the suitable basis allowed us to identify various dynamical regimes in which the quantum walks with Wigner coins can be operated in. As an example, we showed that it is possible to find an initial state which reduces the number of peaks in the probability distribution from generic $2j + 1$ to a single one.

Finally, in the paper [IX] we adopted the ideas developed for quantum walks on a line in [I, V, VI] to quantum walks on a square lattice. We investigated the dependence of the limit density of the two-dimensional quantum walk studied in [38] on the initial coin state. We have shown that similar to [I, V] the eigenvectors of the coin operator form a suitable basis for the description of the properties of the quantum walk. In particular, we found non-generic probability distributions where certain peaks are suppressed.

Chapter 3

Trapping Effect in Quantum Walks

3.1 Introduction

We dedicate this Chapter to the discussion of homogeneous quantum walks for which the unitary evolution operator has a non-empty point spectrum. The existence of point spectrum leads to the so-called trapping effect: part of the wave-function is trapped in the vicinity of the origin which inhibits the spreading of the particle through the lattice. This is a purely quantum-mechanical effect which has no classical counterpart. In the probability distribution of the quantum walk the trapping effect is manifested by an additional peak located at the origin, which does not spread and does not vanish with increasing number of steps. The trapping was first observed in the three-state quantum walk on a line where the coin operator is given by the Grover operator [35, 36]. Later it was identified in quantum walks on higher-dimensional lattices [41–43] and more complicated graph structures [44, 45].

The Chapter is organized as follows: we introduce and explain the trapping effect on the example of the three-state walk on a line with the Grover coin in Section 3.2. We perform the Fourier analysis of the walk in Section 3.3 and show that the trapping effect arises due to the existence of the point spectrum of the evolution operator. The stability of the trapping effect under perturbation of the coin operator is investigated in Section 3.4. For the later discussion we focus on a particular one-parameter family of coins which preserve the trapping nature of the three-state Grover walk. The properties of the considered one-parameter family of quantum walks on a line are analyzed in Section 3.5 and 3.6. In Section 3.5 we investigate the limit density. The trapping probability is evaluated in Section 3.6. In Section 3.7 we consider the three-state quantum walk on a ring graph as a model of quantum transport to an absorbing sink. We conclude in Section 3.8 and discuss the consequences of trapping we have analyzed in the papers [III, IV, V, VII, VIII].

3.2 Three-state Grover Walk on a Line

Let us begin with the formal definition of the three-state Grover walk on a line. The Hilbert space of this quantum walk has the usual form of the tensor product of the position space $\mathcal{H}_P$ and the coin space $\mathcal{H}_C$, i.e.

$$\mathcal{H} = \mathcal{H}_P \otimes \mathcal{H}_C.$$

Since we consider a quantum walk on a line, the position space is the same as for the two-state Hadamard walk which we have discussed in the previous Chapter, i.e.

$$\mathcal{H}_P = \mathrm{Span}\{|x\rangle | x \in \mathbb{Z}\} = l^2(\mathbb{C}),$$

However, the particle is now allowed to remain at its present position. Hence, the coin space is three-dimensional

$$\mathcal{H}_C = \mathrm{Span}\{|L\rangle, |S\rangle, |R\rangle\} = \mathbb{C}^3, \tag{3.1}$$

and the basis state $|S\rangle$ corresponds to the particle staying at its present position.

The discrete-time evolution of the three-state Grover walk is given by the unitary operator $\hat{U}$ according to

$$|\psi(t)\rangle = \hat{U}^t |\psi(0)\rangle, \tag{3.2}$$

where $|\psi(0)\rangle$ is the initial state of the walk. We assume that it has the form

$$|\psi(0)\rangle = |0\rangle \otimes |\psi_C\rangle, \tag{3.3}$$

i.e. the particle starts the walk from the origin $x = 0$ with some initial coin state $|\psi_C\rangle$. Since we consider a homogeneous quantum walk the evolution operator $\hat{U}$ is a product of the displacement operator $\hat{S}$ and the coin operator $\hat{C}$

$$\hat{U} = \hat{S} \cdot \left(\hat{I}_P \otimes \hat{C} \right). \tag{3.4}$$

For the three-state walk on the line the displacement operator is given by

$$\hat{S} = \sum_{x=-\infty}^{\infty} \Big(|x-1\rangle\langle x| \otimes |L\rangle\langle L| + |x\rangle\langle x| \otimes |S\rangle\langle S| + |x+1\rangle\langle x| \otimes |R\rangle\langle R| \Big). \tag{3.5}$$

As the coin we choose the Grover operator $\hat{G}$ on the three-dimensional coin space $\mathcal{H}_C$, which is defined as

$$\hat{G} = 2|w\rangle\langle w| - \hat{I}_C.$$

By $|w\rangle$ we have denoted the uniform superposition of all basis states of the coin space

$$|w\rangle = \frac{1}{\sqrt{3}} \left(|L\rangle + |S\rangle + |R\rangle \right).$$

In the standard basis $\{|L\rangle, |S\rangle, |R\rangle\}$ of the coin space the Grover operator $\hat{G}$ is given by the matrix

$$G = \frac{1}{3}\begin{pmatrix} -1 & 2 & 2 \\ 2 & -1 & 2 \\ 2 & 2 & -1 \end{pmatrix}. \tag{3.6}$$

The state vector after t steps of the three-state Grover walk $|\psi(t)\rangle$ can be written as a superposition

$$|\psi(t)\rangle = \sum_{x=-\infty}^{\infty} \Big(\psi_L(x,t)|x\rangle|L\rangle + \psi_S(x,t)|x\rangle|S\rangle + \psi_R(x,t)|x\rangle|R\rangle \Big),$$

where $\psi_j(x,t)$ are the probability amplitudes of finding the particle at position x with the coin state j $(j = L, S, R)$ after t steps of the walk. Let us denote by $\psi(x,t)$ the vector of probability amplitudes corresponding to the position x after t steps, i.e.

$$\psi(x,t) = (\psi_L(x,t), \psi_S(x,t), \psi_R(x,t))^T.$$

The probability distribution of the particle's position generated by the three-state Grover walk is then given by

$$p(x,t) = ||\psi(x,t)||^2 = |\psi_L(x,t)|^2 + |\psi_S(x,t)|^2 + |\psi_R(x,t)|^2.$$

For illustration, we show in Figure 3.1 a generic probability distribution obtained for the three-state Grover walk with the initial state $|\psi_C\rangle = |S\rangle$ after $t = 50$ steps (blue) and $t = 100$ steps (red).

The probability distribution presented in Figure 3.1 has three characteristic peaks. Two traveling peaks are located at the edges of the probability distribution and their distance from the origin increases linearly with the number of steps t, which shows the ballistic nature of the quantum walk. The height of these peaks decreases with the number of steps. On the other hand, the additional peak at the origin is stationary and it does not vanish even for large number of steps t, as we illustrate in Figure 3.2. Here we present the probability to find the particle at the origin of the walk as a function of the number of steps. One can clearly see that $p(0,t)$ does not vanish even for large t. Moreover, the same holds for any position x on the lattice. We point out that this is a purely quantum-mechanical effect arising from the additional degree of freedom offered in the quantum coin. Indeed, in a classical random walk allowing the particle to stay at its present position does not influence the probability distribution significantly - it will remain a Gaussian. In fact, one step of such a three-state classical random walk is equivalent to two steps of the usual two-state random walk.

In general, we say that a quantum walk shows the trapping effect if

$$\lim_{t\to\infty} p(x,t) \equiv p_\infty(x) \neq 0,$$

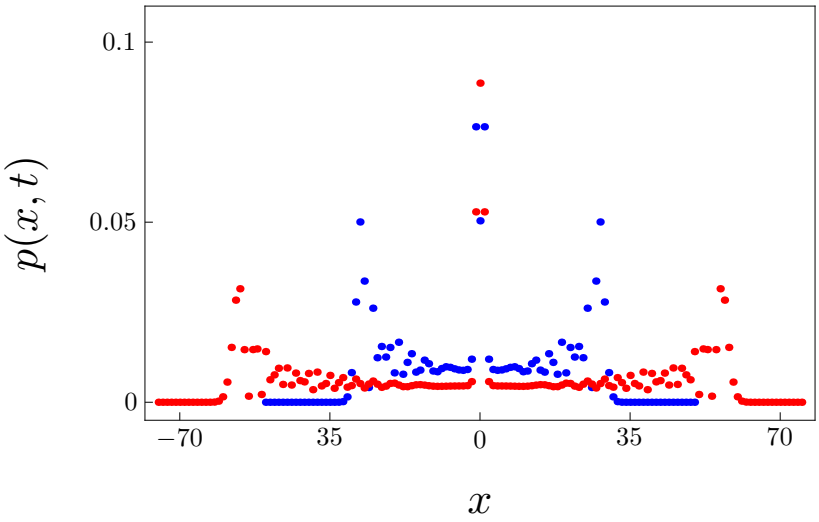

Figure 3.1: Probability distribution of the three-state Grover walk for the initial coin state $|\psi_C\rangle = |S\rangle$ after $t = 50$ steps (blue) and $t = 100$ steps (red).

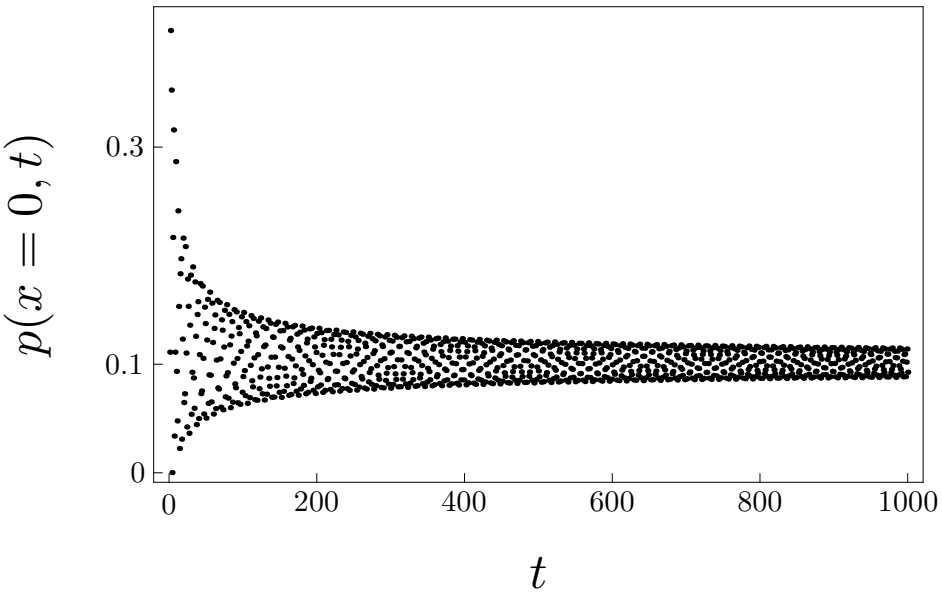

Figure 3.2: Probability to find the particle at the origin $x = 0$ as a function of the number of steps t. The initial coin state was chosen as $|S\rangle$. The plot clearly indicates that the probability $p(0,t)$ converges to a non-zero value.

for some initial coin states. This feature, which is not present in a two-state quantum walk on a line discussed in the previous Chapter, was identified for the first time in [35, 36] and termed localization. However, this is often confused with the Anderson localization

which in the context of quantum walks arises from static phase disorder [60], see [61, 62] for a comprehensive mathematical description. To avoid this confusion we refer to the effect occurring in the three-state Grover walk as trapping. Trapping occurs for homogeneous quantum walks where the time-evolution operator has, apart from the continuous spectrum, also a non-empty point spectrum, as we show in the following Section. The probability distribution of such quantum walk still spreads ballistically ($\Delta x = \Theta(t)$), however, part of the probability distribution is trapped in the vicinity of the starting point, as indicated in Figure 3.1. In contrast, the Anderson localization is a dynamical effect of spatial randomness which reduces the spectrum of the evolution operator to pure point, resulting in the absence of spreading ($\Delta x = \Theta(1)$).

We note that the trapping effect disappears if we choose the initial coin state as the "leaving state" according to [35, 36]

$$|\psi_C\rangle = \frac{1}{\sqrt{6}}|L\rangle - \sqrt{\frac{2}{3}}|S\rangle + \frac{1}{\sqrt{6}}|R\rangle. \tag{3.7}$$

We illustrate this feature in Figure 3.3. The initial coin state (3.7) results in a non-generic probability distribution of the three-state Grover walk. We note that it is an eigenstate of the Grover operator corresponding to the eigenvalue -1. Such states will become useful when we analyze the role of the initial coin state on the probability distribution, as we have shown in the previous Chapter.

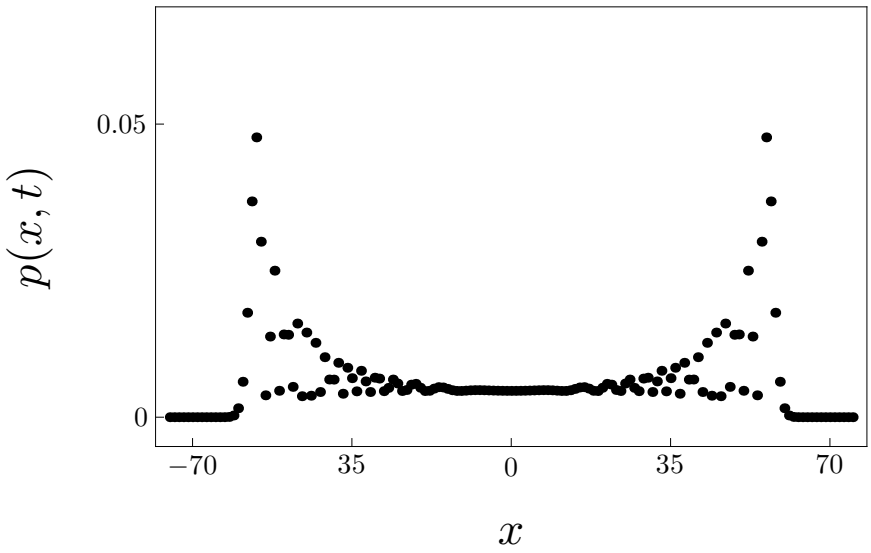

Figure 3.3: Probability distribution of the three-state Grover walk for the leaving state given by (3.7) after $t = 100$ steps. Notice the absence of the central peak in the probability distribution when compared with Figure 3.1.

3.3 Fourier Analysis

In this Section we perform the Fourier analysis of the three-state Grover walk. We show that the trapping effect stems from the fact that the evolution operator of the three-state Grover walk has an infinitely degenerate eigenvalue.

Similarly to Section 2.3 we introduce the Fourier transformation and find that the time-evolution equation (3.2) turns into

$$\tilde{\psi}(k,t) = \tilde{U}(k)^t \tilde{\psi}(k,0). \tag{3.8}$$

Here we have denoted by $\tilde{U}(k)$ the Fourier transformation of the evolution operator which is given by

$$\tilde{U}(k) = D(k) \cdot G, \quad D(k) = \begin{pmatrix} e^{-ik} & 0 & 0 \\ 0 & 1 & 0 \\ 0 & 0 & e^{ik} \end{pmatrix}. \tag{3.9}$$

Since we consider the particle starting the walk from the origin the Fourier transformation of the initial state reads

$$\tilde{\psi}(k,0) = \psi_C = (\psi_L, \psi_S, \psi_R)^T,$$

where ψ_j are the probability amplitudes of $|\psi_C\rangle$ in the standard basis of the coin space.

Let us turn to the spectrum of the evolution operator $\hat{U}$. From (3.9) we find that the eigenvalues of $\tilde{U}(k)$ are given by

$$\lambda_1 = 1, \quad \lambda_{2,3}(k) = e^{\pm i\omega(k)},$$

where $\omega(k)$ is determined by the dispersion relations

$$\omega(k) = \arccos\left(-\frac{1}{3}(2+\cos k)\right). \tag{3.10}$$

We note that $\lambda_{2,3}(k)$ correspond to the continuous spectrum of the evolution operator $\hat{U}$, while $\lambda_1 = 1$ determines its point spectrum. Moreover, $\lambda_1 = 1$ is an eigenvalue of $\hat{U}$ with infinite degeneracy [35, 36]. Indeed, the (non-normalized) eigenvector of $\tilde{U}(k)$ corresponding to λ_1 is easily found to be

$$v_1(k) = \left(1, \frac{1}{2}\left(1+e^{ik}\right), e^{ik}\right)^T. \tag{3.11}$$

Performing the inverse Fourier transformation we find the eigenvector in the position space

$$|s_0\rangle = |0\rangle\left(|L\rangle + \frac{1}{2}|S\rangle\right) + |1\rangle\left(|R\rangle + \frac{1}{2}|S\rangle\right).$$

Moreover, due to the translational invariance of the walk, we can shift the vector $|s_0\rangle$ anywhere on the lattice and obtain an infinite set of eigenvectors

$$|s_x\rangle = |x\rangle \left(|L\rangle + \frac{1}{2}|S\rangle \right) + |x+1\rangle \left(|R\rangle + \frac{1}{2}|S\rangle \right), \quad x \in \mathbb{Z}.$$

One can readily check that they satisfy the equation

$$\hat{U}|s_x\rangle = |s_x\rangle,$$

i.e. they are eigenvectors of the evolution operator with eigenvalue 1.

We show that the existence of the point spectrum of the evolution operator $\hat{U}$ is indeed responsible for the trapping effect. As in the Section 2.3 we find that the solution of the time-evolution equation in the Fourier picture (3.8) can be written in the form

$$\tilde{\psi}(k,t) = v_1(k) f_1(k) + e^{i\omega(k)t} v_2(k) f_2(k) + e^{-i\omega(k)t} v_3(k) f_3(k),$$

where $f_j(k)$ denotes the overlap of the eigenvector $v_j(k)$ with the Fourier transformation of the initial state, i.e.

$$f_j(k) = (v_j(k), \psi_C)\,. \tag{3.12}$$

The explicit form of the eigenvector $v_j(k)$ corresponding to the eigenvalue λ_j is not relevant at the moment. With the help of the inverse Fourier transformation we obtain the solution of the time-evolution equation in the position representation

$$\psi(x,t) = \mathcal{I}_1(x) + \mathcal{I}_2(x,t) + \mathcal{I}_3(x,t),$$

where we have defined the integrals

$$\begin{aligned}
\mathcal{I}_1(x) &= \int_0^{2\pi} \frac{dk}{2\pi} e^{-ixk} v_1(k) f_1(k), \\
\mathcal{I}_2(x,t) &= \int_0^{2\pi} \frac{dk}{2\pi} e^{-ixk} e^{i\omega(k)t} v_2(k) f_2(k), \\
\mathcal{I}_3(x,t) &= \int_0^{2\pi} \frac{dk}{2\pi} e^{-ixk} e^{-i\omega(k)t} v_3(k) f_3(k).
\end{aligned} \tag{3.13}$$

In order to investigate the trapping effect we focus on the asymptotic behaviour of the probability amplitude. As follows from the Riemann-Lebesque lemma the two time-dependent integrals in (3.13) vanish as t approaches infinity. However, the first integral is time-independent. Hence, we find that the probability amplitude at position x in the asymptotic limit $t \to +\infty$ is given by

$$\psi_\infty(x) \equiv \lim_{t \to +\infty} \psi(x,t) = \mathcal{I}_1(x),$$

which can be non-zero. This results in the non-vanishing probability of finding the particle at finite position x in the limit of infinite number of steps

$$\lim_{t\to+\infty} p(x,t) = p_\infty(x) = ||\psi_\infty(x)||^2 \neq 0, \tag{3.14}$$

which we have defined as trapping.

We note that for the initial coin state (3.7) the trapping effect disappears, as we have illustrated in Figure 3.3. This behaviour is straightforward to explain. Indeed, the Fourier transformation of the initial state (3.7)

$$\psi_C = \left(\frac{1}{\sqrt{6}}, -\sqrt{\frac{2}{3}}, \frac{1}{\sqrt{6}}\right)^T,$$

is orthogonal to the eigenvector $v_1(k)$ corresponding to the point spectrum (3.11), i.e. the overlap $f_1(k)$ is zero. Hence, the integral $\mathcal{I}_1(x)$ vanishes, and so does the probability $p(x,t)$ for large t.

We conclude the Fourier analysis of the three-state Grover walk by evaluating the velocity of spreading of the walk through the lattice. This is determined by the continuous part of the spectrum of the evolution operator, i.e. the dispersion relations (3.10). As we have discussed in Section 2.4, the stationary phase approximation indicates that homogeneous quantum walks on a line spread ballistically. The traveling peaks propagate with a constant velocity given by the maximum of the group velocity

$$v = \left|\left.\frac{d\omega}{dk}\right|_{k_0}\right|,$$

where k_0 satisfies

$$\left.\frac{d^2\omega}{dk^2}\right|_{k_0} = 0.$$

From the explicit form of the dispersion relations (3.10) we find that for the three-state Grover walk the velocity of the traveling peaks is given by

$$v = \frac{1}{\sqrt{3}}.$$

This is in accordance with Figure 3.1, which shows the traveling peaks at positions approximately ± 29 after 50 steps (blue dots) and ± 58 after 100 steps (red dots).

3.4 Stability of the Trapping Effect

Let us now turn to the problem of stability of the trapping effect under the change of the coin operator. As we have shown in the previous Section, the trapping effect in the three-state

Grover walk arises from the fact that the evolution operator of the walk has a non-empty point-spectrum. It may be anticipated that the presence of the point spectrum is highly sensitive to the choice of the coin operator. It might not be limited to isolated examples such as the Grover coin, however, even a small perturbation of the coin in a wrong direction can eliminate the eigenvalue. This can be crucial for experimental realizations of such quantum walks, since imperfections in all operations have to be taken into account.

We have addressed this issue for three-state quantum walks in [III] and [IV]. In [III] we have derived two one-parameter families of coins which preserve the point spectrum. The sets were obtained by a suitable parametrization either of the eigenvalues or of the eigenvectors of the Grover matrix. Later, in the paper [IV] we have provided a full classification of $U(3)$ coins which lead to the trapping effect for three-state quantum walks on a line.

Let us now illustrate the approach how to find the sets of coins preserving the trapping effect which we have pursued in [III]. We focus on the parametrization of eigenvectors of the Grover matrix. This was inspired by the work of Watabe et al. [38] where a one-parameter family of 2D quantum walks which contained the four-state Grover walk was studied. This set of quantum walks preserves the trapping effect of the four-state Grover walk. The particular property of the corresponding one-parameter set of 4×4 coin operators is that they have the same spectrum as the Grover matrix. In [III] we have adopted this feature to construct a similar set of 3×3 coins.

We begin with the spectral decomposition of the 3×3 Grover coin. The eigenvalues of the Grover matrix are given by

$$\nu_1 = \nu_2 = -1, \quad \nu_3 = 1.$$

The corresponding eigenvectors can be chosen as

$$\begin{aligned} |\gamma_1^-\rangle &= \frac{1}{\sqrt{6}} \left(|L\rangle - 2|S\rangle + |R\rangle \right), \\ |\gamma_2^-\rangle &= \frac{1}{\sqrt{2}} \left(|L\rangle - |R\rangle \right), \\ |\gamma^+\rangle &= \frac{1}{\sqrt{3}} \left(|L\rangle + |S\rangle + |R\rangle \right). \end{aligned} \tag{3.15}$$

The 3×3 Grover operator can be thus decomposed in the form

$$\hat{G} = -|\gamma_1^-\rangle\langle\gamma_1^-| - |\gamma_2^-\rangle\langle\gamma_2^-| + |\gamma^+\rangle\langle\gamma^+|.$$

Let us now consider two rather trivial coin operators which have the same spectrum as the Grover matrix and which also lead to trapping of the corresponding three-state quantum walk. One of such coin operators is in the standard basis of the coin space given by the matrix

$$G' = \begin{pmatrix} 0 & 0 & 1 \\ 0 & -1 & 0 \\ 1 & 0 & 0 \end{pmatrix}.$$

Using this matrix as a coin for a three-state quantum walk results in a trivial evolution - the particle either stays at the origin, or jumps to the left or right but immediately returns back in the next step. Such a walk does not spread through the lattice. Indeed, one can readily check that the spectrum of the corresponding evolution operator is pure point, i.e. the continuous spectrum is absent.

The second coin operator we consider is given by the matrix

$$G'' = \begin{pmatrix} -1 & 0 & 0 \\ 0 & 1 & 0 \\ 0 & 0 & -1 \end{pmatrix}.$$

The dynamics of the resulting quantum walk is also simple. The $|S\rangle$ component of the initial state remains forever at the origin which corresponds to trapping. The $|L\rangle$ ($|R\rangle$) component moves in every step to the left (right). After t steps the particle can be found only on three lattice points - either $x = 0$ or $x = \pm t$. In contrast to the walk driven by the coin G' the walk with coin G'' spreads through the lattice with the maximal possible velocity of the traveling peaks $v = 1$.

In order to connect the Grover matrix and the matrices G' and G'' we examine their eigenvectors. The eigenvectors of the Grover operator were given in (3.15). The eigenvectors of $\hat{G}'$ are

$$\begin{aligned} |\alpha_1^-\rangle &= -|S\rangle, \\ |\alpha_2^-\rangle &= \frac{1}{\sqrt{2}}\left(|L\rangle - |R\rangle\right), \\ |\alpha^+\rangle &= \frac{1}{\sqrt{2}}\left(|L\rangle + |R\rangle\right). \end{aligned}$$

Finally, the eigenvectors of $\hat{G}''$ are given by

$$\begin{aligned} |\beta_1^-\rangle &= \frac{1}{\sqrt{2}}\left(|L\rangle + |R\rangle\right), \\ |\beta_2^-\rangle &= \frac{1}{\sqrt{2}}\left(|L\rangle - |R\rangle\right), \\ |\beta^+\rangle &= |S\rangle. \end{aligned}$$

In all three cases the first two eigenvectors correspond to the eigenvalue -1 while the third one has the eigenvalue $+1$. Notice that the second eigenvector can be chosen such that it is always the same. We parameterize the first and the third eigenvector so that they continuously change from $|\alpha^\pm\rangle$ through $|\gamma^\pm\rangle$ to $|\beta^\pm\rangle$ while remaining mutually orthogonal

and normalized. This parametrization is given by

$$\begin{aligned} |\sigma_1^-\rangle &= \frac{\rho}{\sqrt{2}}|L\rangle - \sqrt{1-\rho^2}|S\rangle + \frac{\rho}{\sqrt{2}}|R\rangle, \\ |\sigma_2^-\rangle &= \frac{1}{\sqrt{2}}(|L\rangle - |R\rangle), \\ |\sigma^+\rangle &= \sqrt{\frac{1-\rho^2}{2}}|L\rangle + \rho|S\rangle + \sqrt{\frac{1-\rho^2}{2}}|R\rangle. \end{aligned} \tag{3.16}$$

With these vectors we construct the following one-parameter set of coin operators

$$\hat{G}(\rho) = -|\sigma_1^-\rangle\langle\sigma_1^-| - |\sigma_2^-\rangle\langle\sigma_2^-| + |\sigma^+\rangle\langle\sigma^+|,$$

which is in the standard basis of the coin space represented by the matrix

$$G(\rho) = \begin{pmatrix} -\rho^2 & \rho\sqrt{2(1-\rho^2)} & 1-\rho^2 \\ \rho\sqrt{2(1-\rho^2)} & 2\rho^2-1 & \rho\sqrt{2(1-\rho^2)} \\ 1-\rho^2 & \rho\sqrt{2(1-\rho^2)} & -\rho^2 \end{pmatrix}. \tag{3.17}$$

The matrices G' and G'' correspond to the values $\rho = 0$ and $\rho = 1$, respectively. The Grover matrix G is given by the coin parameter $\rho = \frac{1}{\sqrt{3}}$.

Due to the construction described above we will refer to the three-state quantum walks with the one-parameter set of coins (3.17) as the eigenvector family of walks. Let us now show that they exhibit the trapping effect and that the coin parameter ρ directly determines the velocity of the traveling peaks. In order to prove this we investigate the spectrum of the evolution operator, which is readily found to be

$$\lambda_1 = 1, \quad \lambda_{2,3}(k,\rho) = e^{\pm i\omega(k,\rho)}.$$

The existence of k-independent eigenvalue $\lambda_1 = 1$ shows that indeed the one-parameter family of coins (3.17) leads to the trapping effect. Let us now investigate the physical meaning of the parameter ρ. For this reason we examine the continuous spectrum of the evolution operator, which is determined by the dispersion relations

$$\omega(k,\rho) = \arccos\left(\rho^2 - 1 - \rho^2\cos k\right).$$

We see that the parameter ρ alters the dispersion relations and therefore it influences the rate of spreading of the corresponding quantum walk. To determine the velocity of the traveling peaks we have to identify the maximum of the group velocity $\frac{d\omega}{dk}$. We find that the second derivative

$$\frac{d^2\omega}{dk^2} = \frac{\rho(\rho^2-1)\sqrt{1-\cos k}}{(2-\rho^2+\rho^2\cos k)^{\frac{3}{2}}},$$

vanishes for $k_0 = 0$. Hence, the velocity of the traveling peaks is given by

$$v(\rho) = \left| \left. \frac{d\omega}{dk} \right|_{k_0} \right| = \rho,$$

i.e. it is directly determined by the coin parameter. Since ρ can be varied from zero to one we can achieve faster or slower spreading than for the Grover walk corresponding to the value $\rho = \frac{1}{\sqrt{3}}$.

The one-parameter set of coins (3.17) does not exhaust all $U(3)$ matrices that lead to the trapping effect for the three-state quantum walks on a line. We gave full classification of such coins in the paper [IV] where we have also investigated their main physical properties. However, to keep the discussion simple we focus on the eigenvector family of three-state quantum walks. In the following Sections we investigate their properties in more detail.

3.5 Weak-limit Theorem

By analogy with the two-state Hadamard walk studied in the previous Chapter it can be shown that for the eigenvector family of walks the moments of the re-scaled position $\frac{x}{t}$ also converge in the limit of large number of steps t. This fact allows one to derive a weak limit theorem using the steps we have outlined in Section 2.5. One can show that the following statement holds

$$\lim_{t\to\infty} \left\langle \left(\frac{x}{t}\right)^n \right\rangle = \int_{-\rho}^{\rho} v^n w(v) dv, \tag{3.18}$$

however, only for $n \geq 1$, as we discuss later. The explicit form of the limit density $w(v)$ was derived in [39] for the particular case of the three-state Grover walk corresponding to the parameter $\rho = \frac{1}{\sqrt{3}}$ and in [40] for general value of ρ. It was shown that the limit density has the form

$$w(v) = \frac{\sqrt{1-\rho^2}}{2\pi(1-v^2)\sqrt{\rho^2-v^2}} \mathcal{M},$$

where the weight function $\mathcal{M}$ is a second-order polynomial in v

$$\mathcal{M} = \mathcal{M}_0 + \mathcal{M}_1 v + \mathcal{M}_2 v^2.$$

The coefficients $\mathcal{M}_j$ depend on the initial coin state of the walk. A drawback of [39, 40] was that they presented the results in terms of the standard basis of the coin space $\{|L\rangle, |S\rangle, |R\rangle\}$ in which the coefficients $\mathcal{M}_j$ have a rather lengthy form. This can be remedied by using a more suitable basis of the coin space, as we have discussed in the previous Chapter. We have addressed this issue in [V] where we have shown that the suitable basis can be built from the eigenvectors of the coin operator given in (3.16). Let us now briefly review the results of [V].

Instead of using the standard basis we decompose the initial coin state $|\psi_C\rangle$ into the eigenstate basis (3.16) in the form

$$|\psi_C\rangle = g_+|\sigma^+\rangle + g_1|\sigma_1^-\rangle + g_2|\sigma_2^-\rangle.$$

The probability amplitudes g_+ and $g_{1,2}$ are restricted by the normalization condition

$$|g_+|^2 + |g_1|^2 + |g_2|^2 = 1.$$

In terms of the amplitudes g_+ and $g_{1,2}$ the coefficients $\mathcal{M}_j$ are given by

$$\begin{aligned}
\mathcal{M}_0 &= 2(1-|g_2|^2), \\
\mathcal{M}_1 &= -\frac{2}{\rho}\left(g_1\overline{g_2} + \overline{g_1}g_2\right), \\
\mathcal{M}_2 &= \frac{2}{\rho^2}\left(|g_2|^2 - |g_+|^2\right).
\end{aligned}$$

The limit density then reads

$$w(v) = \frac{\sqrt{1-\rho^2}}{\pi(1-v^2)\sqrt{\rho^2-v^2}}\left(1-|g_2|^2 - (g_1\overline{g_2} + \overline{g_1}g_2)\frac{v}{\rho} + (|g_2|^2 - |g_+|^2)\frac{v^2}{\rho^2}\right). \tag{3.19}$$

We note that the limit density (3.19) is not normalized to unity. Indeed, we obtain the following result

$$\int_{-\rho}^{\rho} w(v)dv = 1 - |g_2|^2 - \frac{\sqrt{1-\rho^2}-1}{\rho^2}(|g_2|^2 - |g_+|^2). \tag{3.20}$$

This is smaller than one unless $g_2 = g_+ = 0$ and $g_1 = 1$, i.e. the initial coin state is chosen as $|\sigma_1^-\rangle$. It can be shown [V] that the state $|\sigma_1^-\rangle$ is the leaving state, i.e. it results in the absence of trapping as we have illustrated in Figure 3.3 for the particular case of the Grover walk ($\rho = \frac{1}{\sqrt{3}}$). Hence, the formula (3.18) does not hold for the zeroth moment. The limit density is not sufficient to fully describe the probability distribution as it was in Chapter 2 for the two-state Hadamard walk. This is due to the fact that the limit density captures only the spreading part of the probability distribution which is determined by the continuous spectrum of the evolution operator. However, the evolution operator of the eigenvector family of quantum walks has also a point spectrum which leads to the trapping effect, i.e. the probability to find a particle at a finite position x has a non-vanishing limit for large t given by the trapping probability (3.14). As we show in the following Section, the trapping probability $p_\infty(x)$ decreases exponentially with the distance from the origin. Due to this sharp decay it does not contribute to the moments of the re-scaled position (3.18), except

for $n = 0$. The approximation of the exact probability distribution of the eigenvector family of three-state quantum walks with the limit density

$$p(x,t) \approx \frac{1}{t} w\left(\frac{x}{t}\right),$$

holds only for sufficiently large $|x|$. In the vicinity of the origin the exact probability distribution is dominated by the trapping probability which we evaluate in the following Section. Note that in comparison with the approximation (2.27) of the probability distribution of the two-state Hadamard walk the factor of 2 is missing in front of the limit density. The reason is that the three-state quantum walks we consider in the present Chapter are not bipartite.

Simple form of the limit density (3.19) in terms of the basis (3.16) allows us to easily identify extremal regimes in which the eigenvector family of walks can be operated in. As we have illustrated in Figure 3.1 a generic probability distribution has two traveling peaks, which correspond to the divergencies of the limit density (3.19) for v approaching $\pm\rho$. However, there are various initial states leading to non-generic probability distribution. As for the two-state Hadamard walk studied in the previous Chapter it is possible to construct states for which one of the traveling peaks disappears. Indeed, consider e.g. the coin state

$$|\sigma_L\rangle = \frac{1}{\sqrt{2}}\left(|\sigma_1^-\rangle + |\sigma_2^-\rangle\right). \tag{3.21}$$

From the relation (3.19) we find that the limit density for this initial state reads

$$w_{|\sigma_L\rangle}(v) = \frac{\sqrt{1-\rho^2}\sqrt{(\rho-v)^3}}{2\pi\rho^2(1-v^2)\sqrt{\rho+v}}. \tag{3.22}$$

Such a density tends to zero for v approaching ρ. Nevertheless, the divergency at $v = -\rho$ remains. We illustrate this feature in Figure 3.4 where we display the distribution after 100 steps for the coin parameter $\rho = 0.3$.

Moreover, both traveling peaks can be eliminated by a proper choice of the initial state. This is not possible for two-state Hadamard walk. Indeed, choosing the initial coin state as the eigenvector $|\sigma^+\rangle$ leads to the limit density of the form

$$w_{|\sigma^+\rangle}(v) = \frac{\sqrt{1-\rho^2}\sqrt{\rho^2-v^2}}{\pi\rho^2(1-v^2)}. \tag{3.23}$$

We see that the density does not diverge for v approaching $\pm\rho$ but rather tends to zero. Hence, both traveling peaks on the edges of the probability distribution vanish. We illustrate this effect in Figure 3.5, where we display the probability distribution after 100 steps.

Finally, let us discuss the behaviour of the limit density (3.19) for small values of v. For the two-state Hadamard walk analyzed in the previous Chapter the limit density is flat in the vicinity of the origin, irrespective of the initial condition. In contrast, for the eigenvector

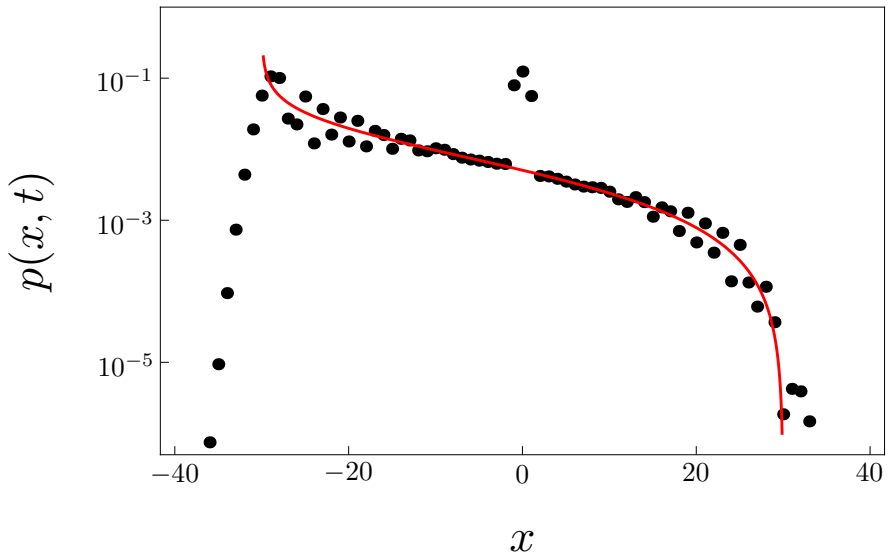

Figure 3.4: Probability distribution $p(x,t)$ of the three-state quantum walk with the coin parameter $\rho = 0.3$ after 100 steps. As the initial state we have chosen $|\sigma_L\rangle$ given by equation (3.21). The peak on the right-hand side of the probability distribution vanishes, as predicted by the limit density (3.22). We use logarithmic scale on the y-axis to highlight this feature.

family of walks the limit density can have a significant dip for small v. Indeed, for the eigenstate $|\sigma_2^-\rangle$ the limit density is given by

$$w_{|\sigma_2^-\rangle}(v) = \frac{\sqrt{1-\rho^2}v^2}{\pi\rho^2(1-v^2)\sqrt{\rho^2-v^2}}. \tag{3.24}$$

We see that the density vanishes as v tends to zero. To illustrate this effect we plot in Figure 3.6 the distribution after 100 steps on a logarithmic scale. The coin parameter was chosen as $\rho = 0.7$. The plot indicates that the probability distribution tends to zero for small $|x|$, except for a very small neighbourhood of the origin where the trapping effects dominates.

Before we turn to the detailed analysis of the trapping probability let us point out another benefit of the description of the considered family of quantum walks in terms of the eigenvector basis (3.16). The form of the limit density (3.19) makes it clear that they have the same properties for all values of $\rho \in (0,1)$. More precisely, for a given amplitudes g_+, g_1 and g_2 the shape of the resulting probability distribution is the same for any value of ρ. Indeed, ρ is just a scaling parameter determining the width of the probability distribution. This result is far from obvious in the standard basis description given in [40].

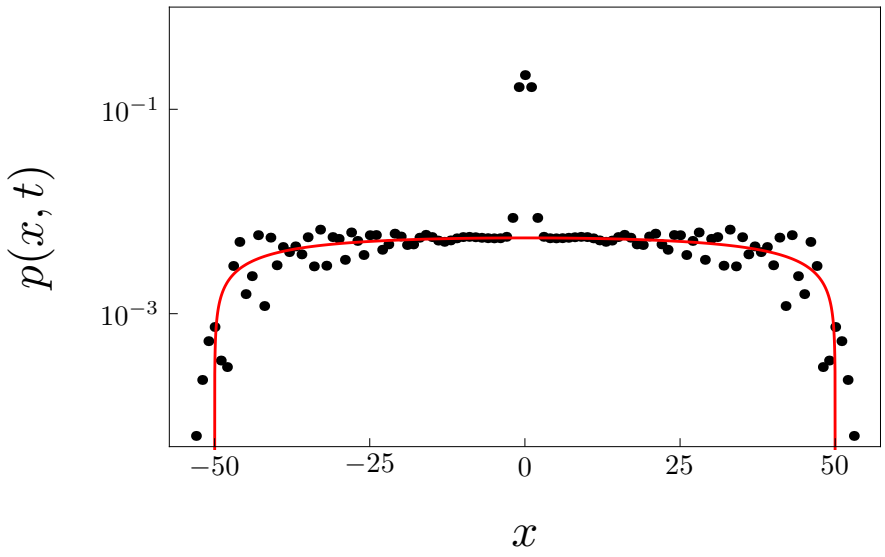

Figure 3.5: Probability distribution $p(x,t)$ of the three-state quantum walk with the coin parameter $\rho = 0.5$ after 100 steps. The initial state was chosen as $|\psi_C\rangle = |\sigma^+\rangle$. The black dots are obtained from the numerical simulation. The red curve corresponds to the limit density (3.23). Notice the absence of the traveling peaks on the edges of the probability distribution. Instead, the probability distribution approximated with the limit density (3.23) tend to zero for $x \to \pm\rho t$. To unravel this effect we display the plot on the logarithmic scale.

3.6 Evaluation of the Trapping Probability

To conclude the analysis of the probability distribution generated by the eigenvector family of walks we evaluate the trapping probability $p_\infty(x)$, i.e. the probability that we find the particle at position x in the limit of $t \to \infty$. The trapping probability $p_\infty(x)$ is determined from the limiting probability amplitude $\psi_\infty(x)$ according to (3.14). The limiting probability amplitude is given by the following integral

$$\psi_\infty(x) = \int_0^{2\pi} \frac{dk}{2\pi} e^{-ixk} f_1(k) v_1(k), \tag{3.25}$$

where $v_1(k)$ is an eigenvector of the evolution operator in the Fourier picture $\tilde{U}(k)$ corresponding to the k-independent eigenvalue 1 and $f_1(k)$ denotes its overlap with the Fourier transformation of the initial state (3.12). For the considered family of walks the explicit form of the eigenvector $v_1(k)$ is easily found to be

$$v_1(k) = \frac{1}{n(k)} \left(\sqrt{1-\rho^2}, \frac{\rho}{\sqrt{2}}(1+e^{ik}), e^{ik}\sqrt{1-\rho^2} \right)^T,$$

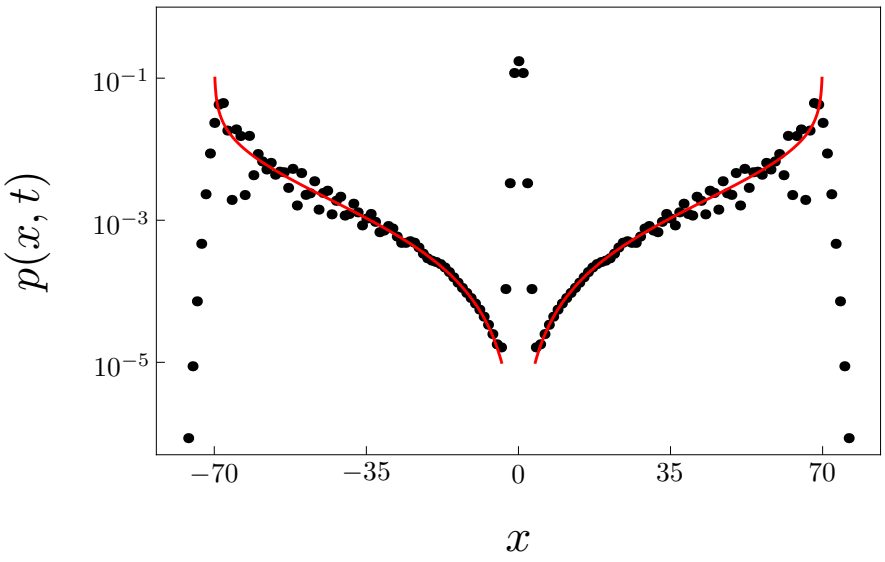

Figure 3.6: Probability distribution $p(x,t)$ of the three-state quantum walk with the coin parameter $\rho = 0.7$ after 100 steps. The initial state was chosen as $|\psi_C\rangle = |\sigma_2^-\rangle$. Notice that the probability distribution is not flat. There is a significant dip for small $|x|$, in accordance with the prediction obtained from the limit density (3.24). For better visibility of the dip we use logarithmic scale on the y-axis. The sharp peak at the origin corresponds to the trapping effect.

where $n(k)$ denotes the normalization factor given by

$$n(k) = \sqrt{2 - \rho^2(1 - \cos k)}.$$

The integrand of (3.25) then reads

$$e^{-ixk} f_1(k) v_1(k) = \frac{e^{-ixk}}{2 - \rho^2(1 - \cos k)} \begin{pmatrix} \sqrt{\frac{1-\rho^2}{2}} \left(1 + e^{-ik}\right) g_+ + \frac{1-\rho^2}{\sqrt{2}} \left(1 - e^{-ik}\right) g_2 \\ \frac{\rho}{2} \left(e^{ik} + 2 + e^{-ik}\right) g_+ + \frac{\rho\sqrt{1-\rho^2}}{2} \left(e^{ik} - e^{-ik}\right) g_2 \\ \sqrt{\frac{1-\rho^2}{2}} \left(1 + e^{ik}\right) g_+ - \frac{1-\rho^2}{\sqrt{2}} \left(1 - e^{ik}\right) g_2 \end{pmatrix}.$$

Hence, the limiting probability amplitude (3.25) can be decomposed into integrals of the form

$$I(x) = \int_0^{2\pi} \frac{dk}{2\pi} \frac{e^{-ixk}}{2 - \rho^2(1 - \cos k)}.$$

Following the method of residues we obtain the result

$$I(x) = \left\{ \begin{array}{c} z = e^{ik} \\ \frac{dz}{iz} = dk \end{array} \right\} = \frac{1}{\pi i} \oint\limits_{|z|=1} \frac{z^{-x}}{z^2 + 2\frac{2-\rho^2}{\rho^2} z + 1} dz = \frac{(-1)^{|x|}}{2\sqrt{1-\rho^2}} Q^{|x|},$$

where the factor Q depends on the coin parameter ρ according to

$$Q = \frac{2 - \rho^2 - 2\sqrt{1-\rho^2}}{\rho^2}.$$

The limiting probability amplitude is thus given by

$$\psi_\infty(x) = \left(\begin{array}{c} \sqrt{\frac{1-\rho^2}{2}} \left(I(x) + I(x+1) \right) g_+ + \frac{1-\rho^2}{\sqrt{2}} \left(I(x) - I(x+1) \right) g_2 \\ \\ \frac{\rho}{2} \left(I(x-1) + 2I(x) + I(x+1) \right) g_+ + \frac{\rho\sqrt{1-\rho^2}}{2} \left(I(x-1) - I(x+1) \right) g_2 \\ \\ \sqrt{\frac{1-\rho^2}{2}} \left(I(x) + I(x-1) \right) g_+ - \frac{1-\rho^2}{\sqrt{2}} \left(I(x) - I(x-1) \right) g_2 \end{array} \right).$$

The trapping probability is determined by the square norm of the limiting probability amplitude. After some algebra we find that it reduces into

$$p_\infty(x) = \left\{ \begin{array}{c} \frac{2-2\rho^2}{\rho^4} Q^{2|x|} |g_+ - g_2|^2, \quad x < 0, \\ \\ \frac{1}{\rho^2} Q \left(|g_+|^2 + (1-\rho^2)|g_2|^2 \right), \quad x = 0, \\ \\ \frac{2-2\rho^2}{\rho^4} Q^{2x} |g_+ + g_2|^2, \quad x > 0 \end{array} \right. \tag{3.26}$$

This result shows that the trapping probability indeed decays exponentially with the distance from the origin $|x|$. Hence, it does not contribute to higher moments of the re-scaled position $\frac{x}{t}$, as we have discussed in the previous Section. In the eigenvector basis (3.16) only two amplitudes of the initial coin state, namely g_+ and g_2, are relevant for the determination of the trapping probability. Indeed, for the leaving state $|\sigma_1^-\rangle$ the trapping effect does not emerge. This reduces the complexity of the expression for the trapping probability tremendously in comparison with the standard basis description [40]. We clearly see that the trapping probability can be highly asymmetric, since the dependence on the initial coin state is different for positive and negative x. In fact, the asymmetry can be made such that the trapping appears only for $x \geq 0$ (or only for $x \leq 0$) by a proper choice of the initial coin state. We illustrate this in Figure 3.7 where we display the probability distribution near the origin for the initial coin state

$$|\psi_C\rangle = \frac{1}{\sqrt{2}} \left(|\sigma^+\rangle + |\sigma_2^-\rangle \right). \tag{3.27}$$

For such an initial state the trapping probability (3.26) reduces to

$$p_\infty(x) = \begin{cases} 0, & x < 0 \\ \left(\frac{1}{\rho^2} - \frac{1}{2}\right) Q, & x = 0 \\ \frac{4-4\rho^2}{\rho^4} Q^{2x}, & x > 0 \end{cases} \tag{3.28}$$

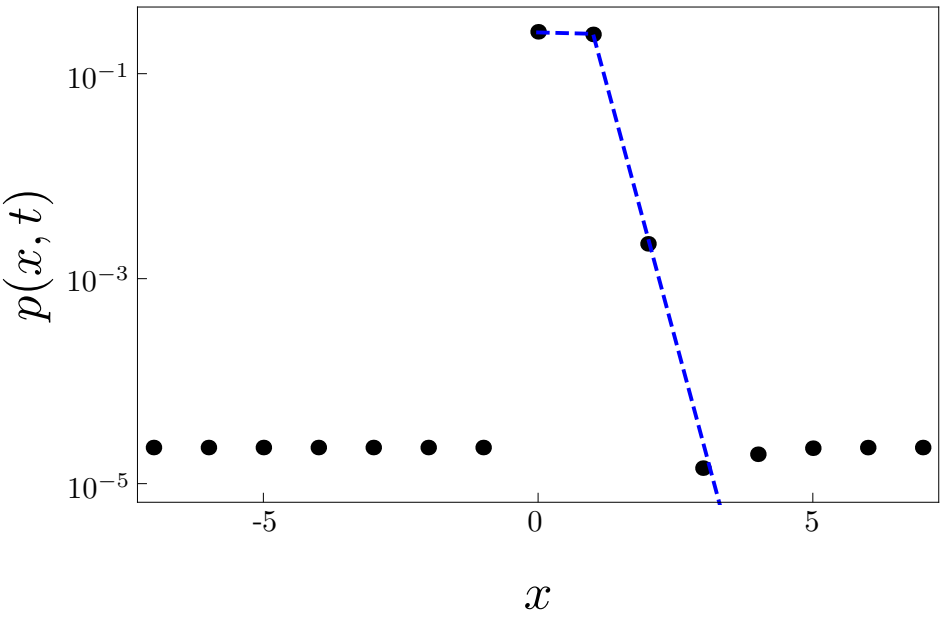

Figure 3.7: Probability distribution after $t = 10000$ steps of the three-state Grover walk ($\rho = \frac{1}{\sqrt{3}}$) with the initial coin state (3.27). We see that the trapping probability is non-zero only for $x \geq 0$, in accordance with the analytical prediction (3.28). To highlight this feature we evolved the walk for more steps and focused only on a small neighbourhood of the origin.

The trapping probability (3.26) together with the limit density (3.19) can be used to approximate the exact probability distribution of the eigenvector family of walks according to

$$p(x,t) \approx \frac{1}{t} w\left(\frac{x}{t}\right) + p_\infty(x). \tag{3.29}$$

The trapping probability $p_\infty(x)$ dominates in the vicinity of the origin, while the limit density governs the behaviour at larger distances. We note that one can easily check that

$$\sum_{m=-\infty}^{\infty} p_\infty(m) = |g_2|^2 + \frac{\sqrt{1-\rho^2}-1}{\rho^2}\left(|g_2|^2 - |g_+|^2\right).$$

This together with (3.20) results in

$$\sum_{m=-\infty}^{\infty} p_{\infty}(m) + \int_{-\rho}^{\rho} w(v)\, dv = 1,$$

i.e. within the approximation (3.29) the probability distribution is properly normalized to unity.

3.7 Transport in Three-state Quantum Walk

In this Section we investigate the three-state quantum walk as a model of coherent excitation transport to an absorbing center, which we refer to as sink. We consider a ring graph with the excitation starting the walk opposite to the sink. We show that the trapping effect restricts the transport of excitation, i.e. the particle has a chance to remain on the ring without ever reaching the sink.

Let us now formally describe our model of excitation transport. We first adopt the eigenvector family of walks on an infinite line investigated in the previous Sections to a finite-size ring with $2N$ vertices labeled from $-N+1$ to N. The position space $\mathcal{H}_P$ is now finite-dimensional

$$\mathcal{H}_P = \mathrm{Span}\{|x\rangle | x = -N+1, \dots N\} = \mathbb{C}^{2N},$$

while the coin space $\mathcal{H}_C$ remains the same (3.1). The step operator of the three-state quantum walk on an infinite line (3.5) has to be replaced with

$$\hat{S}_{\mathrm{ring}} = \sum_{x=-N+1}^{N} \Big(|x-1\rangle\langle x| \otimes |L\rangle\langle L| + |x\rangle\langle x| \otimes |S\rangle\langle S| + |x+1\rangle\langle x| \otimes |R\rangle\langle R| \Big),$$

where we consider periodic boundary condition $N \equiv -N$. The excitation enters the ring at the vertex 0, i.e. the initial state is of the form (3.3). However, the time evolution of the walk is not given purely by the unitary operator $\hat{U}$ (3.4). Indeed, there is a sink located opposite the starting point, i.e. at the vertex N, which takes the excitation away from the ring. Mathematically, the action of the sink is described by the projection operator

$$\hat{\pi} = \Big(\hat{I}_P - |N\rangle\langle N| \Big) \otimes \hat{I}_C.$$

Hence, the complete time evolution is not unitary and the state of the excitation after t steps is described by the vector

$$|\psi(t)\rangle = \Big(\hat{\pi} \cdot \hat{U} \Big)^t |\psi(0)\rangle,$$

with norm generally less than unity.

In the following we analyze the properties of the survival probability $\mathcal{P}(t)$, i.e. the probability that the excitation remains on the ring until time t, which is given by

$$\mathcal{P}(t) = \langle\psi(t)|\psi(t)\rangle.$$

We also consider the asymptotic transport efficiency η defined as

$$\eta = 1 - \lim_{t\to\infty} \mathcal{P}(t).$$

Let us derive an approximation of the asymptotic behaviour of the survival probability $\mathcal{P}(t)$ for large t. We begin with the estimate

$$\mathcal{P}(t) \leq \left\| \left(\hat{\pi}\cdot\hat{U}\right)^t \right\|^2 = \exp\left(2t \ln\left(\left\| \left(\hat{\pi}\cdot\hat{U}\right)^t \right\|^{\frac{1}{t}}\right)\right).$$

For large t the argument of the logarithm can be approximated according to

$$\left\| \left(\hat{\pi}\cdot\hat{U}\right)^t \right\|^{\frac{1}{t}} \approx |\lambda_l|,$$

where λ_l is the leading eigenvalue of $\hat{\pi}\cdot\hat{U}$, i.e. the largest eigenvalue in absolute value. In the case of $|\lambda_l| < 1$ we can make the first-order Taylor expansion of the logarithm

$$\ln\left(\left\| \left(\hat{\pi}\cdot\hat{U}\right)^t \right\|^{\frac{1}{t}}\right) \approx \ln|\lambda_l| \approx -(1-|\lambda_l|),$$

and find that the survival probability behaves in the asymptotic limit as an exponential

$$\mathcal{P}(t) \sim c\ e^{-\gamma t}, \tag{3.30}$$

where the decay rate γ reads

$$\gamma = 2(1-|\lambda_l|).$$

In such a case, the asymptotic transport efficiency η is unity. This occurs e.g. when the excitation dynamic is modeled by a two-state quantum walk, as we have shown in [VII]. However, for the three-state walk model with the coin (3.17) we find that $|\lambda_l| = 1$. Indeed, the unitary evolution operator $\hat{U}$ of the three-state quantum walk on a ring (without the sink) has an eigenvalue 1 with $2N$-fold degeneracy. The corresponding eigenvectors (linearly independent but overlapping) are easily found to be

$$|s_x\rangle = |x\rangle\left(\sqrt{1-\rho^2}|L\rangle + \frac{\rho}{\sqrt{2}}|S\rangle\right) + |x+1\rangle\left(\frac{\rho}{\sqrt{2}}|S\rangle + \sqrt{1-\rho^2}|R\rangle\right), \tag{3.31}$$

where x ranges from $-N+1$ to N. Notice that only two of these vectors, namely $|s_{N-1}\rangle$ and $|s_N\rangle$, have support on the vertex N where the sink is located. Hence, the vectors $|s_n\rangle$

with $n \in \{-N+1, \ldots, N-2\}$ are not affected by the presence of the sink and they are eigenvectors of $\hat{\pi} \cdot \hat{U}$ with eigenvalue one, i.e. $\lambda_l = 1$. Consequently, the trapping effect in the three-state quantum walk persists even in the presence of the sink. This result indicates that the survival probability does not vanish and the excitation transport is not efficient.

We have investigated the transport properties of the eigenvector family of walks on a ring in full detail in [VII]. With the knowledge of the stationary states (3.31) one can evaluate the asymptotic transport efficiency η explicitly for small rings, i.e. small values of N. However, the calculation requires the use of Gramm-Schmidt orthogonalization procedure to form an orthonormal basis in the degenerate subspace corresponding to $\lambda_l = 1$. This becomes rather tedious for larger values of N. Nevertheless, we can estimate the transport efficiency using the results we have obtained for the trapping probability in the case of the walk on an infinite line (3.26). Within this approximation the limiting value of the survival probability is given by summing the trapping probabilities over all vertices of the ring excluding the sink

$$\lim_{t\to\infty} \mathcal{P}(t) = \sum_{x=-N+1}^{N-1} p_\infty(x).$$

From the explicit form of the trapping probability for the infinite line (3.26) the asymptotic transport efficiency η is found to be [VII]

$$\begin{aligned} \eta &= 1 - \sum_{x=-N+1}^{N-1} p_\infty(x) \\ &= 1 - \frac{Q}{\rho^2}\left(\sqrt{1-\rho^2}\left(1-Q^{2(N-1)}\right)\left(|g_2|^2+|g_+|^2\right) + (1-\rho^2)|g_2|^2 + |g_+|^2\right). \end{aligned} \quad (3.32)$$

We see that the transport efficiency depends crucially on the initial coin state. It follows that the smallest value of η is obtained when the initial coin state is chosen as the eigenstate $|\sigma^+\rangle$. To illustrate this result we show in Figure 3.8 the course of the survival probability $\mathcal{P}(t)$ as a function of the number of steps. The considered ring has 10 vertices, i.e. $N = 5$. The coin parameter is chosen as $\rho = \frac{1}{\sqrt{3}}$ corresponding to the three-state Grover walk. In this case the asymptotic transport efficiency is approximately $\eta \approx 0.45$.

We note that for the leaving state $|\sigma_1^-\rangle$ the asymptotic transport efficiency (3.32) reaches unity. Indeed, for $|\sigma_1^-\rangle$ trapping effect disappears and the survival probability decays exponentially according to (3.30). The decay rate γ can be estimated using the sub-leading eigenvalue λ_{sl} of $\hat{\pi} \cdot \hat{U}$ according to

$$\gamma = 2(1 - |\lambda_{sl}|). \quad (3.33)$$

We illustrate this behaviour in Figure 3.9 where we consider the three-state Grover walk ($\rho = \frac{1}{\sqrt{3}}$) on a ring with 10 vertices. The plot shows the survival probability as a function of the number of steps t on a logarithmic scale.

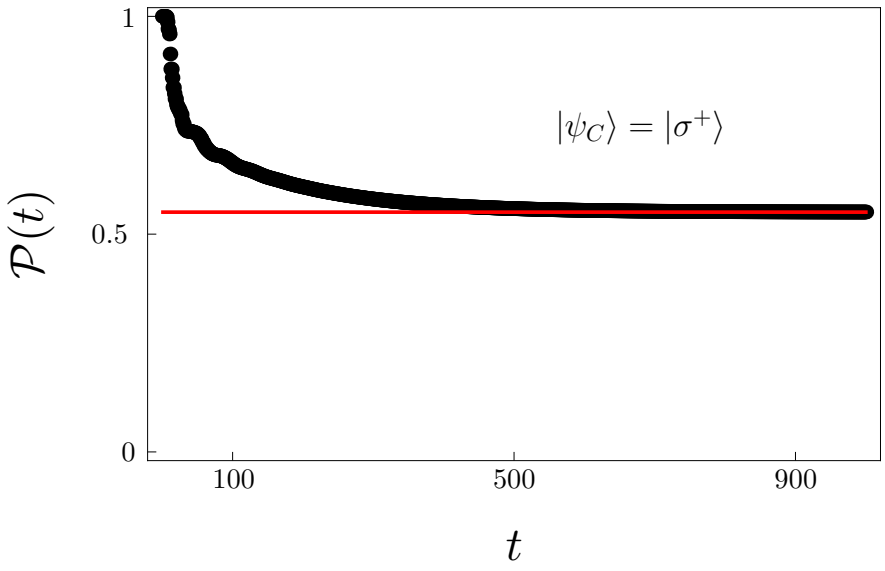

Figure 3.8: Survival probability for the three-state Grover walk ($\rho = \frac{1}{\sqrt{3}}$) on a ring with 10 vertices, i.e. $N = 5$, in dependence on the number of steps. As the initial coin state we have chosen the eigenvector $|\sigma^+\rangle$ for which the trapping effect is the strongest. The survival probability $\mathcal{P}(t)$ approaches the red line given by $\sum_{x=-N+1}^{N-1} p_\infty(x) \approx 0.55$.

3.8 Discussion

In this Chapter we have illustrated the trapping effect on the example of the three-state Grover walk on a line and its one-parameter extension, i.e. the eigenvector family of walks which we derived in [III]. However, the one-parameter set of coins (3.17) does not exhaust all $U(3)$ matrices which lead to the trapping effect for three-state quantum walks. In the paper [III] we have constructed another one-parameter set of coins by a suitable parametrization of the eigenvalues of the Grover matrix, which we refer to as eigenvalue family. The construction was based on the fact that by definition the Grover matrix (3.6) commutes with all permutations. The eigenvectors of the Grover operator (3.15) are chosen in such a way that they are also eigenvectors of the permutation matrix

$$\Pi = \begin{pmatrix} 0 & 0 & 1 \\ 0 & 1 & 0 \\ 1 & 0 & 0 \end{pmatrix}.$$

Using this matrix as a coin for a three-state quantum walk trivially results in trapping, since the particle either stays at the origin, or jumps to the left or right but immediately returns back in the next step. Notice that the eigenvector $|\sigma_2^-\rangle$ corresponds to the same eigenvalue -1 for both the Grover matrix G and the permutation matrix Π. The same applies to $|\sigma_+\rangle$.

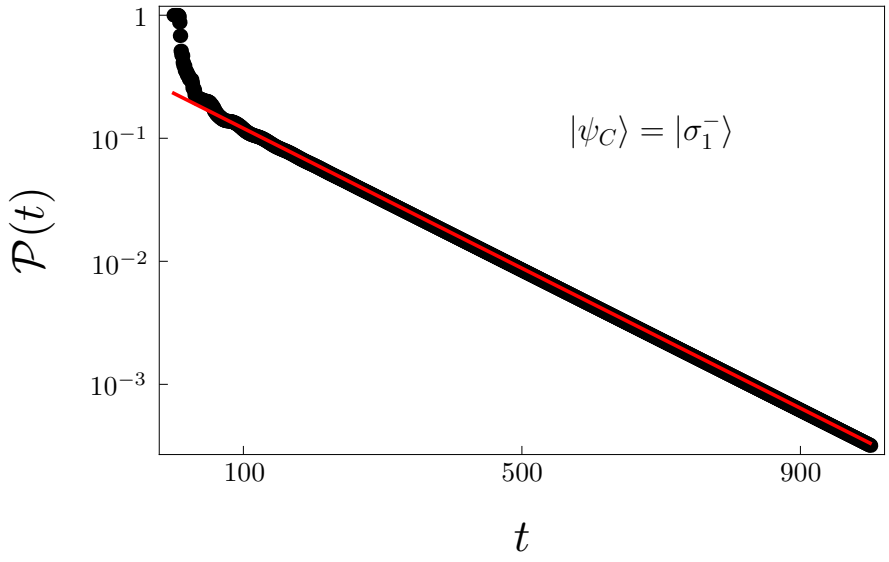

Figure 3.9: Survival probability for the three-state Grover walk ($\rho = \frac{1}{\sqrt{3}}$) on a ring with 10 vertices, i.e. $N = 5$, in dependence on the number of steps. As the initial coin state we have chosen the eigenvector $|\sigma_1^-\rangle$ for which the trapping effect is absent. In such a case the survival probability $\mathcal{P}(t)$ vanishes exponentially, as highlighted by the log-scale. The red line corresponds to the decay rate γ determined by (3.33).

However, for the eigenvector $|\sigma_1^-\rangle$ the eigenvalues of $\hat{G}$ and $\hat{\Pi}$ differ, since

$$\begin{aligned} \hat{G}|\sigma_1^-\rangle &= -|\sigma_1^-\rangle, \\ \hat{\Pi}|\sigma_1^-\rangle &= |\sigma_1^-\rangle. \end{aligned}$$

Hence, we can continuously change from the Grover coin to the permutation matrix Π by parameterizing the eigenvalue corresponding to $|\sigma_1^-\rangle$. We thus arrive at the following one-parameter family (eigenvalue family) of coin operators

$$\hat{C}(\varphi) = -e^{2i\varphi}|\gamma_1^-\rangle\langle\gamma_1^-| - |\gamma_2^-\rangle\langle\gamma_2^-| + |\gamma^+\rangle\langle\gamma^+|, \tag{3.34}$$

where the factor of 2 was added for convenience. In [III] we have shown that the eigenvalue family of quantum walks preserves the trapping effect. The coin parameter φ also determines the speed of spreading of the walks through the lattice. In contrast to the eigenvector family the relation between φ and the velocity of the peaks is more involved.

We elaborated on the results of [III] in the paper [IV] where we have determined all coin operators for which the three-state quantum walk on a line has a non-empty point spectrum. Our construction was based on explicit calculation of the spectrum of the evolution operator in the Fourier space. We have determined sufficient and necessary conditions on the coin operator which guarantees the existence of a point spectrum of the evolution operator of the

quantum walk. These requirements were solved with the help of a particular parametrization of the unitary group, leading us to two sets of non-trivial solutions. The one-parameter families of trapping walks identified in [III] are special cases of these more general solutions. Our results imply that trapping is a rare feature, since trapping coins represent a set of zero measure in the unitary group $U(3)$. Physical implications of our results were discussed. As representative physical parameters we have chosen the propagation velocity and trapping probability at the origin. We have shown that the peak velocity as well as the strength of trapping depend only on few parameters defining the coin. Moreover, we have shown that for any $U(3)$ trapping coin there exists a leaving state for which the trapping vanishes.

The properties of the probability distributions for both families of three-state quantum walks introduced in [III] were analyzed in full detail in [V]. The results for the eigenvector family were illustrated in Sections 3.5 and 3.6 where we have discussed the limit density and the trapping probability in the eigenvector basis. We have shown that all walks from the eigenvector family have the same properties and the coin parameter ρ simply sets the scale, i.e. it determines the width of the distribution but does not affect its overall shape. This fact is rather hidden in the standard basis description. Concerning the eigenvalue family of walks the limit density and the trapping probability can be found in [V]. The limit density for the coin (3.34) is much more involved. In contrast with the eigenvector family the shape of the limit density changes dramatically with the coin parameter, i.e. φ is not a simple scaling parameter. On the other hand, the trapping probability does not depend on φ, i.e. it is the same for all walks from the eigenvalue family.

The results of [V] were extensively used in [VII] and [VIII]. In the paper [VII] we have studied the excitation transport to an absorbing center on a ring graph. The propagation of excitation was modeled by a discrete-time quantum walk with an absorbing sink opposite the starting vertex, which we have briefly reviewed in Section 3.7. We have shown that for a two-state quantum walk model, where the excitation has to leave its actual position to the neighboring sites, the survival probability decays exponentially and the transport efficiency is unity. The decay rate of the survival probability is estimated with the leading eigenvalue of the evolution operator. However, if the propagation of excitation is modeled by a three-state quantum walk which shows the trapping effect then part of the wave-packet never reaches the sink. In such a case, the survival probability does not vanish and the excitation transport is not efficient, as we have discussed in Section 3.7 for the eigenvector family of three-state quantum walks. We have also analyzed the effect of dynamical percolation of the ring on the transport efficiency. Improving transport by allowing the edges to break randomly seems to be a bit counterintuitive at the first sight. However, percolation can in some situations eliminate the trapping effect and thus improve the asymptotic transport efficiency to unity. In particular, we have considered an extension of the eigenvector family of coins (3.17) with

an additional phase parameter α of the form

$$C(\rho,\alpha)=\begin{pmatrix} -\rho^2 & \rho\sqrt{2-2\rho^2} & e^{-i\alpha}\,(1-\rho^2) \\ \rho\sqrt{2-2\rho^2} & 2\rho^2-1 & e^{-i\alpha}\rho\sqrt{2-2\rho^2} \\ e^{i\alpha}\,(1-\rho^2) & e^{i\alpha}\rho\sqrt{2-2\rho^2} & -\rho^2 \end{pmatrix}.$$

The phase parameter α does not influence the dynamics of the unperturbed walk (i.e. without percolation). However, the situation changes when we consider dynamical percolation of the ring where any edge occurs in a given time step with some probability p, and the edge configuration changes in time. The evolution of a quantum walk on a dynamically percolated graph is described within the framework of random unitary channels [67, 68]. It simplifies considerably in the asymptotic regime where it is described by the attractor space. We have shown that the stationary states of the unperturbed walk, which have the form

$$|s_x\rangle=|x\rangle\left(\sqrt{1-\rho^2}|L\rangle+\frac{\rho}{\sqrt{2}}|S\rangle\right)+|x+1\rangle\left(\frac{\rho}{\sqrt{2}}|S\rangle+e^{i\alpha}\sqrt{1-\rho^2}|R\rangle\right),$$

belong to the attractor space only for $\alpha=0$. Hence, for $\alpha\neq 0$ dynamical percolation of the ring eliminates the trapping effect which makes the transport of excitation efficient, i.e. $\eta=1$ for all initial coin states. In such a case, the survival probability vanishes exponentially. We have investigated the dependence of the decay rate on the phase α and the edge probability p.

In the paper [VIII] we have analyzed the behaviour of persistence of unvisited sites for quantum walks on a line. The results for the two-state quantum walks were briefly discussed in the previous Chapter. We have also analyzed persistence for the eigenvector family of three-state quantum walks. We have found that the persistence of site x is given by

$$\mathcal{P}_x(T)\sim c\,\left(\frac{T}{|x|}\right)^{-\lambda}e^{-p_\infty(x)T},$$

where $p_\infty(x)$ is the trapping probability (3.26) and the exponent λ is given by

$$\lambda=\frac{\sqrt{1-\rho^2}}{\pi\rho}\left(1-|g_2|^2\right).$$

We see that in contrast to two-state quantum walks the scaling of persistence is not given solely by the inverse power law. The second contribution to the asymptotic behavior of persistence is an exponential decay coming from the trapping nature of the studied family of quantum walks. Moreover, both the exponent of the inverse power-law λ and the decay constant of the exponential decay given by the trapping probability $p_\infty(x)$ depend also on the initial coin state and its coherence. We have shown that various regimes of persistence are achieved by altering the initial condition, ranging from purely exponential decay to purely inverse power-law behavior. Moreover, one can employ the asymmetry of the trapping effect to achieve different asymptotic scaling of persistence for sites on the positive and negative half line.

Chapter 4

Quantum Walk Approach to Perfect State Transfer

4.1 Introduction

In this Chapter we illustrate the application of quantum walks to perfect state transfer [191] between two vertices of a graph which we have investigated in [X, XI]. Our approach is based on a modification of the quantum walk search algorithm on a given graph. The quantum walk search algorithm is closely related to the Grover's algorithm for searching an unsorted database. For this reason we first review in Section 4.2 the Grover's algorithm and show that it yields an optimal solution. In Section 4.3 we discuss the quantum walk search algorithm. In particular, we show that for the star graph the quantum walk search is exactly equivalent to the Grover's algorithm. The approach to the perfect state transfer based on the modification of the quantum walk search algorithm is addressed in Section 4.4. As an example, we show that it achieves perfect state transfer between two vertices of a star graph. Finally, in Section 4.5 we discuss the extension of the quantum walk based state transfer to different graph structures which we have investigated in [X, XI].

4.2 Grover's Search Algorithm

Consider an unstructured search space of N elements with indexes from 0 to $N-1$. For convenience we assume that $N = 2^n$, i.e. the index can be stored using n bits. We can always add empty entries into the database to make sure that its size is a power of two. We will identify the integer index x with its binary representation $x_{n-1} \dots x_1 x_0$, $x_j \in \{0, 1\}$. For simplicity we consider that there is one marked item with index m which is the only solution of the search problem. Extensions to search with more solutions are also possible [192].

Marking of the item can be represented by a function f defined by

$$f(x) = \begin{cases} 0, & x \neq m \\ 1, & x = m \end{cases}$$

Suppose that we have access to an oracle O_m which is a black-box with the ability to recognize the solution to the search problem. In the classical setting the oracle simply implements the function f. Since the database we search is unstructured, it is clear that to find the marked item we need to query the classical oracle $\Theta(N)$ times. Remarkably, Grover has shown [86,87] that quantum mechanics helps to reduce the number of oracle queries to $\Theta(\sqrt{N})$. Let us now briefly review the main ingredients of the Grover's search algorithm. We follow closely the approach detailed in [193].

The database has $N = 2^n$ entries and so it can be represented using n qubits. To every index $x = 0, \ldots, N-1$ we assign a vector $|x\rangle$ which coincides with one vector of the computational basis according to

$$|x\rangle \equiv |x_{n-1} \ldots x_1 x_0\rangle, \quad x = x_{n-1}2^{n-1} + \ldots + x_1 2^1 + x_0 2^0.$$

The quantum oracle $\hat{O}_m$ utilizes another ancilla qubit which changes value if $x = m$. More precisely, the action of the oracle on the computational basis is given by

$$\hat{O}_m |x\rangle|q\rangle = |x\rangle|q \oplus f(x)\rangle,$$

where $|q\rangle$ corresponds to the state of the ancilla qubit and $\oplus$ denotes addition modulo 2. We can check whether x is the solution of the search problem by applying the oracle to the state $|x\rangle|0\rangle$ and measuring the oracle qubit - it will have the value 1 if and only if $x = m$. However, it is more convenient to consider the ancilla qubit to be initially in the superposition

$$|q\rangle = \frac{1}{\sqrt{2}}(|0\rangle - |1\rangle).$$

Indeed, we find that for $x \neq m$ the state $|x\rangle|q\rangle$ does not change after the application of the oracle. On the other hand, for $x = m$ the oracle only multiplies the state $|m\rangle|q\rangle$ by a factor -1. In both cases the state of the ancilla qubit remains unchanged and it can be omitted from from further discussion of the Grover's search algorithm. With this convention the action of the quantum oracle on the basis states $|x\rangle$ is given by

$$\hat{O}_m |x\rangle = (-1)^{f(x)} |x\rangle.$$

The oracle thus marks the solution by shifting its phase by π. Since we consider one marked item with index m the unitary operator corresponding to the oracle reads

$$\hat{O}_m = \hat{I} - 2|m\rangle\langle m|.$$

In addition to the oracle $\hat{O}_m$ the Grover's search algorithm utilizes the Grover operator $\hat{G}$ which we have already seen in the previous Chapter for a particular case of a three-dimensional Hilbert space. For a system composed of n qubits the Grover operator can be decomposed into three elementary steps. First, we apply the Hadamard transformation $\hat{H}$, whose matrix representation is given in (2.4), to all n individual qubits. Second, we perform a conditional phase shift such that all states except $|0\rangle$ are multiplied by -1. Finally, we again apply the Hadamard transformation to all n qubits. The combined action of these three operations can be written as

$$\hat{G} = \hat{H}^{\otimes n}(2|0\rangle\langle 0| - I)\hat{H}^{\otimes n} = 2|w\rangle\langle w| - \hat{I},$$

where $|w\rangle$ denotes the equal-weight superposition of all basis states, i.e.

$$|w\rangle = \frac{1}{\sqrt{N}} \sum_{x=0}^{N} |x\rangle.$$

The steps of the Grover's search algorithm are as follows:

1. Initialize the system in the equal-weight superposition of all basis states

$$|\psi(0)\rangle = |w\rangle.$$

2. Apply the Grover iteration $\hat{U}$ given by

$$\hat{U} = \hat{G}\hat{O}_m,$$

on the system T-times.

3. Measure the system in the computational basis.

Let us now prove that the runtime of the Grover's algorithm is $\Theta(\sqrt{N})$.

First, we show that for a proper choice of $T = O(\sqrt{N})$ the system will be with high probability in the marked state $|m\rangle$. We note that the evolution of the database under the Grover iteration $\hat{U}$ is quite simple since the states $|w\rangle$ and $|m\rangle$ span an invariant subspace of $\hat{U}$, and $\hat{U}$ acts in this two-dimensional space as a rotation. Indeed, consider the two-dimensional space $\mathcal{H}_{inv}$ spanned by the vectors $|m\rangle$ and

$$|\overline{m}\rangle = \frac{1}{\sqrt{N-1}} \sum_{x \neq m} |x\rangle.$$

Clearly, the vector $|w\rangle$ also belongs to $\mathcal{H}_{inv}$, since we find

$$|w\rangle = \frac{1}{\sqrt{N}}|m\rangle + \sqrt{\frac{N-1}{N}}|\overline{m}\rangle. \tag{4.1}$$

From the definition of the Grover iteration $\hat{U}$ we see that it is a product of two reflections. The oracle $\hat{O}_m$ performs a reflection about the vector $|m\rangle$. Similarly, the Grover operator performs a reflection about the vector $|w\rangle$. Since both $|m\rangle$ and $|w\rangle$ belong to $\mathcal{H}_{inv}$ we find that their product is a rotation in the plane spanned by $|m\rangle$ and $|\overline{m}\rangle$. This shows that $\mathcal{H}_{inv}$ is indeed an invariant subspace of $\hat{U}$ and that

$$|\psi(t)\rangle = \hat{U}^t|w\rangle,$$

remains in $\mathcal{H}_{inv}$ for all t. More precisely, the action of $\hat{U}$ on the vectors $|m\rangle$, $|\overline{m}\rangle$ is easily found to be

$$\begin{aligned} \hat{U}|m\rangle &= \frac{N-2}{N}|m\rangle - \frac{2\sqrt{N-1}}{N}|\overline{m}\rangle, \\ \hat{U}|\overline{m}\rangle &= \frac{2\sqrt{N-1}}{N}|m\rangle + \frac{N-2}{N}|\overline{m}\rangle. \end{aligned} \tag{4.2}$$

The effective evolution operator $\hat{U}_{eff}$, i.e. the restriction of the operator $\hat{U}$ on the invariant subspace $\mathcal{H}_{inv}$, is in the orthonormal basis $\{|m\rangle, |\overline{m}\rangle\}$ represented by the following 2×2 rotation matrix

$$U_{eff} = \begin{pmatrix} \cos\theta & \sin\theta \\ -\sin\theta & \cos\theta \end{pmatrix},$$

where the angle θ is determined by the formulas

$$\cos\theta = \frac{N-2}{N}, \quad \sin\theta = \frac{2\sqrt{N-1}}{N}.$$

With this convention we can rewrite the initial state of the database (4.1) into the form

$$|w\rangle = \sin\left(\frac{\theta}{2}\right)|m\rangle + \cos\left(\frac{\theta}{2}\right)|\overline{m}\rangle.$$

We find that after t iterations of the Grover's algorithm the state of the system is given by

$$|\psi(t)\rangle = \hat{U}^t|w\rangle = \sin\left(\frac{(2t+1)\theta}{2}\right)|m\rangle + \cos\left(\frac{(2t+1)\theta}{2}\right)|\overline{m}\rangle.$$

Therefore, the probability to detect the system in the marked state $|m\rangle$ after t iterations of the Grover's algorithm reads

$$p(t) = \cos^2\left(\frac{(2t+1)\theta}{2}\right). \tag{4.3}$$

Hence, the number of iterations of the Grover's algorithm required to find the marked item with high probability should be chosen as the closest integer to

$$T = \frac{\pi}{2\theta} - 1.$$

We find that for large N the number of iterations scales according to

$$T = \frac{\pi}{4}\sqrt{N} + O\left(\frac{1}{\sqrt{N}}\right).$$

For such T the probability of success (4.3) approaches 1 for large N since

$$p(T) = 1 - O\left(\frac{1}{N}\right).$$

We conclude that the Grover's search algorithm finds the marked item after $O(\sqrt{N})$ oracle queries, i.e. it offers a quadratic speed-up over the classical search. Next, we show that the Grover's search is optimal, since any quantum search on an unsorted database requires at least $\Omega(\sqrt{N})$ oracle queries [194].

In general, the oracle based quantum search alternates the oracle and some other unitaries $\hat{U}_j$ which might be different from each other. Suppose that the search starts in the state $|\phi(0)\rangle$ and we apply the oracle t times. We consider the marked item to have an index x. Between the oracle queries we apply the unitary operations $\hat{U}_1$, $\hat{U}_2$, ..., $\hat{U}_t$. The state of the system is then given by

$$|\phi_x(t)\rangle = \hat{U}_t\hat{O}_x \ldots \hat{U}_1\hat{O}_x|\phi(0)\rangle.$$

The subscript x denotes the fact that we apply the oracle $\hat{O}_x$. We also introduce the vector

$$|\phi(t)\rangle = \hat{U}_t \ldots \hat{U}_1|\phi(0)\rangle,$$

corresponding to the applications of the unitaries $\hat{U}_j$ without the oracle. Let us define

$$D(t) = \sum_x \|\phi_x(t) - \phi(t)\|^2,$$

where we write ϕ instead of $|\phi\rangle$ to simplify the notation. The quantity $D(t)$ indicates the deviation caused by the oracle after t iterations from the evolution solely due to the unitaries $\hat{U}_j$. First, we prove that $D(t)$ cannot grow faster than $O(t^2)$. On the other hand, we show that to successfully identify the marked item $D(t)$ has to be of the order of $\Omega(N)$. These two results combined provide the lower bound $\Omega(\sqrt{N})$ on the number of oracle queries required.

We first prove by induction that $D(t) \leq 4t^2$. For $t = 0$ we find that the inequality holds since $D(0) = 0$. Let us now turn to $D(t+1)$. We express it in the form

$$\begin{aligned} D(t+1) &= \sum_x \|\phi_x(t+1) - \phi(t+1)\|^2 = \sum_x \left\|\hat{U}_{t+1}\left(\hat{O}_x\phi_x(t) - \phi(t)\right)\right\|^2 \\ &= \sum_x \left\|\hat{O}_x\phi_x(t) - \phi(t)\right\|^2 = \sum_x \left\|\hat{O}_x(\phi_x(t) - \phi(t)) + (\hat{O}_x - \hat{I})\phi(t)\right\|^2, \end{aligned}$$

where we have used the unitarity of the operation $\hat{U}_{t+1}$. Now we use the inequality

$$\|a+b\|^2 \leq \|a\|^2 + 2\|a\|\|b\| + \|b\|^2,$$

where we consider

$$\begin{aligned} a &= \hat{O}_x(\phi_x(t) - \phi(t)), \\ b &= (\hat{O}_x - \hat{I})\phi(t) = -2\langle x|\phi(t)\rangle|x\rangle. \end{aligned}$$

We find the upper bound

$$\begin{aligned} D(t+1) &\leq \sum_x \left(\|\phi_x(t) - \phi(t)\|^2 + 4\|\phi_x(t) - \phi(t)\||\langle x|\phi(t)\rangle| + 4|\langle x|\phi(t)\rangle|^2\right) \\ &\leq D(t) + 4\sum_x \|\phi_x(t) - \phi(t)\||\langle x|\phi(t)\rangle| + 4, \end{aligned}$$

where we have used the fact that

$$\sum_x |\langle x|\phi(t)\rangle|^2 = \|\phi(t)\|^2 = 1.$$

Now we use the Cauchy-Schwartz inequality to estimate the second term

$$\sum_x \|\phi_x(t) - \phi(t)\||\langle x|\phi(t)\rangle| \leq \left(\sum_x \|\phi_x(t) - \phi(t)\|^2\right)^{\frac{1}{2}} \left(\sum_x |\langle x|\phi(t)\rangle|^2\right)^{\frac{1}{2}} = \sqrt{D(t)}.$$

Hence, we obtain the inequality

$$D(t+1) \leq D(t) + 4\sqrt{D(t)} + 4.$$

By induction hypothesis we assume that $D(t) \leq 4t^2$ and therefore we find

$$D(t+1) \leq 4t^2 + 8t + 4 = 4(t+1)^2,$$

which completes the first part of the proof.

To complete the proof we have to show that the success probability of at least $\frac{1}{2}$, i.e.

$$|\langle x|\phi_x(t)\rangle|^2 \geq \frac{1}{2},$$

can only be reached if $D(t)$ is $\Omega(N)$. Without loss of generality we may assume that

$$|\langle x|\phi_x(t)\rangle| = \langle x|\phi_x(t)\rangle,$$

which leads us to the estimate

$$\|\phi_x(t) - x\|^2 = 2 - 2|\langle x|\phi_x(t)\rangle| \leq 2 - \sqrt{2}. \tag{4.4}$$

We find the lower bound for $D(t)$

$$D(t) = \sum_x \|(\phi_x(t) - x) + (x - \phi(t))\|^2 \geq E(t) - 2\sum_x \|\phi_x(t) - x\|\|x - \phi(t)\| + F(t),$$

where we have defined the quantities

$$\begin{aligned} E(t) &= \sum_x \|\phi_x(t) - x\|^2, \\ F(t) &= \sum_x \|x - \phi(t)\|^2. \end{aligned}$$

The Cauchy-Schwartz inequality implies that

$$\sum_x \|\phi_x(t) - x\|\|x - \phi(t)\| \leq \left(\sum_x \|\phi_x(t) - x\|^2\right)^{\frac{1}{2}} \left(\sum_x \|x - \phi(t)\|^2\right)^{\frac{1}{2}} = \sqrt{E(t)F(t)},$$

and therefore for $D(t)$ we obtain

$$D(t) \geq F(t) - 2\sqrt{E(t)F(t)} + E(t) = \left(\sqrt{F(t)} - \sqrt{E(t)}\right)^2$$

Let us now estimate the quantities $E(t)$ and $F(t)$. From (4.4) we see that

$$E(t) \leq (2 - \sqrt{2})N. \tag{4.5}$$

Concerning $F(t)$ we find

$$F(t) = \sum_x \|x - \phi(t)\|^2 \geq \sum_x (2 - 2\mathrm{Re}\langle x|\phi(t)\rangle) \geq 2N - 2\sum_x |\langle x|\phi(t)\rangle|.$$

The sum can be estimated with the Cauchy-Schwartz inequality

$$\sum_x |\langle x|\phi(t)\rangle| \leq \left(\sum_x |\langle x|\phi(t)\rangle|^2\right)^{\frac{1}{2}} \left(\sum_x 1\right)^{\frac{1}{2}} = \sqrt{N},$$

and we obtain the lower bound for $F(t)$ in the form

$$F(t) \geq 2N - 2\sqrt{N}.$$

Combining this result with the estimate (4.5) we find that for sufficiently large N and $c < (\sqrt{2} - \sqrt{2 - \sqrt{2}})^2$ the inequality

$$D(t) \geq cN,$$

holds. Since we have shown that $D(t) \leq 4t^2$ we conclude that

$$t \geq \sqrt{\frac{cN}{4}},$$

i.e. to find the marked item with probability at least one-half we have to query the oracle $\Omega(\sqrt{N})$ times. This completes the proof of optimality of the Grover's search algorithm and we conclude that it requires $\Theta(\sqrt{N})$ iterations.

4.3 Quantum Walk Search Algorithm

In this Section we turn to the search algorithm based on quantum walks. We introduce the main ideas and discuss the relation to the Grover's search. Then we analyze in detail the coined quantum walk search on the star graph.

For the quantum walk based search we represent the database with a graph $G = (V, E)$. Each vertex $v \in V$ of the graph corresponds to a particular item of the database. The solution to the search problem is represented by a marked vertex. Our task is to find the marked vertex with high probability by evolving a quantum walker on the graph. Marking the vertex corresponds to changing the dynamics of the quantum walk on that particular node, such as choosing a different coin operator in the coined quantum walk or setting a different on-site energy in the continuous-time quantum walk. The walker is initialized in an equal-weight superposition of all computational basis states to ensure that no additional information is added into the system. We evolve the walker for t steps (or time t in the continuous-time quantum walk) and then measure its position on the graph. The maximum probability of finding the walker on the marked vertex and the runtime t depends on the number of vertices of the graph G, which is equal to the size of the database N, and also on its structure.

The advantage of the quantum walk based search algorithm when compared with the Grover's search is that it allows to represent the database by various graphs, which might be easier to implement in future experiments. However, the optimality of the quantum walk search depends crucially on the structure of the graph. Coined quantum walk search algorithm was shown to be optimal for hypercube [71] and for lattices [74] of dimensions d greater than 2, i.e. it finds the marked node after $O(\sqrt{N})$ steps of the walk. Another variant of discrete-time coinless quantum walk capable of optimal search on regular graphs was proposed by Szegedy [19]. Continuous-time quantum walk was shown to be optimal [72] for search on the complete graph, hypercube and lattices with $d > 4$. Moreover, including the coin degree of freedom the continuous-time quantum walk search is optimal for lattices with $d > 2$ [73]. Later it was found that high symmetry or connectivity of the graph is in fact not required for the optimal runtime of the continuous-time quantum walk search algorithm [88–90]. In fact, Chakraborty et al. [91] have shown that continuous-time quantum walk search algorithm is optimal for almost all graphs.

Let us now illustrate the quantum walk search algorithm on the particular example of the search on the star graph. The star is a bipartite graph consisting of a central vertex labeled as 0 connected to N external vertices with labels 1 to N. One of the external vertices is marked and we want to find it by means of a quantum walk. We consider a coined quantum walk where the particle jumps from the external vertices to the central vertex and back. The position space is spanned by the vectors $|j\rangle_p$, with $j = 0, \ldots, N$, corresponding to the particle being at the vertex j. The coin space has to be defined separately for the external vertices and for the central vertex, since they have different degrees. At the external nodes the coin

space is one-dimensional, since the particle can jump only to the central vertex 0. We denote the coin state as $|0\rangle_c$. At the central node the coin space is N-dimensional, as the particle is allowed to jump to any external vertex j, with $j = 1, \ldots, N$. We denote the corresponding coin states as $|j\rangle_c$. The complete Hilbert space of the coined quantum walk on the star graph is therefore spanned by vectors

$$\begin{aligned} |j\rangle_p \otimes |0\rangle_c &\equiv |j, 0\rangle, \\ |0\rangle_p \otimes |j\rangle_c &\equiv |0, j\rangle, \end{aligned}$$

where j runs from 1 to N. The first index corresponds to the vertex and the second index corresponds to the coin state.

The evolution operator of a single step of the walk can be written as a product of the step operator $\hat{S}$ and the coin operator $\hat{C}$

$$\hat{U} = \hat{S} \cdot \hat{C}. \tag{4.6}$$

The walk describes the particle hopping between the external vertices and the central node. Hence, the step operator is given by

$$\hat{S} = \sum_{j=1}^{N} \left(|j, 0\rangle\langle 0, j| + |0, j\rangle\langle j, 0| \right).$$

Let us now turn to the coin operator. At the external nodes, where the coin space is one-dimensional, we choose the coin operator to act as identity. However, at the marked vertex m the coin acts as a phase shift of π. At the central node the states $|j\rangle_c$ form an N-dimensional space, and we choose the coin operator to act there as the Grover operator

$$\hat{G} = 2|w\rangle_c\langle w| - \hat{I},$$

where $|w\rangle_c$ denotes the symmetric superposition of all basis states $|j\rangle_c$

$$|w\rangle_c = \frac{1}{\sqrt{N}} \sum_{j=1}^{N} |j\rangle_c.$$

Hence, the coin operator has the form

$$\hat{C} = \left(\hat{I}_N - 2|m\rangle_p\langle m| \right) \otimes |0\rangle_c\langle 0| + |0\rangle_p\langle 0| \otimes \hat{G}.$$

After some algebra we find that the evolution operator (4.6) can be re-written as

$$\hat{U} = \sum_{j=1}^{N} |0, j\rangle\langle j, 0| - 2|0, m\rangle\langle m, 0| + \frac{2}{N} \sum_{i,j=1}^{N} |i, 0\rangle\langle 0, j| - \sum_{j=1}^{N} |j, 0\rangle\langle 0, j|. \tag{4.7}$$

We start the walk in an equal-weight superposition of states corresponding to the external vertices

$$|\psi(0)\rangle = \frac{1}{\sqrt{N}} \sum_{j=1}^{N} |j, 0\rangle.$$

The state of the walk after t steps is given by

$$|\psi(t)\rangle = \hat{U}^t |\psi(0)\rangle.$$

We show that after $O(\sqrt{N})$ steps the particle will be with high probability on the marked vertex. In fact, we prove that for the star graph two steps of the coined quantum walk are exactly equivalent to one Grover iteration. Clearly, the walk is bipartite, since the particle hops between the external vertices to the central vertex and back. Hence, it is sufficient to focus on the square of the unitary evolution operator of the walk (4.7). We find that the action of $\hat{U}^2$ on the states $|j, 0\rangle$ is given by

$$\begin{aligned} \hat{U}^2|j,0\rangle &= \frac{2}{N}\sum_{i\neq j}|i,0\rangle - \frac{N-2}{N}|j,0\rangle, \quad j \neq m, \\ \hat{U}^2|m,0\rangle &= \frac{N-2}{N}|m,0\rangle - \frac{2(N-1)}{N}\sum_{i\neq m}|i,0\rangle. \end{aligned} \tag{4.8}$$

It is then straightforward to see that the states $|m, 0\rangle$ and

$$|\overline{m}, 0\rangle = \frac{1}{\sqrt{N-1}} \sum_{j\neq m}^{N} |j, 0\rangle,$$

form an invariant subspace of $\hat{U}^2$. Indeed, using (4.8) we obtain

$$\begin{aligned} \hat{U}^2|m,0\rangle &= \frac{N-2}{N}|m,0\rangle - \frac{2\sqrt{N-1}}{N}|\overline{m},0\rangle, \\ \hat{U}^2|\overline{m},0\rangle &= \frac{2\sqrt{N-1}}{N}|m,0\rangle + \frac{N-2}{N}|\overline{m},0\rangle, \end{aligned}$$

which is identical to the action of the Grover iteration (4.2). Hence, two steps of the coined quantum walk on the star graph are exactly equivalent to one Grover iteration. Using the results for the Grover's search we conclude that we find the marked vertex m with high probability when we chose the number of steps of the quantum walk as an even integer closest to

$$T = \frac{\pi}{2}\sqrt{N} + O\left(\frac{1}{\sqrt{N}}\right).$$

4.4 Perfect State Transfer by Means of Quantum Walks

Finally, let us turn to the perfect state transfer based on a quantum walk. We consider a graph with N vertices where two of them, a sender and a receiver, want to communicate. One possibility to achieve this is based on a simple modification of the quantum walk search algorithm [104]. First, we mark both the sender and the receiver vertex, i.e. we use different coin on these two distinguished locations. Second, we start the walk on the sender vertex in an equal-weight superposition of all coin states. We then evolve the quantum walk and after $O(\sqrt{N})$ steps the particle should reach the receiver vertex.

Let us illustrate this approach to perfect state transfer on the example of the star graph with N external vertices which we have investigated in detail in [X]. Two of the external vertices, the sender labeled s and the receiver labeled r, are marked by a using a different coin operation. The coin operator is therefore given by

$$\hat{C} = \left(\hat{I}_N - 2|s\rangle_p\langle s| - 2|r\rangle_p\langle r|\right) \otimes |0\rangle_c\langle 0| + |0\rangle_p\langle 0| \otimes \hat{G},$$

which corresponds to phase shift of π on the sender and the receiver. The evolution operator determining a single step of the coined quantum walk then reads

$$\hat{U} = \sum_{j=1}^{N} |0,j\rangle\langle j,0| - 2|0,s\rangle\langle s,0| - 2|0,r\rangle\langle r,0| + \frac{2}{N}\sum_{i,j=1}^{N} |i,0\rangle\langle 0,j| - \sum_{j=1}^{N} |j,0\rangle\langle 0,j|. \tag{4.9}$$

We initialize the walk in the sender vertex, i.e. the initial state is

$$|\psi(0)\rangle = |s,0\rangle.$$

We show that after $O(\sqrt{N})$ steps of the coined quantum walk the particle will be with high probability located on the receiver vertex r. We again make use of the bipartiteness of the graph and focus on the square of the evolution operator (4.9). Its action on the computational basis states is given by

$$\begin{aligned}
\hat{U}^2|s,0\rangle &= -\frac{2}{N}\sum_{i\neq s} |i,0\rangle + \left(1 - \frac{2}{N}\right)|s,0\rangle, \\
\hat{U}^2|r,0\rangle &= -\frac{2}{N}\sum_{i\neq r} |i,0\rangle + \left(1 - \frac{2}{N}\right)|r,0\rangle, \\
\hat{U}^2|j,0\rangle &= \frac{2}{N}\sum_{i\neq j} |i,0\rangle - \left(1 - \frac{2}{N}\right)|j,0\rangle, \quad j \neq s,r.
\end{aligned} \tag{4.10}$$

Using these expressions it is straightforward to show that the three orthogonal states $|s,0\rangle$, $|r,0\rangle$ and

$$|\overline{sr},0\rangle = \frac{1}{\sqrt{N-2}}\sum_{j\neq s,r} |j,0\rangle,$$

form an invariant subspace with respect to $\hat{U}^2$. Indeed, from (4.10) we find

$$\begin{aligned}
\hat{U}^2|s,0\rangle &= \frac{N-2}{N}|s,0\rangle - \frac{2}{N}|r,0\rangle - \frac{2\sqrt{N-2}}{N}|\overline{sr},0\rangle, \\
\hat{U}^2|r,0\rangle &= -\frac{2}{N}|s,0\rangle + \frac{N-2}{N}|r,0\rangle - \frac{2\sqrt{N-2}}{N}|\overline{sr},0\rangle, \\
\hat{U}^2|\overline{sr},0\rangle &= \frac{2\sqrt{N-2}}{N}(|s,0\rangle + |r,0\rangle) - \frac{N-4}{N}|\overline{sr},0\rangle.
\end{aligned}$$

Hence, the time evolution of the walk for the fixed initial state $|s,0\rangle$ is described by the effective evolution operator $\hat{U}_{eff}$, which is in the $\{|s,0\rangle, |r,0\rangle, |\overline{sr},0\rangle\}$ basis given by the following 3x3 matrix

$$U_{eff} = \begin{pmatrix} \frac{N-2}{N} & -\frac{2}{N} & \frac{2\sqrt{N-2}}{N} \\ -\frac{2}{N} & \frac{N-2}{N} & \frac{2\sqrt{N-2}}{N} \\ -\frac{2\sqrt{N-2}}{N} & -\frac{2\sqrt{N-2}}{N} & \frac{N-4}{N} \end{pmatrix}.$$

Diagonalization of $\hat{U}_{eff}$ is straightforward. We find that it has an eigenvector

$$|\chi_0\rangle = \frac{1}{\sqrt{2}}\left(|s,0\rangle - |r,0\rangle\right),$$

corresponding to the eigenvalue $\lambda = 1$. The remaining two eigenvectors have the form

$$|\chi^{\pm}\rangle = \frac{1}{2}\left(|s,0\rangle + |r,0\rangle\right) \pm \frac{i}{\sqrt{2}}|\overline{sr},0\rangle.$$

They correspond to a pair of conjugated eigenvalues

$$\lambda^{\pm} = e^{\pm i\omega},$$

where the phase ω is given by

$$\omega = \arccos\left(\frac{N-4}{N}\right). \tag{4.11}$$

Let us now analyze the evolution of the initial state $|s,0\rangle$ under the effective evolution operator $\hat{U}_{eff}$. We find that the initial condition $|s,0\rangle$ and the desired target state $|r,0\rangle$ can be decomposed into the eigenbasis of $\hat{U}_{eff}$ as

$$\begin{aligned}
|s,0\rangle &= \frac{1}{\sqrt{2}}|\chi_0\rangle + \frac{1}{2}\left(|\chi^+\rangle + |\chi^-\rangle\right), \\
|r,0\rangle &= -\frac{1}{\sqrt{2}}|\chi_0\rangle + \frac{1}{2}\left(|\chi^+\rangle + |\chi^-\rangle\right).
\end{aligned}$$

After t applications of the effective evolution operator $\hat{U}_{eff}$, i.e. after $2t$ steps of the walk, we obtain

$$|\psi(2t)\rangle = \frac{1}{\sqrt{2}}|\chi_0\rangle + \frac{e^{i\omega t}}{2}\left(|\chi^+\rangle + e^{-2i\omega t}|\chi^-\rangle\right). \tag{4.12}$$

For $\omega t = \pi$ the state reduces to $-|r,0\rangle$, i.e. the receiver state up to an irrelevant global phase factor. We conclude that the walk achieves (almost) perfect state transfer between the sender and the receiver provided that we choose the number of steps as the closest even integer to $2\pi/\omega$, i.e.

$$T = \frac{2\pi}{\arccos\left(\frac{N-4}{N}\right)}. \tag{4.13}$$

With the Taylor expansion we find that the number of steps required for the state transfer scales with the size of the star graph according to

$$T = \frac{\pi}{\sqrt{2}}\sqrt{N} + O\left(\frac{1}{\sqrt{N}}\right).$$

For illustration we display in Figure 4.1 the fidelity between the state of the walk (4.12) and the target state $|r,0\rangle$ as a function of the number of steps. From (4.12) we find that it is given by

$$\mathcal{F}(2t) = |\langle\psi(2t)|r,0\rangle|^2 = \sin^4\left(\frac{\omega t}{2}\right). \tag{4.14}$$

Note that for odd time steps the fidelity is zero since the walk is bipartite. In Figure 4.1 the number of vertices of the star graph was chosen as $N = 100$. As follows from (4.13) the first maximum of the fidelity is reached after 22 steps of the walk.

4.5 Discussion

The efficiency of the state transfer, i.e. the probability that the particle is actually found at the receiver vertex, depends crucially on the type of the graph where the quantum walk takes place. For the quantum walk search this is not a problem: as far as the probability of finding the marked vertex does not vanish with increasing N, one can repeat the search algorithm k times to find the solution with probability $1-\varepsilon$. The number of repetitions k depends on the error tolerance ε and not on the size of the graph N. Hence, the optimality of the search algorithm, i.e. the ability to find the marked vertex in $O(\sqrt{N})$ steps, is preserved. However, for the sake of perfect state transfer we want to succeed in a single trial, i.e. the probability of the particle reaching the receiver vertex should be as high as possible, ideally reaching unity. This is possible only on few types of graphs, such as the star which we have discussed in the previous Section. In [X] we have shown that the coined quantum walk achieves perfect state transfer on a complete graph with additional self-loop on each vertex. In this case the invariant subspace is five-dimensional, nevertheless, the problem is still analytically tractable. We have found that the spectrum of the effective evolution operator in the invariant subspace

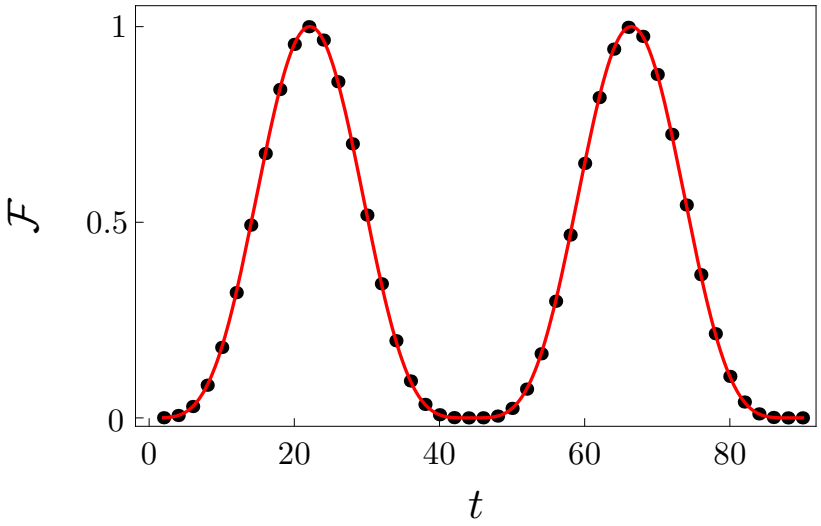

Figure 4.1: Fidelity between the state of the walk (4.12) and the target state $|r, 0\rangle$ for the walk on the star graph as a function of the number of steps t. The black dots correspond to the numerical simulation and the red line is given by (4.14). Fidelity is plotted only at even number of steps, since it vanishes when t is odd. We have considered the star graph with $N = 100$ external vertices. The first maximum of fidelity is reached after 22 steps, in accordance with (4.13).

is given by the eigenvalues

$$\begin{aligned} \lambda_0 &= 1, \\ \lambda_1^{\pm} &= e^{\pm i\omega}, \\ \lambda_2^{\pm} &= e^{\pm 2i\omega}, \end{aligned}$$

where the phase ω is the same as for the star graph (4.11). This implies that the number of steps required for perfect state transfer on the complete graphs with self-loops is the same as for the star graph. Moreover, we have considered perfect state transfer by means of Szegedy's walk with queries [82] on a complete graph. Here the invariant subspace is seven-dimensional and the problem can be treated analytically only in the asymptotic limit $N \to +\infty$. We have found that for large N the dynamics of the Szegedy's walk with queries on the complete graph reduces to that of the coined walk on the star graph, i.e. the perfect state transfer with high fidelity can be achieved in the asymptotic limit.

The results for the star graph were extended in [XI] to complete bipartite graphs $K_{m,n}$ of m plus n vertices. Indeed, the star graph is a special case of a complete bipartite graph with a single vertex in one of the parts, i.e. $K_{m,1}$. We have shown that when both the sender and the receiver vertices are located in the same part of the graph the perfect state transfer is achieved. The size of the second part is irrelevant, since the dynamics in the invariant

subspace is identical to the one for the star graph. On the other hand, when the sender and the receiver are in the opposite parts the particle is found at the receiver vertex with certainty only when the parts of the bipartite graph have the same size, i.e. $m = n$. When their sizes differ the fidelity of state transfer decreases, and the maximal attainable value of fidelity is given by

$$\mathcal{F}_{\max} = \left(\frac{\sqrt{(m-1)(n-1)} + \sqrt{mn}}{m+n-1} \right)^2 .$$

We note that there exists another approach to perfect state transfer based on quantum walks where one defines dynamics at each individual vertex in order to achieve state transfer between two the sender and the receiver. This method was applied to achieve perfect state transfer on a circle [101, 103] and a square lattice [102]. However, it requires considerably more control over the graph in comparison with the approach based on the modification of the quantum walk search, where we have to adjust the dynamics only at the sender and receiver vertex.

Chapter 5

Conclusions

Over the years quantum walks have established a solid position in quantum information theory. They have been successfully applied to various tasks from quantum information processing, quantum communication or quantum simulations. We believe that our work has contributed to this effort.

We concentrated mostly on homogeneous quantum walks where the Fourier analysis is applicable. For certain models it is possible to diagonalize the evolution operator and derive the weak-limit theorem. However, the explicit form of the limit density is often rather complicated, in particular, due to the dependence on the initial coin state. We showed that this issue can be remedied by utilizing a more suitable basis of the coin space [I, V, VI, IX] which reduces the complexity of the formulas tremendously. This allows one to easily identify features which are hidden in the standard basis description. The subsequent analysis of applications of quantum walks is considerably simplified, as we demonstrated on the examples of quantum transport on a ring [VII] or persistence of unvisited sites [VIII]. We plan to investigate the potential of our approach for higher-dimensional quantum walks with more internal degrees of freedom. In addition, we will discuss its application to quantum walks without translational invariance.

Large part of our work was focused on the effect of trapping [III,IV,V]. We provided a full classification of $U(3)$ coins which lead to the trapping effect for three-state quantum walks on a line [IV]. Physical properties of the trapping walks in dependence on the coin parameters were analyzed. We were able to analytically solve the dynamics of particular families of three-state walks. The explicit form of their limit density and trapping probability was derived [V]. At the moment we are preparing a similar classification of $U(4)$ trapping coins for four-state quantum walks on a square lattice [196]. The approach we pursued for $U(3)$ coins in [IV], i.e. a direct construction of the coin operator from the conditions on the existence of the point spectrum, is not convenient for larger matrices. Instead, we employ the properties of the stationary states to reconstruct the coin operator. We also prove that this construction is exhaustive, i.e. we indeed obtain all $U(4)$ trapping coins. The additional degrees of freedom

offered by larger coin space results in features which do not exist for three-state walks. As an example, the effect of strong trapping was identified in [195]. It was found that for certain $U(4)$ coins the leaving state, i.e. an initial state for which the trapping vanishes, does not exist. Hence, in strong trapping walks the trapping effect is always present, irrespective of the initial condition. This is not possible in three-state walks where the leaving state always exists [IV]. We plan to investigate the trapping probability in four-state walks on a square grid in full detail. It would be interesting to see if the trapping probability can be made asymmetric and directionally dependent, in a similar way as for the three-state walks. The identification of suitable bases of the coin space will be crucial for this analysis.

We investigated quantum walks as models of coherent excitation transport to an absorbing sink on a simple ring graph [VII]. Our results show that the trapping effect seriously inhibits transport. However, we found that in certain cases the trapping effect can be eliminated by dynamical percolation, since the stationary states of the trapped walk do not belong to the attractor space of the walk on the dynamically changing ring. Hence, allowing the edges to break randomly might improve the efficiency of transport, which is quite a counterintuitive result. We plan to extend this analysis to more complicated graphs, such as torus, trees or regular graphs. In such cases the topology of the graph might play a non-trivial role, since it certainly affects the structure of the stationary states of the trapped walk. Moreover, it can lead to existence of additional attractors of the walk when we consider dynamical percolation of the graph. We plan to investigate the interplay between these two effects in more detail.

The application of quantum walks to the problem of perfect state transfer between two vertices of a graph was addressed in [X, XI]. Our approach relies on a simple modification of the quantum walk search algorithm. Its efficiency depends crucially on the structure of the underlying graph. We proved by explicit calculation that one can achieve perfect state transfer with unit fidelity on a star graph and complete graph with self-loops. In the case of the Szegedy's walk on a complete graph the perfect state transfer is achieved with high fidelity in the asymptotic limit. For complete bipartite graphs we showed that the unit fidelity of perfect state transfer is ensured when the sender and the receiver vertices are in the same part of the graph. Otherwise, unit fidelity is achieved only when the two parts have the size. It is of interest to identify additional graphs where perfect state transfer can be performed with high fidelity, at least in the limit of large size of the graph. In addition, we plan to investigate perfect state transfer by means of quantum walks under the influence of imperfections, such as phase noise, coin inhomogeneity or percolation.

Finally, let us mention the advancements in the experimental realizations of quantum walks. We have a close collaboration with the experimental group of prof. Christine Silberhorn at the University of Paderborn, Germany. Her group realizes discrete-time quantum walks by utilizing photonic time-multiplexing and loop architecture [176] which significantly reduces the number of required optical elements. The photonic platform is intrinsically coherent and stable. Moreover, with the incorporation of programmable electro-optical mod-

ulators it is possible to simulate dynamical effects, such as Anderson localization [177] or quantum transport in random media [178]. We have collaborated with them extensively on the first optical implementation of a 2D quantum walk [II] which was able to simulate a walk of two particles on a line, including the case of interacting particles. In these experiments the measurement process was somewhat limited, since it was performed through a probabilistic out-coupling. Indeed, after the step of a quantum walk is executed the light pulse passes through a weakly reflective beam-splitter which most likely sends it back into the loop to continue the quantum walk evolution, however, with a probability of a few percent it is coupled out to a polarization resolving detection via avalanche photodiodes. The time of detection of the light pulse uniquely determines the number of steps performed and the position on the lattice. One can then reconstruct the probability distribution at any desired time-step by normalizing the frequencies of detection appropriately. However, the probabilistic nature of this measurement scheme does not allow us to focus on a particular site or a particular time step. Moreover, it increases the photon loss per round-trip which reduces the visibility and limits the achievable number of steps. The group of prof. Silberhorn devised a deterministic out-coupling scheme which solves these issues. This measurement setup employs programmable electro-optical modulators to couple-out on demand a light pulse corresponding to the desired time and position without affecting the coherence of the rest of the wave-packet. In addition to improved visibility at higher number of steps the deterministic out-coupling enables us to implement an absorbing sink. Recently [197] we have used the setup to experimentally demonstrate the role of the measurement scheme on the recurrence probability in quantum walks [189, 198, 199]. In the nearest future we plan to apply the experiment to simulate quantum transport to an absorbing sink.

References

List of Author's Publications

[I] M. Štefaňák, S. M. Barnett, B. Kollár, T. Kiss and I. Jex, New J. Phys. **13**, 033029 (2011).

[II] A. Schreiber, A. Gábris, P. P. Rohde, K. Laiho, M. Štefaňák, V. Potoček, C. Hamilton, I. Jex and C. Silberhorn, Science **336**, 55 (2012).

[III] M. Štefaňák, I. Bezděková and I. Jex, Eur. Phys. J. D **66**, 142 (2012).

[IV] M. Štefaňák, I. Bezděková, I. Jex and S. M. Barnett, Quantum Inf. Comput. **14**, 1213 (2014).

[V] M. Štefaňák, I. Bezděková and I. Jex, Phys. Rev. A **90**, 012342 (2014).

[VI] I. Bezděková, M. Štefaňák and I. Jex, Phys. Rev. A **92**, 022347 (2015).

[VII] M. Štefaňák, J. Novotný and I. Jex, New J. Phys. **18**, 023040 (2016).

[VIII] M. Štefaňák and I. Jex, Phys. Rev. A **93**, 032321 (2016).

[IX] M. Štefaňák, I. Bezděková and I. Jex, Interd. Inf. Sci. **23**, 19 (2017).

[X] M. Štefaňák and S. Skoupý, Phys. Rev. A **94**, 022301 (2016).

[XI] M. Štefaňák and S. Skoupý, Quantum Inf. Process. **16**, 72 (2017).

References

[1] Y. Aharonov, L. Davidovich and N. Zagury, Phys. Rev. A **48**, 1687 (1993).

[2] R. P. Feynman and A. R. Hibbs, *Quantum mechanics and path integrals*, International series in pure and applied physics, McGraw-Hill, New York (1965).

[3] S. P. Gudder, Found. Phys. **18**, 751 (1988).

[4] S. Gudder, *Quantum Probability*, Academic Press Inc., (1988).

[5] E. Farhi and S. Gutmann, Phys. Rev. A **58**, 915 (1998).

[6] D. Meyer, J. Stat. Phys. **85**, 551, (1996).

[7] A. M. Childs, E. Farhi and S. Gutmann, Quantum Inf. Process. **1**, 35 (2002).

[8] F. W. Strauch, Phys. Rev. A **74**, 030301 (2006).

[9] A. M. Childs, Comm. Math. Phys. **294**, 581 (2010).

[10] Y. Shikano, J. Comput. Theor. Nanosci. **10**, 1558 (2013).

[11] A. Ambainis, E. Bach, A. Nayak, A. Vishwanath and J. Watrous, in *Proc. 33th STOC (New York: ACM)*, 60 (2001).

[12] P. L. Knight, E. Roldan and J. E. Sipe, Phys. Rev. A **68**, 020301(R) (2003).

[13] T. D. Mackay, S. D. Bartlett, L. T. Stephenson and B. C. Sanders, J. Phys. A **35**, 2745 (2002).

[14] M. Hillery, J. Bergou and E. Feldman, Phys. Rev. A **68**, 032314 (2003).

[15] E. Feldman and M. Hillery, Phys. Lett. A **324**, 277 (2004).

[16] E. Feldman and M. Hillery, J. Phys. A **40**, 11343 (2007).

[17] F. M. Andrade and M. G. E. da Luz, Phys. Rev. A **80**, 052301 (2009).

[18] B. F. Venancio, F. M. Andrade and M. G. E. da Luz, J. Phys. A **46**, 165302 (2013).

[19] M. Szegedy, in *Proc. 45th Symp. Found. Comp. Science*, 3241 (2004).

[20] R. Portugal, Quantum Inf. Process **15**, 1387 (2016).

[21] T. G. Wong, Quantum Inf. Process. **16**, 215 (2017).

[22] A. Patel, K. S. Raghunathan and P. Rungta, Phys. Rev. A **71**, 032347 (2005).

[23] A. Patel, K. S. Raghunathan and Md. A. Rahaman, Phys. Rev. A **82**, 032331 (2010).

[24] A. Ambainis, R. Portugal and N. Nahimov, Quantum Inf. Comput. **15**, 1233 (2015).

[25] R. Portugal, S. Boettcher and S. Falkner, Phys. Rev. A **91**, 052319 (2015).

[26] R. A. M. Santos, R. Portugal and S. Boettcher, Quantum Inf. Process. **14**, 3179 (2015).

[27] R. Portugal, R. A. M. Santos, T. D. Fernandes and D.N. Gonalves, Quantum Inf. Process. **15**, 85 (2016).

[28] R. Portugal, Phys. Rev. A **93**, 062335 (2016).

[29] S. Attal, F. Petruccione, C. Sabot and I. Sinayskiy, J. Stat. Phys. **147**, 832 (2012).

[30] I. Sinayskiy and F. Petruccione, J. Phys.: Conf. Ser. **442**, 012003 (2013).

[31] G. Grimmett, S. Janson and P. F. Scudo, Phys. Rev. E **69**, 026119 (2004).

[32] N. Konno, Quantum Inform. Comput. **2**, 578 (2002).

[33] N. Konno, J. Math. Soc. Jpn. **57**, 1179 (2005).

[34] N. Konno, Phys. Rev. E **72**, 026113 (2005).

[35] N. Inui and N. Konno, Physica A **353**, 133 (2005).

[36] N. Inui, N. Konno and E. Segawa, Phys. Rev. E **72**, 056112 (2005).

[37] T. Miyazaki, M. Katori, and N. Konno, Phys. Rev. A **76**, 012332 (2007).

[38] K. Watabe, N. Kobayashi, M. Katori and N. Konno, Phys. Rev. A **77**, 062331 (2008).

[39] S. Falkner and S. Boettcher, Phys. Rev. A **90**, 012307 (2014).

[40] T. Machida, Quantum Inf. Comput. **15**, 406 (2015).

[41] N. Inui, Y. Konishi and N. Konno, Phys. Rev. A **69**, 052323 (2004).

[42] N. Konno, N. Obata and E. Segawa, Commun. Math. Phys. **322**, 667 (2013).

[43] Y. Higuchi, N. Konno, I. Sato and E. Segawa, J. Funct. Anal. **267**, 4197 (2014).

[44] Y. Ide, N. Konno, E. Segawa and X. Xu, Entropy **16**), 1501 (2014).

[45] C. Lyu, L. Yu and S. Wu, Phys. Rev. A **92**, 052305 (2015).

[46] M. Cantero, F. Grünbaum, L. Moral and Velázquez, Rev. Math. Phys. **24** 1250002 (2012).

[47] A. Wojcik, T. Luczak, P. Kurzynski, A. Grudka, T. Gdala and M. Bednarska-Bzdega, Physical Review A **85**, 012329 (2012).

[48] T. Endo and N. Konno, Yokohama Math. J. **60**, 33 (2015).

[49] T. Endo and N. Konno, Quantum Inf. Comput. **15**, 105 (2015).

[50] T. Endo and N. Konno, Yokohama Math. J. **61**, 87 (2015).

[51] N. Konno and E. Segawa, Quantum Inf. Comput. **11**, 485 (2011).

[52] M. J. Cantero, F. A. Grünbaum, L. Moral and L. Velázquez, Commun. Pure App. Math. **63**, 464 (2010).

[53] N. Konno and E. Segawa, Quantum Inf. Comput. **14**, 1165 (2014).

[54] D. Damanik, J. Erickson, J. Fillman, G. Hinkle and A. Vu, J. Approx. Theory **208**, 59 (2016).

[55] N. Konno, Quantum Inf. Process. **9**, 405 (2010).

[56] C. Cedzich, T. Rybár, A. H. Werner, A. Alberti, M. Genske and R. F. Werner, Phys. Rev. Lett. **111**, 160601 (2013).

[57] I. Yalcinkaya and Z. Gedik, Phys. Rev. A **92**, 042324 (2015).

[58] T. A. Brun, H. A. Carteret and A. Ambainis, Phys. Rev. A 67, 032304 (2003).

[59] V. Kendon, Math. Struct. Comp. Sci. **17**, 1169 (2006).

[60] Y. Yin, D. E. Katsanos and S. N. Evangelou, Phys. Rev. A **77**, 022302 (2008).

[61] A. Joye and M. Merkli, J. Stat. Phys. **140**, 1025 (2010).

[62] A. Ahlbrecht, V. B. Scholz, A. H. Werner, J. Math. Phys. **52**, 102201 (2011).

[63] G. Leung, P. Knott, J. Bailey and V. Kendon, New J. Phys. **12**, 123018 (2010).

[64] J. Novotný, G. Alber and I. Jex, J. Phys. A **42**, 282003 (2009).

[65] J. Novotný, G. Alber and I. Jex, Cent. Eur. J. Phys. **8**, 1001 (2010).

[66] J. Novotný, G. Alber and I. Jex, J. Phys. A **45**, 485301 (2012).

[67] B. Kollár, T. Kiss, J. Novotný and I. Jex, Phys. Rev. Lett. **108**, 230505 (2012).

[68] B. Kollár, J. Novotný, T. Kiss T and I. Jex, Eur. Phys. J. Plus **129**, 103 (2014).

[69] B. Kollár, J. Novotný, T. Kiss T and I. Jex, New J. Phys. **16**, 23002 (2014).

[70] D. Aharonov, A. Ambainis, J. Kempe and U. Vazirani, in *Proc. 33th STOC (New York: ACM)*, 50 (2001).

[71] N. Shenvi, J. Kempe and K. B. Whaley, Phys. Rev. A **67**, 052307 (2003).

[72] A. M. Childs and J. Goldstone, Phys. Rev. A **70**, 022314 (2004).

[73] A. M. Childs and J. Goldstone, Phys. Rev. A **70**, 042312 (2004).

[74] A. Ambainis, J. Kempe and A. Rivosh, in *Proceedings of the 16th ACM-SIAM Symposium on Discrete Algorithms*, 10991108 (2005).

[75] V. Potoček, A. Gábris, T. Kiss and I. Jex, Phys. Rev. A **79**, 012325 (2009).

[76] D. Reitzner, M. Hillery, E. Feldman and V. Bužek, Phys. Rev. A **79**, 012323 (2009).

[77] B. Hein and G. Tanner, J. Phys. A **42**, 085303 (2009).

[78] T. G. Wong, J. Phys. A **48**, 435304 (2015).

[79] T. G. Wong, A. Ambainis, Phys. Rev. A **92**, 022338 (2015).

[80] T. G. Wong, J. Phys. A, **48**, 405303 (2015).

[81] T. G. Wong, Phys. Rev. A **92**, 032320 (2015).

[82] R. A. M. Santos, Quantum Inf. Process. **15**, 4461 (2016).

[83] T. G. Wong, Quantum Inf. Process. **15**, 1411 (2016).

[84] K. Prusis, J. Vihrovs and T. G. Wong, J. Phys. A **49**, 455301 (2016).

[85] T. G. Wong, L. Tarrataca, N. Nahimov, Quantum Inf. Process. **15**, 4029 (2016).

[86] L. Grover, In *Proceedings of 28th ACM Symposium on Theory of Computing*, 212219, (1996).

[87] L. K. Grover, Phys. Rev. Lett. **78**, 325 (1997).

[88] J. Janmark, D. A. Meyer and T. G. Wong, Phys. Rev. Lett. **112**, 210502 (2014).

[89] L. Novo, S. Chakraborty, M. Mohseni, H. Neven and Y. Omar, Scientific Rep. **5**, 13304 (2014).

[90] D. A. Meyer and T. G. Wong, Phys. Rev. Lett. **114**, 110503 (2015).

[91] S. Chakraborty, L. Novo, A. Ambainis and Y. Omar, Phys. Rev. Lett. **116**, 100501 (2016).

[92] B. L. Douglas and J. B. Wang, J. Phys. A **41**, 075303 (2008).

[93] J. K. Gamble, M. Friesen, D. Zhou, R. Joynt and S. N. Coppersmith, Phys. Rev. A **81**, 052313 (2010).

[94] S. D. Berry and J. B. Wang, Phys. Rev. A **83**, 042317 (2011).

[95] K. Rudinger, J. K. Gamble, M. Wellons, E. Bach, M. Friesen, R. Joynt and S. N. Coppersmith, Phys. Rev. A **86**, 022334 (2012).

[96] K. Rudinger, J. K. Gamble, E. Bach, M. Friesen, R. Joynt and S. N. Coppersmith, J. Comut. Theor. Nanos. **10**, 1653 (2013).

[97] M. Bruderer and M. B. Plenio, Phys. Rev. A **94**, 062317 (2016).

[98] M. Hillery, H. Zheng, E. Feldman, D. Reitzner and V. Bužek, Phys. Rev. A **85**, 062325 (2012).

[99] E. Feldman, M. Hillery, H. W. Lee, D. Reitzner, H. Zheng and V. Bužek, Phys. Rev. A **82**, 040301(R) (2010).

[100] S. Cottrell and M. Hillery, Phys. Rev. Lett. **112**, 030501 (2014).

[101] P. Kurzynski and A. Wojcik, Phys. Rev. A **83**, 062315 (2011).

[102] X. Zhan, H. Qin, Z. H. Bian, J. Li and P. Xue, Phys. Rev. A **90**, 012331 (2014).

[103] I. Yalcinkaya and Z. Gedik, J. Phys. A **48**, 225302 (2015).

[104] B. Hein and G. Tanner, Phys. Rev. Lett. **103**, 260501 (2009).

[105] V. M. Kendon and C. Tamon, J. Comput. Theor. Nanosc. **8**, 422 (2011).

[106] K. Barr, T. Proctor, D. Allen and V. Kendon, Quantum Inform. Comput. **14**, 417 (2014).

[107] S. Attal, F. Petruccione and I. Sinayskiy, Phys. Lett. A **376**, 1545 (2012).

[108] I. Sinayskiy and F. Petruccione, Quantum Inf. Process. **11**, 1301 (2012).

[109] A. M. Childs, Phys. Rev. Lett. **102**, 180501 (2009).

[110] N. B. Lovett, S. Cooper, M. Everitt, M. Trevers and V. Kendon, Phys. Rev. A **81**, 042330 (2010).

[111] O. Mülken, V. Bierbaum and A. Blumen, J. Chem. Phys. **124**, 124905 (2006).

[112] O. Mülken, V. Pernice and A. Blumen, Phys. Rev. E **76**, 051125 (2007).

[113] O. Mülken and A. Blumen, Phys. Rep. **502**, 37 (2011).

[114] P. Schijven, J. Kohlberger, A. Blumen and O. Mülken, J. Phys. A **45**, 215003 (2012).

[115] A. Anishchenko, A. Blumen and O. Mülken, Phys. Rev. E **88**, 062126 (2013).

[116] Z. Darázs, A. Anishchenko, T. Kiss, A. Blumen and O. Mülken, Phys. Rev. E **90**, 032113 (2014).

[117] N. Konno, T. Namiki, T. Soshi and A. Sudbury, J. Phys. A **36**, 241 (2003).

[118] E. Bach, S. Coppersmith, M. P. Goldschen, R. Joynt and J. Watrous, J. Comput. System Sci. **69**, 562 (2004).

[119] T. Yamasaki, H. Kobayashi and H. Imai, Phys. Rev. A **68**, 012302 (2003)

[120] L. C. Kwek and Setiawan, Phys. Rev. A **84**, 032319 (2011).

[121] C. M. Chandrashekar and T. Busch, Quantum Inf. Process. **13**, 1313 (2014).

[122] J. K. Asboth and J. M. Edge, Phys. Rev. A **91**, 022324 (2015).

[123] M. Katori, S. Fujino and N. Konno, Phys. Rev. A **72**, 012316 (2005).

[124] G. M. D'Ariano, N. Mosco, P. Perinotti and A. Tosini, Eur. Phys. Lett. **109**, 40012 (2015).

[125] F. W. Strauch, Phys. Rev. A **73**, 054302 (2006).

[126] P. Kurzynski, Phys. Lett. A **372**, 6125 (2008).

[127] F. Sato and M. Katori, Phys. Rev. A **81**, 012314 (2010).

[128] C. M. Chandrashekar, S. Banerjee, R. Srikanth, Phys. Rev. A **81**, 062340 (2010).

[129] G. Di Molfetta Giuseppe, M. E. Brachet and F. Debbasch, Phys. Rev. A **88**, 042301 (2013).

[130] P. Arrighi, M. Forets and V. Nesme, J. Phys. A **47**, 465302 (2014).

[131] G. Di Molfetta, L. Honter, B. B. Luo, T. Wada and Y. Shikano, Quantum Stud.: Math. Found. **2**, 243 (2015).

[132] C. W. Lee, P. Kurzynski, H. Nha, Phys. Rev. A **92**, 052336 (2015).

[133] A. Mallick and C. M. Chandrashekar, Sci. Rep. **6**, 25779 (2016).

[134] T. Kitagawa, M. S. Rudner, E. Berg and E. Demler, Phys. Rev. A **82**, 033429 (2010).

[135] H. Obuse and N. Kawakami, Phys. Rev. B **84**, 195139 (2011).

[136] T. Kitagawa, M. A. Broome, A. Fedrizzi, M. S. Rudner, E. Berg, I. Kassal,A. Aspuru-Guzik, A Aspuru-Guzik, E. Demler and A. G. White, Nature Comm. **3**, 882 (2012).

[137] T. Kitagawa, Quantum Inf. Process. **11**, 1107 (2012).

[138] J. K. Asboth, Phys. Rev. B **86**, 195414 (2012).

[139] S. Moulieras, M. Lewenstein and G. Puentes, J. Phys. B **46**, 104005 (2013).

[140] J. K. Asboth and H. Obuse, Phys. Rev. B **88**, 121406 (2013).

[141] B. Tarasinski, J. K. Asboth and J. P. Dahlhaus, Phys. Rev. A **89**, 042327 (2014).

[142] H. Obuse, J. K. Asboth, Y. Nishimura and N. Kawakami, Phys. Rev. B **92**, 045424 (2015).

[143] T. Rakovszky and J. K. Asboth, Phys. Rev. A **92**, 052311 (2015).

[144] H. T. Lam, Y. Yu and K. Y. Szeto, Phys. Rev. A **93**, 052319 (2016).

[145] C. Cedzich, F. A. Grünbaum, C. Stahl, L. Velázquez, A. H. Werner and R. F. Werner, J. Phys. A **49**, 21 (2016).

[146] T. Groh, S. Brakhane, W. Alt, D. Meschede, J. Asbth and A. Alberti, Phys. Rev. A **94**, 013620 (2016).

[147] S. Mugel, A. Celi, P. Massignan, J. K. Asbth, M. Lewenstein and C. Lobo, Phys. Rev. A **94**, 023631 (2016).

[148] B. C. Travaglione and G. J. Milburn, Phys. Rev. A **65**, 032310 (2002).

[149] W. Dr, R. Raussendorf, V. M. Kendon, and H.-J. Briegel, Phys. Rev. A **66**, 052319 (2002).

[150] K. Eckert, J. Mompart, G. Birkl, and M. Lewenstein, Phy. Rev. A **72**, 012327 (2005).

[151] R. Cote, A. Russell, E. E. Eyler and P. L. Gould, New J. Phys. **8**, 156 (2006).

[152] B. C. Sanders, S. D. Bartlett, B. Tregenna and P. L. Knight, Phys. Rev. A **67**, 042305 (2003).

[153] T. Di, M. Hillery and M. S. Zubairy, Phys. Rev. A **70**, 032304 (2004).

[154] P. L. Knight, E. Roldn and J. E. Sipe, Opt. Comm. **227**, 147 (2003).

[155] H. Jeong, M. Paternostro and M. Kim, Phys. Rev. A **69**, 012310 (2004).

[156] P. Pathak and G. Agarwal, Phys. Rev. A **75**, 032351 (2007).

[157] C. Chandrashekar, Phys. Rev. A **74**, 032307 (2006).

[158] K. Manouchehri and J. Wang, J. Phys. A **41**, 065304 (2008).

[159] O. Kalman, T. Kiss and P. Földi, Phys. Rev. B **80**, 035327 (2009).

[160] C. S. Hamilton, A. Gabris, I. Jex and S. M. Barnett, New J. Phys. **13**, 013015 (2011).

[161] C. S. Hamilton, R. Kruse, L. Sansoni, C. Silberhorn and I. Jex, Phys. Rev. Lett. **113**, 083602 (2014).

[162] J. Ghosh, Phys. Rev. A **89**, 022309 (2014).

[163] J. Wang and K. Manouchehri, *Physical Implementation of Quantum Walks*, Springer, (2013).

[164] M. Karski, L. Förster, J.-M. Choi, A. Steffen, W. Alt, D. Meschede and A. Widera, Science **325**, 174 (2009).

[165] H. Schmitz, R. Matjeschk, C. Schneider, J. Glueckert, M. Enderlein, T. Huber, and T. Schaetz, Phys. Rev. Lett. **103**, 090504 (2009).

[166] M. Genske, W. Alt, A. Steffen, A. H. Werner, R. F. Werner, D. Meschede and A. Alberti, Phys. Rev. Lett. **110**, 190601 (2013).

[167] F. Zähringer, G. Kirchmair, R. Gerritsma, E. Solano, R. Blatt and C. F. Roos, Phys. Rev. Lett. **104**, 100503 (2010).

[168] A. Peruzzo et al., Science **329**, 1500 (2010).

[169] L. Sansoni, F. Sciarrino, G. Vallone, P. Mataloni, A. Crespi, R. Ramponi and R. Osellame, Phys. Rev. Lett. **108**, 010502 (2012).

[170] J. D. A. Meinecke, K. Poulios, A. Politi, J. C. F. Matthews, A. Peruzzo, N. Ismail, K. Wrhoff, J. L. O'Brien and M. G. Thompson, Phys. Rev. A **88**, 012308 (2013).

[171] K. Poulios et al., Phys. Rev. Lett. **112**, 143604 (2014).

[172] D. Bouwmeester, I. Marzoli, G. Karman, W. Schleich and J. Woerdman, Phys. Rev. A **61**, 013410 (1999).

[173] M. A. Broome, A. Fedrizzi, B. P. Lanyon, I. Kassal, A. Aspuru-Guzik and A. G. White, Phys. Rev. Lett. **104**, 153602 (2010).

[174] P. Xue, H. Qin, B. Tang and B. C. Sanders, New J. Phys. **16**, 053009 (2014).

[175] P. Xue, R. Zhang, H. Qin, X. Zhan, Z. H. Bian, J. Li and B. C. Sanders, Phys. Rev. Lett. **114**, 140502 (2015).

[176] A. Schreiber, K. N. Cassemiro, V. Potoček, A. Gabris, P. J. Mosley, E. Andersson, I. Jex, and C. Silberhorn, Phys. Rev. Lett. **104**, 050502 (2010).

[177] A. Schreiber, K. N. Cassemiro, V. Potoček, A. Gabris, Abris, I. Jex and C. Silberhorn, Phys. Rev. Lett. **106**, 180403 (2011).

[178] F. Elster, S. Barkhofen, T. Nitsche, J. Novotný, A. Gábris, I. Jex and C. Silberhorn, Sci. Rep. **5**, 13495 (2015).

[179] A. Crespi, R. Osellame, R. Ramponi, V. Giovannetti, R. Fazio, L. Sansoni, F. De Nicola, F. Sciarrino and P. Mataloni, Nat. Phot. **7**, 322 (2013).

[180] F. Cardano et al., Nature Commun. **8**, 15516 (2017).

[181] E. Flurin, V. V. Ramasesh, S. Hacohen-Gourgy, L. S. Martin, N. Y. Yao and I. Siddiqi, Phys. Rev. X **7**, 031023 (2017).

[182] H. A. Carteret, M. E. H. Ismail and B. Richmond, J. Phys. A **36**, 8775 (2003).

[183] P. L. Knight, E. Roldan and J. E. Sipe, J. Mod. Opt. **51**, 1761 (2004).

[184] H. A. Carteret, B. Richmond and N. M. Temme, J. Phys. A **38**, 8641 (2005).

[185] R. Wong, *Asymptotic Approximations of Integrals*, SIAM, Philadelphia (2001).

[186] A. Kempf and R. Portugal, Phys. Rev. A **79**, 052317 (2009).

[187] S. Chandrasekhar, Rev. Mod. Phys. **15**, 1 (1943).

[188] S. Goswami, P. Sen, and A. Das, Phys. Rev. E **81**, 021121 (2010).

[189] M. Štefaňák, I. Jex and T. Kiss, Phys. Rev. Lett. **100**, 020501 (2008).

[190] A. Ahlbrecht, A. Alberti, D. Meschede, V. B. Scholz, A. H. Werner and R. F. Werner, New J. Phys. **14**, 073050 (2012).

[191] S. Bose, Phys. Rev. Lett. **91**, 207901 (2003).

[192] M. Boyer, G. Brassard, P. Hoyer and A. Tapp, Fortsch. Phys. - Prog. Phys. **46**, 493, (1998).

[193] M. A. Nielsen and I. L. Chuang, *Quantum Computation and Quantum Information: 10th Anniversary Edition*, Cambridge University Press (Cambridge), (2011).

[194] C. H. Bennett, E Bernstein, G. Brassard, U. Vazirani, SIAM J. Computing. **26**, 1510 (1997).

[195] B. Kollár, T. Kiss, I. Jex, Phys. Rev. A **91**, 022308 (2015).

[196] B. Kollár, I. Bezděková, A. Gilyén, T. Kiss, M. Štefaňḱ and I. Jex, in prepartion

[197] T. Nitsche, R. Kruse, L. Sansoni, S. Barkhofen, M. Štefaňák, A. Gábris, V. Potoček, T. Kiss, I. Jex and C. Silberhorn, in preparation

[198] T. Kiss, L. Kecskes, M. Štefaňák and I. Jex, Phys. Scr. **T135**, 014055 (2009).

[199] F. A. Grünbaum, L. Velázquez, A. H. Werner and R. F. Werner, Commun. Math. Phys. **320**, 543 (2013).

starting the walk in a separable state. We determine the limits for the directional correlations and show that, for any value within these limits, one can design a corresponding separable initial state. Next, we prove that the bounds cannot be exceeded by considering entanglement in the initial state. On the other hand, introducing quantum walks with δ-interactions, we show that the directional correlations can be increased above the limit for non-interacting particles.

Our paper is organized as follows: we briefly review the quantum walk on a line with one and two non-interacting particles in Section II and introduce the probability to be on the same side of the lattice P_s. In Section III we analyze the probability P_s for separable initial states. Entangled initial states are considered in Section IV. In Section V we study the influence of the indistinguishability on the probability P_s. In Section VI we introduce the concept of δ-interacting quantum walks to break the limits of non-interacting quantum walks. We summarize our results in Section VII.

II. QUANTUM WALK ON A LINE WITH ONE AND TWO PARTICLES

Let us first briefly review the quantum walk of a single particle on a line (see e.g. Ref. [67] for a more detailed introduction). The Hilbert space of the particle is given by a tensor product

$$\mathcal{H} = \mathcal{H}_P \otimes \mathcal{H}_C$$

of the position space

$$\mathcal{H}_P = \ell^2(\mathbb{Z}) = \mathrm{Span}\,\{|m\rangle|\ m \in \mathbb{Z}\}$$

and the two-dimensional coin space

$$\mathcal{H}_C = \mathrm{Span}\,\{|L\rangle, |R\rangle\}\ .$$

We consider a particle starting the quantum walk from the origin, i.e. the initial state has the form

$$|\psi(0)\rangle = |0\rangle \otimes |\psi_C\rangle,$$

where $|\psi_C\rangle$ denotes the initial state of the coin. After t steps of the quantum walk the state of the particle is given by

$$|\psi(t)\rangle \equiv \sum_m \Big(\ \psi_L(m,t)|m\rangle|L\rangle + \psi_R(m,t)|m\rangle|R\rangle\Big) = U^t|\psi(0)\rangle\,, \tag{1}$$

where the unitary propagator U has the form

$$U = S\,(I \otimes C)\ . \tag{2}$$

The coin operator C flips the state of the coin before the particle is displaced. In principle, C can be an arbitrary unitary operation on the coin space $\mathcal{H}_C$. We choose the most studied case of the Hadamard coin, denoted by C_H, which is defined by its action on the basis states

$$C_H|L\rangle = \frac{1}{\sqrt{2}}(|L\rangle + |R\rangle), \quad C_H|R\rangle = \frac{1}{\sqrt{2}}(|L\rangle - |R\rangle).$$

After the coin flip the step operator S displaces the particle from its current position according to its coin state

$$S|m\rangle|L\rangle \longrightarrow |m-1\rangle|L\rangle, \quad S|m\rangle|R\rangle \longrightarrow |m+1\rangle|R\rangle.$$

The coefficients $\psi_{L,(R)}(m,t)$ in (1) represent the probability amplitudes of finding the particle at position m after t steps of the quantum walk with the coin state $|L(R)\rangle$. The probability distribution generated by the quantum walk is given by

$$p(m,t) = |\langle m|\langle L|\psi(t)\rangle|^2 + |\langle m|\langle R|\psi(t)\rangle|^2 = |\psi_L(m,t)|^2 + |\psi_R(m,t)|^2\,.$$

The extension of the formalism described above to two distinguishable particles has been given in [58]. One should consider the bipartite Hilbert state as a tensor product

$$\mathcal{H}_{12} = \mathcal{H}_1 \otimes \mathcal{H}_2$$

of the single particle Hilbert spaces. We consider non-interacting particles, i.e. their time evolution is independent. Hence, the propagator of the two-particle quantum walk can be written in a factorized form

$$U_{12} = U_1 \otimes U_2, \tag{3}$$

where U_1 (U_2) is the propagator of the first (second) particle given by Eq. (2). Note that this factorized time evolution cannot increase entanglement between the particles. In this paper we consider particles starting from the same lattice point (the origin). Hence, the initial state of the two-particle quantum walk has the shape

$$|\Psi(0)\rangle = |0,0\rangle \otimes |\Psi_C\rangle,$$

where $|\Psi_C\rangle$ is the initial coin state of the two particles.

Let us first consider the case when the initial coin state is separable, i.e.

$$|\Psi_C\rangle = |\psi_1\rangle \otimes |\psi_2\rangle\,. \tag{4}$$

Since entanglement is not induced in the process of time evolution, the two-particle state remains factorized and the joint probability distribution $p(m,n,t)$ of finding the first particle at the mth and the second at the nth site at time t is reduced to the product of single particle distributions

$$p(m,n,t) = p_1(m,t) \cdot p_2(n,t)\,. \tag{5}$$

Here, $p_i(m,t)$ is the probability distribution of a single-particle quantum walk given that the initial coin state was $|\psi_i\rangle$. Hence, the two-particle quantum walk with initially separable coin state is fully determined by the single-particle quantum walk.

We turn to the situation when the initial coin state $|\Psi_C\rangle$ does not factorize. In such a case, the joint probability distribution $p(m,n,t)$ cannot be written in a product form (5). Nevertheless, we can map the two-particle walk on a line to a quantum walk of a single particle on a square lattice. Indeed, we can write the two-particle propagator (3) in the following form

$$U_{12} = S_{12}(I_{P_{12}} \otimes (C_H \otimes C_H)), \tag{6}$$

where $I_{P_{12}}$ is the identity on the joint position space and the joint step operator S_{12} is given by the tensor product of the single particle step operators S_i. The relation (6) implies that we can consider the two-particle propagator U_{12} as a propagator of single-particle walk on a plane with the coin given by the tensor product of two Hadamard operators. Hence, the two quantum walks in consideration are equivalent. This correspondence allows us to treat the joint probability distribution of the two-particle walk with the tools developed for the single-particle quantum walks.

Finally, let us briefly comment on a quantum walk with indistinguishable particles. It is natural to use the second quantization formalism. We denote the bosonic creation operators by $\hat{a}^\dagger_{(m,i)}$ and the fermionic creation operators by $\hat{b}^\dagger_{(n,j)}$, e.g. $\hat{a}^\dagger_{(m,i)}$ creates one bosonic particle at position m with the internal state $|i\rangle$, $i = L, R$. The dynamics of the quantum walk with indistinguishable particles is defined on a one-particle level, i.e. a single step is given by the following transformation of the creation operators

$$\hat{a}^\dagger_{(m,L)} \longrightarrow \frac{1}{\sqrt{2}}\left(\hat{a}^\dagger_{(m-1,L)} + \hat{a}^\dagger_{(m+1,R)}\right)\,, \quad \hat{a}^\dagger_{(m,R)} \longrightarrow \frac{1}{\sqrt{2}}\left(\hat{a}^\dagger_{(m-1,L)} - \hat{a}^\dagger_{(m+1,R)}\right)\,,$$

for bosonic particles, similarly for fermions. The difference is that the bosonic operators fulfill the commutation relations

$$\left[\hat{a}_{(m,i)}, \hat{a}_{(n,j)}\right] = 0\,, \qquad \left[\hat{a}_{(m,i)}, \hat{a}^\dagger_{(n,j)}\right] = \delta_{mn}\delta_{ij}\,, \tag{7}$$

while the fermionic operators satisfy the anti-commutation relations

$$\left\{\hat{b}_{(m,i)}, \hat{b}_{(n,j)}\right\} = 0\,, \qquad \left\{\hat{b}_{(m,i)}, \hat{b}^\dagger_{(n,j)}\right\} = \delta_{mn}\delta_{ij}\,. \tag{8}$$

Since the dynamics is defined on a single-particle level, one can describe the state of the two indistinguishable particles after t steps of the quantum walk in terms of the single-particle probability amplitudes (see Ref. [59] for a more detailed discussion).

In the present paper we focus on the directional correlations between the two particles. We quantify this property by the probability P_s that both particles are found after t steps of the quantum walk on the same side of the line. For distinguishable particles it is given by

$$P_s(t) = \sum_{m=-t}^{0} \sum_{n=-t}^{0} p(m,n,t) + \sum_{m=1}^{t} \sum_{n=1}^{t} p(m,n,t)\,. \tag{9}$$

For indistinguishable particles $p(m,n,t) \equiv p(n,m,t)$, i.e. these two probabilities correspond to the same physical event. Hence, the sums in (9) have to be restricted over an ordered pair (m,n) with $m \geq n$, i.e.

$$P_s(t) = \sum_{n=-t}^{0} \left(\sum_{m=n}^{0} p(m,n,t) \right) + \sum_{n=1}^{t} \left(\sum_{m=n}^{t} p(m,n,t) \right)\,. \tag{10}$$

In particular, we will be interested in the asymptotic limits of the probability P_s in its dependence on the initial coin state of the two particles. We consider both separable and entangled coin states, as well as indistinguishability of the particles, in the following Sections.

III. SEPARABLE INITIAL STATES

Let us now specify the probability P_s for two distinguishable particles which start the quantum walk with a separable coin state (4). As discussed in the previous Section the joint probability distribution $p(m,n,t)$ factorizes (5). Therefore, the probability to be on the same side of the lattice P_s simplifies into

$$P_s(t) = P_1^-(t) \cdot P_2^-(t) + P_1^+(t) \cdot P_2^+(t)\,, \tag{11}$$

Here we have denoted by $P_i^{\pm}(t)$ the probability that the particle which have started the quantum walk with the coin state $|\psi_i\rangle$ is on the positive or negative half-axis after t steps, i.e.

$$P_i^-(t) = \sum_{m=-t}^{0} p_i(m,t), \quad P_i^+(t) = \sum_{m=1}^{t} p_i(m,t).$$

In Figure 1 we plot the course of the probability $P_s(t)$ with the number of steps t. To unravel the dependence on the initial coin state $|\Psi_C\rangle$ we consider three cases - (i) $|\Psi_C\rangle = |L\rangle \otimes |R\rangle$ (black dots), (ii) $|\Psi_C\rangle = |L\rangle \otimes |L\rangle$ (open circles), and (iii) $|\Psi_C\rangle = \frac{1}{\sqrt{2}}\left(|L\rangle + i|R\rangle\right) \otimes \frac{1}{\sqrt{2}}\left(|L\rangle + i|R\rangle\right)$ (open diamonds). We find that after some initial oscillations the probability P_s quickly approach steady values which are determined by the initial coin state.

Let us now determine the asymptotic value of the probability P_s in dependence of the initial coin state. Consider a general separable coin state of the form

$$|\Psi_C\rangle = (a_1|L\rangle + b_1|R\rangle) \otimes (a_2|L\rangle + b_2|R\rangle)\,.$$

The asymptotic probability distribution for a single particle is given by [24]

$$p(x,t,a_i,b_i) = \frac{1 - \frac{x}{t}((a_i+b_i)\overline{a_i} + (a_i - b_i)\overline{b_i})}{\pi t \sqrt{1 - 2\frac{x^2}{t^2}(1 - \frac{x^2}{t^2})}}\,. \tag{12}$$

The probability that the particle is on the negative or positive half-axis is obtained by integrating the probability density over the corresponding interval

$$\begin{aligned} P_i^-(a_i,b_i) &= \int_{-\frac{t}{\sqrt{2}}}^{0} p(x,t,a_i,b_i)dx = \frac{1}{4}(2 + ((a_i+b_i)\overline{a_i} + (a_i-b_i)\overline{b_i}))\,, \\ P_i^+(a_i,b_i) &= \int_{0}^{\frac{t}{\sqrt{2}}} p(x,t,a_i,b_i)dx = \frac{1}{4}(2 - ((a_i+b_i)\overline{a_i} + (a_i-b_i)\overline{b_i}))\,. \end{aligned} \tag{13}$$

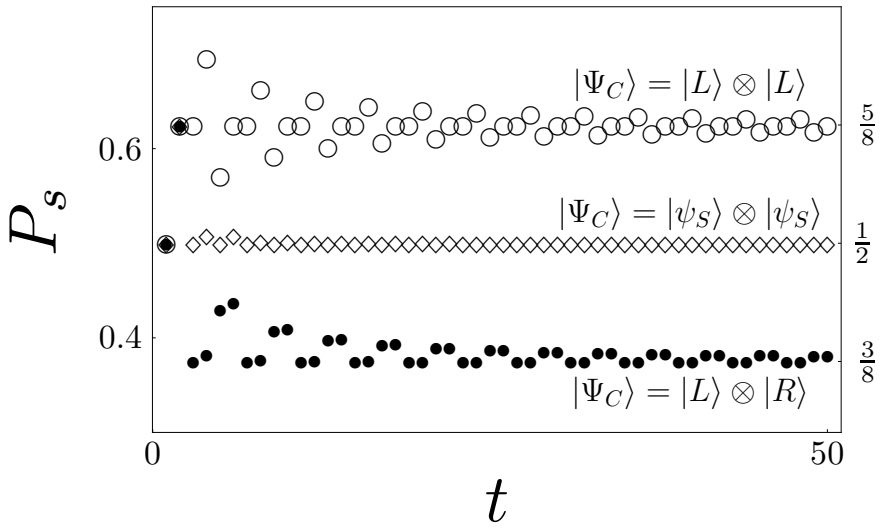

FIG. 1: The probability P_s that two distinguishable particles performing a quantum walk on a line end on the same side as a function of time. Both particles start the quantum walk from the origin. As the initial coin state $|\Psi_C\rangle$ we choose one of the three factorized states - (i) $|L\rangle$ for the first particle and $|R\rangle$ for the second particle (black dots), (ii) $|L\rangle$ for both particles (open circles), and (iii) $|\psi_S\rangle \equiv \frac{1}{\sqrt{2}}(|L\rangle + i|R\rangle)$ for both particles (open diamonds). We find that for the initial coin state (i) the particles are more likely to be on the opposite side, since $P_s < 1/2$. Indeed, due to the choice of the coin state $|LR\rangle$ the probability distribution of the first particle is biased to the left while the probability distribution of the second particle is biased to the right. On the other hand, for the initial state $|LL\rangle$ both probability distributions are biased to the left. Hence, the particles are more likely to be found on the same side. Finally, for the initial state (iii) which results in the symmetric single-particle probability distribution the particles are equally likely to be on the same or the opposite side of the line. The asymptotic values of P_s for all three initial states are in agreement with the analytic estimation of Eq.(15).

Note that within the approximation of Eq. (12) the resulting integrals are time-independent, i.e. we immediately obtain the asymptotic values of the probabilities $P_i^{\pm}$. This is due to the fact that the asymptotic probability density depends only on the ratio x/t.

Inserting the results of (13) into the Eq.(11) we find that the probability P_s is given by

$$P_s^{(sep)} = \frac{1}{8}\Big(\, 4 + \big((a_1+b_1)\overline{a_1} + (a_1-b_1)\overline{b_1}\big)\,\big((a_2+b_2)\overline{a_2} + (a_2-b_2)\overline{b_2}\big)\,\Big)\,. \tag{14}$$

In particular, for the initial states $(i-iii)$ considered in Figure 1, we find the asymptotic values

$$\begin{aligned} P_s^{(LR)} &\equiv P_s(1,0,0,1) = \frac{3}{8}\,, \quad P_s^{(LL)} \equiv P_s(1,0,1,0) = \frac{5}{8}\,, \\ P_s^{(S)} &\equiv P_s(\frac{1}{\sqrt{2}}, \frac{i}{\sqrt{2}}, \frac{1}{\sqrt{2}}, \frac{i}{\sqrt{2}}) = \frac{1}{2}\,. \end{aligned} \tag{15}$$

These results are in perfect agreement with the numerical simulations presented in Figure 1.

Let us now analyze the probability $P_s^{(sep)}$ in more detail. First, we recast the formula (14) in a simpler form by a change of the basis of the coin space. Consider the basis formed by the eigenstates of the Hadamard coin

$$C_H|\chi^{\pm}\rangle = \pm|\chi^{\pm}\rangle\,,$$

which have the following expression in the standard basis

$$|\chi^{\pm}\rangle = \frac{\sqrt{2\pm\sqrt{2}}}{2}|L\rangle \pm \frac{\sqrt{2\mp\sqrt{2}}}{2}|R\rangle\,. \tag{16}$$

We decompose the single-particle coin state in the Hadamard basis

$$|\psi_i\rangle = h_i^+|\chi^+\rangle + h_i^-|\chi^-\rangle\,.$$

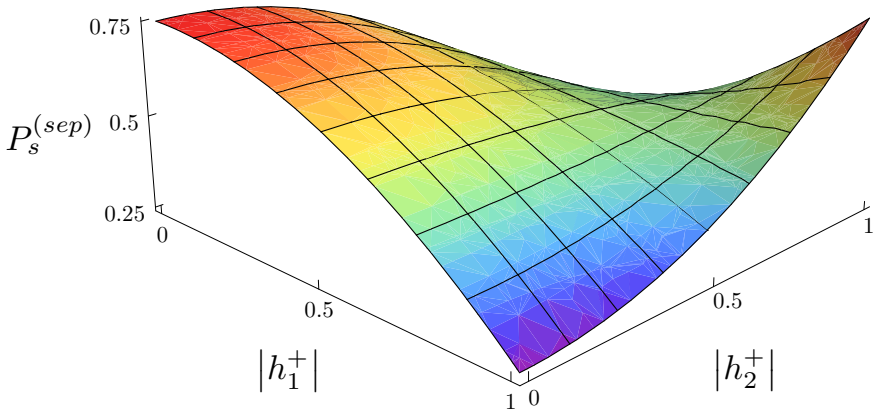

FIG. 2: The probability to be on the same side $P_s^{(sep)}$ in its dependence on the coefficients of the initial coin states. The parameters h_i^+ are given by the overlap of the coin state $|\psi_i\rangle$ with the eigenstate $|\chi^+\rangle$ of the Hadamard coin. We find that the probability $P_s^{(sep)}$ reaches the maximum value 3/4 when both $h_{1,2}^+$ equals either zero or one. The minimum value 1/4 is obtained if one the h_i^+ is zero while the other one is unity.

From the expression (16) we find the transformation between the coefficients in the standard and the Hadamard basis

$$a_i = \frac{\sqrt{2+\sqrt{2}}}{2} h_i^+ + \frac{\sqrt{2-\sqrt{2}}}{2} h_i^- \,, \quad b_i = \frac{\sqrt{2-\sqrt{2}}}{2} h_i^+ - \frac{\sqrt{2+\sqrt{2}}}{2} h_i^- \,.$$

With the help of these relations we find that the formula (14) for the probability $P_s^{(sep)}$ simplifies in the Hadamard basis into

$$P_s^{(sep)} = \frac{1}{4}\left(2 + (2\,|h_1^+|^2 - 1)(2\,|h_2^+|^2 - 1)\right) \,. \tag{17}$$

Here we have used the normalization of the single-particle coin state $|\psi_i\rangle$, i.e. the condition

$$|h_i^+|^2 + |h_i^-|^2 = 1 \,. \tag{18}$$

We display the probability to be on the same side $P_s^{(sep)}$ in its dependence on the parameters h_i^+ in Figure 2. We find that $P_s^{(sep)}$ reaches the maximum value 3/4 provided that both h_i^+ equals zero or unity, i.e. when both particles start the walk in the same eigenstate of the Hadamard coin. Indeed, starting the single-particle walk in the eigenstate $|\chi^+\rangle$ ($|\chi^-\rangle$) leads to a probability distribution which is maximally biased towards left (right). We illustrate this feature in Figure 3. Note that this effect has been identified numerically in [26]. Hence, when both particles start the walk in the same eigenstate of the Hadamard coin, their probability distributions are maximally biased towards the same direction and, consequently, the particles are the most likely to be on the same side. On the other hand, if the particles start the walk in the different eigenstates (e.g. the first one in $|\chi^+\rangle$ and the second one in $|\chi^-\rangle$, which corresponds to $h_1^+ = 1$ and $h_2^+ = 0$), the probability distributions are maximally biased in the opposite directions. In such a case, the particles are the most likely to be on the opposite side of the lattice and $P_s^{(sep)}$ reaches the minimum 1/4.

IV. ENTANGLED INITIAL STATES

Let us now analyze the probability that the particles will be on the same side of the lattice P_s for the initial coin states $|\Psi_C\rangle$ which are not factorized. We follow two approaches. First, we analyze the particular case of maximally entangled Bell states. We express the two-particle state in terms of single-particle amplitudes. In this way, we decompose the joint probability distribution into single-particle distributions plus an interference term. We then use the results of the previous section to find the asymptotic value of the probability P_s. By this approach we emphasize the role of the interference of probability amplitudes. Second, we employ the equivalence between the two-particle walk on a line and single-particle walk on a square lattice discussed in Section II. This correspondence allows us to

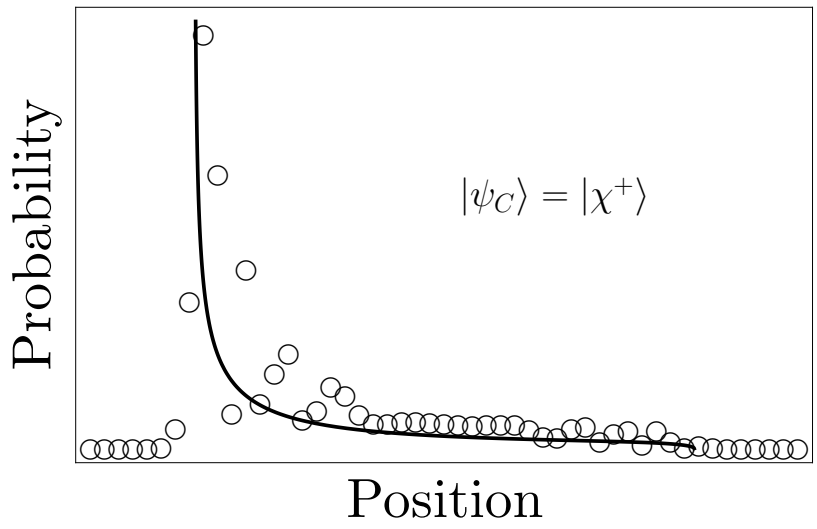

FIG. 3: Single-particle probability distribution for the initial coin state $|\psi_C\rangle = |\chi^+\rangle$. We find only one peak on the left side of the lattice, the peak on the right side has disappeared. Consequently, the resulting probability distribution is maximally biased towards left. Choosing the initial coin state as $|\psi_C\rangle = |\chi^-\rangle$ will flip the plot around the origin and the resulting probability distribution will be maximally biased to the right.

use the tools developed for the quantum walks with a single particle, namely the weak limit theorems [23], to find the asymptotic probability density for the two-particle walk on a line. We leave the details of the calculation for the A. With the explicit form of the probability density we finally derive the asymptotic value of the probability P_s for an arbitrary two-particle coin state.

We start by examining the particular case of maximally entangled Bell states

$$|\psi^{\pm}\rangle = \frac{1}{\sqrt{2}}\left(|LR\rangle \pm |RL\rangle\right) , \quad |\phi^{\pm}\rangle = \frac{1}{\sqrt{2}}\left(|LL\rangle \pm |RR\rangle\right) . \tag{19}$$

Obviously, the joint probability distribution $p(m,n,t)$ is no longer a product of the single-particle probability distributions. However, we can still express it in terms of the single-particle probability amplitudes. Let us denote by $\psi_i^{(L)}(m,t)$ the amplitude of the particle being after t steps at the position m with the coin state $|i\rangle$, $i = L, R$, provided that the initial coin state was $|L\rangle$. Similarly, let $\psi_i^{(R)}(m,t)$ be the amplitude for the initial coin state $|R\rangle$. With this notation we express the joint probability distributions generated by quantum walk of two particles with initially entangled coins by

$$\begin{aligned} p^{(\psi^{\pm})}(m,n,t) &= \frac{1}{2}\sum_{i,j=L,R}\left|\psi_i^{(L)}(m,t)\psi_j^{(R)}(n,t) \pm \psi_i^{(R)}(m,t)\psi_j^{(L)}(n,t)\right|^2 , \\ p^{(\phi^{\pm})}(m,n,t) &= \frac{1}{2}\sum_{i,j=L,R}\left|\psi_i^{(L)}(m,t)\psi_j^{(L)}(n,t) \pm \psi_i^{(R)}(m,t)\psi_j^{(R)}(n,t)\right|^2 , \end{aligned}$$

where the superscript indicates the initial coin state. We now make use of the fact that the amplitudes $\psi_i^{(L,R)}(m,t)$ are real valued. Indeed, both the Hadamard coin and the initial states have only real entries. Hence, the amplitudes cannot attain any imaginary part during the time evolution. Therefore, we can replace the absolute values by simple brackets and expand the joint probability distributions in the form

$$\begin{aligned} p^{(\psi^{\pm})}(m,n,t) &= \frac{1}{2}\left(p^{(L)}(m,t)p^{(R)}(n,t) + p^{(R)}(m,t)p^{(L)}(n,t)\right) \pm \\ &\quad \pm\varphi(m,t)\varphi(n,t) , \\ p^{(\phi^{\pm})}(m,n,t) &= \frac{1}{2}\left(p^{(L)}(m,t)p^{(L)}(n,t) + p^{(R)}(m,t)p^{(R)}(n,t)\right) \pm \\ &\quad \pm\varphi(m,t)\varphi(n,t) . \end{aligned} \tag{20}$$

Here, we have used the notation

$$\varphi(m,t) = \psi_L^{(L)}(m,t)\psi_L^{(R)}(m,t) + \psi_R^{(L)}(m,t)\psi_R^{(R)}(m,t)$$

to shorten the formulas. When we insert the expressions (20) into the definition (9) of the probability P_s we find that the later one can be written in the form

$$P_s^{(\psi^\pm)}(t) = P_s^{(LR)}(t) \pm I(t),\ P_s^{(\phi^\pm)}(t) = P_s^{(LL)}(t) \pm I(t)\,.$$

The interference term $I(t)$ is given by

$$I(t) = \Big(\varphi^-(t)\Big)^2 + \Big(\varphi^+(t)\Big)^2\,,$$

where we have denoted

$$\varphi^-(t) = \sum_{m=-t}^{0} \varphi(m,t), \quad \varphi^+(t) = \sum_{m=1}^{t} \varphi(m,t)\,.$$

Let us now turn to the asymptotic values of P_s in dependence on the choice of the Bell state. The limits of $P_s^{(LR)}$ and $P_s^{(LL)}$ are given in (15). We obtain the asymptotic value of the interference term $I(t)$ from the numerical simulation, which indicates

$$I(t \to +\infty) = \frac{1}{8}\,.$$

Finally, for the limiting values of the probability P_s we find

$$P_s^{(\psi^+)} = \frac{1}{2}, \quad P_s^{(\psi^-)} = \frac{1}{4}, \quad P_s^{(\phi^+)} = \frac{3}{4}, \quad P_s^{(\phi^-)} = \frac{1}{2}\,. \tag{21}$$

We display the dependence of P_s on the number of steps and the choice of the initial coin state in Figure 4. We find that the probability P_s quickly approach the steady values, similarly as for the factorized coin states which we have shown in Figure 1. For $|\psi^+\rangle$ (open circles) and $|\phi^-\rangle$ (black dots) the particles are asymptotically equally likely to be on the same or on the opposite side. For the Bell state $|\phi^+\rangle$ (stars) the particles are more likely to be on the same side of the line. Finally, for the singlet state $|\psi^-\rangle$ (open diamonds) the particles are more likely to be on the opposite side. The asymptotic values of the probabilities P_s are in agreement with the results of (21).

After we have analyzed the particular case of the Bell states we turn to a general initial coin state. As in the previous Section, we make use of the asymptotic probability density $p(x_1, x_2, t)$ and replace the sums in (9) by integrals. We derive the explicit form of the asymptotic probability density in the A. Performing the integrations we arrive at the following expression

$$P_s = \frac{1}{4}\Big(\,2 + |h_{(++)}|^2 + |h_{(--)}|^2 - |h_{(+-)}|^2 - |h_{(-+)}|^2\Big)$$

for the probability to be on the same side. Here we have denoted by $h_{(\alpha\beta)}$ the coefficients of the decomposition of the initial coin state $|\Psi_C\rangle$ into the basis formed by the tensor product of the eigenvectors $|\chi^\pm\rangle$ of the Hadamard coin C_H, i.e.

$$|\Psi_C\rangle = \sum_{\alpha,\beta=\pm} h_{(\alpha\beta)}|\chi^\alpha\rangle|\chi^\beta\rangle. \tag{22}$$

Finally, using the normalization condition for the initial coin state $|\Psi_C\rangle$

$$|h_{(++)}|^2 + |h_{(-+)}|^2 + |h_{(+-)}|^2 + |h_{(--)}|^2 = 1,$$

we can simplify the expression for the probability $P_s^{(ent)}$ into the form

$$P_s^{(ent)} = \frac{1}{4}\Big(\,1 + 2(|h_{(++)}|^2 + |h_{(--)}|^2)\Big)\,. \tag{23}$$

The dependence of the probability $P_s^{(ent)}$ on the initial coin state is illustrated in Figure 5. We find that the probability to be on the same side for entangled initial coin states $P_s^{(ent)}$ satisfies exactly the same bounds as the

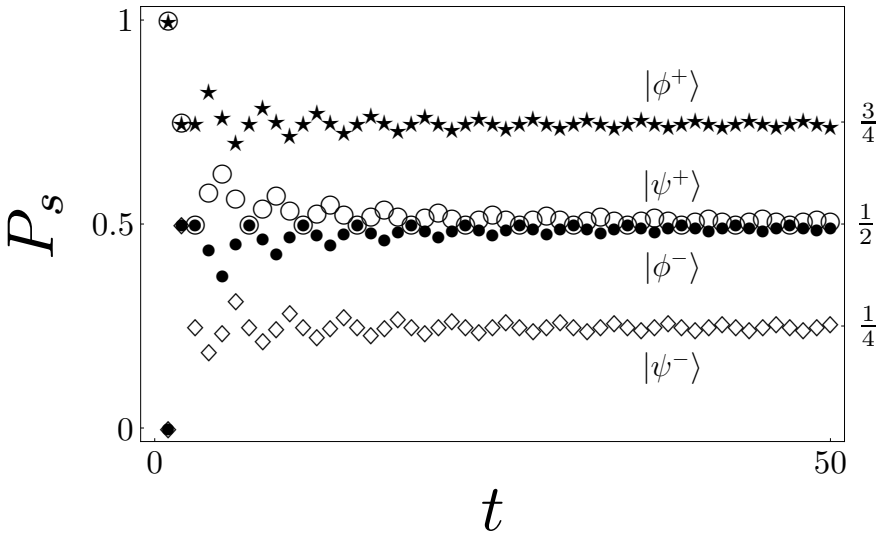

FIG. 4: The probability that two distinguishable particles performing a quantum walk on a line with initially entangled coins end on the same side as a function of time. Both particles start the quantum walk from the origin. As the initial coin state $|\Psi_C\rangle$ we choose one of the Bell states (19). For the Bell states $|\psi^+\rangle$ (open circles) and $|\phi^-\rangle$ (black dots) the particles are equally likely to be found on the same or on the opposite side of the line in the long time limit. For finite times they are more likely to be on the same side for $|\psi^+\rangle$ and more likely on the opposite side for $|\phi^-\rangle$. For the other two Bell states $|\psi^-\rangle$ (open diamonds) and $|\phi^+\rangle$ (stars) the differences remain in the asymptotic limit. The particles are more likely to be on the opposite side for the singlet state $|\psi^-\rangle$ and more likely to be on the same side for $|\phi^+\rangle$. The asymptotic values of the probability P_s agree with the findings of (21).

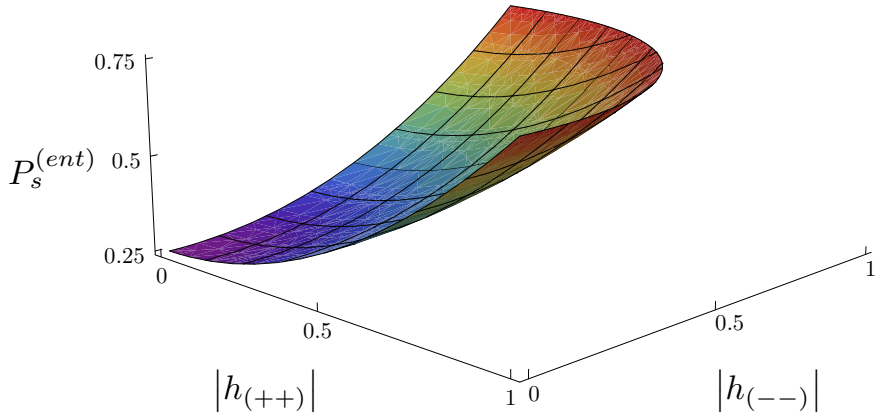

FIG. 5: The probability to be on the same side of the lattice $P_s^{(ent)}$ in its dependence on the choice of the initial coin state. We find that $P_s^{(ent)}$ is bounded in the same way as $P_s^{(sep)}$ displayed in Figure 2. The maximum is obtained for states satisfying the condition $|h_{(++)}|^2 + |h_{(--)}|^2 = 1$, while the minimum is reached when $h_{(++)} = h_{(--)} = 0$.

probability $P_s^{(sep)}$ derived in the previous Section for separable initial coin states. The maximum value of 3/4 is reached when $|h_{(++)}|^2 + |h_{(--)}|^2 = 1$. In such a case, the initial coin state $|\Psi_C\rangle$ is an eigenstate of the two-particle coin $C_H \otimes C_H$ corresponding to the eigenvalue $+1$. On the other hand, the minimum value 1/4 of the probability $P_s^{(ent)}$ is attained when both $h_{(++)}$ and $h_{(--)}$ vanishes. This corresponds to $|\Psi_C\rangle$ being the eigenstate of the coin $C_H \otimes C_H$ with the eigenvalue -1.

Finally, we note that for separable coin states the formula (23) reduces to Eq. (17) which we have derived in the previous Section. Indeed, for separable states we have the relation

$$h_{(++)} = h_1^+ h_2^+, \quad h_{(--)} = h_1^- h_2^-,$$

which together with the normalization (18) implies

$$\begin{aligned} P_s &= \frac{1}{4}\Big(1+2|h_1^+|^2|h_2^+|^2+2|h_1^-|^2|h_2^-|^2\Big) \\ &= \frac{1}{4}\Big(1+2|h_1^+|^2|h_2^+|^2+2(1-|h_1^+|^2)(1-|h_2^+|^2)\Big) \\ &= \frac{1}{4}\Big(2+(2\left|h_1^+\right|^2-1)(2\left|h_2^+\right|^2-1)\Big) = P_s^{(sep)}\,. \end{aligned}$$

V. INDISTINGUISHABLE PARTICLES

Let us now briefly discuss the probability to be on the same side P_s for indistinguishable particles. We show that for a particular choice of the initial state of the two bosons or fermions the problem reduces to the case of distinguishable particles with maximally entangled coins.

As the initial state of the quantum walk we choose

$$|\Psi(0)\rangle = |1_{(0,L)}1_{(0,R)}\rangle\,,$$

i.e. both particles are initially at the origin with the opposite coin states. Recalling the amplitudes $\psi_i^{(L)}$ ($\psi_i^{(R)}$) for the single particle performing the quantum walk with the initial coin state $|L\rangle$ ($|R\rangle$) we express the state of two bosons and fermions in the following form

$$\begin{aligned} |\Psi^{(B)}(t)\rangle &= \sum_{m,n}\sum_{i,j=L,R}\psi_i^{(L)}(m,t)\psi_j^{(R)}(n,t)\hat{a}^\dagger_{(m,i)}\hat{a}^\dagger_{(n,j)}|vac\rangle\,, \\ |\Psi^{(F)}(t)\rangle &= \sum_{m,n}\sum_{i,j=L,R}\psi_i^{(L)}(m,t)\psi_j^{(R)}(n,t)\hat{b}^\dagger_{(m,i)}\hat{b}^\dagger_{(n,j)}|vac\rangle\,, \end{aligned} \tag{24}$$

where $|vac\rangle$ denotes the vacuum state. Note that in (24) both summation indexes m and n run over all possible sites. Using the commutation (7) and anti-commutation (8) relations we can restrict the sums in (24) over an ordered pair (m,n) with $m \geq n$. The resulting wave-function will be symmetric or antisymmetric.

We turn to the joint probabilities $p(m,n,t)$ that after t steps we detect a particle at site m and simultaneously a particle at site n, with $m \geq n$. First, for $m \neq n$ we find

$$\begin{aligned} p^{(B,F)}(m,n,t) &= \left|\langle 1_{(m,i)}1_{(n,j)}|\Psi^{(B,F)}(t)\rangle\right|^2 \\ &= \sum_{i,j=L,R}\left|\psi_i^{(L)}(m,t)\psi_j^{(R)}(n,t)\pm\psi_i^{(R)}(m,t)\psi_j^{(L)}(n,t)\right|^2\,, \end{aligned}$$

where the $+$ sign on the right hand side corresponds to the bosonic (B) , and the $-$ sign to the fermionic (F). Comparing these expressions with the results for Bell states (20) we identify the relation

$$p^{(B)}(m,n,t) = 2p^{(\psi^+)}(m,n,t)\,, \quad p^{(F)}(m,n,t) = 2p^{(\psi^-)}(m,n,t)\,. \tag{25}$$

For $m=n$ we obtain for bosons

$$\begin{aligned} p^{(B)}(m,m,t) &= \left|\langle 2_{(m,L)}|\Psi^{(B)}(t)\rangle\right|^2+\left|\langle 2_{(m,R)}|\Psi^{(B)}(t)\rangle\right|^2+ \\ &\quad+\left|\langle 1_{(m,L)}1_{(m,R)}|\Psi^{(B)}(t)\rangle\right|^2 \\ &= 2\left|\psi_L^{(L)}(m,t)\psi_L^{(R)}(m,t)\right|^2+2\left|\psi_R^{(L)}(m,t)\psi_R^{(R)}(m,t)\right|^2+ \\ &\quad+\left|\psi_L^{(L)}(m,t)\psi_R^{(R)}(m,t)+\psi_R^{(L)}(m,t)\psi_L^{(R)}(m,t)\right|^2\,, \end{aligned}$$

and for fermions

$$p^{(F)}(m,m,t) = \left|\langle 1_{(m,L)}1_{(m,R)}|\Psi^{(F)}(t)\rangle\right|^2 = \left|\psi_L^{(L)}(m,t)\psi_R^{(R)}(m,t)-\psi_R^{(L)}(m,t)\psi_L^{(R)}(m,t)\right|^2\,.$$

We note that relations similar to (25) hold as well for $m = n$. Indeed, we find the following for bosons

$$\begin{aligned} p^{(B)}(m,m,t) &= \frac{1}{2}\sum_{i,j=L,R}\left|\psi_i^{(L)}(m,t)\psi_j^{(R)}(m,t)+\psi_i^{(R)}(m,t)\psi_j^{(L)}(m,t)\right|^2 \\ &= p^{(\psi^+)}(m,m,t)\,, \end{aligned} \tag{26}$$

and for fermions

$$\begin{aligned} p^{(F)}(m,m,t) &= \frac{1}{2}\sum_{i,j=L,R}\left|\psi_i^{(L)}(m,t)\psi_j^{(R)}(m,t)-\psi_i^{(R)}(m,t)\psi_j^{(L)}(m,t)\right|^2 \\ &= p^{(\psi^-)}(m,m,t)\,. \end{aligned} \tag{27}$$

Finally, we derive the probability P_s that the bosons (or fermions) are on the same side of the line. As we have already discussed, for indistinguishable particles we have used the formula (10) where the summation is restricted to an ordered pair (m,n) with $m \geq n$. However, using the results of (25), (26) and (27) we can replace $p^{(B,F)}(m,n,t)$ by $p^{(\psi^\pm)}(m,n,t)$ in (10) and extend the summation over all pairs of m and n. Hence, we find that

$$P_s^{(B)}(t) = P_s^{(\psi^+)}(t)\,, \qquad P_s^{(F)}(t) = P_s^{(\psi^-)}(t)\,.$$

In summary, the results for bosons (resp. fermions) are the same as for distinguishable particle which have started the quantum walk with entangled coin state $|\psi^+\rangle$ (resp. $|\psi^-\rangle$). This is a direct consequence, of course, of the required symmetry properties of two-particle boson and fermion states. We note that also the fact that the particles have started the walk from the same lattice point is important. However, when the two indistinguishable particles start the walk spatially separated their evolution differs from that of distinguishable particles with entangled coin states [59]. Indeed, indistinguishability starts to play a role when the wave-functions begin to overlap, whereas entanglement is a non-local property.

VI. QUANTUM WALKS WITH δ-INTERACTIONS

We have seen in the preceding sections that entanglement in two-particle non-interacting quantum walks cannot break the limit of probabilities we found for separable particles. A natural question arises: What happens if we consider interacting particles? This motivates us to introduce the concept of two-particle quantum walks with δ-interaction. To do that, we change the factorized time evolution operator defined in (3). In the original time evolution the coin was the same factorized coin in all lattice point pairs (m,n), in the δ-interaction quantum walk we change the coin to a non-factorized one C_δ, when the particles are at the same lattice point $m = n$.

Considering the above, we define the unitary time evolution operator for quantum walks with δ-interacting particles on a line as

$$U_\delta = S_{12}(\bar{P}_\delta \otimes (C_H \otimes C_H)) + S_{12}(P_\delta \otimes C_\delta)\,,$$

where P_δ is the projector on the joint position state

$$P_\delta = \sum_m |m\rangle|m\rangle\langle m|\langle m|\,,$$

and

$$\bar{P}_\delta = I_{P_{12}} - P_\delta\,.$$

As an example, we consider the entangling δ-interaction coin C_δ of the following form

$$C_\delta = \frac{1}{2}\begin{pmatrix} 1 & 1 & 1 & 1 \\ 1 & -1 & -1 & 1 \\ -1 & 1 & -1 & 1 \\ -1 & -1 & 1 & 1 \end{pmatrix}. \tag{28}$$

In Figure 6 we present the results of a numerical simulation of the corresponding quantum walk with δ-interaction. The initial coin state was chosen to be the Bell state $|\phi^-\rangle$. From the upper plot we find that the joint probability distribution is concentrated on the diagonal, thus the particles are likely to be found on the same side. The lower plot clearly indicate that quantum walks on a line with δ-interactions can break the upper limit of $P_s = 3/4$ which we have derived for non-interacting particles.

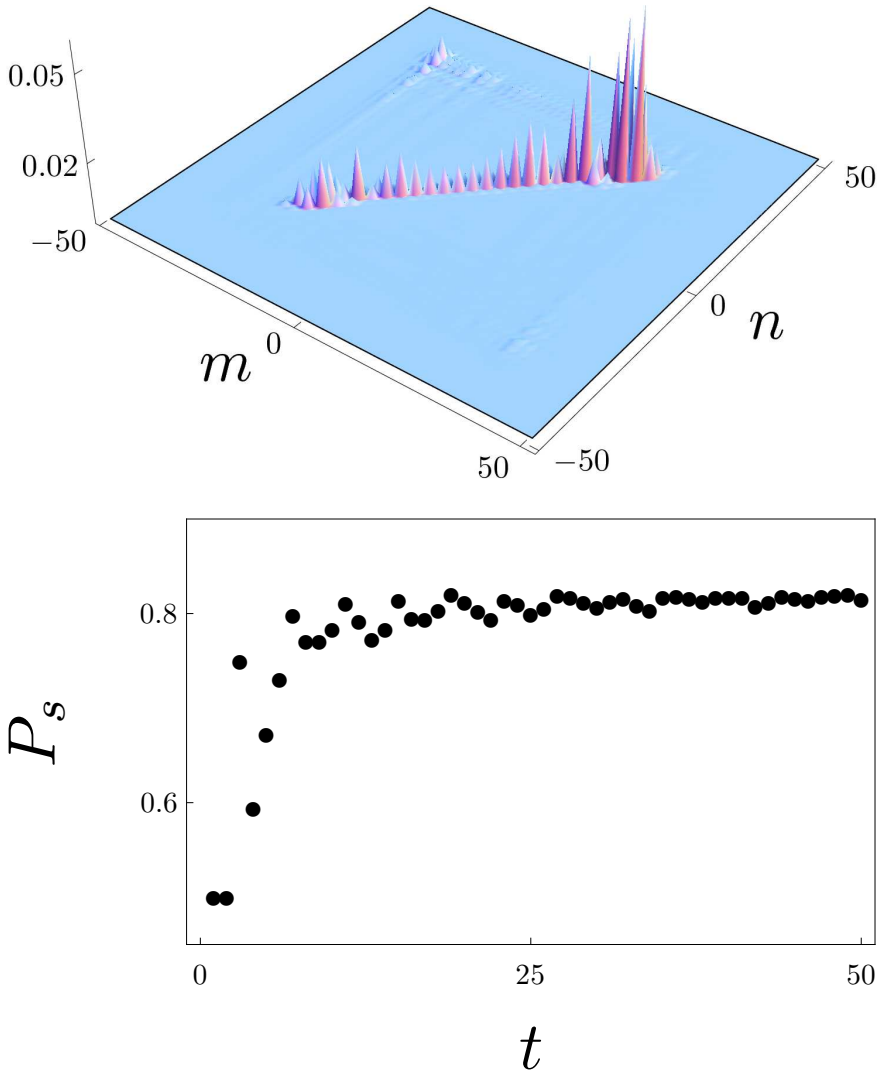

FIG. 6: Joint probability distribution (upper plot) and the probability to be on the same side of the lattice P_s (lower plot) for two interacting particles performing a quantum walk on a line. The δ-interaction coin C_δ is realized by a matrix (28). As the initial coin state we have chosen one of the Bell states, namely $|\Psi_C\rangle = |\phi^-\rangle$. The resulting joint probability distribution is mostly concentrated on the diagonal, as can be seen from the upper plot. Consequently, the particles are very likely to be on the same side of the lattice. Indeed, the lower plot indicates that the asymptotic value of the probability P_s exceeds 0.8.

VII. CONCLUSIONS

We have analyzed the two-particle quantum walk on a line focusing on the directional correlations between the particles. The directional correlation of two non-interacting particles on the line is shown to be confined in an interval, independent of wether the initial state is entangled or not. The bounds of the interval are reached when the initial states coincide with the eigenstates of the coin operator.

Introducing a δ-interaction one can exceed the limit we derived for non-interacting particles. The δ-interaction breaks the translational symmetry, thus new analytical tools are needed to investigate the properties of the introduced model. In the picture of the joint time evolution, this scheme could be considered as an inhomogeneous two-dimensional quantum walk, where the coin is changed on the diagonal line $m = n$.

Acknowledgments

The financial support by MSM 6840770039, MŠMT LC 06002 and the Czech-Hungarian cooperation project (KONTAKT,CZ-11/2009) is gratefully acknowledged. SMB thanks the Royal Society and the Wolfson Foundation for their support.

APPENDIX A: ASYMPTOTIC PROBABILITY DISTRIBUTION FOR A QUANTUM WALK WITH TWO ENTANGLED PARTICLES

In this appendix we derive the asymptotic probability density for a quantum walk on a line with two particles for an arbitrary initial coin state $|\Psi_C\rangle$. We make use of the close relation between the two-particle walk on a line and a single-particle walk on a plane discussed in Section II. We then employ the weak limit theorem [23].

The time-evolution of the Hadamard walk on a plane is in the Fourier representation determined by the propagator

$$\widetilde{U}_{12}(k_1,k_2) = \widetilde{U}_1(k_1) \otimes \widetilde{U}_2(k_2)\,.$$

Here, $\widetilde{U}_j(k)$ denotes the single-particle propagator of the Hadamard walk on a line, which is given by

$$\widetilde{U}_j(k) = \mathcal{D}\left(e^{-ik}, e^{ik}\right) \cdot C_H\,.$$

Since $\widetilde{U}_{12}(k_1,k_2)$ has a structure of a tensor product of two unitary matrices we write its eigenvalues in the form

$$\lambda_{ij}(k_1,k_2) = e^{i\omega_{ij}(k_1,k_2)} = e^{i(\omega_i(k_1)+\omega_j(k_2))},\ i,j=1,2\,, \tag{A1}$$

where $e^{i\omega_i(k)}$ are the eigenvalues of the matrix $\widetilde{U}_j(k)$. Their phases $\omega_i(k)$ are determined by

$$\omega_1(k) = \arcsin\left(\frac{\sin k}{\sqrt{2}}\right), \quad \omega_2(k) = \pi - \omega_1(k)\,. \tag{A2}$$

Similarly, we write the corresponding eigenvectors of $\widetilde{U}_{12}(k_1,k_2)$ in the form of a tensor product

$$v_{ij}(k_1,k_2) = v_i(k_1) \otimes v_j(k_2)$$

of the eigenvectors of the matrices $\widetilde{U}_j(k_j)$

$$\begin{aligned} v_1(k) &= \frac{1}{\sqrt{n_1(k)}}\left(e^{ik}, \sqrt{2}e^{i\omega_1(k)} - e^{ik}\right)^T, \\ v_2(k) &= \frac{1}{\sqrt{n_2(k)}}\left(-e^{ik}, \sqrt{2}e^{-i\omega_1(k)} + e^{ik}\right)^T. \end{aligned} \tag{A3}$$

The normalization of the eigenvectors is given by

$$\begin{aligned} n_1(k) &= 2\left(1+\cos^2 k - \cos k\sqrt{1+\cos^2 k}\right), \\ n_2(k) &= 2\left(1+\cos^2 k + \cos k\sqrt{1+\cos^2 k}\right). \end{aligned}$$

The weak limit theorem [23] states that the cumulative distribution function equals

$$F\left(\widetilde{x}_1,\widetilde{x}_2\right) = \sum_{i,j=1}^{2} \int_{\nabla\omega_{i,j}^{-1}\left((-\infty,\widetilde{x}_1)\times(-\infty,\widetilde{x}_2)\right)} d\mu_{ij}\,, \tag{A4}$$

where we have denoted $\widetilde{x}_i = \frac{x_i}{t}$. The probability measure μ_{ij} is determined by

$$\mu_{ij} = \left|(v_{ij}(k_1,k_2),\psi_C)\right|^2 \frac{dk_1}{2\pi}\frac{dk_2}{2\pi}\,.$$

The four-component vector ψ_C corresponds to the initial state of the coin $|\Psi_C\rangle$. From the explicit form of the eigenvectors $v_{ij}(k_1,k_2)$ given in (A3) we find that the probability measures μ_{ij} equal

$$\begin{aligned}\mu_{ij} &= \frac{1}{4}\Big[\,1+(-1)^{i+1}\Big(\,C_1\mathcal{C}(k_1)+S_1\mathcal{S}(k_1)\Big)+\\ &\quad +(-1)^{j+1}\Big(\,C_2\mathcal{C}(k_2)+S_2\mathcal{S}(k_2)\Big)+\\ &\quad +(-1)^{i+j}\Big(\,C_{12}\mathcal{C}(k_1)\mathcal{C}(k_2)+S_{12}\mathcal{S}(k_1)\mathcal{S}(k_2)+\\ &\quad +X_1\mathcal{C}(k_1)\mathcal{S}(k_2)+X_2\mathcal{S}(k_1)\mathcal{C}(k_2)\,\Big)\Big]\,\frac{dk_1}{2\pi}\frac{dk_2}{2\pi}\,. \end{aligned} \tag{A5}$$

Here, we have used the notation

$$\mathcal{C}(k)=\frac{\cos k}{\sqrt{1+\cos^2 k}},\quad \mathcal{S}(k)=\frac{\sin k}{\sqrt{1+\cos^2 k}}\,,$$

to shorten the formulas. The coefficients C, S and X entering the expressions (A5) can be determined from the initial state of the coin $|\Psi_C\rangle$.

To obtain the cumulative distribution function (A4) we also have to find the integration domains. These are determined by the gradients of the phases $\omega_{i,j}(k_1,k_2)$ of the eigenvalues of the propagator $\widetilde{U}_{12}(k_1,k_2)$. From their explicit form given in (A1) and (A2) we find that the gradients are

$$\nabla\omega_{ij}(k_1,k_2)=\big((-1)^{i+1}\mathcal{C}(k_1),\ (-1)^{j+1}\mathcal{C}(k_2)\big)\ .$$

Using the above derived results and the substitution

$$\mathcal{C}(k_i)=\frac{\cos k_i}{\sqrt{1+\cos^2 k_i}}=q_i,\quad dk_i=\frac{dq_i}{(1-q_i^2)\sqrt{1-2q_i^2}}\,,$$

we can simplify the cumulative distribution function into the form

$$F(\widetilde{x}_1,\widetilde{x}_2)=\frac{1}{\pi^2}\int\limits_{-\frac{1}{\sqrt{2}}}^{\widetilde{x}_1}\frac{dq_1}{(1-q_1^2)\sqrt{1-2q_1^2}}\int\limits_{-\frac{1}{\sqrt{2}}}^{\widetilde{x}_2}\frac{dq_2}{(1-q_2^2)\sqrt{1-2q_2^2}}\Big[\,1-C_1q_1-C_2q_2+C_{12}q_1q_2\Big]\ .$$

With the help of the relation

$$p(x,y)=\frac{\partial^2 F}{\partial x\partial y}$$

between the cumulative distribution $F(x,y)$ and the probability density $p(x,y)$ we find that the later one is given by

$$p(x_1,x_2,t)=\frac{1}{\pi^2(1-\frac{x_1^2}{t^2})\sqrt{1-2\frac{x_1^2}{t^2}}(1-\frac{x_2^2}{t^2})\sqrt{1-2\frac{x_2^2}{t^2}}}\Big[\,1-C_1\frac{x_1}{t}-C_2\frac{x_2}{t}+C_{12}\frac{x_1x_2}{t^2}\Big]\ .$$

Finally, we give the explicit form of the coefficients C_1, C_2 and C_{12}. We find that they have a particularly simple form in the basis formed by the tensor product of eigenvectors of the Hadamard coin $|\chi^{\pm}\rangle$, which have been given in (16). With the decomposition of the initial coin state in the Hadamard basis as given in (22) we obtain the following expressions for the coefficients $C_{1,2}$ and C_{12}:

$$\begin{aligned}C_1 &= \sqrt{2}\left(|h_{(++)}|^2+|h_{(+-)}|^2-|h_{(-+)}|^2-|h_{(--)}|^2\right)\ ,\\ C_2 &= \sqrt{2}\left(|h_{(++)}|^2+|h_{(-+)}|^2-|h_{(+-)}|^2-|h_{(--)}|^2\right)\ ,\\ C_{12} &= 2\left(|h_{(++)}|^2+|h_{(--)}|^2-|h_{(+-)}|^2-|h_{(-+)}|^2\right)\ .\end{aligned}$$

---

[1] Aharonov Y, Davidovich L and Zagury N 1993 *Phys. Rev. A* **48** 1687

[2] Hughes B D 1995 *Random walks and random environments, Vol. 1: Random walks* (Oxford: Oxford University Press)
[3] Meyer D 1996 *J. Stat. Phys.* **85** 551
[4] Farhi E and Gutmann S 1998 *Phys. Rev. A* **58** 915
[5] Strauch F W 2006 *Phys. Rev. A* **74** 030301
[6] Chandrashekar C M 2008 *Phys. Rev. A* **78** 052309
[7] Childs A M 2010 *Commun. Math. Phys.* **294** 581
[8] Childs A M 2009 *Phys. Rev. Lett.* **102** 180501
[9] Lovett N B, Cooper S, Everitt M, Trevers M and Kendon V 2010 *Phys. Rev. A* **81** 042330
[10] Mülken O, Blumen A, Amthor T, Giese C, Reetz-Lamour M and Weidemüller M 2007 *Phys. Rev. Lett.* **99** 090601
[11] Aharonov D, Ambainis A, Kempe J and Vazirani U 2001 *Proceedings of the 33th STOC* (New York) p 50
[12] Shenvi N, Kempe J and Whaley K 2003 *Phys. Rev. A* **67** 052307
[13] Ambainis A 2007 *SIAM J. Comput.* **37** 210
[14] Childs A and Goldstone J 2004 *Phys. Rev. A* **70** 022314
[15] Kendon V M 2006 *Philos. Trans. R. Soc. A-Math. Phys. Eng. Sci.* **364** 3407
[16] Gábris A, Kiss T and Jex I 2007 *Phys. Rev. A* **76** 062315
[17] Magniez F, Nayak A, Roland J and Santha M 2007 *Proceedings of the 33th STOC* (New York) p 575
[18] Reitzner D, Hillery M, Feldman E and Bužek V 2009 *Phys. Rev. A* **79** 012323
[19] Potoček V, Gábris A, Kiss T and Jex I 2009 *Phys. Rev. A* **79** 012325
[20] Hein B and Tanner G 2009 *J. Phys. A* **42** 085303
[21] Hein B and Tanner G 2010 *Phys. Rev. A* **82** 012326
[22] Santha M 2008 Quantum walk based search algorithms *Theory and Applications of Models of Computation* (*Lecture Notes in Computer Science* vol 4978) ed Agrawal, M and Du, DZ and Duan, ZH and Li, AS (Berlin: Springer) p 31
[23] Grimmett G, Janson S and Scudo P 2004 *Phys. Rev. E* **69** 026119
[24] Konno N 2002 *Quantum Inform. Process.* **1** 345
[25] Konno N 2005 *J. Math. Soc. Jpn.* **57** 1179
[26] Tregenna B, Flanagan W, Maile R and Kendon V 2003 *New J. Phys.* **5** 83
[27] Chandrashekar C M, Srikanth R and Laflamme R 2008 *Phys. Rev. A* **77** 032326
[28] Miyazaki T, Katori M and Konno N 2007 *Phys. Rev. A* **76** 012332
[29] Konno N 2008 Quantum Walks *Quantum Potential Theory* (*Lecture Notes In Mathematics* vol 1954) ed Schurmann, M and Franz, U (Berlin: Springer) p 309
[30] Krovi H and Brun T 2006 *Phys. Rev. A* **73** 032341
[31] Krovi H and Brun T A 2006 *Phys. Rev. A* **74** 042334
[32] Mackay T, Bartlett S, Stephenson L and Sanders B 2002 *J. Phys. A* **35** 2745
[33] Inui N, Konishi Y and Konno N 2004 *Phys. Rev. A* **69** 052323
[34] Inui N, Konno N and Segawa E 2005 *Phys. Rev. E* **72** 056112
[35] Inui N and Konno N 2005 *Physica A* **353** 133
[36] Watabe K, Kobayashi N, Katori M and Konno N 2008 *Phys. Rev. A* **77** 062331
[37] Konno N 2010 *Quantum Inf. Process.* **9** 405
[38] Shikano Y and Katsura H 2010 *Phys. Rev. E* **82** 031122
[39] Pólya G 1921 *Math. Ann.* **84** 149
[40] Štefaňák M, Jex I and Kiss T 2008 *Phys. Rev. Lett.* **100** 020501
[41] Štefaňák M, Kiss T and Jex I 2008 *Phys. Rev. A* **78** 032306
[42] Štefaňák M, Kiss T and Jex I 2009 *New J. Phys.* **11** 043027
[43] Kiss T, Kecskes L, Štefaňák M and Jex I 2009 *Phys. Scr.* **T135** 014055
[44] Kollár B, Štefaňák M, Kiss T and Jex I 2010 *Phys. Rev. A* **82** 012303
[45] Chandrashekar C M 2010 *Cent. Eur. J. Phys.* **8** 979
[46] Goswami S, Sen P and Das A 2010 *Phys. Rev. E* **81** 021121
[47] Travaglione B C and Milburn G J 2002 *Phys. Rev. A* **65** 032310
[48] Dür W, Raussendorf R, Kendon V M and Briegel H J 2002 *Phys. Rev. A* **66** 052319
[49] Eckert K, Mompart J, Birkl G and Lewenstein M 2005 *Phys. Rev. A* **72** 012327
[50] Sanders B C, Bartlett S D, Tregenna B and Knight P L 2003 *Phys. Rev. A* **67** 042305
[51] Knight P, Roldan E and Sipe J 2003 *Opt. Commun.* **227** 147
[52] Chandrashekar C M 2006 *Phys. Rev. A* **74** 032307
[53] Karski M, Förster L, Choi J M, Steffen A, Alt W, Meschede D and Widera A 2009 *Science* **325** 174
[54] Schmitz H, Matjeschk R, Schneider C, Glueckert J, Enderlein M, Huber T and Schaetz T 2009 *Phys. Rev. Lett.* **103** 090504
[55] Zähringer F, Kirchmair G, Gerritsma R, Solano E, Blatt R and Roos C F 2010 *Phys. Rev. Lett.* **104** 100503
[56] Schreiber A, Cassemiro K N, Potoček V, Gábris A, Mosley P J, Andersson E, Jex I and Silberhorn C 2010 *Phys. Rev. Lett.* **104** 050502
[57] Broome M A, Fedrizzi A, Lanyon B P, Kassal I, Aspuru-Guzik A and White A G 2010 *Phys. Rev. Lett.* **104** 153602
[58] Omar Y, Paunkovic N, Sheridan L and Bose S 2006 *Phys. Rev. A* **74** 042304
[59] Štefaňák M, Kiss T, Jex I and Mohring B 2006 *J. Phys. A* **39** 14965
[60] Pathak P K and Agarwal G S 2007 *Phys. Rev. A* **75** 032351
[61] Shiau S, Joynt R and Coppersmith S 2005 *Quantum Inform. Comput.* **5** 492
[62] Gamble J K, Friesen M, Zhou D, Joynt R and Coppersmith S N 2010 *Phys. Rev. A* **81** 052313

[63] Alles B, Gunduc S and Gunduc Y 2010 *Preprint arXiv:1011.6023*
[64] Peruzzo A, Lobino M, Matthews J C F, Matsuda N, Politi A, Poulios K, Zhou X Q, Lahini Y, Ismail N, Worhoff K, Bromberg Y, Silberberg Y, Thompson M G and O'Brien J L 2010 *Science* **329** 1500
[65] Rohde P P, Schreiber A, Štefaňák M, Jex I and Silberhorn C 2011 *New J. Phys.* **13** 013001
[66] Knight P, Roldan E and Sipe J 2003 *Phys. Rev. A* **68** 020301
[67] Kempe J 2003 *Contemp. Phys.* **44** 307

A 2D Quantum Walk Simulation of Two-Particle Dynamics

Andreas Schreiber,[1,2,*] Aurél Gábris,[3,4] Peter P. Rohde,[5] Kaisa Laiho,[1,2] Martin Štefaňák,[3] Václav Potoček,[3] Craig Hamilton,[3] Igor Jex,[3] and Christine Silberhorn[1,2]

[1] *University of Paderborn, Applied Physics,Warburger Straße 100, 33098 Paderborn, Germany*
[2] *Max Planck Institute for the Science of Light, Günther-Scharowsky-Straße 1/Bau 24,91058 Erlangen, Germany*
[3] *Department of Physics, Faculty of Nuclear Sciences and Physical Engineering, Czech Technical University in Prague, Břehová 7, 115 19 Praha, Czech Republic*
[4] *Wigner Research Centre for Physics, Hungarian Academy of Sciences, H-1525 Budapest, P.O.Box 49, Hungary*
[5] *Centre for Engineered Quantum Systems, Department of Physics and Astronomy, Macquarie University, Sydney NSW 2113, Australia*

Multi-dimensional quantum walks can exhibit highly non-trivial topological structure, providing a powerful tool for simulating quantum information and transport systems. We present a flexible implementation of a 2D optical quantum walk on a lattice, demonstrating a scalable quantum walk on a non-trivial graph structure. We realized a coherent quantum walk over 12 steps and 169 positions using an optical fiber network. With our broad spectrum of quantum coins we were able to simulate the creation of entanglement in bipartite systems with conditioned interactions. Introducing dynamic control allowed for the investigation of effects such as strong non-linearities or two-particle scattering. Our results illustrate the potential of quantum walks as a route for simulating and understanding complex quantum systems.

Quantum simulation constitutes a paradigm for developing our understanding of quantum mechanical systems. A current challenge is to find schemes, that can be readily implemented in the laboratory to provide insights into complex quantum phenomena. Quantum walks [1–3] serve as an ideal test-bed for studying the dynamics of such systems. Examples include understanding the role of entanglement and interactions between quantum particles, the occurrence of localization effects [4], topological phases [5], energy transport in photosynthesis [6, 7], and the mimicking of the formation of molecule states [8]. While theoretical investigations already take advantage of complex graph structures in higher dimensions, experimental implementations are still limited by the required physical resources.

All demonstrated quantum walks have so far been restricted to evolution in one dimension. They have been realized in a variety of architectures, including photonic [9–12] and atomic [13–15] systems. Achieving increased dimensionality in a quantum walk [16] is of practical interest as many physical phenomena cannot be simulated with a single walker in a one-dimensional quantum walk, such as multi-particle entanglement and non-linear interactions. Furthermore, in quantum computation based on quantum walks [17, 18] search algorithms exhibit a speed-up only in higher dimensional graphs [19–22]. The first optical approaches to increasing the complexity of a linear quantum walk [23–25] showed that the dimensionality of the system is effectively expanded by using two walkers, keeping the graph one-dimensional. While adding additional walkers to the system is promising, introducing conditioned interactions and in particular controlled non-linear interactions at the single photon level is technologically very challenging. Interactions between walkers typically result in the appearance of entanglement, and have been shown to improve certain applications, such as the graph isomorphism problem [26]. In the absence of such interactions, the two walkers remain effectively independent, which severely limits observable quantum features.

We present a highly scalable implementation of an optical quantum walk on two spatial dimensions for quantum simulation, using frugal physical resources. One major advance of a two-dimensional system is the possibility to simulate a discrete evolution of two-particles including controlled interactions. In particular, one walker, in our case a coherent light pulse, on a 2D lattice is topologically equivalent to two-walkers acting on a one-dimensional graph. Thus, despite using an entirely classical light source, our experiment is able to demonstrate several archetypal two-particle quantum features. For our simulations we exploit the similarity between coherent processes in quantum mechanics and classical optics [27, 28], as it was used for example to demonstrate Grover's quantum search algorithm [29].

A quantum walk consists of a walker, such as a photon or an atom, which coherently propagates between discrete vertices on a graph. A walker is defined as a bipartite system consisting of position (x) and a quantum coin (c). The position value indicates at which vertex in the graph the walker resides, while the coin is an ancillary quantum state determining the direction of the walker at the next step. In a two-dimensional quantum walk the basis states of a walker are of the form $|x_1, x_2, c_1, c_2\rangle$ describing its position $x_{1,2}$ in spatial dimension 1 and 2 and the corresponding two-sided coin parameters with $c_{1,2} = \pm 1$. The evolution takes place in discrete steps, each of which has two stages,

*Electronic address: Andreas.Schreiber@upb.de

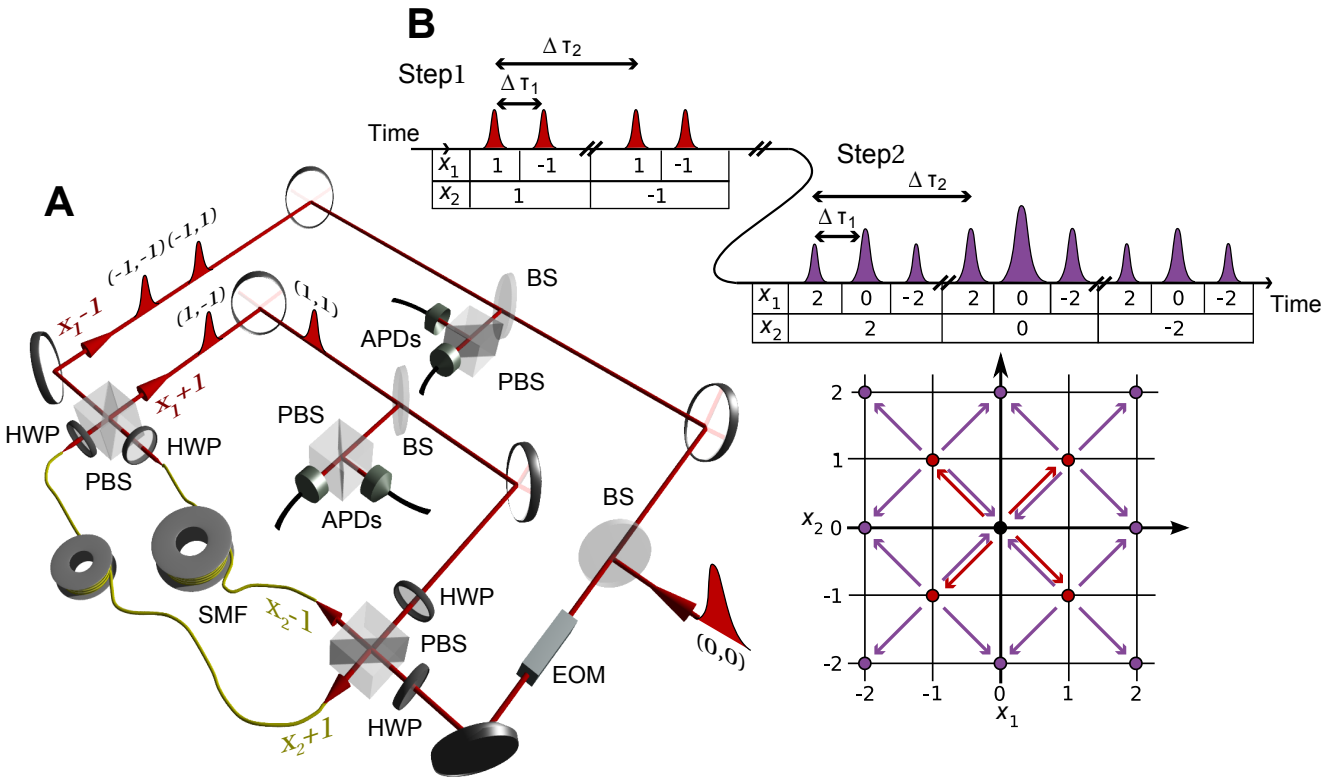

FIG. 1: (**A**) Experimental setup. Our photon source is a pulsed diode laser with pulse width 88ps, wavelength 805nm and repetition rate 110kHz. The photons are initialized at position $|x_1, x_2\rangle = |0, 0\rangle$ in horizontal polarization (corresponding to coin state $|c_1, c_2\rangle = |-1, -1\rangle$). Once coupled into the setup through a low reflectivity beam splitter (BS, reflectivity 3%), their polarization state is manipulated with an EOM and a half-wave plate (HWP). The photonic wave packets are split by a polarizing beam splitter (PBS) and routed through single-mode fibres (SMF) of length 135m or 145m, implementing a temporal step in the x_2 direction. Additional HWPs and a second PBS perform a step in the x_1 direction based on the same principle. The split wave packet after the first step with equal splitting is indicated in the picture. At each step the photons have a probability of 12% (4%) in loops $x_1 - 1$ ($x_1 + 1$) of being coupled out to a polarization and hence coin state resolving detection of the arrival time via four avalanche photodiodes (APDs). Including losses and detection efficiency, the probability of a photon continuing the walk after one step is 52% (12%) without (with) the EOM. (**B**) Projection of the spatial lattice onto a one-dimensional temporally encoded pulse chain for step one and two. Each step consists of a shift in both x_1 direction, corresponding to a time difference of $\Delta\tau_1 = 3.11$ns, and x_2 direction with $\Delta\tau_2 = 46.42$ns.

defined by coin ($\hat{C}$) and step ($\hat{S}$) operators. The coin operator coherently manipulates the coin parameter, leaving the position unchanged, whereas the step operator updates the position according to the new coin value. Explicitly, with a so-called Hadamard coin $\hat{C}_H = \hat{H}_1 \otimes \hat{H}_2$, a single step in the evolution is defined by the operators,

$$\begin{aligned} \hat{H}_i|x_i, \pm 1\rangle &\rightarrow (|x_i, 1\rangle \pm |x_i, -1\rangle)/\sqrt{2}, \quad \forall i = 1, 2 \\ \hat{S}|x_1, x_2, c_1, c_2\rangle &\rightarrow |x_1 + c_1, x_2 + c_2, c_1, c_2\rangle. \end{aligned} \tag{1}$$

The evolution of the system proceeds by repeatedly applying coin and step operators on the initial state $|\psi_{\text{in}}\rangle$, resulting in $|\psi_n\rangle = (\hat{S}\hat{C})^n|\psi_{\text{in}}\rangle$ after n steps. The step operator $\hat{S}$ hereby translates superpositions and entanglement between the coin parameters directly to the spatial domain, imprinting signatures of quantum effects in the final probability distribution.

We performed 2D quantum walks with photons obtained from attenuated laser pulses. The two internal coin states are represented by two polarization modes (horizontal and vertical) in two different spatial modes [App. 1], similar to the proposal in [30]. Incident photons follow, depending on their polarization, four different paths in a fiber network (Fig. 1A). The four paths correspond to the four different directions a walker can take in one step on a 2D lattice. Different path lengths in the circuit generate a temporally encoded state, where different position states

are represented by discrete time-bins (Fig. 1B). Each round trip in the setup implements a single step operation while the quantum coin operation is performed with linear optical elements (half-wave plates, HWP) [App. 1]. In order to adjust the coin operator independently at each position we employed a fast-switching electro-optic modulator (EOM). A measurement with time-resolving single-photon counting modules allowed for the reconstruction of the output photo-statistics [App. 2].

We have implemented two different kinds of quantum coins in our 2D quantum walks. First we investigated quantum walks driven only by separable coin operations, $\hat{C} = \hat{C}_1 \otimes \hat{C}_2$. Here the separability can directly be observed in the spatial spread over the lattice, when initializing the walker in a separable state. As an example we measured a Hadamard walk with photons initially localized at position $|x_1, x_2\rangle = |0, 0\rangle$. The probability distribution showing at which position the photons were detected after ten steps (Fig. 2A+B) can be factorized into two independent distributions of one-dimensional quantum walks [16], stating no conceptual advantage of a 2D-quantum walk. However, two-dimensional quantum walks allow for much greater complexity using controlled operations. These operations condition the transformation of one coin state on the actual state of the other. Due to the induced quantum correlations one obtains a non-trivial evolution resulting in an inseparable final state. The probability distribution for a Hadamard walk with an additional controlling operation can be seen in Fig. 2C+D. We compare the ideal theoretical distribution with the measured photo-statistics via the similarity, $S = (\sum_{x_1,x_2} \sqrt{P_{\text{th}}(x_1,x_2) P_{\text{exp}}(x_1,x_2)})^2$, quantifying the equality of two classical probability distributions ($S = 0$ for a completely orthogonal distributions and $S = 1$ for identical distributions). For the Hadamard walk (Fig. 2A+B) we observe $S = 0.957 \pm 0.003$, and for the quantum walk with controlling gates (Fig. 2C+D) $S = 0.903 \pm 0.018$ (after 10 steps, across 121 positions).

Increasing the number of walkers in a quantum walk effectively increases its dimensionality [23]. Specifically, for a given 1D quantum walk with N positions and two walkers, there exists an isomorphic square lattice walk of size N^2 with one walker. By this topological analogy, a measured spatial distribution from a 2D lattice with positions (x_1, x_2) can be interpreted as a coincidence measurement for two walkers at positions x_1 and x_2 propagating on the same linear graph. Hereby each combined coin operation of both particles, including controlled operations, has an equivalent coin operation in a 2D quantum walk. This allows us to interpret the 2D walk in Fig. 2C+D as a quantum walk with controlled two-particle operations, a system typically creating two-particle entanglement. The inseparability of the final probability distribution is then a direct signature of the simulated entanglement.

In Fig. 2E we show a lower bound for the simulated entanglement between the two particles during the stepwise evolution with four different coin operations. We quantified the simulated entanglement via the von Neumann entropy E, assuming pure final states after the quantum walk [App. 4]. For this calculation the relative phases between the positions and coins were reconstructed from the obtained interference patterns, while phases between the four coin states were chosen to minimize the entanglement value. Without conditioned operations the two particles evolve independently ($E = 0$), whereas an evolution including controlled operations reveals a probability distribution characterized by bipartite entanglement. We found that the interactions presented in Fig. 2C+D exhibit an entropy of at least $E = 2.63 \pm 0.01$ after 12 steps, which is 56% of the maximal entropy (given by a maximally entangled state). The non-zero entropies obtained in the higher steps of the separable Hadamard walk are attributed to the high sensitivity of the entropy measure to small errors in the distribution for $E \approx 0$.

The investigated interactions can be interpreted as long-distance interactions with the interaction strength being independent of the spatial distance of the particles. This is a unique effect and highly non-trivial to demonstrate in actual two-particle quantum systems.

Contrary to the position independent interactions is the evolution of two-particle quantum walks with short-range interactions, that is interactions occurring only when both particles occupy the same position. These interactions can be interpreted as two-particle scattering or non-linear interactions. When utilizing a 2D quantum walk to simulate two walkers, all vertices on the diagonal of the 2D-lattice correspond to both walkers occupying the same position. Hence, we can introduce non-linear interactions by modifying the coin operator on the diagonal positions while keeping all other positions unaffected. As an example of a two-particle quantum walk with non-linear interactions (Fig. 3), the coin operator on the diagonal is in the form $C_{\text{nl}} = (H_1 \otimes H_2) C_Z$, where C_Z is a controlled phase operation implemented by a fast switching EOM. The chosen operation simulates a quantum scenario of particular interest – the creation of bound molecule states, predicted as a consequence of two-particle scattering [8]. Evidently, the quantum walk is to a large extent confined to the main diagonal ($\sum_x P(x,x) = 0.317 \pm 0.006$ as opposed to the Hadamard walk $\sum_x P(x,x) = 0.242 \pm 0.001$), a signature of the presence of a bound molecule state. In general, using a coin invariant under particle exchange, bosonic or fermionic behavior can be simulated, depending on whether the initial states are chosen to be symmetric or anti-symmetric with respect to particle permutations. With our initial state being invariant under particle exchange we simulated an effective Bose-Hubbard type non-linearity for two bosons [31]. We have demonstrated an efficient implementation of a two-dimensional quantum walk and proved the experimental feasibility to simulate a diversity of interesting multi-particle quantum effects. Our experiment

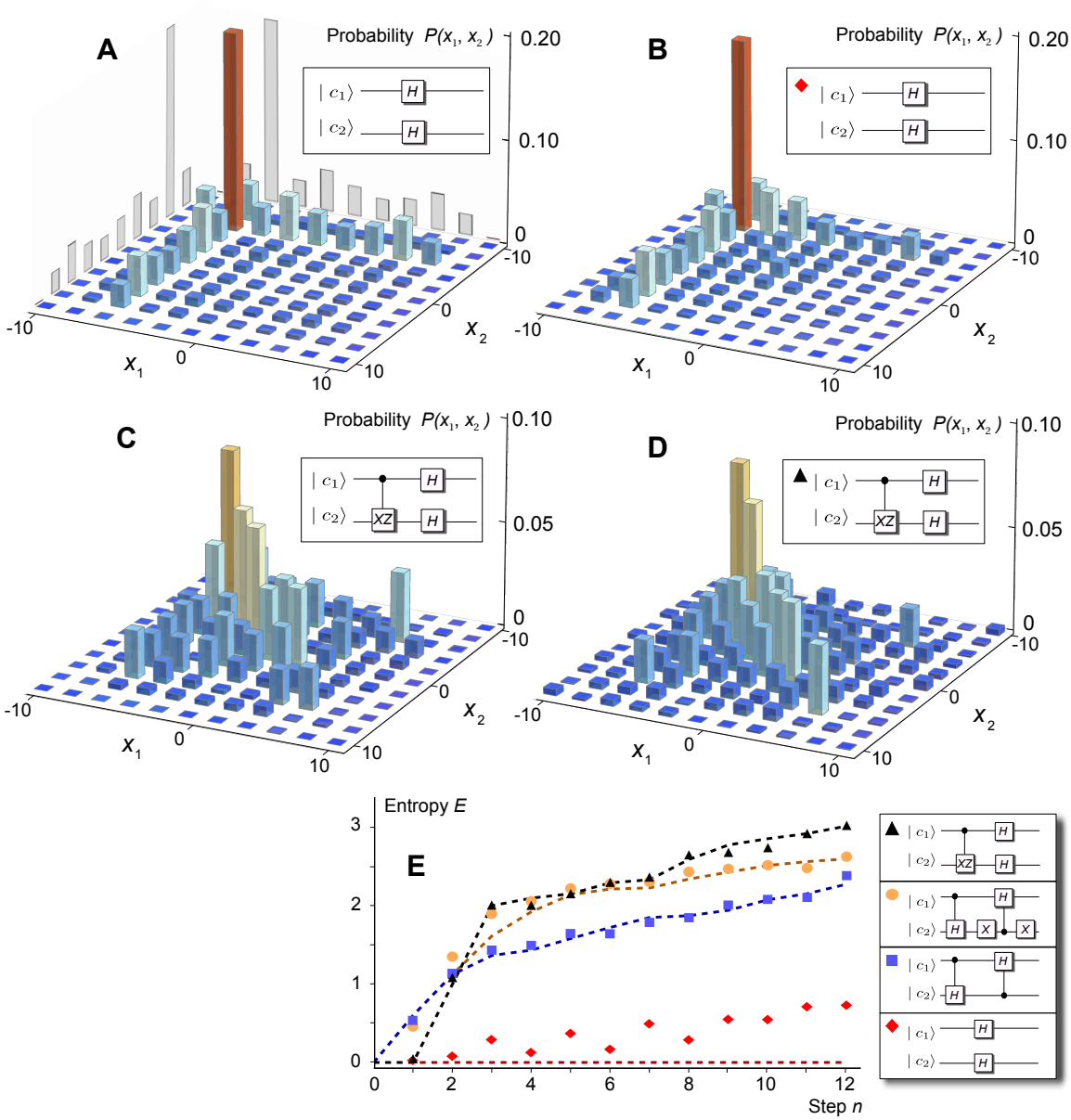

FIG. 2: Measured and simulated probability distribution $P(x_1, x_2)$ (traced over the coin space) after ten steps of a 2D quantum walk with initial state $|0, 0, -1, -1\rangle$. Theoretical (**A**) and measured (**B**) probability distribution of a 2D Hadamard walk using the operation $\hat{C}_H$ (Eq. 1). As only separable coin operations were performed (inset), the distribution is separable, given by a product of two one-dimensional distributions (gray). Theoretical (**C**) and measured (**D**) probability distribution of a 2D walk with controlled-Not X and controlled-phase operation Z, resulting in an unfactorizable distribution. Here c_2 is only transformed by $XZ|\pm 1\rangle \rightarrow \pm|\mp 1\rangle$ if $c_1 = -1$. The results (**B**) and (**D**) are obtained by detecting over 7×10^3 events and calibrated by the detection efficiencies of all four coin basis states. (**E**) Dynamic evolution of the Von Neumann entropy E generated by quantum walks (**B**) and (**D**) and quantum walks using controlled Hadamard coin operations (inset). The experimental values (dots) and theoretical predictions (dashed lines) mark a lower boundary for simulated two-particle entanglement. Statistical errors are smaller than the dot size.

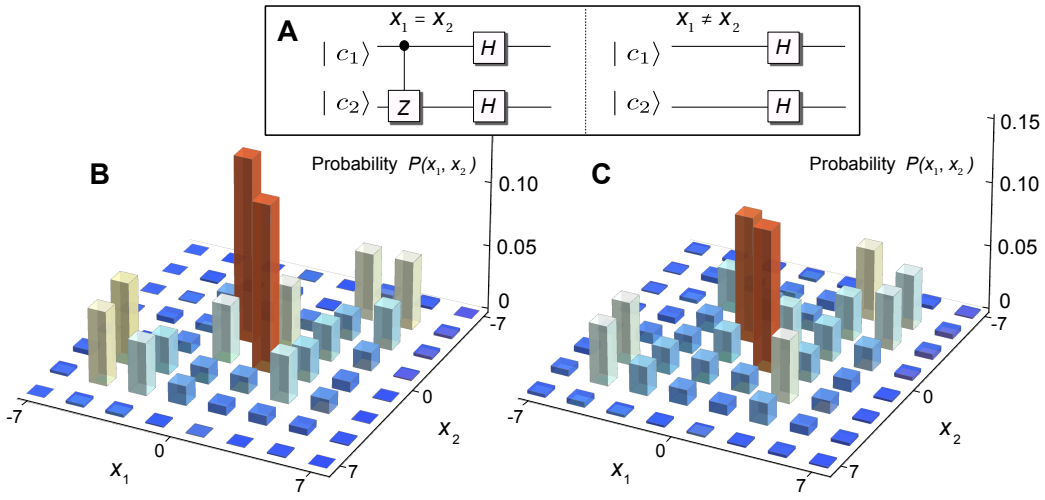

FIG. 3: (**A**) Circuit representation of coin operations simulating non-linear interactions via 2D quantum walk. Only when the two virtual particles meet ($x_1 = x_2$) a controlled operation is applied. Theoretical (**B**) and measured (**C**) coincidence distribution $P(x_1, x_2)$ (traced over the coin space) after seven steps of a simulated two-particle quantum walk with initial state $|0, 0, -1, -1\rangle$. The high probability that both particles are at the same position (diagonal) is a striking signature of bound states. The measured distribution is reconstructed by detecting over 8×10^3 events and has a similarity of $S = 0.957 \pm 0.013$. Adding the EOM to the setup for dynamical control limits the step number to $n = 7$ due to the higher losses per step. Small imperfections of the EOM are included in the theoretical plot.

overcomes the technical challenges of two-particle experiments, while exhibiting very high similarity and scalability. Combined with the flexibility in the choice of input state, controlling the coin at each position independently allows for simulations of a broad spectrum of dynamic quantum systems under different physical conditions.

Our experimental architecture can be generalized to more than two dimensions, with the addition of extra loops and orbital angular momentum modes as coin states [32]. This opens a largely unexplored field of research, facilitating quantum simulation applications with multiple walkers, including bosonic and fermionic behavior, and non-linear interactions. It may be possible to study the effects of higher dimensional localization, graph percolations or utilize the network topology in conjunction with single- or two-photon states. Additionally, a foreseeable future application for our system is the implementation of a quantum search algorithm. We demonstrated that, with a physical resource overhead, a classical experiment can simulate many genuine quantum features. While our experiment is important for simulation applications, it is equally interesting for understanding fundamental physics at the border between classical and quantum coherence theory.

Acknowledgements: We acknowledge financial support from the German Israel Foundation (Project No. 970/2007). AG, MŠ, VP, CH and IJ acknowledge grant support from MSM6840770039 and MSMT LC06002, SGS10/294/OHK4/3T/14, GA ČR 202/08/H078 and OTKA T83858. PR acknowledges support from the Australian Research Council Centre of Excellence for Engineered Quantum Systems (Project number CE110001013).

APPENDIX A: APPENDIX 1: QUANTUM GATES WITH OPTICAL ELEMENTS

We realized the four internal coin states $|\pm 1, \pm 1\rangle$ with the linear polarization states, horizontal $|H\rangle$ and vertical $|V\rangle$, and two spatial modes $|a\rangle$ and $|b\rangle$, similar to the four spatial modes proposed in (*27*). The spatial modes correspond to the two input ports of the first polarizing beam splitter (Fig. A.1)). We encoded the states by

$$\begin{aligned} |H,a\rangle &\rightarrow |-1,-1\rangle;\ |V,a\rangle \rightarrow |-1,+1\rangle; \\ |H,b\rangle &\rightarrow |+1,+1\rangle;\ |V,b\rangle \rightarrow |+1,-1\rangle. \end{aligned} \tag{A1}$$

To implement our quantum operations in the four-dimensional Hilbert space of the quantum coin we decomposed the $U(4)$ unitary coin operation into products of multiple $U(2)$ operations (*31*). Each $U(2)$ transformation is implemented either by half-wave plates (HWP) or an electro-optic modulator (EOM).

In the basis of the four coin states the transformations are given by

$$\begin{aligned} \hat{C}_{\mathrm{HWP}_1} &= \begin{pmatrix} \cos(2\theta_1) & \sin(2\theta_1) & 0 & 0 \\ \sin(2\theta_1) & -\cos(2\theta_1) & 0 & 0 \\ 0 & 0 & 1 & 0 \\ 0 & 0 & 0 & 1 \end{pmatrix}, \\ \hat{C}_{\mathrm{HWP}_2} &= \begin{pmatrix} 1 & 0 & 0 & 0 \\ 0 & 1 & 0 & 0 \\ 0 & 0 & \cos(2\theta_2) & \sin(2\theta_2) \\ 0 & 0 & \sin(2\theta_2) & -\cos(2\theta_2) \end{pmatrix}, \\ \hat{C}_{\mathrm{HWP}_3} &= \begin{pmatrix} \cos(2\theta_3) & 0 & 0 & \sin(2\theta_3) \\ 0 & 1 & 0 & 0 \\ 0 & 0 & 1 & 0 \\ \sin(2\theta_3) & 0 & 0 & -\cos(2\theta_3) \end{pmatrix}, \\ \hat{C}_{\mathrm{HWP}_4} &= \begin{pmatrix} 1 & 0 & 0 & 0 \\ 0 & -\cos(2\theta_4) & \sin(2\theta_4) & 0 \\ 0 & \sin(2\theta_4) & \cos(2\theta_4) & 0 \\ 0 & 0 & 0 & 1 \end{pmatrix}, \\ \hat{C}_{\mathrm{EOM}} &= \begin{pmatrix} e^{i\phi(x_1,x_2)} & 0 & 0 & 0 \\ 0 & 1 & 0 & 0 \\ 0 & 0 & 1 & 0 \\ 0 & 0 & 0 & 1 \end{pmatrix}, \end{aligned} \tag{A2}$$

with θ_i being the angle of HWP_i, $i = \{1, .., 4\}$, relative to its optical axis and $\phi(x_1, x_2)$ a tunable phase.

Depending on the position of the four HWPs in the setup (Fig. A.1A) they operate on different coin state pairs, due to the spatial switch via polarizing beam splitters (PBS). The Hadamard coin (Fig. 2B+E) was obtained for the configurations $\theta_i = \pi/8, \forall i$, while the coin used in Fig. 2D+E was given by $\theta_1 = -\pi/8$, $\theta_{2-4} = \pi/8$. To implement controlled-Hadamard gates either $\mathrm{HWP}_{2,3}$ or $\mathrm{HWP}_{2,4}$ were aligned to their optical axis ($\theta = 0$), while the remaining plates were set to $\theta = \pi/8$ (Fig. 2E). The transformation of the EOM with $\phi(x_1, x_2) = \pi$ corresponds to a controlled-Z operation.

Additional static phase factors changing the relative phase between the four coin states can occur during the propagation through the setup. However, these phases do not influence the final propability distribution due to the property of the coin operators that can be implemented with the used optical elements. Given precise phase control, two additional HWPs and a PBS would allow the implementation of arbitrary $U(4)$ coin operators.

APPENDIX B: APPENDIX 2: QUANTUM WALK IMPLEMENTATION VIA TIME-MULTIPLEXING

Our experiment simulates a 2D quantum walk on a regular square lattice, which means that a walker can move in four possible directions from a given site. The direction of the movement is determined by the current coin state of the walker. To implement the quantum walk in a 2D topology we use the time-multiplexing technique (*9*). This method maps each individual position of the 2D graph on the one-dimensional time line. In contrast to determining the direction of the following step in space, the coin state defines a fixed time delay in the time-multiplexed system.

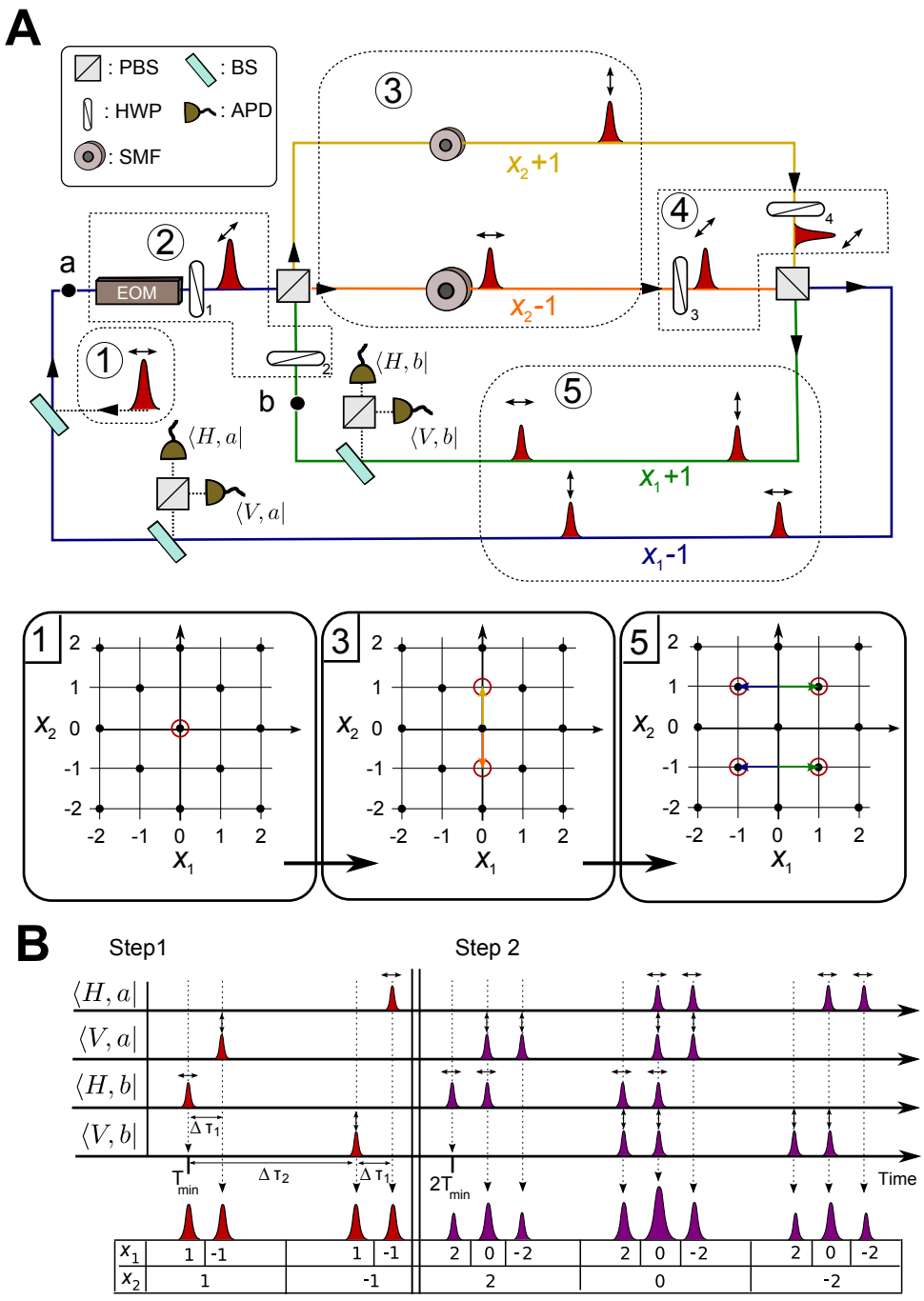

FIG. A.1: (**A**) Schematic setup including five time stages during the first step of a Hadamard walk. The laser pulse is initialized at (1) in horizontal polarization (arrow). After the coin operation $\hat{C}_2$ (2) the vertical step (3) is implemented via two single-mode fibers (SMF) of different lengths. Subsequently $\hat{C}_1$ (4) performs the coin operation for the horizontal direction, followed by the step operation implemented in free space (5). We compensate for different losses in arms a and b via different splitting ratios of the according BS. The corresponding spatial spread on a 2D lattice is shown for part (1), (3) and (5). (**B**) Mapping of the timing information of detected events onto spatial coordinates. The minimal time for a round trip T_{min} is 676ns. For more details see text.

Fig. A.1 shows the first step of a quantum walk in our system and the corresponding mapping of the temporal spread on the 2D lattice. The propagation of the initial pulse representing the walker through the setup is split into five parts:

(1) We initialize the photonic input state in the coin state $|H, a\rangle$ with the starting time corresponding to position $|x_1, x_2\rangle = |0, 0\rangle$.

(2) After launching the pulse into the setup we perform the coin operation $\hat{C}_2 = \hat{C}_{\mathrm{HWP}_2}\hat{C}_{\mathrm{HWP}_1}\hat{C}_{\mathrm{EOM}}$, as defined in Eq. A2.

(3) Split by a polarizing beam splitter (PBS) the pulse travels through two fibers of different lengths. The resulting time separation $\Delta\tau_2$ can be interpreted as a step in vertical (x_2) direction. We hereby define the transformation $x_2 \to x_2 - 1$ for pulses passing the longer fiber, while the pulses in the shorter arm acquire the transformation $x_2 \to x_2 + 1$. Additional retardation plates hereby compensate for unwanted polarization effects in the fibers.

(4) Subsequently HWP_3 and HWP_4 implement the coin operation $\hat{C}_1 = \hat{C}_{\mathrm{HWP}_3}\hat{C}_{\mathrm{HWP}_4}$ (Eq. A2), determining the coin state for the horizontal (x_1) direction.

(5) The step operator in the horizontal (x_1) direction is performed with a second PBS and a temporal shift $\Delta\tau_1$, obtained by traveling in two free space paths of different lengths.

As a result one step in our quantum walk setup combines both a shift in vertical and horizontal direction, restricting the translation on a 2D grid to the diagonal neighbors (Fig. 1B). Starting in the origin, this leads to a spread over maximally $(n+1)^2$ positions after n steps.

After each step a time resolving measurement gives information about the location of the photon. The detection times for the first and second step of a Hadamard walk are shown in Fig. A.1B. At the first detection the photons can arrive at four different times, which is either the minimal time T_{min} (corresponding to position state $|1, 1\rangle$), $T_{\mathrm{min}} + \Delta\tau_1$ stating position $|1, -1\rangle$, $T_{\mathrm{min}} + \Delta\tau_2$ ($|-1, 1\rangle$) or $T_{\mathrm{min}} + \Delta\tau_1 + \Delta\tau_2$ ($|-1, -1\rangle$). At the second step on the other hand, multiple pulses can arrive simultaneously at the detectors. Independent of the coin state and, hence, spatial and polarization modes of the photons, all coinciding detections correspond to the same position state $|x_1, x_2\rangle$. In the following step wave packets in the same time bin and spatial mode interfere at $\mathrm{HWP}_{1,2}$ ($\hat{C}_2$), while wave packets in different spatial modes can interfere at $\mathrm{HWP}_{3,4}$ ($\hat{C}_1$).

APPENDIX C: APPENDIX 3: LIMITS AND IMPERFECTIONS

During the time evolution, the area of the grid covered by the quantum walker grows quadratically with the number of steps. The use of the time-multiplexing technique guarantees that the number of elements stays constant independent of the size of the simulated grid. In the experimental implementation it is only the lengths of the optical paths that needs to be adjusted to the maximum number of steps that are to be realized. In addition, the performance of our time-multiplexed setup is limited only by imperfections of the optical components resulting in errors, decoherence and losses. In the following we want to discuss each point individually.

A sharp limitation for the maximal step number is given by the design of the experiment. If the minimal time for one round trip T_{min} is shorter than the temporal expansion of all positions in a single step, temporal overlaps between different steps can occur. We choose our experimental parameters T_{min} and $\Delta\tau_{1,2}$ without EOM such that $\Delta\tau_2 > 13 \cdot \Delta\tau_1$ and $T_{\mathrm{min}} > 13 \cdot \Delta\tau_2$ to prevent temporal overlaps of different positions for the first 12 steps. An occurring additional delay induced by the modulator changed the conditions without inducing unwanted temporal overlaps. However, by simply changing the fiber lengths or the path differences the step number can easily be increased.

The most significant source of systematic errors in the setup is the EOM. Due to the architecture of the modulator the applied phase is not only affecting the horizontal polarization component, as shown in Eq. A2, but also the vertical component with a factor 1/3.5. This decreases the achievable similarities for quantum walks where controlled-Z coin operations are used. Additionally, the wave front of pulses passing the modulator are distorted differently for both polarizations, which influences the occurring interferences. Both effects are included in the theory presented in Fig. 3B. A replacement of the EOM with an optimized modulator would improve the achievable similarity at higher number of steps.

Decoherence in the time-multiplexed setup can occur if mechanical vibrations of the optical elements influence the interference properties. Typically mirrors vibrate with a frequency below 500Hz, corresponding to a time scale of 2ms. The duration of twelve steps in the current setup is less than $10\mu s$, a factor of 200 faster compared to mirror vibrations. This suggests that decoherence effects will not influence the time-multiplexed quantum walk up to at least 100 steps.

At the present stage the main factor limiting the scalability is given by the losses per step. These are induced by the probabilistic detection method and losses at optical elements. To counter the effect of losses one can either start with an increased intensity or use optical amplifiers, as shown in (*32*). While the first approach requires an active protection of the single-photon detectors, the second prohibits the use of the experiment with single-photon sources. A third method to reduce the losses is a change from probabilistic to a deterministic coupling mechanism with additional polarization modulators. This technique combined with a change-over to a low-loss wavelength regime (1550nm), makes the setup interesting for single photon input states. Using one of the described methods to circumvent the losses can increase the number of steps significantly.

APPENDIX D: APPENDIX 4: ENTANGLEMENT

To quantify the two-particle entanglement simulated in the system we assumed that the quantum walk evolution results in a pure state $|\psi_n\rangle = \sum_{x_1,x_2,c_1,c_2} a_{x_1,x_2,c_1,c_2}|x_1,x_2,c_1,c_2\rangle$ after n steps, with the complex parameters $a_{x_1,x_2,c_1,c_2} \in \mathbb{C}$. The assumption is based on the fact that the system does not show signs of decoherence for any of the coin operators, confirmed by the high values of the measured similarities.

The von Neumann entropy E, which quantifies the entanglement (*33*) is given by

$$E(\rho_1) = -\sum_i \lambda_i \log_2 \lambda_i, \tag{A3}$$

with the eigenvalues λ_i of the reduced density matrix $\rho_1 = \mathrm{Tr}_2(\rho) = \mathrm{Tr}_2(|\psi_n\rangle\langle\psi_n|)$, given by the trace over one subsystem. For details see (*23*).

By individually measuring the arrival probability in each coin and position state we obtain the absolute squared of the parameters $|a_{x_1,x_2,c_1,c_2}|^2$, hence no direct extraction of the phase information is possible. However, we can obtain information about the relative phases between position and coin states from the final interference pattern. As a result we can reconstruct the phase distribution with the help of the theoretical model up to three undetermined relative phases between the four different coin states and a global phase factor. By choosing the phases inducing the minimal entropy, we are able to give a lower bound for the simulated entanglement in the experiment.

[1] Y. Aharonov, L. Davidovich, N. Zagury, *Phys. Rev. A* **48**, 1687 (1993).
[2] D. Aharonov, A. Ambainis, J. Kempe, U. Vazirani, in *Proceedings of the Thirty-Third Annual ACM Symposium on Theory of Computing*, STOC '01, Hersonissos, Greece, 6 to 8 July 2001 (ACM, New York, NY, USA, 2001), pp. 50–59.
[3] J. Kempe, *Contemporary Physics* **44**, 307 (2003).
[4] N. Inui, Y. Konishi, N. Konno, *Phys. Rev. A* **69**, 052323 (2004).
[5] T. Kitagawa, M. S. Rudner, E. Berg, E. Demler, *Phys. Rev. A* **82**, 033429 (2010).
[6] M. Mohseni, P. Rebentrost, S. Lloyd, A. Aspuru-Guzik, *J. Chem. Phys.* **129**, 174106 (2008).
[7] M. B. Plenio, S. F. Huelga, *N. J. Phys.* **10**, 113019 (2008).
[8] A. Ahlbrecht, *et al.*, *arxiv: quant-ph/1105.1051* (2011).
[9] D. Bouwmeester, I. Marzoli, G. P. Karman, W. Schleich, J. P. Woerdman, *Phys. Rev. A* **61**, 013410 (1999).
[10] A. Schreiber, *et al.*, *Phys. Rev. Lett.* **104**, 050502 (2010).
[11] M. A. Broome, *et al.*, *Phys. Rev. Lett.* **104**, 153602 (2010).
[12] A. Schreiber, *et al.*, *Phys. Rev. Lett.* **106**, 180403 (2011).
[13] H. Schmitz, *et al.*, *Phys. Rev. Lett.* **103**, 090504 (2009).
[14] M. Karski, *et al.*, *Science* **325**, 174 (2009).
[15] F. Zähringer, *et al.*, *Phys. Rev. Lett.* **104**, 100503 (2010).
[16] T. D. Mackay, S. D. Bartlett, L. T. Stephenson, B. C. Sanders, *J. Phys. A* **35**, 2745 (2002).
[17] A. M. Childs, *Phys. Rev. Lett.* **102**, 180501 (2009).
[18] N. B. Lovett, S. Cooper, M. Everitt, M. Trevers, V. Kendon, *Phys. Rev. A* **81**, 042330 (2010).
[19] A. M. Childs, *et al.*, in *Proceedings of the thirty-fifth ACM symposium on Theory of computing* - STOC '03 (San Diego, CA, USA, 2003), p. 59.
[20] N. Shenvi, J. Kempe, K. B. Whaley, *Phys. Rev. A* **67**, 052307 (2003).
[21] A. Ambainis, J. Kempe, A. Rivosh, in *Proceedings of the Sixteenth ACM-SIAM Symposium on Discrete Algorithms*, SODA '05, Vancouver, Canada, 23 to 25 January 2005 (Society for Industrial and Applied Mathematics, Philadelphia, 2005), p. 1099-1108.
[22] M. Hillery, D. Reitzner, V. Bužek, *Phys. Rev. A* **81**, 062324 (2010).
[23] A. Peruzzo, *et al.*, *Science* **329**, 1500 (2010).

[24] J. C. F. Matthews, *et al.*, *arxiv: quant-ph/1106.1166* (2011).
[25] L. Sansoni, *et al.*, *Phys. Rev. Lett.* **108**, 010502 (2012).
[26] S. D. Berry, J. B. Wang, *Phys. Rev. A* **83**, 042317 (2011).
[27] R. J. C. Spreeuw, *Found. Phys.* **28**, 361 (1998).
[28] N. J. Cerf, C. Adami, P. G. Kwiat, *Phys. Rev. A* **57**, R1477 (1998).
[29] N. Bhattacharya, H. B. van Linden van den Heuvell, R. J. C. Spreeuw, *Phys. Rev. Lett.* **88**, 137901 (2002).
[30] E. Roldan, J. C. Soriano, *J. Mod. Opt.* **52**, 2649 (2005).
[31] Y. Lahini, *et al.*, *arxiv: quant-ph/1105.2273* (2011).
[32] C. S. Hamilton, A. Gábris, I. Jex, S. M. Barnett, *N. J. Phys.* **13**, 013015 (2011).
[33] M. Reck, A. Zeilinger, H. J. Bernstein, P. Bertani, *Phys. Rev. Lett.* **73**, 58 (1994).
[34] A. Regensburger, *et al.*, *Phys. Rev. Lett.* **107**, 233902 (2011).
[35] S. M. Barnett, S. J. D. Phoenix, *Phys. Rev. A* **40**, 2404 (1989).

Continuous deformations of the Grover walk preserving localization

M. Štefaňák,[1] I. Bezděková,[1] and I. Jex[1]

[1]*Department of Physics, Faculty of Nuclear Sciences and Physical Engineering, Czech Technical University in Prague, Břehová 7, 115 19 Praha 1 - Staré Město, Czech Republic*

The three-state Grover walk on a line exhibits the localization effect characterized by a non-vanishing probability of the particle to stay at the origin. We present two continuous deformations of the Grover walk which preserve its localization nature. The resulting quantum walks differ in the rate at which they spread through the lattice. The velocities of the left and right-traveling probability peaks are given by the maximum of the group velocity. We find the explicit form of peak velocities in dependence on the coin parameter. Our results show that localization of the quantum walk is not a singular property of an isolated coin operator but can be found for entire families of coins.

I. INTRODUCTION

Quantum walks have been introduced by Aharonov et al. [1] as a generalization of a classical random walk [2] to a unitary discrete-time evolution of a quantum particle. The particle moves on a graph or a lattice in discrete time-steps according to its internal degree of freedom, which is usually refer to as coin. In analogy with the coin tossing which tells the classical particle where to go the state of the coin is altered by the coin operator before the displacement itself. However, in a quantum walk each trajectory is assigned a certain probability amplitude and not a probability. Different trajectories interfere which leads to a ballistic spreading of a probability density of a quantum particle. Indeed, quantum walk can be considered as a wave phenomena [3]. This analogy allowed to adopt and develop a number of concepts used in wave propagation in material media for quantum walks. For instance, Kempf and Portugal defined the hitting time based on the concept of group velocity [4].

The application of quantum walks for quantum information processing have been proposed [5]. In particular, one can use the quantum walk to implement the quantum search algorithm [6]. The performance of the search algorithm crucially depends on the choice of the coin operator [7]. A review of quantum walk based algorithms can be found in [8].

For a two-state walk on a line the coin operator is given by a $U(2)$ matrix. Nevertheless, it has been shown [9] that it is sufficient to consider the one-parameter family of coins

$$C(\rho) = \begin{pmatrix} \rho & \sqrt{1-\rho^2} \\ \sqrt{1-\rho^2} & -\rho \end{pmatrix},$$

with $0 \leq \rho \leq 1$. The phases in a general $U(2)$ matrix turn out to be either irrelevant for the quantum walk evolution or can be compensated by the choice of the initial state. The choice of $\rho = 1/\sqrt{2}$ corresponds to the most studied case of the Hadamard walk [10]. The coin parameter determines the rate at which the walk spreads through the lattice. For unbiased walks the peaks of the probability density propagates with constant velocity $\pm\rho$. This also illustrates the ballistic nature of a quantum walk. Biasing the walk by allowing the particle to make longer jumps in one direction speeds up one of the peaks and slows down the other [11]. This has a crucial impact on the recurrence properties of the quantum walk [12]. The understanding of recurrence requires the knowledge of the asymptotic properties of a quantum walk. For two-state quantum walks these characteristics can be obtained from the limit theorems derived by Konno [13, 14]. Grimmett et al. [15] have extended the weak limit theorems to higher-dimensional quantum walks. For a review of asymptotic methods in quantum walks see [16].

Allowing the particle to stay at its actual position we have to extend the coin to a $U(3)$ matrix. The resulting three-state quantum walks lead to dynamics which cannot occur in the two-state walk. As an example, the intriguing effect of localization has been found in the three-state Grover walk on a line [17, 18]. Here the particle has a non-vanishing probability to stay at the origin. However, the localization effect is sensitive to the dimensionality of the lattice. There is no localization in the three-state Grover walk on a triangular lattice [19]. Nevertheless, localization is not limited to quantum walks which allow the particle to stand still. The Grover walk on a 2D square lattice represents such an example [20].

We note that there are two types of localization in the context of quantum walks. The one we have just discussed and which we will focus on in the present paper is inherent to certain quantum walks without any perturbations. It stems from the fact that the unitary propagator of the walk has a non-empty point spectrum. As the wave packet spreads it overlaps with the corresponding bound states which results in partial trapping of the particle in the vicinity of the origin. The second kind is the Anderson localization which arises e.g. from static phase disorder [21] or spatial

coin inhomogeneity [22]. This dynamical localization was experimentally observed in the photonic implementation of quantum walk on a line [23]. For a comprehensive mathematical description of this effect we refer to the literature [24, 25].

In contrast to the two-state walk the properties of a three-state walk with a general $U(3)$ coin operator are not fully understood. The present paper is a step in classification of the three-state quantum walks. By deforming the Grover matrix we find two families of coins which lead to a localizing quantum walk. The first one-parameter family of coins is based on the variation of the spectrum of the Grover matrix. Another one-parameter family of coin operators is obtained by modifying the eigenvectors of the Grover matrix. In both cases we show how does the coin parameter determine the rate of spreading of the corresponding quantum walk by calculating the explicit form of the peak velocities. While for the first family of walks the peak velocities can only decrease when compared to the Grover walk, the second deformation allows to increase them to the maximum possible value.

Our manuscript is organized as follows: In Section II we briefly review the properties of the three-state Grover walk on a line following the Fourier analysis. We determine the peak velocities of the Grover walk by applying the stationary phase approximation in Section III. In Section IV we introduce two deformations of the Grover walk which preserves its localization nature and analyze their peak velocities. We conclude and present an outlook in Section V.

II. THREE-STATE GROVER WALK ON A LINE

Let us first review the three-state Grover walk on a line [17, 18]. The Hilbert space of the particle is given by the tensor product

$$\mathcal{H} = \mathcal{H}_P \otimes \mathcal{H}_C$$

of the position space

$$\mathcal{H}_P = \mathrm{Span}\left\{|\mathrm{m}\rangle, \mathrm{m} \in \mathbb{Z}\right\}$$

and the coin space $\mathcal{H}_C$. In each step the particle has three possibilities - it can move to the left or right or stay at its current location. To each of these options we assign a vector of the standard basis of the coin space $\mathcal{H}_C$, i.e. the coin space is three-dimensional

$$\mathcal{H}_C = \mathbb{C}^3 = \mathrm{Span}\left\{|\mathrm{L}\rangle, |\mathrm{S}\rangle, |\mathrm{R}\rangle\right\}.$$

A single step of the quantum walk is realized by the propagator U given by

$$U = S \cdot (I_P \otimes C),$$

where S is the conditional step operator, I_P denotes the identity on the position space and C is the coin operator. For our three-state walk the conditional step operator S has the following form

$$S = \sum_{m=-\infty}^{+\infty} \Big(|m-1\rangle\langle m| \otimes |L\rangle\langle L| + |m\rangle\langle m| \otimes |S\rangle\langle S| + |m+1\rangle\langle m| \otimes |R\rangle\langle R| \Big).$$

As the coin operator we choose the 3×3 Grover matrix

$$C = C_G = \frac{1}{3}\begin{pmatrix} -1 & 2 & 2 \\ 2 & -1 & 2 \\ 2 & 2 & -1 \end{pmatrix}.$$

The state of the particle after t steps is given by the successive application of the unitary propagator on the initial state

$$|\psi(t)\rangle = \sum_m |m\rangle \Big(\psi_L(m,t)|L\rangle + \psi_S(m,t)|S\rangle + \psi_R(m,t)|R\rangle \Big) = U^t|\psi(0)\rangle. \tag{1}$$

The probability distribution of the particle's position after t steps of quantum walk is obtained by tracing out the coin degree of freedom

$$\begin{aligned} p(m,t) &= |\psi_L(m,t)|^2 + |\psi_S(m,t)|^2 + |\psi_R(m,t)|^2 \\ &= ||\psi(m,t)||^2. \end{aligned}$$

Here we have introduced the vector of probability amplitudes

$$\psi(m,t) = (\psi_L(m,t), \psi_S(m,t), \psi_R(m,t))^T .$$

Since the walk we consider is translationally invariant the time evolution equation (1) greatly simplifies using the Fourier transformation

$$\tilde{\psi}(k,t) = \sum_{m=-\infty}^{+\infty} e^{imk} \psi(m,t), \tag{2}$$

where the momentum k ranges from 0 to 2π. Indeed, applying the Fourier transformation (2) to the time evolution equation (1), we find

$$\tilde{\psi}(k,t) = \tilde{U}(k)\tilde{\psi}(k,t-1) = \tilde{U}^t(k)\tilde{\psi}(k,0). \tag{3}$$

Here $\tilde{\psi}(k,0)$ denotes the Fourier transformation of the initial state of the particle. It equals the initial coin state ψ_C of the particle provided that it starts the walk from the origin. The momentum representation of the time evolution operator $\tilde{U}(k)$ is given by

$$\tilde{U}(k) = \mathrm{Diag}\left(\mathrm{e}^{-\mathrm{ik}}, 1, \mathrm{e}^{\mathrm{ik}}\right) \cdot \mathrm{C_G}. \tag{4}$$

The time evolution equation in the momentum representation (3) is readily solved by diagonalizing the propagator (4). We express the eigenvalues of $\tilde{U}(k)$ in the form $\lambda_j = \exp(i\omega_j(k))$ and denote the corresponding eigenvectors by $v_j(k)$. For the three-state Grover walk the phases read

$$\begin{aligned} \omega_{1,2}(k) &= \pm \arccos\left(-\frac{1}{3}(2+\cos k)\right), \\ \omega_3(k) &= 0. \end{aligned} \tag{5}$$

Since the phase ω_3 vanishes we find that the corresponding eigenvalue λ_3 equals 1 independent of k. In other words, the propagator of the Grover walk has a non-empty point spectrum. This leads to the localization effect [17, 18]. Finally, the solution of the time evolution equation in the momentum representation (3) has the form

$$\tilde{\psi}(k,t) = \sum_{j=1}^{3} e^{i\omega_j(k)t} \left(v_j(k), \psi_C\right) v_j(k).$$

After the inverse Fourier transformation we obtain the solution in the position representation

$$\psi(m,t) = \sum_{j=1}^{3} \int_0^{2\pi} \frac{dk}{2\pi} e^{i\left(\omega_j(k) - \frac{m}{t}k\right)t} \left(v_j(k), \psi_C\right) v_j(k). \tag{6}$$

III. PEAK VELOCITY OF THE GROVER WALK

Let us now determine the rate at which the three-state Grover walk spreads through the lattice. We employ the stationary phase approximation [26] which determines the behavior of the amplitude (6) for $t \to +\infty$. Accordingly, the rate of the decay is given by the order of the stationary points of the phase

$$\tilde{\omega}_j(k) \equiv \omega_j(k) - \frac{m}{t}k. \tag{7}$$

The peak corresponds to the stationary point of the second order - both the first and the second derivatives of the phase (7) with respect to k vanish. Thus we have to solve a set of equations

$$\begin{aligned} \frac{d\tilde{\omega}_j}{dk} &= \frac{d\omega_j}{dk} - \frac{m}{t} = 0, \\ \frac{d^2\tilde{\omega}_j}{dk^2} &= \frac{d^2\omega_j}{dk^2} = 0, \end{aligned} \tag{8}$$

for k and m. Assume that k_0 satisfies the second equation in (8). From the first equation in (8) we find that the position of the peak after t steps is

$$m = \left.\frac{d\omega_j}{dk}\right|_{k_0} t.$$

The peak thus propagates with constant velocity which is given by $\left.\frac{d\omega_j}{dk}\right|_{k_0}$.

We find that there is a simple analogy with wave theory. Indeed, consider k as wavenumber and $\omega_j(k)$ as frequency. Equations (5) represent the dispersion relations. Taking the derivative with respect to k we obtain the group velocity [4]. The wavefront, i.e. the peak in the probability distribution, propagates with the maximal group velocity.

Let us specify the results for the three-state Grover walk. From the explicit form of the dispersion relations (5) we find that the second equation in (8) reads

$$\frac{d^2\omega_{1,2}}{dk^2} = \pm 2\sqrt{\frac{1-\cos k}{(5+\cos k)^3}} = 0.$$

This relation is satisfied for $k_0 = 0$. Evaluating the first derivative of $\omega_j(k)$ at this point we obtain the velocities of the left and right-traveling peaks

$$\begin{aligned} v_R &= \lim_{k\to 0^+} \frac{d\omega_2}{dk} = \frac{1}{\sqrt{3}}, \\ v_L &= \lim_{k\to 0^+} \frac{d\omega_1}{dk} = -\frac{1}{\sqrt{3}}. \end{aligned} \tag{9}$$

Note that from the constant phase $\omega_3 \equiv 0$ one immediately obtains $v_S = 0$. Indeed, the constant eigenvalue results in the central peak of the probability distribution which does not propagate.

To illustrate our results we plot in Figure 1 the probability distribution of the three-state Grover walk after $T = 50$ steps. The probability distribution contains three dominant peaks. Their positions are determined by the velocities $v_{L,R}$ and v_S.

IV. DEFORMATIONS OF THE GROVER WALK

We begin with the spectral decomposition of the Grover coin. Consider the following orthonormal basis

$$\begin{aligned} v_1 &= \frac{1}{\sqrt{6}}\left(1,-2,1\right)^T, \\ v_2 &= \frac{1}{\sqrt{2}}\left(1,0,-1\right)^T, \\ v_3 &= \frac{1}{\sqrt{3}}\left(1,1,1\right)^T, \end{aligned} \tag{10}$$

formed by the eigenvectors of the Grover coin with eigenvalues $\lambda_1 = \lambda_2 = -1$ and $\lambda_3 = 1$. The Grover coin can be thus decomposed in the form

$$C_G = \sum_{j=1}^{3} \lambda_j P_j = -P_1 - P_2 + P_3, \tag{11}$$

where P_j is the projection on the subspace spanned by the corresponding eigenvector.

In the following we introduce two deformations of the three-state Grover walk which preserves its localization nature. First, we modify the eigenvalues of the coin and keep the eigenvectors constant. Second, we leave the spectrum unchanged and deform the eigenvectors.

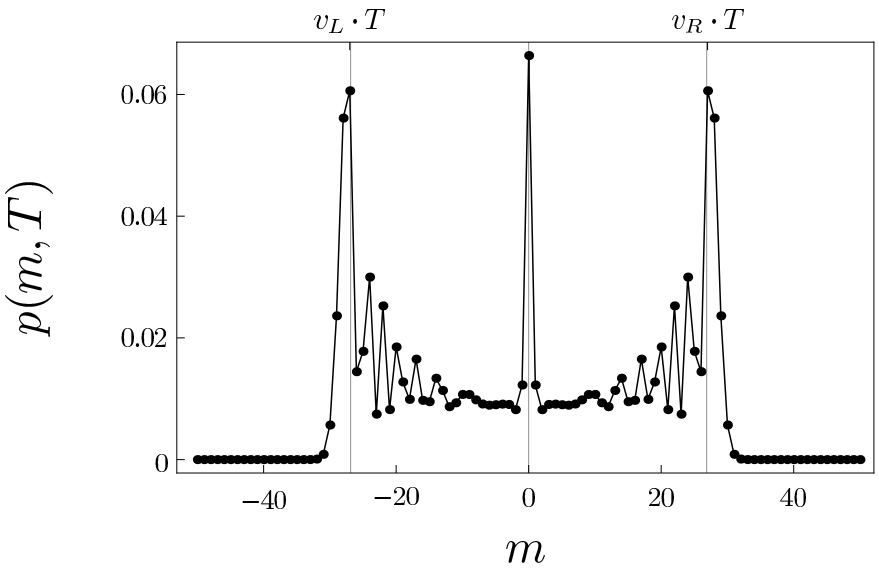

FIG. 1: The probability distribution of the three-state Grover walk after $T = 50$ steps. The initial coin state of the walk was $\psi_C = \frac{1}{\sqrt{3}}(1, -1, 1)$. One can clearly identify three dominant peaks in the probability distribution. The peak at the origin corresponds to the localization nature of the Grover walk and does not propagate. The peaks on the sides travel with constant velocities $v_{L,R} = \pm\frac{1}{\sqrt{3}}$. The grid-lines corresponding to $Tv_{L,R} \approx \pm 29$ coincides with the positions of the peaks obtained from the numerical simulation.

A. Deforming the eigenvalues

The Grover matrix is very symmetric - it is invariant under all permutations of the basis states. Hence, we can diagonalize it together with any permutation matrix. The eigenvectors of the Grover matrix presented in Eq. (10) are chosen in such a way that they are also eigenvectors of the permutation matrix

$$\Pi = \begin{pmatrix} 0 & 0 & 1 \\ 0 & 1 & 0 \\ 1 & 0 & 0 \end{pmatrix}.$$

The corresponding eigenvalues are $\mu_1 = \mu_3 = 1$ and $\mu_2 = -1$. The permutation Π interchanges the $|L\rangle$ and $|R\rangle$ coin states and preserves the $|S\rangle$ state. Using this matrix as a coin for a three-state quantum walk results in a trivial evolution - the particle either stays at the origin, or jumps to the left or right but immediately returns back in the next step. Such a walk does not spread through the lattice and the velocities vanish.

Notice that the eigenvector v_2 corresponds to the same eigenvalue $\lambda_2 = \mu_2 = -1$ for both the Grover and the permutation matrix Π. The same applies to v_3 since $\lambda_3 = \mu_3 = 1$. However, for v_1 we have $\lambda_1 = -1$ and $\mu_1 = 1$. This suggest to introduce a phase factor in front of the projector P_1 in the spectral decomposition of the Grover coin (11). In this way we can continuously change from the Grover coin to the permutation matrix Π. We thus arrive at the following one-parameter family of coin operators

$$\begin{aligned} C_1(\varphi) &= -e^{2i\varphi}P_1 - P_2 + P_3 \\ &= \frac{1}{6}\begin{pmatrix} -1-e^{2i\varphi} & 2(1+e^{2i\varphi}) & 5-e^{2i\varphi} \\ 2(1+e^{2i\varphi}) & 2(1-2e^{2i\varphi}) & 2(1+e^{2i\varphi}) \\ 5-e^{2i\varphi} & 2(1+e^{2i\varphi}) & -1-e^{2i\varphi} \end{pmatrix}. \end{aligned} \tag{12}$$

The factor of 2 in the exponent was included for convenience. We show that the family of three-state quantum walks with the coin operator (12) posses the localization property of the Grover walk. The phase parameter φ determines the rate of spreading of the probability distribution through the lattice.

The dispersion relations for the one-parameter family of quantum walks with the coin operator (12) are

$$\begin{aligned} \omega_{1,2}(k,\varphi) &= \varphi \pm \arccos\left(-\frac{1}{3}(2+\cos k)\cos\varphi\right), \\ \omega_3(k,\varphi) &= 0. \end{aligned}$$

As for the original Grover walk we find that one frequency is independent of k. This ensures that the localization effect is preserved.

Let us now determine the velocities of the peaks, i.e. the maximal group velocity. The second derivatives of the frequencies $\omega_{1,2}(k,\varphi)$

$$\frac{\partial^2\omega_{1,2}}{\partial k^2} = \mp\frac{9\cos k - \cos^2\varphi(2+5\cos k+2\cos^2 k)}{(9-\cos^2\varphi(2+\cos k)^2)^{\frac{3}{2}}}\cos\varphi$$

vanish for

$$k_0 = \arccos\left(\frac{1}{4\cos^2\varphi}\left(9-5\cos^2\varphi - 3\sqrt{9-10\cos^2\varphi+\cos^4\varphi}\right)\right).$$

Evaluating the group velocities $\frac{\partial\omega_{1,2}}{\partial k}$ at the stationary point k_0 we obtain the velocities of the left and right-going peaks

$$\begin{aligned} v_R(\varphi) &= \left.\frac{\partial\omega_2}{\partial k}\right|_{k_0} = \frac{1}{\sqrt{6}}\sqrt{3-\cos^2\varphi-\sin\varphi\sqrt{9-\cos^2\varphi}}, \\ v_L(\varphi) &= \left.\frac{\partial\omega_1}{\partial k}\right|_{k_0} = -v_R(\varphi). \end{aligned} \tag{13}$$

We illustrate our results in Figures 2 and 3. In Figure 2 we display the velocity $v_R(\varphi)$ as a function of the coin parameter φ. It turns out that the dependence is almost linear

$$v_R(\varphi) \approx \frac{1}{\sqrt{3}}\left(1-\frac{2\varphi}{\pi}\right).$$

The inset shows the variation of $v_R(\varphi)$ from this linear approximation. We find that from the one-parameter family of quantum walks with the coin operator $C_G(\varphi)$ the Grover walk is the fastest one, as $v_R(\varphi)$ attains the maximal value $\frac{1}{\sqrt{3}}$ for $\varphi = 0$. With increasing φ the velocity of the right peak drops down and it becomes zero for $\varphi = \pi/2$.

In Figure 3 we show the probability distribution of the generalized three-state localizing walk with the parameter $\varphi = \pi/4$ after $T = 50$ steps. In comparison with the original Grover walk displayed in Figure 1 we find that the distribution spreads much slower.

B. Deforming the eigenvectors

Our second approach to the deformation of the Grover walk is inspired by the work of Watabe et al. [27]. The authors have studied a one-parameter family of 2D four-state quantum walks which contained the Grover walk. This set of quantum walks also preserves the localization effect. The particular property of the corresponding one-parameter set of 4×4 coin operators is that they have the same spectrum as the Grover matrix. We show that this feature can be employed to construct a similar set of 3×3 coins.

Let us first consider two rather trivial coin operators which have the same spectrum as the Grover matrix and which also preserve localization of the corresponding quantum walk. One of such matrices is similar to the permutation matrix Π introduced in the previous section, namely

$$C = \begin{pmatrix} 0 & 0 & 1 \\ 0 & -1 & 0 \\ 1 & 0 & 0 \end{pmatrix}.$$

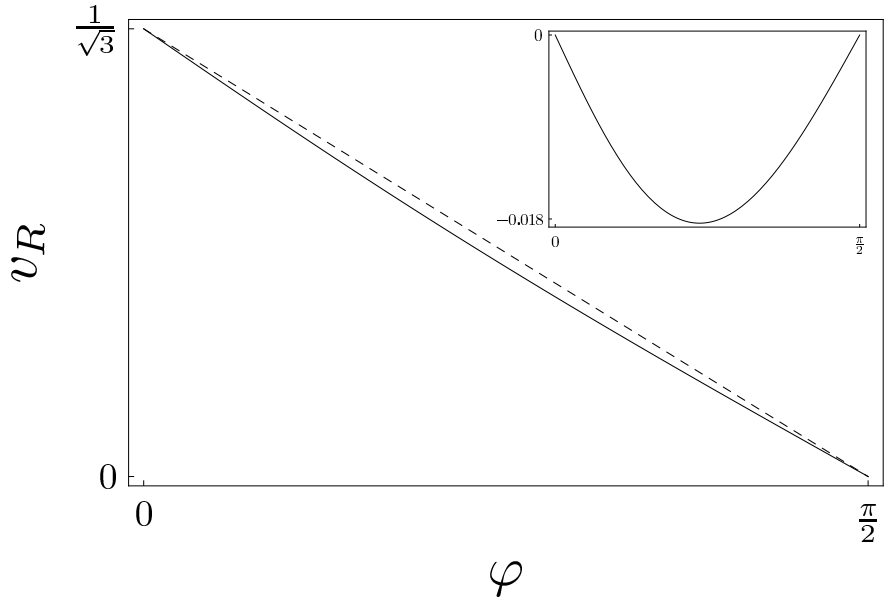

FIG. 2: The velocity of the $v_R(\varphi)$ for the one-parameter family of quantum walks defined by the coin operator $C_G(\varphi)$ (12). Despite the rather complicated formula (13) for $v_R(\varphi)$ we see that it decreases almost linearly with φ. The dashed curve corresponds to the straight line $\frac{1}{\sqrt{3}}(1-2\varphi/\pi)$. The inset shows the difference of the two curves.

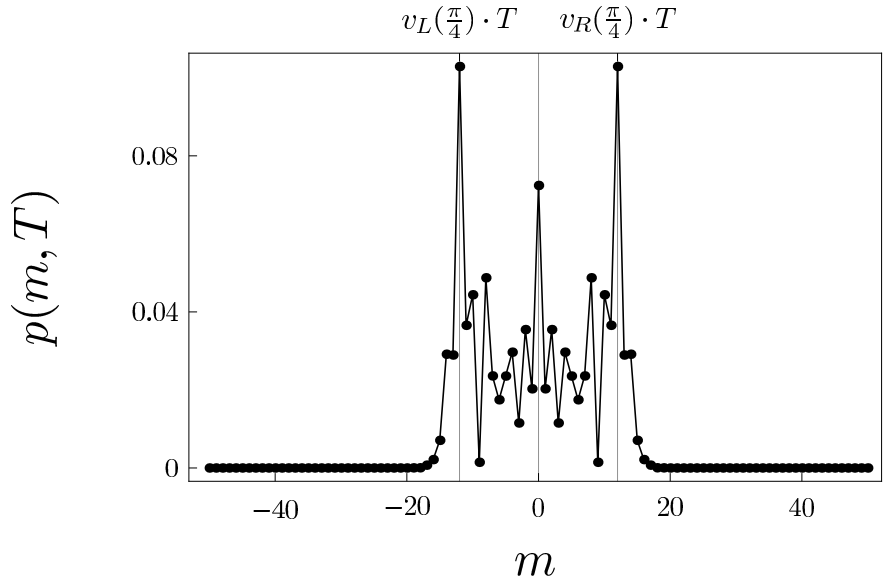

FIG. 3: The probability distribution of the three-state walk with the coin operator $C_1(\pi/4)$ after $T = 50$ steps. As for the Grover walk we have chosen the initial coin state according to $\psi_C = \frac{1}{\sqrt{3}}(1,-1,1)$. When compared with Figure 1 we find that the spreading of the probability distribution is much slower than for the Grover walk. Indeed, for $\varphi = \pi/4$ the peak velocities drops down to $v_{L,R}(\pi/4) \approx \pm 0.27$, which is less than a half of the velocities for the Grover walk.

We have only changed the sign of the diagonal element which ensures that C has the same spectrum as the Grover matrix. Nevertheless, the corresponding quantum walk is the same as the walk with the permutation coin Π. The

walk is trivially localizing and the peak velocities equal zero. The second coin operator we consider is given by

$$C' = \begin{pmatrix} -1 & 0 & 0 \\ 0 & 1 & 0 \\ 0 & 0 & -1 \end{pmatrix}.$$

The dynamics of the resulting quantum walk is simple. The $|S\rangle$ component of the initial state remains at the origin which corresponds to localization. The $|L\rangle$ ($|R\rangle$) component moves in every step to the left (right). After t steps the particle can be found only on three lattice points - either $m = 0$ or $m = \pm t$. In contrast to the walk driven by the coin C the walk with coin C' spreads through the lattice with the maximal possible peak velocities $v_{L,R} = \pm 1$.

In order to connect the Grover matrix and the matrices C and C' we examine their eigenvectors. The eigenvectors of the Grover matrix were given in (10). The eigenvectors of C are

$$\begin{aligned} u_1 &= (0,-1,0)^T, \\ u_2 &= \frac{1}{\sqrt{2}}(1,0,-1)^T, \\ u_3 &= \frac{1}{\sqrt{2}}(1,0,1)^T. \end{aligned}$$

Finally, the eigenvectors of C' are given by

$$\begin{aligned} w_1 &= \frac{1}{\sqrt{2}}(1,0,1)^T, \\ w_2 &= \frac{1}{\sqrt{2}}(1,0,-1)^T, \\ w_3 &= (0,1,0)^T. \end{aligned}$$

The first two eigenvectors correspond to the eigenvalue -1 while the third one has the eigenvalue 1. Notice that the second eigenvector can be chosen such that it is always the same. We parameterize the eigenvectors in such a way that they continuously change from $u_{1,3}$ to $w_{1,3}$ while remaining mutually orthogonal and normalized. This parametrization is given by

$$\begin{aligned} v_1(\rho) &= \left(\frac{\rho}{\sqrt{2}}, -\sqrt{1-\rho^2}, \frac{\rho}{\sqrt{2}}\right)^T, \\ v_2(\rho) &= \frac{1}{\sqrt{2}}(1,0,-1)^T, \\ v_3(\rho) &= \left(\sqrt{\frac{1-\rho^2}{2}}, \rho, \sqrt{\frac{1-\rho^2}{2}}\right)^T. \end{aligned}$$

With these vectors we construct the following one-parameter set of coin operators

$$\begin{aligned} C_2(\rho) &= -P_1(\rho) - P_2(\rho) + P_3(\rho) \\ &= \begin{pmatrix} -\rho^2 & \rho\sqrt{2(1-\rho^2)} & 1-\rho^2 \\ \rho\sqrt{2(1-\rho^2)} & 2\rho^2-1 & \rho\sqrt{2(1-\rho^2)} \\ 1-\rho^2 & \rho\sqrt{2(1-\rho^2)} & -\rho^2 \end{pmatrix}. \end{aligned} \tag{14}$$

The matrices C and C' correspond to the values $\rho = 0$ and $\rho = 1$, respectively. The Grover matrix is given by the coin parameter $\rho = \frac{1}{\sqrt{3}}$.

We now show that the three-state quantum walks with the one-parameter family of coins (14) exhibits the localization effect and that the coin parameter ρ directly determines the peak velocities. In order to prove this we analyze the dispersion relations

$$\begin{aligned} \omega_{1,2}(k,\rho) &= \pm \arccos\left(\rho^2 - 1 - \rho^2 \cos k\right), \\ \omega_3(k,\rho) &= 0. \end{aligned} \tag{15}$$

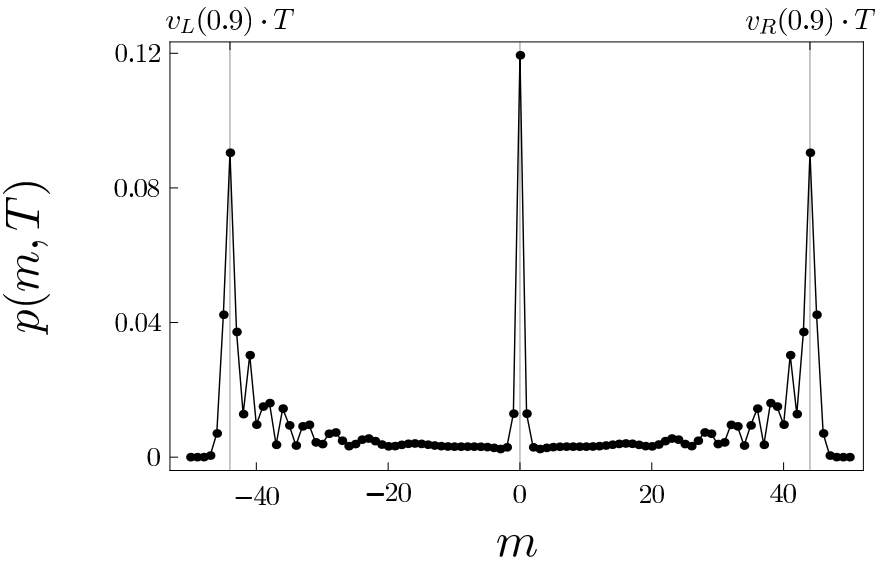

FIG. 4: The probability distribution of the three-state walk with the coin operator $C_2(\rho)$ after $T = 50$ steps. The initial coin state of the walk is $\psi_C = \frac{1}{\sqrt{2}}(1, 0, 1)$. As the coin parameter we have chosen $\rho = 0.9$. This results in much faster spreading of the probability distribution. The peaks appear at the position $\pm\rho \cdot T = \pm 45$, in accordance with the analytical result (16).

One of the frequencies is independent of the wavenumber, which guarantees the localization property of the corresponding one-parameter family of quantum walks with coin operator (14). Concerning the peak velocities, we have to determine for which wavenumber do the second derivatives of $\omega_{1,2}$ vanish. From their explicit form

$$\frac{\partial^2 \omega_{1,2}}{\partial k^2} = \pm \frac{\rho(\rho^2 - 1)\sqrt{1 - \cos k}}{(2 - \rho^2 + \rho^2 \cos k)^{\frac{3}{2}}}$$

we see that they are both equal to zero for $k_0 = 0$. Hence, the peak velocities are given by

$$\begin{aligned} v_R(\rho) &= \lim_{k \to 0^+} \frac{\partial \omega_2}{\partial k} = \rho, \\ v_L(\rho) &= \lim_{k \to 0^+} \frac{\partial \omega_1}{\partial k} = -\rho. \end{aligned} \tag{16}$$

Since ρ can be varied from zero to one we can achieve faster spreading than for the Grover walk. We illustrate these results in Figure 4.

V. CONCLUSIONS

We have introduced two deformations of the Grover walk which preserve its localization nature. The coin parameters determine the velocities of the peaks in the probability distributions of the particle's position. The two families of walks differ in the achievable rate of spreading across the lattice. For the first one the upper limit is given by the original Grover walk. In the second case this limit on the peak velocity can be broken.

The presented construction of two sets of coins can be extended to higher-dimensional quantum walks in a straightforward way. In fact, the family of 2D quantum walks studied in [27] can be obtained by the deformation of the eigenvectors of the 4×4 Grover matrix. Concerning the deformation based on the modification of the spectrum, one has to diagonalize the Grover matrix together with a permutation matrix which interchanges the displacements that mutually cancels each other. There is a unique eigenvector corresponding to eigenvalue -1 for the Grover matrix and eigenvalue 1 for the permutation. A construction similar to the one given in (12) yields a one-parameter set of coins preserving localization.

Our results show that localization effect can be found for a set of quantum walks. The presented construction is a step in a systematic classification of localizing quantum walks not only on a line but also in higher dimensions. It remains an open question if there exist coin operators outside the two families we have identified which also lead to localization.

Acknowledgments

We acknowledge the financial support from MSM 6840770039, MSMT LC06002 and SGS11/132/OHK4/2T/14.

[1] Y. Aharonov, L. Davidovich, N. Zagury, Phys. Rev. A **48**, 1687 (1993)
[2] B.D. Hughes, *Random walks and random environments, Vol. 1: Random walks* (Oxford University Press, Oxford, 1995)
[3] P. Knight, E. Roldan, J. Sipe, Phys. Rev. A **68**, 020301 (2003)
[4] A. Kempf, R. Portugal, Phys. Rev. A **79**, 052317 (2009)
[5] D. Aharonov, A. Ambainis, J. Kempe, U. Vazirani, , in *Proceedings of the 33th STOC* (ACM, New York, NY, 2001), p. 50
[6] N. Shenvi, J. Kempe, K. Whaley, Phys. Rev. A **67**, 052307 (2003)
[7] A. Ambainis, J. Kempe, A. Rivosh, , in *Proceedings of the 16th Annual ACM-SIAM Symposium on Discrete Algorithms* (2005), p. 1099
[8] M. Santha, *Quantum walk based search algorithms*, in *Theory and Applications of Models of Computation*, edited by M. Agrawal, D. Z. Du, Z. H. Duan and A. S. Li (Springer, Berlin, 2008), Vol. 4978 of *Lecture Notes in Computer Science*, p. 31
[9] B. Tregenna, W. Flanagan, R. Maile, V. Kendon, New J. Phys. **5**, 83 (2003)
[10] A. Ambainis, E. Bach, A. Nayak, A. Vishwanath, J. Watrous, , in *Proceedings of the 33th STOC* (ACM, New York, NY, 2001), p. 60
[11] M. Štefaňák, T. Kiss, I. Jex, New J. Phys. **11**, 043027 (2009)
[12] M. Štefaňák, I. Jex, T. Kiss, Phys. Rev. Lett. **100**, 020501 (2008)
[13] N. Konno, Quantum Inform. Comput. **2**, 578 (2002)
[14] N. Konno, J. Math. Soc. Jpn. **57**, 1179 (2005)
[15] G. Grimmett, S. Janson, P. Scudo, Phys. Rev. E **69**, 026119 (2004)
[16] N. Konno, *Quantum Walks*, in *Quantum Potential Theory*, edited by M. Schurmann and U. Franz (Springer, Berlin, 2008), Vol. 1954 of *Lecture Notes In Mathematics*, p. 309
[17] N. Inui, N. Konno, E. Segawa, Phys. Rev. E **72**, 056112 (2005)
[18] N. Inui, N. Konno, Physica A **353**, 133 (2005)
[19] B. Kollár, M. Štefaňák, T. Kiss, I. Jex, Phys. Rev. A **82**, 012303 (2010)
[20] N. Inui, Y. Konishi, N. Konno, Phys. Rev. A **69**, 052323 (2004)
[21] Y. Yin, D.E. Katsanos, S.N. Evangelou, Phys. Rev. A **77**, 022302 (2008)
[22] N. Konno, Quantum Inf. Process. **9**, 405 (2010)
[23] A. Schreiber, K.N. Cassemiro, V. Potoček, A. Gábris, I. Jex, C. Silberhorn, Phys. Rev. Lett. **106**, 180403 (2011)
[24] A. Joye, M. Merkli, J. Stat. Phys. **140**, 1025 (2010)
[25] A. Ahlbrecht, V.B. Scholz, A.H. Werner, J. Math. Phys. **52**, 042201 (2011)
[26] R. Wong, *Asymptotic Approximations of Integrals* (SIAM, Philadelphia, 2001)
[27] K. Watabe, N. Kobayashi, M. Katori, N. Konno, Phys. Rev. A **77**, 062331 (2008)

Stability Of Point Spectrum For Three-State Quantum Walks On A Line

M. Štefaňák,[1] I. Bezděková,[1] I. Jex,[1] and S. M. Barnett[2]

[1] *Department of Physics, Faculty of Nuclear Sciences and Physical Engineering, Czech Technical University in Prague, Břehová 7, 115 19 Praha 1 - Staré Město, Czech Republic*
[2] *School of Physics & Astronomy, University of Glasgow, Glasgow G12 8QQ, Scotland, U.K.*

Evolution operators of certain quantum walks possess, apart from the continuous part, also point spectrum. The existence of eigenvalues and the corresponding stationary states lead to partial trapping of the walker in the vicinity of the origin. We analyze the stability of this feature for three-state quantum walks on a line subject to homogenous coin deformations. We find two classes of coin operators that preserve the point spectrum. These new classes of coins are generalizations of coins found previously by different methods and shed light on the rich spectrum of coins that can drive discrete-time quantum walks.

I. INTRODUCTION

Quantum walks [1] have become quite popular in the last few years. This is motivated by their potential applications in quantum information theory [2], statistical physics [3, 4] and transport theory [5]. Additional interest in quantum walks was stimulated by the now considerable number of experiments [6–13] which have demonstrated the basic properties of quantum walks. They have shown in an impressive way the quantum coherence which is needed for their realization. Among the basic effects associated with quantum walks is the fast spreading of the walker across the underlying grid.

The key role in the analysis of the quantum walk plays the determination of the spectrum of the unitary evolution operator. For quantum walks with homogeneous coin on infinite lattice one can employ Fourier analysis [14], which reduces this problem to that of finding the eigenvalues of a finite-size matrix dependent on the wave-number k. The ballistic spreading of the quantum walk can be deduced from the analogy with wave theory. The continuous spectrum of the evolution operator corresponds to the k-dependent eigenvalues which can be described by dispersion relations. This allows one to find the group velocity and its distribution [15] which determines the propagation of the wave packets. The peaks in the probability distribution of the quantum walk propagate at constant rate given by the maximum of the group velocity [16]. However, the evolution operators of certain quantum walks also have a non-empty point spectrum, which is represented by k-independent eigenvalues. In such a case, the evolution does not consist of purely ballistic spreading. Indeed, as the walker spreads through the lattice its wave-function overlaps with the stationary states. The walker is therefore partially trapped in the vicinity of the origin. This feature, also known as localization, was found in the three-state walk on a line with the Grover coin operator [17, 18], where the evolution operator has one eigenvalue equal to unity. Similarly, Grover walk on a square lattice also has a point spectrum [19] consisting of ± 1. This can be exploited for a number of effects. The form of the spectrum can be used to sculpture the shape of the walker's wave packet, the walker can be trapped at particular position and can also lead to the effect of full revival [20], where the walker's wave-packet undergoes a periodic time-evolution. It may be anticipated, however, that the presence of the point spectrum will be highly sensitive to the choice of the coin operator. Even a small perturbation in a wrong direction can eliminate the eigenvalues. This can be crucial for experimental realizations of such quantum walks, where the imperfections in all operations has to be taken into account. In [21] the authors have analyzed a one-parameter modification of the Grover walk on a square lattice which preserves the point spectrum. The coin parameter controls the rate at which the particle spread through the lattice. We have extended this idea to three-state walk [22] on a line and found two one-parameter families of walks with point spectrum. Their coin operators are constructed as either eigenvalue or eigenvector deformations of the Grover coin. It is not clear, however, whether the two sets exhaust all possible three-state walks with point spectrum. The present paper aims to address this issue. The determination of coin families with a point spectrum contribute significantly to the classification of coins with respect to their physical properties, i.e. to localizing and non-localizing coins. Even though this is a very crude classification it certainly helps and in addition it simplifies experimental considerations when the wave packet propagating as a quantum walk is of interest.

The paper is organized as follows: In Section II we find the conditions on the coin operator which guarantees that the evolution operator of the quantum walk has a point spectrum. We solve these requirements in Section III with the help of a particular parametrization of the unitary group. We find three trivial solutions and two non-trivial ones. In Section IV we analyze the dependence of the rate of spreading of the walk through the lattice on the remaining coin parameters. Finally, we study the trapping of the walker in Section V. We conclude and present an outlook in Section VI.

II. CHARACTERISTIC EQUATION AND CONDITIONS ON THE COIN OPERATOR

We consider a three-state discrete-time quantum walk on a line with a homogeneous coin operator $\hat{C}$. We denote the basis coin states as $|L\rangle$, $|S\rangle$ and $|R\rangle$, which correspond to the step to the left, staying at the present position and the step to the right. The simplest way to solve the dynamics is to analyze it in the momentum representation [14]. In the Fourier representation the evolution operator has the form

$$\tilde{U}(k) = D\left(e^{-ik}, 1, e^{ik}\right) \cdot C, \tag{1}$$

where D denotes a diagonal matrix and C is the matrix representation of the coin operator with matrix elements

$$C_{ij} = \langle i|\hat{C}|j\rangle, \text{ with } i,j = L,\ S,\ R. \tag{2}$$

We are interested in quantum walks which show the localization effect. This feature corresponds to the fact that the evolution operator in the Fourier representation (1) has an eigenvalue independent of k. Note that if (1) has two eigenvalues independent of k, the third one has to be also constant. This follows immediately from the fact that the determinant of (1) is the same as determinant of C which is independent of k. The case when the evolution operator (1) has all three eigenvalues independent of k leads to a trivial quantum walk with no spreading. Let us therefore assume that only one eigenvalue of the evolution operator is independent of k. Then we can always put the eigenvalues into the form

$$\lambda_0 = e^{i\varphi}, \quad \lambda_{1,2}(k) = e^{\pm i\omega(k)}, \tag{3}$$

simply by multiplying the coin operator by a global phase factor, which does not influence the overall dynamics. The function $\omega(k)$ has to be real for all k, since the evolution operator $\tilde{U}(k)$ is unitary and its eigenvalues must be of modulus 1. Consider the characteristic equation

$$\det\left(\tilde{\mathrm{U}}(\mathrm{k}) - \lambda\right) = (\lambda_0 - \lambda)(\lambda_1 - \lambda)(\lambda_2 - \lambda) = 0. \tag{4}$$

The terms with same power of λ on the left and the right hand side of the equation give the following relations

λ^0: $\quad e^{i\varphi} = \det C$

λ^1: $\quad 1 + e^{i\varphi}\left(e^{i\omega(k)} + e^{-i\omega(k)}\right) = m_L e^{ik} + m_S + m_R e^{-ik}.$

λ^2: $\quad e^{i\varphi} + e^{i\omega(k)} + e^{-i\omega(k)} = C_{LL}e^{-ik} + C_{SS} + C_{RR}e^{ik}$

Here we have denoted by m_i the minors of the coin operator, i.e.

$$m_L = \det\begin{pmatrix} C_{SS} & C_{SR} \\ C_{RS} & C_{RR} \end{pmatrix}, \quad \mathrm{m_S} = \det\begin{pmatrix} C_{LL} & C_{LR} \\ C_{RL} & C_{RR} \end{pmatrix}, \quad \mathrm{m_R} = \det\begin{pmatrix} C_{LL} & C_{LS} \\ C_{SL} & C_{SS} \end{pmatrix}. \tag{5}$$

The third equation leads to the dispersion relations determining the $\omega(k)$ in the form

$$2\cos\omega(k) = C_{LL}e^{-ik} + C_{SS} + C_{RR}e^{ik} - e^{i\varphi}. \tag{6}$$

This function has to be real for all k, which is only possible if

$$C_{LL} = C_{RR}^* = \rho e^{i\gamma}, \quad C_{SS} = e^{i\varphi} - 2\mu, \quad \rho,\ \gamma,\ \mu \in \mathbb{R}, \tag{7}$$

where the star denotes the complex conjugation. The dispersion relations then attain a simple form

$$\cos\omega(k) = \rho\cos(k - \gamma) - \mu. \tag{8}$$

Note that they are fully determined by the diagonal elements of the coin operator. Moreover, if $\rho = 0$, i.e. when $C_{LL} = C_{RR} = 0$, then ω is constant. In such a case the evolution operator has purely point spectrum and the quantum walk is trivial - it does not spread at all.

Let us now consider the terms with λ^1 which lead us to the dispersion relations in the form

$$2\cos\omega(k) = e^{-i\varphi}\left(m_L e^{ik} + m_S + m_R e^{-ik} - 1\right). \tag{9}$$

Comparing this formula with (6) we find the following conditions involving the off-diagonal elements of C

$$C_{LL} = e^{-i\varphi}\left(C_{LL}C_{SS} - C_{LS}C_{SL}\right), \tag{10}$$

$$C_{RR} = e^{-i\varphi}\left(C_{RR}C_{SS} - C_{SR}C_{RS}\right) = C_{LL}^*, \tag{11}$$

$$C_{SS} - e^{i\varphi} = e^{-i\varphi}\left(C_{LL}C_{RR} - C_{LR}C_{RL} - 1\right). \tag{12}$$

Moreover, the matrix C has to be unitary.

III. PARAMETRIZATION OF THE UNITARY GROUP

In order to find coins which satisfy the conditions (10)-(12) we first parameterize the three-dimensional unitary group, which has a dimension nine, in the following way [23]

$$C = D\left(e^{i\alpha_1}, e^{i\alpha_2}, e^{i\alpha_3}\right) \cdot V \cdot D\left(e^{i\beta_1}, e^{i\beta_2}, e^{i\beta_3}\right). \tag{13}$$

Here the matrix V is the quark mixing matrix

$$V = \begin{pmatrix} c_{12}c_{13} & c_{13}s_{12} & e^{-i\delta}s_{13} \\ -c_{23}s_{12} - e^{i\delta}c_{12}s_{13}s_{23} & c_{12}c_{23} - e^{i\delta}s_{12}s_{13}s_{23} & c_{13}s_{23} \\ s_{12}s_{23} - e^{i\delta}c_{12}c_{23}s_{13} & -c_{12}s_{23} - e^{i\delta}c_{23}s_{12}s_{13} & c_{13}c_{23} \end{pmatrix}, \tag{14}$$

familiar from the Standard model [24]. For brevity we have used the notation

$$c_{ij} = \cos\theta_{ij}, s_{ij} = \sin\theta_{ij}. \tag{15}$$

The mixing matrix has four real parameters $\theta_{12}, \theta_{13}, \theta_{23}$ and δ. The five remaining independent parameters are

$$\gamma_1 = \alpha_1 + \beta_1,\ \gamma_2 = \alpha_1 + \beta_2,\ \gamma_3 = \alpha_1 + \beta_3,\ \gamma_4 = \alpha_2 + \beta_1,\ \gamma_5 = \alpha_3 + \beta_1. \tag{16}$$

With this parametrization a general 3x3 unitary matrix is given by

$$C = \begin{pmatrix} e^{i\gamma_1}c_{12}c_{13} & e^{i\gamma_2}c_{13}s_{12} & e^{-i(\delta-\gamma_3)}s_{13} \\ -e^{i\gamma_4}\left(c_{23}s_{12} + e^{i\delta}c_{12}s_{13}s_{23}\right) & e^{-i(\gamma_1-\gamma_2-\gamma_4)}\left(c_{12}c_{23} - e^{i\delta}s_{12}s_{13}s_{23}\right) & e^{-i(\gamma_1-\gamma_3-\gamma_4)}c_{13}s_{23} \\ e^{i\gamma_5}\left(s_{12}s_{23} - e^{i\delta}c_{12}c_{23}s_{13}\right) & -e^{-i(\gamma_1-\gamma_2-\gamma_5)}\left(c_{12}s_{23} + e^{i\delta}c_{23}s_{12}s_{13}\right) & e^{-i(\gamma_1-\gamma_3-\gamma_5)}c_{13}c_{23} \end{pmatrix}. \tag{17}$$

Note that the determinant of C equals

$$\det C = e^{i\varphi} = e^{-i(\gamma_1-\gamma_2-\gamma_3-\gamma_4-\gamma_5)}. \tag{18}$$

Let us now turn to the requirements for the non-empty point spectrum of the evolution operator. The relations (10) and (11) lead to the condition

$$c_{13}\left(c_{12} - e^{i(\gamma_3+\gamma_5)}c_{23}\right) = 0. \tag{19}$$

This is satisfied in the following cases:

1. $c_{13} = 0$, i.e. $\theta_{13} = \frac{\pi}{2}$ - trivial solution, no dynamics

   The coin operator has the form

   $$C = \begin{pmatrix} 0 & 0 & e^{-i(\delta-\gamma_3)} \\ -e^{i\gamma_4}\left(c_{23}s_{12} + e^{i\delta}c_{12}s_{23}\right) & e^{-i(\gamma_1-\gamma_2-\gamma_4)}\left(c_{12}c_{23} - e^{i\delta}s_{12}s_{23}\right) & 0 \\ e^{i\gamma_5}\left(s_{12}s_{23} - e^{i\delta}c_{12}c_{23}\right) & -e^{-i(\gamma_1-\gamma_2-\gamma_5)}\left(c_{12}s_{23} + e^{i\delta}c_{23}s_{12}\right) & 0 \end{pmatrix}. \tag{20}$$

   Since $C_{LL} = C_{RR} = 0$, the evolution operator does not have a continuous spectrum.

   We note that the alternative choice of $\theta_{13} = -\frac{\pi}{2}$ results in an equivalent matrix (in the sense of the properties of the quantum walk). The same will apply to other solutions of equation (19) given bellow. We will therefore always treat only one possible choice of the angles in the range $(-\pi, \pi)$.

2. $c_{12} = c_{23} = 0$, i.e. $\theta_{12} = \theta_{23} = \frac{\pi}{2}$ - trivial solution, no dynamics

   The coin operator has the form

   $$C = \begin{pmatrix} 0 & e^{i\gamma_2}c_{13} & e^{-i(\delta-\gamma_3)}s_{13} \\ 0 & -e^{i(\delta-\gamma_1+\gamma_2+\gamma_4)}s_{13} & e^{-i(\gamma_1-\gamma_3-\gamma_4)}c_{13} \\ e^{i\gamma_5} & 0 & 0 \end{pmatrix}. \tag{21}$$

   Since $C_{LL} = C_{RR} = 0$, the evolution operator does not have a continuous spectrum.

3. $\gamma_3 = -\gamma_5$, $c_{12} = c_{23}$

From the equation (12) follows the condition

$$(\sin(\gamma_1 - \gamma_2 - \gamma_4) - \sin(\delta - \gamma_1 + \gamma_2 + \gamma_4)s_{13})s_{23} = 0. \tag{22}$$

This requires that one of the following is satisfied:

(a) $s_{23} = 0$, i.e. $\theta_{23} = 0$ - trivial solution, decoupling

$$C = \begin{pmatrix} e^{i\gamma_1}c_{13} & 0 & e^{-i(\delta+\gamma_5)}s_{13} \\ 0 & e^{-i(\gamma_1-\gamma_2-\gamma_4)} & 0 \\ -e^{i(\delta+\gamma_5)}s_{13} & 0 & e^{-i\gamma_1}c_{13} \end{pmatrix} \tag{23}$$

In this case the state of the coin $|S\rangle$ is decoupled from the other two states $|L, R\rangle$. The walk reduces to a two-state walk and the $|S\rangle$ component of the initial state remains at the origin.

(b) $\delta = 0$, $\gamma_1 = \gamma_2 + \gamma_4$ - nontrivial solution

In this case the coin operator is given by the following matrix

$$C_1 = \begin{pmatrix} e^{i(\gamma_2+\gamma_4)}c_{13}c_{23} & e^{i\gamma_2}c_{13}s_{23} & e^{-i\gamma_5}s_{13} \\ -e^{i\gamma_4}c_{23}(1+s_{13})s_{23} & c_{23}^2 - s_{13}s_{23}^2 & e^{-i(\gamma_2+\gamma_5)}c_{13}s_{23} \\ e^{i\gamma_5}\left(-c_{23}^2 s_{13} + s_{23}^2\right) & -e^{-i(\gamma_4-\gamma_5)}c_{23}(1+s_{13})s_{23} & e^{-i(\gamma_2+\gamma_4)}c_{13}c_{23} \end{pmatrix}, \tag{24}$$

which depends on five parameters $\gamma_2, \gamma_4, \gamma_5, \theta_{13}$ and θ_{23}. The dispersion relations (8) now reads

$$\omega(k) = \arccos\left[c_{13}c_{23}\cos(k - \gamma_2 - \gamma_4) - \frac{1}{2}s_{23}^2(1 + s_{13})\right]. \tag{25}$$

Notice that for

$$\gamma_2 = \gamma_4 = \gamma_5 = 0, \quad \theta_{13} = \arcsin(1 - \rho^2), \quad \theta_{23} = \arccos\left(-\frac{\rho}{\sqrt{2-\rho^2}}\right)$$

the coin operator (24) reduces to

$$C_\rho = \begin{pmatrix} -\rho^2 & \rho\sqrt{2-2\rho^2} & 1-\rho^2 \\ \rho\sqrt{2-2\rho^2} & -1+2\rho^2 & \rho\sqrt{2-2\rho^2} \\ 1-\rho^2 & \rho\sqrt{2-2\rho^2} & -\rho^2 \end{pmatrix}.$$

This is the family of coin operators we have found in [22] through the deformation of eigenvectors of the Grover matrix.

(c) $\delta \neq \gamma_1 - \gamma_2 - \gamma_4$, $s_{13} = \frac{\sin(\gamma_1-\gamma_2-\gamma_4)}{\sin(\delta-\gamma_1+\gamma_2+\gamma_4)}$ - nontrivial solution

In this case, the coin operator equals

$$C_2 = \begin{pmatrix} e^{i\gamma_1}c_{23}B & e^{i\gamma_2}Bs_{23} & -e^{-i(\delta+\gamma_5)}A\sin\kappa \\ -e^{i(\gamma_1-\gamma_2)}As_{23}c_{23}\sin\delta & e^{i\kappa}\left(c_{23}^2 + e^{i\delta}As_{23}^2\sin\kappa\right) & e^{-i(\gamma_1-\gamma_4+\gamma_5)}Bs_{23} \\ e^{i\gamma_5}\left(s_{23}^2 + e^{i\delta}c_{23}^2 A\sin\kappa\right) & -e^{-i(\gamma_4-\gamma_5)}As_{23}c_{23}\sin\delta & e^{-i\gamma_1}c_{23}B \end{pmatrix}. \tag{26}$$

For brevity we have used the notation

$$\kappa = \gamma_2 + \gamma_4 - \gamma_1, \quad A = \frac{1}{\sin(\delta+\kappa)}, \quad B = \sqrt{A^2\sin\delta\sin(\delta+2\kappa)}. \tag{27}$$

The set of solutions C_2 depends on six parameters, namely $\gamma_1, \gamma_2, \gamma_4, \gamma_5, \delta$ and θ_{23}. We note that this class of coins is well defined only when the condition

$$-1 \leq s_{13} \leq 1, \text{ i.e. } -1 \leq \frac{\sin\kappa}{\sin(\delta+\kappa)} \leq 1, \tag{28}$$

is satisfied. The dispersion relations are now determined by

$$\omega(k) = \arccos\left[Bc_{23}\cos(k-\gamma_1) - \frac{1}{2}As_{23}^2\sin\delta\right]. \tag{29}$$

Notice that for the choice of the parameters

$$\gamma_1 = \gamma_2 = \pi, \quad \theta_{23} = -\arctan 2, \quad \gamma_4 = \gamma_5 = -\varphi, \quad \delta = \varphi + \operatorname{arccotan}\left(\frac{2\cot\varphi}{3}\right)$$

the coin operator (26) reduces to

$$C_\varphi = \begin{pmatrix} -\frac{\cos\varphi}{3} & \frac{2\cos\varphi}{3} & \frac{2\cos\varphi}{3} - i\sin\varphi \\ \frac{2\cos\varphi}{3} & -\frac{\cos\varphi}{3} - i\sin\varphi & \frac{2\cos\varphi}{3} \\ \frac{2\cos\varphi}{3} - i\sin\varphi & \frac{2\cos\varphi}{3} & -\frac{\cos\varphi}{3} \end{pmatrix}.$$

This set is up to a global phase factor $e^{i\varphi}$ equal to the one-parameter family we have found in [22] by the deformation of eigenvalues of the Grover matrix.

The solutions C_1 and C_2 represents all coin operators which result in three-state quantum walk with point spectrum. Before we proceed with the analysis of their physical properties we point out that the derived results imply that the existence of point spectrum is a rather rare feature. Indeed, the found solutions depend on five, respectively six parameters, while a general coin operator depends on nine parameters. Hence, both families of coins C_1 and C_2 represent a set of zero measure in the unitary group $U(3)$.

IV. PEAK VELOCITIES OF THE RESULTING QUANTUM WALKS

Let us now analyze the coin operators we have found in more detail. As a first physical parameter we consider the peak velocity [16] which describes the rate of spreading of the quantum walk through the lattice. The peak velocity is determined as the maximum of the group velocity $v = \frac{d\omega}{dk}$. Notice that for both sets of coins C_1 and C_2 the dispersion relations are of the form

$$\omega(k) = \arccos\left(\rho\cos(k-\gamma) - \mu\right). \tag{30}$$

To determine the peak velocity of the corresponding quantum walk we have to find k_0 such that the second derivative of ω vanishes. This leads us to the equation

$$\rho\mu(1+\cos^2(k_0-\gamma)) + (1-\rho^2-\mu^2)\cos(k_0-\gamma) = 0. \tag{31}$$

The solutions are given by

$$k_0 = \gamma \pm \arccos\Delta, \tag{32}$$

where we have denoted

$$\Delta = \frac{\rho^2+\mu^2-1+\sqrt{(1-\rho^2-\mu^2)^2-4\rho^2\mu^2}}{2\rho\mu}. \tag{33}$$

The peak velocities are then found by evaluating the first derivative of ω at the point k_0. We obtain the following result

$$v_{peak} = \frac{\rho\sqrt{1-\Delta^2}}{\sqrt{1-(\mu-\rho\Delta)^2}}. \tag{34}$$

Note that neither Δ nor v_{peak} depend on γ, so this parameter does not have a dynamical consequence.

A. The class C_1

For the set of coin operators C_1 the parameters ρ and μ are given by

$$\rho = \cos\theta_{13}\cos\theta_{23}, \quad \mu = \frac{1}{2}(1+\sin\theta_{13})\sin^2\theta_{23}. \tag{35}$$

We find that for the five-parameter family of coins C_1 the peak velocity depends only on two, namely θ_{13} and θ_{23}. The choice of the parameters $\gamma_2, \gamma_4, \gamma_5$ does not influence the dynamics of the quantum walk.

The peak velocity as a function of θ_{13} and θ_{23} is displayed in Figure 1. As expected, the peak velocity is zero for $\theta_{13} = \pm\pi/2$ and $\theta_{23} = \pm\pi/2$, since these parameters correspond to the trivial solutions. The peak velocity is smooth except for the curve determined by

$$\cos\theta_{23} = \pm\frac{\cos\theta_{13}}{1+\sin\theta_{13}}, \tag{36}$$

where it has a discontinuous derivative. For a given θ_{23} the maximum of the peak velocity lies on this curve and is given by

$$v_{max} = \sqrt{\cos\theta_{23}\cos\left(2\arctan\left(\frac{1-\cos\theta_{23}}{1+\cos\theta_{23}}\right)\right)} \tag{37}$$

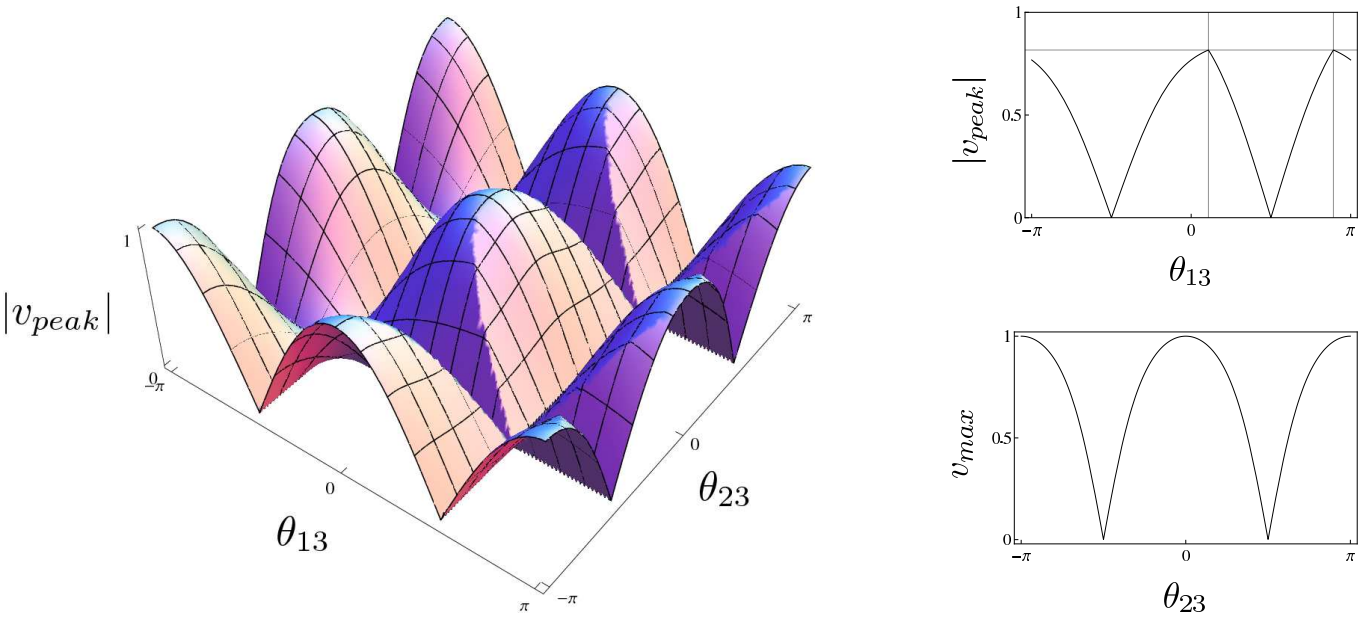

FIG. 1: On the left we show the absolute value of the peak velocity for the set of coin operators C_1 in dependence on the parameters θ_{13} and θ_{23}. The upper right plot displays the cut for θ_{23} equal to $\pi/4$. Notice the two spikes at the values of θ_{13} determined by Eq. (36). The lower right plot shows the maximum peak velocity for a given θ_{23} which is determined by Eq. (37).

B. The class C_2

In the second case the coefficients are equal to

$$\rho = \sqrt{\frac{\sin\delta\sin(\delta+2\kappa)}{\sin^2(\delta+\kappa)}}\cos\theta_{23}, \quad \mu = \frac{\sin\delta}{2\sin(\delta+\kappa)}\sin^2\theta_{23}. \tag{38}$$

We see that for the six-parameter family of coins C_2 the peak velocity depends only on three, namely δ, θ_{23} and κ which is a linear combination of γ_1, γ_2 and γ_4, see equation (27).

The peak velocity as a function of the angles δ and θ_{23} is shown in Figure 2 on the left. We fix the value of the remaining parameter $\kappa = \pi/5$. As before, the peak velocity vanishes for $\theta_{23} = \pm\pi/2$. On the right we display the maximum of the peak velocity as a function of κ. For a given κ, the maximum of the peak velocity is reached for $\theta_{23} = 0$ and $\delta = \pi/2 - \kappa$, and reduces to

$$v_{max} = |\cos\kappa|. \tag{39}$$

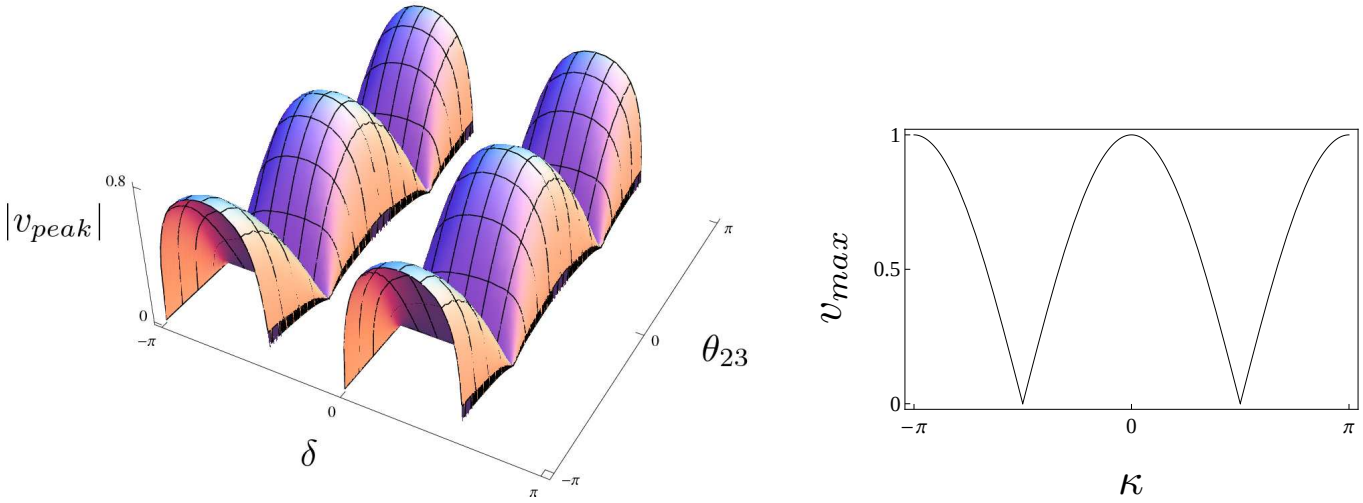

FIG. 2: On the left we show the peak velocity for the set of coin operators C_2. We have chosen the parameter $\kappa = \pi/5$. Due to the condition (28) not all values of δ are admissible. The maximum of the peak velocity as a function of the angle κ is shown on the right. The maximum is reached for the values $\theta_{23} = 0$ and $\delta = \pi/2 - \kappa$.

V. TRAPPING PROBABILITY

As we have already mentioned, the dynamics of the quantum walks we are interested in do not consist of just ballistic spreading. The existence of eigenvalue that is independent of k and the corresponding bound state leads to partial trapping of the walker at the origin. In this section we analyze this feature in more detail.

We denote by $v(k) = \left(v^L(k), v^S(k), v^R(k)\right)^T$ the momentum representation of the (non-normalized) stationary state, i.e. the eigenstate of the evolution operator (1) corresponding to the constant eigenvalue. By $n(k)$ we denote the square norm of this vector. In a similar way, we denote by $v_{1,2}(k)$ the (normalized) eigenvectors of (1) corresponding to eigenvalues $e^{\pm i\omega(k)}$ Let the initial state of the coin be equal to

$$|\varphi\rangle = \varphi^L|L\rangle + \varphi^S|S\rangle + \varphi^R|R\rangle. \tag{40}$$

The momentum representation of the initial state of the walk $|0\rangle \otimes |\varphi\rangle$ is then simply $\varphi = \left(\varphi^L, \varphi^S, \varphi^R\right)^T$. Using Fourier analysis [14] we find that the probability amplitude of particle being at the origin after t steps of the walk is given by

$$\begin{aligned}\psi(0,t) \;=\; & \int_{-\pi}^{\pi} \frac{dk}{2\pi}\, \frac{1}{n(k)}\, (v(k),\varphi)\, v(k) + \int_{-\pi}^{\pi} \frac{dk}{2\pi}\, e^{i\omega(k)t}\, (v_1(k),\varphi)\, v_1(k) + \\ & + \int_{-\pi}^{\pi} \frac{dk}{2\pi}\, e^{-i\omega(k)t}\, (v_2(k),\varphi)\, v_2(k).\end{aligned} \tag{41}$$

With the stationary phase approximation [25] one can show that the time-dependent integrals in (41) behave as $\sim t^{-\frac{1}{2}}$ for large values of t. Hence, in the limit $t \to +\infty$ only the first term in (41) remains and we find

$$\psi^{\varphi}_{\infty} \equiv \lim_{t\to+\infty} \psi(0,t) = \int_{-\pi}^{\pi} \frac{dk}{2\pi} \frac{1}{n(k)}\, (v(k),\varphi)\, v(k). \tag{42}$$

The localization probability is then equal to the square norm of the amplitude. Since we want to focus on the role of the coin operator on the walker trapping, we consider the initial coin state of the walker as the maximally mixed state. In such a case, the trapping probability can be expressed in the form

$$P_\infty = \frac{1}{3}\left(|\psi_\infty^L|^2 + |\psi_\infty^S|^2 + |\psi_\infty^R|^2\right), \tag{43}$$

where ψ_∞^j is the limiting amplitude for the initial coin state $|j\rangle$, i.e.

$$\psi_\infty^j = \int_{-\pi}^{\pi} \frac{dk}{2\pi} \frac{1}{n(k)} v^{j^*}(k) v(k), \quad j = L, S, R. \tag{44}$$

In the following we will see that k-dependence of the stationary state $v(k)$ involves only the term e^{ik}. The product $v^{j^*}(k)v(k)$ will be a linear combination of functions e^{-ik}, 1, e^{ik}. The square norm of the stationary state will be of the form

$$n(k) = a - 2b\cos(k - c). \tag{45}$$

This implies that the amplitudes (44) can be decomposed into integrals

$$I_n = \int_{-\pi}^{\pi} \frac{dk}{2\pi} \frac{e^{ink}}{a - 2b\cos(k-c)}, \quad n = -1, 0, 1. \tag{46}$$

Such an integral can be turned into a contour integral over a unit circle in a complex plane

$$I_n = \left\{ \begin{array}{c} e^{ik} = z \\ dk = \frac{dz}{iz} \end{array} \right\} = -\frac{1}{2\pi i} \oint \frac{z^n dz}{be^{-ic}z^2 - az + be^{ic}}, \tag{47}$$

which is easily evaluated with the help of the residues. We find the following result

$$I_0 = \frac{1}{\sqrt{a^2 - 4b^2}}, \qquad I_1 = I_{-1}^* = \frac{\frac{a}{\sqrt{a^2-4b^2}} - 1}{2b} e^{ic}. \tag{48}$$

Let us now specify the results for the two sets of coin operators.

A. The Class C_1

For the first class of the coins the stationary state is given by

$$v(k) = \begin{pmatrix} -e^{-i\gamma_5}(\sin\frac{\theta_{13}}{2} + \cos\frac{\theta_{13}}{2})s_{23} \\ e^{i(k-\gamma_2-\gamma_5)}(\sin\frac{\theta_{13}}{2} - \cos\frac{\theta_{13}}{2}) + e^{i(\gamma_4-\gamma_5)}(\sin\frac{\theta_{13}}{2} + \cos\frac{\theta_{13}}{2})c_{23} \\ -e^{ik}(\sin\frac{\theta_{13}}{2} + \cos\frac{\theta_{13}}{2})s_{23} \end{pmatrix}. \tag{49}$$

The square of the norm of this vector is equal to

$$n(k) = 2 + (1 + s_{13})s_{23}^2 - 2c_{13}c_{23}\cos(k - \gamma_2 - \gamma_4). \tag{50}$$

The parameters a, b and c are therefore

$$a = 2 + (1 + s_{13})s_{23}^2, \quad b = c_{13}c_{23}, \quad c = \gamma_2 + \gamma_4. \tag{51}$$

We find that the limiting amplitudes at the origin (44) are given by

$$\begin{aligned} \psi_\infty^L &= \begin{pmatrix} I_0(1 + s_{13})s_{23}^2 \\ e^{-i\gamma_2}(|I_1|c_{13} - I_0 c_{23}(1 + s_{13}))s_{23} \\ e^{i\gamma_5}|I_1|(1 + s_{13})s_{23}^2 \end{pmatrix}, \\ \psi_\infty^S &= \begin{pmatrix} e^{i\gamma_2}(|I_1|c_{13}s_{23} - I_0) \\ I_0(1 + c_{23}^2 - s_{13}s_{23}^2) - 2|I_1|c_{13}c_{23} \\ e^{i(\gamma_2+\gamma_5)}(I_0 c_{13}s_{23} - |I_1|(1 + s_{13})s_{23}c_{23}) \end{pmatrix}, \\ \psi_\infty^R &= \begin{pmatrix} e^{-i\gamma_5}|I_1|(1 + s_{13})s_{23}^2 \\ e^{-i(\gamma_2+\gamma_5)}(I_0 c_{13} - |I_1|(1 + s_{13})s_{23}c_{23}) \\ I_0(1 + s_{13})s_{23}^2 \end{pmatrix}. \end{aligned} \tag{52}$$

The trapping probability at the origin for a maximally mixed initial coin state then equals

$$\begin{aligned} P_\infty &= \frac{1}{3}I_0^2\left[1+c_{23}^4+\frac{1}{2}(2+s_{23}^2)^2+(s_{13}^2+2s_{13}-\frac{1}{2})s_{23}^4\right]- \\ &-\frac{4}{3}I_0|I_1|c_{13}c_{23}\left[1+c_{23}^2+(2+s_{13})s_{23}^2\right]- \\ &-\frac{4}{3}|I_1|^2(1+s_{13})(c_{23}^2s_{13}-1) \end{aligned} \tag{53}$$

Notice that the result is independent of the γ_i's. The only relevant parameters are the angles θ_{13} and θ_{23}, i.e. the same parameters which also determine the rate of spreading of the walk. We display the behaviour of the localization probability in Figure 3.

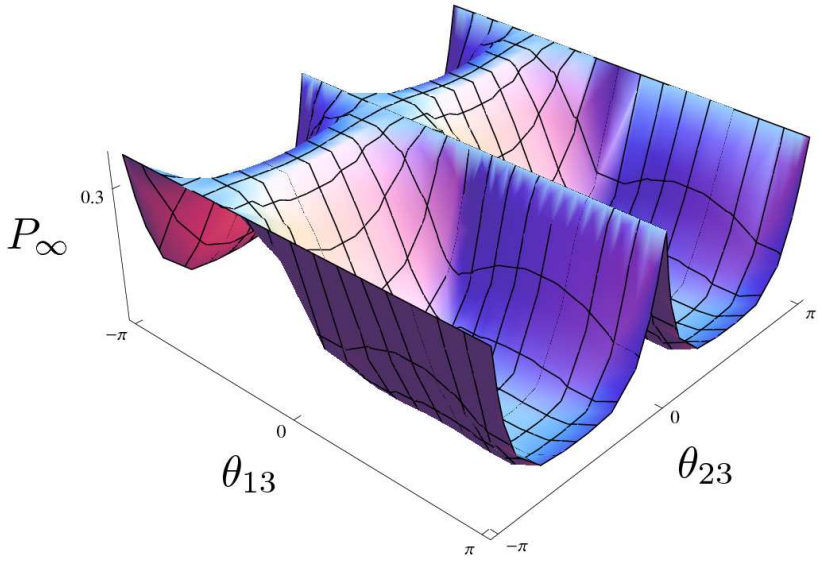

FIG. 3: Localization probability for the first class.

B. The Class C_2

In the second case the stationary state is equal to

$$v(k)=\begin{pmatrix} e^{i(\gamma_2+\gamma_4)}\sin\delta s_{23} \\ -e^{i(\gamma_1+\gamma_4)}\sin\delta c_{23}+e^{i(k+\gamma_4)}\sqrt{\sin\delta\sin(\delta+2\kappa)} \\ e^{i(k+\gamma_1+\gamma_5)}\sin\delta s_{13}\end{pmatrix}. \tag{54}$$

The normalization of this vector is given by the factor

$$n(k)=\sin\delta\left(\sin(\delta+2\kappa)+(1+s_{23}^2)\sin\delta-2c_{23}\sqrt{\sin\delta\sin(\delta+2\kappa)}\cos(k-\gamma_1)\right) \tag{55}$$

The parameters a, b, c are then given by

$$a=\sin\delta(\sin\delta(1+s_{23}^2)+\sin(\delta+2\kappa)),\quad b=\sin\delta c_{23}\sqrt{\sin\delta\sin(\delta+2\kappa)},\quad c=\gamma_1. \tag{56}$$

The probability amplitudes at the origin in the limit $t \to +\infty$ tend to the values

$$\begin{aligned}
\psi_\infty^L &= \begin{pmatrix} I_0 \sin^2\delta s_{23}^2 \\ e^{i(\gamma_1-\gamma_2)} \sin\delta s_{23}(|I_1|\sqrt{\sin\delta\sin(\delta+2\kappa)} - I_0 c_{23}\sin\delta) \\ e^{i(\gamma_1+\gamma_5-\kappa)}|I_1|\sin^2\delta s_{23}^2 \end{pmatrix}, \\
\psi_\infty^S &= \begin{pmatrix} e^{i(\gamma_2-\gamma_1)} \sin\delta s_{23}(|I_1|\sqrt{\sin\delta\sin(\delta+2\kappa)} - I_0 c_{23}\sin\delta) \\ \sin\delta(I_0(c_{23}^2\sin\delta + \sin(\delta+2\kappa)) - 2|I_1|c_{23}\sqrt{\sin\delta\sin(\delta+2\kappa)}) \\ e^{i(\gamma_1+\gamma_5-\gamma_4)} \sin\delta s_{23}(I_0\sqrt{\sin\delta\sin(\delta+2\kappa)} - |I_1|c_{23}\sin\delta) \end{pmatrix}, \\
\psi_\infty^R &= \begin{pmatrix} e^{i(\kappa-\gamma_1-\gamma_5)}|I_1|\sin^2\delta s_{23}^2 \\ e^{i(\gamma_4-\gamma_1-\gamma_5)} \sin\delta s_{23}(I_0\sqrt{\sin\delta\sin(\delta+2\kappa)} - |I_1|c_{23}\sin\delta) \\ I_0\sin^2\delta s_{23}^2 \end{pmatrix}.
\end{aligned} \tag{57}$$

Finally, the probability of finding the particle at the origin is given by

$$\begin{aligned}
P_\infty &= \frac{1}{3} I_0^2 \sin^2\delta \left[(c_{23}^2\sin\delta + \sin(\delta+2\kappa))^2 + 2\sin^2\delta s_{23}^4 + \right. \\
&\quad \left. + 2\sin\delta s_{23}^2 (c_{23}^2\sin\delta + \sin(\delta+2\kappa))\right] + \\
&\quad + \frac{2}{3}|I_1|^2\sin^3\delta\left[\sin\delta s_{23}^2 + (1+c_{23}^2)\sin(\delta+2\kappa)\right] - \\
&\quad - \frac{4}{3} I_0|I_1|c_{23}\sin^2\delta\left[(1+s_{23}^2)\sin\delta + \sin(\delta+2\kappa)\sqrt{\sin\delta\sin(\delta+2\kappa)}\right].
\end{aligned} \tag{58}$$

Note that the result depends on γ_i's only through $\kappa = \gamma_2 + \gamma_4 - \gamma_1$. The localization probability thus depend only on δ, θ_{23} and κ. These parameters also determine the peak velocity of the walk. We show the course of this function in Figure 4

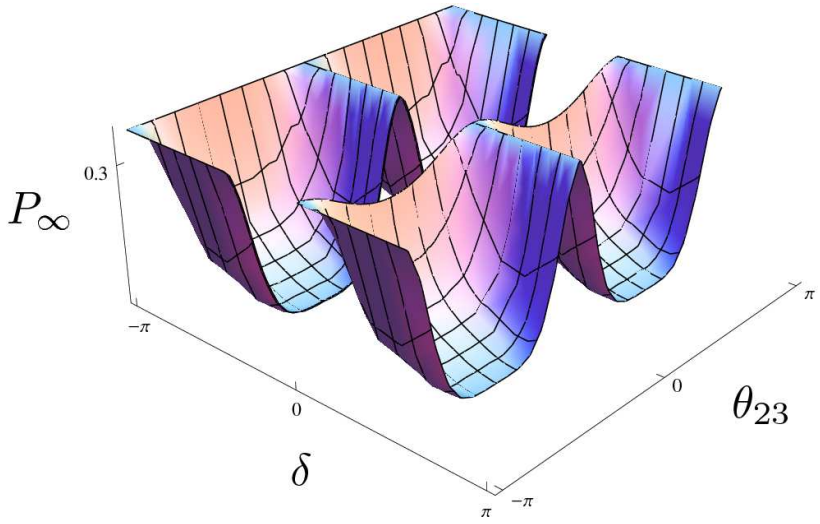

FIG. 4: Localization probability for the second class of coins. The parameter κ has been chosen equal to $\pi/5$. The admissible range of the parameter δ is limited by the condition (28).

VI. CONCLUSIONS

We have found two classes of coins for three state quantum walks on the line which have a point spectrum. Previously found coins [22] having this property are special cases of the defined classes. In this perspective our results complete the classification of three-step quantum walks on a line which exhibit the localization effect. The obtained formulas (24), (26) determine all coin operators leading to localizing quantum walks. The sets of coin operators depend on five, respectively six parameters. Our results imply that localization is a rare feature, since both families of coins represent a set of zero measure in the unitary group $U(3)$.

Physical implications of our results have been discussed. As representative physical parameters we have chosen the propagation velocity and trapping probability at the origin. We have shown that the peak velocity as well as the strength of localization depend only on few parameters defining the coin, namely two for the first class and three for the second. We derived explicit formula specifying the dependencies of the physically relevant parameters on the parameters used to define the coin matrix. Explicit formulas for the velocity and trapping allow to quantify the strength of localization and magnitude of the speed. Hence the extreme regimes of three state walks on the line can be pinpointed. The very moderate dependence of localization and peak velocity on matrix parameters has to be put into contrast with the original coin matrix which has nine independent parameters.

The identification of the two localizing coin classes allows us to estimate the degree of control we need to have over the coin in order to see localization in an experiment. Such an analysis is relevant when considering possible experimental implementations for instance using the optical feedback loop [8]. The coin control, usually realized as an internal degree of freedom of the particle spin or angular momentum [12, 26], must be sufficiently strict because localization exhibited by the coins applies only to a very limited range of parameters when compared to the full parameter size of a general $U(3)$ coin.

Acknowledgments

The financial support from RVO 68407700, SGS13/217/OHK4/3T/14, GAČR 13-33906S and GAČR 14-02901P is gratefully acknowledged.

[1] Y. Aharonov, L. Davidovich and N. Zagury (1993), *Quantum Random Walks*, Phys. Rev. A, 48, 1687
[2] M. Santha (2008), *Quantum walk based search algorithms*, in Theory and Applications of Models of Computation, Lecture Notes in Computer Science, edited by M. Agrawal, D.Z. Du, Z.H. Duan, A.S. Li (Springer, Berlin, 2008), Vol. 4978, p. 31
[3] A. Ahlbrecht, H. Vogts, A. H. Werner and R. F. Werner (2011), *Asymptotic evolution of quantum walks with random coin*, J. Math. Phys., 52, 042201
[4] A. Joye (2012), *Dynamical localization for d-dimensional random quantum walks*, Quant. Inf. Proc., 11, 1251-1269
[5] O. Mülken and A. Blumen (2011), *Continuous-Time Quantum Walks: Models for Coherent Transport on Complex Networks*, Phys. Rep., 502, 37-87
[6] M. Karski, L. Förster, J. Choi, A. Steffen, W. Alt, D. Meschede and A. Widera (2009), *Quantum Walk in Position Space with Single Optically Trapped Atoms*, Science, 325, 174
[7] H. Schmitz, R. Matjeschk, Ch. Schneider, J. Glueckert, M. Enderlein, T. Huber and T. Schaetz (2009), *Quantum Walk of a Trapped Ion in Phase Space*, Phys. Rev. Lett., 103, 090504
[8] A. Schreiber, K. N. Cassemiro, V. Potoček, A. Gábris, P. J. Mosley, E. Andersson, I. Jex and Ch. Silberhorn (2010), *Photons Walking the Line: A Quantum Walk with Adjustable Coin Operations*, Phys. Rev. Lett., 104, 050502
[9] F. Zähringer, G. Kirchmair, R. Gerritsma, E. Solano, R. Blatt and C. F. Roos (2010), *Realization of a Quantum Walk with One and Two Trapped Ions*, Phys. Rev. Lett., 104, 100503
[10] M. A. Broome, A. Fedrizzi, B. P. Lanyon, I. Kassal, A. Aspuru-Guzik and A. G. White (2010), *Discrete Single-Photon Quantum Walks with Tunable Decoherence*, Phys. Rev. Lett., 104, 153602
[11] A. Peruzzo, M. Lobino, J. C. F. Matthews, N. Matsuda, A. Politi, K. Poulios, X. Zhou, Y. Lahini, N. Ismail, K. Worhoff, Y. Bromberg, Y. Silberberg, M. G. Thompson and J. L. O'Brien (2010), *Quantum Walks of Correlated Photons*, Science, 329, 1500
[12] A. Schreiber, A. Gábris, P. P. Rohde, K. Laiho, M. Štefaňák, V. Potoček, C. Hamilton, I. Jex and Ch. Silberhorn (2012), *A 2D Quantum Walk Simulation of Two-Particle Dynamics*, Science, 336, 55
[13] L. Sansoni, F. Sciarrino, G. Vallone, P. Mataloni, A. Crespi, R. Ramponi and R. Osellame (2012), *Two-particle bosonic-fermionic quantum walk via 3D integrated photonics*, Phys. Rev. Lett., 108, 010502
[14] A. Ambainis, E. Bach, A. Nayak, A. Vishwanath and J. Watrous (2001), *One-dimensional quantum walks*, in Proceedings of the 33th STOC, ACM New York, pages 3749
[15] G. Grimmett, S. Janson and P. F. Scudo (2004), *Weak limits for quantum random walks*, Phys. Rev. E, 69, 026119
[16] A. Kempf and R. Portugal (2009), *Group velocity of discrete-time quantum walks*, Phys. Rev. A, 79, 052317
[17] N. Inui, N. Konno and E. Segawa (2005), *One-dimensional three-state quantum walk*, Phys. Rev. E, 72, 056112
[18] N. Inui and N. Konno (2005), *Localization of multi-state quantum walk in one dimension*, Physica A, 353, 133
[19] N. Inui, Y. Konishi and N. Konno (2004), *Localization of two-dimensional quantum walks*, Phys. Rev. A, 69, 052323
[20] M. Štefaňák, B. Kollár, T. Kiss and I. Jex (2010), *Full revivals in 2D quantum walks*, Phys. Scr., T140, 014035
[21] K. Watabe, N. Kobayashi, M. Katori and N. Konno (2008), *Limit distributions of two-dimensional quantum walks*, Phys. Rev. A, 77, 062331
[22] M. Štefaňák, I. Bezděková and I. Jex (2012), *Continuous deformations of the Grover walk preserving localization*, Eur. Phys. J. D, 66, 142

[23] C. Jarlskog (2005), *A recursive parametrisation of unitary matrices*, J. Math. Phys., 46, 103508
[24] K. Nakamura et al. (2010), *Review of Particles Physics: The CKM Quark-Mixing Matrix*, J. Phys. G, 37, 75021
[25] R. Wong (2001), *Asymptotic Approximations of Integrals*, SIAM Philadelphia
[26] C. S. Hamilton, A. Gabris, I. Jex and S. M. Barnett (2011), *Quantum Walk with a four-dimensional coin*, New J. Phys., 13, 013015

Limit distributions of three-state quantum walks: the role of coin eigenstates

M. Štefaňák,[1] I. Bezděková,[1] and I. Jex[1]

[1]*Department of Physics, Faculty of Nuclear Sciences and Physical Engineering, Czech Technical University in Prague, Břehová 7, 115 19 Praha 1 - Staré Město, Czech Republic*

We analyze two families of three-state quantum walks which show the localization effect. We focus on the role of the initial coin state and its coherence in controlling the properties of the quantum walk. In particular, we show that the description of the walk simplifies considerably when the initial coin state is decomposed in the basis formed by the eigenvectors of the coin operator. This allows us to express the limit distributions in a much more convenient form. Consequently, striking features which are hidden in the standard basis description are easily identified. Moreover, the dependence of moments of the position distribution on the initial coin state can be analyzed in full detail. In particular, we find that in the eigenvector basis the even moments and the localization probability at the origin depend only on incoherent combination of probabilities. In contrast, odd moments and localization outside the origin are affected by the coherence of the initial coin state.

I. INTRODUCTION

Quantum walks [1–3] emerged as an extension of a concept of a random walk to a unitary evolution of a quantum particle on a discrete graph or lattice. Soon, their potential for quantum information processing was recognized [4]. The quantum walk based algorithms which outperforms their classical counterparts were implemented for problems such as database search [5] or finding a path in a randomly glued tree graphs [6]. Later it was shown [7, 8] that quantum walks represent a universal tool for quantum computation. More recently quantum walk based algorithms are being developed for problems such as graph isomorphism testing [9–11] or finding structural anomalies in graphs [12–14].

For quite a long time the quantum walk was rather a theoretical concept, even though very fruitful. However, in 2009 the first experimental realization of a quantum walk on a line utilizing optically trapped atoms [15] has been reported. The experiments with cold ions [16, 17] and photons [18, 19] followed shortly afterwards. These experiments were latter expanded to implement a quantum walk on a line with two non-interacting particles [20–22]. More recently, an experiment implementing a quantum walk on a square lattice [23] has been realized which was capable of simulating the walk on a line of two interacting particles [24].

One of the distinctive features of quantum walks when compared with classical random walks is their quadratically faster spreading. This stems from the fact that the quantum walk is a wave phenomenon [25] rather than a diffusion. The probability distributions resulting from quantum walks have typically an inverted-bell shape with characteristic peaks on the edges which propagate through the lattice with constant velocity. For quantum walks with homogeneous coin the probability distribution can be investigated by means of Fourier analysis [26]. Important results are the weak-limit theorems [27] which prove the convergence of the moments of the re-scaled position of the quantum particle in the limit of large number of steps. This allows one to derive the so-called group-velocity density which can be used to approximate the probability distribution generated by the quantum walk and to evaluate the moments of this distribution. More recently, a method based on matrix-valued orthogonal polynomials have been developed [28] which extends the analysis to models with inhomogeneities.

In the present paper we investigate the position distributions of two one-parameter families of three-state quantum walks which we have introduced in [29]. These families of quantum walks were derived as extensions of the three-state Grover walk. This particular model was extensively studied in the literature [30, 31] where it was found that it differs considerably from the two-state walk [32]. Namely, the three-state Grover walk features the so-called localization effect, which means that the particle has a non-vanishing probability to stay at any position even in the limit of infinite number of steps. The reason why does this effect appear is that the evolution operator of the three-state Grover walk possess apart from continuous spectrum also an isolated eigenvalue. The corresponding stationary state is unfolded over the whole lattice. Provided that it has a non-zero overlap with the initial condition, part of the wave-packet describing the quantum particle will remain trapped at the already visited sites and will not evolve anymore. This results in an additional central peak in the probability distribution of the three-state Grover walk which is exponentially decaying with the distance from the origin but is independent of the number of steps. The same holds for the two families of quantum walks we have derived in [29] since they preserve the point spectrum. However, they do not exhaust the set of quantum walks with localization, as we have recently shown in [33]. The probability distribution of such quantum walks is not described solely by the group-velocity density, since this part takes into account only the continuous spectrum. To obtain the full probability distribution one has to include also the localization stemming from the point spectrum. For the three-state Grover walk these two parts of the probability

distribution were derived recently by Falkner and Boettcher in [34], where the authors have also discussed the rate of convergence of the moments of the distribution to the asymptotic values determined by the group-velocity density. At the same time, Machida [35] presented similar results extended to one of the families of quantum walks with localization we have introduced in [29] and discussed the application of the three-state walk for preparation of discrete uniform measures. However, both results [34, 35] have a significant drawback. Namely, the dependence of both the group-velocity density and the localization probability on the initial coin state is rather involved. The reason for this inconvenience is that the initial coin state is expressed in the standard basis of the coin space. However, we can describe the initial state in a different basis which proves to be more suitable for the analysis of the quantum walk. In [36] we have shown that for the Hadamard walk on a line this suitable basis is given by the eigenstates of the coin operator. The approach resembles the transformation from bare states to dressed states familiar from quantum optics [37]. In the present paper we explore the transformation to the basis formed by the eigenstates of the coin operator further and apply it to the two families of three-state quantum walks introduced in [29].

The paper is organized as follows: In Section II we analyze the family of quantum walks constructed in [29] as a parametrization of eigenvectors of the Grover coin. We show that the results [34, 35] simplify considerably when the initial coin state is expressed in basis formed by eigenvectors of the coin operator. This allows us to determine the dependence of the moments of the distribution on the initial coin state. We also discuss the extremal regimes of quantum walks in consideration. In Section III we turn to the second family of quantum walks from [29] which was constructed as a parametrization of eigenvalues of the Grover matrix. The details of the derivation of the localization probability and the group-velocity density are left for the Appendix A. Finally, we conclude and present an outlook in Section IV.

II. EIGENVECTOR FAMILY

Let us begin with a family of quantum walks which was introduced in [29] and recently analyzed in [34, 35]. The coin operators are in the standard basis of the coin space $\{|L\rangle,\ |S\rangle,\ |R\rangle\}$ given by the following matrix [38]

$$C(\rho) = \begin{pmatrix} -\rho^2 & \rho\sqrt{2-2\rho^2} & 1-\rho^2 \\ \rho\sqrt{2-2\rho^2} & 2\rho^2-1 & \rho\sqrt{2-2\rho^2} \\ 1-\rho^2 & \rho\sqrt{2-2\rho^2} & -\rho^2 \end{pmatrix}, \tag{1}$$

with the coin parameter $\rho \in (0,1)$. We exclude the boundary points from our consideration since they result in trivial walks. Indeed, for $\rho = 0$ the coin (1) reduces to a permutation matrix with an additional phase shift to the state $|S\rangle$. Walk with such a coin can merely hop back and forth between the origin and its nearest neighbours. For the choice of $\rho = 1$ the coin (1) reduces to an identity matrix with an additional phase shift to the states $|L\rangle$ and $|R\rangle$. Such a coin is not mixing the coin states and the walk is simple - the $|L\rangle$ component of the initial coin state keeps hopping to the left, the $|R\rangle$ component keeps hopping to the right and the $|S\rangle$ component remains at the origin. Both quantum walks with $\rho = 0$ and $\rho = 1$ can be analyzed in a straightforward way without the need for the week-limit theorems.

The set of coin operators (1) was constructed in [29] by a special parametrization of the eigenvectors of the 3x3 Grover matrix which is a member of this family corresponding to the choice of the coin parameter $\rho = \frac{1}{\sqrt{3}}$. One can show [29] that the evolution operators of the quantum walks with the coin (1) have a non-empty point spectrum for all values of $\rho \in (0,1)$. Consequently, the quantum walks show the localization effect in a similar way as found originally for the three-state Grover walk [30, 31]. The coin parameter ρ determines directly the peak velocity of the walk [29], i.e. the positions of the peaks after t steps of the quantum walk will be $\pm\rho t$.

The group-velocity density of quantum walks with the coin (1) was recently derived by Falkner and Boettcher [34] for the special case of the Grover walk corresponding to $\rho = \frac{1}{\sqrt{3}}$, and by Machida [35] for a general value of ρ. For a particle starting the walk from the origin with the initial coin state $|\psi_C\rangle$ the density has the form

$$w(v) = \frac{\sqrt{1-\rho^2}(d_0 + d_1 v + d_2 v^2)}{2\pi(1-v^2)\sqrt{\rho^2 - v^2}}. \tag{2}$$

With the group-velocity density (2) one can determine the asymptotic value of the re-scaled moments of the particle's position m in the limit of large number of steps t. Namely, the following relations hold for all $n \in \mathbb{N}$

$$\lim_{t\to+\infty} \left\langle \left(\frac{m}{t}\right)^n \right\rangle = \langle v^n \rangle = \int_{-\rho}^{\rho} v^n \ w(v)\ dv. \tag{3}$$

The group-velocity density can be also used to approximate the probability distribution after a finite number of steps t. We have to replace v in (2) with $\frac{m}{t}$ and simultaneously re-normalize the distribution by $\frac{1}{t}$. This will be applied later in the Figures where we will compare the analytical results with a finite time numerical simulation.

Note that the density (2) looks relatively simple. However, we have yet to specify the terms d_i which involve the dependence on the initial coin state $|\psi_C\rangle$. Machida [35] found that they are given by

$$\begin{aligned} d_0 &= |\alpha+\gamma|^2+2|\beta|^2, \\ d_1 &= 2\Big\{ -|\alpha-\beta|^2+|\gamma-\beta|^2- \\ &\quad -\left(2-\frac{\sqrt{2-2\rho^2}}{\rho}\right)\mathrm{Re}\left((\alpha-\gamma)\overline{\beta}\right)\Big\}, \\ d_2 &= |\alpha|^2-2|\beta|^2+|\gamma|^2- \\ &\quad -2\left\{\frac{\sqrt{2-2\rho^2}}{\rho}\mathrm{Re}\left((\alpha+\gamma)\overline{\beta}\right)+\frac{2-\rho^2}{\rho^2}\mathrm{Re}\left(\alpha\overline{\gamma}\right)\right\} \end{aligned} \tag{4}$$

where α, β and γ are the coefficients of $|\psi_C\rangle$ in the standard basis, i.e.

$$|\psi_C\rangle = \alpha|L\rangle+\beta|S\rangle+\gamma|R\rangle. \tag{5}$$

However, if we decompose the initial coin state in a more suitable basis it will simplify the relations (4) considerably. It can be anticipated that such a suitable basis is the one formed by the eigenstates of the coin operator. The eigenvectors of the coin operator (1) read [29]

$$\begin{aligned} |\sigma^+\rangle &= \sqrt{\frac{1-\rho^2}{2}}|L\rangle+\rho|S\rangle+\sqrt{\frac{1-\rho^2}{2}}|R\rangle, \\ |\sigma_1^-\rangle &= \frac{\rho}{\sqrt{2}}|L\rangle-\sqrt{1-\rho^2}|S\rangle+\frac{\rho}{\sqrt{2}}|R\rangle, \\ |\sigma_2^-\rangle &= \frac{1}{\sqrt{2}}(|L\rangle-|R\rangle). \end{aligned} \tag{6}$$

They satisfy the eigenvalue equations

$$C(\rho)|\sigma^+\rangle = |\sigma^+\rangle, \qquad C(\rho)|\sigma_i^-\rangle = -|\sigma_i^-\rangle, i=1,2.$$

We decompose the initial coin state into the eigenstate basis in the form

$$|\psi_C\rangle = g_+|\sigma^+\rangle+g_1|\sigma_1^-\rangle+g_2|\sigma_2^-\rangle, \tag{7}$$

where the probability amplitudes g_+ and $g_{1,2}$ are restricted by the normalization condition

$$|g_+|^2+|g_1|^2+|g_2|^2 = 1. \tag{8}$$

From the relations (6) we find that the coefficients in the standard basis α, β, γ are in the eigenstate basis given by

$$\begin{aligned} \alpha &= \frac{1}{\sqrt{2}}\left(\sqrt{1-\rho^2}g_+ + \rho g_1 + g_2\right), \\ \beta &= g_+\rho - \sqrt{1-\rho^2}g_1, \\ \gamma &= \frac{1}{\sqrt{2}}\left(\sqrt{1-\rho^2}g_+ + \rho g_1 - g_2\right). \end{aligned}$$

Plugging these expressions into (4) and using the normalization condition (8) we obtain much more convenient formulas for the terms d_i, namely

$$\begin{aligned} d_0 &= 2(1-|g_2|^2), \\ d_1 &= -\frac{2}{\rho}\left(g_1\overline{g_2}+\overline{g_1}g_2\right), \\ d_2 &= \frac{2}{\rho^2}\left(|g_1|^2+2|g_2|^2-1\right). \end{aligned} \tag{9}$$

Finally, the group-velocity density reads

$$w(v) = \frac{\sqrt{1-\rho^2}}{\pi(1-v^2)\sqrt{\rho^2-v^2}}\left(1-|g_2|^2 - \right. \tag{10}$$
$$\left. -(g_1\overline{g_2}+\overline{g_1}g_2)\frac{v}{\rho}+(|g_1|^2+2|g_2|^2-1)\frac{v^2}{\rho^2}\right).$$

This result allows us to determine the dependence of the moments (3) on the initial coin state in a straightforward way. Namely, odd moments of the group-velocity have the form

$$\langle v^{2n+1}\rangle = O_n(\rho)\left(g_1\overline{g_2}+\overline{g_1}g_2\right),$$

where we have denoted

$$O_n(\rho) = -\frac{\sqrt{1-\rho^2}}{\rho}\int\limits_{-\rho}^{\rho}\frac{v^{2n+2}}{\pi(1-v^2)\sqrt{\rho^2-v^2}}\,dv.$$

We see that in the eigenstate basis the odd moments are determined by the coherent combination of the probability amplitudes g_1 and g_2. On the other hand, the even moments (3) depend only on the probabilities $|g_1|^2$ and $|g_2|^2$ of finding the particle initially in the coin state $|\sigma_1^-\rangle$ or $|\sigma_2^-\rangle$. This means that the mixed initial coin state of the form

$$\rho_C = |g_+|^2|\sigma^+\rangle\langle\sigma^+| + |g_1|^2|\sigma_1^-\rangle\langle\sigma_1^-| + |g_2|^2|\sigma_2^-\rangle\langle\sigma_2^-|,$$

results in a distribution with the same even moments as the pure coin state (7). In particular, the second moment is given by

$$\langle v^2\rangle = \left(|g_1|^2+1\right)\Delta_1(\rho) + \left(|g_2|^2-1\right)\Delta_2(\rho), \tag{11}$$

where we have used the notation

$$\Delta_1(\rho) = \frac{1+\rho^2-\sqrt{1-\rho^2}}{2+2\sqrt{1-\rho^2}},$$
$$\Delta_2(\rho) = \frac{2-\rho^2-2\sqrt{1-\rho^2}}{\rho^2}.$$

One can easily check that the inequalities

$$\Delta_1(\rho) > \Delta_2(\rho) > 0,$$

hold for all $\rho\in(0,1)$. It is then straightforward to show that the state giving rise to the distribution with the smallest variance is the one corresponding to $g_1 = g_2 = 0$, i.e. the eigenstate $|\sigma^+\rangle$. Analogously, the eigenstate $|\sigma_1^-\rangle$ yields the distribution with the greatest variance. We display the second moment (11) as a function of the probabilities $|g_1|^2$ and $|g_2|^2$ in Fig. 1 for the choice of the coin parameter $\rho = 0.5$. The plot indicates that $|\sigma^+\rangle$ yields the smallest variance while $|\sigma_1^-\rangle$ gives the greatest.

We note that the group-velocity density (10) is not normalized to unity, as was found in [34, 35]. Indeed, we obtain the following result

$$\int\limits_{-\rho}^{\rho} w(v)dv = 1-|g_2|^2 - \frac{\sqrt{1-\rho^2}-1}{\rho^2}\left(|g_1|^2+2|g_2|^2-1\right). \tag{12}$$

The remaining part of the probability is in the exponential peak corresponding to localization. This was also recently calculated by Falkner and Boettcher [34] for $\rho = \frac{1}{\sqrt{3}}$ corresponding to the Grover walk, and by Machida [35] for a general value of ρ. The probability to find the particle at position m in the limit $t\to+\infty$ is given by [35]

$$p_\infty(m) = \frac{1}{128(1-\rho^2)^2}\left\{2(1-\rho^2)\left|B\nu^{|m+1|}+A\nu^{|m|}\right|^2 + \right.$$
$$+\rho^2\left|B\nu^{|m+1|}+(A+B)\nu^{|m|}+A\nu^{|m-1|}\right|^2 +$$
$$\left. 2(1-\rho^2)\left|B\nu^{|m|}+A\nu^{|m-1|}\right|^2\right\}.$$

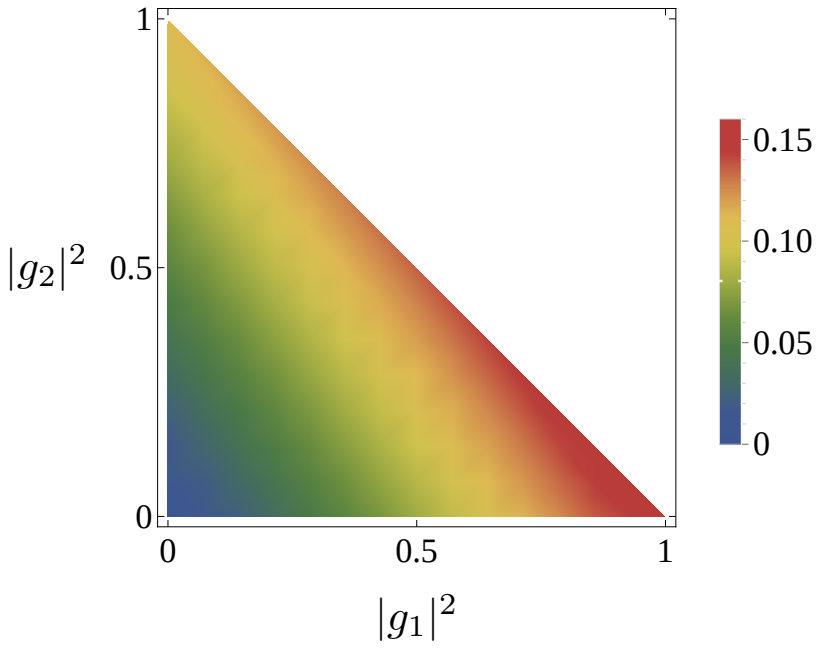

FIG. 1: (Color online) Second moment of the three-state walk with the coin operator (1) as a function of $|g_1|^2$ and $|g_2|^2$. We have chosen the coin parameter $\rho = 0.5$. The plot indicates that the greatest variance is achieved for the initial state $|\sigma_1^-\rangle$, while the smallest results from $|\sigma^+\rangle$. The domain of the plot is restricted to the lower triangle since the probabilities $|g_1|^2$ and $|g_2|^2$ are limited by the normalization condition (8).

Here ν depends on the coin parameter

$$\nu = -\frac{2-\rho^2-2\sqrt{1-\rho^2}}{\rho^2},$$

and A, B involves the initial coin state

$$\begin{aligned} A &= 4\left(1-\rho^2\right)\alpha + 2\rho\sqrt{2-2\rho^2}\beta, \\ B &= 4\left(1-\rho^2\right)\gamma + 2\rho\sqrt{2-2\rho^2}\beta. \end{aligned}$$

The simplification of this result by turning into the eigenvector basis (6) is perhaps even more significant than the one achieved for the group-velocity density (10). Indeed, after some algebra we find that the localization probability $p_\infty(m)$ is given by

$$p_\infty(m) = \begin{cases} \frac{2-2\rho^2}{\rho^4}\nu^{2m}|g_+ + g_2|^2, & m > 0, \\ \frac{1}{\rho^2}|\nu|\left\{|g_+|^2 + (1-\rho^2)|g_2|^2\right\}, & m = 0, \\ \frac{2-2\rho^2}{\rho^4}\nu^{2|m|}|g_+ - g_2|^2, & m < 0 \end{cases} \tag{13}$$

This result shows that the central peak is indeed an exponential with the base ν^2, except for the origin. Moreover, the dependence on the initial coin state is particularly simple in the eigenvector basis. For the origin the localization probability is given by an incoherent combination of $|g_+|^2$ and $|g_2|^2$, while outside the dependence is determined by a coherent combination of amplitudes g_+ and g_2. Moreover, the dependence differs for positive and negative m. This fact can be exploited to force the particle to localize only on the positive or negative half-line by a proper choice of the initial coin state. As an example, consider the initial coin state

$$|\psi_C\rangle = \frac{1}{\sqrt{2}}\left(|\sigma^+\rangle + |\sigma_2^-\rangle\right).$$

Using the expression (13) we find that in this case the localization probability equals

$$p_\infty(m) = \begin{cases} \frac{4-4\rho^2}{\rho^4}\nu^{2m}, & m > 0 \\ \left(\frac{1}{\rho^2} - \frac{1}{2}\right)|\nu|, & m = 0 \\ 0, & m < 0 \end{cases} \tag{14}$$

Localization thus appears only on the positive half-line. We illustrate this effect in Figure 2 where we present the probability distribution of the Grover walk corresponding to $\rho = \frac{1}{\sqrt{3}}$ after $t = 1000$ steps. To unravel the unusual behaviour of localization we display only a small neighbourhood of the origin.

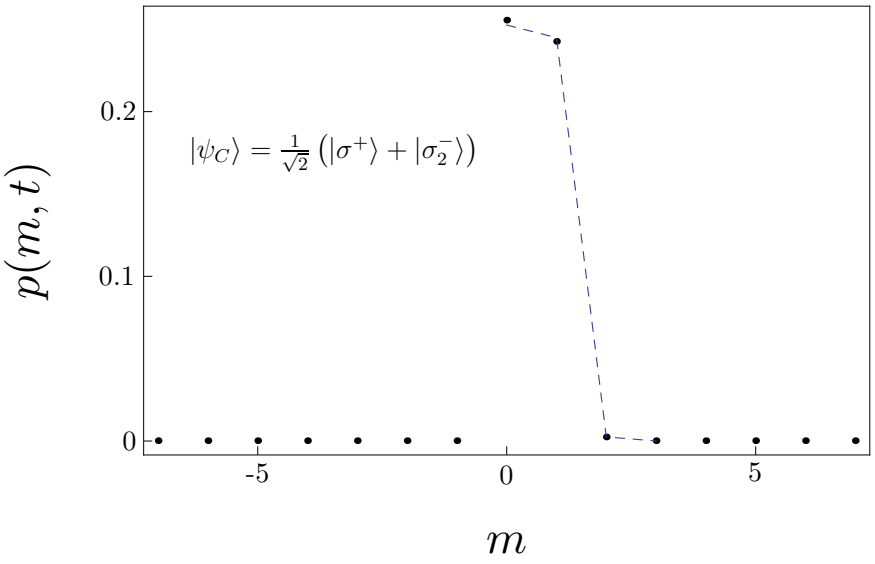

FIG. 2: (Color online) Probability distribution in the vicinity of the origin for the three-state Grover walk starting with the initial state $|\psi_C\rangle = \frac{1}{\sqrt{2}}\left(|\sigma^+\rangle + |\sigma_2^-\rangle\right)$ after $t = 1000$ steps. The localization depicted by the blue-dashed line appears only for positive m, as predicted by (14).

We note that one can easily check that

$$\sum_{m=-\infty}^{\infty} p_\infty(m) = |g_2|^2 + \frac{\sqrt{1-\rho^2}-1}{\rho^2}\left(|g_2|^2 - |g_+|^2\right).$$

This together with (12) and the normalization condition (8) results in

$$\sum_{m=-\infty}^{\infty} p_\infty(m) + \int_{-\rho}^{\rho} w(v)\, dv = 1,$$

i.e. the complete probability density is properly normalized to unity.

Let us now illustrate our findings on several examples. A typical distribution resulting from the three-state walk with the coin (1) has three characteristic peaks. Two are on the edges of the distribution and correspond to the divergency of the group-velocity density (10) for v approaching $\pm\rho$. The third one is the exponential peak at the origin corresponding to localization (13). However, these characteristics will be altered considerably when we chose one of the eigenvectors of the coin operator as the initial state of the walk.

First, consider the eigenstate $|\sigma^+\rangle$ as the initial coin state of the walk. From the relation (10) we find that the group-velocity density is given by

$$w_{|\sigma^+\rangle}(v) = \frac{\sqrt{1-\rho^2}\sqrt{\rho^2-v^2}}{\pi\rho^2(1-v^2)}. \tag{15}$$

We see that the density does not diverge for v approaching $\pm\rho$. Hence, both peaks on the edges of the distribution disappear. We illustrate this effect in Fig. 3, where we display the distribution after 100 steps. The coin parameter was chosen as $\rho = 0.7$.

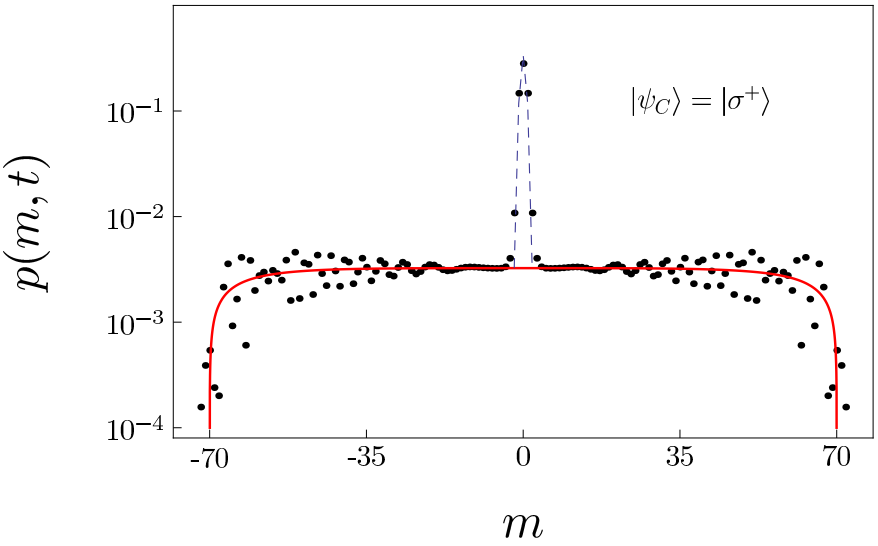

FIG. 3: (Color online) Probability distribution of the three-state walk with the coin parameter $\rho = 0.7$ after $t = 100$ steps. As the initial state we have chosen the coin eigenstate $|\sigma^+\rangle$. For this initial coin state both peaks on the edges of the distribution vanish. This corresponds to the fact that the group-velocity density (15), depicted by the red curve, tends to zero for v approaching $\pm\rho$. To unravel this feature we plot the probability distribution on the logarithmic scale. The blue-dashed line depicts the localization probability (13).

Let us turn to the eigenstate $|\sigma_1^-\rangle$. From the relation (13) we see that for the choice of the parameters $g_1 = 1$ and $g_2 = g_+ = 0$ the localization probability equals zero for all m. Hence, for this initial state the localization disappears, in accordance with the findings of [35]. We illustrate this effect in Fig. 4, where we show the distribution after 100 steps and the coin parameter $\rho = 0.8$. We can clearly see that there are only two peaks on the edges of the distribution. Consequently, the state $|\sigma_1^-\rangle$ yields the distribution with the greatest variance, as indicated by Fig. 1.

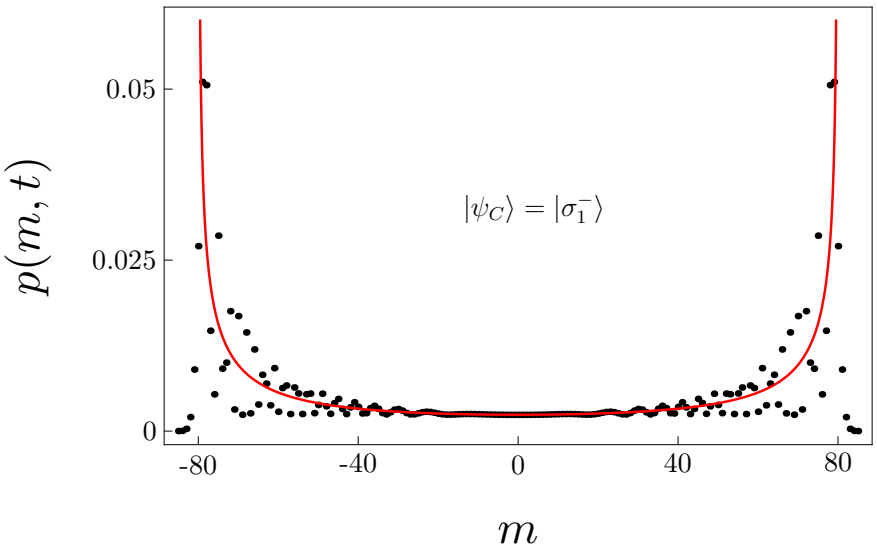

FIG. 4: (Color online) Probability distribution of the three-state walk with the coin parameter $\rho = 0.8$ after $t = 100$ steps. As the initial state we have chosen the coin eigenstate $|\sigma_1^-\rangle$. For this initial coin state the localization effect disappears. The red curve corresponds to the density (10).

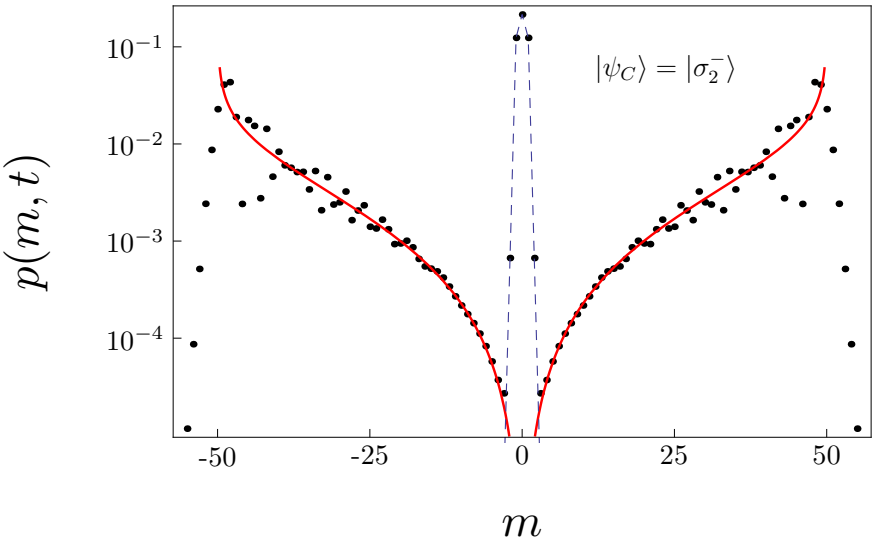

FIG. 5: (Color online) Probability distribution of the three-state walk with the coin parameter $\rho = 0.5$ after $t = 100$ steps. As the initial state we have chosen the coin eigenstate $|\sigma_2^-\rangle$. The probability density (16) depicted by the red curve tends to zero near the origin. To unravel this effect we use logarithmic scale on the y-axis. The blue-dashed line corresponds to the localization probability (13).

Concerning the last eigenstate $|\sigma_2^-\rangle$, we find that the group-velocity density is given by

$$w_{|\sigma_2^-\rangle}(v) = \frac{\sqrt{1-\rho^2}v^2}{\pi\rho^2(1-v^2)\sqrt{\rho^2-v^2}}. \tag{16}$$

We see that the density vanishes as v tends to zero. To illustrate this effect we plot in Fig. 5 the distribution after 100 steps on a logarithmic scale. The coin parameter was chosen as $\rho = 0.5$. The plot indicates that the distribution tends to zero around the origin, except for a very small neighbourhood where the localization dominates.

We have seen that for the initial coin state $|\sigma^+\rangle$ both peaks on the edges of the distribution vanish. However, it is possible to construct a state for which only one of the peaks disappears. Indeed, consider the coin state

$$|\sigma_L\rangle = \frac{1}{\sqrt{2}}\left(|\sigma_1^-\rangle + |\sigma_2^-\rangle\right). \tag{17}$$

From the relation (10) we find that the group-velocity density for this initial state reads

$$w_{|\sigma_L\rangle}(v) = \frac{\sqrt{1-\rho^2}\sqrt{(\rho-v)^3}}{2\pi\rho^2(1-v^2)\sqrt{\rho+v}}. \tag{18}$$

Such a density tends to zero for v approaching ρ. Nevertheless, the divergency at $v = -\rho$ remains. We illustrate this feature in Fig. 6 where we display the distribution after 100 steps for the coin parameter $\rho = 0.6$.

To conclude this Section, we note that the characteristic features of this family of quantum walks are maintained for all values of the coin parameter $\rho \in (0, 1)$, which scales the rate at which the walk spreads through the lattice. The three-state Grover walk is a particular case corresponding to the case $\rho = \frac{1}{\sqrt{3}}$. The change of the basis of the coin space to the one formed by the eigenstates of the coin operator (1) allowed us to simplify the description of the walk considerably. Consequently, interesting dynamical regimes which are otherwise hidden were easily identified.

III. EIGENVALUE FAMILY

Let us turn to the second family of quantum walks we have introduced in [29]. The coin operators are in the standard basis of the coin space represented by the following matrix

$$C(\varphi) = \frac{1}{6}\begin{pmatrix} -1-e^{2i\varphi} & 2(1+e^{2i\varphi}) & 5-e^{2i\varphi} \\ 2(1+e^{2i\varphi}) & 2(1-2e^{2i\varphi}) & 2(1+e^{2i\varphi}) \\ 5-e^{2i\varphi} & 2(1+e^{2i\varphi}) & -1-e^{2i\varphi} \end{pmatrix}, \tag{19}$$

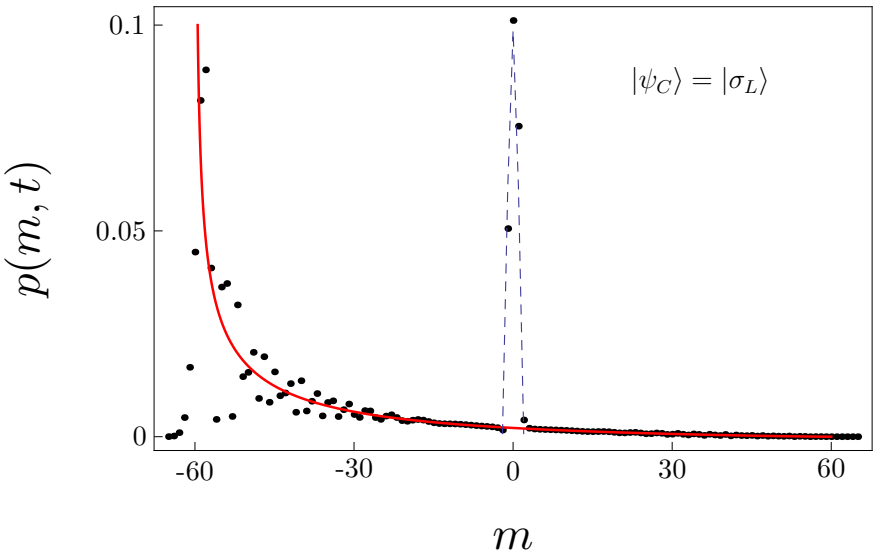

FIG. 6: (Color online) Probability distribution of the three-state walk with the coin parameter $\rho = 0.6$ after $t = 100$ steps. As the initial coin state we have chosen $|\sigma_L\rangle$ given by equation (17). In this case the peak on the right hand side of the lattice disappears, as predicted by the density (18) illustrated with the red curve. The blue-dashed line depicts the localization probability (13).

with the coin parameter $\varphi \in \langle 0, \frac{\pi}{2})$. For the choice of $\varphi = 0$ the coin operator turns to the 3x3 Grover matrix. We exclude the other boundary point $\varphi = \frac{\pi}{2}$ from our consideration since in such a case the coin operator (19) reduces to a permutation matrix and the resulting quantum walk is trivial.

The set of matrices (19) was constructed in [29] as a special parametrization of the eigenvalues of the 3x3 Grover matrix. It was shown that the evolution operators of quantum walks with the coin operators (19) maintain a point spectrum for all values of $\varphi \in \langle 0, \frac{\pi}{2})$. Hence, the family of quantum walks driven by such coins show the localization effect. The parameter φ determines the rate at which the walk spreads through the lattice. Namely, we have shown in [29] that the positions of the peaks after t steps of the walk will be $\pm\eta t$, where the peak velocity η is given by

$$\eta = \frac{1}{\sqrt{6}}\sqrt{3 - \cos^2\varphi - \sin\varphi\sqrt{9 - \cos^2\varphi}}. \tag{20}$$

Before we proceed with the analysis of this family of quantum walks, we first choose a suitable basis in the coin space. We again employ the eigenstates of the coin operator (19) which are given by

$$\begin{aligned} |\gamma^+\rangle &= \frac{1}{\sqrt{3}}\left(|L\rangle + |S\rangle + |R\rangle\right), \\ |\gamma_1^-\rangle &= \frac{1}{\sqrt{6}}\left(|L\rangle - 2|S\rangle + |R\rangle\right), \\ |\gamma_2^-\rangle &= \frac{1}{\sqrt{2}}\left(|L\rangle - |R\rangle\right). \end{aligned}$$

They satisfy the following eigenvalue equations

$$\begin{aligned} C(\varphi)|\gamma^+\rangle &= |\gamma^+\rangle, \\ C(\varphi)|\gamma_1^-\rangle &= -e^{2i\varphi}|\gamma_1^-\rangle, \\ C(\varphi)|\gamma_2^-\rangle &= -|\gamma_2^-\rangle. \end{aligned}$$

We decompose the initial coin state $|\psi_C\rangle$ into the eigenvector basis in the following form

$$|\psi_C\rangle = g_+|\gamma^+\rangle + g_1|\gamma_1^-\rangle + g_2|\gamma_2^-\rangle, \tag{21}$$

where the probability amplitudes g_+ and $g_{1,2}$ satisfy the normalization condition (8).

Let us now turn to the group-velocity density of the family of quantum walks with coin operators (19). We leave the details of the derivation for the Appendix, where we show that it can be expressed in the following form

$$\begin{aligned} w(v) &= \frac{1}{6\pi(1-v^2)\Theta}\Big[\left(3|g_1|^2+5|g_2|^2-2\right)\Lambda_+ + \\ &+ \left(1-|g_1|^2-2|g_2|^2\right)\Omega - \\ &-\sqrt{3}v(g_1\overline{g_2}+\overline{g_1}g_2+i(g_1\overline{g_2}-\overline{g_1}g_2)\tan\varphi)\Lambda_+ + \\ &+iv(g_2\overline{g_+}-\overline{g_2}g_+)\Xi\Big]. \end{aligned} \tag{22}$$

Here we have denoted

$$\begin{aligned} \Lambda_\pm &= \Phi_+ \pm \Phi_-, \\ \Phi_\pm &= \sqrt{9(1-v^2)-(5+3v^2)\cos^2\varphi \pm 12\Theta\cos\varphi}, \\ \Omega &= 4\cos\varphi\frac{(5-3v^2)\cos\varphi\Lambda_+ + 3\Theta\Lambda_-}{8\cos^2\varphi+3v^2\sin^2\varphi}, \\ \Xi &= 3\sqrt{6}\tan\varphi\frac{(v^2+\cos^2\varphi)\Lambda_+ - \Theta\cos\varphi\Lambda_-}{8\cos^2\varphi+3v^2\sin^2\varphi}, \\ \Theta &= \sqrt{(\eta^2-v^2)\left(\eta^2-v^2+\sin\varphi\sqrt{1-\frac{\cos^2\varphi}{9}}\right)}. \end{aligned} \tag{23}$$

The formula for the group-velocity (22) is much more involved than the one derived in the previous Section (see equation (10)). Nevertheless, the dependence on the initial coin state is still relatively simple in the eigenvector basis. In particular, one can show that the even moments depend only on the probabilities $|g_1|^2$ and $|g_2|^2$ of finding the particle initially in the coin state $|\gamma_1^-\rangle$ or $|\gamma_2^-\rangle$. Indeed, note that all expressions defined in (23) are even functions of v. Consequently, the first two terms in the group-velocity density (22) are even in v, while the remaining two are odd. Hence, only the first two terms of (22) contribute to the calculation of even moments. As an example, for the second moment we obtain the result

$$\begin{aligned} \langle v^2\rangle &= \left(3|g_1|^2+5|g_2|^2-2\right)\Delta_1(\varphi) + \\ &+ \left(1-|g_1|^2-2|g_2|^2\right)\Delta_2(\varphi), \end{aligned} \tag{24}$$

where $\Delta_i(\varphi)$ denotes the following integrals

$$\begin{aligned} \Delta_1(\varphi) &= \int_{-\eta}^{\eta}\frac{v^2}{6\pi(1-v^2)\Theta}\,\Lambda_+\,dv, \\ \Delta_2(\varphi) &= \int_{-\eta}^{\eta}\frac{v^2}{6\pi(1-v^2)\Theta}\,\Omega\,dv, \end{aligned}$$

which have to be evaluated numerically for a given value of φ. We display the second moment as a function of the probabilities $|g_1|^2$ and $|g_2|^2$ in Fig. 7. The coin parameter φ was chosen as $\frac{\pi}{4}$. The plot indicates that the greatest second moment is achieved for the eigenstate $|\gamma_1^-\rangle$, while the smallest results from $|\gamma_+\rangle$.

We note that the odd moments are determined by the last two terms of the group-velocity density (22). Hence, they are influenced by the coherence of the initial coin state.

Similarly to the previous model the group-velocity density (22) is not normalized since we find

$$\int_{-\eta}^{\eta} w(v)\,dv = \sqrt{6}-2+(3-\sqrt{6})|g_1|^2+(5-2\sqrt{6})|g_2|^2, \tag{25}$$

which differs from one unless $g_1=1$. The remaining part of the probability is in the localization. Concerning this part of the probability distribution we show in the Appendix that it is completely independent of φ. Hence, it coincides

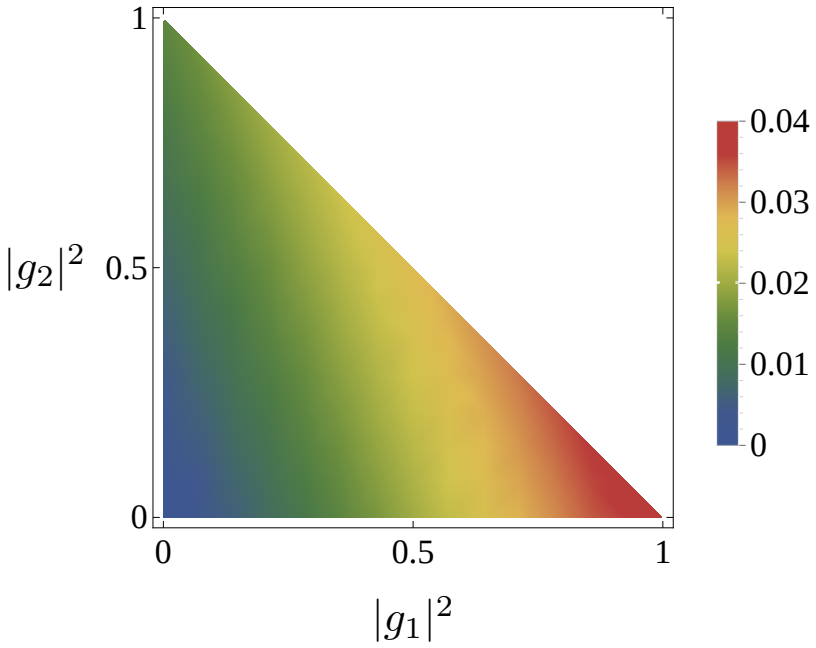

FIG. 7: (Color online) Second moment of the three-state walk with the coin (19) as a function of $|g_1|^2$ and $|g_2|^2$. We have chosen the coin parameter $\varphi = \frac{\pi}{4}$. Note the different scale in comparison with Fig. 1. The domain of the plot is restricted due to the normalization condition (8).

with the result for the three-state Grover walk corresponding to the choice of $\varphi = 0$. As we have mentioned earlier, the Grover walk also belongs to the eigenvector family we have studied in the previous Section. Using the result (13) for $\rho = \frac{1}{\sqrt{3}}$ corresponding to the Grover walk we find that the localization probability for three-state quantum walks with the coin (19) reads

$$p_\infty(m) = \begin{cases} 12(5-2\sqrt{6})^{2m}|g_+ + g_2|^2, & m > 0, \\ (5-2\sqrt{6})(3|g_+|^2 + 2|g_2|^2), & m = 0, \\ 12(5-2\sqrt{6})^{2|m|}|g_+ - g_2|^2, & m < 0. \end{cases} \tag{26}$$

We can easily check that

$$\sum_{m=-\infty}^{\infty} p_\infty(m) = (\sqrt{6}-2)|g_2|^2 + (3-\sqrt{6})|g_+|^2,$$

which together with (25) and the normalization condition (8) guarantees that

$$\sum_{m=-\infty}^{\infty} p_\infty(m) + \int_{-\eta}^{\eta} w(v)\, dv = 1.$$

Let us now illustrate our findings on several examples. For the choice of the coin parameter $\varphi = 0$ the walk reduces to the three-state Grover walk and the group velocity density (22) simplifies enormously to

$$\begin{aligned} w(v) \;=\; & \frac{\sqrt{2}}{\pi(1-v^2)\sqrt{1-3v^2}} \Big(1 - |g_2|^2 - \\ & -\sqrt{3}(g_1\overline{g_2} + \overline{g_1}g_2)v + 3(|g_1|^2 + 2|g_2|^2 - 1)v^2\Big). \end{aligned}$$

Note that this formula coincides with the result (10) of the previous Section for the particular choice of $\rho = \frac{1}{\sqrt{3}}$. Hence, all features we have discussed in Section II apply to the choice of $\varphi = 0$. In particular, the coin eigenstates

will play a special role since they result in an extremal regime of the walk. For $\varphi > 0$ the role of coin eigenstates will be less prominent and most of the features we have found in Section II diminish. The only exception is the behaviour of localization (26) which is completely independent of φ. As a consequence, choosing the eigenvector $|\gamma_1^-\rangle$ as the initial coin state of the walk will cancel localization for any value of the coin parameter φ.

Let us first consider the eigenstate $|\gamma^+\rangle$. In the special case of $\varphi = 0$ the distribution will not have peaks at the edges, see Fig. 3 for comparison. For very small values of the coin parameter, such as $\varphi = 0.01$ illustrated in the upper plot of Fig. 8, the density bends down as v approaches $\pm\eta$. Nevertheless, the density depicted by the red curve does not converge to zero. Instead, it diverges at $v = \pm\eta$ for any non-zero value of the coin parameter φ. With increasing value φ the bending of the density diminish and it attains the familiar inverted-bell shape. This is illustrated in the lower plot of Fig. 8 where we choose the coin parameter $\varphi = \frac{\pi}{4}$.

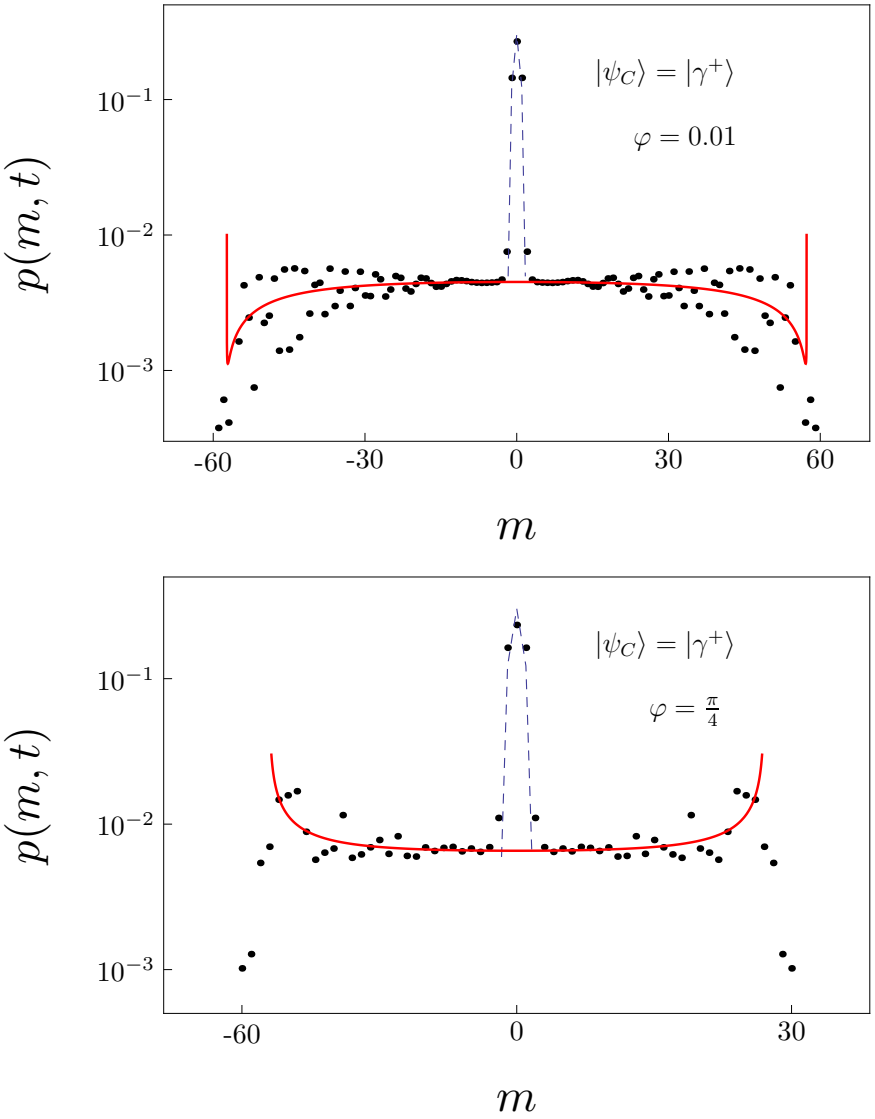

FIG. 8: (Color online) Probability distribution of the three-state walk after $t = 100$ steps on a logarithmic scale. The red curve denotes the density (22) and the blue-dashed line corresponds to the localization probability (26). As the initial state we have chosen the coin eigenstate $|\gamma^+\rangle$. For small values of the coin parameter, such as $\varphi = 0.01$ depicted in the upper plot, the density bends to zero for v approaching $\pm\eta$. However, for any $\varphi > 0$ the density diverges as these points. For increasing values of φ the density obtains the inverted-bell shape common for quantum walks. This is illustrated in the lower plot where we choose the coin parameter $\varphi = \frac{\pi}{4}$.

In Fig. 9 we illustrate the probability distribution after 100 steps for the initial coin state $|\gamma_1^-\rangle$. The coin parameter φ was chosen as $\frac{\pi}{6}$. As we have discussed before, choosing this eigenvector as the initial coin state results in the absence of localization for all values of the coin parameter φ.

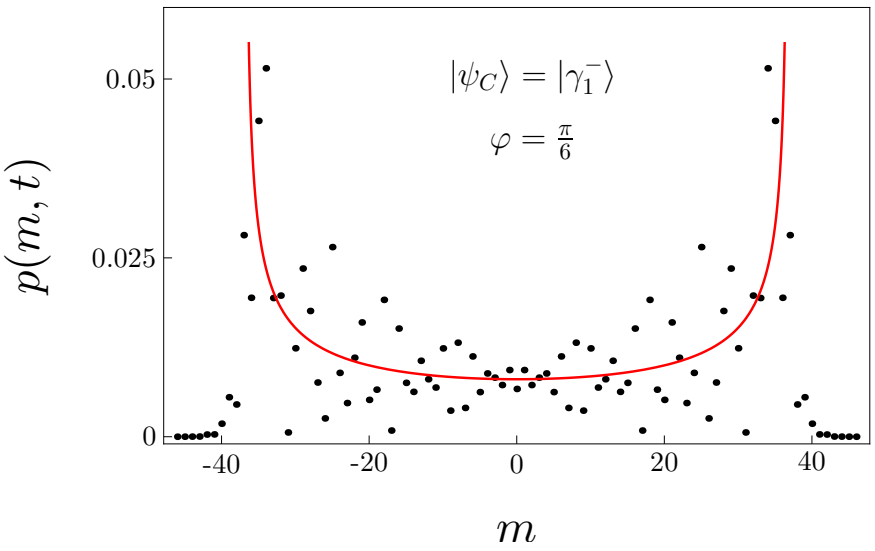

FIG. 9: (Color online) Probability distribution of the three-state walk with the coin parameter $\varphi = \frac{\pi}{6}$ after $t = 100$ steps. The red curve corresponds to the density (22). As the initial state we have chosen the coin eigenstate $|\gamma_1^-\rangle$. For this initial coin state the localization effect disappears for all values of φ.

As a last scenario we consider the eigenstate $|\gamma_2^-\rangle$. In the particular case of $\varphi = 0$ the distribution will resemble the one illustrated in Fig. 5, i.e. the density tends to zero at the origin. For small values of the coin parameter, such as $\varphi = 0.01$ depicted in the upper plot of Fig. 10, the density maintains a significant dip at the origin. However, it does not converge to zero for any positive φ. With increasing values of the coin parameter the dip at the origin diminish. This is illustrated in the lower plot of Fig. 10 where we choose the coin parameter $\varphi = \frac{\pi}{3}$.

To conclude this Section, we have found that the transformation from the standard basis of the coin space to the eigenstate basis is fruitful also for the quantum walks with coin operators (19). In contrast to the results obtained in the previous Section, the present family does not preserve all features of the three-state Grover walk. The exception is the behaviour of localization which is independent φ.

IV. CONCLUSIONS

The limit distributions of two families of three-state quantum walks closely related to the Grover walk have been derived. The first family of quantum walks we have analyzed maintains all properties of the three-state Grover walk. The coin parameter scales the spreading of the walk through the lattice. In contrast, for the second family of quantum walks the features of the three-state Grover walk gradually diminish as the coin parameter increases. The only exception is the behaviour of localization which is the same for all quantum walks within this family.

We have found that limit distributions of both families of quantum walks obtain a particularly simple form when we express the initial coin state in terms of the eigenvectors of the coin operator. This allowed us to reveal the extremal regimes of quantum walk dynamics. Moreover, the dependence of the moments of the distribution on the initial condition can be analyzed in full detail. We have shown that the even moments and the localization probability at the origin depend only on the probabilities of finding the particle initially in the eigenstates of the coin operator. Hence, an incoherent mixture of eigenstates yields in this respect the same results as a pure initial coin state, provided that the aforementioned probabilities are the same. On the other hand, the odd moments and the localization probability outside the origin are determined by the coherence of the initial coin state.

Changing the basis of the coin space to the one formed by the eigenvectors of the coin operator proved to be a very useful tool for the analysis of both families of quantum walks. We expect that this approach will be fruitful also in other models of quantum walks and that it will allow us to uncover otherwise hidden features.

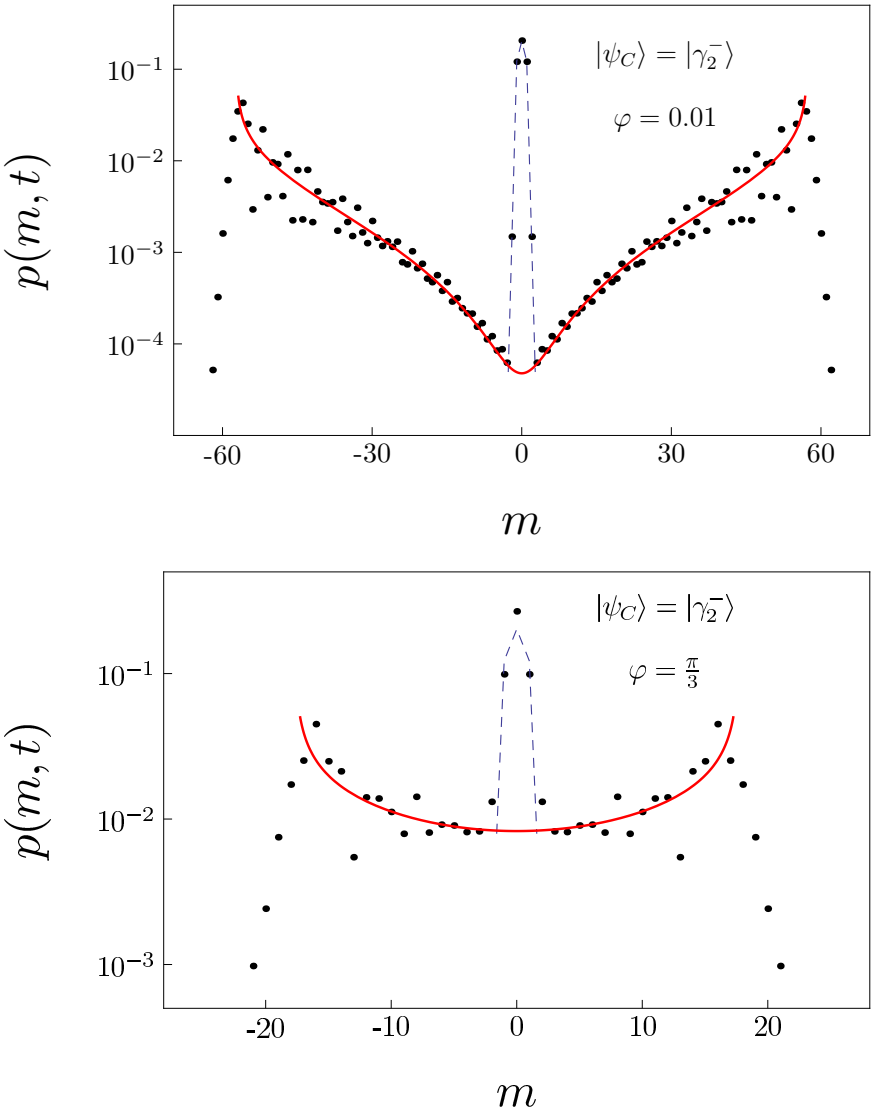

FIG. 10: (Color online) Probability distribution of the three-state walk after $t = 100$ steps on a logarithmic scale. The red curve denotes the density (22) and the blue-dashed line corresponds to the localization probability (26). As the initial state we have chosen the coin eigenstate $|\gamma_2^-\rangle$. For small values of the coin parameter the density has a dip around the origin. This is illustrated in the upper plot where we choose $\varphi = 0.01$. With increasing values of the coin parameter the density flattens, as depicted in the lower plot for $\varphi = \frac{\pi}{3}$.

Acknowledgments

We appreciate the financial support from RVO 68407700. MŠ is grateful for the grant GAČR 14-02901P. IB and IJ are thankful for the financial support from SGS13/217/OHK4/3T/14 and GAČR 13-33906S.

APPENDIX A: FOURIER ANALYSIS OF THE EIGENVALUE FAMILY OF THREE-STATE QUANTUM WALKS

In this appendix we derive the limit distribution of the three-state quantum walk with the coin (19). In the Fourier representation [26] the evolution operator is given by

$$\widetilde{U}(k) = \mathrm{Diag}\left(e^{-ik}, 1, e^{ik}\right) \cdot C(\varphi) = \frac{1}{6}\begin{pmatrix} -e^{-ik}(1+e^{2i\varphi}) & 2e^{-ik}(1+e^{2i\varphi}) & e^{-ik}(5-e^{2i\varphi}) \\ 2(1+e^{2i\varphi}) & 2(1-2e^{2i\varphi}) & 2(1+e^{2i\varphi}) \\ e^{ik}(5-e^{2i\varphi}) & 2e^{ik}(1+e^{2i\varphi}) & -e^{ik}(1+e^{2i\varphi}) \end{pmatrix}.$$

The eigenvalues of this matrix are

$$\lambda_1 = 1, \quad \lambda_{2,3} = e^{i(\varphi \pm \omega(k))},$$

where $\omega(k)$ is determined by the dispersion relations

$$\omega(k) = -\arccos\left(-\frac{1}{3}(2+\cos k)\cos\varphi\right).$$

The corresponding eigenvectors have the form

$$v_1(k) = \sqrt{\frac{2}{5+\cos k}}\begin{pmatrix} 1 \\ \frac{1}{2}\left(1+e^{ik}\right) \\ e^{ik} \end{pmatrix}, \quad v_{2,3}(k) = \frac{1}{\sqrt{n_{2,3}(k)}}\begin{pmatrix} \left(e^{-ik}+e^{-i(\varphi\pm\omega)}\right)\cos\varphi \\ \cos\omega + e^{\pm i\omega} - e^{-i(2\varphi\pm\omega)} + \cos k\cos\varphi \\ \left(e^{-ik}+e^{i(\varphi\pm\omega)}\right)\cos\varphi \end{pmatrix}, \tag{A1}$$

where we have denoted by $n_{2,3}(k)$ the normalization factors which reads

$$\begin{aligned} n_{2,3}(k) \;=\; & \frac{4}{3}\cos^2\varphi\left\{9 - 4\cos^2\varphi \pm 2\sin\varphi\sqrt{9-(2+\cos k)^2\cos^2\varphi} - \right. \\ & \left. - \cos k\left((4+\cos k)\cos^2\varphi \pm \sin\varphi\sqrt{9-(2+\cos k)^2\cos^2\varphi}\right)\right\}. \end{aligned}$$

We note that the first eigenvalue is independent of k. Hence, the eigenvector v_1 is a stationary state. As we will see later this eigenstate will determine the localization probability. The remaining eigenstates $v_{2,3}$ will contribute to the group-velocity density.

Let us begin with the localization probability that the particle will be found at position m in the asymptotic limit $t \to +\infty$. We denote by ψ_C the Fourier transformation of the initial state of the quantum walk $|0\rangle \otimes |\psi_C\rangle$. By $f_j(k)$ we mark the overlaps between the eigenstates $v_j(k)$ and ψ_C , i.e.

$$f_j(k) = (v_j(k), \psi_C).$$

The probability amplitude of the particle being at position m after t steps of the walk is then given by

$$\begin{aligned} \psi(m,t) \;=\; & \int_0^{2\pi} \frac{dk}{2\pi}\; e^{-imk} f_1(k)\; v_1(k) + \\ & + \int_0^{2\pi} \frac{dk}{2\pi}\; e^{-imk} e^{i(\varphi+\omega(k))t} f_2(k)\; v_2(k) + \\ & + \int_0^{2\pi} \frac{dk}{2\pi}\; e^{-imk} e^{i(\varphi-\omega(k))t} f_3(k)\; v_3(k). \end{aligned} \tag{A2}$$

It follows from the Riemann-Lebesque lemma that the two time-dependent integrals in (A2) vanish as t approaches infinity. Hence, in the limit $t \to +\infty$ only the first term in (A2) remains and we find

$$\psi_\infty(m) \equiv \lim_{t\to+\infty} \psi(m,t) = \int_0^{2\pi} \frac{dk}{2\pi}\; e^{-imk} f_1(k)\; v_1(k).$$

The localization probability $p_\infty(m)$ that the particle is trapped at position m as t approaches infinity is then given by $|\psi_\infty(m)|^2$. We see that it depends solely on the stationary state $v_1(k)$. Since $v_1(k)$ is independent of the coin parameter φ the localization probability $p_\infty(m)$ is the same for the whole family of quantum walks. The result coincides with the one for the three-state Grover walk corresponding to the value $\varphi = 0$.

We now turn to the derivation of the group-velocity density. This can be deduced by calculating the moments of the particle's position in the Fourier representation [39]. Let m denote the position of the particle after t steps of the quantum walk. One can show [27] that the n-th moment of the re-scaled position $\frac{m}{t}$ converges in the limit of $t \to +\infty$. Following the approach of [39] we find that the limiting value of the moment is given by

$$\lim_{t\to+\infty} \left\langle \left(\frac{m}{t}\right)^n \right\rangle = \int_0^{2\pi} \left(\frac{d\omega}{dk}\right)^n \left((-1)^n |f_2(k)|^2 + |f_3(k)|^2\right) \frac{dk}{2\pi}. \tag{A3}$$

Let us determine the overlap functions $f_j(k)$, respectively the term $\left((-1)^n |f_2(k)|^2 + |f_3(k)|^2\right)$. We note that

$$v = \frac{d\omega}{dk} = \frac{\cos\varphi \sin k}{\sqrt{9 - (2+\cos k)^2 \cos^2\varphi}}, \tag{A4}$$

is an odd function of k. Hence, for even n it is sufficient to find only the even part of $|f_2(k)|^2 + |f_3(k)|^2$, since the contribution of the odd part to the integral (A3) is zero. Similarly, for odd n it is sufficient to determine the odd part of $-|f_2(k)|^2 + |f_3(k)|^2$. To do this we consider the decomposition of the initial coin state $|\psi_C\rangle$ in the eigenstate basis as in (21). The Fourier transformation of the initial state of the walk $|0\rangle \otimes |\psi_C\rangle$ is then given by

$$\psi_C = \begin{pmatrix} \frac{g_1}{\sqrt{6}} + \frac{g_2}{\sqrt{2}} + \frac{g_+}{\sqrt{3}} \\ \frac{g_+}{\sqrt{3}} - \sqrt{\frac{2}{3}} g_1 \\ \frac{g_1}{\sqrt{6}} - \frac{g_2}{\sqrt{2}} + \frac{g_+}{\sqrt{3}} \end{pmatrix}$$

With the explicit form of the eigenvectors (A1) we then find that the even part of $|f_2(k)|^2 + |f_3(k)|^2$ reads

$$\left\{ |f_1(k)|^2 + |f_2(k)|^2 \right\}_{\text{even}} = 3|g_1|^2 + 5|g_2|^2 - 2 + \left(1 - |g_1|^2 - 2|g_2|^2\right) \frac{12}{5+\cos k}$$

In a similar way, the odd part of $-|f_2(k)|^2 + |f_3(k)|^2$ is given by

$$\begin{aligned} \left\{ -|f_2(k)|^2 + |f_3(k)|^2 \right\}_{\text{odd}} &= \left(-\sqrt{3}(g_1\overline{g_2} + \overline{g_1}g_2 + i(g_1\overline{g_2} - \overline{g_1}g_2)\tan\varphi) + i\sqrt{6}(g_2\overline{g_+} - \overline{g_2}g_+) \frac{2+\cos k}{5+\cos k} \tan\varphi \right) \times \\ &\quad \times \frac{\cos\varphi \sin k}{\sqrt{9 - (2+\cos k)^2 \cos^2\varphi}} \end{aligned}$$

The last part of the derivation of the group-velocity density is to make the substitution $k \to v$ in the integral (A3), where the group-velocity v is defined in (A4). The transformation from k to v is not unique and has to be done separately in two intervals. For $k \in (0, k_0) \cup (2\pi - k_0, 2\pi)$, where

$$k_0 = \arccos\left(\frac{1}{4\cos^2\varphi} (9 - 5\cos^2\varphi - 3\sin\varphi\sqrt{9 - \cos^2\varphi}) \right),$$

we find from (A4) the that the following relations hold

$$\begin{aligned} \cos k &= \frac{2v^2 + \sqrt{1 + 3v^2 - 9v^2 \frac{1-v^2}{\cos^2\varphi}}}{1 - v^2}, \\ \sin k &= v \frac{\sqrt{9(1-v^2)^2 - \cos^2\varphi \left(2 + \sqrt{1 + 3v^2 - 9v^2 \frac{1-v^2}{\cos^2\varphi}}\right)^2}}{\cos\varphi(1-v^2)}. \end{aligned}$$

Similarly, in the interval $k \in (k_0, 2\pi - k_0)$ we find the identities

$$\begin{aligned}\cos k &= \frac{2v^2 - \sqrt{1 + 3v^2 - 9v^2 \frac{1-v^2}{\cos^2\varphi}}}{1 - v^2}, \\ \sin k &= v \frac{\sqrt{9(1-v^2)^2 - \cos^2\varphi \left(2 - \sqrt{1 + 3v^2 - 9v^2 \frac{1-v^2}{\cos^2\varphi}}\right)^2}}{\cos\varphi(1-v^2)}.\end{aligned}$$

Performing all steps of the substitution from k to v is quite tedious but after some algebra we find that the moments (A3) can be re-written in the form

$$\lim_{t\to+\infty} \left\langle \left(\frac{m}{t}\right)^n \right\rangle = \int_{-\eta}^{\eta} v^n \; w(v) \; dv,$$

where η is the maximum of the group velocity $v(k)$ which is achieved at $k = k_0$. We find that it is given by

$$\eta = \frac{1}{\sqrt{6}} \sqrt{3 - \cos^2\varphi - \sin\varphi \sqrt{9 - \cos^2\varphi}}.$$

By $w(v)$ we have labeled the group-velocity density which can be expressed in the form

$$\begin{aligned} w(v) = \frac{1}{6\pi(1-v^2)\Theta} \quad & \Big[\left(3|g_1|^2 + 5|g_2|^2 - 2\right) \Lambda_+ + \left(1 - |g_1|^2 - 2|g_2|^2\right) \Omega - \\ & - \sqrt{3} v (g_1 \overline{g_2} + \overline{g_1} g_2 + i(g_1 \overline{g_2} - \overline{g_1} g_2) \tan\varphi) \Lambda_+ + iv(g_2 \overline{g_+} - \overline{g_2} g_+) \Xi \Big]. \end{aligned}$$

Here we have used the notation

$$\begin{aligned}\Lambda_\pm &= \Phi_+ \pm \Phi_-, \quad \Phi_\pm = \sqrt{9(1-v^2) - (5+3v^2)\cos^2\varphi \pm 12\Theta\cos\varphi}, \\ \Omega &= 4\cos\varphi \frac{(5-3v^2)\cos\varphi \Lambda_+ + 3\Theta\Lambda_-}{8\cos^2\varphi + 3v^2\sin^2\varphi}, \\ \Xi &= 3\sqrt{6}\tan\varphi \frac{(v^2 + \cos^2\varphi)\Lambda_+ - \Theta\cos\varphi\Lambda_-}{8\cos^2\varphi + 3v^2\sin^2\varphi}, \\ \Theta &= \sqrt{(\eta^2 - v^2)\left(\eta^2 - v^2 + \sin\varphi\sqrt{1 - \frac{\cos^2\varphi}{9}}\right)}.\end{aligned}$$

[1] Y. Aharonov, L. Davidovich and N. Zagury, Phys. Rev. A **48**, 1687 (1993)
[2] D. Meyer, J. Stat. Phys. **85**, 551, (1996)
[3] E. Farhi and S. Gutmann, Phys. Rev. A **58**, 915 (1998)
[4] D. Aharonov, A. Ambainis, J. Kempe and U. Vazirani, in *Proceedings of the 33th STOC*, ACM New York, p. 50 (2001)
[5] N. Shenvi, J. Kempe and K. Whaley, Phys. Rev. A **67**, 052307 (2003)
[6] A. M. Childs, R. Cleve, E. Deotto, E. Farhi, S. Gutmann and D. A. Spielman, in *Proc. 35th STOC*, ACM New York, pp. 59 (2003)
[7] A. M. Childs, Phys. Rev. Lett. **102**, 180501 (2009)
[8] N. B. Lovett, S. Cooper, M. Everitt, M. Trevers and V. Kendon, Phys. Rev. A **81**, 042330 (2010)
[9] J. K. Gamble, M. Friesen, D. Zhou, R. Joynt and S. N. Coppersmith, Phys. Rev. A **81**, 052313 (2010)
[10] S. D. Berry and J. B. Wang, Phys. Rev. A **83**, 042317 (2011)
[11] K. Rudinger, J. K. Gamble, M. Wellons, E. Bach, M. Friesen, R. Joynt and S. N. Coppersmith, Phys. Rev. A **86**, 022334 (2012)
[12] M. Hillery, D. Reitzner and V. Bužek, Phys. Rev. A **81**, 062324 (2010)
[13] M. Hillery, H. J. Zheng, E. Feldman, D. Reitzner and V. Bužek, Phys. Rev. A **85**, 062325 (2012)
[14] S. Cottrell and M. Hillery, Phys. Rev. Lett. **112**, 030501 (2014)
[15] M. Karski, L. Förster, J. Choi, A. Steffen, W. Alt, D. Meschede and A. Widera, Science **325**, 174 (2009)

[16] H. Schmitz, R. Matjeschk, Ch. Schneider, J. Glueckert, M. Enderlein, T. Huber and T. Schaetz, Phys. Rev. Lett. **103**, 090504 (2009)
[17] F. Zähringer, G. Kirchmair, R. Gerritsma, E. Solano, R. Blatt and C. F. Roos, Phys. Rev. Lett. **104**, 100503 (2010)
[18] A. Schreiber, K. N. Cassemiro, V. Potoček, A. Gábris, P. J. Mosley, E. Andersson, I. Jex and Ch. Silberhorn, Phys. Rev. Lett. **104**, 050502 (2010)
[19] M. A. Broome, A. Fedrizzi, B. P. Lanyon, I. Kassal, A. Aspuru-Guzik and A. G. White, Phys. Rev. Lett. **104**, 153602 (2010)
[20] A. Peruzzo, M. Lobino, J. C. F Matthews, N. Matsuda, A. Politi, K. Poulios, X. Zhou, Y. Lahini, N. Ismail, K. Worhoff, Y. Bromberg, Y. Silberberg, M. G. Thompson and J. L. O'Brien, Science **3329**, 1500 (2010)
[21] J. O. Owens, M. A. Broome, D. N. Biggerstaff, M. E. Goggin, A. Fedrizzi, T. Linjordet, M. Ams, G. D. Marshall, J. Twamley, M. J. Withford and A. G. White, New J. Phys. **13**, 075003 (2011)
[22] L. Sansoni, F. Sciarrino, G. Vallone, P. Mataloni, A. Crespi, R. Ramponi and R. Osellame, Phys. Rev. Lett. **108**, 010502 (2012)
[23] A. Schreiber, A. Gábris, P. P. Rohde, K. Laiho, M. Štefaňák, V. Potoček, C. Hamilton, I. Jex and Ch. Silberhorn, Science **336**, 55 (2012)
[24] A. Ahlbrecht, A. Alberti, D. Meschede, V. B. Scholz, A. H. Werner and R. F. Werner, New J. Phys. **14**, 073050 (2012)
[25] P. L. Knight, E. Roldan and J. E. Sipe, Phys. Rev. A **68**, 020301 (2003)
[26] A. Ambainis, E. Bach, A. Nayak, A. Vishwanath and J. Watrous, *Proceedings of the 33th STOC*, ACM New York, p. 60 (2001)
[27] G. Grimmett, S. Janson and P. F. Scudo, Phys. Rev. E **69**, 026119 (2004)
[28] M. J. Cantero, F. A. Grünbaum, L. Moral and L. Velázquez, Quantum Inf. Process. **11**, 1149 (2012)
[29] M. Štefaňák, I. Bezděková and I. Jex, Eur. Phys. J. D **66**, 142 (2012)
[30] N. Inui, N. Konno and E. Segawa, Phys. Rev. E **72**, 056112 (2005)
[31] N. Inui and N. Konno, Physica A **353**, 133 (2005)
[32] N. Konno, Quantum Inform. Comput. **2**, 578 (2002)
[33] M. Štefaňák, I. Bezděková, I. Jex and S. M. Barnett, Quantum Inf. Comput. **14**, pp 1213 (2014), arXiv:1309.7835v2
[34] S. Falkner and S. Boettcher, Phys. Rev. A **90**, 012307 (2014)
[35] T. Machida, arXiv:1404.1522
[36] M. Štefaňák, S. M. Barnett, B. Kollár, T. Kiss and I. Jex, New J. Phys. **13**, 033029 (2011)
[37] see e.g. W. P. Schleich, *Quantum optics in phase space*, Wiley-VCH Berlin, (2001)
[38] We note that Machida in [35] uses a different parametrization of the coin operator (1). Our parameter ρ corresponds to the angle θ used in [35] through $\cos\theta = 2\rho^2 - 1$ and $\sin\theta = 2\rho\sqrt{1-\rho^2}$. We prefer to use the parametrization (1) as it was originaly introduced in [29] since ρ has a direct dynamical interpretation as a peak velocity.
[39] K. Watabe, N. Kobayashi, M. Katori and N. Konno, Phys. Rev. A **77**, 062331 (2008)

Suitable bases for quantum walks with Wigner coins

I. Bezděková,[1] M. Štefaňák,[1] and I. Jex[1]

[1]*Department of Physics, Faculty of Nuclear Sciences and Physical Engineering, Czech Technical University in Prague, Břehová 7, 115 19 Praha 1 - Staré Město, Czech Republic*

The analysis of a physical problem simplifies considerably when one uses a suitable coordinate system. We apply this approach to the discrete-time quantum walks with coins given by $2j+1$-dimensional Wigner rotation matrices (Wigner walks), a model which was introduced in T. Miyazaki et al., Phys. Rev. A **76**, 012332 (2007). First, we show that from the three parameters of the coin operator only one is physically relevant for the limit density of the Wigner walk. Next, we construct a suitable basis of the coin space in which the limit density of the Wigner walk acquires a much simpler form. This allows us to identify various dynamical regimes which are otherwise hidden in the standard basis description. As an example, we show that it is possible to find an initial state which reduces the number of peaks in the probability distribution from generic $2j+1$ to a single one. Moreover, the models with integer j lead to the trapping effect. The derived formula for the trapping probability reveals that it can be highly asymmetric and it deviates from purely exponential decay. Explicit results are given up to the dimension five.

I. INTRODUCTION

Quantum walk [1–3] is an extension of the concept of a random walk [4] to unitary evolution of a quantum particle on a graph. Both continuous-time and discrete-time (or coined) quantum walks have found promising applications in quantum information processing, e.g. in quantum search algorithms [5–8], graph isomorphism testing [9–11], finding structural anomalies in graphs [12–14] or as universal tools for quantum computation [15, 16]. Quantum walks were realized in a number of experiments using optically trapped atoms [17], cold ions [18, 19] and photons [20–26].

The dynamics of the discrete-time quantum walks crucially depends on the choice of the coin operator and the initial state [27], which has essential implications for the performance of the search algorithm [28]. The behaviour of two-state quantum walks with homogeneous coin is fully understood [29]. This is not true for quantum walks with higher-dimensional coins, since the complexity of the unitary group grows rapidly with its dimension. Most of the known results were obtained for quantum walks with Grover coin which leads to the so-called trapping (or localization) effect [30, 31]. In contrast to the two-state walk, which show purely ballistic spreading, the particle performing the Grover walk has a non-vanishing probability to remain trapped in the vicinity of the origin. This is represented by a stationary peak in the probability distribution located at the origin, which does not vanish with the increasing number of steps but decays exponentially with the distance from the starting point. The Grover walk and its extensions were intensively studied, either for line [30–36], plane [37–39] or higher dimensional lattices [40, 41].

Among the few models of quantum walks on a line which were solved analytically for arbitrary dimension of the coin operator, i.e. arbitrary number of displacements particle can make in a single time-step, are the Wigner walks introduced in [42]. This model utilizes $2j+1$-dimensional Wigner rotation matrices as coin operators and is closely related to the tensor product model of quantum walks [43–46]. Explicitly, using the Fourier analysis [47] and the weak-limit theorem [48], the limit density of the Wigner walks was derived in [42] for arbitrary j. However, as the authors point out in [42], the dependence of the limit density on the initial coin state is rather involved. The reason for this inconvenience is that the initial coin state is decomposed into the standard basis of the coin space, i.e. the one in which the step operator is defined. The aim of our paper is to present an alternative approach to [42]. Namely, by using a more suitable basis of the coin space we put the results of [42] into much more convenient form. This allows us to identify previously unknown features which are hidden in the standard basis description. As an example, we show that while the generic probability distribution of the $2j+1$-dimensional Wigner walk has $2j+1$ peaks, there exist initial conditions for which the number of peaks reduces to one. Moreover, the models with integer j exhibit the trapping effect similar to the Grover walk. This feature was not analyzed in detail in [42]. We derive the explicit formula for the trapping probability for $j=1$ and $j=2$. Our results show that the trapping probability can be highly asymmetric. Moreover, the decay of the trapping probability with the distance from the origin is not exactly exponential for $j=2$.

The paper is organized as follows. In Section II we review the results on quantum walks with Wigner coin obtained in [42]. We find that when we focus only on the limit density and its moments the number of physically relevant coin parameters can be reduced from three to one. Next, we outline the procedure to determine the suitable basis of the coin space in which the limit density simplifies considerably. Namely, we choose the basis states among those which give rise to non-generic distributions. In Section III the suitable basis is determined for the simplest case of the two-state model. Moreover, we find a recipe for the construction of suitable bases for higher-dimensional models. We

apply this recipe in Section IV to the three-state model and we find that it is equivalent to the three-state Grover walk [30, 31] and its one-parameter generalization [32–35]. In Sections V and VI the four-state and five-state models are studied, respectively. Expressing the limit density in the suitable basis allows us to determine additional non-generic situations. In particular, we find initial conditions such that the number of peaks in the probability distribution is reduced to one. Finally, we summarize our results and present an outlook in Section VII. More technical details of the analysis are left for the Appendices.

II. QUANTUM WALKS WITH WIGNER COINS

In this Section we review the quantum walks on a line with Wigner coins (Wigner walks) following their introduction and analysis in [42]. The Hilbert space of the Wigner walk is given by a tensor product

$$\mathcal{H} = \mathcal{H}_P \otimes \mathcal{H}_C,$$

of the position space

$$\mathcal{H}_P = \mathrm{Span}\left\{|x\rangle | x \in \mathbb{Z}\right\},$$

and the coin space $\mathcal{H}_C$. The dimension of the coin space is $2j+1$, where j is a (half-)integer. The standard basis of the coin space is formed by vectors $|m\rangle$ corresponding to the jumps of length $2m$ where $m = -j, -j+1 \ldots, j$. Single step of the time-evolution is given by a unitary operator

$$\hat{U} = \hat{S} \cdot (\hat{I} \otimes \hat{R}^{(j)}(\alpha, \beta, \gamma)), \tag{1}$$

where $\hat{S}$ is the step operator

$$\hat{S} = \sum_{x=-\infty}^{+\infty} \sum_{m=-j}^{j} |x+2m\rangle\langle x| \otimes |m\rangle\langle m|, \tag{2}$$

and $\hat{R}^{(j)}(\alpha, \beta, \gamma)$ denotes the coin operator which is given by the Wigner rotation matrix [49, 50], i.e. the $2j+1$-dimensional irreducible representation of the rotation group SO(3). The matrix elements of the coin in the standard basis of the coin space

$$R^{(j)}_{mn}(\alpha, \beta, \gamma) = \langle m|\hat{R}^{(j)}(\alpha, \beta, \gamma)|n\rangle,$$

are given by

$$R^{(j)}_{mn}(\alpha, \beta, \gamma) = e^{-i\alpha m} r^{(j)}_{mn}(\beta) e^{-i\gamma n},$$

where

$$r^{(j)}_{mn}(\beta) = \sum_{l} \Gamma(j, m, n, l) \left(\cos\frac{\beta}{2}\right)^{2j+m-n-2l} \left(\sin\frac{\beta}{2}\right)^{2l-m+n}.$$

The factor $\Gamma(j, m, n, l)$ reads

$$\Gamma(j, m, n, l) = (-1)^l \frac{\sqrt{(j+m)!(j-m)!(j+n)!(j-n)!}}{(j-n-l)!(j+m-l)!(l-m+n)!l!}. \tag{3}$$

The summation index l runs over all integers such that all factorials in (3) are well defined.

As the initial state of the Wigner walk we consider

$$|\psi(0)\rangle = |0\rangle \otimes |\psi_C\rangle,$$

i.e. the particle starts from the origin with the initial coin state

$$|\psi_C\rangle = \sum_{m=-j}^{j} q_m |m\rangle. \tag{4}$$

The amplitudes q_m fulfill the normalization condition

$$\sum_{m=-j}^{j} |q_m|^2 = 1.$$

The state of the particle after t steps of the walk reads

$$|\psi(t)\rangle = \hat{U}^t |\psi(0)\rangle,$$

which can be decomposed into the standard basis as

$$|\psi(t)\rangle = \sum_x \sum_{m=-j}^{j} \Psi_m^{(j)}(x,t)|x\rangle \otimes |m\rangle.$$

The probability to find the particle at position x after t steps of the quantum walk is then given by

$$p^{(j)}(x,t) = \sum_{m=-j}^{j} \left|\Psi_m^{(j)}(x,t)\right|^2.$$

We note that all Wigner walks are bipartite, i.e. half of the lattice points are empty at any time step. For integer j the odd sites are never occupied, while for half-integer j the walk oscillates between even and odd sites.

Since the Wigner walks are translationally invariant, their analysis is greatly simplified in the Fourier picture [47]. Moreover, in the asymptotic limit the moments of the particle's re-scaled position (or pseudo-velocity) can be expressed in the form [48]

$$\lim_{t\to+\infty} \left\langle \left(\frac{x}{t}\right)^n \right\rangle = \int v^n \nu^{(j)}(v) dv, \tag{5}$$

where $\nu^{(j)}(v)$ is the limit density. Its explicit form for Wigner walks was derived in [42] where it was shown that it is given by a sum

$$\nu^{(j)}(v) = \sum_{0<m\leq j} \nu^{(j,m)}(v). \tag{6}$$

The summation index m runs over (half-)integers, depending on whether j is half-integer or integer, in unit steps. The individual densities $\nu^{(j,m)}(v)$ have the form

$$\nu^{(j,m)}(v) = \frac{1}{2m}\mu\left(\frac{v}{2m}; \cos\frac{\beta}{2}\right) \mathcal{M}^{(j,m)}\left(\frac{v}{2m}\right) \tag{7}$$

where $\mu(v;a)$ is the Konno's density function [51, 52]

$$\mu(v;a) = \frac{\sqrt{1-a^2}}{\pi(1-v^2)\sqrt{(a-v)(a+v)}}. \tag{8}$$

The symbol $\mathcal{M}^{(j,m)}(v)$ denotes the weight function which is a polynomial of degree $2j$ in v with coefficients determined by the initial state and the coin parameters β and γ. The decomposition (6) of the limit density $\nu^{(j)}(v)$ into $\lceil j \rceil$ densities $\nu^{(j,m)}(v)$ indicates that the $2j+1$-state Wigner walk can be considered as superposition of $\lceil j \rceil$ walks which propagates through the lattice with different velocity given by $2m\cos\frac{\beta}{2}$. In addition to the evaluation of moments (5), the limit density (6) can be used to approximate the shape of the probability distribution of the Wigner walk in finite time according to

$$p^{(j)}(x,t) \approx \frac{2}{t}\nu^{(j)}(\frac{x}{t}). \tag{9}$$

The factor of 2 accounts for the fact that the Wigner walks are bipartite. Note that the Konno's density function $\mu(v;a)$ diverges for $v \to \pm a$. These divergencies correspond to the $2j+1$ peaks ($2j$ if j is an integer) in the probability distribution $p^{(j)}(x,t)$ which are found at $x \approx \pm 2m\cos\frac{\beta}{2}t$, where the range of the index m is the same as in the sum (6).

We note that for integer j the particle is allowed to stay at its actual position, while for half-integer j it has to leave the previously occupied site. This has a crucial impact on the dynamics of the quantum walk, as was found in [42]. Indeed, for half-integer j the spectrum of the evolution operator (1) is purely continuous, while for integer j it has, in addition, an isolated eigenvalue with infinitely-many localized eigenstates. The presence of the point spectrum results in an additional peak in the center of the probability distribution which decays rapidly with the distance from the origin. Moreover, the peak does not vanish with increasing number of time steps, i.e. for integer j the particle has a non-vanishing probability to remain at position x in the asymptotic limit. This feature was first observed for three-state Grover walk on a line [30, 31]. We denote the limiting value of the probability to remain at position x as

$$p_{\infty}^{(j)}(x) = \lim_{t\to\infty} p^{(j)}(x,t), \tag{10}$$

and call it the trapping probability. Its explicit form was not given in [42]. We evaluate the trapping probability in Sections IV and VI, where we treat the Wigner walks with $j = 1$, resp. $j = 2$, following the approach used in [33–35].

In principle, the formulas (6), (7) and the general expression for the weight functions $\mathcal{M}^{(j,m)}(v)$ derived in [42] allow us to calculate the limit density $\nu^{(j)}(v)$ for arbitrary (half-)integer j. However, the actual form of the limit density is rather complicated already for small values of j, as can be observed in [42] where the authors provided the explicit results up to $j = \frac{3}{2}$. This makes further investigation of Wigner walks quite demanding. It is the aim of the paper to simplify the limit density as much as possible. In order to do so, we first discuss which of the coin parameters are physically relevant. Second, we simplify the dependence of the weight function on the initial coin state by choosing a more suitable basis in the coin space. Since we are interested only in the moments and the limit density, we consider two Wigner walks with coins $\hat{R}^{(j)}(\alpha_1,\beta_1,\gamma_1)$ and $\hat{R}^{(j)}(\alpha_2,\beta_2,\gamma_2)$ as equivalent if for any initial coin state $|\psi_{C_1}\rangle$ of the first walk there exists an initial coin state of the second walk $|\psi_{C_2}\rangle$ such that the resulting limit densities are the same. We note that two equivalent Wigner walks, as we have defined them, might exhibit different properties when additional aspects of quantum walks, such as topological phases [53–60], are of interest.

Let us begin with the coin parameters. Notice that Konno's density function depends only on one of them, namely β. Moreover, as was shown in [42] the weight functions $\mathcal{M}^{(j,m)}$ are determined by the initial coin state and the coin parameters β and γ, but they are independent of α. Hence, all quantum walks with different α are equivalent, as far as the limit density and the moments of the particle's position are concerned. Therefore, we consider $\alpha = 0$ from now on. Moreover, the dependence of the weights $\mathcal{M}^{(j,m)}$ on γ is rather simple. As was found in [42] the parameter γ enters only through the terms of the form $q_m\overline{q_n}e^{-i(m-n)\gamma}$. Hence, the Wigner walk with coin $\hat{R}^{(j)}(0,\beta,0)$ and the initial coin state (4) gives the same limit density as the Wigner walk with the coin $\hat{R}^{(j)}(0,\beta,\gamma)$ and the initial coin state

$$|\psi_C^{\gamma}\rangle = \sum_{m=-j}^{j} q_m e^{im\gamma}|m\rangle.$$

Therefore, all models with different γ are equivalent according to our definition and we restrict our further analysis to the case $\gamma = 0$. Hence, we are left with only one physically relevant coin parameter β. We note that for two-state walks the equivalence of the three-parameter set of quantum walks with coins $\hat{R}^{(1/2)}(\alpha,\beta,\gamma)$, which in fact covers all translationally invariant two-state quantum walks, with the single-parameter family $\hat{R}^{(1/2)}(0,\beta,0)$ was already established in [61]. The above discussion shows that within the set of Wigner walks the equivalence hold for arbitrary j.

We now turn to a slightly different parametrization of the coin operator $\hat{R}^{(j)}(0,\beta,0)$ which is more suitable in the context of Wigner walks. Namely, instead of β we consider the parameter ρ given by

$$\rho = \cos\frac{\beta}{2},$$

which corresponds to the divergencies of the limit densities (7). It also directly determines the speed of propagation of the wave-packet through the lattice [62]. Since the Euler angle β is limited to the interval $[0,\pi]$, the new parameter ρ varies from 0 to 1, and the identity

$$\sin\frac{\beta}{2} = \sqrt{1-\rho^2},$$

holds. Finally, we define the coin operator $\hat{R}^{(j)}(\rho) \equiv \hat{R}^{(j)}(0,\beta,0)$ with the matrix elements in the standard basis given by

$$\begin{aligned} R_{mn}^{(j)}(\rho) &= \langle m|\hat{R}^{(j)}(\rho)|n\rangle = \sum_l \Gamma(j,m,n,l) \\ &\quad \times\rho^{2j+m-n-2l}\left(\sqrt{1-\rho^2}\right)^{2l-m+n}. \end{aligned} \tag{11}$$

Let us now turn to the dependence of the limit density on the initial coin state. As was pointed out in [42], the weight functions $\mathcal{M}^{(j,m)}$ are rather involved functions of the coefficients q_i of the initial coin state in the standard basis. The aim of this paper is to simplify these expressions by choosing a more suitable basis of the coin space. Following the common experience of quantum mechanics one would expect that the suitable basis is the one given by the eigenvectors of the operator involved. This is indeed the case of the three-state Grover walk [35]. However, for Wigner walks the eigenvectors do not represent the best choice. To construct the suitable basis we consider one additional property of the eigenvectors of the Grover coin used in [35]. Namely, the basis vectors were chosen such that they result in non-generic distributions of the Grover walk, i.e. they reduce the number of peaks in the probability distribution. We adopt this requirement for Wigner walks and select the suitable basis vectors among such states. The conditions for non-generic distributions are straightforward in the asymptotic limit, since then the peaks correspond to the divergencies of the limit density (6). Therefore, we have to determine the states for which some of the divergencies of (6) vanish. In the following Section we solve these conditions and determine the suitable basis states for the two-state model. We then rewrite the suitable basis in terms of the eigenvectors of the coin operator. This gives us a recipe for construction of suitable bases in higher-dimensional models.

III. TWO-STATE MODEL

We begin with the simplest case of a two-state model where $j = \frac{1}{2}$. The coin space is two-dimensional with the basis states $|1/2\rangle$, $|-1/2\rangle$, which correspond to the jumps of one step to the right and one step to the left. In the standard basis the matrix representation of the coin operator is given by

$$R^{(1/2)}(\rho) = \begin{pmatrix} \rho & -\sqrt{1-\rho^2} \\ \sqrt{1-\rho^2} & \rho \end{pmatrix}. \tag{12}$$

The limiting probability density calculated in [42] reads

$$\nu^{(1/2)}(v) = \mu(v;\rho)\mathcal{M}^{(1/2,1/2)}, \tag{13}$$

where $\mu(v;\rho)$ is the Konno's density function (8) and the weight $\mathcal{M}^{(1/2,1/2)}$ is given by

$$\mathcal{M}^{(1/2,1/2)} = 1 + \mathcal{M}_1^{(1/2,1/2)} v. \tag{14}$$

The linear term $\mathcal{M}_1^{(1/2,1/2)}$ in the weight has the form

$$\begin{aligned} \mathcal{M}_1^{(1/2,1/2)} &= -|q_{1/2}|^2 + |q_{-1/2}|^2 + \\ &+ \frac{\sqrt{1-\rho^2}}{\rho}(q_{1/2}\overline{q_{-1/2}} + \overline{q_{1/2}}q_{-1/2}), \end{aligned} \tag{15}$$

where q_i's represent the coefficients of the initial coin state in the standard basis of the coin space

$$|\psi_C\rangle = q_{1/2}|1/2\rangle + q_{-1/2}|-1/2\rangle. \tag{16}$$

We will now determine the suitable basis for the description of the two-state model. Following the discussion in the previous section, we will construct the suitable basis from the states which lead to non-generic probability distributions, i.e. the states for which one of the divergencies of the limit density (13) vanishes. These divergencies coincide with those of the Konno's density function (8), which appear for $v = \pm\rho$. To eliminate them we have to find such $q_{\pm 1/2}$ that the weight function tends to zero faster than the denominator of the Konno's density function for $v = \pm\rho$, i.e. the weight has to attain the form

$$\mathcal{M}^{(\frac{1}{2},\frac{1}{2})} = 1 \pm \frac{v}{\rho}.$$

Hence, the linear term (15) has to be equal to $\pm\frac{1}{\rho}$. The solutions of these two equations

$$\begin{aligned} 1-\frac{v}{\rho}: \qquad & q_{1/2}=\sqrt{\frac{1+\rho}{2}} \\ & q_{-1/2}=-\sqrt{\frac{1-\rho}{2}}, \\ 1+\frac{v}{\rho}: \qquad & q_{1/2}=\sqrt{\frac{1-\rho}{2}}, \\ & q_{-1/2}=\sqrt{\frac{1+\rho}{2}}, \end{aligned}$$

provide the coefficients of the initial states (16) that eliminate the divergence of the limit density (13) at $v=\pm\rho$. We denote these vectors as $|\chi^{\pm}\rangle$. In the standard basis they have the form

$$\begin{aligned} |\chi^{+}\rangle &= \sqrt{\frac{1+\rho}{2}}|1/2\rangle-\sqrt{\frac{1-\rho}{2}}|-1/2\rangle, \\ |\chi^{-}\rangle &= \sqrt{\frac{1-\rho}{2}}|1/2\rangle+\sqrt{\frac{1+\rho}{2}}|-1/2\rangle. \end{aligned} \tag{17}$$

Clearly, these two states form an orthonormal basis of the coin space. Moreover, we find that in this basis the weight function (14) simplifies considerably. We express the initial coin state in terms of the basis $\{|\chi^{\pm}\rangle\}$ according to

$$|\psi_C\rangle=h^{+}|\chi^{+}\rangle+h^{-}|\chi^{-}\rangle.$$

The correspondence between the amplitudes of the initial coin state in the suitable basis h_i and in the standard basis is then given by

$$\begin{aligned} q_{1/2} &= \sqrt{\frac{1+\rho}{2}}h^{+}+\sqrt{\frac{1-\rho}{2}}h^{-}, \\ q_{-1/2} &= -\sqrt{\frac{1-\rho}{2}}h^{+}+\sqrt{\frac{1+\rho}{2}}h^{-}. \end{aligned}$$

Inserting these relations into the formula (15) we find that the linear term of the weight function reduces into

$$\mathcal{M}_1^{(1/2,1/2)}=\frac{1}{\rho}(1-2|h^{+}|^2).$$

Hence, the limit density for a two-state quantum walk with Wigner coin (12) in the suitable basis $\{|\chi^{\pm}\rangle\}$ reads

$$\nu^{(1/2)}(v)=\frac{\sqrt{1-\rho^2}\left(1+(1-2|h^{+}|^2)\frac{v}{\rho}\right)}{\pi(1-v^2)\sqrt{(\rho-v)(\rho+v)}}. \tag{18}$$

This result shows another benefit of using the basis $\{|\chi^{\pm}\rangle\}$. Namely, by absorbing part of the ρ dependence into the definition of the basis states (17), ρ is effectively reduced to a scaling parameter. Indeed, varying the value of ρ while keeping the amplitudes h^{+} and h^{-} untouched does not affect the shape of the limit density (18). The parameter ρ simply determines how far the density is stretched. We point out that the same will apply for Wigner walks with higher values of j.

To illustrate our results we display in FIG. 1 the probability distribution for the initial coin state $|\chi^{-}\rangle$ after 100 steps. The red curve depicts the limit density which for $|\chi^{-}\rangle$ is given by

$$\nu_{|\chi^{-}\rangle}^{(1/2)}(v)=\frac{\sqrt{1-\rho^2}\sqrt{\rho+v}}{\pi\rho(1-v^2)\sqrt{\rho-v}}.$$

Clearly, the limit density diverges for $v\to\rho$ but tends to zero for $v\to-\rho$. This corresponds to the presence of only one peak in FIG. 1 which we emphasize by using a logarithmic scale on the y-axis [63].

Let us point out that the limit density of any homogeneous two-state quantum walk on a line can be transformed into the form (18). Indeed, the two-dimensional Wigner coins $\hat{R}^{(1/2)}(\alpha,\beta,\gamma)$ covers all SU(2) matrices and the equivalence

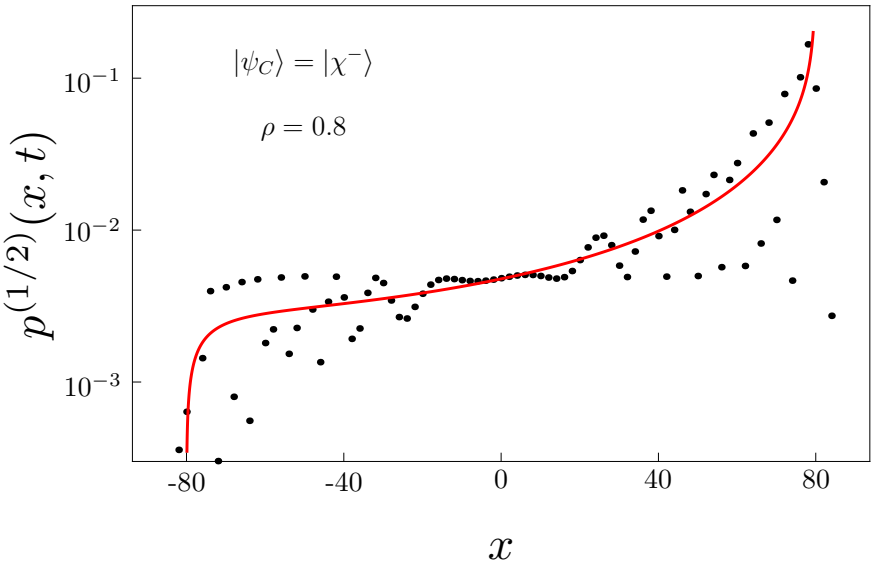

FIG. 1: (Color online) Probability distribution after 100 steps of the two-state Wigner walk with the coin $R^{(1/2)}(\rho)$. The initial state was chosen as $|\chi^-\rangle$. The coin parameter is $\rho = 0.8$. We note that for different values of ρ the probability distribution will have the same shape, only its width will change accordingly. The same applies to all figures.

of a general SU(2) walk to the walk with the coin $\hat{R}^{(1/2)}(\rho)$ was already pointed out in [61]. Hence, for any two-state quantum walk on a line one can find two orthogonal coin states giving rise to non-generic distributions with only one peak.

Finally, let us rewrite the suitable basis $\{|\chi^\pm\rangle\}$ in terms of the eigenvectors of the coin operator (12). This decomposition will be useful in the following Sections where we treat higher-dimensional models. The eigenvectors of the coin operator (12) are given by

$$|\psi^\pm\rangle = \frac{1}{\sqrt{2}}(|1/2\rangle \mp i|-1/2\rangle). \tag{19}$$

They satisfy the eigenvalue equations

$$\hat{R}^{(1/2)}(\rho)|\psi^\pm\rangle = e^{\pm i\varphi}|\psi^\pm\rangle,$$

where the phase of the eigenvalues reads

$$\varphi = \arccos\rho.$$

The decomposition of the suitable basis $\{|\chi^\pm\rangle\}$ into the eigenvectors (19) is easily found to be

$$\begin{aligned} |\chi^+\rangle &= \frac{1}{\sqrt{2}}\left(e^{-i\frac{\varphi}{2}}|\psi^+\rangle + e^{i\frac{\varphi}{2}}|\psi^-\rangle\right), \\ |\chi^-\rangle &= \frac{i}{\sqrt{2}}\left(e^{-i\frac{\varphi}{2}}|\psi^+\rangle - e^{i\frac{\varphi}{2}}|\psi^-\rangle\right). \end{aligned} \tag{20}$$

These relations provide us with a recipe for construction of suitable bases for $j > \frac{1}{2}$.

IV. THREE-STATE MODEL

In this Section we analyze the three-state Wigner walk which is driven by the coin operator

$$R^{(1)}(\rho) = \begin{pmatrix} \rho^2 & -\sqrt{2}\rho\sqrt{1-\rho^2} & 1-\rho^2 \\ \sqrt{2}\rho\sqrt{1-\rho^2} & -1+2\rho^2 & -\sqrt{2}\rho\sqrt{1-\rho^2} \\ 1-\rho^2 & \sqrt{2}\rho\sqrt{1-\rho^2} & \rho^2 \end{pmatrix}.$$

The Wigner matrix $R^{(1)}(\rho)$ is reminiscent of the modified Grover coin which was introduced in [32] and recently analyzed in more detail in [34, 35]. Therefore, it is not surprising that the two models yield the same results, as we identify in the following subsections. In fact, the affinity of the three-state Wigner walk and the three-state Grover walk was already discussed in [42].

In the three-state Wigner walk the particle is allowed to remain at its present position. As we have discussed before, this implies that the probability distribution of the three-state Wigner walk is not described solely by the limit density (6). There is an additional non-vanishing and stationary peak at the origin due to the trapping effect (10). We analyze the limit density in subsection IV A and the trapping probability in subsection IV B. Before we give their explicit forms, we first construct the suitable basis of the coin space. We adopt the recipe provided by Eq. (20), which gives the decomposition of the suitable basis states for the two-state model into the eigenvectors of the coin operator. For the three-state model, the coin $\hat{R}^{(1)}(\rho)$ has two eigenvectors $|\psi^{\pm}\rangle$ satisfying the eigenvalue equations

$$\hat{R}^{(1)}(\rho)|\psi^{\pm}\rangle = e^{\pm i\varphi}|\psi^{\pm}\rangle.$$

The explicit form of the eigenvectors and the phase φ is left for the Appendix A. Following the formula (20) for the two-state model, we construct from $|\psi^{\pm}\rangle$ two orthonormal vectors $|\chi^{\pm}\rangle$ which will serve as part of the new basis. Moreover, the coin $\hat{R}^{(1)}(\rho)$ has an additional eigenvector $|\psi_0\rangle$ corresponding to the eigenvalue one. This vector is indeed orthogonal to both $|\psi^{\pm}\rangle$ and $|\chi^{\pm}\rangle$. Hence, we consider it as the last vector of the new basis which reads

$$\begin{aligned} |\chi_0\rangle &= |\psi_0\rangle, \\ |\chi^{+}\rangle &= \frac{1}{\sqrt{2}}\left(e^{-i\frac{\varphi}{2}}|\psi^{+}\rangle + e^{i\frac{\varphi}{2}}|\psi^{-}\rangle\right), \\ |\chi^{-}\rangle &= \frac{i}{\sqrt{2}}\left(e^{-i\frac{\varphi}{2}}|\psi^{+}\rangle - e^{i\frac{\varphi}{2}}|\psi^{-}\rangle\right). \end{aligned} \tag{21}$$

The initial state is now decomposed in the suitable basis $\{|\chi_0\rangle, |\chi^{\pm}\rangle\}$ according to

$$|\psi_C\rangle = h_0|\chi_0\rangle + h^{+}|\chi^{+}\rangle + h^{-}|\chi^{-}\rangle. \tag{22}$$

The explicit correspondence between the amplitudes of the initial state in the suitable basis h_i and in the standard basis q_i is given in the Appendix A. In the following we show that the limit density and the trapping probability obtain much more convenient forms when expressed in the basis $\{|\chi_0\rangle, |\chi^{\pm}\rangle\}$.

A. Limit density

The limit density for the three-state Wigner walk was derived in [42] and reads

$$\nu^{(1)}(v) = \frac{1}{2}\mu\left(\frac{v}{2};\rho\right)\mathcal{M}^{(1,1)}\left(\frac{v}{2}\right),$$

where $\mathcal{M}^{(1,1)}(v)$ can be expressed as a polynomial of degree two in v

$$\mathcal{M}^{(1,1)}(v) = \mathcal{M}_0^{(1,1)} + \mathcal{M}_1^{(1,1)}v + \mathcal{M}_2^{(1,1)}v^2.$$

The individual terms $\mathcal{M}_i^{(1,1)}$ depend on the coin parameter ρ and the initial coin state. Their explicit form in the standard basis was given in [42], we present it in the Appendix A for comparison. There we also show how the terms $\mathcal{M}_i^{(1,1)}$ simplify when we expand the initial state into the suitable basis according to (22). Indeed, in the suitable basis we obtain

$$\begin{aligned} \mathcal{M}_0^{(1,1)} &= |h^{+}|^2 + |h^{-}|^2, \\ \mathcal{M}_1^{(1,1)} &= \frac{1}{\rho}(h_0\overline{h^{-}} + \overline{h_0}h^{-}), \\ \mathcal{M}_2^{(1,1)} &= \frac{1}{\rho^2}(|h_0|^2 - |h^{+}|^2). \end{aligned}$$

For illustration we show in FIGs. 2,3 and 4 the probability distribution of the three-state Wigner walk with the initial coin state given by one of the suitable basis vectors (21). In FIG. 2 we find that for $|\chi_0\rangle$ the limit density tends

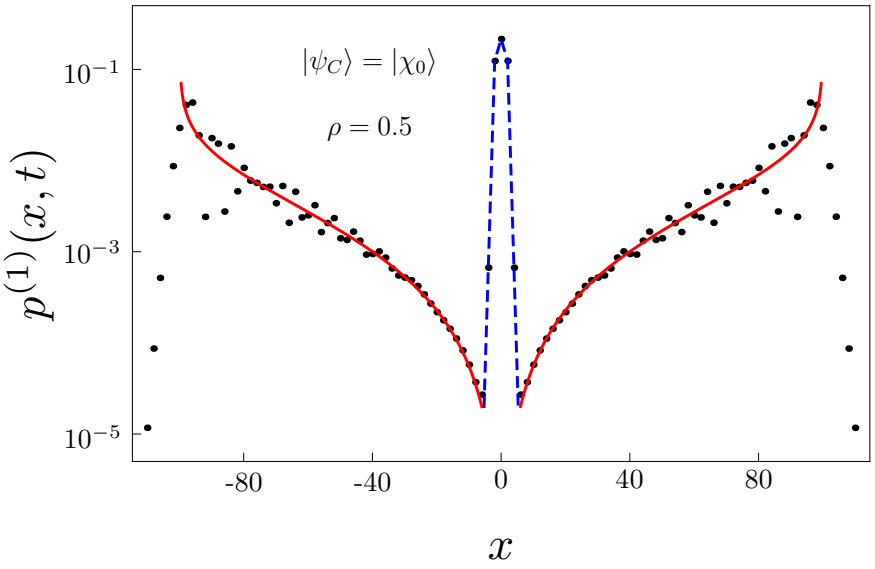

FIG. 2: Probability distribution after 100 steps of the three-state Wigner walk. The initial coin state was chosen as $|\chi_0\rangle$ and the coin parameter is $\rho = 0.5$

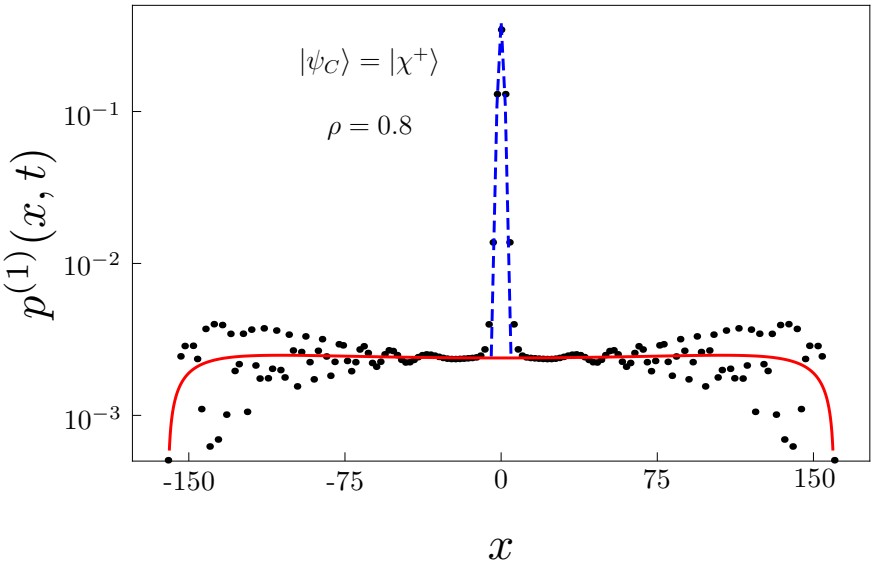

FIG. 3: Probability distribution after 100 steps of the three-state Wigner walk. The initial coin state was chosen as $|\chi^+\rangle$ and the coin parameter is $\rho = 0.8$

to zero at the origin. Indeed, for $h_0 = 1$ the constant term of the limit density $\mathcal{M}_0^{(1,1)}$ vanishes. Nevertheless, the probability distribution at the origin does not vanish due to the trapping effect[64]. For $|\chi^+\rangle$ both peaks at $v \to \pm 2\rho$ vanishes, as we illustrate in FIG. 3. Finally, FIG. 4 indicates that for the last basis vector $|\chi^-\rangle$ the trapping at the origin disappears, which we identify analytically in the Appendix A.

We point out that the limit density of the three-state Grover walk and its one-parameter extension exhibit all of these features [35]. Moreover, in the following subsection we show that also the trapping effect of the three-state Wigner walk is the same as for the three-state Grover walk.

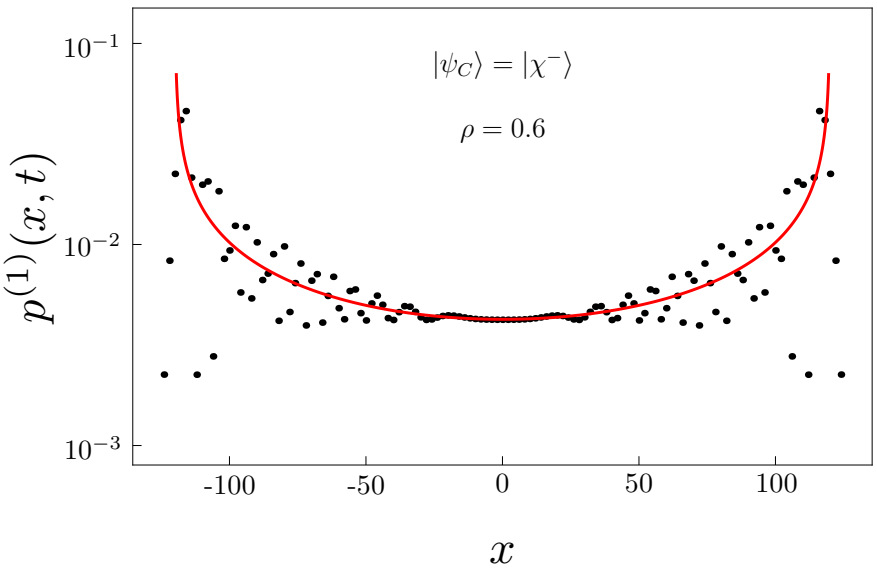

FIG. 4: Probability distribution after 100 steps of the three-state Wigner walk. The initial coin state was chosen as $|\chi^-\rangle$ and the coin parameter is $\rho = 0.6$

B. Trapping probability

Let us now turn to the trapping probability. The details of the calculations are left for the Appendix A. Following the same approach that was used for the three-state Grover walk in [33–35] we find that in the suitable basis (21) the trapping probability reads

$$p_\infty^{(1)}(2x) = \begin{cases} Q^{2|x|}\frac{2(1-\rho^2)}{\rho^4}|h_0 - h^+|^2, & x < 0, \\ \frac{Q}{\rho^2}((1-\rho^2)|h_0|^2 + |h^+|^2), & x = 0, \\ Q^{2x}\frac{2(1-\rho^2)}{\rho^4}|h_0 + h^+|^2, & x > 0. \end{cases} \tag{23}$$

Here we have denoted

$$Q = \frac{2 - \rho^2 - 2\sqrt{1-\rho^2}}{\rho^2}. \tag{24}$$

We note that the trapping probability for the one-parameter extension of the three-state Grover walk has exactly the same form [35].

In the suitable basis (21), the trapping probability (23) is independent of the amplitude h^- of the initial coin state (22). This fact reduces the dependence of the trapping probability to just two amplitudes h_0 and h^+. However, the expression (23) can be simplified further by an additional change of basis. Notice that the dependence of the trapping probability is different for positive and negative positions. In fact, one can choose such an initial state that the trapping effect appears only on positive or negative semi-axis. We note that the same feature was identified for the three-state Grover walk [33] and its one-parameter extension [35]. For the three-state Wigner walk with the initial coin state

$$|\lambda^+\rangle = \frac{1}{\sqrt{2}}\left(|\chi_0\rangle + |\chi^+\rangle\right),$$

the trapping effect appears only for non-negative positions. Similarly, the state

$$|\lambda^-\rangle = \frac{1}{\sqrt{2}}\left(|\chi_0\rangle - |\chi^+\rangle\right)$$

shows trapping only for non-positive x. We illustrate this feature in FIG. 5.

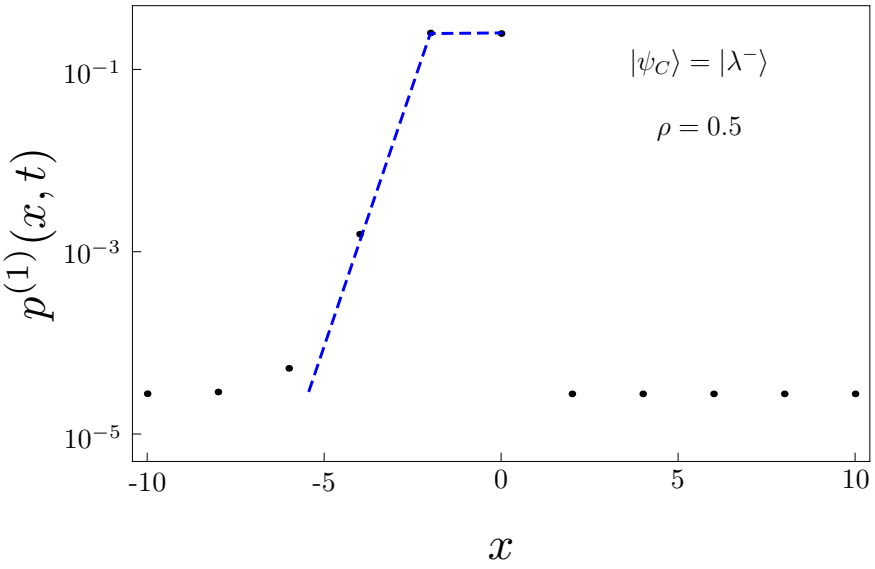

FIG. 5: Probability distribution after 10000 steps of the three-state Wigner walk. The initial coin state was chosen as $|\lambda^-\rangle$ and the coin parameter is $\rho = 0.5$. Only a small vicinity of the origin is displayed to emphasize that for $|\lambda^-\rangle$ the trapping effect appears only for $x \leq 0$. Higher number of steps in comparison with other figures was chosen so that the trapping effect is sufficiently pronounced further from the origin.

The vectors $|\lambda^+\rangle$ and $|\lambda^-\rangle$ are mutually orthogonal. Moreover, they are both orthogonal to $|\chi^-\rangle$ and the triplet $\{|\chi^-\rangle, |\lambda^\pm\rangle\}$ forms an orthonormal basis of the coin space. When we decompose the initial coin state as

$$|\psi_C\rangle = h^-|\chi^-\rangle + l^+|\lambda^+\rangle + l^-|\lambda^-\rangle,$$

we find that the trapping probability turns into

$$p_\infty(2x) = \begin{cases} Q^{2|x|}\frac{2(1-\rho^2)}{\rho^4}|l^-|^2, & x < 0, \\ \frac{Q}{\rho^2}\left(|l^+|^2 + |l^-|^2 - \frac{1}{2\rho^2}|l^+ + l^-|^2\right), & x = 0, \\ Q^{2x}\frac{2(1-\rho^2)}{\rho^4}|l^+|^2, & x > 0. \end{cases}$$

The advantage of the basis $\{|\chi^-\rangle, |\lambda^\pm\rangle\}$ is that the trapping probability outside the origin has a simpler form. Namely, it depends only on one amplitude l^+ (resp. l^-) for positive x (resp. negative x). This additional change of basis becomes crucial in Section VI where we treat the five-state Wigner walk.

V. FOUR-STATE MODEL

For $j = \frac{3}{2}$ we obtain a four state quantum walk model with the coin operator determined by (11). The coin operator $\hat{R}^{(3/2)}(\rho)$ has two pairs of eigenvectors $|\psi_1^\pm\rangle$ and $|\psi_2^\pm\rangle$ with conjugated pairs of eigenvalues

$$\begin{aligned} \hat{R}^{(3/2)}(\rho)|\psi_1^\pm\rangle &= e^{\pm i\varphi_1}|\psi_1^\pm\rangle, \\ \hat{R}^{(3/2)}(\rho)|\psi_2^\pm\rangle &= e^{\pm i\varphi_2}|\psi_2^\pm\rangle. \end{aligned}$$

The explicit form of the eigenvectors and the phases $\varphi_{1,2}$ is given in the Appendix B. Following the formula (20) we construct the suitable basis by combining only the eigenvectors corresponding to the same phase factor φ_1 or φ_2.

Therefore, we consider the suitable basis in the form

$$\begin{aligned}
|\chi_1^+\rangle &= \frac{1}{\sqrt{2}}(e^{-i\frac{\varphi_1}{2}}|\psi_1^+\rangle + e^{i\frac{\varphi_1}{2}}|\psi_1^-\rangle),\\
|\chi_1^-\rangle &= \frac{i}{\sqrt{2}}(e^{-i\frac{\varphi_1}{2}}|\psi_1^+\rangle - e^{i\frac{\varphi_1}{2}}|\psi_1^-\rangle),\\
|\chi_2^+\rangle &= \frac{1}{\sqrt{2}}(e^{-i\frac{\varphi_2}{2}}|\psi_2^+\rangle + e^{i\frac{\varphi_2}{2}}|\psi_2^-\rangle),\\
|\chi_2^-\rangle &= \frac{i}{\sqrt{2}}(e^{-i\frac{\varphi_2}{2}}|\psi_2^+\rangle - e^{i\frac{\varphi_2}{2}}|\psi_2^-\rangle).
\end{aligned} \tag{25}$$

The initial coin state is decomposed in the suitable basis according to

$$|\psi_C\rangle = h_1^+|\chi_1^+\rangle + h_1^-|\chi_1^-\rangle + h_2^+|\chi_2^+\rangle + h_2^-|\chi_2^-\rangle.$$

We present the explicit relation between the amplitudes in the suitable basis h_i and the standard basis q_i in the Appendix B.

Let us now turn to the limit density which for the four-state model is given by a sum of two densities [42]

$$\nu^{(3/2)}(v) = \nu^{(3/2,1/2)}(v) + \nu^{(3/2,3/2)}(v).$$

The individual densities corresponding to a slower walk ($m = \frac{1}{2}$) and a faster walk ($m = \frac{3}{2}$) read

$$\begin{aligned}
\nu^{(3/2,1/2)}(v) &= \mu(v;\rho)\mathcal{M}^{(3/2,1/2)}(v),\\
\nu^{(3/2,3/2)}(v) &= \frac{1}{3}\mu\left(\frac{v}{3};\rho\right)\mathcal{M}^{(3/2,3/2)}\left(\frac{v}{3}\right),
\end{aligned} \tag{26}$$

The weight functions $\mathcal{M}^{(3/2,m)}(v)$ are given by cubic polynomials in v

$$\mathcal{M}^{(3/2,m)}(v) = \sum_{k=0}^{3}\mathcal{M}_i^{(3/2,m)}v^i, \tag{27}$$

with coefficients $\mathcal{M}_i^{(3/2,m)}$ determined by the initial coin state and the coin parameter ρ. Their explicit forms in the standard basis of the coin space are given in [42]. We express them in terms of the suitable basis $\{|\chi_1^\pm\rangle, |\chi_2^\pm\rangle\}$ in the Appendix B. Using the expressions (B3) and (B4) one can show by direct computation that each of the basis states $|\chi_i^\pm\rangle$ eliminates two peaks of the probability distribution - one in each of the individual limit densities $\nu^{(3/2,1/2)}(v)$ and $\nu^{(3/2,3/2)}(v)$. To illustrate our results we present in FIGs. 6 and 7 the probability distributions for the initial states $|\chi_1^+\rangle$ and $|\chi_2^+\rangle$.

We point out that it is possible to eliminate both peaks for each limit density $\nu^{(3/2,m)}(v)$ on its own. In order to do so we have to find an initial coin state such that both divergences provided by the Konno's density $\mu(v;\rho)$ in (26) vanishes. Hence, the weight function have to be of the form

$$\mathcal{M}^{(3/2,m)}(v) = (\rho^2 - v^2)(a + bv),$$

for some arbitrary constants a and b. This is satisfied provided that

$$\begin{aligned}
\mathcal{M}_0^{(3/2,m)} + \rho^2\mathcal{M}_2^{(3/2,m)} &= 0,\\
\mathcal{M}_1^{(3/2,m)} + \rho^2\mathcal{M}_3^{(3/2,m)} &= 0.
\end{aligned} \tag{28}$$

Adding and subtracting these two equations for the weight function $\mathcal{M}^{(3/2,1/2)}(v)$ we obtain the following

$$|h_1^+ + \sqrt{3}h_2^+|^2 = 0, \quad |h_1^- + \sqrt{3}h_2^-|^2 = 0,$$

which lead us to the relations

$$h_2^+ = -\frac{1}{\sqrt{3}}h_1^+, \quad h_2^- = -\frac{1}{\sqrt{3}}h_1^-. \tag{29}$$

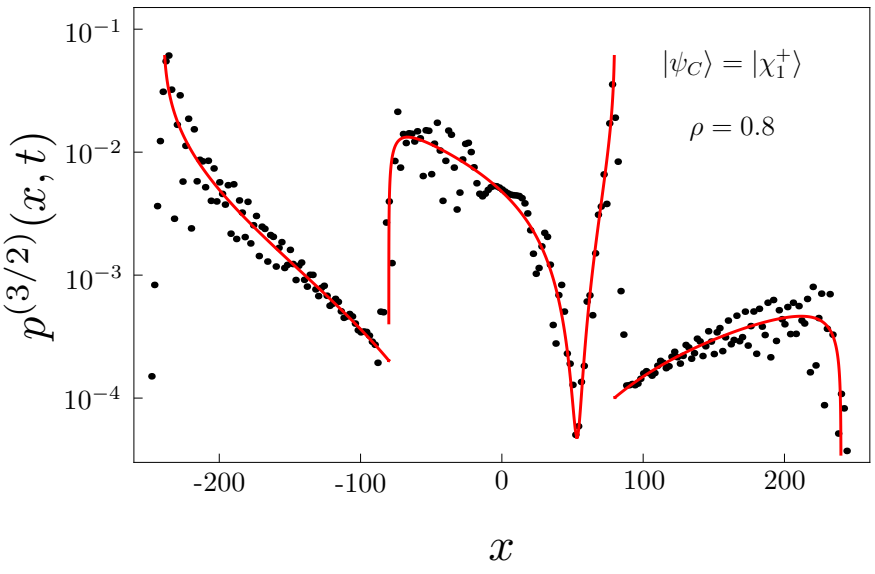

FIG. 6: (Color online) Probability distribution after 100 steps of the four-state Wigner walk. The initial coin state was chosen as $|\chi_1^+\rangle$. The coin parameter is $\rho = 0.8$. The initial state $|\chi_1^-\rangle$ results in a distribution which is a mirror image of the present one.

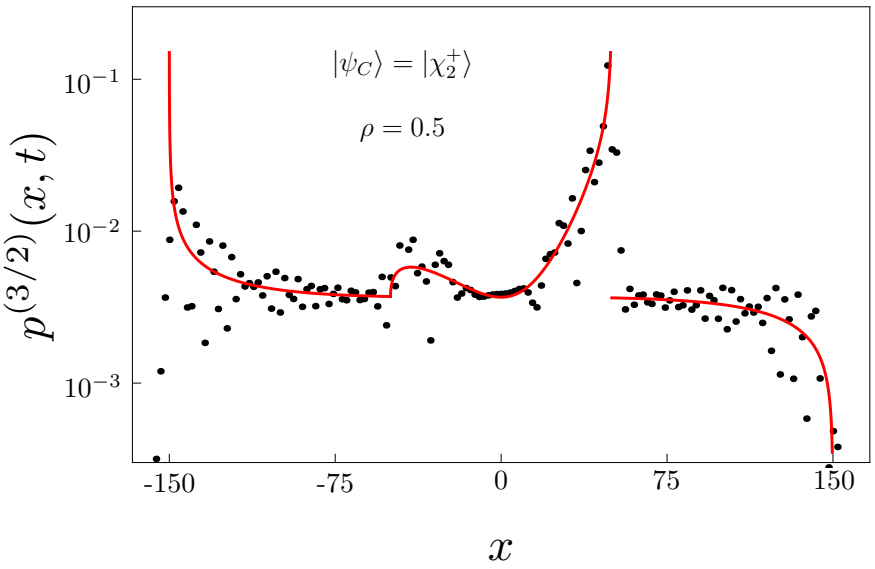

FIG. 7: (Color online) Probability distribution after 100 steps of the four-state Wigner walk. The initial coin state was chosen as $|\chi_2^+\rangle$. The coin parameter is $\rho = 0.5$. For the initial state $|\chi_2^-\rangle$ the probability distribution is a mirror image of the present one.

Hence, we find a two-dimensional subset of states

$$|\psi_C^{(1/2)}\rangle = h_1^+|\chi_1^+\rangle + h_1^-|\chi_1^-\rangle - \frac{h_1^+}{\sqrt{3}}|\chi_2^+\rangle - \frac{h_1^-}{\sqrt{3}}|\chi_2^-\rangle, \tag{30}$$

for which the peaks of the slower walk described by $\nu^{(3/2,1/2)}(v)$ vanishes. We note that for the vectors of the family (30) with either $h_1^+ = h_2^+ = 0$ or $h_1^- = h_2^- = 0$ in addition one of the peaks of the faster walk vanishes, i.e. these states result in a probability distribution with only one peak. We illustrate this result in FIG. 8.

Similarly, we can cancel both divergencies for the second limit density $\nu^{(3/2,3/2)}(v)$ corresponding to the faster peaks in the probability distribution. From the equations (28) for $m = \frac{3}{2}$ we find that both faster peaks vanish provided

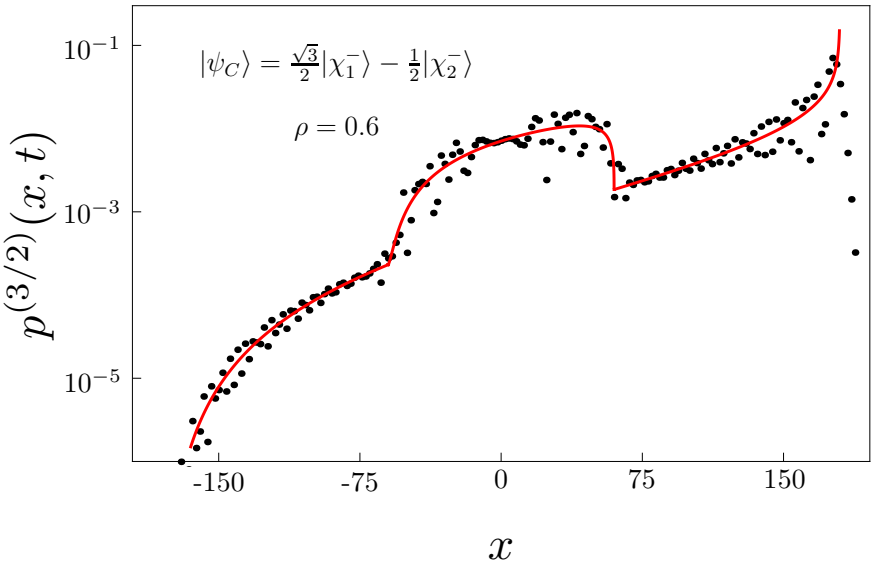

FIG. 8: (Color online) Probability distribution after 100 steps of the four-state Wigner walk. The initial coin state $\frac{\sqrt{3}}{2}|\chi_1^-\rangle - \frac{1}{2}|\chi_2^-\rangle$ was chosen as a part of the set (30) for which the inner peaks in the probability distribution vanishes. Moreover, since $h_1^+ = h_2^+ = 0$, only one of the outer peaks is present. The coin parameter is $\rho = 0.6$

that

$$h_2^+ = \sqrt{3}h_1^+, \quad h_2^- = \sqrt{3}h_1^-. \tag{31}$$

Hence, we obtain a two-dimensional set of initial states

$$|\psi_C^{(3/2)}\rangle = h_1^+|\chi_1^+\rangle + h_1^-|\chi_1^-\rangle + \sqrt{3}h_1^+|\chi_2^+\rangle + \sqrt{3}h_1^-|\chi_2^-\rangle, \tag{32}$$

for which the outer peaks in the probability distribution vanishes. Moreover, the vectors from the family (32) satisfying either $h_1^+ = h_2^+ = 0$ or $h_1^- = h_2^- = 0$ lead to elimination of one additional peak of the slower walk, i.e. they result in a probability distribution with only one peak. We illustrate this result in FIG. 9.

Clearly, it is impossible to fulfill both conditions (29) and (31) simultaneously. Hence, the probability distribution of the four-state Wigner walk has always at least one peak.

VI. FIVE-STATE MODEL

In this Section we analyze the case $j = 2$ which leads to the five-state Wigner walk. Similarly to the three-state model, which we have discussed in Section IV, the probability distribution of the five-state model consists of the limit density and the trapping probability. We treat them in subsections VI A and VI B, but first we construct the suitable basis of the coin space following the recipe (20). The coin operator $\hat{R}^{(2)}(\rho)$ has two pairs of eigenvectors $|\psi_1^\pm\rangle$ and $|\psi_2^\pm\rangle$ corresponding to two pairs of conjugated eigenvalues

$$\begin{aligned} \hat{R}^{(2)}(\rho)|\psi_1^\pm\rangle &= e^{\pm i\varphi_1}|\psi_1^\pm\rangle, \\ \hat{R}^{(2)}(\rho)|\psi_2^\pm\rangle &= e^{\pm i\varphi_2}|\psi_2^\pm\rangle. \end{aligned}$$

The explicit form of the eigenvectors and the phases $\varphi_{1,2}$ is left for the Appendix C. From these two pairs of eigenvectors we construct four basis vectors $|\chi_1^\pm\rangle$ and $|\chi_2^\pm\rangle$ according to (25). In addition, the coin $\hat{R}^{(2)}(\rho)$ has an eigenvalue 1. We include the corresponding eigenvector $|\psi_0\rangle$ as the last basis vector. Hence, we obtain the suitable

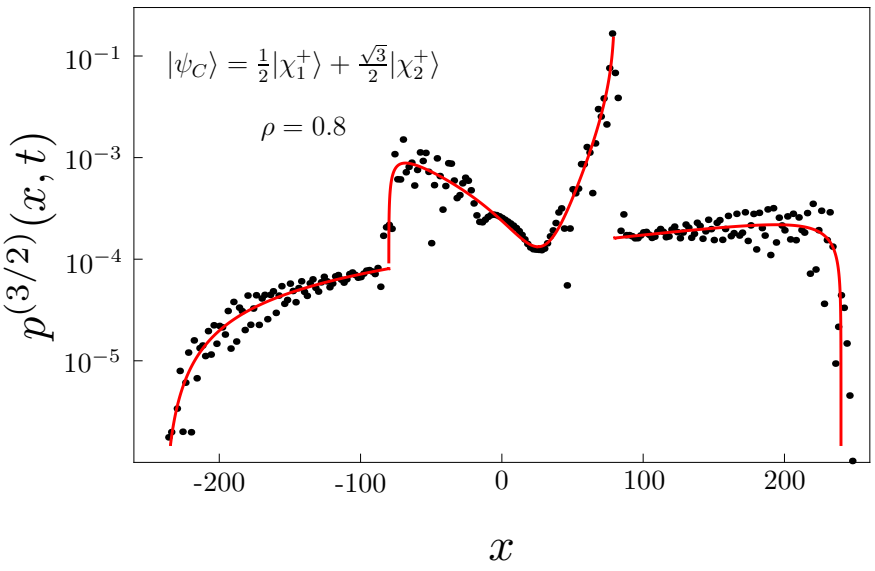

FIG. 9: (Color online) Probability distribution after 100 steps of the four-state Wigner walk. The initial coin state $\frac{1}{2}|\chi_1^+\rangle + \frac{\sqrt{3}}{2}|\chi_2^+\rangle$ is an element of the set (32) for which the outer peaks in the probability distribution vanishes. Since $h_1^- = h_2^- = 0$, only one of the inner peaks is present. The coin parameter is $\rho = 0.8$

basis in the form

$$\begin{aligned}
|\chi_0\rangle &= |\psi_0\rangle, \\
|\chi_1^+\rangle &= \frac{1}{\sqrt{2}}\left(e^{-i\frac{\varphi_1}{2}}|\psi_1^+\rangle + e^{i\frac{\varphi_1}{2}}|\psi_1^-\rangle\right), \\
|\chi_1^-\rangle &= \frac{i}{\sqrt{2}}\left(e^{-i\frac{\varphi_1}{2}}|\psi_1^+\rangle - e^{i\frac{\varphi_1}{2}}|\psi_1^-\rangle\right), \\
|\chi_2^+\rangle &= \frac{1}{\sqrt{2}}\left(e^{-i\frac{\varphi_1}{2}}|\psi_2^+\rangle + e^{i\frac{\varphi_1}{2}}|\psi_2^-\rangle\right), \\
|\chi_2^-\rangle &= \frac{i}{\sqrt{2}}\left(e^{-i\frac{\varphi_1}{2}}|\psi_2^+\rangle - e^{i\frac{\varphi_1}{2}}|\psi_2^-\rangle\right).
\end{aligned} \tag{33}$$

The initial state is decomposed into the suitable basis according to

$$|\psi_C\rangle = h_0|\chi_0\rangle + h_1^+|\chi_1^+\rangle + h_1^-|\chi_1^-\rangle + h_2^+|\chi_2^+\rangle + h_2^-|\chi_2^-\rangle.$$

We present the correspondence between the amplitudes in the suitable basis h_i and in the standard basis q_i in the Appendix C. In the following subsections we illustrate that the change of the basis allows us to identify various interesting regimes of dynamics which are otherwise hidden in the standard basis description.

A. Limit density

Let us first discuss the limit density. As for the four-state walk of Section V, the total limit density (6) is a sum of two densities

$$\nu^{(2)}(v) = \nu^{(2,1)}(v) + \nu^{(2,2)}(v),$$

corresponding to a slower walk

$$\nu^{(2,1)}(v) = \frac{1}{2}\mu\left(\frac{v}{2};\rho\right)\mathcal{M}^{(2,1)}\left(\frac{v}{2}\right)$$

and a faster walk

$$\nu^{(2,2)}(v) = \frac{1}{4}\mu\left(\frac{v}{4};\rho\right)\mathcal{M}^{(2,2)}\left(\frac{v}{4}\right).$$

The weight functions $\mathcal{M}^{(2,m)}(v)$ are polynomials of degree four in v

$$\mathcal{M}^{(2,m)}(v) = \sum_{i=0}^{4}\mathcal{M}_i^{(2,m)}v^i,$$

with coefficients $\mathcal{M}_i^{(2,m)}$ determined by the initial coin state and the coin parameter ρ. Their explicit form in the standard basis of the coin space can be evaluated using the procedure of [42]. In the Appendix C we express them in terms of the coefficients in the suitable basis.

Let us now illustrate the role of individual vectors of the suitable basis $\{|\chi_0\rangle, |\chi_1^{\pm}\rangle, |\chi_2^{\pm}\rangle\}$ on the dynamics of the five-state Wigner walk. Using the explicit form of the weight functions (C3) and (C4) one can show that each of the basis states eliminates two peaks, either in the slower walk described $\nu^{(2,1)}(v)$ or in the faster walk given by $\nu^{(2,2)}(v)$. In FIG. 10 we display the probability distribution for the initial state $|\chi_0\rangle$. We find that both peaks of the slower walk vanishes. In addition, both densities $\nu^{(2,1)}(v)$ and $\nu^{(2,2)}(v)$ tend to zero at the origin, since both weight functions $\mathcal{M}^{(2,m)}(v)$ miss the constant term $\mathcal{M}_0^{(2,m)}$. In FIG. 10 this corresponds to the significant dip of the red curve around the origin. However, the total probability distribution does not vanish at the origin due to the trapping effect, which is illustrated by the blue curve in FIG. 10.

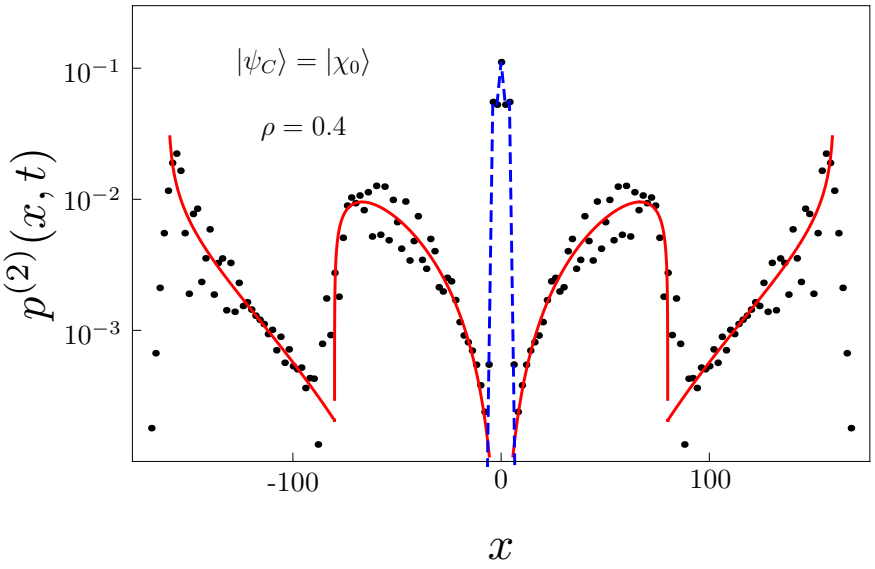

FIG. 10: (Color online) Probability distribution after 100 steps of the five-state Wigner walk. The initial coin state was chosen as $|\chi_0\rangle$. The coin parameter is $\rho = 0.4$

In FIG. 11 we have chosen the initial state as $|\chi_1^+\rangle$. For this particular state both outer peaks vanishes. FIG. 12 displays the probability distribution for the initial state $|\chi_1^-\rangle$. In this situation both inner peaks vanishes and, in addition, the trapping effect disappears. In FIG. 13 we have chosen the initial state as $|\chi_2^+\rangle$. For this initial state both inner peaks vanishes. However, unlike in FIG. 12 the trapping effect is present. Finally, in FIG. 14 we display the probability distribution for the initial state $|\chi_2^-\rangle$. In such a case the outer peaks vanishes. Moreover, the trapping effect is absent, similar to the FIG. 12.

Let us now determine the sets of states for which both peaks of either the slower walk or the faster walk disappear. To achieve this the weight function has to be of the form

$$\mathcal{M}^{(2,m)}(v) = (\rho^2 - v^2)(a + bv + cv^2),$$

for some arbitrary a, b, c. This is satisfied provided that

$$\begin{aligned}\mathcal{M}_1^{(2,m)} + \rho^2\mathcal{M}_3^{(2,m)} &= 0,\\ \mathcal{M}_0^{(2,m)} + \rho^2\mathcal{M}_2^{(2,m)} + \rho^4\mathcal{M}_4^{(2,m)} &= 0.\end{aligned} \tag{34}$$

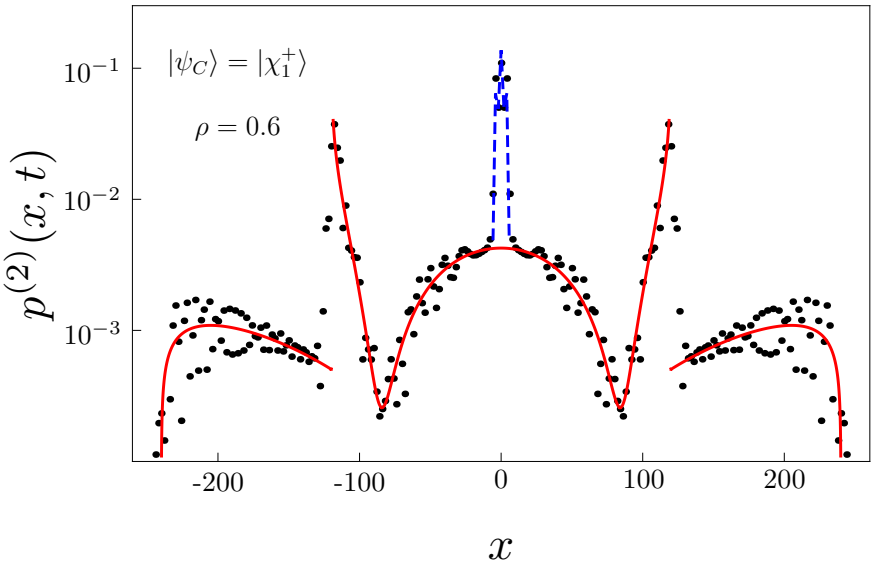

FIG. 11: (Color online) Probability distribution after 100 steps of the five-state Wigner walk. The initial coin state was chosen as $|\chi_1^+\rangle$. The coin parameter is $\rho = 0.6$

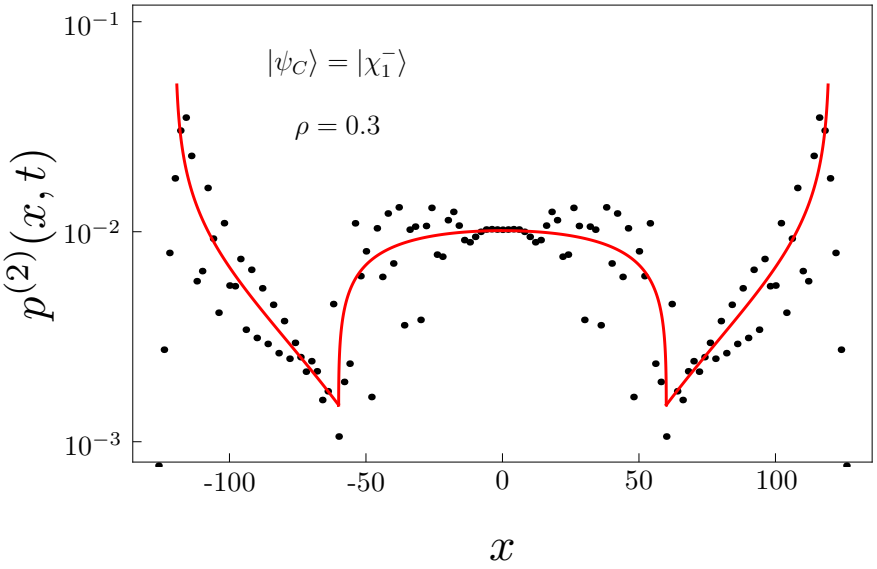

FIG. 12: (Color online) Probability distribution after 100 steps of the five-state Wigner walk. The initial coin state was chosen as $|\chi_1^-\rangle$. The coin parameter is $\rho = 0.3$

Concerning the slower walk described by the limit density $\nu^{(2,1)}(v)$, from the explicit form of the weight function $\mathcal{M}^{(2,1)}(v)$ given in (C3) we obtain the conditions

$$\begin{aligned} h_1^+\overline{h_2^-} + \overline{h_1^+}h_2^- &= 0, \\ |h_1^+|^2 + |h_2^-|^2 &= 0, \end{aligned}$$

which are satisfied for

$$h_1^+ = h_2^- = 0. \tag{35}$$

Thus we have a three-dimensional subspace of initial coin states

$$|\psi_C^{(1)}\rangle = h_0|\chi_0\rangle + h_1^-|\chi_1^-\rangle + h_2^+|\chi_2^+\rangle$$

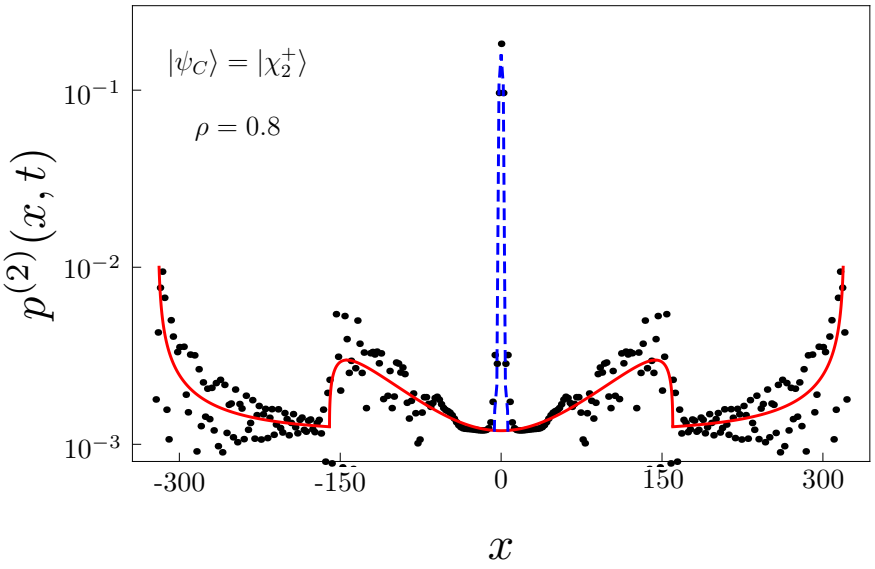

FIG. 13: (Color online) Probability distribution after 100 steps of the five-state Wigner walk. The initial coin state was chosen as $|\chi_2^+\rangle$. The coin parameter is $\rho = 0.8$

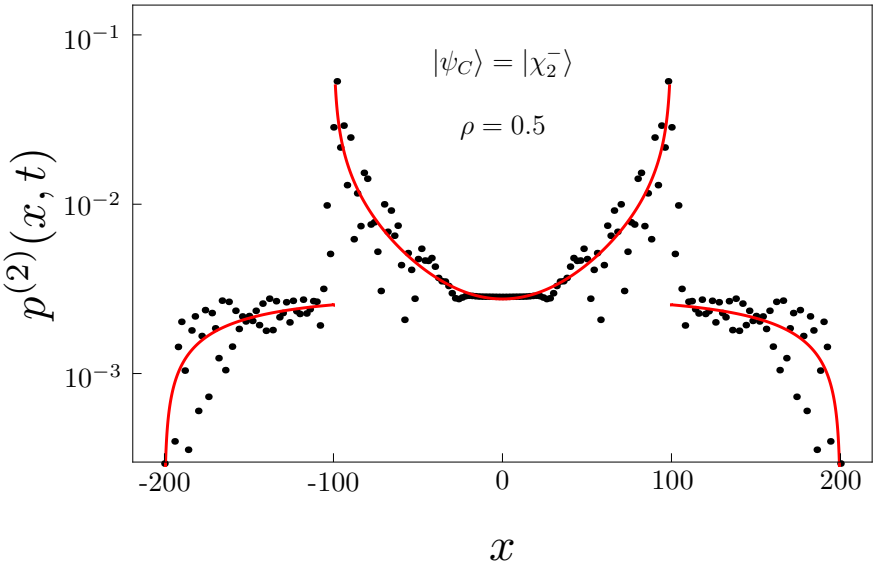

FIG. 14: (Color online) Probability distribution after 100 steps of the five-state Wigner walk. The initial coin state was chosen as $|\chi_2^-\rangle$. The coin parameter is $\rho = 0.5$

for which both divergencies in $\nu^{(2,1)}(v)$ disappear.

For the faster walk described by the limit density $\nu^{(2,2)}(v)$ the condition (34) for the weight $\mathcal{M}^{(2,2)}(v)$ leads us to the relations

$$\begin{aligned} h_1^-(\sqrt{3}\overline{h_0} - \overline{h_2^+}) + \overline{h_1^-}(\sqrt{3}h_0 - h_2^+) &= 0, \\ |\sqrt{3}h_0 - h_2^+|^2 + 4|h_1^-|^2 &= 0. \end{aligned}$$

This is satisfied provided that

$$h_1^- = 0, \quad h_2^+ = \sqrt{3}h_0. \tag{36}$$

Hence, we find a three-dimensional subspace of initial states

$$|\psi_C^{(2)}\rangle = h_0|\chi_0\rangle + h_1^+|\chi_1^+\rangle + \sqrt{3}h_0|\chi^+\rangle + h_2^-|\chi_2^-\rangle$$

for which the density $\nu^{(2,2)}(v)$ has no divergencies.

In contrast to the four-state walk which we have treated in the previous Section, it is now possible to satisfy both conditions (35) and (36) simultaneously, i.e. we can eliminate all four divergencies in both densities. The state for which this situation occurs is given by

$$|\psi_C\rangle = \frac{1}{2}|\chi_0\rangle + \frac{\sqrt{3}}{2}|\chi_2^+\rangle. \tag{37}$$

We point out that this is the only coin state for which the probability distribution of the five-state Wigner walk has only one peak. This peak arises due to the trapping effect which we address in the following subsection. We illustrate this feature in FIG. 15.

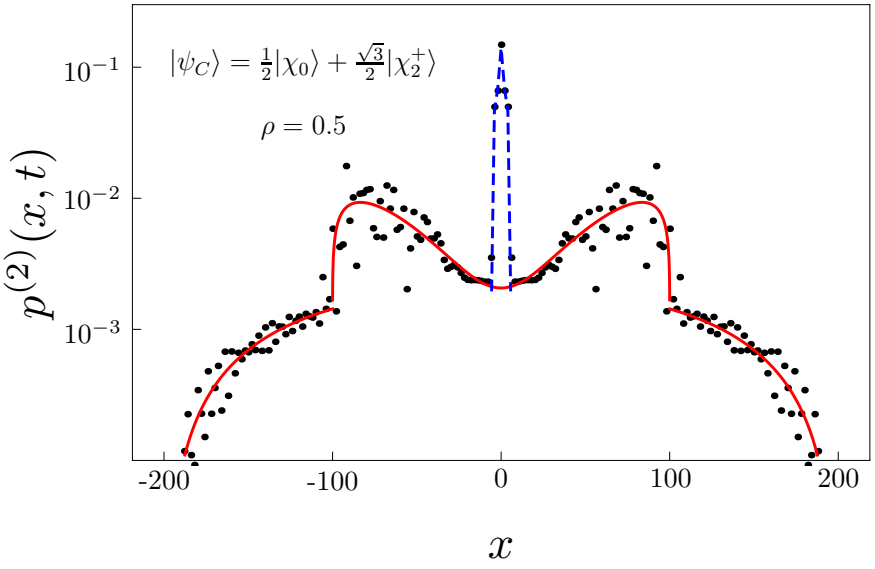

FIG. 15: (Color online) Probability distribution after 100 steps of the five-state Wigner walk. The coin parameter is $\rho = 0.5$. The initial coin state was chosen according to (37), which satisfies both conditions for eliminations of peaks of the slower walk (35) and the faster walk (36) simultaneously. The resulting probability distribution has only one peak at the origin due to the trapping effect.

Finally, we note that the slower walk described by the limit density $\nu^{(2,1)}(v)$ can vanish completely. Indeed, for the state

$$|\psi_C\rangle = \frac{1}{2}|\chi_0\rangle - \frac{\sqrt{3}}{2}|\chi_2^+\rangle, \tag{38}$$

all terms $\mathcal{M}_i^{(2,1)}$ are equal to zero. In such a case the spreading of the five-state Wigner walk is described only by the limit density $\nu^{(2,2)}(v)$. We illustrate this effect in FIG. 16.

B. Trapping probability

Let us now turn to the trapping probability. We leave the details of calculations for the Appendix C and focus on the dependence of the trapping probability on the initial coin state. As we discuss in more detail in the Appendix C, the trapping effect does not occur when the initial state is a linear combination of vectors $|\chi_1^-\rangle$ and $|\chi_2^-\rangle$. This feature was illustrated already in FIGs. 12 and 14. It implies that in the suitable basis $\{|\chi_0\rangle, |\chi_1^\pm\rangle, |\chi_2^\pm\rangle\}$ the trapping probability depends only on three amplitudes of the initial coin state, namely h_0, h_1^+ and h_2^+. However, the explicit form of $p_\infty^{(2)}(x)$ is still rather involved. Nevertheless, this can be overcome by an additional change of basis in the

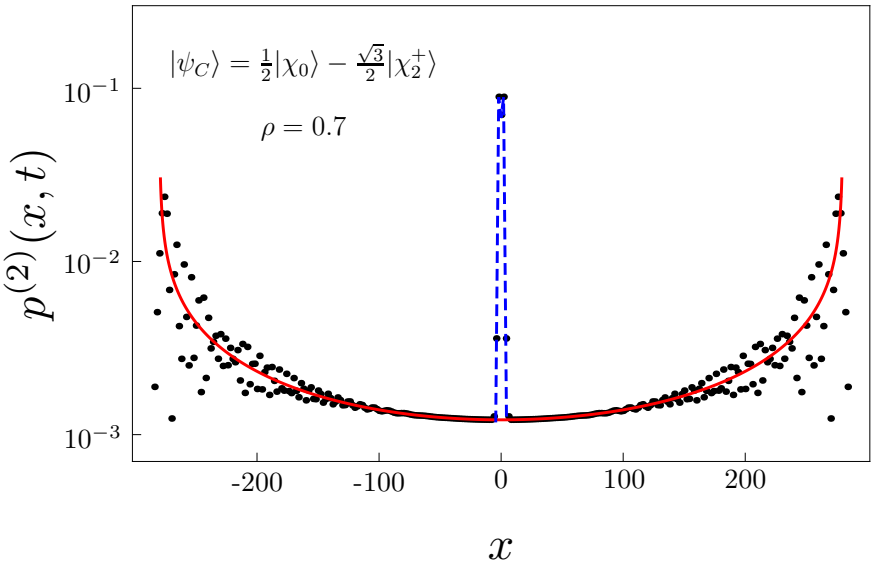

FIG. 16: (Color online) Probability distribution after 100 steps of the five state Wigner walk. The coin parameter is $\rho = 0.7$. The initial state was chosen according to (38). For this particular initial coin state the limit density $\nu^{(2,1)}(v)$ describing the slower walk vanishes.

subspace spanned by $\{|\chi_0\rangle,\ |\chi_1^+\rangle,\ |\chi_2^+\rangle\}$ which affects the trapping effect. Similarly as for the three-state model, which we have treated in Section IV, there are coin states for which the trapping effect appears only for $x \geq 0$, respectively $x \leq 0$. We find that the state resulting in trapping of the particle only at non-negative positions is given by

$$|\lambda^+\rangle = \sqrt{\frac{3}{8}}|\chi_0\rangle + \frac{1}{\sqrt{2}}|\chi_1^+\rangle + \frac{1}{\sqrt{8}}|\chi_2^+\rangle.$$

The second state, which traps the particle only at positions $x \leq 0$ is orthogonal to $|\lambda^+\rangle$ and reads

$$|\lambda^-\rangle = \sqrt{\frac{3}{8}}|\chi_0\rangle - \frac{1}{\sqrt{2}}|\chi_1^+\rangle + \frac{1}{\sqrt{8}}|\chi_2^+\rangle.$$

We find that the orthogonal complement of $|\lambda^\pm\rangle$ within the subspace spanned by $\{|\chi_0\rangle,\ |\chi_1^+\rangle,\ |\chi_2^+\rangle\}$ is given by the vector (38), which we now denote as $|\lambda_0\rangle$. The triplet $\{|\lambda_0\rangle,\ |\lambda^\pm\rangle\}$ forms an orthonormal basis in the subspace affecting the trapping effect, and together with the vectors $|\chi_1^-\rangle$ and $|\chi_2^-\rangle$ it forms an orthonormal basis of the whole coin space. When we express the initial state in the new basis according to

$$|\psi_C\rangle = l_0|\lambda_0\rangle + l^+|\lambda^+\rangle + l^-|\lambda^-\rangle + h_1^-|\chi_1^-\rangle + h_2^-|\chi_2^-\rangle,$$

we find that the trapping probability for positive x reads

$$p_\infty^{(2)}(2x) = Q^{2x}\frac{3(1-\rho^2)}{2\rho^4}\left(|l_0 + f(x)l^+|^2 + |l^+|^2\right), \tag{39}$$

and similarly for negative x we find

$$p_\infty^{(2)}(2x) = Q^{2|x|}\frac{3(1-\rho^2)}{2\rho^4}\left(|l_0 + f(x)l^-|^2 + |l^-|^2\right). \tag{40}$$

Here we have used the notation

$$f(x) \ = \ \frac{\sqrt{6}}{\rho^2}\left(\rho^2 - 2 + 2|x|\sqrt{1-\rho^2}\right).$$

Directly at the origin the trapping probability has a more complicated form

$$\begin{aligned} p_{\infty}^{(2)}(0) \;=\; & \frac{9(1-\rho^2)}{4\rho^4} Q^2 \left(|l_+|^2 + |l_-|^2\right) + \\ & + \frac{3}{8} Q^2 |l_+ + l_-|^2 + \frac{2-\rho^2-\sqrt{1-\rho^2}}{4\rho^2} Q |l_0|^2 - \\ & - \frac{\sqrt{6}\left(2-\rho^2+\frac{1}{2}\sqrt{1-\rho^2}\right)}{8\rho^2} Q^2 \times \\ & \times \left((l_+ + l_-)\overline{l_0} + (\overline{l_+} + \overline{l_-}) l_0\right). \end{aligned} \tag{41}$$

The results (39) and (40) indicate that the decay of the trapping probability with distance from the origin is not purely exponential like for the three-state Wigner walk (23). Nevertheless, the correction to the exponential decay becomes negligible for large x. The state $|\lambda_0\rangle$ is an exception, since for $l^{\pm} = 0$ the terms involving the position-dependent function $f(x)$ vanish and the behaviour of the trapping probability is exactly exponential. Moreover, the decay rate determined by Q is the same as for the three-state Wigner walk.

For illustration, we display in FIG. 17 the probability distribution of the five-state Wigner walk with the initial coin state $|\lambda^+\rangle$. Clearly, the trapping effect appears only for $x \geq 0$. Moreover, the plateau formed by the first three point indicates that the decay of the trapping probability deviates from a pure exponential, in accordance with (39).

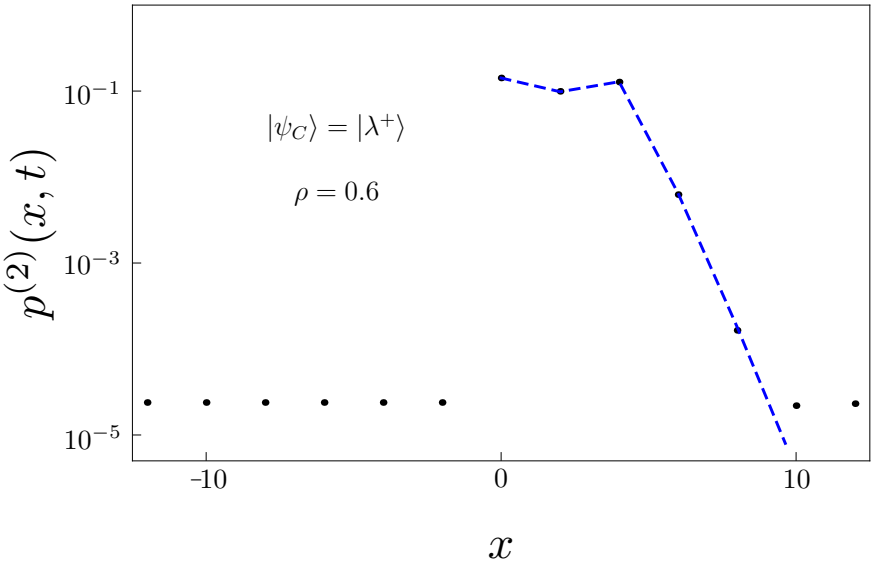

FIG. 17: (Color online) Probability distribution after 10000 steps of the five-state Wigner walk. The initial state was chosen as $|\lambda^+\rangle$. The coin parameter is $\rho = 0.6$. Only a small vicinity of the origin is displayed to emphasize that for $|\lambda^+\rangle$ the trapping effect appears only for $x \geq 0$. Higher number of steps in comparison with other figures was chosen so that the trapping effect is sufficiently pronounced further from the origin. Notice the plateau formed by the first three points exemplifying the fact that for $|\lambda^+\rangle$ the decay of the trapping probability (39) is not purely exponential.

VII. CONCLUSIONS

We have investigated in detail quantum walk models on a line with coin operators given by Wigner rotation matrices $\hat{R}^{(j)}(\alpha, \beta, \gamma)$. We have shown that this three-parameter set of walks is equivalent to a single parameter family $\hat{R}^{(j)}(\rho)$, as far as the shape of the probability distribution and its moments are concerned. The parameter ρ has a simple physical interpretation since it determines the position of the peaks in the probability distribution and its width.

Next, we have simplified the results of [42] by turning to a more suitable basis of the coin space. Unlike for the three-state Grover walk [35], the suitable basis is not directly given by the eigenvectors of the coin operator, however, we have found a recipe which allowed us to construct the suitable basis from them. We presented the explicit form of

Initial state	Properties	Figure
$\|\chi_0\rangle$	density tends to zero at the origin	FIG. 2
$\|\chi^+\rangle$	only one peak due to the trapping	FIG. 3
$\|\chi^-\rangle$	no trapping effect	FIG. 4
$\|\lambda^-\rangle$	no trapping on the positive half-line	FIG. 5

TABLE I: Summary of figures for the three-state model.

Initial state	Properties	Figure
$\|\chi_1^+\rangle$	only one peak in the slower walk only one peak in the faster walk	FIG. 6
$\|\chi_2^+\rangle$	only one peak in the slower walk only one peak in the faster walk	FIG. 7
$\sqrt{3}\|\chi_1^-\rangle - \|\chi_2^-\rangle$	no peaks in the slower walk only one peak in the faster walk	FIG. 8
$\|\chi_1^+\rangle + \sqrt{3}\|\chi_2^+\rangle$	no peaks in the faster walk only one peak in the slower walk	FIG. 9

TABLE II: Summary of figures for the four-state model.

the limit densities for Wigner walks up to $j = 2$. Expressing them in the suitable basis allowed us to identify various interesting regimes which are otherwise hidden in the standard basis description. As an example, we have shown that the number of peaks in the probability distribution can be reduced to one. Moreover, the suitable basis reveals that ρ is a scaling parameter, since varying the value of ρ while keeping the same amplitudes of the initial state in the suitable basis simply changes the width of the probability distribution without distorting its shape.

The Wigner walks with integer j show the trapping effect, which was not explicitly evaluated in [42]. We presented the explicit form of the trapping probability for $j = 1$ and $j = 2$. Our results show that the trapping probability can be highly asymmetric and, moreover, is not purely exponential for $j = 2$.

For clarity the Tables I, II and III summarize the main effects and its graphical representation in the text for three-, four- and five-state Wigner walks.

Based on our explicit results for Wigner walks up to $j = 2$ we make the following conjecture on the suitable basis for models with greater j. For half-integer j the coin operator $\hat{R}^{(j)}(\rho)$ has $\left\lfloor \frac{2j+1}{2} \right\rfloor$ pairs of eigenvectors $|\psi_n^\pm\rangle$ corresponding to eigenvalues of the form $e^{\pm i\varphi_n}$. The suitable basis $\{|\chi_n^\pm\rangle\}$ can be constructed according to the recipe

$$
\begin{aligned}
|\chi_n^+\rangle &= \frac{1}{\sqrt{2}}\left(e^{-i\frac{\varphi}{2}}|\psi_n^+\rangle + e^{i\frac{\varphi}{2}}|\psi_n^-\rangle\right), \\
|\chi_n^-\rangle &= \frac{i}{\sqrt{2}}\left(e^{-i\frac{\varphi}{2}}|\psi_n^+\rangle - e^{i\frac{\varphi}{2}}|\psi_n^-\rangle\right).
\end{aligned}
$$

For integer j there is an additional eigenvector $|\psi_0\rangle \equiv |\chi_0\rangle$ with eigenvalue 1, which we include as the last vector of the suitable basis.

The vectors of the suitable basis were selected among those which result in non-generic probability distribution of the Wigner walk. They point out the extremal regimes in which these quantum walks can be operated. Moreover, they indicate ways in which wave-packet could be shaped using quantum walks with higher-dimensional coins. We assume that this approach will be useful in analyzing the properties of other quantum walk models, especially on higher dimensional lattices.

Initial state	Properties	Figure
$\|\chi_0\rangle$	no peaks in the slower walk density tends to zero at the origin	FIG. 10
$\|\chi_1^+\rangle$	no peaks in the faster walk	FIG. 11
$\|\chi_1^-\rangle$	no peaks in the slower walk no trapping effect	FIG. 12
$\|\chi_2^+\rangle$	no peaks in the slower walk	FIG. 13
$\|\chi_2^-\rangle$	no peaks in the faster walk no trapping effect	FIG. 14
$\|\chi_0\rangle + \sqrt{3}\|\chi_2^+\rangle$	only one peak due to the trapping	FIG. 15
$\|\chi_0\rangle - \sqrt{3}\|\chi_2^+\rangle$	slower walk vanishes	FIG. 16
$\|\lambda^+\rangle$	no trapping on the negative half-line	FIG. 17

TABLE III: Summary of figures for the five-state model.

Acknowledgement

MŠ is grateful for the financial support from GAČR 14-02901P. IB and IJ are grateful for the financial support from SGS13/217/OHK4/3T/14 and GAČR 13-33906S.

APPENDIX A: THREE-STATE MODEL

1. Suitable basis

For the three-state model the explicit form of the eigenvectors of the coin $\hat{R}^{(1)}(\rho)$ reads

$$\begin{aligned} |\psi^{\pm}\rangle &= \frac{1}{2}(\pm i|1\rangle + \sqrt{2}|0\rangle \mp i|-1\rangle), \\ |\psi_0\rangle &= \frac{1}{\sqrt{2}}(|1\rangle + |-1\rangle). \end{aligned} \tag{A1}$$

The eigenvectors satisfy the equations

$$\begin{aligned} \hat{R}^{(1)}(\rho)|\psi^{\pm}\rangle &= e^{\pm i\varphi}|\psi^{\pm}\rangle, \\ \hat{R}^{(1)}(\rho)|\psi_0\rangle &= |\psi_0\rangle, \end{aligned}$$

where the phase φ is given by

$$\varphi = \arccos(2\rho^2 - 1).$$

The suitable basis is then constructed according to the formula (21). We find that the vectors of the suitable basis $\{|\chi_0\rangle, |\chi^{\pm}\rangle\}$ are in terms of the standard basis given by

$$\begin{aligned} |\chi_0\rangle &= \frac{1}{\sqrt{2}}(|1\rangle + |-1\rangle), \\ |\chi^{+}\rangle &= \sqrt{\frac{1-\rho^2}{2}}|1\rangle + \rho|0\rangle - \sqrt{\frac{1-\rho^2}{2}}|-1\rangle, \\ |\chi^{-}\rangle &= -\frac{\rho}{\sqrt{2}}|1\rangle + \sqrt{1-\rho^2}|0\rangle + \frac{\rho}{\sqrt{2}}|-1\rangle. \end{aligned}$$

This leads us to the following relations between the coefficients of the initial state when expressed in the standard basis (q_i) and the suitable basis (h_i)

$$\begin{aligned} q_1 &= \frac{1}{\sqrt{2}}h_0 + \sqrt{\frac{1-\rho^2}{2}}h^+ - \frac{\rho}{\sqrt{2}}h^-, \\ q_0 &= \rho h^+ + \sqrt{1-\rho^2}h^-, \\ q_{-1} &= \frac{1}{\sqrt{2}}h_0 - \sqrt{\frac{1-\rho^2}{2}}h^+ + \frac{\rho}{\sqrt{2}}h^-. \end{aligned} \tag{A2}$$

2. Weight function

The individual terms of the weight $\mathcal{M}^{(1,1)}(v)$ are in the standard basis of the coin space given by [42]

$$\begin{aligned} \mathcal{M}_0^{(1,1)} &= \frac{1}{2}\left(|q_1|^2 + 2|q_0|^2 + |q_{-1}|^2 - q_1\overline{q_{-1}} - \overline{q_1}q_{-1}\right), \\ \mathcal{M}_1^{(1,1)} &= -|q_1|^2 + |q_{-1}|^2 + \\ &\quad + \frac{\sqrt{1-\rho^2}}{\sqrt{2}\rho}(q_1\overline{q_0} + \overline{q_1}q_0 + q_0\overline{q_{-1}} + \overline{q_0}q_{-1}), \\ \mathcal{M}_2^{(1,1)} &= \frac{1}{2}(|q_1|^2 - 2|q_0|^2 + |q_{-1}|^2) - \\ &\quad - \frac{\sqrt{1-\rho^2}}{\sqrt{2}\rho}(q_1\overline{q_0} + \overline{q_1}q_0 - q_0\overline{q_{-1}} - \overline{q_0}q_{-1}) + \\ &\quad + \frac{2-\rho^2}{2\rho^2}(q_1\overline{q_{-1}} + \overline{q_1}q_{-1}). \end{aligned}$$

Using the relations (A2) we find that in the suitable basis $\{|\chi_0\rangle, |\chi^\pm\rangle\}$ the weight function simplifies into

$$\begin{aligned} \mathcal{M}_0^{(1,1)} &= |h^+|^2 + |h^-|^2, \\ \mathcal{M}_1^{(1,1)} &= \frac{1}{\rho}(h_0\overline{h^-} + \overline{h_0}h^-), \\ \mathcal{M}_2^{(1,1)} &= \frac{1}{\rho^2}(|h_0|^2 - |h^+|^2). \end{aligned}$$

3. Trapping probability

The trapping effect arises from the fact that the evolution operator of the three-state Wigner walk has an infinitely degenerate eigenvalue 1. The overlap of the corresponding localized eigenvectors with the initial state leads to the non-vanishing trapping probability (10). The overlap is simple to evaluate in the Fourier picture [47]. Indeed, the Fourier transformation diagonalizes the step operator (2) and the evolution operator (1) reduces into a 3×3 matrix

$$\tilde{U}(k) = \mathrm{Diag}(e^{2ik},\ 1,\ e^{-2ik}) \cdot R^{(1)}(\rho),$$

where k is a continuous quasi-momentum ranging from 0 to 2π. The matrix $\tilde{U}(k)$ has an k-independent eigenvalue 1 with the eigenvector

$$v(k) = \frac{1}{\sqrt{4 - 2\rho^2(1+\cos 2k)}} \begin{pmatrix} \sqrt{2}\sqrt{1-\rho^2} \\ \left(1 - e^{2ik}\right)\rho \\ \sqrt{2}e^{2ik}\sqrt{1-\rho^2} \end{pmatrix}. \tag{A3}$$

The overlap of the eigenvector with the Fourier transformed initial state

$$\tilde{\psi}_C = (q_1, q_0, q_{-1})^T, \tag{A4}$$

where q_i are expressed in (A2), yields the limiting probability amplitude at position x

$$\psi_\infty^{(1)}(x) = \int_0^{2\pi} \frac{dk}{2\pi} e^{-ixk}(v(k), \tilde{\psi}_C)v(k). \tag{A5}$$

Direct evaluation of the scalar product $(v(k), \tilde{\psi}_C)$ reveals that it vanishes when the initial coin state is $|\chi^-\rangle$. Hence, for this particular state the trapping effect does not occur. For other initial states the limiting amplitude can be decomposed into integrals of the form

$$\mathcal{I}^{(1)}(x) = \int_0^{2\pi} \frac{e^{-ixk}}{4\pi(2-\rho^2(1+\cos k))} dk.$$

Using the substitution $z = e^{ik}$ one can turn $\mathcal{I}^{(1)}(x)$ to a contour integral over a unit circle in the complex plane, which can be evaluated explicitly by the method of residues. We find that the result reads

$$\mathcal{I}^{(1)}(x) = \frac{Q^{|x|}}{4\sqrt{1-\rho^2}},$$

where the factor Q is given in (24). Finally, the trapping probability $p_\infty^{(1)}(x)$ is given by the square norm of the amplitude (A5). The final result is presented in (23)

APPENDIX B: FOUR-STATE MODEL

1. Suitable basis

For the four-state model the coin operator $\hat{R}^{(3/2)}(\rho)$ has two pairs of eigenvectors

$$\begin{aligned} |\psi_1^\pm\rangle &= \frac{1}{\sqrt{8}}(\sqrt{3}|3/2\rangle \mp i|1/2\rangle + |-1/2\rangle \mp i\sqrt{3}|-3/2\rangle), \\ |\psi_2^\pm\rangle &= \frac{1}{\sqrt{8}}(|3/2\rangle \pm i\sqrt{3}|1/2\rangle - \sqrt{3}|-1/2\rangle \mp i|-3/2\rangle), \end{aligned} \tag{B1}$$

with conjugated pairs of eigenvalues

$$\begin{aligned} \hat{R}^{(3/2)}(\rho)|\psi_1^\pm\rangle &= e^{\pm i\varphi_1}|\psi_1^\pm\rangle, \\ \hat{R}^{(3/2)}(\rho)|\psi_2^\pm\rangle &= e^{\pm i\varphi_2}|\psi_2^\pm\rangle. \end{aligned}$$

The phases of the eigenvalues are given by

$$\begin{aligned} \varphi_1 &= \arccos\rho, \\ \varphi_2 &= \begin{cases} \arccos\left(\rho(4\rho^2-3)\right), & 0 < \rho \le \frac{1}{2} \\ 2\pi - \arccos\left(\rho(4\rho^2-3)\right), & \frac{1}{2} < \rho \le 1 \end{cases}. \end{aligned}$$

The suitable basis is then constructed according to (25). Using the explicit form of the eigenvectors (B1) we can obtain direct relation between the standard basis $\{|3/2\rangle, |1/2\rangle, |-1/2\rangle, |-3/2\rangle\}$ and the suitable basis $\{|\chi_1^\pm\rangle, |\chi_2^\pm\rangle\}$. From this we find the following correspondence between the coefficients of the initial state in the standard basis (q_i) and in the suitable basis (h_i)

$$
\begin{aligned}
q_{3/2} &= \frac{\sqrt{3(1+\rho)}}{2\sqrt{2}}h_1^+ + \frac{\sqrt{3(1-\rho)}}{2\sqrt{2}}h_1^- + \frac{\sqrt{1+\rho}}{2\sqrt{2}}(1-2\rho)h_2^+ + \frac{\sqrt{1-\rho}}{2\sqrt{2}}(1+2\rho)h_2^-,\\
q_{1/2} &= -\frac{\sqrt{1-\rho}}{2\sqrt{2}}h_1^+ + \frac{\sqrt{1+\rho}}{2\sqrt{2}}h_1^- + \frac{\sqrt{3(1-\rho)}}{2\sqrt{2}}(1+2\rho)h_2^+ - \frac{\sqrt{3(1+\rho)}}{2\sqrt{2}}(1-2\rho)h_2^-,\\
q_{-1/2} &= \frac{\sqrt{1+\rho}}{2\sqrt{2}}h_1^+ + \frac{\sqrt{1-\rho}}{2\sqrt{2}}h_1^- - \frac{\sqrt{3(1+\rho)}}{2\sqrt{2}}(1-2\rho)h_2^+ - \frac{\sqrt{3(1-\rho)}}{2\sqrt{2}}(1+2\rho)h_2^-,\\
q_{-3/2} &= -\frac{\sqrt{3(1-\rho)}}{2\sqrt{2}}h_1^+ + \frac{\sqrt{3(1+\rho)}}{2\sqrt{2}}h_1^- - \frac{\sqrt{1-\rho}}{2\sqrt{2}}(1+2\rho)h_2^+ + \frac{\sqrt{1+\rho}}{2\sqrt{2}}(1-2\rho)h_2^-.
\end{aligned}
\tag{B2}
$$

2. Weight function

The weight functions $\mathcal{M}^{(3/2,1/2)}(v)$ and $\mathcal{M}^{(3/2,3/2)}(v)$ for the four-state model in terms of the standard basis coefficients q_i were given explicitly in [42], we do not reproduce it since it is rather long. With the help of the relations (B2) we can express them in terms of the suitable basis amplitudes h_i. We find that the individual terms of the weight function $\mathcal{M}^{(3/2,1/2)}(v)$ obtain the form

$$
\begin{aligned}
\mathcal{M}_0^{(3/2,1/2)} &= |h_1^+|^2 + |h_1^-|^2,\\
\mathcal{M}_1^{(3/2,1/2)} &= -\frac{1}{\rho}\left[2(|h_1^+|^2 - |h_1^-|^2) + \frac{\sqrt{3}}{2}(h_1^+\overline{h_2^+} + \overline{h_1^+}h_2^+ - h_1^-\overline{h_2^-} - \overline{h_1^-}h_2^-)\right],\\
\mathcal{M}_2^{(3/2,1/2)} &= -\frac{\sqrt{3}}{4\rho^2}\left[\sqrt{3}(|h_1^+|^2 + |h_1^-|^2 - |h_2^+|^2 - |h_2^-|^2) - (h_1^+\overline{h_2^+} + \overline{h_1^+}h_2^+ + h_1^-\overline{h_2^-} + \overline{h_1^-}h_2^-)\right],\\
\mathcal{M}_3^{(3/2,1/2)} &= \frac{3}{4\rho^3}\left[(3|h_1^+|^2 - 3|h_1^-|^2 + |h_2^+|^2 - |h_2^-|^2) + \sqrt{3}(h_1^+\overline{h_2^+} + \overline{h_1^+}h_2^+ - h_1^-\overline{h_2^-} - \overline{h_1^-}h_2^-)\right].
\end{aligned}
\tag{B3}
$$

Similarly, the coefficients of the weight function for $\mathcal{M}^{(3/2,3/2)}(v)$ read

$$
\begin{aligned}
\mathcal{M}_0^{(3/2,3/2)} &= |h_2^+|^2 + |h_2^-|^2,\\
\mathcal{M}_1^{(3/2,3/2)} &= \frac{\sqrt{3}}{2\rho}(h_1^+\overline{h_2^+} + \overline{h_1^+}h_2^+ - h_1^-\overline{h_2^-} - \overline{h_1^-}h_2^-),\\
\mathcal{M}_2^{(3/2,3/2)} &= \frac{\sqrt{3}}{4\rho^2}\left[\sqrt{3}(|h_1^+|^2 + |h_1^-|^2 - |h_2^+|^2 - |h_2^-|^2) - (h_1^+\overline{h_2^+} + \overline{h_1^+}h_2^+ + h_1^-\overline{h_2^-} + \overline{h_1^-}h_2^-)\right],\\
\mathcal{M}_3^{(3/2,3/2)} &= -\frac{1}{4\rho^3}\left[(3|h_1^+|^2 - 3|h_1^-|^2 + |h_2^+|^2 - |h_2^-|^2) + \sqrt{3}(h_1^+\overline{h_2^+} + \overline{h_1^+}h_2^+ - h_1^-\overline{h_2^-} - \overline{h_1^-}h_2^-)\right].
\end{aligned}
\tag{B4}
$$

APPENDIX C: FIVE-STATE MODEL

1. Suitable basis

The eigenvectors of the coin operator $\hat{R}^{(2)}(\rho)$ for the five-state model are given by

$$
\begin{aligned}
|\psi_1^\pm\rangle &= \frac{1}{2}(\pm i|2\rangle + |1\rangle + |-1\rangle \mp i|-2\rangle),\\
|\psi_2^\pm\rangle &= \frac{1}{4}(|2\rangle \pm 2i|1\rangle - \sqrt{6}|0\rangle \mp 2i|-1\rangle + |-2\rangle),\\
|\psi_0\rangle &= \sqrt{\frac{3}{8}}|2\rangle + \frac{1}{2}|0\rangle + \sqrt{\frac{3}{8}}|-2\rangle.
\end{aligned}
\tag{C1}
$$

They satisfy the eigenvalue equations

$$\begin{aligned}\hat{R}^{(2)}(\rho)|\psi_1^{\pm}\rangle &= e^{\pm i\varphi_1}|\psi_1^{\pm}\rangle,\\ \hat{R}^{(2)}(\rho)|\psi_2^{\pm}\rangle &= e^{\pm i\varphi_2}|\psi_2^{\pm}\rangle,\\ \hat{R}^{(2)}(\rho)|\psi_0\rangle &= |\psi_0\rangle,\end{aligned}$$

with phases determined by

$$\begin{aligned}\varphi_1 &= \arccos\left(2\rho^2-1\right),\\ \varphi_2 &= \begin{cases} \arccos\left(8\rho^4-8\rho^2+1\right), & 0<\rho\le\frac{1}{\sqrt{2}}\\ 2\pi-\arccos\left(8\rho^4-8\rho^2+1\right), & \frac{1}{\sqrt{2}}<\rho<1\end{cases}.\end{aligned}$$

The suitable basis $\{|\chi_0\rangle,|\chi_1^{\pm}\rangle,|\chi_2^{\pm}\rangle\}$ for the five-state model is then constructed according to the formula (33). Using the explicit form of the eigenvectors (C1) we can obtain the relation between the vectors of the standard basis and the suitable basis, which leads us to the correspondence between the coefficients of the initial state in the standard basis and the suitable basis

$$\begin{aligned}q_2 &= \frac{\sqrt{3}}{2\sqrt{2}}h_0+\sqrt{\frac{1-\rho^2}{2}}h_1^+-\frac{\rho}{\sqrt{2}}h_1^-+\frac{1-2\rho^2}{2\sqrt{2}}h_2^++\rho\sqrt{\frac{1-\rho^2}{2}}h_2^-,\\ q_1 &= \frac{\rho}{\sqrt{2}}h_1^++\sqrt{\frac{1-\rho^2}{2}}h_1^-+\rho\sqrt{2(1-\rho^2)}h_2^+-\frac{1-2\rho^2}{\sqrt{2}}h_2^-,\\ q_0 &= \frac{1}{2}h_0-\frac{\sqrt{3}}{2}(1-2\rho^2)h_2^+-\rho\sqrt{3(1-\rho^2)}h_2^-,\\ q_{-1} &= \frac{\rho}{\sqrt{2}}h_1^++\sqrt{\frac{1-\rho^2}{2}}h_1^--\rho\sqrt{2(1-\rho^2)}h_2^++\frac{1-2\rho^2}{\sqrt{2}}h_2^-,\\ q_{-2} &= \frac{\sqrt{3}}{2\sqrt{2}}h_0-\sqrt{\frac{1-\rho^2}{2}}h_1^++\frac{\rho}{\sqrt{2}}h_1^-+\frac{1-2\rho^2}{2\sqrt{2}}h_2^++\rho\sqrt{\frac{1-\rho^2}{2}}h_2^-.\end{aligned}\tag{C2}$$

2. Weight function

The weight functions $\mathcal{M}^{(2,1)}(v)$ and $\mathcal{M}^{(2,2)}(v)$ for the five-state model in the standard basis of the coin space can be evaluated using the procedure of [42]. Using the relations (C2) we can transform them into the suitable basis. We find that the coefficients of the weight function $\mathcal{M}^{(2,1)}(v)$ obtain the form

$$\begin{aligned}\mathcal{M}_0^{(2,1)} &= |h_1^+|^2+|h_1^-|^2,\\ \mathcal{M}_1^{(2,1)} &= \frac{1}{\rho}\left[h_1^+\overline{h_2^-}+\overline{h_1^+}h_2^-+h_2^+\overline{h_1^-}+\overline{h_2^+}h_1^-+\sqrt{3}(h_0\overline{h_1^-}+\overline{h_0}h_1^-)\right],\\ \mathcal{M}_2^{(2,1)} &= \frac{1}{\rho^2}\left[3|h_0|^2-4|h_1^+|^2-|h_1^-|^2+|h_2^+|^2+|h_2^-|^2+\sqrt{3}(h_0\overline{h_2^+}+\overline{h_0}h_2^+)\right],\\ \mathcal{M}_3^{(2,1)} &= -\frac{1}{\rho^3}\left[2(h_1^+\overline{h_2^-}+\overline{h_1^+}h_2^-)+h_2^+\overline{h_1^-}+\overline{h_2^+}h_1^-+\sqrt{3}(h_0\overline{h_1^-}+\overline{h_0}h_1^-)\right],\\ \mathcal{M}_4^{(2,1)} &= -\frac{1}{\rho^4}\left[3|h_0|^2-4|h_1^+|^2+|h_2^+|^2+\sqrt{3}(h_0\overline{h_2^+}+\overline{h_0}h_2^+)\right].\end{aligned}\tag{C3}$$

Similarly, the coefficients of the weight function $\mathcal{M}^{(2,2)}(v)$ in the suitable basis are easily found to be

$$\begin{aligned}
\mathcal{M}_0^{(2,2)} &= |h_2^+|^2 + |h_2^-|^2, \\
\mathcal{M}_1^{(2,2)} &= -\frac{1}{\rho}\left[h_1^+\overline{h_2^-} + \overline{h_1^+}h_2^- + h_1^-\overline{h_2^+} + \overline{h_1^-}h_2^+\right], \\
\mathcal{M}_2^{(2,2)} &= \frac{1}{\rho^2}\left[|h_1^+|^2 + |h_1^-|^2 - |h_2^+|^2 - |h_2^-|^2 - \frac{\sqrt{3}}{2}(h_0\overline{h_2^+} + \overline{h_0}h_2^+)\right], \\
\mathcal{M}_3^{(2,2)} &= \frac{1}{2\rho^3}\left[2(h_1^+\overline{h_2^-} + \overline{h_1^+}h_2^-) + (h_1^-\overline{h_2^+} + \overline{h_1^-}h_2^+) + \sqrt{3}(h_0\overline{h_1^-} + \overline{h_0}h_1^-)\right], \\
\mathcal{M}_4^{(2,2)} &= \frac{1}{4\rho^4}\left[(3|h_0|^2 - 4|h_1^+|^2 + |h_2^+|^2) + \sqrt{3}(h_0\overline{h_2^+} + \overline{h_0}h_2^+)\right].
\end{aligned} \tag{C4}$$

3. Trapping probability

The trapping probability for the five-state Wigner walk can be evaluated using the same method described in Appendix A for the three-state model. The asymptotic value of the amplitude at position x is given by

$$\psi_\infty^{(2)}(x) = \int_0^{2\pi} \frac{dk}{2\pi} e^{-ixk}(v(k), \tilde{\psi}_C)v(k), \tag{C5}$$

where $\tilde{\psi}_C$ is the Fourier transformation of the initial state

$$\tilde{\psi}_C = (q_2,\ q_1,\ q_0,\ q_{-1},\ q_{-2})^T,$$

where the coefficients q_i are given by (C2). The vector $v(k)$ is the eigenstate of the evolution operator in the Fourier picture

$$\tilde{U}(k) = \mathrm{Diag}(e^{4ik},\ e^{2ik},\ 1,\ e^{-2ik},\ e^{-4ik}) \cdot R^{(2)}(\rho),$$

corresponding to the eigenvalue 1. Its explicit form is given by

$$v(k) = \frac{1}{n(k)} \begin{pmatrix} e^{2ik}\left(1-\rho^2\right) \\ -\left(1-e^{2ik}\right)\rho\sqrt{1-\rho^2} \\ \sqrt{\frac{2}{3}}\left(\rho^2\cos(2k) - 2\rho^2 + 1\right) \\ \left(1-e^{-2ik}\right)\rho\sqrt{1-\rho^2} \\ e^{-2ik}\left(1-\rho^2\right) \end{pmatrix},$$

where we have denoted by $n(k)$ the normalization factor which reads

$$n(k) = \sqrt{\frac{2}{3}}(2 - \rho^2(1 + \cos(2k))).$$

One can show by direct calculation that if the initial state is a linear combination only of vectors $|\chi_1^-\rangle$ and $|\chi_2^-\rangle$ then $\tilde{\psi}_C$ is orthogonal to $v(k)$. In such a case, the limiting amplitude vanishes and the trapping effect does not occur. Otherwise, the limiting amplitude (C5) can be decomposed into integrals of the form

$$\mathcal{I}^{(2)}(x) = \int_0^{2\pi} \frac{e^{-ixk}}{4\pi(2 - \rho^2(1+\cos k))^2} dk,$$

which is turned into the contour integral over a unit circle in the complex plane and evaluated by the method of residues. We find that the result reads

$$\mathcal{I}^{(2)}(x) = Q^{|x|}\frac{2 - \rho^2 + 2|x|\sqrt{1-\rho^2}}{16(1-\rho^2)^{\frac{3}{2}}},$$

where Q is given by (24). The trapping probability $p_\infty^{(2)}(x)$ is then obtained by the square norm of the amplitude (C5). The final result for positive x, negative x and the origin is presented in (39), (40) and (41).

[1] Y. Aharonov, L. Davidovich and N. Zagury, Phys. Rev. A **48**, 1687 (1993).
[2] D. Meyer, J. Stat. Phys. **85**, 551, (1996).
[3] E. Farhi and S. Gutmann, Phys. Rev. A **58**, 915 (1998).
[4] B. D. Hughes, Random walks and random environments, Vol. 1: Random walks, Oxford University Press, Oxford (1995).
[5] N. Shenvi, J. Kempe and K. Whaley, Phys. Rev. A **67**, 052307 (2003).
[6] A. M. Childs and J. Goldstone, Phys. Rev. A **70**, 022314 (2004).
[7] V. Potoček, A. Gabris, T. Kiss and I. Jex, Phys. Rev. A **79**, 012325 (2009).
[8] A. M. Childs and Y. Ge, Phys. Rev. A **89**, 052337 (2014).
[9] J. K. Gamble, M. Friesen, D. Zhou, R. Joynt and S. N. Coppersmith, Phys. Rev. A **81**, 052313 (2010).
[10] S. D. Berry and J. B. Wang, Phys. Rev. A **83**, 042317 (2011).
[11] K. Rudinger, J. K. Gamble, M. Wellons, E. Bach, M. Friesen, R. Joynt and S. N. Coppersmith, Phys. Rev. A **86**, 022334 (2012).
[12] M. Hillery, D. Reitzner and V. Bužek, Phys. Rev. A **81**, 062324 (2010).
[13] M. Hillery, H. J. Zheng, E. Feldman, D. Reitzner and V. Bužek, Phys. Rev. A **85**, 062325 (2012).
[14] S. Cottrell and M. Hillery, Phys. Rev. Lett. **112**, 030501 (2014).
[15] A. M. Childs, Phys. Rev. Lett. **102**, 180501 (2009).
[16] N. B. Lovett, S. Cooper, M. Everitt, M. Trevers and V. Kendon, Phys. Rev. A **81**, 042330 (2010).
[17] M. Karski, L. Förster, J. Choi, A. Steffen, W. Alt, D. Meschede and A. Widera, Science **325**, 174 (2009).
[18] H. Schmitz, R. Matjeschk, Ch. Schneider, J. Glueckert, M. Enderlein, T. Huber and T. Schaetz, Phys. Rev. Lett. **103**, 090504 (2009).
[19] F. Zähringer, G. Kirchmair, R. Gerritsma, E. Solano, R. Blatt and C. F. Roos, Phys. Rev. Lett. **104**, 100503 (2010).
[20] A. Schreiber, K. N. Cassemiro, V. Potoček, A. Gábris, P. J. Mosley, E. Andersson, I. Jex and Ch. Silberhorn, Phys. Rev. Lett. **104**, 050502 (2010).
[21] M. A. Broome, A. Fedrizzi, B. P. Lanyon, I. Kassal, A. Aspuru-Guzik and A. G. White, Phys. Rev. Lett. **104**, 153602 (2010).
[22] A. Peruzzo, M. Lobino, J. C. F Matthews, N. Matsuda, A. Politi, K. Poulios, X. Zhou, Y. Lahini, N. Ismail, K. Worhoff, Y. Bromberg, Y. Silberberg, M. G. Thompson and J. L. O'Brien, Science **3329**, 1500 (2010).
[23] J. O. Owens, M. A. Broome, D. N. Biggerstaff, M. E. Goggin, A. Fedrizzi, T. Linjordet, M. Ams, G. D. Marshall, J. Twamley, M. J. Withford and A. G. White, New J. Phys. **13**, 075003 (2011).
[24] L. Sansoni, F. Sciarrino, G. Vallone, P. Mataloni, A. Crespi, R. Ramponi and R. Osellame, Phys. Rev. Lett. **108**, 010502 (2012).
[25] A. Schreiber, A. Gábris, P. P. Rohde, K. Laiho, M. Štefaňák, V. Potoček, C. Hamilton, I. Jex and Ch. Silberhorn, Science **336**, 55 (2012).
[26] Y. C. Jeong, C. Di Franco, H. T. Lim, M. S. Kim and Y. H. Kim, Nature Comm. **4**, 2471 (2013).
[27] B. Tregenna, W. Flanagan, R. Maile and V. Kendon, New J. Phys. **5**, 83 (2003).
[28] A. Ambainis, J. Kempe and A. Rivosh, *Proceedings of the 16th Annual ACM-SIAM Symposium on Discrete Algorithms*, SIAM/ACM, p. 1099 (2005).
[29] N. Konno, Quantum Inf. Comput. **2**, 578 (2002).
[30] N. Inui, N. Konno and E. Segawa, Phys. Rev. E **72**, 056112 (2005).
[31] N. Inui and N. Konno, Physica A, **353**, 133 (2005).
[32] M. Štefaňák, I. Bezděková and I. Jex, Eur. Phys. J. D **66**,142 (2012).
[33] S. Falkner and S. Boettcher, Phys. Rev. A **90**, 012307 (2014).
[34] T. Machida, Quantum Inf. Comp. **15**, 0406 (2015).
[35] M. Štefaňák, I. Bezděková and I. Jex, Phys. Rev. A **90**, 012342 (2014).
[36] M. Štefaňák, I. Bezděková, I. Jex and S. M. Barnett, Quantum Inf. Comput. **14**, pp 1213 (2014).
[37] N. Inui, Y. Konishi and N. Konno, Phys. Rev. A **69**, 052323 (2004).
[38] K. Watabe, N. Kobayashi, M. Katori and N. Konno, Phys. Rev. A **77**, 062331 (2008).
[39] B. Kollár, T. Kiss and I. Jex, Phys. Rev. A **91**, 022308 (2015).
[40] M. Hinarejos, A. Prez, E. Roldn, A. Romanelli and G. J. de Valcrcel, New J. Phys. **15**, 073041 (2013).
[41] Y. Higuchi, N. Konno, I. Sato and E. Segawa, J. Funct. Anal. **267**, 4197 (2014).
[42] T. Miyazaki, M. Katori and N. Konno, Phys. Rev. A **76**, 012332 (2007).
[43] T. D. Mackay, S. D. Bartlett, L. T. Stephenson, and B. C. Sanders, J. Phys. A: Math. Gen. **35**, 2745 (2002).
[44] T. A. Brun, H. A. Carteret, and A. Ambainis, Phys. Rev. A **67**, 052317 (2003).
[45] T. A. Brun, H. A. Carteret, and A. Ambainis, Phys. Rev. Lett. **91**, 130602 (2003).
[46] S. E. Venegas-Andraca, J. L. Ball, K. Burnett, and S. Bose, New J. Phys. **7**, 221 (2005).
[47] A. Ambainis, E. Bach, A. Nayak, A. Vishwanath and J. Watrous, *Proceedings of the 33th STOC*, ACM New York, p. 60 (2001).

[48] G. Grimmett, S. Janson and P. F. Scudo, Phys. Rev. E **69**, 026119 (2004).
[49] A. Messiah, *Quantum mechanics,* vol. II, (North Holland, Amsterdam, 1962).
[50] E. P. Wigner, *Group Theory and Its Application to the Quantum Mechanics of Atomic Spectra* (Academic Press, New York, 1959).
[51] N. Konno, Quantum Inf. Process 1, 345 (2002).
[52] N. Konno, J. Math. Soc. Jpn, 57, 1179 (2005).
[53] T. Kitagawa, M. S. Rudner, E. Berg and E. Demler, Phys. Rev. A **82**, 033429 (2010).
[54] H. Obuse and N. Kawakami, Phys. Rev. B **84**, 195139 (2011).
[55] T. Kitagawa, M. A. Broome, A. Fedrizzi, M. S. Rudner, E. Berg, I. Kassal,A. Aspuru-Guzik, A Aspuru-Guzik, E. Demler and A. G. White, Nature Comm. **3**, 882 (2012).
[56] T. Kitagawa, Quantum Inf. Process. **11**, 1107 (2012).
[57] J. K. Asboth, Phys. Rev. B **86**, 195414 (2012).
[58] S. Moulieras, M. Lewenstein and G. Puentes, J. Phys. B **46**, 104005 (2013).
[59] J. K. Asboth and H. Obuse, Phys. Rev. B **88**, 121406 (2013).
[60] B. Tarasinski, J. K. Asboth and J. P. Dahlhaus, Phys. Rev. A **89**, 042327 (2014).
[61] S. K. Goyal, T. Konrad and L. Diosi, Phys. Lett. A **379**, 100 (2015).
[62] A. Kempf and R. Portugal, Phys. Rev. A **79**, 052317 (2009).
[63] We use log-scale in all figures to emphasize the peaks and dips. The black points are given by the numerical simulation of the quantum walk. The full red curves always correspond to the approximation of the probability distribution with the limit density given by (9).
[64] We calculate the explicit form of the trapping probability in the following subsection. The trapping probability is in this and all relevant figures denoted by the dashed blue curve.

initial conditions. The rate of the transport depends on the size of the ring and the coin operator which determines the spreading of the excitation's wave-packet. This case will serve as the reference for the more involved lazy walk. When we consider the transport described by a lazy quantum walk where the particle is allowed to stay at its actual position, the situation becomes more interesting. Indeed, certain lazy quantum walks are able to trap part of the wave-function in the vicinity of the origin [40, 41], i.e. the probability of finding the excitation at finite positions does not vanish in the limit of infinite number of steps. This feature crucially depends on the choice of the coin operator [42, 43]. The consequence of the trapping effect is that the transport of excitation in the lazy quantum walk is not fully efficient. Nevertheless, we show that dynamical percolations [44, 45] of the ring can eliminate the trapping effect and improve the transport efficiency.

The paper is organized as follows: In Section II we describe the model of excitation transport based on a discrete-time quantum walk. The two-state walk model is analyzed in Section III. Section IV is devoted to the lazy walk model. The effect of dynamical percolations on the transport efficiency is discussed in Section V. We conclude and present an outlook in Section VI. More technical details of calculating the survival probability for a two-state walk are left for A.

II. TRANSPORT OF EXCITATION IN DISCRETE-TIME QUANTUM WALK

In this Section we formally describe our model. We consider the transport of excitation to the sink on a finite-size ring described by a discrete-time quantum walk. The vertices of the ring have labels from $-N+1$ to N. The sink, which takes the excitation away from the ring, is located at the vertex N. Note that this configuration is equivalent to a finite line from $-N$ to N with sinks at both ends. The Hilbert space of the quantum walk has the tensor product structure

$$\mathcal{H} = \mathcal{H}_P \otimes \mathcal{H}_C,$$

where $\mathcal{H}_P$ is the position space spanned by the vectors $|m\rangle$, with $m = -N+1, \dots N$, corresponding to the excitation being at the vertex m. By $\mathcal{H}_C$ we denote the coin space which describes the internal degree of freedom of the excitation. The excitation enters the ring exactly opposite the sink with some coin state $|\psi_C\rangle \in \mathcal{H}_C$, i.e. the initial state is

$$|\psi_{in}\rangle = |0\rangle|\psi_C\rangle.$$

A single time-step consists of a quantum walk evolution $\hat{U}$

$$\hat{U} = \hat{S} \cdot (\hat{I}_P \otimes \hat{C}),$$

where the step operator $\hat{S}$ and the coin operator $\hat{C}$ will be specified later. This is followed by a projection

$$\hat{\pi} = \left(\hat{I}_P - |N\rangle\langle N|\right) \otimes \hat{I}_C,$$

corresponding to the effect of the sink. Hence, the complete time evolution is not unitary and the state of the excitation after t steps is described by vector

$$|\psi(t)\rangle = \left(\hat{\pi} \cdot \hat{U}\right)^t |\psi_{in}\rangle,$$

with norm generally less than unity.

In the following we analyze the properties of the survival probability $\mathcal{P}(t)$, i.e. the probability that the excitation remains on the ring until time t, which is given by

$$\mathcal{P}(t) = \langle\psi(t)|\psi(t)\rangle,$$

and the asymptotic transport efficiency η which we define as

$$\eta = 1 - \lim_{t\to\infty} \mathcal{P}(t).$$

In Section III we consider the two-state quantum walk model, while in Section IV we focus on the lazy model. Before we turn to these models we first derive an asymptotic estimate of the survival probability $\mathcal{P}(t)$. We begin with the estimate

$$\mathcal{P}(t) \leq \left\| \left(\hat{\pi} \cdot \hat{U}\right)^t \right\|^2 = \exp\left(2t \ln\left(\left\| \left(\hat{\pi} \cdot \hat{U}\right)^t \right\|^{\frac{1}{t}}\right)\right).$$

For large t the argument of the logarithm can be estimated according to

$$\left\| \left(\hat{\pi} \cdot \hat{U} \right)^t \right\|^{\frac{1}{t}} \approx |\lambda_l|,$$

where λ_l is the leading eigenvalue of $\hat{\pi} \cdot \hat{U}$, i.e. the largest eigenvalue in absolute value. When $|\lambda_l|$ is close to unity (but less than one) we make the first-order Taylor expansion of the logarithm

$$\ln \left(\left\| \left(\hat{\pi} \cdot \hat{U} \right)^t \right\|^{\frac{1}{t}} \right) \approx \ln |\lambda_l| \approx -(1 - |\lambda_l|).$$

Hence, when the absolute value of the leading eigenvalue λ_l of $\hat{\pi} \cdot \hat{U}$ is smaller then one we find that the survival probability behaves in the asymptotic limit as an exponential

$$\mathcal{P}(t) \sim e^{-\gamma t}, \tag{1}$$

where the decay rate γ reads

$$\gamma = 2(1 - |\lambda_l|). \tag{2}$$

In such a case, the asymptotic transport efficiency η is unity. However, when $|\lambda_l| = 1$ the survival probability does not vanish and the transport is not efficient. We will see in Section IV that such situation occurs in certain lazy quantum walks.

III. TWO-STATE WALK MODEL

Let us begin with the two-state walk model, i.e. the particle has to move in each time step from the vertex m to the nearest neighbours $m-1$ or $m+1$. The coin space $\mathcal{H}_C$ is two-dimensional, we denote the basis vectors corresponding to the steps to the left and right as $|L\rangle$ and $|R\rangle$. The step operator of the two-state quantum walk is then given by

$$\hat{S}^{(2)} = \sum_{m=-N+1}^{N} |m-1\rangle\langle m| \otimes |L\rangle\langle L| + |m+1\rangle\langle m| \otimes |R\rangle\langle R|, \tag{3}$$

where we consider periodic boundary condition $N \equiv -N$. As for the coin operator $\hat{C}$, for simplicity we consider a one-parameter family which is in the standard basis of the coin space given by the matrix

$$C^{(2)} = \begin{pmatrix} \rho & \sqrt{1-\rho^2} \\ \sqrt{1-\rho^2} & -\rho \end{pmatrix}, \quad \rho \in (0,1). \tag{4}$$

Nevertheless, this choice in fact covers all $U(2)$ matrices due to unitary equivalence which was recently found in [46]. The coin parameter ρ determines the rate at which the excitation spreads through the ring [47]. The choice of $\rho = \frac{1}{\sqrt{2}}$ corresponds to the familiar and extensively studied case of the Hadamard walk.

In Figure 1 we present the numerical simulation of the survival probability $\mathcal{P}(t)$ for the Hadamard walk ($\rho = \frac{1}{\sqrt{2}}$) on the ring consisting of 10 vertices, i.e. $N = 5$. The left plot shows the survival probability for the first 100 steps. Due to the symmetries of the model we consider, i.e. the excitation enters the ring exactly opposite the sink, the survival probability is exactly the same for all initial coin states $|\psi_C\rangle$. This follows from the results of [34], as we show in A. The right plot displays the survival probability on a longer time scale of 1000 steps. To unravel the asymptotic behavior of $\mathcal{P}(t)$ we use logarithmic scale on the y axis. The plot indicates that the survival probability decays exponentially (1) with the decay rate (2) determined by the leading eigenvalue of $\hat{\pi} \cdot \hat{U}$.

The decay rate γ depends crucially both on the coin parameter ρ and the size of the ring N. We plot the decay rate γ as a function of the coin parameter ρ in Figure 2. For ρ approaching zero the decay rate vanishes. Indeed, for $\rho = 0$ the coin operator (4) turns into a permutation matrix. In such a case, the excitation never leaves the vertices -1, 0 and 1, i.e. it never reaches the sink and the asymptotic transport efficiency η is zero, except for $N = 1$ when the ring consists only of the source and the sink. On the other hand, for ρ approaching unity the decay rate increases rapidly. In the limiting case of $\rho = 1$ the coin operator (4) reduces to an identity with an additional phase shift of π on the $|R\rangle$ state. Hence, the excitation is fully transported into the sink after N steps and the survival probability is a step function, with $\mathcal{P}(t) = 1$ for $t < N$ and $\mathcal{P}(t) = 0$ for $t \geq N$.

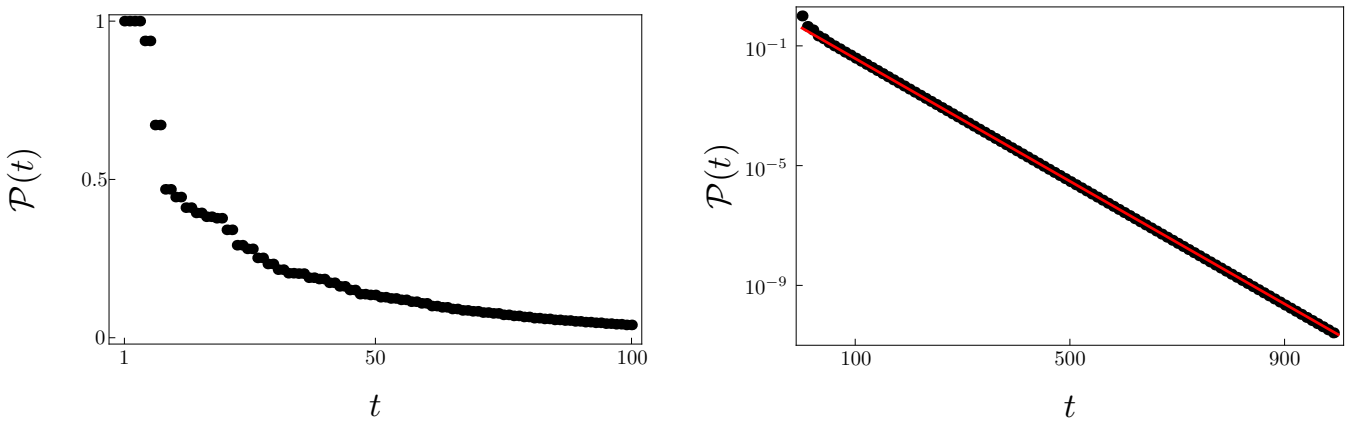

FIG. 1: On the left we display the survival probability $\mathcal{P}(t)$ for the Hadamard walk (i.e. $\rho = \frac{1}{\sqrt{2}}$). Due to the symmetries of the model the survival probability $\mathcal{P}(t)$ is independent of the initial coin state. On the right we show the asymptotic behavior of the survival probability $\mathcal{P}(t)$ for the Hadamard walk. The log-scale reveals that the survival probability decays exponentially. The red curve is given by (1). The size of the ring is given by $N = 5$, i.e. 10 vertices.

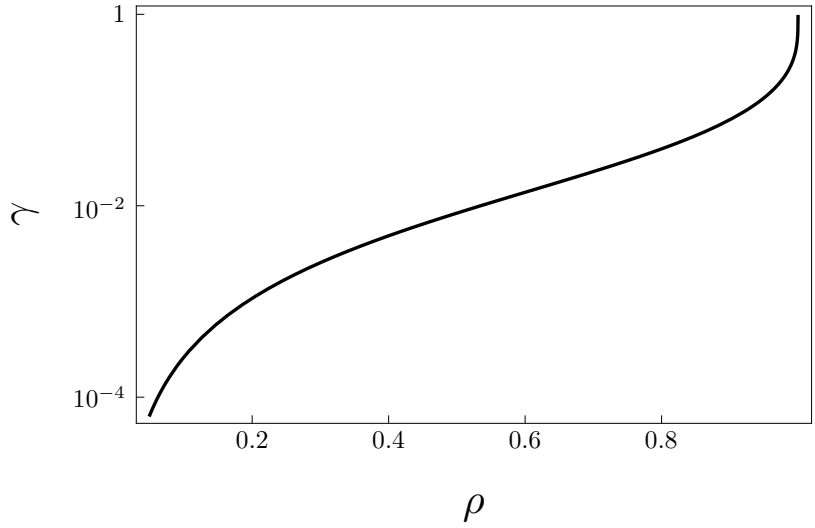

FIG. 2: The decay rate γ as a function of the coin parameter ρ. The size of the ring is given by $N = 5$.

In Figure 3 we consider the decay rate γ as a function of the size of the ring N. For the plot on the left we have chosen the coin parameter $\rho = \frac{1}{\sqrt{2}}$ corresponding to the Hadamard walk, while in the right plot we have considered $\rho = 0.8$. The log-log scale reveals that the decay rate obeys a power law

$$\gamma \sim N^{-3}, \tag{5}$$

independent of the coin parameter ρ.

We point out that for large N the decay rate γ is very small. Hence, it takes a considerable number of steps for the exponential behaviour of the survival probability (1) to set in. As was established and explained at length in Section 4.6 of [35], repeated reflections from the sink (or, in fact, from the adjacent points) slow the decay of the survival probability in the intermediate regime to a power law

$$\mathcal{P}(t) \sim t^{-\frac{1}{2}}. \tag{6}$$

Nevertheless, after an order of N^3 steps the survival probability begins to deviate from the power law (6) and tends to follow the exponential dependence on the number of steps (2). We illustrate this property in Figure 4.

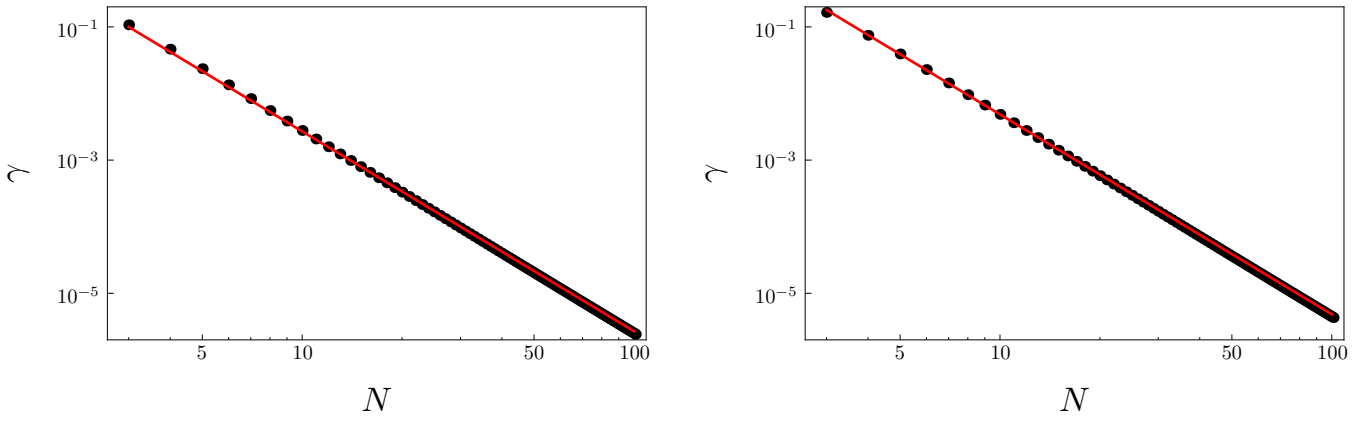

FIG. 3: The decay rate γ as a function of the size of the ring N. Left plot shows the choice $\rho = \frac{1}{\sqrt{2}}$ corresponding to the Hadamard walk, while in the right plot we have chosen $\rho = 0.8$. The plots indicate that the decay rate rate obeys a power law (5). This behaviour is independent of the coin parameter ρ.

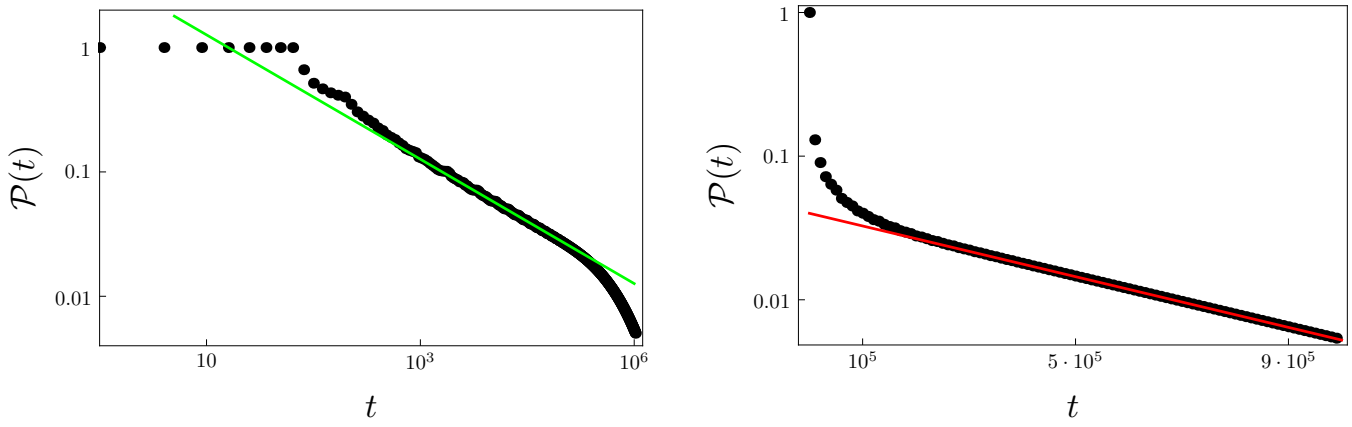

FIG. 4: Survival probability for the Hadamard walk on a ring with 100 vertices, i.e. $N = 50$. On the left we display $\mathcal{P}(t)$ on a log-log scale. The green line corresponds to the power law behavior of (6). We observe that it fits well in the intermediate regime, however, it deviates on the long time scale. Indeed, the plot on the right, where we display the survival probability on a log-scale, shows that in the asymptotic regime the behavior of $\mathcal{P}(t)$ follows the exponential (1) depicted by the red line.

To summarize this section, for the two-state model the survival probability $\mathcal{P}(t)$ is independent of the initial coin state and decays exponentially. Hence, the asymptotic transport efficiency η is unity.

IV. LAZY WALK MODEL

We now turn to the lazy walk model. Let us denote the basis coin states corresponding to the step to the left, stay, and the step to the right as $|L\rangle$, $|S\rangle$ and $|R\rangle$. The step operator of a lazy quantum walk on a ring is then given by the following extension of the step operator for a two-state walk (3)

$$\hat{S}^{(3)} = \hat{S}^{(2)} + \sum_{m=-N+1}^{N} |m\rangle\langle m| \otimes |S\rangle\langle S|.$$

Next, we choose the coin operator which exhibits the trapping effect. The complete set of such coins for a lazy walk was determined in [43]. For simplicity, we consider a two-parameter set of coins which are in the standard basis of

the coin space $\{|L\rangle, |S\rangle, |R\rangle\}$ given by the matrix

$$C^{(3)} = \begin{pmatrix} -\rho^2 & \rho\sqrt{2-2\rho^2} & e^{-i\alpha}\left(1-\rho^2\right) \\ \rho\sqrt{2-2\rho^2} & 2\rho^2-1 & e^{-i\alpha}\rho\sqrt{2-2\rho^2} \\ e^{i\alpha}\left(1-\rho^2\right) & e^{i\alpha}\rho\sqrt{2-2\rho^2} & -\rho^2 \end{pmatrix} \tag{7}$$

where ρ ranges from zero to one and the phase α from 0 to 2π. The parameter ρ has the same interpretation as for the two-state walk of Section III. The phase α will not play a role in this Section, however, it will be crucial when we consider percolations in Section V.

The trapping effect arises when the evolution operator of the quantum walk has a highly degenerate eigenvalue and the corresponding eigenstates are spatially localized [40, 41]. One can show by direct calculation that this is the case for the lazy walk on ring with the coin (7). Indeed, the evolution operator $\hat{U}$ has an eigenvalue $\lambda = 1$ with $2N$-fold degeneracy and the corresponding eigenvectors (linearly independent but overlapping) read

$$\begin{aligned} |s_n\rangle &= |n\rangle\left(\sqrt{1-\rho^2}|L\rangle + \frac{\rho}{\sqrt{2}}|S\rangle\right) + \\ &\quad + |n+1\rangle\left(\frac{\rho}{\sqrt{2}}|S\rangle + e^{i\alpha}\sqrt{1-\rho^2}|R\rangle\right), \end{aligned} \tag{8}$$

where n ranges from $-N+1$ to N. Notice that only two of these vectors, namely $|s_{N-1}\rangle$ and $|s_N\rangle$, have support on the vertex N where the sink is located. Hence, the vectors $|s_n\rangle$ with $n \in \{-N+1, \ldots, N-2\}$ are not affected by the sink and they are eigenvectors of $\hat{\pi}\cdot\hat{U}$ with eigenvalue one. Consequently, the trapping effect remains even in the presence of the sink, the survival probability has a non-vanishing limit and the excitation transport is not fully efficient.

Let us now evaluate the transport efficiency η. Using the Gram-Schmidt procedure one can form an orthonormal basis in the degenerate subspace from the eigenstates (8). We denote the basis vectors by $|\phi_n\rangle$. The probability of trapping the excitation on the vertex m, i.e. the probability of finding the excitation at position m in the limit of infinite number of steps, is obtained from

$$p_T(m) = \sum_{i=L,S,R}\left|\langle m|\langle i|\left(\sum_n |\phi_n\rangle\langle\phi_n|\right)|\psi_{in}\rangle\right|^2. \tag{9}$$

The limiting value of the survival probability is then given by summing the trapping probabilities over all vertices of the ring excluding the sink

$$\lim_{t\to\infty}\mathcal{P}(t) = \sum_{m=-N+1}^{N-1} p_T(m),$$

which can be simplified into

$$\lim_{t\to\infty}\mathcal{P}(t) = \sum_{n=-N+1}^{N-2}|\langle\psi_{in}|\phi_n\rangle|^2.$$

Hence, the asymptotic transport efficiency reads

$$\eta = 1 - \sum_{n=-N+1}^{N-2}|\langle\psi_{in}|\phi_n\rangle|^2.$$

The evaluation of η is readily done for small N. We present the results for $N = 2, \ldots, 5$ in Table I.

In order to reduce the complexity of the formulas we have expressed the initial coin state $|\psi_C\rangle$ in terms of a more suitable basis of the coin space. Following [48] we have chosen the basis formed by the eigenvectors of the coin operator (7)

$$\begin{aligned} |\sigma^+\rangle &= \sqrt{\frac{1-\rho^2}{2}}|L\rangle + \rho|S\rangle + \sqrt{\frac{1-\rho^2}{2}}e^{i\alpha}|R\rangle, \\ |\sigma_1^-\rangle &= \frac{\rho}{\sqrt{2}}|L\rangle - \sqrt{1-\rho^2}|S\rangle + \frac{\rho}{\sqrt{2}}e^{i\alpha}|R\rangle, \\ |\sigma_2^-\rangle &= \frac{1}{\sqrt{2}}(|L\rangle - e^{i\alpha}|R\rangle). \end{aligned} \tag{10}$$

N	η
2	$1-\frac{2(1-\rho^2)}{4-3\rho^2}\lvert h_2\rvert^2-\frac{2}{4-\rho^2}\lvert h_+\rvert^2$
3	$1-4(2-\rho^2)\left(\frac{(1-\rho^2)\lvert h_2\rvert^2}{16-20\rho^2+5\rho^4}+\frac{\lvert h_+\rvert^2}{16-12\rho^2+\rho^4}\right)$
4	$1-2(16-16\rho^2+3\rho^4)\left(\frac{(1-\rho^2)\lvert h_2\rvert^2}{64-7\rho^2(\rho^2-4)^2}+\frac{\lvert h_+\rvert^2}{64-\rho^2(\rho^4-24\rho^2+80)}\right)$
5	$1-8\left(2-\rho^2\right)\left(\rho^4-8\rho^2+8\right)\left(\frac{\left(1-\rho^2\right)\lvert h_2\rvert^2}{\left(3\rho^2-4\right)\left(3\rho^6-36\rho^4+96\rho^2-64\right)}+\frac{\lvert h_+\rvert^2}{\rho^8-40\rho^6+240\rho^4-448\rho^2+256}\right)$

TABLE I: Asymptotic transport efficiency η for small rings up to $N=5$.

The initial coin state is in the eigenbasis decomposed according to

$$|\psi_C\rangle = h_+|\sigma^+\rangle + h_1|\sigma_1^-\rangle + h_2|\sigma_2^-\rangle.$$

There are several advantages of using the basis (10). First, η is independent of the amplitude h_1, as can be seen from Table I. Indeed, for $h_1=1$ and $h_+=h_2=0$ the trapping effect vanishes [48]. Hence, the initial coin state $|\sigma_1^-\rangle$ is the only one for which the transport efficiency η is unity. Next, η does not depend on the phase α which was absorbed into the definition of the eigenbasis (10). Thus, the coins with different values of α are equivalent[**?**]. Finally, the amplitudes h_+ and h_2 enter the formula for the transport efficiency η only as probabilities $|h_+|^2$ and $|h_2|^2$ of finding the particle initially in the coin state $|\sigma^+\rangle$ or $|\sigma_2^-\rangle$. Hence, the efficiency of transfer is given by incoherent contributions from the two relevant basis states. It is then straightforward to show that the worst transport efficiency arises when the initial coin state is chosen as $|\sigma^+\rangle$.

To illustrate our results we display in Figure 5 the survival probability for the Grover walk (i.e. $\rho=\frac{1}{\sqrt{3}}$ and $\alpha=0$), when the initial coin state is chosen as $|\sigma_1^-\rangle$ (left plot) or $|\sigma^+\rangle$ (right plot). For $|\sigma_1^-\rangle$ the trapping effect disappears and the survival probability decays exponentially (1), similarly to the two-state walk of Section III. The decay rate γ can be estimated using the sub-leading eigenvalue λ_{sl} of $\hat{\pi}\cdot\hat{U}$ according to

$$\gamma = 2(1-|\lambda_{sl}|). \tag{11}$$

Nevertheless, for all other initial coin states the trapping effect results in non-vanishing limit of the survival probability. For $|\sigma^+\rangle$ the trapping effect is the strongest. The right plot indicates that the survival probability does not drop below the value $\sum_{m=-N+1}^{N-1} p_T(m) \approx 0.55$, which is depicted by the red line.

For larger rings the Gram-Schmidt procedure becomes tedious and, moreover, the resulting formula for the transport efficiency η is rather lengthy. Nevertheless, we can estimate the transport efficiency following the analysis of the walk on an infinite line. We approximate the trapping probability at position m (9) using the results obtained for infinite line in [48] where it was found

$$p_T(m) = \begin{cases} \frac{2-2\rho^2}{\rho^4}Q^{2m}|h_+ + h_2|^2, & m>0, \\ \frac{Q}{\rho^2}\left\{|h_+|^2+(1-\rho^2)|h_2|^2\right\}, & m=0. \\ \frac{2-2\rho^2}{\rho^4}Q^{2|m|}|h_+ - h_2|^2, & m<0 \end{cases} \tag{12}$$

Here the quotient Q reads

$$Q = \frac{2-\rho^2-2\sqrt{1-\rho^2}}{\rho^2}.$$

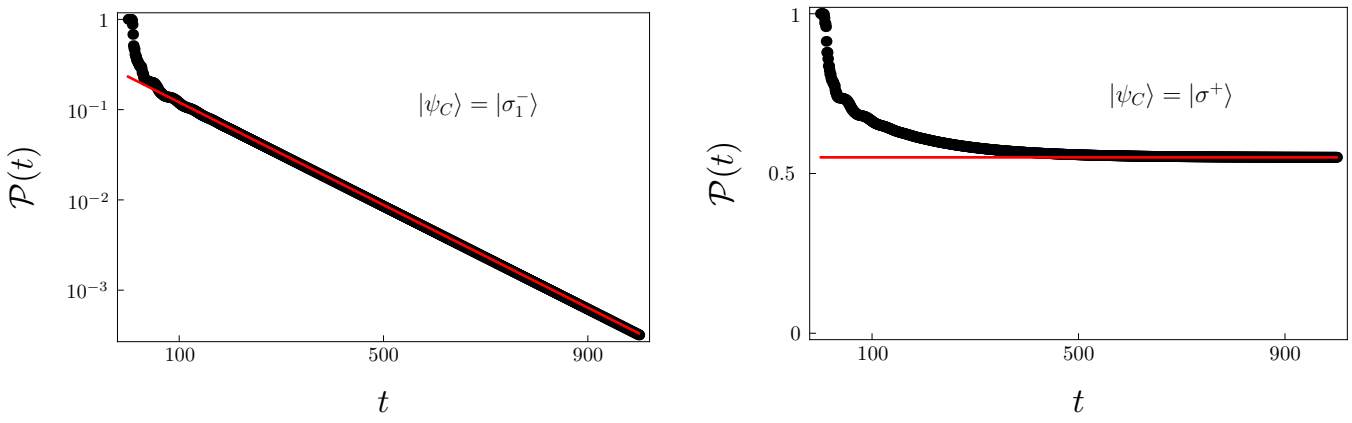

FIG. 5: Survival probability for the Grover walk on a ring with 10 vertices, i.e. $N = 5$ in dependence on the number of steps. On the left we have chosen the initial coin state as $|\sigma_1^-\rangle$ for which the trapping effect disappears. In such a case the survival probability $\mathcal{P}(t)$ vanishes exponentially. This is highlighted by the log-scale. The red line corresponds to the decay rate γ determined by (11). The right plot shows the survival probability when the initial coin state is $|\sigma^+\rangle$ for which the trapping effect is the strongest. The survival probability approaches the red line given by $\sum_{m=-N+1}^{N-1} p_T(m) \approx 0.55$.

Hence, the asymptotic transport efficiency for a ring of size $2N$ can be estimated by

$$\eta \approx 1 - \tfrac{Q}{\rho^2} \left(\sqrt{1-\rho^2} \left(1 - Q^{2(N-1)}\right) \left(|h_2|^2 + |h_+|^2\right) + \right.$$
$$\left. + (1-\rho^2)|h_2|^2 + |h_+|^2 \right).$$

Since the trapping probability (12) decays very fast (exponentially) with the distance from the origin, this approximation is quite good even for small rings. The difference is most profound for the coin parameter ρ close to one. With increasing size of the ring the differences become negligible. This result also confirms that the worst transport efficiency is obtained for the initial coin state $|\sigma^+\rangle$.

V. DYNAMICAL PERCOLATION OF THE RING

In this Section we analyze the effect of dynamical percolation of the ring on the transport efficiency of the lazy quantum walk. Percolation can be viewed as a special (but realistic) noise source and hence the problem at hand can be cast under the headline of noise assisted excitation transfer. Improving transport by allowing the edges to break randomly seems to be a bit counterintuitive at the first sight. However, percolations can in some situations eliminate the localized eigenstates (8) and thus improve the asymptotic transport efficiency to unity.

The evolution of the percolated quantum walk can be described within the framework of random unitary channels [49, 50]. The density matrix of the excitation evolves according to the formula

$$\hat{\rho}'(t+1) = \sum_{\mathcal{K}} p_{\mathcal{K}} \hat{U}_{\mathcal{K}} \hat{\rho}(t) \hat{U}_{\mathcal{K}}^{\dagger}, \tag{13}$$

where $\mathcal{K}$ denotes the possible edge configuration, $p_{\mathcal{K}}$ is the probability of the configuration $\mathcal{K}$ and $\hat{U}_{\mathcal{K}}$ is a quantum walk on a ring with edge configuration $\mathcal{K}$. The random unitary channel (13) is followed by the projection

$$\hat{\rho}(t+1) = \hat{\pi} \hat{\rho}'(t+1) \hat{\pi}^{\dagger}, \tag{14}$$

which corresponds to the action of the sink. For simplicity, we consider that every edge occurs with the same probability p independent of its position. The probability of the edge configuration $\mathcal{K}$ is then given by

$$p_{\mathcal{K}} = p^{|\mathcal{K}|} (1-p)^{2N-|\mathcal{K}|},$$

where $|\mathcal{K}|$ denotes the size of the set $\mathcal{K}$, i.e. the number of edges present in that configuration. The evolution operator $\hat{U}_{\mathcal{K}}$ of the walk on a percolated ring with edge configuration $\mathcal{K}$ has the form

$$\hat{U}_{\mathcal{K}} = \hat{S}_{\mathcal{K}} \cdot (\hat{I}_P \otimes \hat{C}),$$

where $\hat{S}_{\mathcal{K}}$ is the step operator on the percolated ring. If the edge between m and $m+1$ is broken then the jumps from m to $m+1$ and from $m+1$ to m cannot occur. Instead, the coin states corresponding to the jumps undergoes a reflection, i.e.

$$|m\rangle|R\rangle \to |m\rangle|L\rangle, \quad |m+1\rangle|L\rangle \to |m+1\rangle|R\rangle. \tag{15}$$

Hence, the step operator $\hat{S}_{\mathcal{K}}$ on the percolated ring is given by

$$\begin{aligned}\hat{S}_{\mathcal{K}} \;=\; & \sum_{(m,m+1)\in\mathcal{K}} |m\rangle\langle m+1| \otimes |L\rangle\langle L| + |m+1\rangle\langle m| \otimes |R\rangle\langle R| + \\ & + \sum_{(m,m+1)\notin\mathcal{K}} |m\rangle\langle m| \otimes |L\rangle\langle R| + |m+1\rangle\langle m+1| \otimes |R\rangle\langle L| + \\ & + \sum_m |m\rangle\langle m| \otimes |S\rangle\langle S|.\end{aligned}$$

The evolution of a dynamically percolated quantum walk is rather involved. Nevertheless, it simplifies considerably in the asymptotic regime where it is described by the attractors satisfying

$$\hat{U}_{\mathcal{K}}\hat{X}\hat{U}_{\mathcal{K}}^{\dagger} = \lambda\hat{X}, \quad \forall\mathcal{K}, \quad \text{with } |\lambda| = 1.$$

Moreover, substantial part of the attractor space is spanned by the so-called p-attractors [49, 50], which can be constructed from the common eigenstates of all $\hat{U}_{\mathcal{K}}$'s. The common eigenstate $|\xi\rangle$ has to satisfy the equations

$$\hat{U}_{\mathcal{K}}|\xi\rangle = \beta|\xi\rangle,$$

for all possible configurations $\mathcal{K}$. We search for the common eigenstates in the form

$$|\xi\rangle = \sum_m |m\rangle|\xi^m\rangle,$$

where the coin state at position m is given by

$$|\xi^m\rangle = \xi_L^m|L\rangle + \xi_S^m|S\rangle + \xi_R^m|R\rangle.$$

Following [49, 50] we find that the amplitudes of the common eigenstate have to fulfill the shift conditions

$$\xi_L^m = \xi_R^{m+1}, \quad \forall m. \tag{16}$$

Moreover, the common eigenstates have to fulfill the coin conditions

$$\hat{\mathcal{R}}\hat{C}|\xi^m\rangle = \beta|\xi^m\rangle, \quad \forall m, \tag{17}$$

where $\hat{\mathcal{R}}$ is the reflection operator which performs the operation (15). In the standard basis of the coin space it is given by the matrix

$$\mathcal{R} = \begin{pmatrix} 0 & 0 & 1 \\ 0 & 1 & 0 \\ 1 & 0 & 0 \end{pmatrix}.$$

Let us now test when the stationary states of the non-percolated (ideal) walk satisfy the common eigenstates conditions. Form (8) it follows that the amplitudes of the stationary state $|s_n\rangle$ are given by

$$\begin{aligned}\xi_L^m &= \delta_{m,n}\sqrt{1-\rho^2}, \\ \xi_S^m &= (\delta_{m,n} + \delta_{m,n+1})\frac{\rho}{\sqrt{2}}, \\ \xi_R^m &= \delta_{m,n+1}\sqrt{1-\rho^2}e^{i\alpha}.\end{aligned}$$

Hence, we find that the shift conditions (16) are fulfilled only for $\alpha = 0$. One can check that the coin conditions (17) are also satisfied only in this case. Hence, for $\alpha = 0$ the percolations do not eliminate the stationary states (8) - they remain as common eigenstates of all $\hat{U}_{\mathcal{K}}$'s. Moreover, the stationary states $|s_n\rangle$ with $n \in \{-N+1, \ldots, N-2\}$ are not affected by the projection $\hat{\pi}$ corresponding to the effect of the sink. Therefore, for $\alpha = 0$ the trapping effect is preserved in the percolated walk and the efficiency of transport to the sink is not improved, i.e. η depends on the initial coin state in the same way as for the ideal walk. On the other hand, for $\alpha \neq 0$ the stationary states (8) do not satisfy the common eigenstates conditions and they are sensitive to percolations. Hence, for $\alpha \neq 0$ dynamical percolations of the ring eliminate the trapping effect and the transport of excitation is efficient, i.e. $\eta = 1$ for all initial coin states. We see that percolations nullify the equivalence of coins with different values of α which holds for ideal walks.

For illustration we display in Figure 6 the survival probability for one random realization of dynamically percolated quantum walk. On the left we have chosen $\alpha = 0$, for which the stationary states (8) are unaffected by percolations. We find that the survival probability levels at the same value as for the ideal walk (see the right plot of Figure 5 for comparison). The plot on the right shows the survival probability when $\alpha = \pi$. In this case percolations cancel the trapping effect and the survival probability decays exponentially.

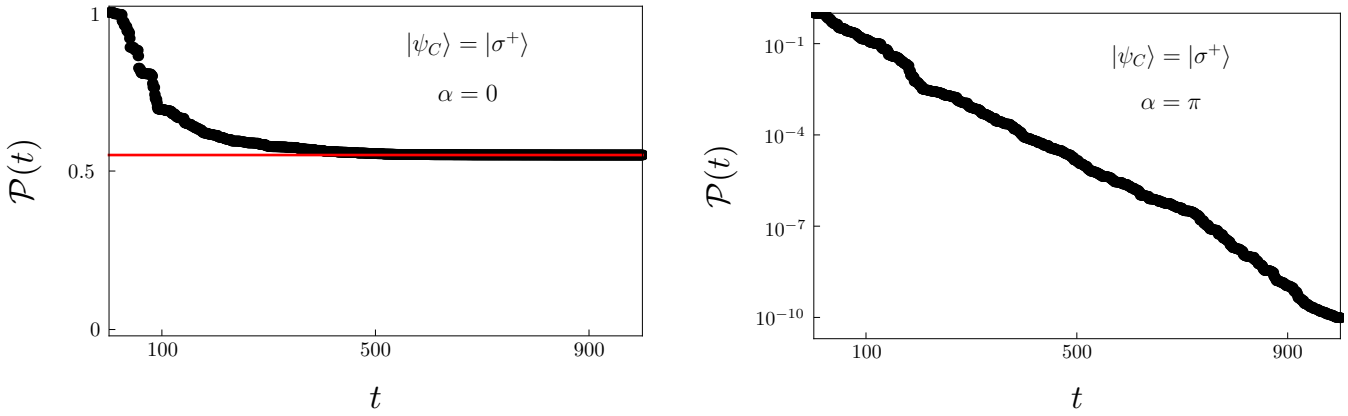

FIG. 6: Survival probability for percolated quantum walk. The initial coin state was chosen as $|\sigma^+\rangle$. The probability of edge presence is $p = \frac{1}{2}$. On the left we have considered the phase $\alpha = 0$. In this case, percolations do not eliminate the trapping effect and the survival probability does not drop below the same value as for the non-percolated walk (see the right plot of Figure 5). On the other hand, for $\alpha = \pi$, which we display in the right plot, the trapping effect vanishes. The survival probability decreases exponentially, which we highlight with the log-scale. The deviations from the straight line stem from the fact that the plot corresponds to a single random realization of the percolated walk.

The decay rate γ of the survival probability depends on both parameters of the coin ρ and α and also on the probability of edge presence p. The numerical simulations indicates that the decay rate can be estimated according to

$$\gamma = 1 - |\lambda_l|, \tag{18}$$

where λ_l is the leading eigenvalue of the superoperator

$$\Phi = \sum_{\mathcal{K}} p_{\mathcal{K}} \left(\hat{\pi}\hat{U}_{\mathcal{K}}\right) \otimes \left(\hat{\pi}\hat{U}^*_{\mathcal{K}}\right), \tag{19}$$

which describes the evolution of the density matrix consisting of the random unitary channel (13) and the projection onto the sink (14). Compared to Eq. (2) the factor 2 is missing due to the use of the superoperator formalism. In (19) star denotes the complex conjugation.

For illustration we display in Figures 7, 8 and 9 the decay rate as a function of the phase α, coin parameter ρ and the edge presence probability p, respectively. The size of the ring is given by $N = 5$. The red curves are given by the formula (18) while the black dots are obtained from numerical simulation where we fit the exponential decay (1) to the survival probability averaged over 1000 random realizations of percolated quantum walk.

In Figure 7 we plot the decay rate as a function of the phase α while fixing the coin parameter $\rho = \frac{1}{\sqrt{3}}$ and the edge presence probability $p = \frac{1}{2}$. For small values of α the decay rate tends to zero, as can be expected. Notice that maximal decay rate is not obtained for $\alpha = \pi$, but rather for $\alpha \approx \frac{47}{50}\pi$. We have not found a simple explanation for

this effect. The numerical simulations indicate that the position of the peak drifts further away from $\frac{\pi}{2}$, however, very mildly. For $\alpha \in (\pi, 2\pi)$ the plot would be the mirror image of the presented one.

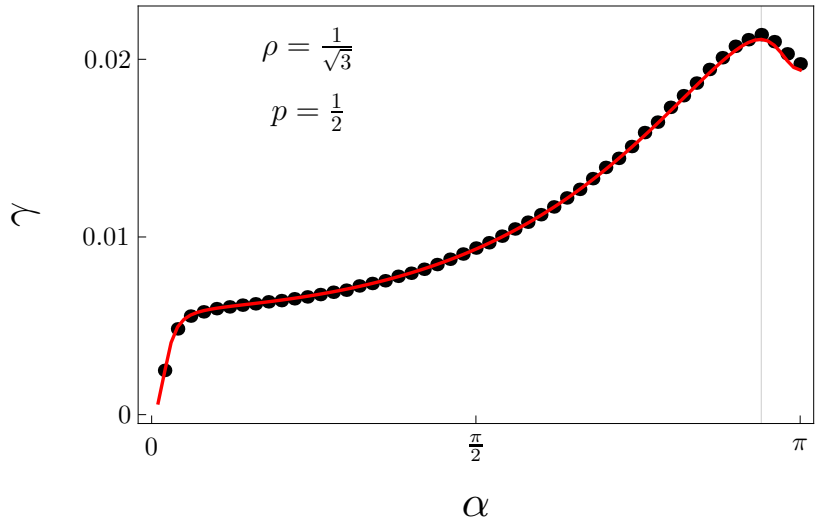

FIG. 7: Decay rate as a function of the phase α. The other parameters have been chosen as $\rho = \frac{1}{\sqrt{3}}$ and $p = \frac{1}{2}$. The maximal decay rate is reached for $\alpha \approx \frac{47}{50}\pi$.

The decay rate in dependence on the coin parameter ρ is displayed in Figure 8. The remaining parameters were chosen as $p = \frac{1}{2}$ and $\alpha = \pi$.

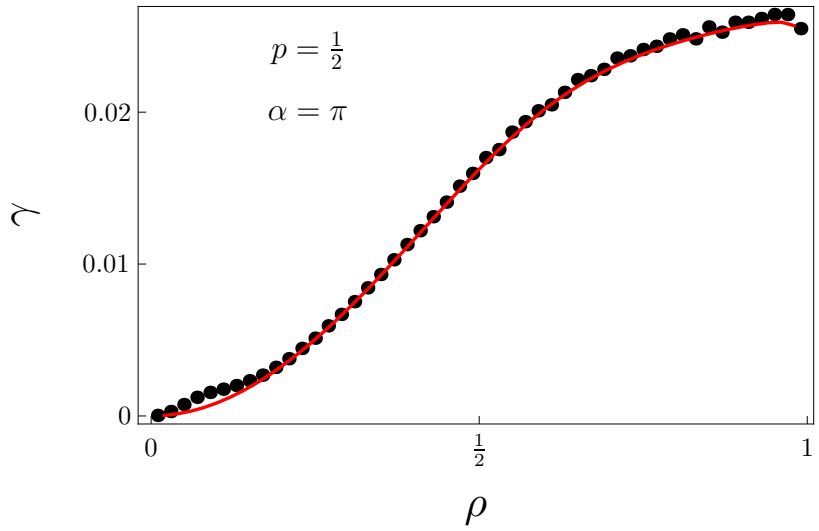

FIG. 8: Decay rate as a function of the probability of the coin parameter ρ. We have considered $p = \frac{1}{2}$ and $\alpha = \pi$.

Figure 9 shows the decay rate as a function of the edge presence probability p for fixed $\rho = \frac{1}{\sqrt{3}}$ and $\alpha = \pi$. Notice the asymmetry of the curve. The maximal decay rate is reached for $p \approx 0.55$. The numerical simulations indicate that with increasing N the position of the maximum tends to $p = 0.5$

In summary, percolations eliminate the trapping effect provided that the coin parameter α is non-zero. This leads to exponential decay of the survival probability with the decay rate determined by the leading eigenvalue of the superoperator (19). However, for $\alpha = 0$ the trapping effect is robust to percolations and the transport efficiency is not improved.

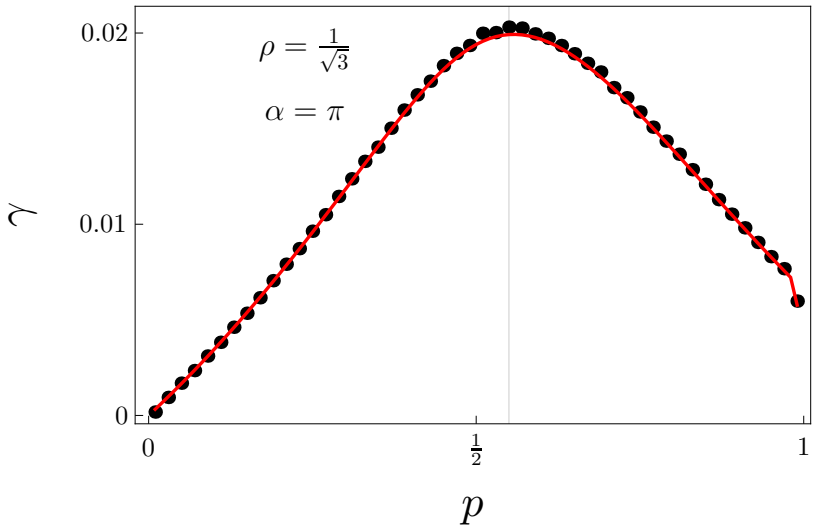

FIG. 9: Decay rate as a function of the probability of edge presence probability p for fixed $\rho = \frac{1}{\sqrt{3}}$ and $\alpha = \pi$. The maximal decay rate is obtained for $p \approx 0.55$.

VI. CONCLUSIONS

We have analyzed the absorption problem for discrete-time quantum walks on a ring. Using both numerical as well analytic methods we determined several properties of this model of transport. For a two-state quantum walk the transport of excitation to the sink is efficient and the survival probability decays exponentially independent of the initial coin state. The decay rate is determined by the coin operator and the size of the ring. In this respect we completed the analysis presented previously.

Next, we have considered a two-parameter set of lazy quantum walk which exhibits the trapping effect. Compared to the two state quantum walk the lazy walk shows a much richer dynamics. Indeed, the survival probability has a non-vanishing lower bound and the excitation transport is inefficient, except for a particular initial coin state. We have determined the dependency of the transport efficiency on the initial coin state, the coin operator and the size of the ring.

Finally, we have shown that the trapping effect can be eliminated by dynamical percolations of the ring provided that the phase parameter α of the coin operator is non-zero. In such a case, the survival probability decays exponentially independent of the initial condition. The decay rate is determined by the parameters of the coin and percolations. However, for $\alpha = 0$ the stationary states are resilient to percolations and the trapping effect is preserved. We note that in the framework of continuous-time quantum walks similar effects have been found in [51–54].

The trapping effect is present also in quantum walks on more complicated graphs driven by higher dimensional coins. It would be interesting to find conditions under which it is robust under percolations, or, on the contrary, what type of percolation is sufficient to eliminate the trapping effect and allow for efficient transfer. In this way studies of percolated quantum walk could contribute to our understanding of transport along complicated molecular structures and ways how to control it.

Finally, let us briefly comment on the possible physical implementations of the lazy walk model. Since the model requires three internal states, usual optical implementations based on polarization are not applicable, at least not in a straightforward way. However, one may employ optical angular momentum [55] or interferometric multiports [56]. Additional candidates might be realizations of quantum walk in phase space [57, 58] or using trapped three-level atoms [59, 60].

Acknowledgments

We acknowledge the financial support from RVO 68407700. MŠ is grateful for the financial support from GAČR 14-02901P. IJ is grateful for the financial support from GAČR 13-33906S.

APPENDIX A: SURVIVAL PROBABILITY FOR A TWO-STATE WALK

In this appendix we show that the survival probability for a two-state quantum walk model which we have discussed in Section III is independent of the initial coin state. The key ingredients of the proof are the results of [34] and the fact that we consider a highly symmetric situation. Namely, the excitation enters the ring exactly opposite of the sink.

In [34] the authors have studied the absorption problem for a two-state quantum walk on a finite line with vertices $\{0,\ldots,n\}$ with sinks on both ends 0 and n. In particular, they have focused on the probability $P_k^{(n)}(t,\psi_C)$ that the excitation starting the walk at the vertex k with the initial state $\psi_C=(\psi_L,\psi_R)^T$ is absorbed at the vertex 0 after t steps of the walk. By $\psi_{L,R}$ we have denoted the amplitudes of the initial coin state in the standard basis, i.e.

$$|\psi_C\rangle=\psi_L|L\rangle+\psi_R|R\rangle.$$

It is straightforward to see that the survival probability $\mathcal{P}(t)$ for the two-state walk on a ring of size $2N$ can be written equivalently as

$$\mathcal{P}(t)=1-\left(P_N^{(2N)}(t,\psi_C)+\tilde{P}_N^{(2N)}(t,\psi_C)\right), \tag{A1}$$

where we have denoted by $\tilde{P}_N^{(2N)}(t,\psi_C)$ the probability of absorption at the vertex $2N$. We now prove that the sum $P_N^{(2N)}(t,\psi_C)+\tilde{P}_N^{(2N)}(t,\psi_C)$ is independent of the initial coin state ψ_C. It was shown in [34] that the probability of absorption at 0 can be expressed in the form

$$P_N^{(2N)}(t,\psi_C)=C_1(t)|\psi_L|^2+C_2(t)|\psi_R|^2+2\mathrm{Re}\left(C_3(t)\psi_L^*\psi_R\right). \tag{A2}$$

The coefficients $C_i(t)$ are determined by the coin operator. For the choice of the coin (4) they read

$$\begin{aligned}
C_1(t) &= \left|\rho p_N^{(2N)}(t)+\sqrt{1-\rho^2}r_N^{(2N)}(t)\right|^2,\\
C_2(t) &= \left|\sqrt{1-\rho^2}p_N^{(2N)}(t)-\rho r_N^{(2N)}(t)\right|^2,\\
C_3(t) &= \left(\rho p_N^{(2N)}(t)+\sqrt{1-\rho^2}r_N^{(2N)}(t)\right)^*\left(\sqrt{1-\rho^2}p_N^{(2N)}(t)-\rho r_N^{(2N)}(t)\right).
\end{aligned}$$

The quantities $p_N^{(2N)}(t)$ and $r_N^{(2N)}(t)$ were analyzed in [34]. They also depend on the coin operator and for the choice of the coin (4) they are real valued. Hence, we can omit the complex conjugation in the formula for $C_3(t)$ since all terms involved are real.

Let us now turn to the probability of absorption at the vertex $2N$. This was not considered in [34], however, it is straightforward to map it to the probability of absorption at the vertex 0. Indeed, by interchanging the coin states $|L\rangle$ and $|R\rangle$ we can express $\tilde{P}_N^{(2N)}(t,\psi_C)$ as the probability of absorption at 0 in a quantum walk with the coin operator

$$\tilde{C}^{(2)}=\begin{pmatrix}-\rho & \sqrt{1-\rho^2}\\ \sqrt{1-\rho^2} & \rho\end{pmatrix},$$

starting with the initial coin state

$$|\tilde{\psi}_C\rangle=\psi_R|L\rangle+\psi_L|R\rangle.$$

Here we also use the symmetry of the problem, i.e. the fact that the distance from the starting point of the walk to sinks at 0 and $2N$ is the same. Modifying the formula (A2) accordingly we find that the probability of absorption at the vertex $2N$ reads

$$\tilde{P}_N^{(2N)}(t,\psi_C)=\tilde{C}_1(t)|\psi_R|^2+\tilde{C}_2(t)|\psi_L|^2+2\mathrm{Re}\left(\tilde{C}_3(t)\psi_L\psi_R^*\right),$$

with coefficients $\tilde{C}_i(t)$ given by

$$\begin{aligned}
\tilde{C}_1(t) &= \left|-\rho\tilde{p}_N^{(2N)}(t)+\sqrt{1-\rho^2}\tilde{r}_N^{(2N)}(t)\right|^2,\\
\tilde{C}_2(t) &= \left|\sqrt{1-\rho^2}\tilde{p}_N^{(2N)}(t)+\rho\tilde{r}_N^{(2N)}(t)\right|^2,\\
\tilde{C}_3(t) &= \left(-\rho\tilde{p}_N^{(2N)}(t)+\sqrt{1-\rho^2}\tilde{r}_N^{(2N)}(t)\right)\left(\sqrt{1-\rho^2}\tilde{p}_N^{(2N)}(t)+\rho\tilde{r}_N^{(2N)}(t)\right).
\end{aligned}$$

Following [34] we find that the quantities $\tilde{p}_N^{(2N)}(t), \tilde{r}_N^{(2N)}(t)$ are related to $p_N^{(2N)}(t), r_N^{(2N)}(t)$ through the formula

$$\begin{aligned}\tilde{p}_N^{(2N)}(t) &= (-1)^{N-1} p_N^{(2N)}(t),\\ \tilde{r}_N^{(2N)}(t) &= (-1)^{N} r_N^{(2N)}(t).\end{aligned}$$

It is then straightforward to show that

$$\begin{aligned}\tilde{C}_1(t) &= C_1(t),\\ \tilde{C}_2(t) &= C_2(t),\\ \tilde{C}_3(t) &= -C_3(t).\end{aligned}$$

Hence, the sum of the probabilities of absorption at vertices 0 and $2N$ reads

$$\begin{aligned}P_N^{(2N)}(t,\psi_C) + \tilde{P}_N^{(2N)}(t,\psi_C) &= C_1(t) + C_2(t) + \\ &\quad +2\mathrm{Re}\left(C_3(t)\left(\psi_L^*\psi_R - \psi_L\psi_R^*\right)\right),\end{aligned} \tag{A3}$$

where we have used the normalization condition of the initial coin state

$$|\psi_L|^2 + |\psi_R|^2 = 1.$$

Moreover, since $C_3(t)$ is real and $\psi_L^*\psi_R - \psi_L\psi_R^*$ is purely imaginary the last term in (A3) vanishes. Hence, we find that (A3) is independent of the initial coin state and through the relation (A1) the same holds for the survival probability $\mathcal{P}(t)$. This completes our proof.

REFERENCES

[1] Aharonov Y, Davidovich L and Zagury N 1993 *Phys. Rev.* A **48** 1687
[2] Meyer D 1996 *J. Stat. Phys.* **85** 551
[3] Farhi E and Gutmann S 1998 *Phys. Rev.* A **58** 915
[4] Shenvi N, Kempe J and Whaley K 2003 *Phys. Rev.* A **67** 052307
[5] Childs A M and Goldstone J 2004 *Phys. Rev.* A **70** 022314
[6] Reitzner D, Hiller M, Feldman E and Bužek V 2009 *Phys. Rev.* A **79** 012323
[7] Potoček V, Gabris A, Kiss T and Jex I 2009 *Phys. Rev.* A **79** 012325
[8] Childs A M and Ge T 2014 *Phys. Rev.* A **89** 052337
[9] Kendon V M and Tamon C 2011 *J. Comput. Theor. Nanosc.* **8** 422
[10] Kurzynski P and Wojcik A 2011 *Phys. Rev.* A **83** 062315
[11] Barr K E, Proctor T J, Allen D and Kendon V M 2014 *Quantum Inf. Comput.* **14** 417
[12] Zhan X, Qin H, Bian Z H, Li J and Xue P 2014 *Phys. Rev.* A **90** 012331
[13] Yalcinkaya I and Gedik Z 2015 *J. Phys.* A **48** 225302
[14] Gamble J K, Friesen M, Zhou D, Joynt R and Coppersmith S N 2010 *Phys. Rev.* A **81** 052313
[15] Berry S D and Wang J B 2011 *Phys. Rev.* A **83** 042317
[16] Rudinger K, Gamble J K, Wellons M, Bach E, Friesen M, Joynt R and Coppersmith S N 2012 *Phys. Rev.* A **86** 022334
[17] Hillery M, Reitzner D and Bužek V 2010 *Phys. Rev.* A **81** 062324
[18] Hillery M, Zheng H J, Feldman E, Reitzner D and Bužek V 2012 *Phys. Rev.* A **85** 062325
[19] Cottrell S and Hillery M 2014 *Phys. Rev. Lett.* **112** 030501
[20] Childs A M 2009 *Phys. Rev. Lett.* **102** 180501
[21] Lovett N B, Cooper S, Everitt M, Trevers M and Kendon V 2010 *Phys. Rev.* A **81** 042330
[22] Karski M, Förster L, Choi J, Steffen A, Alt W, Meschede D and Widera A 2009 *Science* **325** 174
[23] Schmitz H, Matjeschk R, Schneider C, Glueckert J, Enderlein M, Huber T and Schaetz T 2009 *Phys. Rev. Lett.* **103** 090504
[24] Zähringer F, Kirchmair G, Gerritsma R, Solano E, Blatt R and Roos C F 2010 *Phys. Rev. Lett.* **104** 100503
[25] Schreiber A, Cassemiro K N, Potoček V, Gábris A, Mosley P J, Andersson E, Jex I and Silberhorn C 2010 *Phys. Rev. Lett.* **104** 050502
[26] Broome M A, Fedrizzi A, Lanyon B P, Kassal I, Aspuru-Guzik A and White A G 2010 *Phys. Rev. Lett.* **104** 153602
[27] Peruzzo A, Lobino M, Matthews J C F, Matsuda N, Politi A, Poulios K, Zhou X, Lahini Y, Ismail N, Worhoff K, Bromberg Y, Silberberg Y, Thompson M G and O'Brien J L 2010 *Science* **3329** 1500

[28] Owens J O, Broome M A, Biggerstaff D N, Goggin M E, Fedrizzi A, Linjordet T, Ams M, Marshall g D, Twamley J, Withford M J and White A G 2011 *New J. Phys.* **13** 075003
[29] Sansoni L, Sciarrino F, Vallone G, Mataloni P, Crespi A, Ramponi R and Osellame R 2012 *Phys. Rev. Lett.* **108** 010502
[30] Schreiber A, Gábris A, Rohde P P, Laiho K, Štefaňák M, Potoček V, Hamilton C, Jex I and Silberhorn C 2012 *Science* **336** 55
[31] Jeong Y C, Di Franco C, Lim H T, Kim M S and Kim Y H 2013 *Nature Comm.* **4** 2471
[32] Elster F, Barkhofen S, Nitsche T, Novotný J, Gábris A, Jex I and Silberhorn C 2015 *Sci. Rep.* **5** 13495
[33] Ambainis A, Bach E, Nayak A, Vishwanath A and Watrous J 2001 in *Proceedings of the Thirty-Third Annual ACM Symposium on Theory of Computing* 37
[34] Konno N, Namiki T, Soshi T and Sudbury A 2003 *J. Phys.* A **36** 241
[35] Bach E, Coppersmith S, Goldschen M P, Joynt R and Watrous J 2004 *J. Comput. System Sci.* **69** 562
[36] Yamasaki T, Kobayashi H and Imai H 2003 *Phys. Rev.* A **68** 012302
[37] Kwek L C and Setiawan 2011 *Phys. Rev.* A **84** 032319
[38] Chandrashekar C M and Busch T 2014 *Quantum Inf. Proc.* **13** 1313
[39] Asboth J K and Edge J M 2015 *Phys. Rev.* A **91** 022324
[40] Inui N, Konno N and Segawa E 2005 *Phys. Rev.* E **72** 056112
[41] Inui N and Konno N 2005 *Physica* A **353** 133
[42] Štefaňák M, Bezděková I and Jex I 2012 *Eur. Phys. J.* D **66** 142
[43] Štefaňák M, Bezděková I, Jex I and Barnett S M 2014 *Quantum Inf. Comput.* **14** 1213
[44] Grimmett G 1999 *Percolation, Die Grundlehren der mathematischen Wissenschaften in Einzeldarstellungen* (Springer, New York)
[45] Leung G, Knott P, Bailey J and Kendon V 2010 *New J. Phys.* **12** 123018
[46] Goyal S K, Konrad T and Diosi L 2015 *Phys. Lett.* A **379** 100
[47] Kempf A and Portugal R 2009 *Phys. Rev.* A **79** 052317
[48] Štefaňák M, Bezděková I and Jex I 2014 *Phys. Rev.* A **90** 012342
[49] Kollár B, Kiss T, Novotný J and Jex I 2012 *Phys. Rev. Lett.* **108** 230505
[50] Kollár B, Novotný J, Kiss T, and Jex I 2014 *Eur. Phys. J. Plus* **129** 103
[51] Muelken O and Blumen A 2011 *Phys. Rep.* **502** 37
[52] Schijven P, Kohlberger J, Blumen A and Muelken O 2012 *J. Phys.* A **45** 215003
[53] Anishchenko A, Blumen A and Muelken O 2013 *Phys. Rev.* E **88** 062126
[54] Darázs Z, Anishchenko A, Kiss T, Blumen A and Muelken O 2014 *Phys. Rev.* E **90** 032113
[55] Hamilton C S, Gábris A, Jex I and Barnett S M 2011 *New J. Phys.* **13** 013015
[56] Hillery M, Bergou J A and Feldman E 2003 *Phys. Rev.* A **68** 032314
[57] Xue P, Sanders B C, Blais A and Lalumiere K 2008 *Phys. Rev.* A **78** 042334
[58] Xue P and Sanders B C 2008 *New J. Phys.* **10** 053025
[59] Eckert K, Mompart J, Corbalan R, Lewenstein M and Birkl G 2006 *Optics Commun.* **264** 264
[60] Sevincli S et al. 2011 *J. Phys.* B **44** 184018
[61] This is no longer true when we consider percolations of the ring, as we will show in the following Section.

Persistence of unvisited sites in quantum walks on a line

M. Štefaňák[1] and I. Jex[1]

[1]*Department of Physics, Faculty of Nuclear Sciences and Physical Engineering, Czech Technical University in Prague, Břehová 7, 115 19 Praha 1 - Staré Město, Czech Republic*

We analyze the asymptotic scaling of persistence of unvisited sites for quantum walks on a line. In contrast to the classical random walk there is no connection between the behaviour of persistence and the scaling of variance. In particular, we find that for a two-state quantum walks persistence follows an inverse power-law where the exponent is determined solely by the coin parameter. Moreover, for a one-parameter family of three-state quantum walks containing the Grover walk the scaling of persistence is given by two contributions. The first is the inverse power-law. The second contribution to the asymptotic behaviour of persistence is an exponential decay coming from the trapping nature of the studied family of quantum walks. In contrast to the two-state walks both the exponent of the inverse power-law and the decay constant of the exponential decay depend also on the initial coin state and its coherence. Hence, one can achieve various regimes of persistence by altering the initial condition, ranging from purely exponential decay to purely inverse power-law behaviour.

I. INTRODUCTION

Quantum walks [1–3] represent a versatile tool in quantum information processing with applications ranging from search algorithms [4–7], graph isomorphism testing [8–10], finding structural anomalies in graphs [11–13] or perfect state transfer [14–18]. Moreover, quantum walks were shown to be universal tools for quantum computation [19, 20].

One fundamental characterization of classical random walks on infinite lattices [21] is recurrence or transience. Random walk is said to be recurrent when the probability to return to the starting point at some later time (so-called Pólya number) is unity, and transient otherwise. In fact, recurrence ensures that any lattice point is visited with certainty. Pólya has shown [22] that for unbiased random walks this property depends on the dimension of the lattice. In particular, random walks are recurrent in dimensions 1 and 2 and transient on cubic and higher dimensional lattices. This result originates from the diffusive behaviour of a classical random walk.

Since measurement has a non-trivial effect on the state of the quantum system, one has to specify a particular measurement scheme to extend the concept of recurrence to the domain of quantum walks. One possibility is to consider a scheme [23] where the quantum walk is restarted from the beginning after the measurement, and in each iteration one additional step is performed. In this way the effect of measurement on the quantum state is minimized. Within this measurement scheme the Pólya number of a quantum walk depends not only on the dimension of the lattice, but also on the coin operator which drives the walk, and in some cases also on the initial coin state [24]. The ballistic nature of quantum walks implies that most of them are transient already in dimension 2. However, some quantum walks, such as the Grover walk [25–29], show the so-called trapping effect (or localization). This feature can be employed to construct recurrent quantum walks in arbitrary dimension [24].

Another scheme is to continue with the quantum walk evolution after the measurement [30]. The effect of frequent measurement is that the quantum walks are transient already on a one-dimensional lattice, as follows from [31]. Recurrence of quantum state within this measurement scheme has been analyzed for general discrete time unitary evolution in [32]. The authors have found that the expectation value of the first return time is quantized, i.e. it is either infinite or an integer. More recently, it was shown [33] that this property is preserved even in iterated open quantum dynamics, provided that the corresponding superoperator is unital in the relevant part of the Hilbert space. Moreover, the notion of monitored recurrence was extended to a finite-dimensional subspace in [34]. In such case the averaged expected return time is a rational number.

Persistence describes the probability that a given site remains unvisited until certain number of steps. As such, it can be viewed as a complementary event to that of recurrence. For classical random walks on a line and a plane persistence of any site tends to zero for large number of steps. In particular, on one-dimensional lattice persistence obeys an inverse power-law with exponent 1/2, which follows in a straightforward way from the diffusive behaviour of a random walk [35].

In the context of quantum walks persistence was first introduced in [36]. The authors have analyzed persistence for two-state Hadamard walk on a line within the measurement scheme of [23], i.e. when the quantum walk is restarted after the measurement. It was found that persistence of any site follows an inverse power-law with exponent determined numerically as $\lambda \approx 0.318$. In contrast to the classical case, no clear connection of the exponent to the spreading properties of the quantum walk was found.

In the present paper we give analytical explanation of the results found in [36]. The study of persistence is extended to a one-parameter set of two-state quantum walks on a line. We confirm that persistence obeys an inverse power-

law. The exponent is determined solely by the parameter of the coin operator. Hence, there is no connection of the exponent to the scaling of variance like in the classical random walk. Moreover, we analyze persistence of sites for a set of three-state quantum walks [37–39] which involves the familiar Grover walk [26–28] as a special case. We find that persistence exhibits a more complicated asymptotic behaviour. In addition to the inverse power-law there is also an exponential decay which arises from the trapping effect. The analytical results are obtained using the suitable basis of the coin space formed by the eigenvectors of the coin operator [39]. Both the exponent of the inverse power-law and the decay rate of the exponential decay depend on the coin parameter and, in contrast to the two-state walk, on the initial coin state and its coherence. Hence, it is possible to obtain various regimes of persistence, ranging from pure inverse power-law to pure exponential decay, by choosing different initial condition. Moreover, we find that for some initial coin states persistence behave differently for lattice sites on the positive and negative half-lines.

The paper is organized as follows: In Section II we review the definition of persistence of site m within a particular measurement scheme of [23, 36]. We provide an estimate of the asymptotic behaviour of persistence based on the limit density. Section III is dedicated to the analysis of persistence in two-state quantum walks. In Section IV we perform similar analysis for a set of three-state quantum walks. More technical details are left for Appendices A and B. We conclude and present an outlook in Section V.

II. PERSISTENCE OF UNVISITED SITES

In this Section we briefly introduce persistence of a given site and provide and estimate of its asymptotic behaviour. We follow the measurement scheme used in [23, 36], where the quantum walk is restarted from the beginning after each measurement. By persistence of a site m we understand the probability that the particular lattice point remains unvisited until T steps. Since the walk starts at the origin of the lattice we only consider persistence of sites $m \neq 0$. We find that this probability is given by [36]

$$\mathcal{P}_m(T) = \prod_{t=1}^{T} (1 - p(m,t)), \tag{1}$$

where $p(m,t)$ denotes the probability to find the quantum particle at position m after t steps of the quantum walk.

Let us now turn to the approximation of persistence for large T. For this purpose we re-write (1) in the exponential form

$$\begin{aligned} \mathcal{P}_m(T) &= \exp\left(\ln\left(\prod_{t=1}^{T}(1-p(m,t))\right)\right) \\ &= \exp\left(\sum_{t=1}^{T}\ln(1-p(m,t))\right). \end{aligned}$$

We replace the logarithm by the first order Taylor expansion and arrive at

$$\mathcal{P}_m(T) \approx \exp\left(-\sum_{t=1}^{T} p(m,t)\right). \tag{2}$$

Next, we use the limit density $w(v)$ derived from the weak-limit theorem [40] to estimate the exact probability $p(m,t)$ by

$$p(m,t) \approx \frac{1}{t} w\left(\frac{m}{t}\right).$$

Finally, we estimate the sum in (2) with an integral

$$\mathcal{I}_m(T) = \int_1^T \frac{1}{t} w\left(\frac{m}{t}\right) dt \tag{3}$$

and obtain the approximation of persistence

$$\mathcal{P}_m(T) \approx \exp\left(-\mathcal{I}_m(T)\right). \tag{4}$$

In the following we analyze persistence of unvisited sites for two- and three-state quantum walks on a line. Detailed evaluations of the integral (3) are left for the Appendices.

III. TWO-STATE WALK ON A LINE

Let us start our analysis with the two-state quantum walk on a line with the coin operator

$$C(\rho) = \begin{pmatrix} \rho & \sqrt{1-\rho^2} \\ \sqrt{1-\rho^2} & -\rho \end{pmatrix}, \quad 0 < \rho < 1.$$

The coin parameter ρ determines the speed of propagation of the wave packet on the line [41]. For $\rho = 1/\sqrt{2}$ we obtain the familiar Hadamard walk [31].

Suppose that the initial coin state of the particle was

$$|\psi_C\rangle = a|L\rangle + b|R\rangle.$$

The limiting probability density for the two-state quantum walk is given by [42, 43]

$$w(v) = \frac{\frac{\sqrt{1-\rho^2}}{\rho}\left(1 - v\Lambda(a,b)\right)}{\pi\left(1-v^2\right)\sqrt{1-\frac{v^2}{\rho^2}}},$$

where Λ is determined by the initial coin state and the coin parameter

$$\Lambda(a,b) = |a|^2 - |b|^2 + \frac{\sqrt{1-\rho^2}}{\rho}\left(a\bar{b} + b\bar{a}\right).$$

Before we turn to the persistence we first simplify the dependence on the initial coin state Λ by changing the basis of the coin space. Following the idea of [44] we consider the basis formed by the eigenvectors of the coin operator

$$\begin{aligned} |\chi^+\rangle &= \sqrt{\frac{1+\rho}{2}}|L\rangle + \sqrt{\frac{1-\rho}{2}}|R\rangle, \\ |\chi^-\rangle &= -\sqrt{\frac{1-\rho}{2}}|L\rangle + \sqrt{\frac{1+\rho}{2}}|R\rangle, \end{aligned} \tag{5}$$

which satisfy the relations

$$C(\rho)|\chi^\pm\rangle = \pm|\chi^\pm\rangle.$$

We decompose the initial coin state of the walk into the eigenvector basis as

$$|\psi_C\rangle = h_+|\chi^+\rangle + h_-|\chi^-\rangle.$$

From (5) we find that the coefficients of the initial coin state in the standard basis a and b are related to the eigenbasis coefficients $h_\pm$ by

$$\begin{aligned} a &= \frac{\sqrt{1+\rho}}{\sqrt{2}}h_+ - \frac{\sqrt{1-\rho}}{\sqrt{2}}h^-, \\ b &= \frac{\sqrt{1-\rho}}{\sqrt{2}}h_+ + \frac{\sqrt{1+\rho}}{\sqrt{2}}h^-. \end{aligned}$$

In the new basis the factor $\Lambda(a,b)$ becomes

$$\Lambda(h_+,h_-) = \frac{2|h_+|^2 - 1}{\rho}.$$

The asymptotic probability density thus simplifies into

$$w(v) = \frac{\frac{\sqrt{1-\rho^2}}{\rho}\left(1 - \frac{v}{\rho}(2|h_+|^2 - 1)\right)}{\pi\left(1-v^2\right)\sqrt{1-\frac{v^2}{\rho^2}}} \tag{6}$$

Let us now turn to persistence. We leave the details of evaluation of the integral (4) for Appendix A. We find that for large T the function $\mathcal{I}_m(T)$ grows like a logarithm

$$\mathcal{I}_m(T) \sim \lambda \ln\left(\frac{T}{|m|}\right),$$

where the pre-factor reads

$$\lambda = \frac{\sqrt{1-\rho^2}}{\rho\pi}. \tag{7}$$

Hence, we find that in the asymptotic regime persistence of site m follows an inverse power-law

$$\mathcal{P}_m(T) \sim \left(\frac{T}{|m|}\right)^{-\lambda}, \tag{8}$$

The exponent λ is independent of the initial coin state. It is determined solely by the coin operator, i.e. by the value of ρ. Note that for $\rho = 1/\sqrt{2}$, i.e. the Hadamard walk, we find that $\lambda = \frac{1}{\pi} \approx 0.318$, which is in agreement with the numerical result obtained in [36].

Our results are illustrated in Figures 1-3. In Figure 1 we show the influence of the initial coin state. In the first two plots we display the probability distribution of the two-state quantum walk with the coin parameter $\rho = 1/\sqrt{2}$, i.e. the Hadamard walk. In all Figures grey circles represent the data-points obtained from numerical simulation. The red curves correspond to the asymptotic probability density given by (6). For the upper plot we have chosen the initial coin state $|\psi_C^{(1)}\rangle = |\chi^-\rangle$. The resulting probability density shows only one peak on the right. In the middle plot the initial coin state was chosen according to $|\psi_C^{(2)}\rangle = \frac{1}{\sqrt{2}}(|\chi^+\rangle + |\chi^-\rangle)$. This state leads to a symmetric distribution. Despite the differences in the probability distributions the persistence shows the same asymptotic scaling, as we illustrate in the last figure. Here we display the persistence of site $m = 2$ as a function of the number of steps T. To unravel the inverse power-law behavior we use log-log scale. The grey circles correspond to the numerical simulation and the red curves show the inverse power-law (8).

In Figure 2 we illustrate the influence of the coin parameter ρ. In the first two plots we show the probability distribution of the two-state quantum walk with the initial coin state $|\psi_C\rangle = \frac{1}{\sqrt{2}}(|\chi^+\rangle + |\chi^-\rangle)$. For the upper plot the coin parameter is $\rho_1 = 0.2$. In the middle plot we have chosen the coin parameter $\rho_2 = 0.8$. We see that the coin parameter directly affects the speed at which the walk spreads through the lattice [41]. The lower plot shows the difference in the scaling of persistence of site $m = 2$ for different values of ρ. We use log-log scale to unravel the scaling of persistence. We find that the exponent of the inverse power-law decreases with increasing value of ρ, in accordance with (7).

Finally, Figure 3 illustrates that the asymptotic behaviour of persistence is independent of the actual position m. The upper plot displays the probability distribution of the two-state walk with coin parameter $\rho = 0.5$ and the initial coin state $|\psi_C\rangle = |\chi^+\rangle$. This initial condition leads to a density which is the most biased towards left, as indicated by the presence of only one peak. In the lower plot we show persistence of sites $m = 2$ and $m = -2$ on a log-log scale. Despite the differences in the intermediate regime, the slope of both curves is the same, in agreement with (8).

To conclude this Section, we have found that for the two-state quantum walk on a line persistence of unvisited sites obeys an inverse power-law (8) with exponent (7) determined only by the coin parameter.

IV. THREE-STATE WALK ON A LINE

Let us now turn to the three-state walk on a line. Here the particle is allowed to move to the left, stay at its position or move to the right. We denote the corresponding orthogonal coin states by $|L\rangle$, $|S\rangle$ and $|R\rangle$. As for the coin operator we consider the one which was studied in [37–39]. In the standard basis $\{|L\rangle, |S\rangle, |R\rangle\}$ the coin operator is given by the matrix

$$C(\rho) = \begin{pmatrix} -\rho^2 & \rho\sqrt{2-2\rho^2} & 1-\rho^2 \\ \rho\sqrt{2-2\rho^2} & 2\rho^2-1 & \rho\sqrt{2-2\rho^2} \\ 1-\rho^2 & \rho\sqrt{2-2\rho^2} & -\rho^2 \end{pmatrix}, \tag{9}$$

with parameter $\rho \in (0,1)$. Quantum walks with such a coin operator represent a one-parameter extension of the familiar three-state Grover walk [26–28], which corresponds to the choice of $\rho = 1/\sqrt{3}$. Indeed, the results of [39]

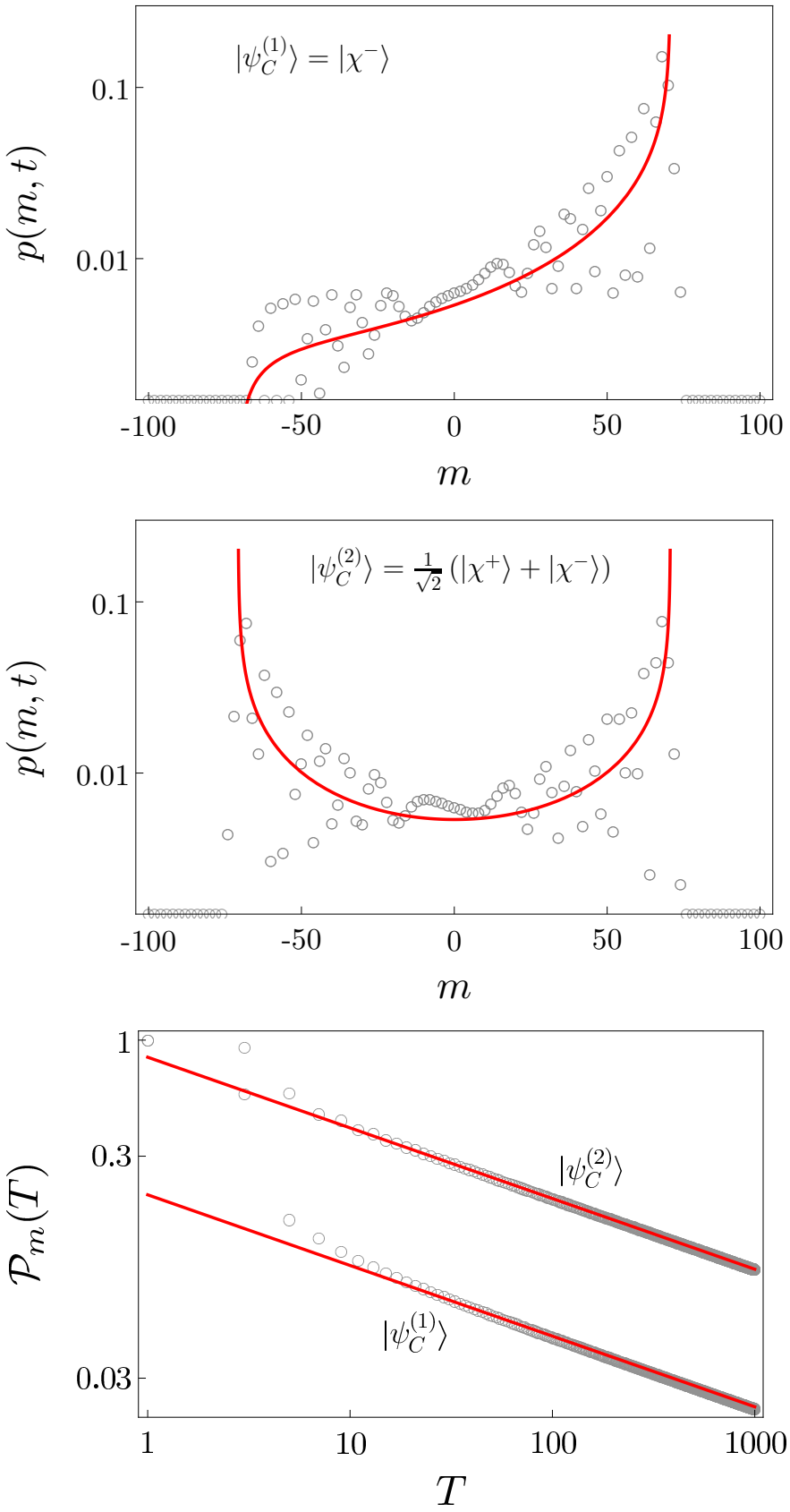

FIG. 1: Probability density and persistence in dependence on the choice of the initial coin state for the Hadamard walk ($\rho = 1/\sqrt{2}$). The first two plots show the probability distribution of the Hadamard walk after $t = 100$ steps for two different initial coin states $|\psi_C^{(1,2)}\rangle$ on a semi-log scale. In the lower plot we display persistence of site $m = 2$ as a function of the number of steps T on a log-log scale. Despite the differences in the probability distributions the asymptotic scaling of persistence is independent of the initial state, in accordance with (8).

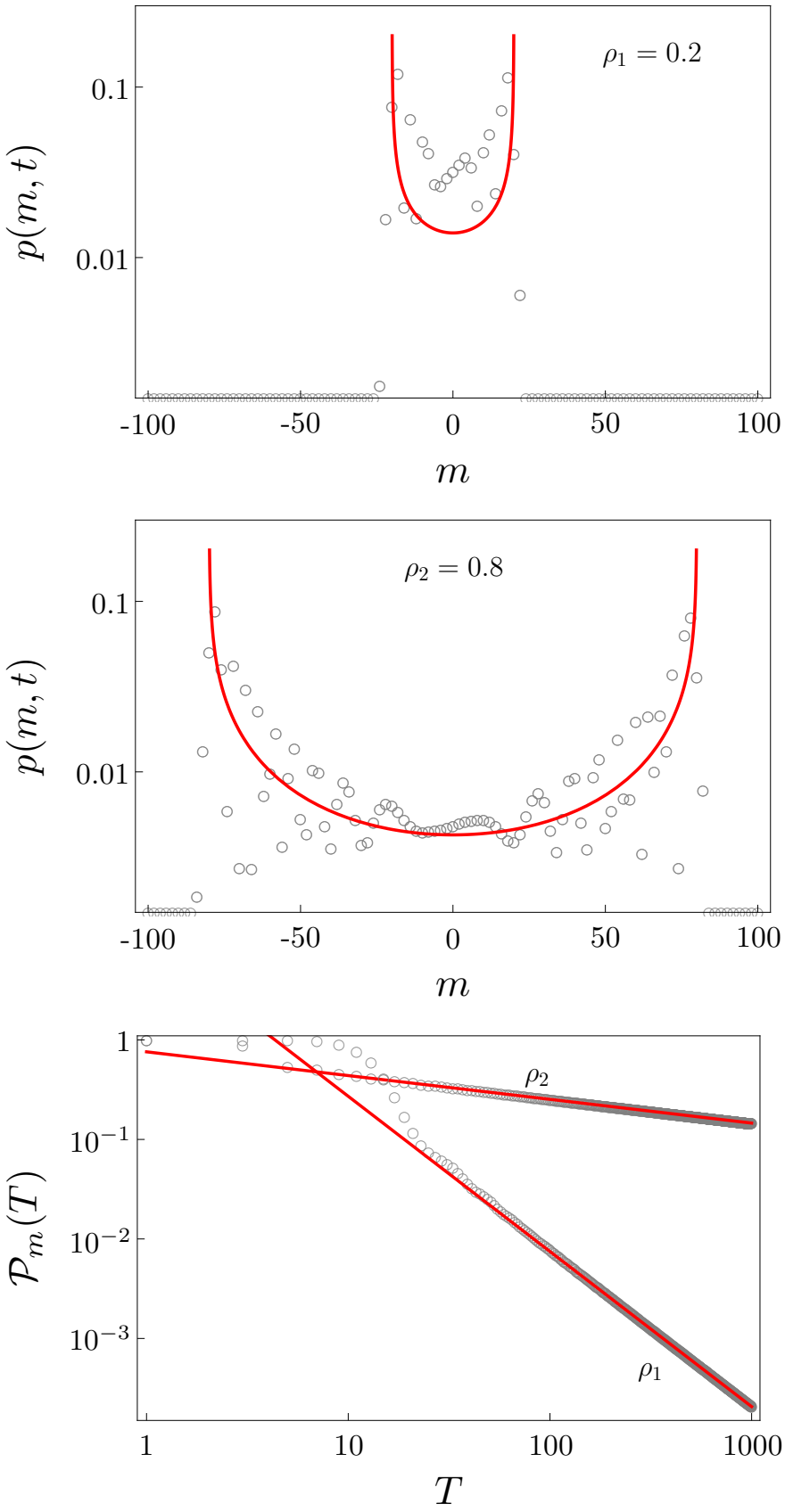

FIG. 2: Probability density and persistence in dependence on the choice of the coin parameter ρ. The first two plots show the probability distribution of the two-state quantum walk on a semi-log scale. In both situations the initial coin state was chosen as $|\psi_C\rangle = \frac{1}{\sqrt{2}}(|\chi^+\rangle + |\chi^-\rangle)$, which leads to symmetric probability distribution. In the upper plot the coin parameter is $\rho_1 = 0.2$ while in the middle plot we have chosen $\rho_2 = 0.8$. The lower plot shows scaling of persistence of site $m = 2$ for different values of $\rho_{1,2}$ on a log-log scale. The exponent of the inverse power-law (8) decreases with increasing value of ρ, as predicted by (7).

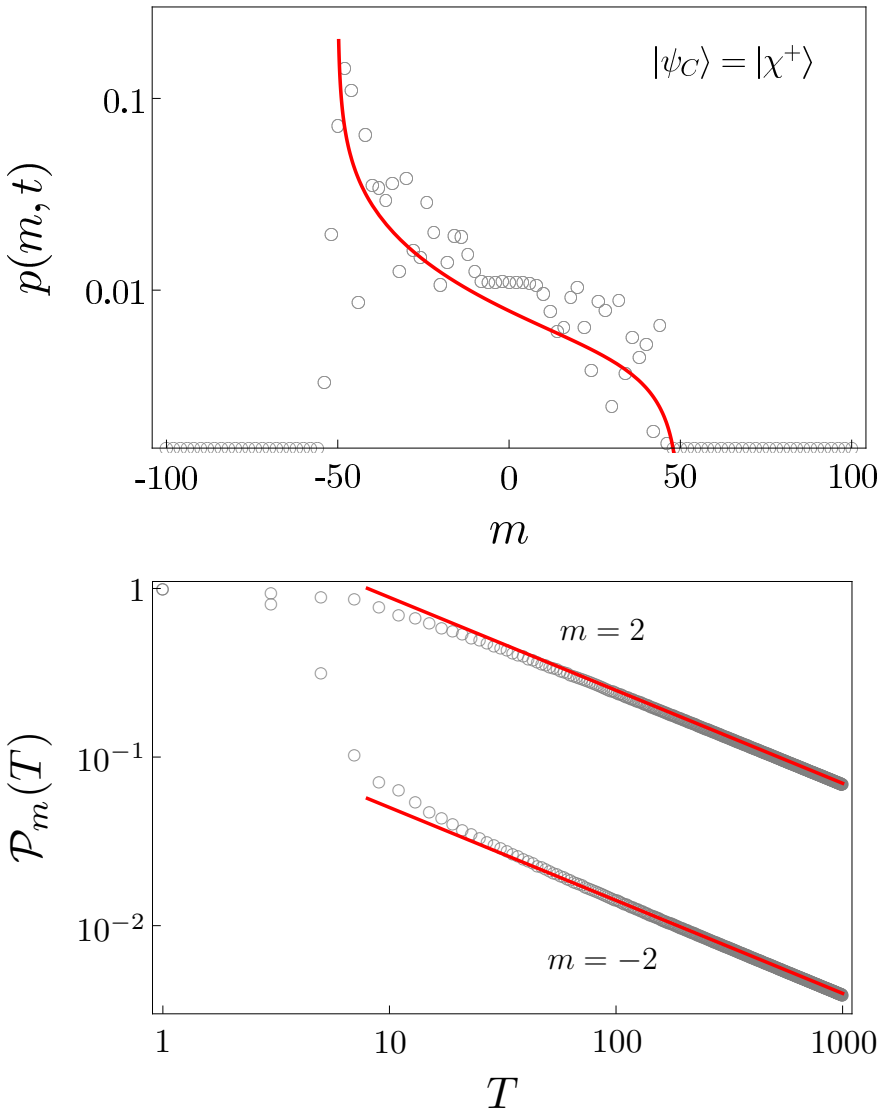

FIG. 3: The first plot shows the probability distribution for the two-state walk with $\rho = 0.5$. The initial coin state is $|\psi_C\rangle = |\chi^+\rangle$, which results in density with only one peak on the left. The lower plot illustrates the behaviour of persistence of sites $m = 2$ and $m = -2$. Both curves have the same slope (7) which is determined solely by the coin parameter ρ.

have shown that the considered quantum walks share the same features and the coin factor ρ is a scaling parameter which determines the rate of spreading of the three-state quantum walk across the line.

To evaluate persistence of unvisited sites we estimate the exact probability distribution $p(m,t)$ for large number of steps t. In contrast to the two-state walk, the properties of the probability distribution are not fully captured by the limit density $w(v)$. Indeed, the three-state quantum walk leads to the trapping effect [26–28, 38, 39], which means that the probability of finding the particle at position m has a non-vanishing limit for t approaching infinity. We denote the limiting value

$$\lim_{t\to\infty} p(m,t) = p_\infty(m),$$

as the trapping probability. Hence, for large t we approximate the probability to find the particle at position m at time t with the sum

$$p(m,t) \approx \frac{1}{t} w\left(\frac{m}{t}\right) + p_\infty(m).$$

The limit density $w(v)$ and the trapping probability $p_\infty(m)$ were analyzed in [38, 39]. We follow the results of [39] since they have simpler form due to the use of a more suitable basis of the coin space. In particular, the basis of the

coin space was constructed from the eigenvectors of the coin operator (9) which reads

$$\begin{aligned}
|\sigma^+\rangle &= \sqrt{\frac{1-\rho^2}{2}}|L\rangle + \rho|S\rangle + \sqrt{\frac{1-\rho^2}{2}}|R\rangle, \\
|\sigma_1^-\rangle &= \frac{\rho}{\sqrt{2}}|L\rangle - \sqrt{1-\rho^2}|S\rangle + \frac{\rho}{\sqrt{2}}|R\rangle, \\
|\sigma_2^-\rangle &= \frac{1}{\sqrt{2}}(|L\rangle - |R\rangle).
\end{aligned}$$

The vectors satisfy the eigenvalue equations

$$C(\rho)|\sigma^+\rangle = |\sigma^+\rangle, \qquad C(\rho)|\sigma_i^-\rangle = -|\sigma_i^-\rangle, i = 1, 2.$$

We decompose the initial coin state into the eigenstate basis according to

$$|\psi_C\rangle = g_+|\sigma^+\rangle + g_1|\sigma_1^-\rangle + g_2|\sigma_2^-\rangle.$$

The limiting probability density then reads [39]

$$\begin{aligned}
w(v) &= \frac{\sqrt{1-\rho^2}}{\pi(1-v^2)\sqrt{\rho^2-v^2}}\left(1-|g_2|^2 - \right. \\
&\left. -(g_1\overline{g_2}+\overline{g_1}g_2)\frac{v}{\rho} + (|g_2|^2-|g_+|^2)\frac{v^2}{\rho^2}\right).
\end{aligned} \tag{10}$$

The trapping probability is given by [39]

$$p_\infty(m) = \begin{cases} \frac{2-2\rho^2}{\rho^4}Q^{2m}|g_+ + g_2|^2, & m > 0, \\ \frac{Q}{\rho^2}\left\{|g_+|^2 + (1-\rho^2)|g_2|^2\right\}, & m = 0, \\ \frac{2-2\rho^2}{\rho^4}Q^{2|m|}|g_+ - g_2|^2, & m < 0 \end{cases} \tag{11}$$

where Q depends on the coin parameter ρ

$$Q = \frac{2-\rho^2-2\sqrt{1-\rho^2}}{\rho^2}.$$

Let us estimate the persistence of site m. We approximate the sum in (2) with

$$\sum_{t=1}^{T} p(m,t) \approx \mathcal{I}_m(T) + \sum_{t=\lceil \frac{|m|}{\rho} \rceil}^{T} p_\infty(m),$$

where $\mathcal{I}_m(T)$ is defined in (3). The sum on the right hand side is trivial

$$\sum_{t=\lceil \frac{|m|}{\rho} \rceil}^{T} p_\infty(m) = \left(T - \left\lceil \frac{|m|}{\rho} \right\rceil\right) p_\infty(m).$$

Here $\lceil x \rceil$ denotes the ceiling of x, i.e. the smallest integer not less than x. The integral $\mathcal{I}_m(T)$ is evaluated in Appendix B. We find that $\mathcal{I}_m(T)$ asymptotically grows like a logarithm

$$\mathcal{I}_m(T) \sim \lambda \ln\left(\frac{T}{|m|}\right),$$

where the pre-factor reads

$$\lambda = \frac{\sqrt{1-\rho^2}}{\pi\rho}\left(1-|g_2|^2\right).$$

We conclude that for the three-state quantum walk on a line persistence of site m behaves asymptotically like

$$\mathcal{P}_m(T) \sim \left(\frac{T}{|m|}\right)^{-\lambda} e^{-p_\infty(m)T}. \tag{12}$$

We see that there are two contributions to persistence. Similarly to the two-state walk there is an inverse power-law. In addition, the trapping effect contributes with the exponential decay. However, the behavior of persistence depends on the initial state, in contrast to the two-state walk. Indeed, both λ and the trapping probability $p_\infty(m)$ are determined by the initial condition. The exponent λ depends only on the probability $|g_2|^2$ to find the initial coin state $|\psi_C\rangle$ in the eigenstate $|\sigma_2^-\rangle$. On the other hand, the rate of the exponential decay is determined by the interference of the amplitudes g_+ and g_2. In the following we discuss various initial conditions to illustrate our result.

Let us first consider the initial coin state $|\psi_C\rangle = |\sigma^+\rangle$. In such a case the general formula (12) for the asymptotic behaviour of persistence turns into

$$\mathcal{P}_m^{(g_+)}(T) \sim \left(\frac{T}{|m|}\right)^{-\lambda} e^{-\gamma(m)T}, \tag{13}$$

with the exponent given by

$$\lambda = \frac{\sqrt{1-\rho^2}}{\pi\rho}, \tag{14}$$

and the decay constant

$$\gamma(m) = \frac{2(1-\rho^2)}{\rho^4} Q^{2|m|}. \tag{15}$$

We see that both contributions, namely the inverse power-law and the exponential decay, are present. For illustration of this result, we show in Figure 4 the probability distribution and persistence for the three-state walk with the coin parameter $\rho = 0.8$. The first plot displays the probability distribution after $t = 100$ steps. The grey circles corresponds to the numerical simulation, the red curve depicts the asymptotic probability density (10) and the blue dashed curve corresponds to the trapping probability (11). The second plot illustrates persistence of sites $m = 2$ and $m = 10$ on the log-log scale. For $m = 2$ the decay of persistence is faster than inverse power-law. Indeed, for large number of steps the exponential decay starts to play a dominant role. On the other hand, for $m = 10$ we do not observe any deviation from the inverse power-law at the considered time-scale. This is due to the fact that the decay constant (15) itself decreases exponentially with the distance from the origin. The last plot, where we display persistence of site $m = 2$ on the logarithmic scale, illustrates that $\mathcal{P}_m(T)$ decays exponentially in the long-time limit.

Let us now turn to the initial coin state $|\psi_C\rangle = |\sigma_2^-\rangle$. The general formula for persistence of site m (12) for $g_2 = 1$ reduces into purely exponential decay

$$\mathcal{P}_m^{(g_2)}(T) \sim e^{-\gamma(m)T}, \tag{16}$$

where the decay rate $\gamma(m)$ is given by (15). To illustrate this effect, we display in Figure 5 the probability distribution and persistence for the Grover walk, i.e. $\rho = 1/\sqrt{3}$. The first plot shows the probability distribution after $t = 100$ steps. The second plot displays persistence of sites $m = 1$, $m = 2$ and $m = 5$. The decay rate (15) decreases exponentially with the growing distance from the origin. Hence, already for $m = 5$ persistence essentially saturates on the considered time-scale. The last plot shows persistence of site $m = 2$ on a log-scale. The figure illustrates that the decay of persistence is indeed purely exponential.

Next, we consider the initial coin state $|\psi_C\rangle = |\sigma_1^-\rangle$. In such a case the expression (12) reduces to a pure inverse power-law

$$\mathcal{P}_m^{(g_1)}(T) \sim \left(\frac{T}{|m|}\right)^{-\lambda}, \tag{17}$$

with the exponent λ given by (14). To illustrate this feature, we show in Figure 6 the probability distribution and persistence for the three-state walk with the coin parameter $\rho = 0.6$. The upper plot displays the probability distribution after 100 steps. We find that for the particular initial state $|\psi_C\rangle = |\sigma_1^-\rangle$ the trapping effect disappears. Indeed, according to (11) we find that $p_\infty(m)$ vanishes if $g_+ = g_2 = 0$. The lower plot displays persistence of sites $m = 2$ and $m = 5$. The log-log scale unravels that the scaling is given only by the inverse power-law (17).

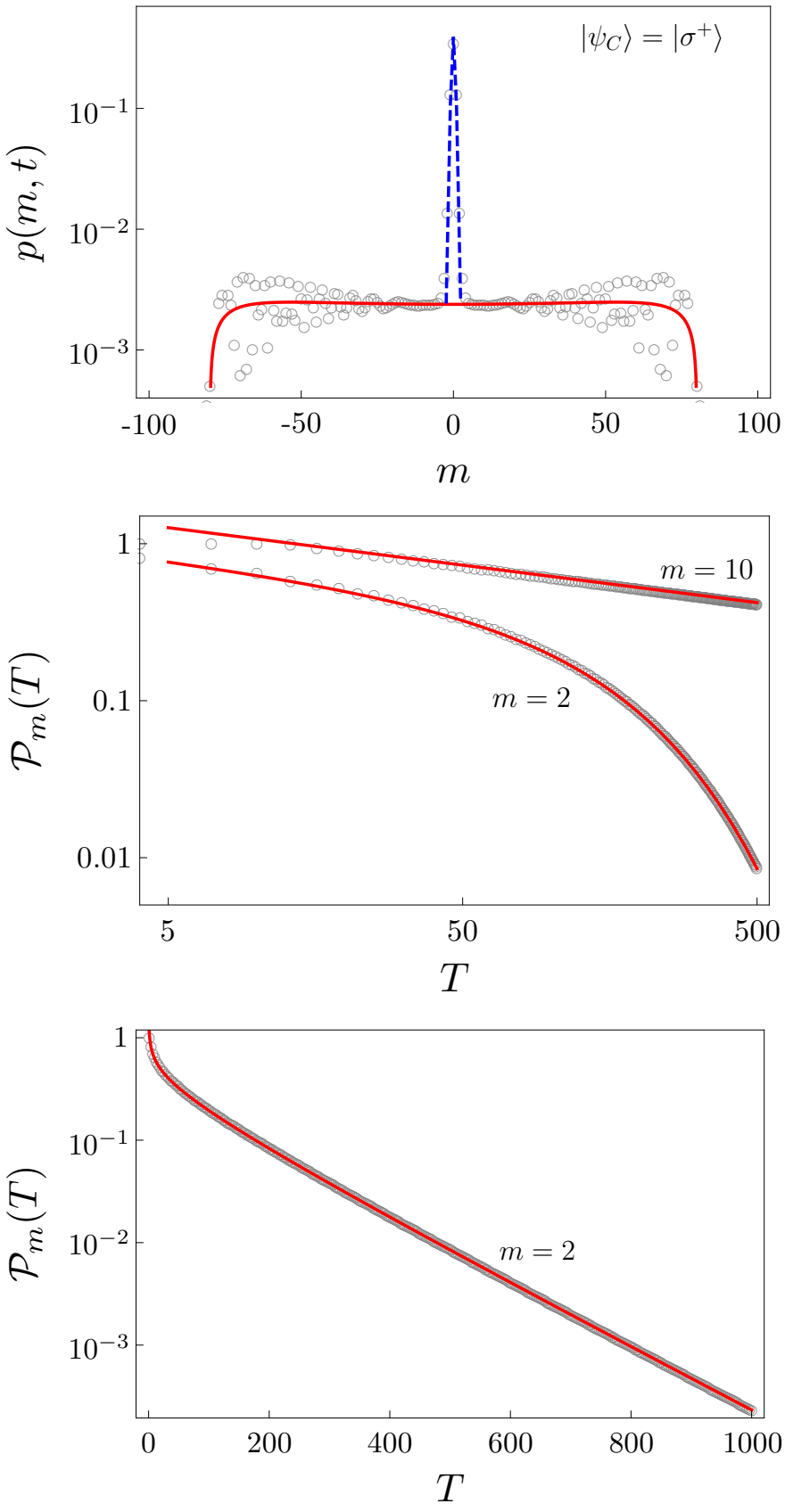

FIG. 4: Probability distribution and persistence for the three-state walk with $\rho = 0.8$ starting with the coin state $|\psi_C\rangle = |\sigma^+\rangle$. In the first plot we show the probability distribution after $t = 100$ steps. The second plot displays persistence (13) of sites $m = 2$ and $m = 10$ on the log-log scale. For $m = 2$ the decay of persistence is faster than the inverse power-law. The deviation is due to the exponential decay which starts to play a dominant role for large T. We do not observe this effect for $m = 10$, since the decay constant decreases exponentially with the distance from the origin. The third plot, which shows persistence of site $m = 2$ on the log-scale, confirms that $\mathcal{P}_m(T)$ decays exponentially.

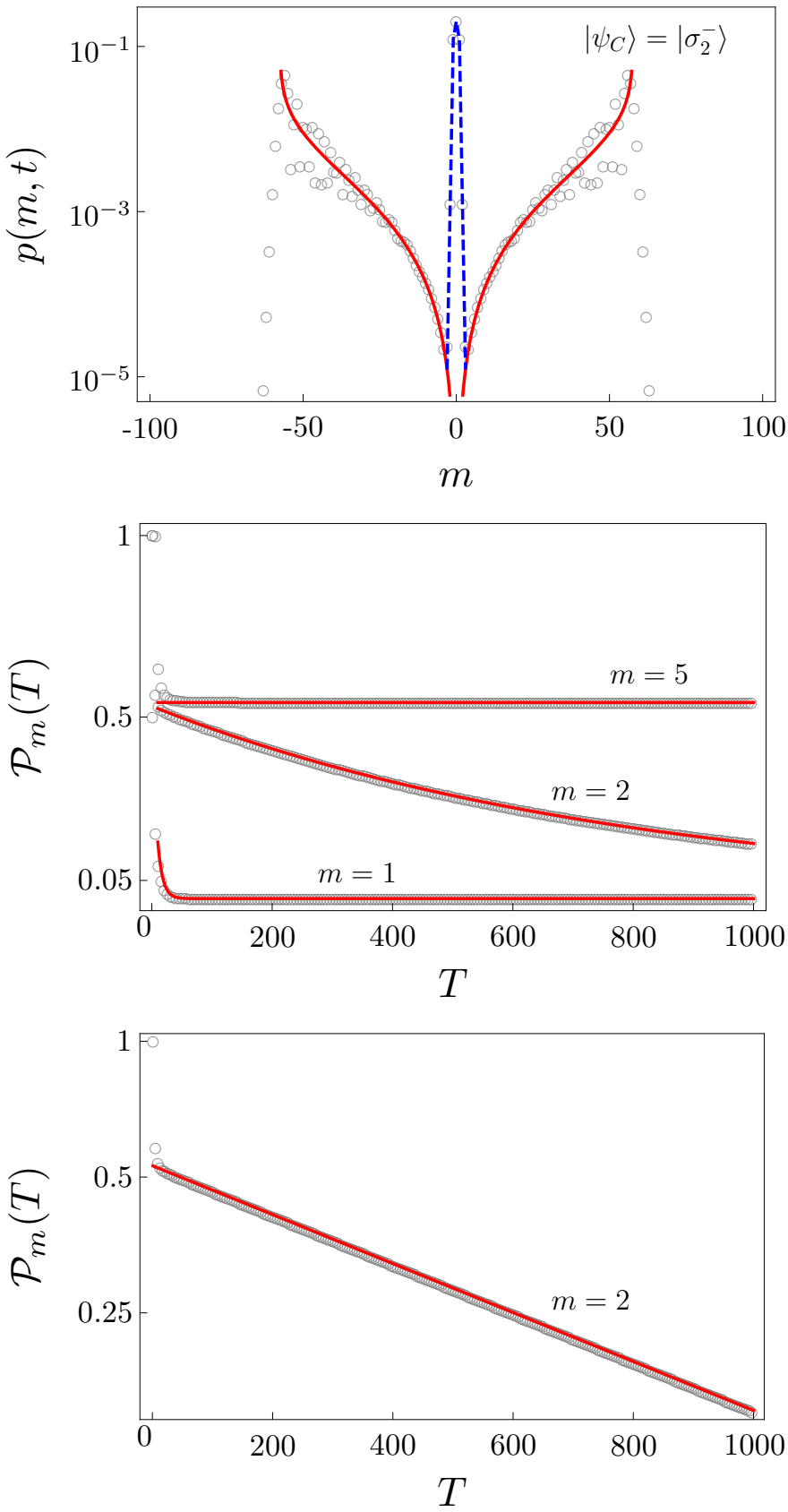

FIG. 5: Probability distribution and persistence for the three-state Grover walk starting with the coin state $|\psi_C\rangle = |\sigma_2^-\rangle$. In the upper plot we show the probability distribution after $t = 100$ steps. The middle plot displays persistence (16) of sites $m = 1$, $m = 2$ and $m = 5$. The decay is exponential but the rate drops down very fast with the growing distance from the origin. The lower plot with the log-scale on the y-axis illustrates that the decay of persistence is indeed purely exponential (16).

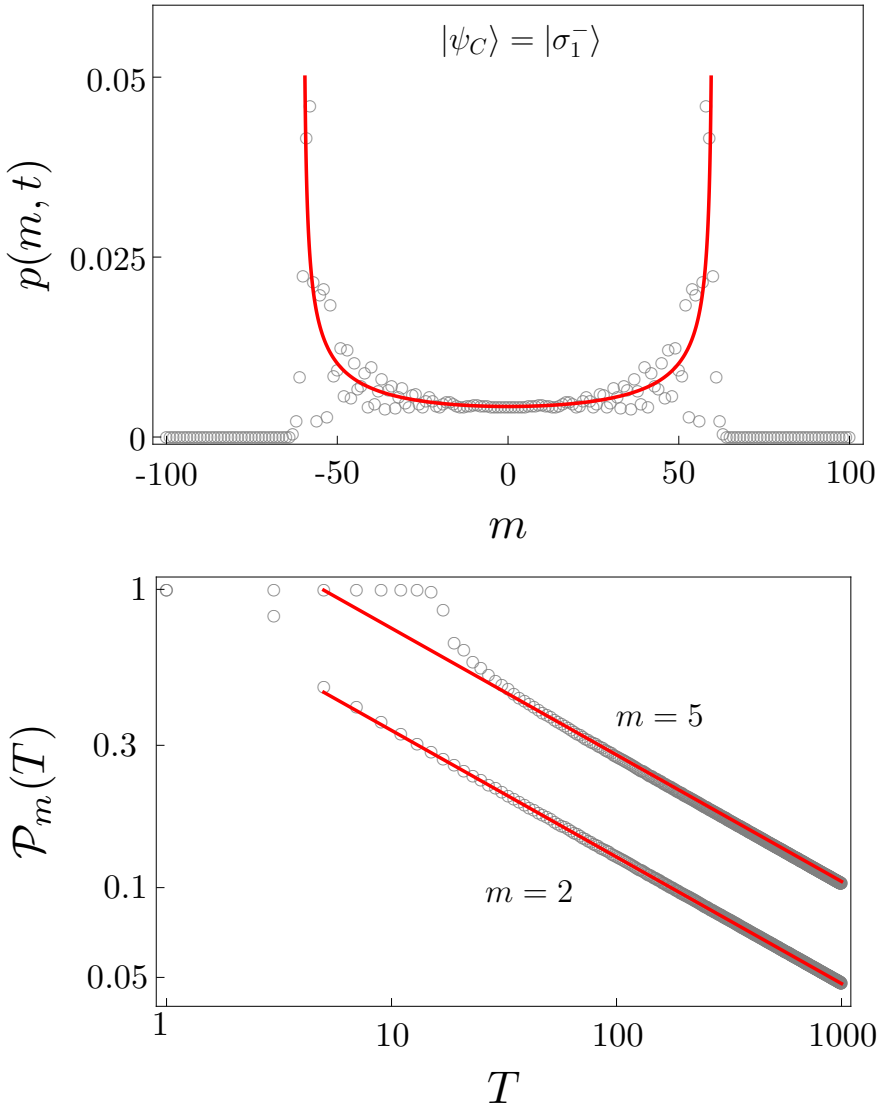

FIG. 6: Probability distribution and persistence for the three-state walk with $\rho = 0.6$ starting with the coin state $|\psi_C\rangle = |\sigma_1^-\rangle$. The upper plot shows the probability distribution after $t = 100$ steps. For this particular initial state the trapping effect disappears. The lower plot displays persistence of sites $m = 2$ and $m = 5$ on a log-log scale. We find that the scaling is given by the inverse power-law (17).

Finally, let us point out that the dependence of the trapping probability (11) on the initial coin state can be different for positive and negative m. This leads to different behavior of persistence for sites on positive and negative half-lines. As an example, consider the initial coin state

$$|\psi_C\rangle = \frac{1}{\sqrt{2}}\left(|\sigma^+\rangle + |\sigma_2^-\rangle\right). \tag{18}$$

We find that persistence of sites on positive half-line ($m > 0$) behaves like

$$\mathcal{P}_m^+(T) \sim \left(\frac{T}{m}\right)^{-\lambda} e^{-\gamma(m)T}, \tag{19}$$

where the exponent reads

$$\lambda = \frac{\sqrt{1-\rho^2}}{2\pi\rho}, \tag{20}$$

and the decay rate is given by

$$\gamma(m) = \frac{4(1-\rho^2)}{\rho^4} Q^{2m}.$$

Hence, for positive m persistence decays exponentially in the asymptotic regime. However, for sites on the negative half-line ($m < 0$) persistence obeys only the inverse power-law

$$\mathcal{P}_m^-(T) \sim \left(\frac{T}{|m|}\right)^{-\lambda}, \tag{21}$$

with the exponent λ given by (20). We point out that coherence of the initial coin state is crucial for this effect. Indeed, consider the initial coin state given by an incoherent mixture of the basis states

$$\rho_C = \frac{1}{2}|\sigma^+\rangle\langle\sigma^+| + \frac{1}{2}|\sigma_2^-\rangle\langle\sigma_2^-|.$$

In such a case persistence is given by the sum of the expressions (16) and (17) with the corresponding exponent (14) and decay rate (15), independent of the sign of the position m. Hence, there is no asymmetry between negative and positive m and persistence of all lattice sites decays exponentially in the asymptotic regime. Compared to the coherent superposition (18) the exponent (14) is larger by a factor of two while the decay rate (15) is smaller by a factor of two.

We illustrate the results for the initial coin state (18) in Figure 7 where we consider the three-state quantum walk with the coin parameter $\rho = 0.5$. In the upper plot we display the probability distribution after 100 steps of the walk. Notice that the trapping probability, highlighted by the dashed blue curve, is non-zero only on the positive half-line. The lower plot illustrates the difference in the scaling of persistence for sites on the positive or negative half-lines. Here we show persistence of sites $m = 2$ and $m = -2$ on the log-log scale. We find that for $m = -2$ the behavior of persistence is determined only by the inverse power-law (21). On the other hand, for $m = 2$ the decrease of persistence is faster. Indeed, for positive m the behavior of persistence is dominated by the exponential decay (19) in the long-time limit. This is illustrated in the last plot, where we show persistence of site $m = 2$ on the log-scale.

V. CONCLUSIONS

In the present paper persistence of unvisited sites for two- and three-state quantum walks on a line was analyzed. We have found that in contrast to the classical random walk there is no connection between the asymptotic behavior of persistence and scaling of the variance with the number of steps. Concerning the two-state walk, we have analytically confirmed the numerical result obtained in [36] for the Hadamard walk. Moreover, we have extended the analysis to a one-parameter set of two-state quantum walks. In particular, we have shown that persistence of unvisited sites obeys an inverse power-law independent of the initial condition and the actual position of the site. The exponent of the inverse power-law is determined by the parameter of the coin operator.

The main result of the paper is the behaviour of persistence for three-state quantum walks. We have focused on a one-parameter family of walks which includes the familiar three-state Grover walk. Due to the trapping effect displayed by the considered set of quantum walks, the behaviour of persistence is more involved than for the two-state quantum walks. In particular, we have shown that the asymptotic scaling of persistence is in general determined by a combination of an inverse power-law and an exponential decay. However, both the exponent of the inverse power-law and the decay rate of the exponential decline depend on the initial coin state. Therefore, it is possible to obtain various asymptotic regimes of persistence by choosing proper initial conditions. Moreover, one can employ the asymmetry of the trapping effect to achieve different asymptotic scaling of persistence for sites on the positive and negative half-line. All obtained results have been facilitated by using a suitable basis formed by the eigenvectors of the coin operator. This allows to express persistence in closed and compact form and trace back the ways it is influenced by the initial state and its coherence.

The present study is limited to the quantum walks on a line. A natural extension is to consider persistence of unvisited sites in quantum walks on higher-dimensional lattices. It would be interesting if similar effects, such as the dependency of persistence on the initial condition and various regimes of persistence for different lattice sites, can be found on more complicated lattices.

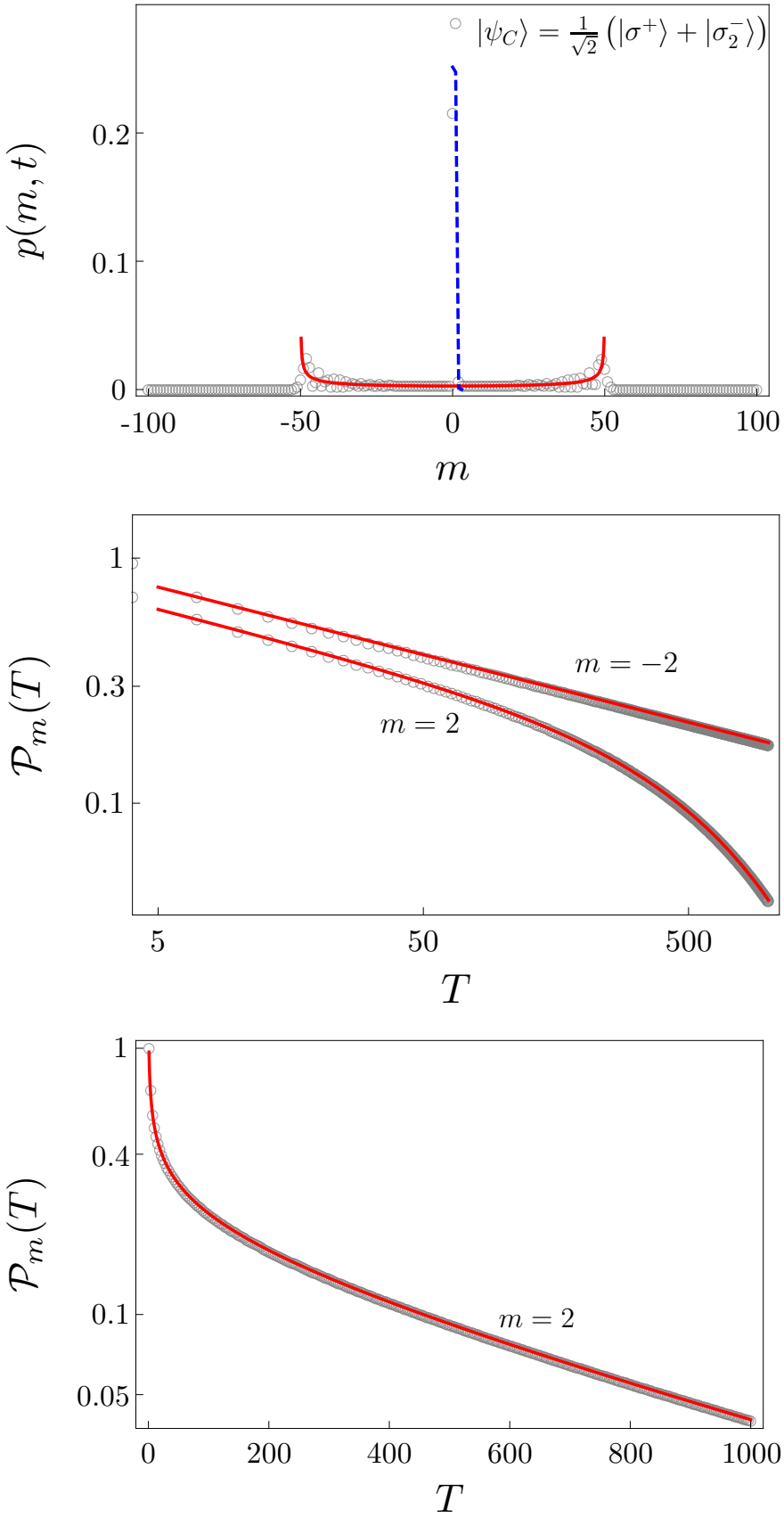

FIG. 7: Probability distribution and persistence for the three-state walk starting with the coin state (18). The coin parameter was chosen as $\rho = 0.5$. In the upper plot we display the probability distribution after $t = 100$ steps. Note that the trapping probability is non-zero only on the positive half-line. The lower plot shows persistence of sites $m = 2$ and $m = -2$ on the log-log scale. For $m = -2$ the behavior of persistence is determined only by the inverse power-law (21). However, for $m = 2$ the decrease of persistence is exponential (19), as we illustrate in the last plot with the logarithmic scale.

Acknowledgments

We appreciate the financial support from RVO 68407700. MŠ is grateful for the financial support from GAČR under Grant No. 14-02901P. IJ is grateful for the financial support from GAČR under Grant No. 13-33906S.

APPENDIX A: INTEGRAL $\mathcal{I}_m(T)$ FOR A TWO-STATE WALK

We dedicate this appendix to evaluating integral $\mathcal{I}_m(T)$ defined in (3) for the two-state walk. The limit density $w(v)$ is given by the formula (6). Since the limit density (6) is non-zero only for $|v| \leq \rho$, we replace the lower bound in the integral (3) with $|m|/\rho$. With the substitution $u = \frac{m}{\rho t}$ we rewrite $\mathcal{I}_m(T)$ into the form

$$\mathcal{I}_m(T) = \frac{\sqrt{1-\rho^2}}{\rho\pi} \int\limits_{\frac{|m|}{\rho T}}^{1} \frac{1 - \mathrm{sgn}(m) u (2|h_+|^2 - 1)}{u\left(1-\rho^2 u^2\right)\sqrt{1-u^2}} du.$$

Evaluating the integral we obtain

$$\begin{aligned}\mathcal{I}_m(T) \;=\; & \frac{\sqrt{1-\rho^2}}{\rho\pi} \ln\left(\frac{\rho T}{|m|}\left(1+\sqrt{1-\frac{m^2}{\rho^2 T^2}}\right)\right) + \frac{1}{\pi}\arctan\left(\frac{\rho}{\sqrt{1-\rho^2}}\sqrt{1-\frac{m^2}{\rho^2 T^2}}\right) + \\ & + \mathrm{sgn}(m)\frac{2|h_+|^2-1}{\rho}\left(\frac{1}{\pi}\arctan\left(\frac{|m|}{\rho T}\sqrt{\frac{1-\rho^2}{1-\frac{m^2}{\rho^2 T^2}}}\right) - \frac{1}{2}\right).\end{aligned}$$

Moreover, for large number of steps T this function tends to

$$\mathcal{I}_m(T) \approx \frac{\sqrt{1-\rho^2}}{\rho\pi}\ln\left(\frac{2\rho T}{|m|}\right) - \frac{\arcsin\rho}{\pi} + \mathrm{sgn}(m)\frac{2|h_+|^2-1}{2\rho}.$$

Therefore, for large T the function $\mathcal{I}_m(T)$ grows like a logarithm

$$\mathcal{I}_m(T) \sim \lambda \ln\left(\frac{T}{|m|}\right),$$

where the pre-factor reads

$$\lambda = \frac{\sqrt{1-\rho^2}}{\rho\pi}.$$

APPENDIX B: INTEGRAL $\mathcal{I}_m(T)$ FOR A THREE-STATE WALK

In this appendix we evaluate the integral (3) for a three-state quantum walk, i.e. the limit density is given by (10). Using the substitution $u = \frac{m}{\rho t}$ we rewrite $\mathcal{I}_m(T)$ into the form

$$\mathcal{I}_m(T) = \frac{\sqrt{1-\rho^2}}{\rho\pi} \int\limits_{\frac{|m|}{\rho T}}^{1} \frac{1 - |g_2|^2 - (g_1\overline{g_2} + \overline{g_1}g_2)u + (|g_2|^2 - |g_+|^2)u^2}{u(1-u^2)\sqrt{1-u^2}} du.$$

Evaluating the integral we obtain the following result

$$\begin{aligned}\mathcal{I}_m(T) &= \frac{\sqrt{1-\rho^2}}{\pi\rho}\left(1-|g_2|^2\right)\left(\ln\left(\frac{\rho T}{|m|}\right)+\ln\left(1+\sqrt{1-\frac{m^2}{\rho^2T^2}}\right)\right)- \\ &-\frac{1}{2\pi}\left(1-|g_2|^2\right)\arctan\left(\frac{2\rho\sqrt{\left(1-\frac{m^2}{\rho^2T^2}\right)(1-\rho^2)}}{\left(2-\frac{m^2}{\rho^2T^2}\right)\rho^2-1}\right)+\frac{1}{\pi\rho^2}\left(|g_2|^2-|g_+|^2\right)\arctan\left(\rho\sqrt{\frac{1-\frac{m^2}{\rho^2T^2}}{1-\rho^2}}\right)- \\ &-\frac{1}{2\pi\rho}\left(\overline{g_1}g_2+g_1\overline{g_2}\right)\left(\pi-2\arctan\left(\frac{\frac{|m|}{\rho T}\sqrt{1-\rho^2}}{\sqrt{1-\frac{m^2}{\rho^2T^2}}}\right)\right).\end{aligned}$$

For large number of steps T this function approaches

$$\begin{aligned}\mathcal{I}_m(T) &\approx \frac{\sqrt{1-\rho^2}}{\pi\rho}\left(1-|g_2|^2\right)\ln\left(\frac{2\rho T}{|m|}\right)+\frac{1}{2\pi}\left(1-|g_2|^2\right)\arctan\left(\frac{2\rho\sqrt{1-\rho^2}}{1-2\rho^2}\right)+ \\ &+\frac{1}{\pi\rho^2}\left(|g_2|^2-|g_+|^2\right)\arctan\left(\rho\sqrt{\frac{1}{1-\rho^2}}\right)-\frac{1}{2\rho}\left(\overline{g_1}g_2+g_1\overline{g_2}\right)\end{aligned}$$

Wee see that $\mathcal{I}_m(T)$ asymptotically grows like a logarithm

$$\mathcal{I}_m(T)\sim\lambda\ln\left(\frac{T}{|m|}\right),$$

where the pre-factor reads

$$\lambda=\frac{\sqrt{1-\rho^2}}{\pi\rho}\left(1-|g_2|^2\right).$$

---

[1] Y. Aharonov, L. Davidovich and N. Zagury, Phys. Rev. A **48**, 1687 (1993).
[2] D. Meyer, J. Stat. Phys. **85**, 551, (1996).
[3] E. Farhi and S. Gutmann, Phys. Rev. A **58**, 915 (1998).
[4] N. Shenvi, J. Kempe and K. Whaley, Phys. Rev. A **67**, 052307 (2003).
[5] A. M. Childs and J. Goldstone, Phys. Rev. A **70**, 022314 (2004).
[6] V. Potoček, A. Gabris, T. Kiss and I. Jex, Phys. Rev. A **79**, 012325 (2009).
[7] A. M. Childs and Y. Ge, Phys. Rev. A **89**, 052337 (2014).
[8] J. K. Gamble, M. Friesen, D. Zhou, R. Joynt and S. N. Coppersmith, Phys. Rev. A **81**, 052313 (2010).
[9] S. D. Berry and J. B. Wang, Phys. Rev. A **83**, 042317 (2011).
[10] K. Rudinger, J. K. Gamble, M. Wellons, E. Bach, M. Friesen, R. Joynt and S. N. Coppersmith, Phys. Rev. A **86**, 022334 (2012).
[11] M. Hillery, D. Reitzner and V. Bužek, Phys. Rev. A **81**, 062324 (2010).
[12] M. Hillery, H. J. Zheng, E. Feldman, D. Reitzner and V. Bužek, Phys. Rev. A **85**, 062325 (2012).
[13] S. Cottrell and M. Hillery, Phys. Rev. Lett. **112**, 030501 (2014).
[14] V. M. Kendon and C. Tamon, J. Comput. Theor. Nanosc. **8**, 422 (2011).
[15] P. Kurzynski and A. Wojcik, Phys. Rev. A **83**, 062315 (2011).
[16] K. E. Barr, T. J. Proctor, D. Allen and V. M. Kendon, Quantum Inf. Comput. **14**, 417 (2014).
[17] X. Zhan, H. Qin, Z. H. Bian, J. Li and P. Xue, Phys. Rev. A **90**, 012331 (2014).
[18] I. Yalcinkaya and Z. Gedik, J. Phys. A **48**, 225302 (2015).
[19] A. M. Childs, Phys. Rev. Lett. **102**, 180501 (2009).
[20] N. B. Lovett, S. Cooper, M. Everitt, M. Trevers and V. Kendon, Phys. Rev. A **81**, 042330 (2010).
[21] E.W. Montroll, in *Random Walks on Lattices*, edited by R. Bellman (American Mathematical Society, Providence, RI), Vol. **16**, 193 (1964).
[22] G. Pólya, Mathematische Annalen **84**, 149 (1921).
[23] M. Štefaňák, I. Jex and T. Kiss, Phys. Rev. Lett. **100**, 020501 (2008).
[24] M. Štefaňák, T. Kiss and I. Jex, Phys. Rev. A **78**, 032306 (2008).

[25] N. Inui, Y. Konishi and N. Konno, Phys. Rev. A **69**, 052323 (2004).
[26] N. Inui, N. Konno and E. Segawa, Phys. Rev. E **72**, 056112 (2005).
[27] N. Inui and N. Konno, Physica A, **353**, 133 (2005).
[28] S. Falkner and S. Boettcher, Phys. Rev. A **90**, 012307 (2014).
[29] K. Watabe, N. Kobayashi, M. Katori and N. Konno, Phys. Rev. A **77**, 062331 (2008).
[30] T. Kiss, L. Kecskes, M. Štefaňák and I. Jex, Phys. Scr. **T135**, 014055 (2009).
[31] A. Ambainis, E. Bach, A. Nayak, A. Vishwanath and J. Watrous, in *Proceedings of the 33th STOC*, ACM New York, p. 60 (2001).
[32] F. A. Grünbaum, L. Velázquez, A. H. Werner and R. F. Werner, Commun. Math. Phys. **320**, 543 (2013).
[33] P. Sinkovicz, Z. Kurucz, T. Kiss and J. K. Asbóth, Phys. Rev. A **91**, 042108 (2015).
[34] J. Bourgain, F. A. Grünbaum, L. Velázquez and J. Wilkening, Commun. Math. Phys. **329**, 1031 (2014).
[35] S. Chandrasekhar, Rev. Mod. Phys. 15, 1 (1943)
[36] S. Goswami, P. Sen, and A. Das, Phys. Rev. E **81**, 021121 (2010).
[37] M. Štefaňák, I. Bezděková and I. Jex, Eur. Phys. J. D **66**, 142 (2012).
[38] T. Machida, Quantum Inf. Comp. **15**, 0406 (2015).
[39] M. Štefaňák, I. Bezděková and I. Jex, Phys. Rev. A **90**, 012342 (2014).
[40] G. Grimmett, S. Janson and P. F. Scudo, Phys. Rev. E **69**, 026119 (2004).
[41] A. Kempf and R. Portugal, Phys. Rev. A **79**, 052317 (2009).
[42] N. Konno, Quantum Inf. Process. **1**, 345 (2002).
[43] N. Konno, J. Math. Soc. Jpn. **57**, 1179 (2005).
[44] M. Štefaňák, S. M. Barnett, B. Kollár, T. Kiss and I. Jex, New J. Phys. **13**, 033029 (2011).

Limit density of 2D quantum walk: zeroes of the weight function

M. Štefaňák,[1] I. Bezděková,[1] and I. Jex[1]

[1]*Department of Physics, Faculty of Nuclear Sciences and Physical Engineering, Czech Technical University in Prague, Břehová 7, 115 19 Praha 1 - Staré Město, Czech Republic*

Properties of the probability distribution generated by a discrete-time quantum walk, such as the number of peaks it contains, depend strongly on the choice of the initial condition. In the present paper we discuss from this point of view the model of the two-dimensional quantum walk analyzed in K. Watabe et al., Phys. Rev. A **77**, 062331, (2008). We show that the limit density can be altered in such a way that it vanishes on the boundary or some line. Using this result one can suppress certain peaks in the probability distribution. The analysis is simplified considerably by choosing a more suitable basis of the coin space, namely the one formed by the eigenvectors of the coin operator.

I. INTRODUCTION

Quantum walks [1–3] were proposed as extensions of the concept of a classical random walk to the unitary evolution of a quantum particle on a discrete graph or lattice. They have found promising applications in quantum information processing, e.g. in search algorithms [4], graph isomorphism testing [5], finding structural anomalies in graphs [6], and perfect state transfer [7]. Moreover, quantum walks were shown to be universal tools for quantum computation [8].

Suitable tools for the analysis of homogeneous quantum walks on infinite lattice are the Fourier transformation [9] and the weak-limit theorems [10]. While the properties of many quantum walks on a line are well understood [11–14], less is know about quantum walks on higher-dimensional latices. Indeed, there are many technical difficulties, e.g. diagonalization of the evolution operator. One of the few models of 2D quantum walks which is well understood is the one analyzed in [15]. This model is a one-parameter extension of the 2D Grover walk which preserves its key feature, namely the trapping effect (or localization) [16]. The coin parameter controls the area covered by the quantum walk, which in general is an elliptic disc and reduces to a circle for the 2D Grover walk.

In the present paper we focus on the role of the initial conditions on the shape of the probability distribution resulting from the 2D quantum walk of [15]. We are interested in initial states which lead to non-generic probability distributions, such as those with reduced number of peaks. In order to find them we first simplify the results of [15] by converting them to a more suitable basis of the coin space. Following [14] we choose the basis formed by the eigenvectors of the coin operator. We then discuss various initial coin states which result in non-generic probability distribution. In particular, we show that the limit density can be set to zero on some line. This can be used to suppress peaks in the probability distribution.

The paper is organized as follows: First, in Section II the results of [15] are briefly reviewed. Next, we convert them into more suitable basis to simplify the following analysis. In Section III various initial states which lead to non-generic probability distributions are discussed. We conclude and present an outlook in Section IV.

II. 2D QUANTUM WALK

Let us first briefly review the results of [15]. The authors have considered a quantum walk on a two-dimensional square lattice where the particle can in each step move from its present position (x, y) to the nearest neighbours $(x \pm 1, y)$ and $(x, y \pm 1)$. These displacements correspond to the four states $|R\rangle$, $|L\rangle$, $|U\rangle$ and $|D\rangle$ which form the standard basis of the coin space $\mathcal{H}_C$. In this standard basis the coin operator is given by the following matrix

$$C = \begin{pmatrix} -p & 1-p & \sqrt{p(1-p)} & \sqrt{p(1-p)} \\ 1-p & -p & \sqrt{p(1-p)} & \sqrt{p(1-p)} \\ \sqrt{p(1-p)} & \sqrt{p(1-p)} & p-1 & p \\ \sqrt{p(1-p)} & \sqrt{p(1-p)} & p & p-1 \end{pmatrix}, \tag{1}$$

where the parameter p ranges from 0 to 1. For $p = \frac{1}{2}$ the coin operator (1) reduces to the familiar 4×4 Grover matrix. This particular model was analyzed in detail in [16]. Using the Fourier analysis and the weak limit theorem [10] the authors have derived the limit density $\nu(v_x, v_y)$ of the 2D quantum walk. This allows one to evaluate the asymptotic

values of all moments of re-scaled position (or pseudo-velocity) through the formula

$$\lim_{t\to+\infty}\left\langle\left(\frac{x}{t}\right)^m\left(\frac{y}{t}\right)^n\right\rangle=\int v_x^m v_y^n \nu(v_x,v_y)dv_xdv_y.$$

The limit density of the 2D quantum walk is given by [15]

$$\nu(v_x,v_y)=\mu(v_x,v_y)\mathcal{M}(v_x,v_y)+\Delta\delta_0(v_x)\delta_0(v_y). \tag{2}$$

Here $\mu(v_x,v_y)$ denotes the fundamental density which reads [15]

$$\mu(v_x,v_y)=\frac{2}{\pi^2(1-v_x+v_y)(1+v_x-v_y)(1-v_x-v_y)(1+v_x+v_y)}\mathbf{1}_{\mathcal{E}}, \tag{3}$$

where $\mathbf{1}_{\mathcal{E}}$ denotes the indicator function of the elliptic disc

$$\mathcal{E}=\left\{(v_x,v_y)\,\middle|\,\frac{v_x^2}{p}+\frac{v_y^2}{1-p}\le 1\right\}.$$

The function $\mathbf{1}_{\mathcal{E}}$ equals 1 if the point (v_x,v_y) belongs to $\mathcal{E}$ and zero otherwise. The symbol $\mathcal{M}(v_x,v_y)$ denotes the weight function which is a second order polynomial in v_x and v_y

$$\mathcal{M}(v_x,v_y)=\mathcal{M}_1+\mathcal{M}_2v_x+\mathcal{M}_3v_y+\mathcal{M}_4v_x^2+\mathcal{M}_5v_y^2+\mathcal{M}_6v_xv_y, \tag{4}$$

with coefficients $\mathcal{M}_j$ determined by the coin parameter p and the initial coin state. Its explicit form in the standard basis is given in [15]. Finally, δ_0 denotes the Dirac delta function and Δ corresponds to the localization probability around the origin. The second term in (2) ensures that the limit density is properly normalized

$$\int_{\mathcal{E}}\nu(v_x,v_y)dv_xdv_y=1.$$

As we illustrate in Fig. 1, generic probability distribution $w(x,y,t)$ resulting from the studied 2D quantum walk has five characteristic peaks. Four of them are propagating and after t steps of the quantum walk they are located at positions

$$x=\pm pt,\quad y=\pm(1-p)t. \tag{5}$$

The propagating peaks correspond to the divergencies of the limit density (2) at points

$$v_x=\pm p,\quad v_y=\pm(1-p). \tag{6}$$

These points lie at the boundary $\partial\mathcal{E}$ of the elliptic disc. In addition, the probability distribution $w(x,y,t)$ contains a stationary peak located at the origin. On the level of the limit density (2) the stationary peak is described by the Dirac delta function. The peak does not vanish in the asymptotic limit $t\to+\infty$. Hence, this feature is usually called trapping (or localization), since the particle has a non-zero probability to remain close to the origin even in the limit of large number of steps. The trapping effect arises from the fact that the evolution operator of the studied 2D quantum walk has, apart from the continuous spectrum, two eigenvalues ±1 with infinite degeneracy [15]. The exact form of the trapping probability is not know, however, it decays rapidly (exponentially) with the distance from the origin. However, we will not analyze this feature in the present paper, since we focus on the properties of the limit density (2).

In the following we consider various initial conditions resulting in non-generic probability distributions. We show that the weight function (4) can be altered such that it vanishes on the boundary ellipse $\partial\mathcal{E}$ or on some line in the v_x, v_y plane. Using this result we can suppress certain peaks in the probability distribution. Before we turn to the detailed analysis of the weight function we first simplify it by turning into a more suitable basis of the coin space. For this purpose we consider the orthonormal basis formed by the eigenvectors of the coin operator (1), which can be expressed in the following form

$$\begin{aligned}
|\sigma_+\rangle &= \sqrt{\frac{1-p}{2}}(|R\rangle+|L\rangle)+\sqrt{\frac{p}{2}}(|U\rangle+|D\rangle),\\
|\sigma_1\rangle &= \sqrt{\frac{p}{2}}(|R\rangle+|L\rangle)-\sqrt{\frac{1-p}{2}}(|U\rangle+|D\rangle),\\
|\sigma_2\rangle &= \frac{1}{\sqrt{2}}(|R\rangle-|L\rangle),\\
|\sigma_3\rangle &= \frac{1}{\sqrt{2}}(|D\rangle-|U\rangle).
\end{aligned} \tag{7}$$

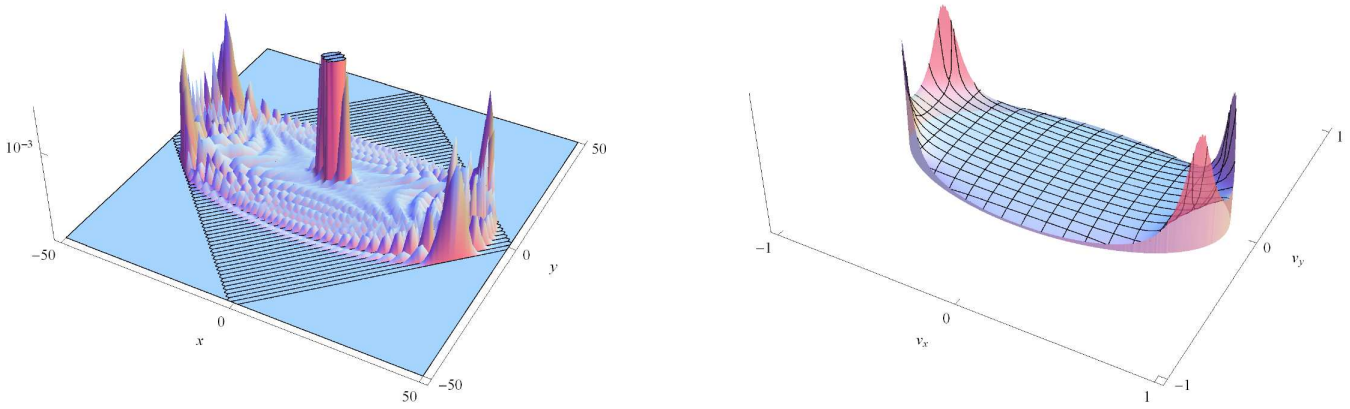

FIG. 1: 2D quantum walk with the initial coin state $1/2(|R\rangle + |L\rangle + |U\rangle + |D\rangle)$. The coin parameter was chosen as $p = 0.8$. On the left we display the probability distribution after 50 steps. The right plot shows the limit density (2). Notice the four peaks in the probability distribution located at positions given by (5) which correspond to the divergencies of the limit density (6). The central peak in the left figure corresponds to the trapping probability which is not discussed in the present paper.

The eigenvectors satisfy the relations

$$\begin{aligned} C|\sigma_+\rangle &= |\sigma_+\rangle, \\ C|\sigma_j\rangle &= -|\sigma_j\rangle, \ j = 1, 2, 3. \end{aligned} \tag{8}$$

The initial coin state is decomposed into the eigenvector basis according to

$$|\psi_C\rangle = g_+|\sigma_+\rangle + g_1|\sigma_1\rangle + g_2|\sigma_2\rangle + g_3|\sigma_3\rangle. \tag{9}$$

Simple algebra reveals that the coefficients of the weight function in terms of the amplitudes g_j are given by

$$\begin{aligned} \mathcal{M}_1 &= |g_+|^2 + |g_1|^2, \\ \mathcal{M}_2 &= \frac{1}{\sqrt{p}}(g_1\overline{g_2} + \overline{g_1}g_2), \\ \mathcal{M}_3 &= \frac{1}{\sqrt{1-p}}(g_1\overline{g_3} + \overline{g_1}g_3), \\ \mathcal{M}_4 &= \frac{1}{p}(|g_2|^2 - |g_+|^2), \\ \mathcal{M}_5 &= \frac{1}{1-p}(|g_3|^2 - |g_+|^2), \\ \mathcal{M}_6 &= \frac{1}{\sqrt{p(1-p)}}(g_2\overline{g_3} + \overline{g_2}g_3). \end{aligned} \tag{10}$$

We see that the terms $\mathcal{M}_1$, $\mathcal{M}_4$ and $\mathcal{M}_5$ are determined by pairs of probabilities, while $\mathcal{M}_2$, $\mathcal{M}_3$ and $\mathcal{M}_6$ depend on the interference of a pair of amplitudes, i.e. the coherences between the $|\sigma_j\rangle$ states. The simple form of (10) allows us to identify initial coin states which lead to non-generic probability distributions in a straight-forward way.

III. NON-GENERIC PROBABILITY DISTRIBUTIONS

Let us now discuss the role of the initial coin state on the shape of the probability distribution. We begin with the eigenstate $|\sigma_+\rangle$. In such a case the weight function reduces to

$$\mathcal{M}(v_x, v_y) = 1 - \frac{v_x^2}{p} - \frac{v_y^2}{1-p}, \tag{11}$$

which vanishes on the boundary ellipse $\partial\mathcal{E}$. Hence, the divergencies of the limit density are suppressed and all propagating peaks will be absent in the resulting probability distribution. We illustrate this effect in Fig. 2, where we choose the coin parameter $p = 0.4$.

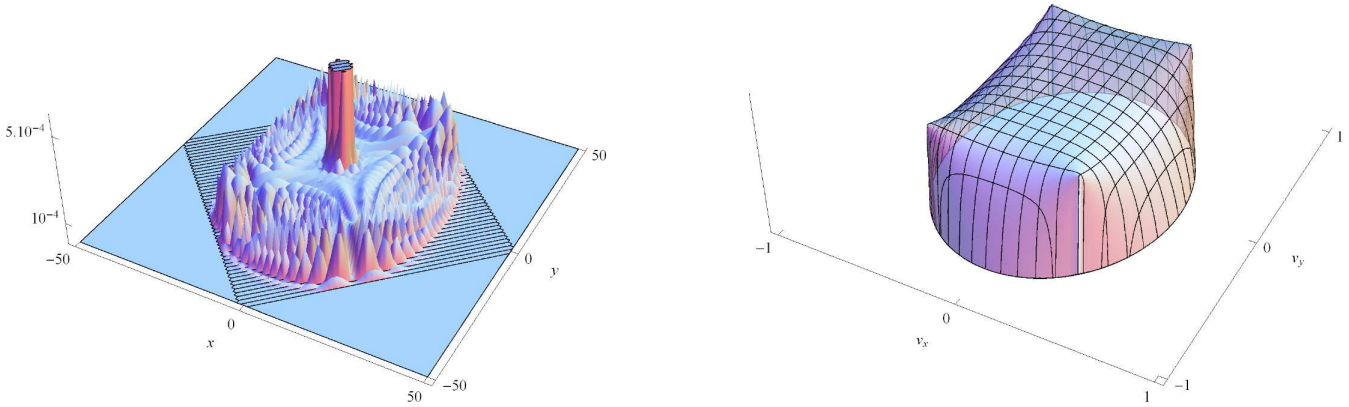

FIG. 2: 2D quantum walk with the initial coin state $|\sigma_+\rangle$. The coin parameter was chosen as $p = 0.4$. On the left we display the probability distribution after 50 steps. Notice the absence of the peaks on ellipse. Indeed, the limit density vanishes at the boundary, which we illustrate on the right. The central peak corresponds to the trapping effect.

Next, we consider the eigenstate $|\sigma_1\rangle$. For this particular initial coin state the trapping effect vanishes, as was identified already in [15]. We illustrate this feature in Fig. 3 where we take the coin parameter $p = 0.6$.

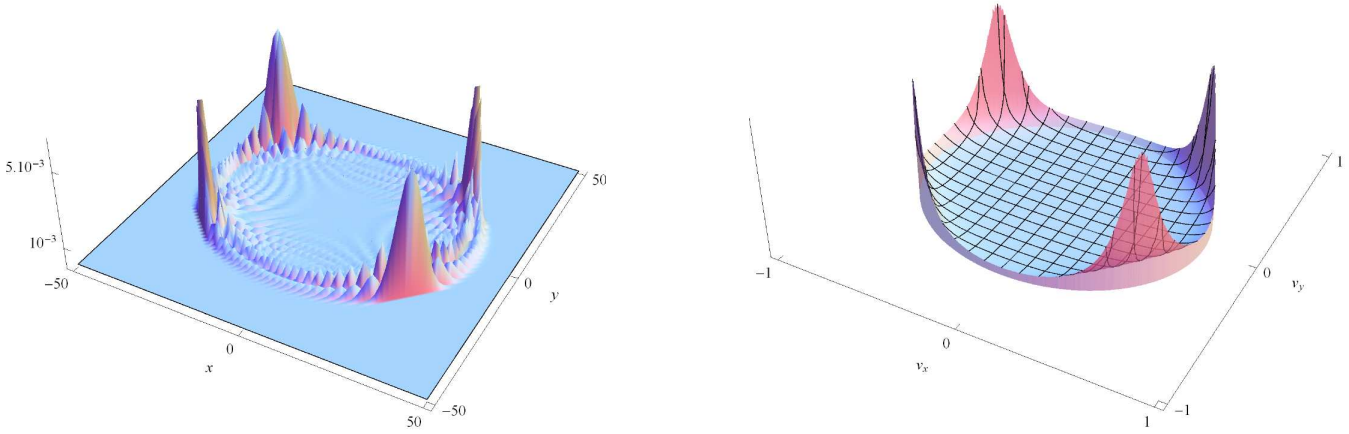

FIG. 3: 2D quantum walk with the initial coin state $|\sigma_1\rangle$. The coin parameter was chosen as $p = 0.6$. The left plot shows the probability distribution after 50 steps. Notice the absence of the central peak. Indeed, for the initial coin state $|\sigma_1\rangle$ the trapping effect vanishes. The right plot illustrates the limit density.

Let us now consider the eigenstate $|\sigma_2\rangle$ as the initial coin state. We find that the weight function reduces to

$$\mathcal{M}(v_x, v_y) = \frac{v_x^2}{p}. \tag{12}$$

Hence, the limit density vanishes on the line $v_x = 0$. This effect is illustrated in Fig. 4 for the coin parameter $p = 0.8$.

In a similar way, the choice of the initial coin state $|\psi_C\rangle = |\sigma_3\rangle$ leads to the weight function of the form

$$\mathcal{M}(v_x, v_y) = \frac{v_y^2}{1-p}. \tag{13}$$

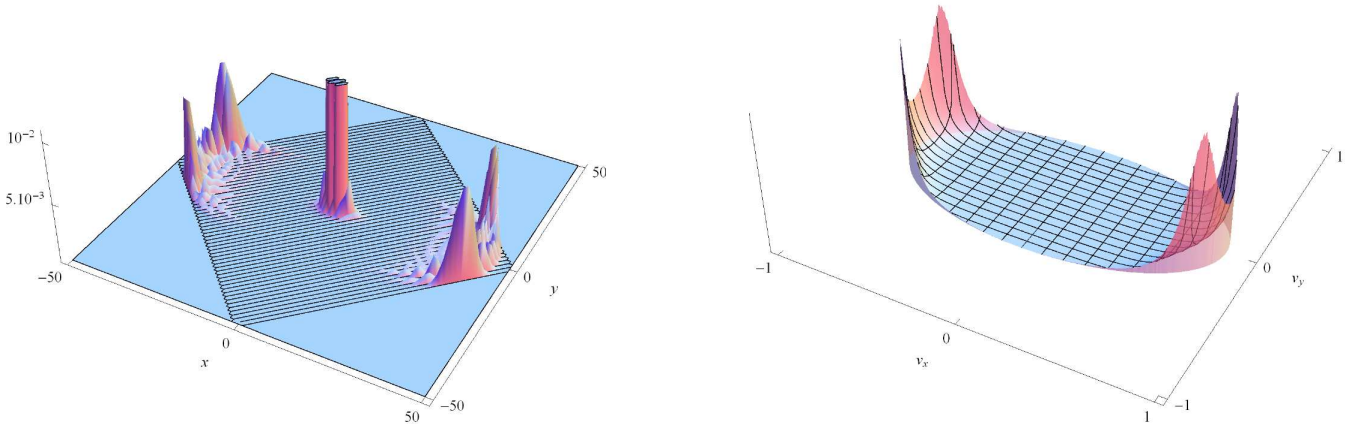

FIG. 4: 2D quantum walk with the initial coin state $|\sigma_2\rangle$. The coin parameter was chosen as $p = 0.8$. On the left we display the probability distribution after 50 steps of the quantum walk. Notice the suppression of the probability near the line $x = 0$. Indeed, the limit density vanishes for $v_x = 0$, as we illustrate in the right plot.

Therefore, for $|\sigma_3\rangle$ the density vanishes for $v_y = 0$. This feature is depicted Fig. 5.

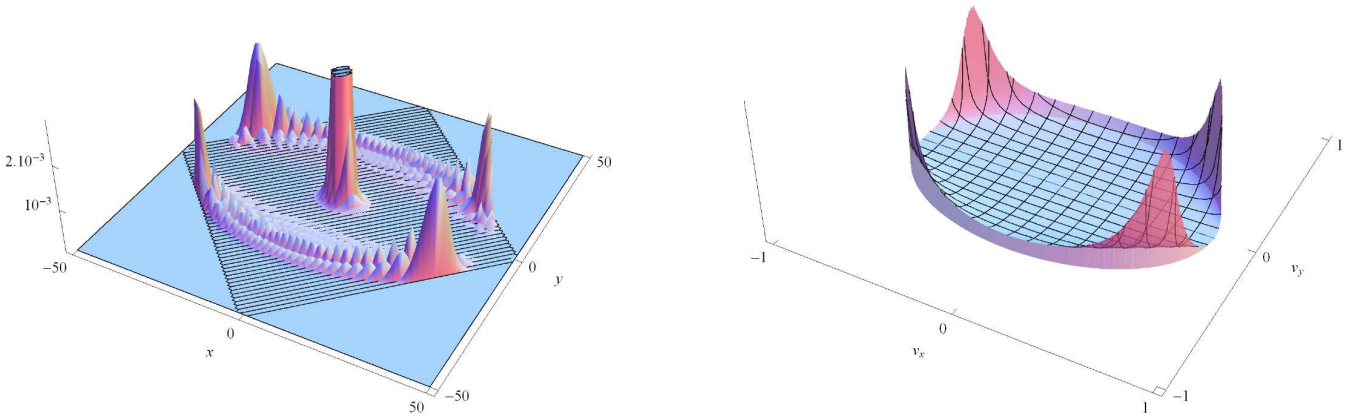

FIG. 5: 2D quantum walk with the initial coin state $|\sigma_3\rangle$. The coin parameter was chosen as $p = 0.7$. On the left we display the probability distribution after 50 steps of the quantum walk. The probability distribution is considerably suppressed along the $y = 0$ line, as predicted by the limit density which is present in the right figure.

More generally, when we choose the initial coin state of the form

$$|\psi_C\rangle = g_2|\sigma_2\rangle + g_3|\sigma_3\rangle,$$

the weight function reduces into

$$\mathcal{M}(v_x, v_y) = \left| \frac{g_2}{\sqrt{p}} v_x + \frac{g_3}{\sqrt{1-p}} v_y \right|^2 .$$

Hence, when both g_2 and g_3 are real the weight functions vanishes on the line determined by

$$\frac{g_2}{\sqrt{p}} v_x = -\frac{g_3}{\sqrt{1-p}} v_y. \tag{14}$$

We can use this fact to suppress two peaks of the probability distribution. Indeed, choosing the initial coin state as

$$|\psi_C\rangle = \sqrt{1-p}|\sigma_2\rangle + \sqrt{p}|\sigma_3\rangle, \tag{15}$$

eliminates the peaks at $v_x = p, v_y = -(1-p)$ and $v_x = -p, v_y = 1-p$. Similarly, for the initial coin state

$$|\psi_C\rangle = \sqrt{1-p}|\sigma_2\rangle - \sqrt{p}|\sigma_3\rangle,$$

the peaks at $v_x = p, v_y = 1-p$ and $v_x = -p, v_y = -(1-p)$ vanishes. For illustration of this effect we display in Fig. 6 the probability distribution of the 2D quantum walk with the initial coin state (15) and the coin parameter $p = 0.3$.

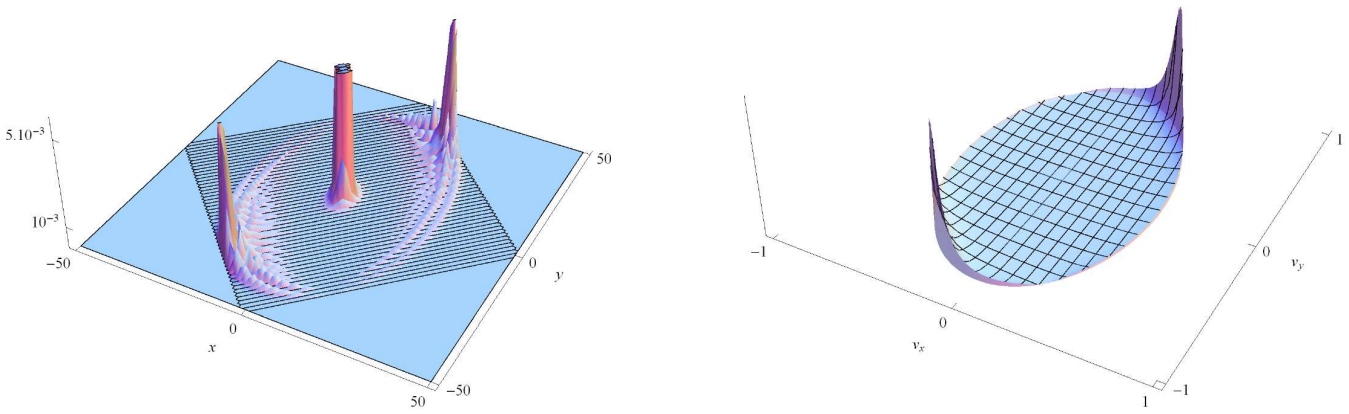

FIG. 6: 2D quantum walk with the initial coin state given by (15). The coin parameter was chosen as $p = 0.3$. On the left we display the probability distribution after 50 steps of the quantum walk. Notice that there are only two peaks on the boundary ellipse. The remaining two are suppressed since they lie on the line (14) where the limit density vanishes. This is illustrated in the right plot.

Finally, we consider a situation when the weight function reduces to a polynomial only in one variable, either v_x or v_y. We find that for $g_+ = g_3 = 0$ the weight function reduces to

$$\mathcal{M}(v_x, v_y) = \left| g_1 + \frac{g_2}{\sqrt{p}} v_x \right|^2.$$

This means that the weight function vanishes on the line

$$v_x = -\frac{g_1}{g_2}\sqrt{p},$$

provided that both g_1 and g_2 are real. Hence, we can eliminate the peaks on the line $v_x = \pm p$ by choosing the initial state

$$|\psi_C\rangle = \frac{1}{\sqrt{1+p}}(\sqrt{p}|\sigma_1\rangle \mp |\sigma_2\rangle).$$

Similarly, when we choose $g_+ = g_2 = 0$ the weight function reduces to

$$\mathcal{M}(v_x, v_y) = \left| g_1 + \frac{g_3}{\sqrt{1-p}} v_y \right|^2.$$

This means that the weight function vanishes on the line

$$v_y = -\frac{g_1}{g_3}\sqrt{1-p},$$

provided that both g_1 and g_3 are real. Hence, we can eliminate the peaks on the line $v_y = \pm(1-p)$ by choosing the initial state

$$|\psi_C\rangle = \frac{1}{\sqrt{2-p}}(\sqrt{1-p}|\sigma_1\rangle \mp |\sigma_3\rangle).$$

We illustrate this feature in Fig. 7 where we consider the 2D quantum walk with the initial coin state

$$|\psi_C\rangle = \frac{1}{\sqrt{1+p}}(\sqrt{p}|\sigma_1\rangle + |\sigma_2\rangle), \tag{16}$$

and the coin parameter $p = 0.5$.

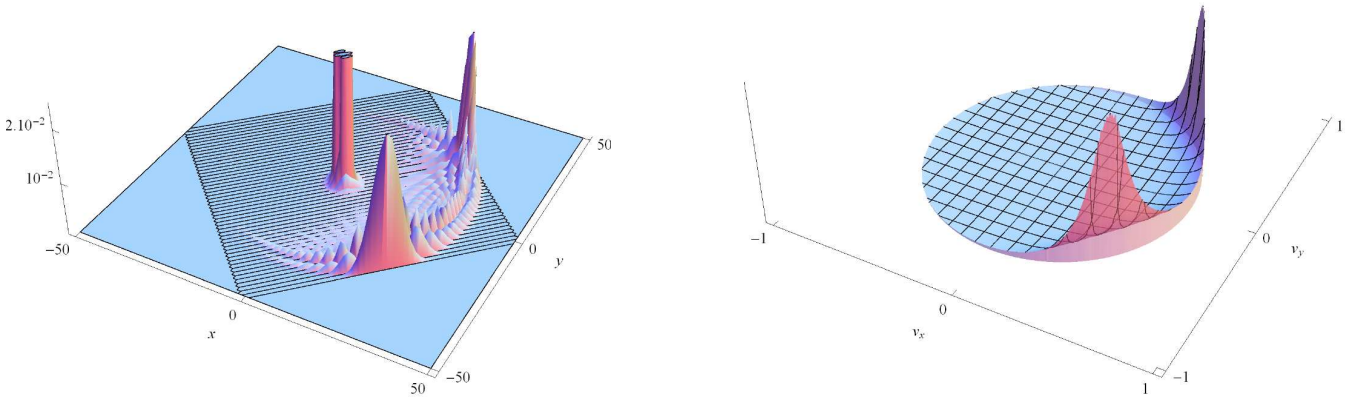

FIG. 7: 2D quantum walk with the initial coin state given by (16). The coin parameter was chosen as $p = 0.5$. On the left we display the probability distribution after 50 steps of the quantum walk. Notice that there are only two peaks on the right-hand side of the probability distribution. The remaining two are suppressed since they lie on the line $v_x = -p$ where the limit density vanishes. This is illustrated in the right plot.

IV. CONCLUSIONS

We have discussed in detail the role of the initial conditions on the shape of the probability distribution generated by the 2D quantum walk model analyzed in [15]. The analysis is simplified considerably by converting the results of [15] into the basis formed by the eigenvectors of the coin operator. It was found that the weight function can vanish on a certain line in the v_x, v_y plane. Using this fact one can eliminate a pair of peaks in the probability distribution with a proper choice of the initial coin state. Moreover, the weight function can vanish on the boundary which leads to elimination of all propagating peaks.

The properties of the trapping effect were not discussed in the present contribution and remain an open question. In principle, the explicit form of the trapping probability can be obtained using similar methods as for quantum walks on a line. There it was found that the trapping probability can be highly asymmetric [13, 14]. In fact, it might be present on one half-line and vanish completely on the other. It would be interesting to see if similar features can be found in the present 2D quantum walk model.

Acknowledgments

We appreciate the financial support from RVO 14000 and from Czech Technical University in Prague under Grant No. SGS16/241/OHK4/3T/14. MŠ is grateful for the financial support from GAČR under Grant No. 14-02901P. IB

and IJ are grateful for the financial support from GAČR under Grant No. 13-33906S.

---

[1] Aharonov, Y., Davidovich, L., and Zagury, N., *Quantum random walk*, Phys. Rev. A **48** 1687, (1993)
[2] Meyer, D., *From quantum cellular automata to quantum lattice gases*, J. Stat. Phys. **85**, 551 (1996)
[3] Farhi, E., and Gutmann, S., *Quantum computation and decision trees*, Phys. Rev. A **58**, 915 (1998)
[4] Shenvi, N., Kempe J., and Whaley, K., *Quantum random-walk search algorithm*, Phys. Rev. A **67**, 052307 (2003)
[5] Gamble, J. K., Friesen, M., Zhou, D., Joynt, R., and Coppersmith, S. N., *Two-particle quantum walks applied to the graph isomorphism problem*, Phys. Rev. A **81**, 052313 (2010)
[6] Cottrell, S., and Hillery, M., *Finding structural anomalies in star graphs using quantum walks*, Phys. Rev. Lett. **112**, 030501 (2014)
[7] Kendon, V. M., and Tamon, C., *Perfect state transfer in quantum walks on graphs*, J. Comput. Theor. Nanosc. **8**, 422 (2011)
[8] Childs, A. M., *Universal computation by quantum walk*, Phys. Rev. Lett. **102**, 180501 (2009)
[9] Ambainis, A., Bach, E., Nayak, A., Vishwanath, A., and Watrous, J., *One-dimensional quantum walks*, Proceedings of the 33th STOC, ACM New York, 60 (2001)
[10] Grimmett, G., Janson, S., and Scudo, P. F., *Weak limits for quantum random walks*, Phys. Rev. E **69**, 026119 (2004)
[11] Konno, N., *A new type of limit theorems for the one-dimensional quantum random walk*, J. Math. Soc. Jpn. **57**, 1179 (2005)
[12] Miyazaki, T., Katori, M., and Konno, N., *Wigner formula of rotation matrices and quantum walks*, Phys. Rev. A **76**, 012332 (2007)
[13] Falkner, S., and Boettcher, S., *Weak limit of the three-state quantum walk on the line*, Phys. Rev. A **90**, 012307 (2014)
[14] Štefaňák, M., Bezděková, I., and Jex, I., *Limit distributions of three-state quantum walks: The role of coin eigenstates*, Phys. Rev. A **90**, 012342 (2014)
[15] Watabe, K., Kobayashi, N., Katori, M., and Konno, N., *Limit distributions of two-dimensional quantum walks*, Phys. Rev. A **77**, 062331 (2008)
[16] Inui, N., Konishi, Y., and Konno, N., *Localization of two-dimensional quantum walks*, Phys. Rev. A **69**, 052323 (2004)

Perfect state transfer by means of discrete-time quantum walk search algorithms on highly symmetric graphs

M. Štefaňák[1] and S. Skoupý[1]

[1]*Department of Physics, Faculty of Nuclear Sciences and Physical Engineering, Czech Technical University in Prague, Břehová 7, 115 19 Praha 1 - Staré Město, Czech Republic*

Perfect state transfer between two marked vertices of a graph by means of discrete-time quantum walk is analyzed. We consider the quantum walk search algorithm with two marked vertices, sender and receiver. It is shown by explicit calculation that for the coined quantum walks on star graph and complete graph with self-loops perfect state transfer between the sender and receiver vertex is achieved for arbitrary number of vertices N in $O(\sqrt{N})$ steps of the walk. Finally, we show that Szegedy's walk with queries on complete graph allows for state transfer with unit fidelity in the limit of large N.

I. INTRODUCTION

Quantum walks [1] have emerged as quantum analogues of a classical random walk on a discrete lattice or a graph. Both discrete-time [2] and continuous time [3] quantum walks were proposed. Soon, the potential of quantum walks in quantum information processing was identified [4]. In fact, it was found that both continuous-time [5] and discrete-time [6] quantum walks are universal models of quantum computation.

One of the most prominent application of quantum walks in quantum information processing is the spatial search of the unsorted database of N items represented by a graph with a marked vertex. Marking the vertex corresponds to different dynamics on that node, i.e. different coin operator in the discrete-time quantum walk or different on-site energy in the continuous-time quantum walk. Discrete-time quantum walk search algorithm was shown to be optimal for hypercube [7] and for lattices [8] of dimensions d greater than 2, i.e. it finds the marked node after $O(\sqrt{N})$ steps of the walk. Continuous-time quantum walk was shown to be optimal [9] for search on the complete graph, hypercube and lattices with $d > 4$. Moreover, including the coin degree of freedom the continuous-time quantum walk search is optimal for lattices with $d > 2$ [10]. Later it was found that high symmetry or connectivity of the graph is in fact not required for the optimal runtime of the continuous-time quantum walk search algorithm [11–13]. In fact, Chakraborty et al. [14] have shown that continuous-time quantum walk search algorithm is optimal for almost all graphs. Another variant of discrete-time coinless quantum walk capable of optimal search was proposed by Szegedy [15]. Szegedy's walk on complete graph finds the marked vertex with probability 1/2. Recently, Santos [16] have found that adding queries to the Szegedy's walk on the complete graph increases the probability of finding the marked vertex to 1 in the limit of large N.

Another promising application of quantum walks is the perfect state transfer between two vertices of a graph or a lattice. There exist two different approaches to the problem. In the first one defines dynamics at each individual vertex in order to achieve state transfer between two selected vertices. This approach was pursued by Kurzynski and Wojcik [17], who have designed the local coin operators to achieve perfect state transfer with discrete-time quantum walk on a circle. The method of [17] is essentially the discrete-time variant of the engineered coupling protocol [18] in spin chains. In a similar way, Zhan et al. [19] have designed paths using local coin operators of discrete time quantum walk, either identity matrices or tensor product of Pauli σ_x, which leads to state transfer on a square lattice. Yalcinkaya and Gedik [20] have analyzed the state transfer on a circle with fixed coin operator. They have shown that only identity or Pauli σ_x achieves state transfer with unit fidelity over arbitrary distance, while Hadamard operator or other mixing coins allow for perfect state transfer over finite distances only. In these models [17, 19, 20] the transfer of the internal coin state is also possible. Second approach, where one modifies the dynamics only at vertices which want to communicate the quantum state, was proposed by Hein and Tanner [21]. The authors have considered discrete-time quantum walk search algorithm on a lattice with two marked vertices, sender and receiver, and showed that initializing the algorithm on the sender vertex the walk will reach the receiver vertex with high probability. In this scenario only the transfer of particle from one vertex to the other is considered, instead of the transfer of arbitrary internal coin state. For finite graphs, especially cycles and their variants, this approach was analyzed by [22, 23] in both discrete-time and continuous-time models. More recently, Chakraborty et al. [14] have shown that in the continuous-time quantum walk scenario it is possible to achieve perfect state transfer for almost any graph in the limit of large size of the graph N.

In the present paper we follow the idea of Hein and Tanner [21] for perfect state transfer by means of discrete-time quantum walk on highly symmetric graphs. We focus on such graphs where the discrete-time quantum walk search algorithm succeeds in finding the marked vertex with certainty, namely the star graph and complete graph with self-loops [8, 25]. We also consider Szegedy's walk with queries on the complete graph [16] where unit success probability

is reached in the limit of large size of the graph N. We explicitly show that the algorithms are capable of state transfer between the sender and the receiver vertices in $O(\sqrt{N})$ steps. The method is analogous to the analysis of the search algorithms on the corresponding graphs [8, 16, 24, 25]. Namely, we determine the invariant subspace of the evolution operator of the walk which includes the sender and the receiver states. Since the distance between the sender and the receiver vertices in the models discussed in the present paper is independent of the size of the graph N the dimension of the invariant subspace is also independent of N. Similar dimensional reduction due to the high symmetry of the graph [26] was also applied previously in analysis of anomaly identification on star graphs [27, 28] and continuous-time quantum walk search algorithms [12]. In particular, the invariant subspace has dimension 3 for the star graph, 5 for the complete graph with self-loops and 7 for the Szegedy's walk with queries on the complete graph. This fact greatly reduces the complexity of the problem. Indeed, we only have to deal with the effective evolution operator which is a fixed size matrix with matrix elements depending on the size of the graph N. For star graph and complete graph with self-loops the effective evolution operator can be diagonalized analytically and the problem of state transfer can be solved exactly. We show that for both graphs the quantum walk achieves perfect state transfer, i.e. the particle is transferred with unit probability, for arbitrary size of the graph N. In the case of the Szegedy's walk with queries on complete graph we show that the particle is transferred with unit probability in the limit of large N.

Our manuscript is organized as follows: In Section II we analyze the perfect state transfer in the coined quantum walk on the star graph. Section III is devoted to perfect state transfer in the coined quantum walk on the complete graph with self-loops. Finally, state transfer in the Szegedy's walk with queries on the complete graph is discussed in Section IV. We summarize our results in the conclusions of Section V.

II. STAR GRAPH

Let us begin with the state transfer between two vertices of a star graph by means of a discrete-time quantum walk. Discrete-time quantum walk search algorithm on the star graph is exactly equivalent to the Grover search algorithm [29], hence, it finds the marked vertex with unit probability. We show by explicit calculation that the algorithm also achieves perfect state transfer.

Star graph consists of a central vertex labeled as 0 which is connected to N external vertices with labels 1 to N. Discrete-time quantum walk on the star graph can be defined as a scattering walk [27, 28] or as the usual coined quantum walk. Both models are equivalent [30, 31], and since the coined walk will be used in the following Section III we pursue this approach. We consider a quantum walk where the particle jumps from the external vertices to the central vertex and back. The position space is spanned by the vectors $|j\rangle_p$, with $j = 0, \ldots, N$, corresponding to the particle being at the vertex j. The coin space has to be defined separately for the external vertices and for the central vertex. At the external nodes the coin space is one-dimensional, since the particle can jump only to the central vertex 0. We denote the coin state as $|0\rangle_c$. At the central node the coin space has a dimension N, as the particle is allowed to jump to any external vertex j, with $j = 1, \ldots, N$. We denote the corresponding coin states as $|j\rangle_c$. The complete Hilbert space of the discrete-time quantum walk on the star graph is therefore spanned by vectors

$$\begin{aligned} |j\rangle_p \otimes |0\rangle_c &\equiv |j, 0\rangle, \\ |0\rangle_p \otimes |j\rangle_c &\equiv |0, j\rangle, \end{aligned}$$

where j runs from 1 to N. The first index corresponds to the vertex and the second index corresponds to the coin state.

The evolution operator of a single step of the walk can be written as a product of the step operator S and the coin operator C

$$U = S \cdot C. \tag{1}$$

The walk describes the particle hopping between the external vertices and the central node. Hence, the step operator is given by

$$S = \sum_{j=1}^{N} \left(|j, 0\rangle\langle 0, j| + |0, j\rangle\langle j, 0| \right).$$

Let us now turn to the coin operator. At the external nodes, where the coin space is one-dimensional, we choose the coin operator to act as identity. However, for the sake of state transfer, we have two marked vertices s (sender) and r (receiver), where the coin acts as a phase shift of π. At the central node the states $|j\rangle_c$ form an N-dimensional space, and we choose the coin operator to act there as the Grover diffusion operator

$$G = 2|\psi_S\rangle_c\langle\psi_S| - I_N, \tag{2}$$

where $|\psi_S\rangle_c$ denotes the symmetric superposition of all basis states $|j\rangle_c$

$$|\psi_S\rangle_c = \frac{1}{\sqrt{N}} \sum_{j=1}^{N} |j\rangle_c, \tag{3}$$

and I_N is the identity operator on the Hilbert space of dimension N. Hence, the coin operator is defined as

$$C = (I_N - 2|s\rangle_p\langle s| - 2|r\rangle_p\langle r|) \otimes |0\rangle_c\langle 0| + |0\rangle_p\langle 0| \otimes G.$$

After some algebra we find that the evolution operator (1) can be re-written as

$$\begin{aligned} U &= \sum_{j=1}^{N} |0,j\rangle\langle j,0| - 2|0,s\rangle\langle s,0| - 2|0,r\rangle\langle r,0| + \\ &+ \frac{2}{N} \sum_{i,j=1}^{N} |i,0\rangle\langle 0,j| - \sum_{j=1}^{N} |j,0\rangle\langle 0,j|. \end{aligned} \tag{4}$$

We start the walk in the sender vertex, i.e. the initial state is

$$|\psi(0)\rangle = |s,0\rangle.$$

The state of the walk after t steps is given by

$$|\psi(t)\rangle = U^t|\psi(0)\rangle.$$

We will show that after $O(\sqrt{N})$ steps the particle will be on the receiver vertex, i.e. in the state $|r,0\rangle$. Clearly, the walk is bipartite, since in the odd steps the particle is at the central node and in the even steps it is at the external nodes. Since we want to analyze the possibility of state transfer between two external nodes s and r we focus only on the square of the evolution operator. From the expression (4) the action of U^2 on the states $|j,0\rangle$ is then easily found to be

$$\begin{aligned} U^2|j,0\rangle &= \frac{2}{N} \sum_{i \neq j} |i,0\rangle - \left(1 - \frac{2}{N}\right) |j,0\rangle, \quad j \neq s,r \\ U^2|s,0\rangle &= -\frac{2}{N} \sum_{i \neq s} |i,0\rangle + \left(1 - \frac{2}{N}\right) |s,0\rangle, \\ U^2|r,0\rangle &= -\frac{2}{N} \sum_{i \neq r} |i,0\rangle + \left(1 - \frac{2}{N}\right) |r,0\rangle. \end{aligned} \tag{5}$$

Using these expressions one shows that the following three orthogonal states

$$\begin{aligned} |\alpha_1\rangle &= |s,0\rangle, \\ |\alpha_2\rangle &= |r,0\rangle, \\ |\alpha_3\rangle &= \frac{1}{\sqrt{N-2}} \sum_{j \neq s,r} |j,0\rangle, \end{aligned} \tag{6}$$

form an invariant subspace with respect to U^2. Indeed, from (5) we find

$$\begin{aligned} U^2|\alpha_1\rangle &= \left(1 - \frac{2}{N}\right) |\alpha_1\rangle - \frac{2}{N}|\alpha_2\rangle - \frac{2\sqrt{N-2}}{N}|\alpha_3\rangle, \\ U^2|\alpha_2\rangle &= -\frac{2}{N}|\alpha_1\rangle + \left(1 - \frac{2}{N}\right) |\alpha_2\rangle - \frac{2\sqrt{N-2}}{N}|\alpha_3\rangle, \\ U^2|\alpha_3\rangle &= \frac{2\sqrt{N-2}}{N}(|\alpha_1\rangle + |\alpha_2\rangle) - \left(1 - \frac{4}{N}\right) |\alpha_3\rangle. \end{aligned}$$

Hence, the time evolution of the walk for the fixed initial state $|\alpha_1\rangle$ is described by the effective evolution operator U_{eff}, which is in the $|\alpha_i\rangle$ basis (6) given by the following 3x3 matrix

$$U_{eff} = \begin{pmatrix} 1-\frac{2}{N} & -\frac{2}{N} & \frac{2\sqrt{N-2}}{N} \\ -\frac{2}{N} & 1-\frac{2}{N} & \frac{2\sqrt{N-2}}{N} \\ -\frac{2\sqrt{N-2}}{N} & -\frac{2\sqrt{N-2}}{N} & 1-\frac{4}{N} \end{pmatrix}.$$

Diagonalization of U_{eff} is straightforward. We find that it has an eigenvector

$$|\chi_0\rangle = \frac{1}{\sqrt{2}}\left(|\alpha_1\rangle - |\alpha_2\rangle\right), \tag{7}$$

corresponding to the eigenvalue $\lambda = 1$. The remaining two eigenvectors have the form

$$|\chi^{\pm}\rangle = \frac{1}{2}\left(|\alpha_1\rangle + |\alpha_2\rangle\right) \pm \frac{i}{\sqrt{2}}|\alpha_3\rangle. \tag{8}$$

They correspond to a pair of conjugated eigenvalues

$$\lambda^{\pm} = e^{\pm i\omega},$$

where the phase ω is given by

$$\omega = \arccos\left(\frac{N-4}{N}\right). \tag{9}$$

Let us now analyze the evolution of the initial state $|\alpha_1\rangle$ under the effective evolution operator U_{eff}. We find that the initial condition $|\alpha_1\rangle$ and the desired target state $|\alpha_2\rangle$ can be decomposed into the eigenbasis of U_{eff} as

$$\begin{aligned} |\alpha_1\rangle &= \frac{1}{\sqrt{2}}|\chi_0\rangle + \frac{1}{2}\left(|\chi^+\rangle + |\chi^-\rangle\right), \\ |\alpha_2\rangle &= -\frac{1}{\sqrt{2}}|\chi_0\rangle + \frac{1}{2}\left(|\chi^+\rangle + |\chi^-\rangle\right). \end{aligned}$$

After t applications of the effective evolution operator U_{eff}, i.e. after $2t$ steps of the walk, we obtain

$$|\psi(2t)\rangle = \frac{1}{\sqrt{2}}|\chi_0\rangle + \frac{e^{i\omega t}}{2}\left(|\chi^+\rangle + e^{-2i\omega t}|\chi^-\rangle\right). \tag{10}$$

For $\omega t = \pi$ the state reduces to $-|\alpha_2\rangle$, i.e. the receiver state up to an irrelevant global phase factor. We conclude that the walk achieves (almost) perfect state transfer between the sender and receiver vertices after T steps, provided that we choose T as the closest integer to $2\pi/\omega$, i.e.

$$T \approx \frac{2\pi}{\arccos\left(\frac{N-4}{N}\right)}. \tag{11}$$

With the Taylor expansion we find that the number of steps required for the state transfer scales with the size of the star graph according to

$$T \sim \frac{\pi}{\sqrt{2}}\sqrt{N} + O(N^{-\frac{1}{2}}).$$

For illustration we display in Figure 1 the fidelity between the state of the walk (10) and the target state $|\alpha_2\rangle$ as a function of the number of steps. From (10) we find that it is given by

$$\mathcal{F}(2t) = |\langle\psi(2t)|\alpha_2\rangle|^2 = \sin^4\left(\frac{\omega t}{2}\right). \tag{12}$$

Note that for odd time steps the fidelity is zero since the walk is bipartite. In Figure 1 the number of vertices of the star graph was chosen as $N = 100$. As follows from (11) the first maximum of the fidelity is reached after 22 steps of the walk.

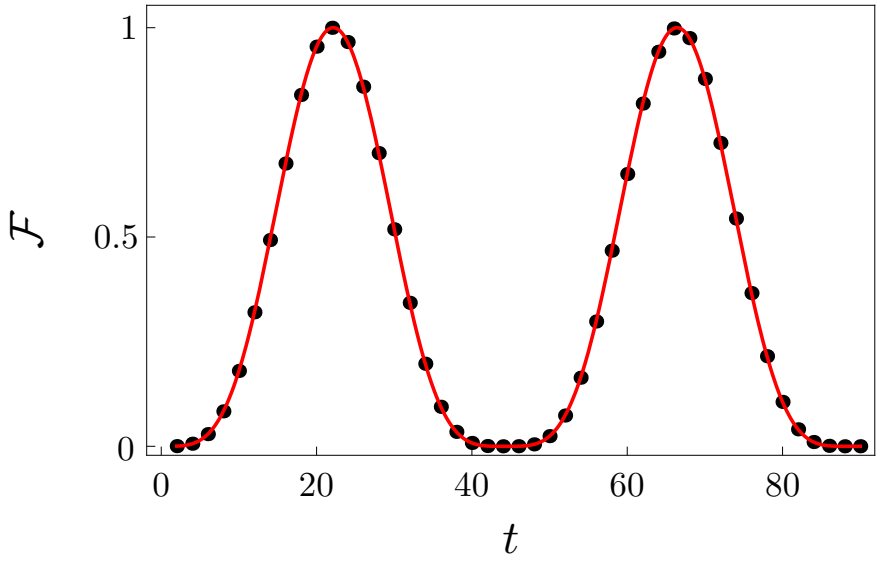

FIG. 1: Fidelity between the state of the walk (10) and the target state $|\alpha_2\rangle$ for the walk on the star graph as a function of the number of steps t. The black dots correspond to the numerical simulation and the red line is given by (12). Fidelity is plotted only at even number of steps, since it vanishes when t is odd. We have considered the star graph with $N = 100$ external vertices. The first maximum of fidelity is reached after 22 steps, in accordance with (11).

III. COMPLETE GRAPH WITH SELF-LOOPS

Let us now turn to the state transfer on the complete graph of N vertices with additional self-loop on each vertex. The reason we consider the additional self-loops is that the discrete-time quantum walk search algorithm on the complete graph does not find the marked vertex with unit probability. Nevertheless, it was shown [8, 25] that adding self-loops makes two steps of the discrete-time quantum walk equivalent to the Grover search algorithm and increases probability of finding the marked vertex to one. In the following we show explicitly that the algorithm achieves state transfer with unit fidelity independent of the size of the graph.

The Hilbert space of the walk is given by

$$\mathcal{H} = \mathcal{H}_P \otimes \mathcal{H}_C,$$

where both position space and coin space have dimension N. We denote the basis vectors of $\mathcal{H}_P$ as $|1\rangle_p, \ldots, |N\rangle_p$. Similarly, the basis vectors of $\mathcal{H}_C$ are denoted as $|1\rangle_c, \ldots, |N\rangle_c$. The basis of $\mathcal{H}$ is then formed by the vectors $|i\rangle_p \otimes |j\rangle_c \equiv |i, j\rangle$, where the first index corresponds to the position (vertex), and the second index corresponds to the coin state.

The evolution operator of the walk is given by the product of the step operator and the coin operator

$$U = S \cdot C.$$

The step operator reads

$$S = \sum_{i,j=1}^{N} |j, i\rangle\langle i, j|.$$

As for the coin operator, we choose it to act as the Grover operator (2) on all non-marked vertices, with an additional phase shift of π on the marked vertices s and r. Hence, C can be written as

$$C = (I_N - 2|s\rangle_p\langle s| - 2|r\rangle_p\langle r|) \otimes G,$$

where G is given in (2).

Concerning the initial state of the walk, we choose the particle to be localized on the sender vertex s with the equal weight superposition of all coin states (3), i.e.

$$|\psi(0)\rangle = |s\rangle_p \otimes |\psi_S\rangle_c = \frac{1}{\sqrt{N}} \sum_{j=1}^{N} |s,j\rangle.$$

We again denote this state as $|\alpha_1\rangle$ since it will be the first basis vector of the invariant subspace. We now show that after $O(\sqrt{N})$ steps of the walk the particle will be in the state

$$|\alpha_2\rangle = |r\rangle_p \otimes |\psi_S\rangle_c = \frac{1}{\sqrt{N}} \sum_{j=1}^{N} |r,j\rangle,$$

i.e. localized on the receiver vertex r. Similarly like for the star graph, it is sufficient to consider U^2, since [8, 25] have shown that two steps of the walk are equivalent to one iteration of the Grover search algorithm on the position Hilbert space $\mathcal{H}_P$. First, let us determine the invariant subspace of U^2 which includes $|\alpha_{1,2}\rangle$. Simple algebra reveals that the following four orthonormal vectors

$$\begin{aligned}
|\alpha'_3\rangle &= \frac{1}{\sqrt{2(N-2)}} \sum_{i\neq s,r} \left(|i,s\rangle + |i,r\rangle\right), \\
|\alpha'_4\rangle &= \frac{1}{N-2} \sum_{i,j\neq s,r} |i,j\rangle, \\
|\alpha'_5\rangle &= \sqrt{\frac{2}{N-2}}|\alpha_1\rangle - \sqrt{\frac{N}{2(N-2)}}(|s,s\rangle + |s,r\rangle), \\
|\alpha'_6\rangle &= \sqrt{\frac{2}{N-2}}|\alpha_2\rangle - \sqrt{\frac{N}{2(N-2)}}(|r,s\rangle + |r,r\rangle),
\end{aligned} \tag{13}$$

complement $|\alpha_{1,2}\rangle$ to the invariant subspace of U^2. However, we can reduce the dimension of the invariant subspace further from 6 to 5. Indeed, one can show that U^2 has an eigenvector

$$|\chi\rangle = \frac{1}{\sqrt{N}}|\alpha'_3\rangle + \sqrt{\frac{N-2}{2N}}|\alpha'_4\rangle + \frac{1}{2}|\alpha'_5\rangle + \frac{1}{2}|\alpha'_6\rangle,$$

corresponding to the eigenvalue 1, which is orthogonal to $|\alpha_{1,2}\rangle$. Hence, $|\chi\rangle$ is also orthogonal to $U^2|\alpha_{1,2}\rangle$, and thus it can be subtracted from the invariant subspace. The orthogonal complement of $|\chi\rangle$ in the subspace spanned by vectors (13) then completes $|\alpha_{1,2}\rangle$ to the invariant subspace of of U^2. We choose the orthonormal basis as

$$\begin{aligned}
|\alpha_3\rangle &= \sqrt{\frac{N-2}{N}}|\alpha'_3\rangle - \sqrt{\frac{2}{N}}|\alpha'_4\rangle = \frac{1}{\sqrt{2N}} \sum_{i=1}^{N}(|i,s\rangle + |i,r\rangle) - \frac{\sqrt{2}}{(N-2)\sqrt{N}} \sum_{i,j\neq s,r} |i,j\rangle, \\
|\alpha_4\rangle &= \frac{1}{\sqrt{2}}|\alpha'_5\rangle - \frac{1}{\sqrt{2}}|\alpha'_6\rangle = \frac{1}{\sqrt{N(N-2)}} \sum_{j\neq s,r} \left(|s,j\rangle - |r,j\rangle\right) + \sqrt{\frac{N-2}{4N}} \left(|r,r\rangle + |r,s\rangle - |s,s\rangle - |s,s\rangle\right), \\
|\alpha_5\rangle &= \frac{1}{\sqrt{N}}|\alpha'_3\rangle + \sqrt{\frac{N-2}{2N}}|\alpha'_4\rangle - \frac{1}{2}|\alpha'_5\rangle - \frac{1}{2}|\alpha'_6\rangle \\
&= \frac{1}{\sqrt{2N(N-2)}} \left(\sum_{i,j\neq s,r} |i,j\rangle + \sum_{i\neq s,r} \left(|i,s\rangle + |i,r\rangle\right) - \sum_{j\neq s,r} \left(|s,j\rangle + |r,j\rangle\right) \right) + \\
&\quad + \sqrt{\frac{N-2}{8N}} \left(|s,r\rangle + |s,s\rangle + |r,s\rangle + |r,r\rangle\right).
\end{aligned}$$

The effective evolution operator in the $|\alpha_i\rangle$ basis is given by the matrix

$$U_{eff} = \begin{pmatrix} \frac{(N-4)(N-2)}{N^2} & -\frac{2(N-4)}{N^2} & \frac{4\sqrt{2}(N-2)}{N^2} & -\frac{2\sqrt{N-2}}{N} & \frac{2\sqrt{2}(N-4)\sqrt{N-2}}{N^2} \\ -\frac{2(N-4)}{N^2} & \frac{(N-4)(N-2)}{N^2} & \frac{4\sqrt{2}(N-2)}{N^2} & \frac{2\sqrt{N-2}}{N} & \frac{2\sqrt{2}(N-4)\sqrt{N-2}}{N^2} \\ \frac{4\sqrt{2}(N-2)}{N^2} & \frac{4\sqrt{2}(N-2)}{N^2} & \frac{(N-4)^2}{N^2} & 0 & -\frac{4(N-4)\sqrt{N-2}}{N^2} \\ \frac{2\sqrt{N-2}}{N} & -\frac{2\sqrt{N-2}}{N} & 0 & \frac{N-4}{N} & 0 \\ -\frac{2\sqrt{2}(N-4)\sqrt{N-2}}{N^2} & -\frac{2\sqrt{2}(N-4)\sqrt{N-2}}{N^2} & \frac{4(N-4)\sqrt{N-2}}{N^2} & 0 & \frac{N^2-16N+32}{N^2} \end{pmatrix}$$

We find that the spectrum of U_{eff} consists of eigenvalues

$$\begin{aligned} \lambda_0 &= 1, \\ \lambda_1^{\pm} &= e^{\pm i\omega}, \\ \lambda_2^{\pm} &= e^{\pm 2i\omega}, \end{aligned} \tag{14}$$

where the phase ω is given in (9). The corresponding eigenvectors are found to be

$$\begin{aligned} |\chi_0\rangle &= \frac{1}{2}|\alpha_1\rangle + \frac{1}{2}|\alpha_2\rangle + \frac{1}{\sqrt{2}}|\alpha_3\rangle, \\ |\chi_1^{\pm}\rangle &= \frac{1}{2}|\alpha_1\rangle - \frac{1}{2}|\alpha_2\rangle \mp \frac{i}{\sqrt{2}}|\alpha_4\rangle, \\ |\chi_2^{\pm}\rangle &= \frac{1}{2\sqrt{2}}|\alpha_1\rangle + \frac{1}{2\sqrt{2}}|\alpha_2\rangle - \frac{1}{2}|\alpha_3\rangle \pm \frac{i}{\sqrt{2}}|\alpha_5\rangle. \end{aligned} \tag{15}$$

The initial state of the walk $|\alpha_1\rangle$ and the desired target state $|\alpha_2\rangle$ are decomposed into the eigenbasis (15) of effective evolution operator according to

$$\begin{aligned} |\alpha_1\rangle &= \frac{1}{2}|\chi_0\rangle + \frac{1}{2}\left(|\chi_1^+\rangle + |\chi_1^-\rangle\right) + \frac{1}{2\sqrt{2}}\left(|\chi_2^+\rangle + |\chi_2^-\rangle\right), \\ |\alpha_2\rangle &= \frac{1}{2}|\chi_0\rangle - \frac{1}{2}\left(|\chi_1^+\rangle + |\chi_1^-\rangle\right) + \frac{1}{2\sqrt{2}}\left(|\chi_2^+\rangle + |\chi_2^-\rangle\right) \end{aligned}$$

After $2t$ steps of the walk the state can be written as

$$\begin{aligned} |\psi(2t)\rangle &= U_{eff}^t|\alpha_1\rangle \\ &= \frac{1}{2}|\chi_0\rangle + \frac{e^{i\omega t}}{2}\left(|\chi_1^+\rangle + e^{-2i\omega t}|\chi_1^-\rangle\right) + \\ &\quad + \frac{e^{2i\omega t}}{2\sqrt{2}}\left(|\chi_2^+\rangle + e^{-4i\omega t}|\chi_2^-\rangle\right). \end{aligned} \tag{16}$$

We find that for $\omega t = \pi$ the state reduces to the desired target state $|\alpha_2\rangle$. Hence, to achieve perfect state transfer we have to choose the number of steps T as the closest integer to $\frac{2\pi}{\omega}$, which is exactly the same as for the star graph (11). We note that the perfect state transfer in this model is possible for arbitrary N thanks to the perfect matching of the spectrum (14), i.e. the fact that the phases of eigenvalues $\lambda_2^{\pm}$ are exactly twice the phases of the eigenvalues of $\lambda_1^{\pm}$.

For illustration we display in Figure 2 the fidelity between the state of the walk (16) and the target state $|\alpha_2\rangle$ as a function of the number of steps, which is given by

$$\mathcal{F}(2t) = |\langle\psi(2t)|\alpha_2\rangle|^2 = \cos^2(\omega t)\sin^4\left(\frac{\omega t}{2}\right). \tag{17}$$

In comparison to the result for the star graph (12) we find that there is an additional modulation with $\cos^2(\omega t)$ arising from the eigenvectors $|\chi_2^{\pm}\rangle$ that oscillate at double frequency. In Figure 2 the number of vertices was chosen as $N = 30$. The first maximum of fidelity is reached after 12 steps of the walk, in agreement with the analytical prediction of (11).

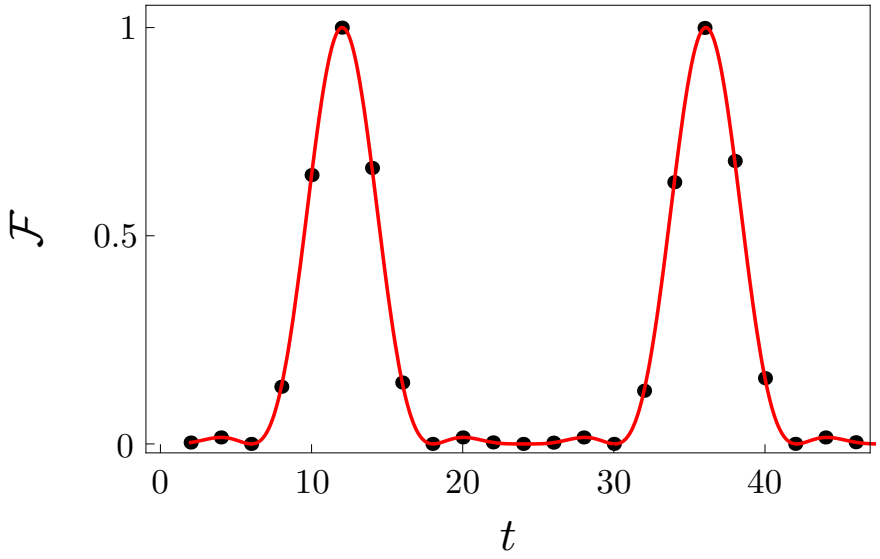

FIG. 2: Fidelity between the state of the walk (16) and the target state $|\alpha_2\rangle$ for the walk on the complete graph with self-loops as a function of the number of steps t. The black dots correspond to the numerical simulation and the red line is given by (17). Fidelity is plotted only at even number of steps. We have considered the complete graph with self-loops with $N = 30$ vertices. The first maximum of fidelity is reached after 12 steps, in accordance with (11).

IV. SZEGEDY'S WALK WITH QUERIES ON THE COMPLETE GRAPH

Finally, let us consider the state transfer in Szegedy's walk, which is a coinless discrete-time quantum walk model driven by reflection operators in a bipartite graph [32]. In the original proposal of the Szegedy's walk [15] the search algorithm finds the marked vertex of the complete graph with probability $\frac{1}{2}$. However, Santos [16] have shown that adding phase shifts of π on the marked vertices (i.e. queries), increases the success probability to one in the limit of large number of vertices N. Therefore, we consider the Szegedy's walk with queries on the complete graph with two marked vertices s and r. We show that in the limit of large N the walk achieves perfect state transfer between the sender and the receiver.

Let us briefly review the definition of the Szegedy's walk [15] on the graph $G(X, E)$, where $X = \{1, \ldots, N\}$ is the set of vertices and E is the set of edges. We turn it to bipartite graph of $N + N$ vertices, i.e. duplicate the graph G, remove all edges in the original graph and its copy, and add edges between the vertices in the two sets as in the original graph. The Hilbert space of the Szegedy's walk is given by tensor product of two N-dimensional Hilbert spaces $\mathcal{H}_N$

$$\mathcal{H} = \mathcal{H}_N \otimes \mathcal{H}_N,$$

corresponding to the vertices of the original graph and its copy. We denote the vectors of computational basis of $\mathcal{H}$ as

$$|i\rangle \otimes |j\rangle \equiv |i, j\rangle, \quad i, j = 1, \ldots, N,$$

where the first index corresponds to the vertex of the original graph and the second index denotes the vertex in the copy. Szegedy's walk [15] is driven by reflections around subspaces generated by vectors $|\Phi_i\rangle$ and $|\Psi_j\rangle$

$$\begin{aligned} \mathcal{R}_A &= 2\sum_{i=1}^{N} |\Phi_i\rangle\langle\Phi_i| - I_{N^2}, \\ \mathcal{R}_B &= 2\sum_{j=1}^{N} |\Psi_j\rangle\langle\Psi_j| - I_{N^2}, \end{aligned}$$

which are defined as

$$|\Phi_i\rangle = |i\rangle \otimes \left(\sum_j \sqrt{p_{ij}} |j\rangle \right),$$
$$|\Psi_j\rangle = \left(\sum_i \sqrt{p_{ij}} |i\rangle \right) \otimes |j\rangle. \quad (18)$$

Here p_{ij} denotes components of a stochastic matrix associated to the graph G. We consider G to be the complete graph and for simplicity take the stochastic matrix as

$$p_{ij} = \frac{1}{N-1} \left(1 - \delta_{ij}\right).$$

Hence, in our model the vectors (18) are given by

$$|\Phi_i\rangle = \frac{1}{\sqrt{N-1}} \sum_{j \neq i} |i,j\rangle,$$
$$|\Psi_j\rangle = \frac{1}{\sqrt{N-1}} \sum_{i \neq j} |i,j\rangle.$$

Santos [16] has extended the evolution of the Szegedy's walk with queries, i.e phase shift of π on the marked vertices. Since we have two marked vertices s and r, the action of the queries is described by the following operator

$$\mathcal{R}_M = (I_N - 2|s\rangle\langle s| - 2|r\rangle\langle r|) \otimes I_N.$$

The complete evolution operator of the Szegedy's walk with queries is then given by [16]

$$U = \mathcal{R}_B \mathcal{R}_A \mathcal{R}_M. \quad (19)$$

We show that for large N, starting the walk in the state

$$|\alpha_1\rangle = |\Phi_s\rangle = \frac{1}{\sqrt{N-1}} \sum_{j \neq s} |s,j\rangle,$$

and performing $O(\sqrt{N})$ steps we will obtain with high probability the state

$$|\alpha_2\rangle = |\Phi_r\rangle = \frac{1}{\sqrt{N-1}} \sum_{j \neq r} |r,j\rangle.$$

Notice that in the first vector the first index is s, while in the second vector the first index r. In this sense, we achieve the state transfer from the vertex s to vertex r.

First, we determine the invariant subspace which includes the initial and the final states $|\alpha_1\rangle$ and $|\alpha_2\rangle$. Using the definition of the evolution operator (19) we find that the invariant subspace includes five additional orthonormal vectors

$$|\alpha_3\rangle = \frac{1}{\sqrt{(N-2)(N-3)}} \sum_{\substack{i,j \neq s,r \\ i \neq j}} |i,j\rangle,$$
$$|\alpha_4\rangle = \frac{1}{\sqrt{(N-1)(N-2)}} \sum_{j \neq s,r} |s,j\rangle - \sqrt{\frac{N-2}{N-1}} |s,r\rangle,$$
$$|\alpha_5\rangle = \frac{1}{\sqrt{(N-1)(N-2)}} \sum_{j \neq s,r} |r,j\rangle - \sqrt{\frac{N-2}{N-1}} |r,s\rangle,$$
$$|\alpha_6\rangle = \frac{1}{\sqrt{N-2}} \sum_{i \neq s,r} |i,s\rangle,$$
$$|\alpha_7\rangle = \frac{1}{\sqrt{N-2}} \sum_{i \neq s,r} |i,r\rangle.$$

The effective evolution operator is in the $|\alpha_i\rangle$ basis given by the following 7x7 matrix

$$U_{eff} = \begin{pmatrix} \frac{N-3}{N-1} & -\frac{2(N-2)}{(N-1)^2} & \frac{2(N-3)^{3/2}\sqrt{N-2}}{(N-1)^{5/2}} & 0 & \frac{2\sqrt{N-2}}{(N-1)^2} & \frac{4(N-2)^{3/2}}{(N-1)^{5/2}} & \frac{2(N-3)\sqrt{N-2}}{(N-1)^{5/2}} \\ -\frac{2(N-2)}{(N-1)^2} & \frac{N-3}{N-1} & \frac{2(N-3)^{3/2}\sqrt{N-2}}{(N-1)^{5/2}} & \frac{2\sqrt{N-2}}{(N-1)^2} & 0 & \frac{2(N-3)\sqrt{N-2}}{(N-1)^{5/2}} & \frac{4(N-2)^{3/2}}{(N-1)^{5/2}} \\ -2\sqrt{\frac{(N-3)(N-2)}{(N-1)^3}} & -2\sqrt{\frac{(N-3)(N-2)}{(N-1)^3}} & \frac{(N-5)^2}{(N-1)^2} & \frac{2\sqrt{N-3}}{(N-1)^{3/2}} & \frac{2\sqrt{N-3}}{(N-1)^{3/2}} & \frac{2(N-5)\sqrt{N-3}}{(N-1)^2} & \frac{2(N-5)\sqrt{N-3}}{(N-1)^2} \\ 0 & -\frac{2\sqrt{N-2}}{(N-1)^2} & -\frac{2\sqrt{N-3}(N+1)}{(N-1)^{5/2}} & -\frac{N-3}{N-1} & \frac{2}{(N-1)^2} & -\frac{4}{(N-1)^{5/2}} & \frac{2(N-3)N}{(N-1)^{5/2}} \\ -\frac{2\sqrt{N-2}}{(N-1)^2} & 0 & -\frac{2\sqrt{N-3}(N+1)}{(N-1)^{5/2}} & \frac{2}{(N-1)^2} & -\frac{N-3}{N-1} & \frac{2(N-3)N}{(N-1)^{5/2}} & -\frac{4}{(N-1)^{5/2}} \\ 0 & -2\sqrt{\frac{N-2}{(N-1)^3}} & \frac{2(N-3)^{3/2}}{(N-1)^2} & 0 & -\frac{2(N-2)}{(N-1)^{3/2}} & -\frac{(N-3)^2}{(N-1)^2} & \frac{2(N-3)}{(N-1)^2} \\ -2\sqrt{\frac{N-2}{(N-1)^3}} & 0 & \frac{2(N-3)^{3/2}}{(N-1)^2} & -\frac{2(N-2)}{(N-1)^{3/2}} & 0 & \frac{2(N-3)}{(N-1)^2} & -\frac{(N-3)^2}{(N-1)^2} \end{pmatrix}.$$

Direct diagonalization of U_{eff} is rather difficult, however, the eigenvalues can be determined analytically. Indeed, the characteristic equation

$$\det\left(U_{eff} - e^{i\omega} I_7\right) = 0$$

can be written in the form

$$\left(5 + N(N-4) + (N-1)^2\cos\omega\right)\left(-N^2 + 8N - 17 + 2(N-4)\cos\omega + (N-1)^2\cos^2\omega\right)\sin\left(\frac{\omega}{2}\right) = 0.$$

We find the solutions

$$\begin{aligned} \omega_0 &= 0, \\ \omega_1 &= \arccos\left(\frac{4 - N + \Delta}{(N-1)^2}\right), \\ \omega_2 &= \arccos\left(\frac{4 - N - \Delta}{(N-1)^2}\right), \\ \omega_3 &= \arccos\left(\frac{4N - N^2 - 5}{(N-1)^2}\right), \end{aligned} \tag{20}$$

where Δ is given by

$$\Delta = \sqrt{N^4 - 10N^3 + 35N^2 - 50N + 33}.$$

The spectrum of the effective evolution operator U_{eff} is then given by

$$\begin{aligned} \lambda_0 &= e^{i\omega_0} = 1, \\ \lambda_1^{\pm} &= e^{\pm i\omega_1}, \\ \lambda_2^{\pm} &= e^{\pm i\omega_2}, \\ \lambda_3^{\pm} &= e^{\pm i\omega_3}. \end{aligned}$$

The eigenvector corresponding to the eigenvalue $\lambda_0 = 1$ can be also determined analytically. We find that it reads

$$\begin{aligned} |\chi_0\rangle &= \frac{1}{\sqrt{2}}\sqrt{\frac{N(N-3)+2}{N(N-3)+3}}(|\alpha_1\rangle - |\alpha_2\rangle) + \\ &+ \frac{1}{\sqrt{2(N(N-3)+3)}}(|\alpha_6\rangle - |\alpha_7\rangle). \end{aligned}$$

We point out that this eigenvector has a large overlap with the initial state of the walk $|\alpha_1\rangle$ and the desired target state $|\alpha_2\rangle$. Indeed, for large N we can write

$$|\chi_0\rangle = \frac{1}{\sqrt{2}}(|\alpha_1\rangle - |\alpha_2\rangle) + O(N^{-1}). \tag{21}$$

Notice that for $N \to \infty$ the vector (21) has the same shape as the eigenvector of the walk on the star graph (7) corresponding to the eigenvalue $\lambda = 1$.

The explicit form of the eigenvectors $|\chi_i^{\pm}\rangle$ is quite lengthy. However, it turns out that for large N only $|\chi_1^{+}\rangle$ and $|\chi_1^{-}\rangle$, i.e. the eigenvectors corresponding to $\lambda_1^{\pm} = e^{\pm i\omega_1}$, are relevant, since the overlaps of $|\alpha_{1,2}\rangle$ with $|\chi_j^{\pm}\rangle$ vanishes as $O(N^{-\frac{1}{2}})$ for $j = 2, 3$. We find that for large N the eigenvectors $|\chi_1^{\pm}\rangle$ are given by

$$|\chi_1^{\pm}\rangle = \frac{1}{2}(|\alpha_1\rangle + |\alpha_2\rangle) \pm \frac{i}{\sqrt{2}}|\alpha_3\rangle + O(N^{-\frac{1}{2}}). \tag{22}$$

Again, for $N \to \infty$ the eigenvectors (22) have the same shape as the eigenvectors of the walk on the star graph (8). Moreover, we find that the phase ω_1 (20) approaches (9) as N tends to infinity, i.e. also the corresponding eigenvalues coincides with those for the star graph. Hence, in the limit of large N the dynamics of the Szegedy's walk with queries on the complete graph reduces to the dynamics of the coined walk on the star graph. Since we have shown in Section II that the latter model achieves perfect state transfer, the same applies to the former, however, only in the limit of large N. We conclude that the Szegedy's walk with queries on the complete graph achieves almost perfect state transfer between the sender and the receiver vertex when we choose the number of steps T as the closest integer to $\frac{\pi}{\omega_1}$, i.e.

$$T \approx \frac{\pi}{\arccos\left(\frac{4-N+\Delta}{(N-1)^2}\right)}, \tag{23}$$

which approaches half the value (11) required for the star graph and complete graph with self-loops as N tends to infinity.

For illustration we display in Figure 3 the fidelity between the state of the walk and the target state $|\alpha_2\rangle$ for the Szegedy's walk with queries on the complete graph with $N = 30$ vertices. Within the approximations made in (21), (22) the fidelity is given by

$$\mathcal{F}(t) = |\langle\psi(t)|\alpha_2\rangle|^2 \approx \sin^4\left(\frac{\omega_1 t}{2}\right). \tag{24}$$

For the complete graph with $N = 30$ vertices the first maximum of fidelity is reached after 6 steps of the walk, in agreement with the analytical prediction of (23).

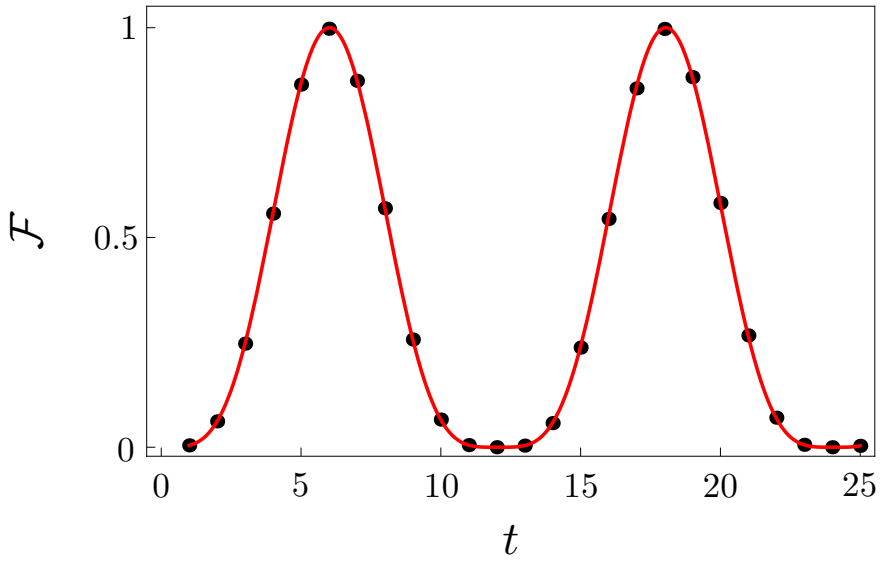

FIG. 3: Fidelity for the Szegedy's walk with queries on the complete graph as a function of the number of steps t. The black dots correspond to the numerical simulation and the red line is given by (24). We have considered the complete graph with $N = 30$ vertices. The first maximum of the fidelity is reached after 6 steps, in accordance with (23).

V. CONCLUSIONS

State transfer between two vertices of a graph by means of discrete-time quantum walk search algorithm with two marked vertices was analyzed. In particular, we have shown that the coined quantum walk on a star graph and

complete graph with self-loops achieve perfect state transfer between the sender and receiver vertex for arbitrary number of vertices N. On the other hand, Szegedy's walk with queries on complete graph achieves perfect state transfer only in the limit of large N. All three algorithms require $O(\sqrt{N})$ steps.

The present model does not allow for the transfer of the internal coin state of the particle which is possible in other discrete-time models [17, 19, 20]. Indeed, there is either no non-trivial internal state as for the walk on the star graph, or it has to be fixed as for the coined walk on the complete graph with self-loops and Szegedy's walk on the complete graph. On the other hand, the present method requires less control over the system, since we only have to adjust the coin at the sender and receiver vertex.

It is of interest to determine additional graphs where perfect state transfer is possible by means of discrete-time quantum walks. Our preliminary numerical analysis indicates that the modification of the Szegedy's walk where the receiver vertex is in the copy of the original graph also achieves state transfer with high fidelity. This result suggests that discrete-time quantum walks are suitable for perfect state transfer on complete bipartite graphs. We plan to thoroughly investigate this model in the near future.

Finally, let us point out that in the continuous-time quantum walk scenario Chakraborty et al. [14] have shown that state transfer with fidelity approaching unity is achieved for almost all graphs in the limit of large number of vertices N. It would be interesting to prove similar statement in the discrete-time case. Moreover, Chakraborty et al. [14] have also considered entanglement generation between two vertices. The protocol uses a non-adjacent third party vertex, which has to tune its nearest neighbor couplings. We plan to identify the discrete-time counterpart of this protocol.

Acknowledgments

We appreciate the financial support from RVO 68407700 and from Czech Technical University in Prague under Grant No. SGS16/241/OHK4/3T/14. MŠ is grateful for the financial support from GAČR under Grant No. 14-02901P.

[1] Y. Aharonov, L. Davidovich and N. Zagury, Phys. Rev. A **48**, 1687 (1993).
[2] D. Meyer, J. Stat. Phys. **85**, 551, (1996).
[3] E. Farhi and S. Gutmann, Phys. Rev. A **58**, 915 (1998).
[4] D. Aharonov, A. Ambainis, J. Kempe and U. Vazirani, in Proceedings of the 33th STOC (ACM Press, New York, 2001), p. 50
[5] A. M. Childs, Phys. Rev. Lett. **102**, 180501 (2009).
[6] N. B. Lovett, S. Cooper, M. Everitt, M. Trevers and V. Kendon, Phys. Rev. A **81**, 042330 (2010)
[7] N. Shenvi, J. Kempe and K. B. Whaley, Phys. Rev. A **67**, 052307 (2003).
[8] A. Ambainis, J. Kempe and A. Rivosh, in *Proceedings of the 16th ACM-SIAM Symposium on Discrete Algorithms*, 10991108 (2005).
[9] A. M. Childs and J. Goldstone, Phys. Rev. A **70**, 022314 (2004).
[10] A. M. Childs and J. Goldstone, Phys. Rev. A **70**, 042312 (2004)
[11] J. Janmark, D. A. Meyer and T. G. Wong, Phys. Rev. Lett. **112**, 210502 (2014).
[12] L. Novo, S. Chakraborty, M. Mohseni, H. Neven and Y. Omar, Scientific Rep. **5**, 13304 (2014).
[13] D. A. Meyer and T. G. Wong, Phys. Rev. Lett. **114**, 110503 (2015).
[14] S. Chakraborty, L. Novo, A. Ambainis and Y. Omar, Phys. Rev. Lett. **116**, 100501 (2016).
[15] M. Szegedy, in *Proceedings of the 45th Symposium on Foundations of Computer Science*, 3241 (2004).
[16] R. A. M. Santos, arXiv:1603.05473v2.
[17] P. Kurzynski and A. Wojcik, Phys. Rev. A **83**, 062315 (2011).
[18] M. Christandl, N. Datta, A. Ekert and A. J. Landahl, Phys. Rev. Lett. **92**, 187902 (2004).
[19] X. Zhan, H. Qin, Z. H. Bian, J. Li and P. Xue, Phys. Rev. A **90**, 012331 (2014).
[20] I. Yalcinkaya and Z. Gedik, J. Phys. A **48**, 225302 (2015).
[21] B. Hein and G. Tanner, Phys. Rev. Lett. **103**, 260501 (2009).
[22] V. M. Kendon and C. Tamon, J. Comput. Theor. Nanosc. **8**, 422 (2011).
[23] K. Barr, T. Proctor, D. Allen and V. Kendon, Quantum Inform. Comput. **14**, 417 (2014).
[24] D. Reitzner, M. Hillery, E. Feldman and V. Bužek, Phys. Rev. A **79**, 012323 (2009).
[25] T. G. Wong, J. Phys. A **48**, 435304 (2015).
[26] H. Krovi and T. A. Brun, Phys. Rev. A **75**, 062332 (2007).
[27] M. Hillery, H. Zheng, E. Feldman, D. Reitzner and V. Bužek, Phys. Rev. A **85**, 062325 (2012).
[28] E. Feldman, M. Hillery, H. W. Lee, D. Reitzner, H. Zheng and V. Bužek, Phys. Rev. A **82**, 040301(R) (2010).
[29] L. K. Grover, Phys. Rev. Lett. **79**, 325 (1997).
[30] F. M. Andrade and M. G. E. da Luz, Phys. Rev. A **80**, 052301 (2009).

[31] B. F. Venancio, F. M. Andrade and M. G. E. da Luz, J. Phys. A **46**, 165302 (2013).
[32] R. Portugal, Quantum Inform. Process. **15**, 1387 (2016).

Perfect state transfer by means of discrete-time quantum walk on complete bipartite graphs

M. Štefaňák[1] and S. Skoupý[1]

[1]*Department of Physics, Faculty of Nuclear Sciences and Physical Engineering, Czech Technical University in Prague, Břehová 7, 115 19 Praha 1 - Staré Město, Czech Republic*

We consider a quantum walk with two marked vertices, sender and receiver, and analyze its application to perfect state transfer on complete bipartite graphs. First, the situation with both the sender and the receiver vertex in the same part of the graph is considered. We show that in this case the dynamics of the quantum walk is independent of the size of the second part and reduces to the one for the star graph where perfect state transfer is achieved. Second, we consider the situation where the sender and the receiver vertex are in the opposite parts of the graph. In such a case the state transfer with unit fidelity is achieved only when the parts have the same size.

I. INTRODUCTION

Quantum walks [1] were proposed as quantum mechanical extensions of classical random walks on a graph or lattice. The time evolution of the quantum walk can be either continuous [2] or discrete [3]. The relation between the continuous-time and discrete-time quantum walks was studied intensively [4–6].

In continuous-time quantum walk [2, 7] the evolution of the particle is governed by the Schrödinger equation where the Hamiltonian is given by the discrete Laplacian of the graph. Continuous-time quantum walks have found promising applications in quantum search algorithms [8, 9] and modeling of coherent transport on graphs and networks [10–12]. Moreover, continuous-time quantum walks were shown to be universal tools for quantum computation [13]. While the original continuous-time quantum walk search algorithms were analyzed on symmetric lattices or graphs, such as hypercube or a complete graph, later it was found [14–16] that high symmetry is not required for the optimal runtime of the algorithm. More recently, it was shown [17] that the continuous-time quantum walk search algorithm is optimal for almost all graphs.

For discrete-time quantum walks Meyer has shown [3] that in order to obtain a non-trivial evolution the system cannot be scalar. A straight-forward way to overcome this constraint is to embed the particle with an additional internal degree of freedom, usually called the coin, which governs the displacements of the particle [18, 19]. However, several variants of coinless discrete-time quantum walks were proposed. In scattering quantum walks [20–22], which were introduced following the analogy with interferometers, the states of the quantum particle corresponds to the directed edges of the graph. Equivalence between the scattering and coined quantum walks was analyzed in detail [23, 24]. Szegedy [25] proposed a construction of discrete-time quantum walks based on quantization of classical Markov chains. In the staggered quantum walk model [26–31] the evolution of the particle is governed by reflections that correspond to tessellations of the underlying graph. The staggered quantum walk model was recently proven to be more general than both the coined and the Szegedy's walk [32, 33]. Discrete-time quantum walks were applied to various quantum information tasks including quantum search [25, 34–39] or detecting anomalies in graphs [40–42], and were shown to be universal models of quantum computation [43].

Quantum walks were also applied to the problem of perfect state transfer [44] between two vertices of a graph or lattice, which we call sender and receiver. One approach relies on defining the dynamics at each individual vertex in order to achieve state transfer between the sender and the receiver. This method was analyzed in discrete-time quantum walks on a circle [45, 46] and a square lattice [47]. Another possibility is to modify the dynamics only at the sender and the receiver. This method was proposed for wave communication on regular lattices [48] and was further analyzed on various types of finite graphs in [49–51]. Typically, it does not allow for the transfer of the internal state of the particle which is possible in other discrete-time models [45–47]. On the other hand, the method requires less control over the system, since we only have to adjust the coin operators at the sender and the receiver vertices. In the continuous-time quantum walk framework it was shown [17] that this protocol achieves perfect state transfer for almost any graph.

In the present paper we extend the results of [51], where we have among others considered the perfect state transfer on a star graph by means of discrete-time quantum walk, to complete bipartite graphs. Indeed, star graph is a particular example of a complete bipartite graph where one of the parts has only one vertex. Two different scenarios are considered, namely the sender and the receiver vertex are either located in the same part or in the opposite parts. We show that when both the sender and the receiver vertex are located in the same part the dynamics of the walk is independent of the size of the second part. Hence, the effective evolution operator is the same as for the star graph, where the perfect state transfer is achieved with unit fidelity [51]. Next, we analyze the situation where the sender

and the receiver vertex are in the opposite parts. We show that in such a case the perfect state transfer with unit fidelity is achieved only when the parts are of the same size.

The rest of the paper is organized as follows: In Section II we introduce the notation and review the basic ideas of state transfer by means of discrete-time quantum walk. The case where both the sender and the receiver vertex are located in the same part is considered in Section III. In Section IV the situation where the sender and the receiver vertex are in the opposite parts is analyzed. We summarize our results and present an outlook in the conclusions of Section V.

II. PRELIMINARIES

In this Section we introduce the notation that will be used later on in the paper. We analyze the state transfer between two vertices of a complete bipartite graph of m plus n vertices $K_{m,n}$ by means of a discrete-time quantum walk. We consider the coined quantum walk model. Alternatively, one can employ the scattering quantum walk formalism [20–22]. Nevertheless, both models are equivalent [23, 24] and lead to exactly the same dynamics. To distinguish between the vertices of different parts of the complete bipartite graph we label them with latin letters in the first part and greek letters in the second.

Let us begin with the definition of the Hilbert space of the quantum walk we consider. Since the graph is bipartite the Hilbert space can be written as a direct sum

$$\mathcal{H} = \mathcal{H}^{(1)} \oplus \mathcal{H}^{(2)},$$

where the states from $\mathcal{H}^{(1)}$ ($\mathcal{H}^{(2)}$) corresponds to the particle located in the first (second) part accompanied with some coin state. The Hilbert spaces $\mathcal{H}^{(i)}$ have the form of tensor product

$$\mathcal{H}^{(i)} = \mathcal{H}_P^{(i)} \otimes \mathcal{H}_C^{(i)},$$

of the position space $\mathcal{H}_P^{(i)}$ and the coin space $\mathcal{H}_C^{(i)}$. In the first part, which has m vertices, the position space $\mathcal{H}_P^{(1)}$ is spanned by vectors $|i\rangle_p$ with i ranging from 1 to m. The coin space $\mathcal{H}_C^{(1)}$ is determined by the neighboring vertices, i.e. the vertices where the particle can move in a single step. Since we consider complete bipartite graph, the neighbors of any vertex from the first part are all vertices from the second part. Hence, the coin space $\mathcal{H}_C^{(1)}$ is n-dimensional and we denote the basis vectors as $|\alpha\rangle_c$ with α ranging from 1 to n. To shorten the notation we denote the basis vectors of $\mathcal{H}^{(1)}$ by $|i,\alpha\rangle \equiv |i\rangle_p \otimes |\alpha\rangle_c$. The state $|i,\alpha\rangle$ corresponds to the particle located at the vertex i that will move to the vertex α after the application of the shift operator, which will be defined later. Similarly, for the second part the position space $\mathcal{H}_P^{(2)}$ is spanned by vectors $|\alpha\rangle_p$ with α ranging from 1 to n and the coin space $\mathcal{H}_C^{(2)}$ is spanned by vectors $|i\rangle_c$ with i ranging from 1 to m. We denote the basis vectors of $\mathcal{H}^{(2)}$ by $|\alpha,i\rangle \equiv |\alpha\rangle_p \otimes |i\rangle_c$.

The evolution operator which propagates the quantum walk by one step can be decomposed into a sum of two operators

$$U = U_1 + U_2 \tag{1}$$

where U_i acts nontrivially only on the states from $\mathcal{H}^{(i)}$. The operators U_i have the form

$$U_i = S_i \cdot C_i,$$

where S_i denotes the shift operator and C_i is the coin operator. The shift operators displace the particle from one part of the complete bipartite graph to the other according to its coin state. We define them by

$$\begin{aligned} S_1 &= \sum_i \sum_\alpha |\alpha,i\rangle\langle i,\alpha|, \\ S_2 &= \sum_i \sum_\alpha |i,\alpha\rangle\langle\alpha,i| = S_1^\dagger, \end{aligned}$$

where the summation over i runs from 1 to m and the summation over α runs from 1 to n. This will hold throughout the paper unless otherwise specified.

Let us now turn to the coin operators C_i which alter the internal coin states before the shift itself. For the purpose of state transfer we consider two marked vertices, sender and receiver, between which we want to communicate the quantum state. On the marked vertices the coin operator will act in a different way then on the non-marked vertices. In the present paper we consider the coin operator on the non-marked vertices to act as a Grover diffusion operator

[52] of appropriate dimension, while on the marked vertices it will act as minus identity. The explicit form of the coin operators C_1 and C_2 will be given latter depending on the location of the marked vertices. The sender vertex will be always located in the first part and we label it as s. The receiver vertex will be either in the same part as the sender vertex, in which case we label it as r, or in the second part and we label it as ρ.

In the following Sections we analyze the transfer of the particle from the sender vertex to the receiver vertex by means of the discrete-time quantum walk defined above. We start the walk in the initial state

$$|init\rangle = \frac{1}{\sqrt{n}} \sum_{\alpha} |s, \alpha\rangle, \tag{2}$$

i.e. the particle is located at the sender vertex with equal-weight superposition of all basis coin states. We analyze its evolution towards the target state, where the particle is located at the receiver vertex. The explicit form of the target state will be given latter depending on the location of the receiver vertex. Our analysis is based on the determination of the invariant subspace of the effective evolution operator which greatly reduces the complexity of the problem. Similar dimensional reduction due to the high symmetry of the graph [53] was applied previously in both discrete-time [40, 41, 51] and continuous-time quantum walks [15].

III. SENDER AND RECEIVER IN THE SAME PART

Let us begin our analysis with the situation where both the sender and the receiver vertex are in the first part. The coin operator C_1 is then given by

$$C_1 = -(|s\rangle_p\langle s| + |r\rangle_p\langle r|) \otimes I_n + \sum_{i \neq s,r} |i\rangle_p\langle i| \otimes G_n,$$

where I_n denotes the identity and G_n is the Grover diffusion operator

$$G_n = \frac{2}{n} \sum_{\alpha,\beta} |\alpha\rangle_c\langle\beta| - \sum_{\alpha} |\alpha\rangle_c\langle\alpha|, \tag{3}$$

both acting on the n-dimensional coin space $\mathcal{H}_C^{(1)}$. Hence, we find that the part of the evolution operator acting on $\mathcal{H}^{(1)}$ reads

$$U_1 = \frac{2}{n} \sum_{i \neq s,r} \sum_{\alpha,\beta} |\alpha, i\rangle\langle i, \beta| - \sum_{i} \sum_{\alpha} |\alpha, i\rangle\langle i, \alpha|.$$

On the second part, which does not contain any marked vertices, the coin operator is given by

$$C_2 = \sum_{\alpha} |\alpha\rangle_p\langle\alpha| \otimes G_m,$$

where G_m is the Grover diffusion operator on the m-dimensional coin space $\mathcal{H}_C^{(2)}$

$$G_m = \frac{2}{m} \sum_{i,j} |i\rangle_c\langle j| - \sum_{i} |i\rangle_c\langle i|. \tag{4}$$

The part of the evolution operator acting on $\mathcal{H}^{(2)}$ then reads

$$U_2 = \frac{2}{m} \sum_{i,j} \sum_{\alpha} |i, \alpha\rangle\langle\alpha, j| - \sum_{i} \sum_{\alpha} |i, \alpha\rangle\langle\alpha, i|.$$

We start the walk in the state (2) and analyze its evolution towards the target state

$$|target\rangle = \frac{1}{\sqrt{n}} \sum_{\alpha} |r, \alpha\rangle. \tag{5}$$

Note that both states (2) and (5) belong to $\mathcal{H}^{(1)}$. Since the walk is bipartite, it is sufficient to consider only the square of the evolution operator, and in fact we can restrict to the part which acts non-trivially on the initial state. We find that the effective two-step evolution operator is given by

$$\begin{aligned} U_{eff} &= U_2 \cdot U_1 = \frac{4}{mn} \sum_i \sum_{j\neq s,r} \sum_{\alpha,\beta} |i,\alpha\rangle\langle j,\beta| - \frac{2}{m} \sum_{i,j} \sum_{\alpha} |i,\alpha\rangle\langle j,\alpha| - \\ &-\frac{2}{n} \sum_{i\neq s,r} \sum_{\alpha,\beta} |i,\alpha\rangle\langle i,\beta| + \sum_i \sum_{\alpha} |i,\alpha\rangle\langle i,\alpha| \end{aligned} \tag{6}$$

In the following we show that the evolution of the quantum walk on the complete bipartite graph $K_{m,n}$ is the same as for the star graph $K_{m,1}$ where the perfect state transfer is achieved [51].

First, we determine the invariant subspace of the effective evolution operator (6) which contains the initial (2) and target (5) states. Clearly, the initial and target states are orthogonal and can be used as the first two basis states of the invariant subspace

$$|\phi_1\rangle = |init\rangle, \quad |\phi_2\rangle = |target\rangle.$$

To complete the invariant subspace we choose the last basis state as

$$|\phi_3\rangle = \frac{1}{\sqrt{n(m-2)}} \sum_{i\neq s,r} \sum_{\alpha} |i,\alpha\rangle.$$

Simple algebra reveals that the action of the effective evolution operator (6) on the basis states $|\phi_j\rangle$ is given by

$$\begin{aligned} U_{eff}|\phi_1\rangle &= \left(1-\frac{2}{m}\right)|\phi_1\rangle - \frac{2}{m}|\phi_2\rangle - \frac{2\sqrt{m-2}}{m}|\phi_3\rangle, \\ U_{eff}|\phi_2\rangle &= -\frac{2}{m}|\phi_1\rangle + \left(1-\frac{2}{m}\right)|\phi_2\rangle - \frac{2\sqrt{m-2}}{m}|\phi_3\rangle, \\ U_{eff}|\phi_3\rangle &= \frac{2\sqrt{m-2}}{m}|\phi_1\rangle + \frac{2\sqrt{m-2}}{m}|\phi_2\rangle + \left(1-\frac{4}{m}\right)|\phi_3\rangle. \end{aligned}$$

Hence, in the invariant subspace spanned by $|\phi_j\rangle$ the evolution operator (6) reduces to the following matrix

$$U_{eff} = \begin{pmatrix} 1-\frac{2}{m} & -\frac{2}{m} & \frac{2\sqrt{m-2}}{m} \\ -\frac{2}{m} & 1-\frac{2}{m} & \frac{2\sqrt{m-2}}{m} \\ -\frac{2\sqrt{m-2}}{m} & -\frac{2\sqrt{m-2}}{m} & 1-\frac{4}{m} \end{pmatrix}, \tag{7}$$

which is independent of the size of the second part. In fact, the effective evolution operator (7) is exactly the same as for the star graph $K_{m,1}$ where it was shown [51] that perfect state transfer is achieved when we choose the number of steps of the quantum walk as the closest even integer to

$$T = \frac{2\pi}{\arccos\left(\frac{m-4}{m}\right)}.$$

IV. SENDER AND RECEIVER IN OPPOSITE PARTS

Let us now turn to the case where the sender and the receiver vertices are in the opposite part. To be specific, we consider the sender vertex (labeled s) located in the first part and the receiver vertex (labeled ρ) in the second part. The coin operator C_1 is given by

$$C_1 = -|s\rangle_p\langle s| \otimes I_n + \sum_{i\neq s} |i\rangle_p\langle i| \otimes G_n,$$

where G_n is given in (3). The part of the evolution operator acting on $\mathcal{H}^{(1)}$ then reads

$$U_1 = \frac{2}{n} \sum_{i\neq s} \sum_{\alpha,\beta} |\alpha,i\rangle\langle i,\beta| - \sum_i \sum_{\alpha} |\alpha,i\rangle\langle i,\alpha|.$$

Similarly, the coin operator C_2 reads

$$C_2 = -|\rho\rangle_p\langle\rho| \otimes I_m + \sum_\alpha |\alpha\rangle_p\langle\alpha| \otimes G_m,$$

where I_m denotes the identity on the m-dimensional coin space $\mathcal{H}_C^{(2)}$ and G_m is given in (4). The part of the evolution operator acting on $\mathcal{H}^{(2)}$ then reads

$$U_2 = \frac{2}{m}\sum_{i,j}\sum_{\alpha\neq\rho}|i,\alpha\rangle\langle\alpha,j| - \sum_i\sum_\alpha |i,\alpha\rangle\langle\alpha,i|.$$

We again begin the walk in the initial state (2) and analyze its evolution towards the target state, which now reads

$$|target_2\rangle = \frac{1}{\sqrt{m}}\sum_i |\rho,i\rangle. \tag{8}$$

Since the sender and the receiver vertices are located in the opposite parts of the graph the initial state (2) and the target state (8) do not belong to the same subspace of $\mathcal{H}$. Hence, it is suitable first to apply the evolution operator of the walk (1) once on the initial state (2). The state of the walk after one step is given by

$$|init_2\rangle = U|init\rangle = -\frac{1}{\sqrt{n}}\sum_\alpha |\alpha,s\rangle, \tag{9}$$

which belongs to $\mathcal{H}^{(2)}$, i.e. the same subspace as the target state (8). From now on we can again employ the bipartitness of the walk and consider the effective two-step evolution operator

$$\begin{aligned} U_{eff} &= U_1\cdot U_2 = \frac{4}{mn}\sum_{i\neq s}\sum_j\sum_{\alpha\neq\rho}\sum_\beta |\beta,i\rangle\langle\alpha,j| - \frac{2}{n}\sum_{i\neq s}\sum_{\alpha,\beta}|\beta,i\rangle\langle\alpha,i| - \\ &-\frac{2}{m}\sum_{i,j}\sum_{\alpha\neq\rho}|\alpha,i\rangle\langle\alpha,j| + \sum_i\sum_\alpha|\alpha,i\rangle\langle\alpha,i|. \end{aligned} \tag{10}$$

In the following we analyze how close we can get from the state (9) towards the target state (8) by successive applications of the effective evolution operator (10).

We begin with the determination of the invariant subspace of (10) which includes the vectors (8) and (9). In contrast to the previous Section, these two vectors are no longer orthogonal and therefore they cannot be directly used as basis vectors of the invariant subspace. One possibility to choose the basis of the invariant subspace is given by [54]

$$\begin{aligned} |\phi_1\rangle &= |\rho,s\rangle, \\ |\phi_2\rangle &= \frac{1}{\sqrt{m-1}}\sum_{i\neq s}|\rho,i\rangle, \\ |\phi_3\rangle &= \frac{1}{\sqrt{n-1}}\sum_{\alpha\neq\rho}|\alpha,s\rangle, \\ |\phi_4\rangle &= \frac{1}{\sqrt{(m-1)(n-1)}}\sum_{i\neq s}\sum_{\alpha\neq\rho}|\alpha,i\rangle. \end{aligned} \tag{11}$$

Clearly we find

$$\begin{aligned} |init_2\rangle &= -\frac{1}{\sqrt{n}}|\phi_1\rangle - \sqrt{\frac{n-1}{n}}|\phi_3\rangle, \\ |target_2\rangle &= \frac{1}{\sqrt{m}}|\phi_1\rangle + \sqrt{\frac{m-1}{m}}|\phi_2\rangle, \end{aligned}$$

i.e. both the target state (8) and the state (9) are included in the subspace spanned by $|\phi_j\rangle$. Simple algebra reveals that the action of the effective two-step evolution operator (10) on the basis states (11) is given by

$$\begin{aligned}
U_{eff}|\phi_1\rangle &= |\phi_1\rangle, \\
U_{eff}|\phi_2\rangle &= \left(1-\frac{2}{n}\right)|\phi_2\rangle - 2\frac{\sqrt{n-1}}{n}|\phi_4\rangle, \\
U_{eff}|\phi_3\rangle &= 4\frac{\sqrt{(m-1)(n-1)}}{mn}|\phi_2\rangle + \left(1-\frac{2}{m}\right)|\phi_3\rangle + \\
&\quad +2\frac{(n-2)\sqrt{m-1}}{mn}|\phi_4\rangle, \\
U_{eff}|\phi_4\rangle &= 2\frac{(m-2)\sqrt{n-1}}{mn}|\phi_2\rangle - 2\frac{\sqrt{m-1}}{m}|\phi_3\rangle + \\
&\quad +\frac{(m-2)(n-2)}{mn}|\phi_4\rangle.
\end{aligned}$$

Hence, the effective evolution operator (10) is in the invariant subspace spanned by the vectors $|\phi_j\rangle$ given by the matrix

$$U_{eff} = \begin{pmatrix} 1 & 0 & 0 & 0 \\ 0 & 1-\frac{2}{n} & 4\frac{\sqrt{(m-1)(n-1)}}{mn} & 2\frac{(m-2)\sqrt{n-1}}{mn} \\ 0 & 0 & 1-\frac{2}{m} & -2\frac{\sqrt{m-1}}{m} \\ 0 & -2\frac{\sqrt{n-1}}{n} & 2\frac{(n-2)\sqrt{m-1}}{mn} & \frac{(m-2)(n-2)}{mn} \end{pmatrix}. \tag{12}$$

Let us now determine the eigenvalues and eigenvectors of the matrix (12). We find that the eigenvalues are 1 which has a two-fold degeneracy and $e^{\pm i\omega}$, where the phase ω is given by

$$\omega = \arccos\left(\frac{mn-2m-2n+2}{mn}\right).$$

The eigenvectors corresponding to eigenvalue 1 are given by

$$\begin{aligned}
|\chi_1\rangle &= |\phi_1\rangle, \\
|\chi_2\rangle &= \frac{1}{\sqrt{m+n-1}}\left(\sqrt{n-1}|\phi_2\rangle + \sqrt{m-1}|\phi_3\rangle - |\phi_4\rangle\right).
\end{aligned}$$

Eigenvectors corresponding to $\lambda_{3,4} = e^{\pm i\omega}$ are given by

$$\begin{aligned}
|\chi_3\rangle &= a|\phi_2\rangle + b|\phi_3\rangle + c|\phi_4\rangle, \\
|\chi_4\rangle &= \overline{a}|\phi_2\rangle + b|\phi_3\rangle + \overline{c}|\phi_4\rangle,
\end{aligned}$$

where the coefficients a, b and c read

$$\begin{aligned}
a &= -\frac{mn-m-n+1}{\sqrt{2n(m-1)(n-1)(m+n-1)}} - \frac{i}{\sqrt{2n}}, \\
b &= \sqrt{\frac{n}{2(m+n-1)}}, \\
c &= \frac{m-1}{\sqrt{2n(m-1)(m+n-1)}} - i\sqrt{\frac{n-1}{2n}}.
\end{aligned}$$

Let us now analyze the evolution of the state (9) towards the target state (8) under the effective evolution operator (12). The decomposition of the state (9) into the eigenbasis $|\chi_i\rangle$ is given by

$$\begin{aligned}
|init_2\rangle &= -\frac{1}{\sqrt{n}}|\chi_1\rangle - \sqrt{\frac{mn-m-n+1}{n(m+n-1)}}|\chi_2\rangle - \\
&\quad -\sqrt{\frac{n-1}{2(m+n-1)}}\left(|\chi_3\rangle + |\chi_4\rangle\right).
\end{aligned}$$

Hence, the state of the walk after t iterations of the effective two-step evolution operator, i.e. after $2t+1$ steps of the quantum walk, reads

$$\begin{aligned} |\psi(2t+1)\rangle &= -\frac{1}{\sqrt{n}}|\chi_1\rangle - \sqrt{\frac{mn-m-n+1}{n(m+n-1)}}|\chi_2\rangle - \\ &-\sqrt{\frac{n-1}{2(m+n-1)}}\left(e^{i\omega t}|\chi_3\rangle + e^{-i\omega t}|\chi_4\rangle\right). \end{aligned} \tag{13}$$

We find that the decomposition of the target state (8) into the eigenbasis $|\chi_i\rangle$ is given by

$$\begin{aligned} |target_2\rangle &= \frac{1}{\sqrt{m}}|\chi_1\rangle + \sqrt{\frac{(m-1)(n-1)}{m(m+n-1)}}|\chi_2\rangle + \\ &+\sqrt{\frac{m-1}{m}}\left(\overline{a}|\chi_3\rangle + a|\chi_4\rangle\right). \end{aligned}$$

Therefore, the fidelity between the state of the particle after $2t+1$ steps of the quantum walk (13) and the desired target state equals

$$\begin{aligned} \mathcal{F}(2t+1) &= |\langle\psi(2t+1)|target_2\rangle|^2 \\ &= \frac{1}{mn(m+n-1)^2}\left[mn-(m-1)(n-1)\cos(\omega t)+\right. \\ &\left.+\sqrt{(m-1)(n-1)(m+n-1)}\sin(\omega t)\right]^2. \end{aligned} \tag{14}$$

Note that for even number of steps the particle is located in the first part of the graph and hence the fidelity vanishes. We find that the first maximum of the fidelity is reached for

$$\omega t = \arccos\left(-\sqrt{\frac{(m-1)(n-1)}{mn}}\right),$$

i.e. in order to achieve the state transfer with highest possible probability we have to choose the number of steps of the quantum walk equal to odd integer closest to

$$T = 2t+1 = \frac{2\arccos\left(-\sqrt{\frac{(m-1)(n-1)}{mn}}\right)}{\arccos\left(\frac{mn-2m-2n+2}{mn}\right)} + 1. \tag{15}$$

The maximal value of fidelity is given by

$$\mathcal{F}_{\max} = \left(\frac{\sqrt{(m-1)(n-1)}+\sqrt{mn}}{m+n-1}\right)^2. \tag{16}$$

We note that the maximal fidelity is less than one unless $m=n$, i.e. perfect state transfer with unit probability can be achieved only when both parts have the same number of vertices.

We illustrate these results in Figures 1-4. In Figure 1 we consider state transfer on the complete bipartite graph $K_{100,100}$. The plot shows the fidelity as a function of the number of steps. Since the parts of the graph have the same number of vertices it is possible to achieve perfect state transfer with unit fidelity.

In Figure 2 we show the fidelity as a function of the number of steps for state transfer on the complete bipartite graph $K_{100,50}$, i.e. the parts have different number of vertices. In such a case it is not possible to achieve state transfer with unit fidelity. According to (16) the maximal attainable value of fidelity is $\mathcal{F}_{\max} \approx 0.89$.

In Figure 3 we display the maximal value of fidelity (16) as a function of the size of the parts m and n of the complete bipartite graph $K_{m,n}$.

Finally, in Figure 4 we show the maximal value of fidelity for the complete bipartite graph $K_{100,n}$ as a function of the size of the part containing the receiver vertex n.

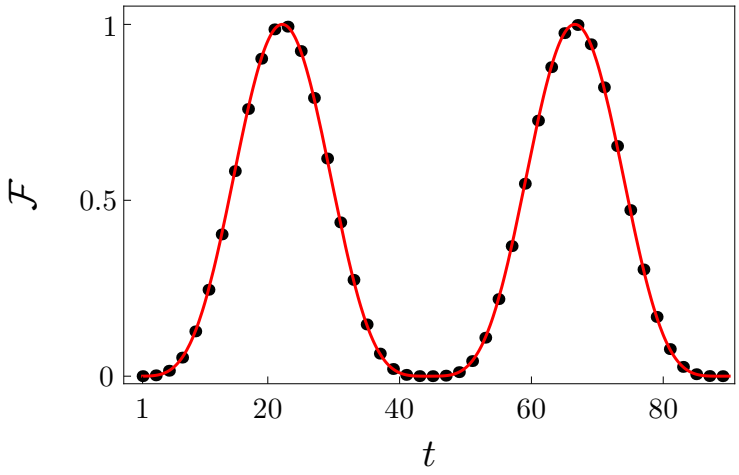

FIG. 1: Fidelity as a function of the number of steps t for state transfer on the complete bipartite graph $K_{100,100}$. The red line denotes the analytical expression (14) and the black dots corresponds to the numerical simulation. The black dots are plotted only for odd time steps, since for even steps the fidelity vanishes. Since $m = n$ perfect state transfer with unit fidelity is possible. The number of steps required to achieve unit fidelity is given by $T = 23$ steps, in accordance with the analytical results of (15).

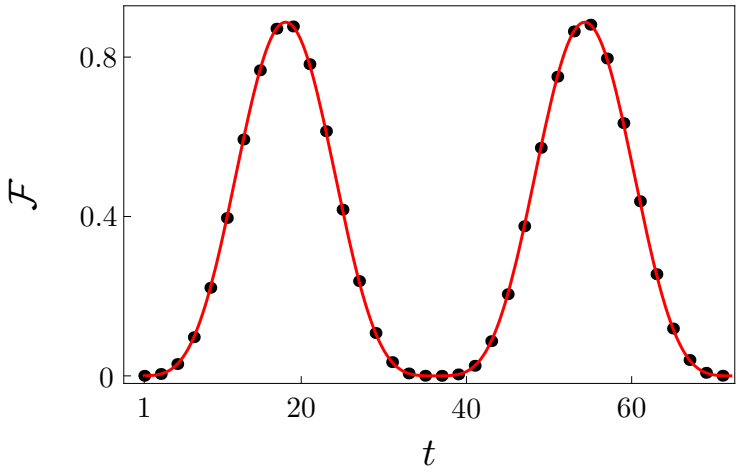

FIG. 2: Fidelity as a function of the number of steps for state transfer on the complete bipartite graph $K_{100,50}$. The red line denotes the analytical expression (14) and the black dots corresponds to the numerical simulation. Fidelity reaches the maximal value of $\mathcal{F}_{\max} \approx 0.89$ after $T = 19$ steps of the walk, in accordance with the analytical results of (16) and (15).

V. CONCLUSIONS

State transfer between two vertices of a complete bipartite graph by means of discrete-time quantum walk was analyzed. We have shown that when the sender and the receiver vertices are located in the same part the perfect state transfer is achievable independent of the size of the second component. However, when the sender and the receiver vertices are located in the opposite parts of the graph the state transfer with unit fidelity is achieved only when the two parts of the graph have exactly the same number of vertices. The maximal value of fidelity of state transfer in dependence on the number of vertices of the respective parts of the complete bipartite graph was determined.

In the present model we have discussed state transfer in a closed system, where the dynamics is purely unitary. However, one can consider interactions of the particle with environment, i.e. open quantum dynamics which inevitably

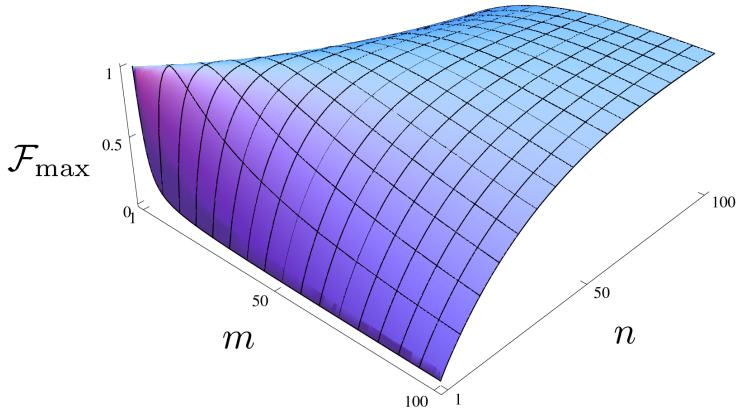

FIG. 3: Maximal value of the fidelity (16) in dependence on the size of the parts m and n of the complete bipartite graph $K_{m,n}$.

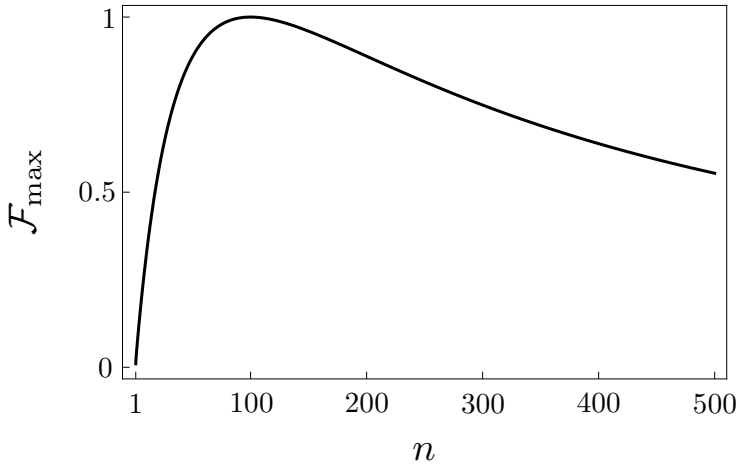

FIG. 4: Maximal value of fidelity (16) in dependence on the size of the part which contains the receiver vertex n. The size of the part which contains the sender vertex is taken as $m = 100$. We see that $\mathcal{F}_{\max}$ reaches unity for $m = n = 100$ and then declines gradually.

leads to decoherence. It would be interesting to analyze how strong interaction one can tolerate in order to achieve state transfer with a desired fidelity. We plan to investigate the effects of decoherence on the state transfer efficiency in the near future.

Acknowledgments

We acknowledge the financial support from RVO 14000 and from Czech Technical University in Prague under Grant No. SGS16/241/OHK4/3T/14. MŠ is grateful for the financial support from GAČR under Grant No. 14-02901P.

[1] Y. Aharonov, L. Davidovich and N. Zagury, Quantum random walks, Phys. Rev. A **48**, 1687 (1993)
[2] E. Farhi and S. Gutmann, Quantum computation and decision trees, Phys. Rev. A **58**, 915 (1998)

[3] D. Meyer, From quantum cellular automata to quantum lattice gases, J. Stat. Phys. **85**, 551, (1996)
[4] F. W. Strauch, Connecting the discrete-and continuous-time quantum walks, Phys. Rev. A 74, 030301 (2006)
[5] A. M. Childs, On the relationship between continuous- and discrete-time quantum walk, Comm. Math. Phys. **294**, 581 (2010)
[6] Y. Shikano, From discrete time quantum walk to continuous time quantum walk in limit distribution, J. Comput. Theor. Nanosci. **10**, 1558 (2013)
[7] A. M. Childs, E. Farhi and S. Gutmann, An example of the difference between quantum and classical random walks, Quantum Inf. Process. **1**, 35 (2002)
[8] A. M. Childs and J. Goldstone, Spatial search by quantum walk, Phys. Rev. A **70**, 022314 (2004).
[9] A. M. Childs and J. Goldstone, Spatial search and the Dirac equation, Phys. Rev. A **70**, 042312 (2004)
[10] O. Mülken, V. Bierbaum and A. Blumen, Coherent exciton transport in dendrimers and continuous-time quantum walks, J. Chem. Phys. **124**, 124905 (2006)
[11] O. Mülken, V. Pernice and A. Blumen, Quantum transport on small-world networks: A continuous-time quantum walk approach, Phys. Rev. E **76**, 051125 (2007)
[12] O. Mülken and A. Blumen, Continuous-time quantum walks: Models for coherent transport on complex networks, Phys. Rep. **502**, 37 (2011)
[13] A. M. Childs, Universal Computation by Quantum Walk, Phys. Rev. Lett. **102**, 180501 (2009)
[14] J. Janmark, D. A. Meyer and T. G. Wong, Global Symmetry is Unnecessary for Fast Quantum Search, Phys. Rev. Lett. **112**, 210502 (2014)
[15] L. Novo, S. Chakraborty, M. Mohseni, H. Neven and Y. Omar, Systematic Dimensionality Reduction for Quantum Walks: Optimal Spatial Search and Transport on Non-Regular Graphs, Scientific Rep. **5**, 13304 (2014)
[16] D. A. Meyer and T. G. Wong, Connectivity is a Poor Indicator of Fast Quantum Search, Phys. Rev. Lett. **114**, 110503 (2015)
[17] S. Chakraborty, L. Novo, A. Ambainis and Y. Omar, Spatial Search by Quantum Walk is Optimal for Almost all Graphs, Phys. Rev. Lett. **116**, 100501 (2016)
[18] A. Ambainis, E. Bach, A. Nayak, A. Vishwanath and J. Watrous, One-dimensional quantum walks, Proc. 33rd Ann. Symp. on Theory of Computing (New York: ACM), 37 (2001)
[19] T. D. Mackay, S. D. Bartlett, L. T. Stephenson and B. C. Sanders, Quantum walks in higher dimensions, J. Phys. A **35**, 2745 (2002)
[20] M. Hillery, J. Bergou and E. Feldman, Quantum walks based on an interferometric analogy, Phys. Rev. A **68**, 032314 (2003)
[21] E. Feldman and M. Hillery, Scattering theory and discrete-time quantum walks, Phys. Lett. A **324**, 277 (2004)
[22] E. Feldman and M. Hillery, Modifying quantum walks: a scattering theory approach, J. Phys. A **40**, 11343 (2007)
[23] F. M. Andrade and M. G. E. da Luz, Equivalence between discrete quantum walk models in arbitrary topologies, Phys. Rev. A **80**, 052301 (2009)
[24] B. F. Venancio, F. M. Andrade and M. G. E. da Luz, Unveiling and exemplifying the unitary equivalence of discrete time quantum walk models, J. Phys. A **46**, 165302 (2013)
[25] M. Szegedy, Quantum Speed-Up of Markov Chain Based Algorithms, in *Proceedings of the 45th Symposium on Foundations of Computer Science*, 3241 (2004)
[26] A. Patel, K. S. Raghunathan and P. Rungta, Quantum random walks do not need a coin toss, Phys. Rev. A **71**, 032347 (2005)
[27] A. Patel, K. S. Raghunathan and Md. A. Rahaman, Search on a hypercubic lattice using a quantum random walk. II. d=2, Phys. Rev. A 82, 032331 (2010)
[28] M. Falk, Quantum search on the spatial grid. arXiv:1303.4127, (2013)
[29] A. Ambainis, R. Portugal and N. Nahimov, Spatial search on grids with minimum memory, Quantum Inf. Comput. **15**, 1233 (2015)
[30] R. Portugal, S. Boettcher and S. Falkner, One-dimensional coinless quantum walks, Phys. Rev. A **91**, 052319 (2015)
[31] R. A. M. Santos, R. Portugal and S. Boettcher, Moments of coinless quantum walks on lattices, Quantum Inf. Process. **14**, 3179 (2015)
[32] R. Portugal, R.A.M. Santos, T.D. Fernandes and D.N. Gonalves, The Staggered Quantum Walk Model, Quantum Inf. Process. **15**, 85 (2016)
[33] R. Portugal, Staggered quantum walks on graphs, Phys. Rev. A **93**, 062335 (2016)
[34] N. Shenvi, J. Kempe and K. B. Whaley, Quantum random-walk search algorithm, Phys. Rev. A **67**, 052307 (2003)
[35] A. Ambainis, J. Kempe and A. Rivosh, Coins make quantum walks faster, in *Proceedings of the 16th ACM-SIAM Symposium on Discrete Algorithms*, 10991108 (2005)
[36] V. Potoček, A. Gábris, T. Kiss and I. Jex, Optimized quantum random-walk search algorithms, Phys. Rev. A **79**, 012325 (2009)
[37] B. Hein and G. Tanner, Quantum search algorithms on the hypercube, J. Phys. A **42**, 085303 (2009)
[38] D. Reitzner, M. Hillery, E. Feldman and V. Bužek, Quantum searches on highly symmetric graphs, Phys. Rev. A **79**, 012323 (2009)
[39] R. A. M. Santos, Szegedys quantum walk with queries, Quantum Inf. Process., 1 (2016)
[40] E. Feldman, M. Hillery, H. W. Lee, D. Reitzner, H. Zheng and V. Bužek, Finding structural anomalies in graphs by means of quantum walks, Phys. Rev. A **82**, 040301(R) (2010).
[41] M. Hillery, H. Zheng, E. Feldman, D. Reitzner and V. Bužek, Quantum walks as a probe of structural anomalies in graphs,

Phys. Rev. A **85**, 062325 (2012)
[42] S. Cottrell and M. Hillery, Finding structural anomalies in star graphs: A general approach, Phys. Rev. Lett. **112**, 030501 (2014)
[43] N. B. Lovett, S. Cooper, M. Everitt, M. Trevers and V. Kendon, Universal quantum computation using the discrete-time quantum walk, Phys. Rev. A **81**, 042330 (2010)
[44] S. Bose, Quantum communication through an unmodulated spin chain, Phys. Rev. Lett. **91**, 207901 (2003)
[45] P. Kurzynski and A. Wojcik, Discrete-time quantum walk approach to state transfer, Phys. Rev. A **83**, 062315 (2011)
[46] I. Yalcinkaya and Z. Gedik, Qubit state transfer via discrete-time quantum walks, J. Phys. A **48**, 225302 (2015)
[47] X. Zhan, H. Qin, Z. H. Bian, J. Li and P. Xue, Perfect state transfer and efficient quantum routing: A discrete-time quantum-walk approach, Phys. Rev. A **90**, 012331 (2014)
[48] B. Hein and G. Tanner, Wave Communication across Regular Lattices, Phys. Rev. Lett. **103**, 260501 (2009)
[49] V. M. Kendon and C. Tamon, Perfect State Transfer in Quantum Walks on Graphs, J. Comput. Theor. Nanosci. **8**, 422 (2011)
[50] K. Barr, T. Proctor, D. Allen and V. Kendon, Periodicity and perfect state transfer in quantum walks on variants of cycles, Quantum Inform. Comput. **14**, 417 (2014)
[51] M. Štefaňák and S. Skoupý, Perfect state transfer by means of discrete-time quantum walk search algorithms on highly symmetric graphs, Phys. Rev. A **94**, 022301 (2016)
[52] L. K. Grover, Quantum mechanics helps in searching for a needle in a haystack, Phys. Rev. Lett. **79**, 325 (1997)
[53] H. Krovi and T. A. Brun, Quantum walks on quotient graphs, Phys. Rev. A **75**, 062332 (2007)
[54] We note that the dimension of the invariant subspace can be reduced to three, however, the construction of the basis is more invovlved. Moreover, the subsequent analysis is not simpler than the one presented in the paper.